

Accn. 7377

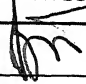
657 823

1129

**J.R.D. TATA MEMORIAL LIBRARY**  
**INDIAN INSTITUTE OF SCIENCE**  
BANGALORE - 560 012.

Accn. No. ....

This Journal / Reference publication ought to be  
returned on or before the date last marked below,  
or fines will be incurred.

DUE DATE	TICKET NO.	INTLS
24 JUN 2012		
33010100		


# ELECTRICAL VIBRATION INSTRUMENTS

AN ELEMENTARY TEXTBOOK

ON

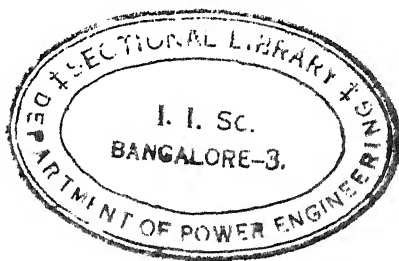
*The Behavior and Tests of Telephone Receivers,  
Oscillographs, and Vibration Galvanometers*

BY

A. E. KENNELLY

A.M. HON. (HARVARD) Sc.D. HON. (PITTSBURGH  
AND TOULOUSE)

PROFESSOR OF ELECTRICAL ENGINEERING, HARVARD UNIVERSITY AND  
THE MASSACHUSETTS INSTITUTE OF TECHNOLOGY, MEMBER NA-  
TIONAL ACADEMY OF SCIENCES, HONORARY MEMBER INSTITUTE  
OF ELECTRICAL ENGINEERS, LONDON, AND OF SOCIÉTÉ  
FRANÇAISE DES ÉLECTRICIENS, PARIS, PAST PRESI-  
DENT AMERICAN INSTITUTE OF ELECTRICAL EN-  
GINEERS, INSTITUTE OF RADIO ENGINEERS  
AND ILLUMINATING ENGINEERING  
SOCIETY.



*New York*

THE MACMILLAN COMPANY

1923

*All rights reserved*



COPYRIGHT, 1923,  
By THE MACMILLAN COMPANY

---

Set up and electrotyped. Published July, 1923.



## PREFACE

THE Bell telephone receiver is a marvelous instrument. It has undergone remarkably little change in structure since the first manufacturing model was produced by the inventor. It is reported that there were over 12,500,000 telephone receivers in public service at the end of 1920 in connection with the Bell system of the United States alone, or about one to every nine individuals in the then existing population. Nevertheless, there has been singularly little available information concerning the nature and properties of the telephone receiver as a machine. In order to understand quantitatively the delivery of speech by a receiver, its behavior as a machine must first be clearly understood.

It is the object of this book to present, from an electrical engineering standpoint, the characteristics of telephone receivers (and of other vibrational instruments) as reciprocating electric motors, based on researches which have been carried on in the electrical engineering laboratories at the Massachusetts Institute of Technology and at Harvard University during the past fourteen years.

The central idea in the preparation of the material for this book has been the wonderful and fascinating analogy between the laws of mechanics for a simple vibrational system, and the laws of electromagnetics for a simple alternating-current or oscillating-current system. An insight into one of these two systems provides a vision of the other. If electrical engineers received their fundamental training in the dynamics of mechanical vibrating systems, their conceptions of alternating-current circuits would doubtless be speedily grafted thereon. Actually, they almost always receive their fundamental training on these matters in the study of the electromagnetics of alternating-current circuits, so that their views of vibrating mechanical systems are most readily received through electric analogies. It is believed that the study of vibrating systems is not only made easy to electrical engineering students in this manner, but that

this study in turn aids and clarifies their knowledge of alternating-current systems.

Another basic idea in the presentation of the subject matter is that every electrical vibration instrument necessarily possesses a readily determinable motional-impedance diagram, which in its fundamental form is a simple circle, and which is capable of disclosing many electromechanical characteristics of the instrument.

It has been the aim of the work to offer a textbook to students of telephone engineering, as well as a reference book to telephone engineers on the subject of the receiver. Moreover, the same principles have been extended to cover the behavior and tests of oscillographs and vibration galvanometers, for the benefit of workers in electrical engineering laboratories generally.

An effort has been made to keep the main text of the book on a nearly uniform level of mathematical simplicity. Propositions of relative complexity, such as may be of interest for further investigation, have been collected into appendices.

The author has coöperated in some manner with a number of research workers in successive portions of this quest. While expressing his indebtedness to all, he desires to mention his particular indebtedness to the following collaborators: Professor W. L. Upson in 1908, Professor G. W. Pierce in 1912; Mr. H. A. Affel in 1914-15; Dr. H. O. Taylor in 1915-16; Messrs. R. N. Hunter and A. A. Prior in 1918-19; Professor H. Nukiyama in 1918; Professor H. Mori in 1919 and Professor K. Kurokawa in 1920. A large part of the experimental work described in the book has been performed by these coöperators, and it has been the welcome task of the author to collate and combine their contributions. Whatever credit there may be in the accomplishment of the task, he desires placed to their account. For such errors and defects as may exist in the work, he desires to accept personal responsibility. It has not been practicable to consult them in the preparation of the book. Sections of the work have been published already, however, in joint papers before technical societies since 1908.

The author is also under indebtedness to various members of the engineering staffs of the American Telephone and Telegraph Co. and the Western Electric Co. for special parts, for telephone receivers, for illustrative material, and for valuable suggestions. A considerable part of the laboratory research work was carried

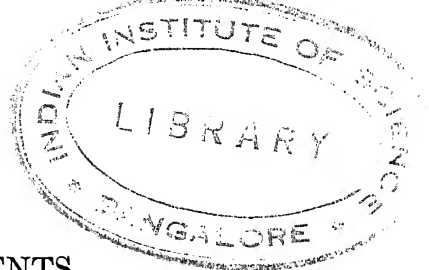
out under appropriations to the Massachusetts Institute of Technology from the American Telephone and Telegraph Company, for the encouragement of research; but the conduct of the work was left entirely to the officers of the Electrical Engineering Department of the Institute, and the MSS. of the book has not been submitted to the company for consideration before printing. In one sense this is a drawback, for the experience and knowledge of telephone apparatus acquired during many years by the excellent research engineers of that company has placed them in a position of unequalled technical advantages.

The author is also indebted to Professor V. Karapetoff for experimental material relating to the modes of vibration of steel diaphragms, to Mr. L. W. Chubb for data on circular zero oscillograms, and to Professor F. S. Dellenbaugh for transient oscillograms.

The MSS. of the book was completed in March, 1921; but its printing has been delayed by a variety of circumstances, including a year of exchange service in France, until the present time. The author desires to express his indebtedness to his colleagues, the editors, Professors D. C. Jackson and E. R. Hedrick, for their valuable suggestions and aid in preparing the MSS. and proofs for the press.

CAMBRIDGE, MASS.

*May, 1923*



## CONTENTS

CHAPTER	PAGE
I TELEPHONE RECEIVERS . . . . .	1
II THE PERMANENT MAGNET OF THE RECEIVER AND ITS FUNCTIONS . . . . .	6
III MODE OF VIBRATION OF A TELEPHONE DIAPHRAGM . . . . .	12
IV EQUIVALENT MASS OF A DIAPHRAGM VIBRATING IN ITS FUNDAMENTAL MODE . . . . .	32
V EQUIVALENT SINGLE CENTRAL ELASTIC FORCE, OR STIFF- NESS COEFFICIENT $s$ , OF A DIAPHRAGM . . . . .	37
VI FORCED VIBRATIONS OF A RECEIVER DIAPHRAGM UNDER A SIMPLE IMPRESSED VIBROMOTIVE FORCE . . . . .	42
VII THE ELECTRIC IMPEDANCE OF TELEPHONE RECEIVERS, AND ITS MEASUREMENT . . . . .	61
VIII THE VECTOR FORCE DIAGRAMS OF THE TELEPHONE RECEIVER . . . . .	80
IX THE ANALYSIS OF THE MOTIONAL-IMPEDANCE CIRCLE . . . . .	99
X METHODS FOR DETERMINING THE FUNDAMENTAL CON- STANTS OF A RECEIVER . . . . .	115
XI INFLUENCES THAT AFFECT THE CONSTANTS OF A RE- CEIVER . . . . .	134
XII SECONDARY DISTORTIONS OF MOTIONAL-IMPEDANCE CIRCLES . . . . .	142
XIII ACOUSTIC IMPEDANCE . . . . .	167
XIV INFLUENCE OF THE DIMENSIONS OF THE DIAPHRAGM UPON ITS CONSTANTS . . . . .	191
XV OSCILLOGRAPHS . . . . .	196
XVI ANGULAR VELOCITY OF A ROTATIONAL VIBRATING SYSTEM . . . . .	206
XVII BLUNTNESS AND SHARPNESS OF RESONANCE IN A VIBRATOR . . . . .	217
XVIII DISPLACEMENT IMPEDANCE AND ADMITTANCE . . . . .	221
XIX OSCILLOGRAPHMETERS . . . . .	237
XX OSCILLOGRAPH TESTS . . . . .	243
XXI TESTS OF OSCILLOGRAPHS . . . . .	250
XXII VIBRATION GALVANOMETERS . . . . .	265
XXIII THE HUMMING TELEPHONE . . . . .	287

## APPENDICES

	PAGE
I APPLICATION OF BESSEL FUNCTIONS TO THE ELEMENTARY THEORY OF PLATE VIBRATION . . . . .	303
II OUTLINE THEORY OF EQUIVALENT MASS OF A DIAPHRAGM . . . . .	307
III ELEMENTARY THEORY OF A SIMPLE VIBRATOR, WITH ESPECIAL REFERENCE TO A TELEPHONE-RECEIVER DIAPHRAGM . . . . .	311
IV ANGULAR VELOCITIES OF A SIMPLE MECHANICAL OR ELECTRIC SYSTEM . . . . .	325
V FREE DAMPED VIBRATIONS OF A SIMPLE MECHANICAL OR ELECTRIC SYSTEM. PERIODIC VIBRATION . . . . .	336
VI FREE UNDAMPED VIBRATION. LIMITING CASE OF NEGLIGIBLE RESISTANCE . . . . .	356
VII FREE OVERDAMPED VIBRATION OF A SIMPLE SYSTEM. ULTRAPERIODIC VIBRATION . . . . .	365
VIII FREE CRITICALLY DAMPED VIBRATION. APERIODIC VIBRATION . . . . .	379
IX ON THE ANALOGIES BETWEEN SOUND-WAVE TRANSMISSION ALONG A UNIFORM ACOUSTIC TUBE CONDUCTOR AND ELECTROMAGNETIC-WAVE TRANSMISSION ALONG A UNIFORM ELECTRIC LINE CONDUCTOR . . . . .	389
X RELATIONS BETWEEN TWO PLANE VECTORS WITH DISPLACED REFERENCE AXES . . . . .	397
XI GRAPHS OF SCALAR VELOCITIES AND DISPLACEMENTS . . . . .	399
XII DATA ON PROPORTIONALITY BETWEEN FRICTIONAL TORQUE AND ANGULAR VELOCITY IN VIBRATION INSTRUMENTS . . . . .	411
XIII HARMONIC ANALYSIS SCHEDULES . . . . .	413
XIV FURTHER EXPERIMENTAL TESTS OF MODES OF DIAPHRAGM VIBRATION . . . . .	426
LIST OF SYMBOLS EMPLOYED . . . . .	428
BIBLIOGRAPHY . . . . .	438
INDEX OF SUBJECTS . . . . .	443
INDEX OF NAMES . . . . .	449

# ELECTRICAL VIBRATION INSTRUMENTS



# ELECTRICAL VIBRATION INSTRUMENTS

## CHAPTER I

### TELEPHONE RECEIVERS

**Introduction.** — The electromagnetic telephone receiver of Bell is an electric motor of the reciprocating type. It receives alternating electric power from the telephone circuit with which it is connected, and transforms this into magnetic power in a magnetic circuit in the instrument. This alternating magnetic power is again transformed into alternating mechanical power, for the production of useful and recognizable acoustic vibrations. When supplied with electric power of a single frequency and suitable steady amplitude, the efficiency of a telephone receiver, considered as a motor, is the ratio of the acoustic power delivered into the adjacent air in sound, to the electric power received at its terminals. This efficiency differs greatly at different impressed frequencies.

When the receiver is employed as a detector of feeble alternating currents of a single frequency, a relatively high efficiency at that particular frequency is desirable — to the exclusion, perhaps, of high efficiency at other frequencies. When it is employed, however, as an instrument for reproducing speech, over a range of frequency from say 100 ~ to 2500 ~, a sharply tuned, or highly selective response of high efficiency at a single frequency is undesirable. In order to produce the best speech reproduction, moderately good efficiency, as a reciprocating motor, over a relatively wide range of frequency is to be preferred. This behavior is likely to be at variance with the production of the highest efficiency over a relatively small frequency range. The best telephonic alternating-current detector is therefore unlikely to be the best telephonic reproducer of speech.

Electromagnetic telephone receivers made at the present time may be divided into two classes:

(1) Receivers in which an alternating electromagnet operates directly upon an acoustic vibratory diaphragm armature of steel.



(2) Receivers in which an alternating electromagnet operates upon a vibratory steel armature, mechanically connected to a separate acoustic vibratory diaphragm.

To class (1) belong the ordinary Bell telephone receivers, which constitute the vast majority of receivers in service. To class (2) belong Baldwin receivers.

**Bell Receivers.** — Bell receivers are subdivided into two classes: namely, (a) *monopolar receivers* and (b) *bipolar receivers*.

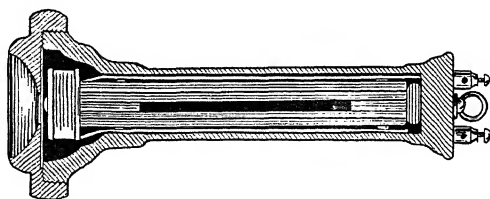


FIG. 1. Unipolar Bell telephone receiver of the year 1877.

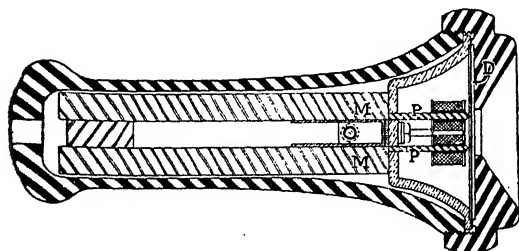
(a) The monopolar receiver was the form in which the Bell receiver was first manufactured for general industrial service, although both monopolar and bipolar receivers were made by Bell. The monopolar receiver has now been superseded almost entirely by the bipolar type. A monopolar receiver is illustrated in Fig. 1.

(b) The bipolar receiver is made in a variety of forms which differ, as a rule, only in relatively small mechanical details. They are divided into two subclasses: namely (b1) *hand receivers*, such as are provided with desk-



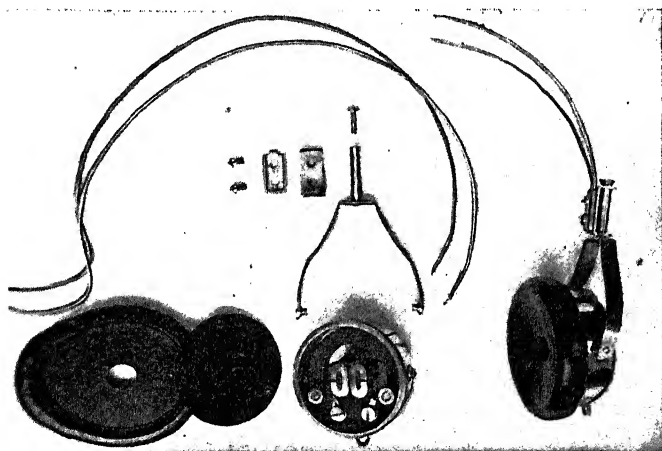
FIG. 2. Parts of a standard type of Western Electric Company's Bell telephone receiver, separated and assembled.

being held in the hand against the ear, and (b2), *head or watch-case receivers*, commonly supported in pairs by a metallic band, so as to be held one against each ear.



standard Bell telephone receiver for subscriber's sets. Longitudinal section.

and bipolar Western Electric receiver is illustrated in Fig. 2A. The bipolar permanent magnet *MM* carries a thinner polar extensions *PP*, on which the exciting coils are mounted. The electromagnetic system is firmly maintained at a distance from the japanned steel diaphragm *D*.



Western Electric watch-case receiver, assembled and with cover removed.

Fig. 3 illustrates a standard type of Western Electric watch-case receiver, both as assembled and with the cover removed. The relative positions between the parts is shown in Fig. 3A.

**Baldwin Receivers.** — A particular form of Baldwin receiver construction is indicated in Fig. 4. Here a single coil  $C$  receiving the telephone current, magnetizes an iron plate  $AA$ , which is supported within the coil and is free to oscillate about an axis through  $O$ . This plate is held between permanent magnet pole-pieces  $N S N' S'$ , by the elastic forces of a spring  $B$  at one end, and a light rod  $RR$  at the other, which rod is fastened to the

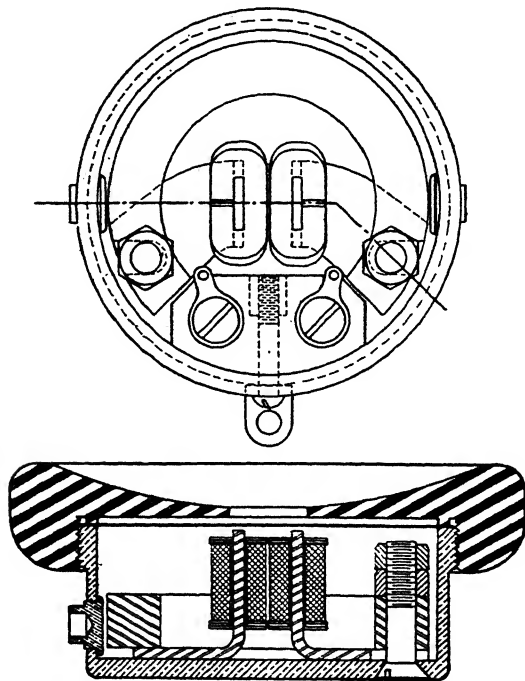


FIG. 3A. A standard Bell watch-case receiver. Plan and section along axis.

center of a mica diaphragm  $DD$ . The plate  $AA$  remains in equilibrium, under combined magnetic and elastic forces, until alternating currents in the coil set up alternating magnetization in the plate and cause the end  $R$  of the latter to be alternately raised and lowered, in synchronism with the alternating-current impulses, thus communicating vibration to the diaphragm  $DD$ .

**Conclusion.** — In what follows, we shall confine ourselves mainly to a consideration of the type of instrument in class 1; and, in particular, to bipolar instruments of the types represented

in Figs. 2 and 3. However, instruments of class 2 come within the principles, analyses, and tests to be described, so that although only class 1 receivers are referred to, yet receivers of class 2 will be included by inference. It is proposed to analyze the behavior

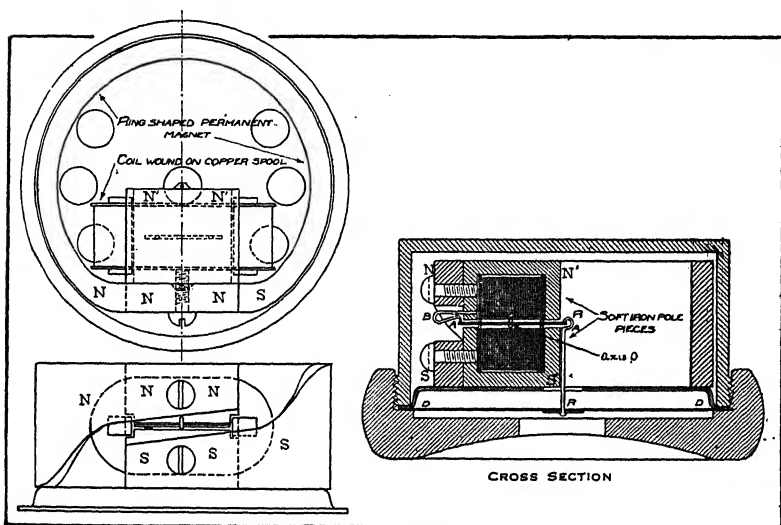


FIG. 4. Mica diaphragm telephone receiver. Air gap (including armature) = 0.11 cm. Thickness of armature = 0.03 cm.

of the telephone receiver as an electromagnetic motor — at least to a first approximation — and to describe a technique by which the characteristic constants of a receiver can be measured in the laboratory.

## CHAPTER II

### THE PERMANENT MAGNET OF THE RECEIVER AND ITS FUNCTIONS

**Introduction.** — The part played by the permanent magnet in a telephone receiver is very important, and has been recognized by various writers\* since the early days of the Bell invention. We shall see that it not only synchronizes the attractive vibromotive force (vmf.) on the armature, with the vmf. of the alternative current, but it also greatly enhances the magnitude of the vmf.

In Fig. 5,  $DD'$  represents a steel diaphragm clamped around its edge. In its initial position, this diaphragm lies in the plane of

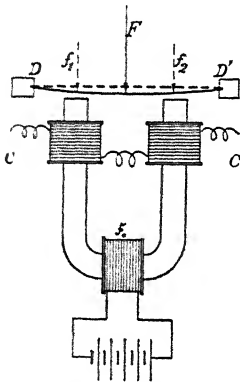


FIG. 5. Diagram of magnetic circuit in a bipolar telephone receiver.

the clamping edge, as indicated by the dotted line. When the permanent bipolar magnet is presented symmetrically to the lower surface of the diaphragm, however, a pair of parallel magnetic attracting forces are brought to act upon the latter, perpendicularly to its plane, along the dotted lines  $f_1 f_2$ , Fig. 5. Their effect is substantially the same as would be produced by  $F$ , their sum, acting downwards at the center of the diaphragm. This force flexes the diaphragm convexly towards the poles, although the actual deflection is usually only of the order of a tenth of a millimeter at the center. Consequently, for

practical purposes, we may disregard the curvature of the diaphragm in the presence of the poles, and consider that the diaphragm in the normal position has its lower surface parallel to the upper surface of each pole, as in Fig. 6, at a normal distance of  $X$  cm. from that surface. This air-gap length, or entrefer  $X$ , lies

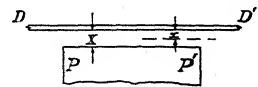


FIG. 6. Diagram of polar air gap of receiver.

\* Heavside, Bibliography 7. Meyer and Whitehead, Bibliography 39.

ordinarily between 0.1 mm. and 0.4 mm. It is commonly about 0.3 mm.

If the active surface area of each pole is  $S$  sq. cm., the air-gap reluctance at each gap, if we neglect magnetic fringing around the polar edge, is  $X/S$  oersteds; so that the total reluctance in the two air gaps of the permanent magnetic circuit will be

$$(1) \quad \mathcal{R}_0 = \frac{2 X}{S} \quad \text{oersteds.}$$

This is the principal reluctance in the circuit, because the rest of the magnetic circuit is metallic, even though it is of low permeability.

With the instrument in proper mechanical adjustment, there is a certain active permanent or structural magnetomotive force (mmf.),  $\mathcal{F}_0$  gilberts, resident in the molecular structure of the permanent magnet, as though produced by an exciting winding  $\mathcal{F}_0$  (Fig. 5) on a soft iron magnet. Neglecting magnetic leakage between the limbs, and also the magnetic reluctance in the diaphragm and other ferric parts of the circuit, we see that this mmf. produces a permanent magnetic flux through each air gap of

$$(2) \quad \phi_0 = \frac{\mathcal{F}_0}{\mathcal{R}_0} \quad \text{maxwells,}$$

and a corresponding permanent magnetic flux density in each gap of

$$(3) \quad \mathcal{B}_0 = \frac{\phi_0}{S} = \frac{\mathcal{F}_0}{\mathcal{R}_0 S} \quad \text{gausses.}$$

**Demagnetizing Force.** — The counter-magnetomotive force (cmf.) in the permanent magnetic circuit, due to the  $\phi \mathcal{R}$  drop of potential in the two air gaps, will be, to a first approximation,

$$(4) \quad \mathcal{F}_c = \phi_0 \mathcal{R}_0 = 2 \mathcal{B}_0 X \quad \text{gilberts,}$$

and the average counter-magnetic force, or demagnetizing force, in the magnetic circuit, will be

$$(5) \quad \mathcal{H}_c = \frac{\mathcal{F}_c}{L} = \mathcal{B}_0 \cdot \frac{2 X}{L} \quad \frac{\text{gilberts}}{\text{cm}},$$

where  $L$  is the mean length of flux path in the permanent magnet in cm. If  $\mathcal{F}_{im}$  is the maximum cyclic mmf. produced by the alternating current in the coils  $CC$  (Fig. 5), then the maximum cyclic

total demagnetizing force averaged over the whole length of the permanent magnet is

$$(6) \quad \mathcal{H}_c' = \frac{\mathcal{F}_c + \mathcal{F}_{im}}{L} = (\mathcal{B}_0 + \mathcal{B}_{im}) \frac{2X}{L} \quad \frac{\text{gilberts}}{\text{cm}}.$$

This demagnetizing force must be materially less than the coercive force of the steel in the permanent magnet at the flux density in the main cross-section of that magnet, as taken from the  $\mathcal{H}$ - $\mathcal{B}$  Ewing diagram, if demagnetization is to be safely resisted.\* This reasoning does not take into account the increased demagnetizing force that is produced when the diaphragm is lifted from the poles. This force is also much more difficult to assign numerically, owing to the lack of available experimental data. If the linear cmf.  $\phi_0 \mathcal{R}/L$  of the flux  $\phi_0$  through the reluctance  $\mathcal{R}$ , with diaphragm removed, exceeds the value of  $\mathcal{H}$  with which, in the diagram, the  $\mathcal{B}$  in the steel is associated, further demagnetization must instantly occur.

$\mathcal{F}_0$  in an ordinary type of hand receiver appears to be commonly in the neighborhood of 200 gilberts; that of  $\mathcal{R}_0$  about 0.6 oersted, and therefore  $\phi_0$  is about 330 maxwells. With  $S = 0.25$  sq. cm., this corresponds to  $\mathcal{B}_0 = 1320$  gausses.

The law of specific magnetic tractive force, as enunciated by Maxwell,† is

$$(7) \quad f = \frac{\mathcal{B}^2}{8\pi} \quad \frac{\text{dynes}}{\text{sq. cm.}},$$

which is directed along the flux paths. If  $S$  is the active surface of each pole in the entrefer over which the flux density  $\mathcal{B}_0$  exists uniformly, the total pull in a bipolar system is

$$(8) \quad F_0 = 2Sf = \frac{2S\mathcal{B}^2}{8\pi} = \frac{S\mathcal{B}^2}{4\pi} \quad \frac{\text{dynes}}{\text{sq. cm.}}$$

With  $\mathcal{B} = \mathcal{B}_0 = 1300$  gausses say, and  $2S = 0.5$  sq. cm., the specific force  $f$  would be 67250 dynes per sq. cm., or 68.5 gm. weight per sq. cm., and the total magnetic pull would be 33,625 dynes, or 34.3 gm. weight.

If now an alternating current of  $I_m$  maximum cyclic amperes be sent through the winding of the receiver, and  $N$  is the number

\* Ewing, Bibliography 6; also Bibliography 16.

† Bibliography 4.

of turns in this winding, including both coils, then the maximum cyclic mmf. produced by the excitation will be

$$(9) \quad \mathcal{F}_{im} = 4 \pi N I_m \quad \text{max. cy. gilberts.}$$

This mmf. will not develop exactly the same magnetic flux in the air gaps as the same number of structural gilberts in the permanent magnet, or as the same number of gilberts produced by an equivalent continuous current excitation  $\mathcal{F}_0$  (Fig. 5), because of leakage in the magnetic circuit. To a first approximation, however, we may ignore this leakage disturbance, and assume that the reluctance  $\mathcal{R}_0$  of the magnetic circuit, which resides mainly in the air gaps, is the same to both mmfs. The maximum cyclic flux produced by the alternating excitation will then be

$$(10) \quad \phi_{im} = \frac{4 \pi N I_m}{\mathcal{R}_0} \quad \text{max. cy. maxwells,}$$

and the corresponding flux density in the air gaps will be

$$(11) \quad \mathcal{B}_{im} = \frac{4 \pi N I_m}{S \mathcal{R}_0} \quad \text{max. cy. gaussses.}$$

With a current of 1 maximum cyclic milliampere in a winding of say 1300 turns (650 on each spool),

$$4 \pi N I_m = 1.63 \quad \text{max. cy. gilberts.}$$

With  $\mathcal{R}_0 = 0.6$  oersted, the flux  $\phi_{im}$  produced would be 2.7 max. cy. maxwells. The flux density  $\mathcal{B}_{im}$  in the air gaps, with  $S = 0.25$ , would be 10.8 max. cy. gaussses. This alternating flux density would be superposed upon the permanent magnetic flux density  $\mathcal{B}_0$ , which we have assumed as 1300 gaussses. The resultant flux density in the air gaps, with the alternating current applied, would thus vary between 1289.2 and 1310.8 gaussses, once in each current cycle.

Applying equation (8) we have for the total pull on the diaphragm

$$(12) \quad F = \frac{S}{4 \pi} (\mathcal{B}_0 + \mathcal{B}_{im})^2 \\ = \frac{S}{4 \pi} (\mathcal{B}_0^2 + 2 \mathcal{B}_0 \mathcal{B}_{im} + \mathcal{B}_{im}^2) \quad \text{max. alt. dynes.}$$

Referring to the terms within the bracket,  $\mathcal{B}_{im}^2$  may be neglected



in comparison with either  $\mathcal{B}_0^2$  or  $2 \mathcal{B}_0 \mathcal{B}_{im}$ . Consequently, we may write (12) in the form

$$\begin{aligned}
 (13) \quad F &= \frac{S}{4\pi} \mathcal{B}_0^2 + \frac{2S}{4\pi} \mathcal{B}_0 \mathcal{B}_{im} \\
 &= F_0 + \frac{2S}{4\pi} \mathcal{B}_0 \mathcal{B}_{im} = F_0 + \frac{\phi_0}{2\pi} \mathcal{B}_{im} \\
 &= F_0 + \frac{\mathcal{B}_0 \phi_{im}}{2\pi} = F_0 + 2 \mathcal{B}_0 \frac{N I_m}{\mathcal{R}_0} \quad \text{max. cyc. dynes.}
 \end{aligned}$$

This means that the pull on the diaphragm changes from  $F_0 - \mathcal{B}_0 \phi_{im}/2\pi$  to  $F_0 + \mathcal{B}_0 \phi_{im}/2\pi$  dynes and back, in each current cycle. In the case considered, the value of  $\pm \phi_0 \mathcal{B}_{im}/2\pi$ , the maximum alternating pull delivered by the current would be  $\pm 557$  dynes, superposed on  $F_0 = 33625$ ; or the total pull would vary between 33068 and 34182, a difference of 1114 dynes, once in each cycle.

If there were no permanent magnetic flux, and the alternating mmf. acted alone, it would produce, unaided, a pull of

$$(14) \quad F_{im} = \frac{2S}{8\pi} \mathcal{B}_{im}^2 \quad \text{max. cy. dynes,}$$

which, in the case considered, with 1 milliampere, and  $\mathcal{B}_{im} = 10.8$  gauss, would amount to only 2.32 dynes, twice in each current cycle. The maximum cyclic change in pull due to the current is thus increased, by the presence of the permanent magnet, in the ratio

$$(15) \quad \frac{2(F - F_0)}{F_{im}} = \frac{4\mathcal{B}_0}{\mathcal{B}_{im}},$$

which in this case is 481. The permanent magnet not only magnifies the magnetic pull 481 times, but it keeps the pitch of the diaphragm vibration in unison with the pitch of the alternating current. If the permanent magnetic flux were removed, the pitch of the diaphragm would be one octave above the pitch of the current. A receiver with a large permanent magnetic flux density in the air gaps is, therefore, other things being equal, a receiver of large magnetic amplifying power on the pull produced by the alternating current.

**Vibromotive Force.** — The alternating mechanical force produced on the diaphragm of a receiver is described as the *vibromotive force* (abbreviated vmf.). In the instance considered, the vmf. has a maximum cyclic value of 557 dynes, and an effective

(root-mean-square\*) value of  $557/\sqrt{2} = 394$  dynes. It is a simple harmonic quantity, if the impressed alternating current is simply harmonic (sinusoidal), and if the ratio  $\mathcal{B}_0/\mathcal{B}_{im}$  remains large. If the permanent flux density  $\mathcal{B}_0$  is unduly weakened, or if  $\mathcal{B}_{im}$  is unduly increased, an examination of equation (12) will show that the last term  $\mathcal{B}_{im}$  in the bracket can no longer be neglected. The result is that the vibromotive force  $F - F_0$  is no longer simply harmonic, when  $\mathcal{B}_{im}$  is sinusoidal; but is asymmetric with respect to its zero line, or contains even harmonics. Such harmonics appear in some oscillograms which were produced by the vibratory motion of a receiver diaphragm actuated by relatively strong alternating currents.†

The theory of magnetic amplification outlined above, although qualitatively acceptable, and in line with the literature of the subject, does not seem to have been quantitatively checked by experiment. It would be useful to obtain a check on formula (15) by experimental investigation.

\* That is, the square root of the average square, an expression well known in the theory of alternating electric currents. Hereafter we shall denote this by the abbreviation rms.

† Meyer and Whitehead, Bibliography 39.

## CHAPTER III

### MODE OF VIBRATION OF A TELEPHONE DIAPHRAGM

**Introduction.** — A symmetric monopolar telephone receiver produces, under the influence of an impressed alternating current, a vibromotive force at the center of the diaphragm, and perpendicular to its plane. A symmetric bipolar telephone receiver produces a parallel pair of equal forces, one on each side of the diaphragm center, which may be regarded for present purposes as equivalent to a single force equal to their sum acting at the center. The question then arises as to what kind of vibratory motion will be produced in the diaphragm by the action of this single equivalent central vmf.

**Classification of Diaphragms.** — In the theory of elastic vibrations, there are two kinds of diaphragms; namely, membranes and plates. A membrane is assumed to admit of being both bent and stretched by the action of small distorting forces, acting perpendicularly to its plane. It tends to return to its normal undisturbed position under the action of both antiflexural restoring forces across its plane, and of antistretching restoring forces in its plane. A plate is assumed to admit of being bent, but not stretched, by the action of small distorting forces. It tends to return to its normal undisturbed position solely under the action of antiflexural restoring forces across its plane. In practice, a diaphragm may behave mainly as a plate, but also partly as a membrane, the degree of mixture depending on its specific elasticities, its dimensions, and on the nature of the clamping. A plate powerfully stretched by radial forces at its boundary, tends to develop membranous behavior. The laws of vibration of membranes and plates are distinct, although they have resemblances.\* In the case of the steel diaphragm of a telephone receiver, clamped at the edge in the ordinary way, without stretch, the diaphragm may be considered as a simple plate, and only plate vibrations need here be discussed.

\*Rayleigh, Bibliography 12.

**Modes of Vibration.** — When a circular plate is clamped at the edge and is subjected to a blow perpendicular to its plane, it is shown in textbooks on acoustics\* that it is able to vibrate freely in three modes, and either singly or in any combination of these modes:

- (1) As a whole, and without nodal diameters or nodal circles.
- (2) In circular sectors with nodal diameters.
- (3) In circular segments with nodal circles.

The first mode is not only the simplest but it is also the mode of lowest natural or free pitch. That is, it is the gravest mode.

In the second mode, the plate breaks up into vibrating sectors separated by nodal diameters, or diameters which remain at rest. Theoretically, there may be any number of such pairs of ventral sectors and intermediate nodal diameters. The simplest case of the second mode is that of one diameter,† dividing the flat plate into two semicircular ventral sectors *A* and *B*. When *A* is moving up, *B* is moving down at the same velocity reversed, and to the same extent or displacement. The next simplest case has two mutually perpendicular nodal diameters, dividing the plate into four quadrantal ventral sectors *A*, *B*, *C*, and *D*. When *A* and *C* are moving up, *B* and *D* are moving down, to like displacements, and with like velocities. The pitch of the vibration increases with the number of nodal diameters; but not in simple proportion. In other words, the overtones of the plate produced by nodal sectoring are not in harmonic numerical ratios. Their numerical ratios are more complex and involve *Bessel overtones*.

In the third mode, the plate breaks up into concentric vibrating circular segments separated by nodal concentric circles, or circles which remain at rest. Theoretically, there may be any number of such ventral segments and intermediate nodal circles. The simplest case of the third mode is that in which there is one nodal circle, dividing the plate into an interior circle *A* and an external circular ring *B*. When *A* is moving up, *B* is moving down symmetrically, and *vice versa*.

The next simplest case of the third mode has two nodal circles, dividing the plate into three concentric circular areas *A*, *B*, and *C*. When *B* moves up *A* and *C* move down symmetrically, and so on.

\* Rayleigh, Bibliography 12; Barton, Bibliography 28.

† Lamb, Bibliography 35.

The pitch of vibration increases with the number of nodal circles; but not in simple proportion. The overtones or "partials" of the third mode again are not harmonic to the fundamental, or to one another.\*

The subject of free vibration in the first mode is discussed further in Appendices I and II.

A uniform circular plate, clamped at the edge, is thus able to vibrate freely in three modes, *i.e.*, in any one singly, or all together, and with an indefinitely large number of ascending pitches in either of the last two modes. Any free vibration must occur in one of these modes. The number of free pitches within a given musical compass of say 3 octaves is limited. It will have a fundamental pitch in the first mode, then a certain number within the three octaves in the second mode, and also a certain number in the third mode. When the plate is set into free vibration, any or all of these free pitches may be present in the resultant tone, the prominence of the individual overtones depending upon the nature and geometric distribution of the initial disturbance, as well as upon the geometric constraints imposed on the plate. Thus, touching the plate at a point tends to favor the mode or modes of vibration that form a nodal line through that point.

If, instead of disturbing the plate and allowing it to vibrate freely towards its normal position of rest, we impress forced vibrations upon the plate, by a simple harmonic vmf., how will the plate respond? It will vibrate; but will it vibrate in the first, second, or third mode, or in all three? It is evident that it is possible to set up vibrations in any of three modes, and in any of the overtones of the two last modes. Theoretically, it can always respond in the first mode, the whole plate bulging alternately up and down with the maximum displacement at the center. On the other hand, there is no bar to the setting up of a vibration of a certain amplitude in the second or third mode, or in a particular overtone of either.

It is easy to realize that if the impressed vmf. happens to have the precise pitch of one of the overtones of the second or third modes, there will be an inducement for the plate to assume that mode and overtone; but it might also, while so doing, retain part of its energy of motion in the first mode.

It is also easy to realize that small mechanical or geometric

\* Lamb, Bibliography 35.

asymmetries or nonuniformities in the plate system may appreciably influence the partition of vibrational energy into modes of motion. Moreover, the amplitude and the distribution of the vmf. over the plate enter into the action. Very feeble and symmetrically distributed vmfs. favor the first or fundamental mode. Vigorous and asymmetrically distributed vmfs. favor departures towards overtones generally, or particular individual overtones. See also Appendix XIV.

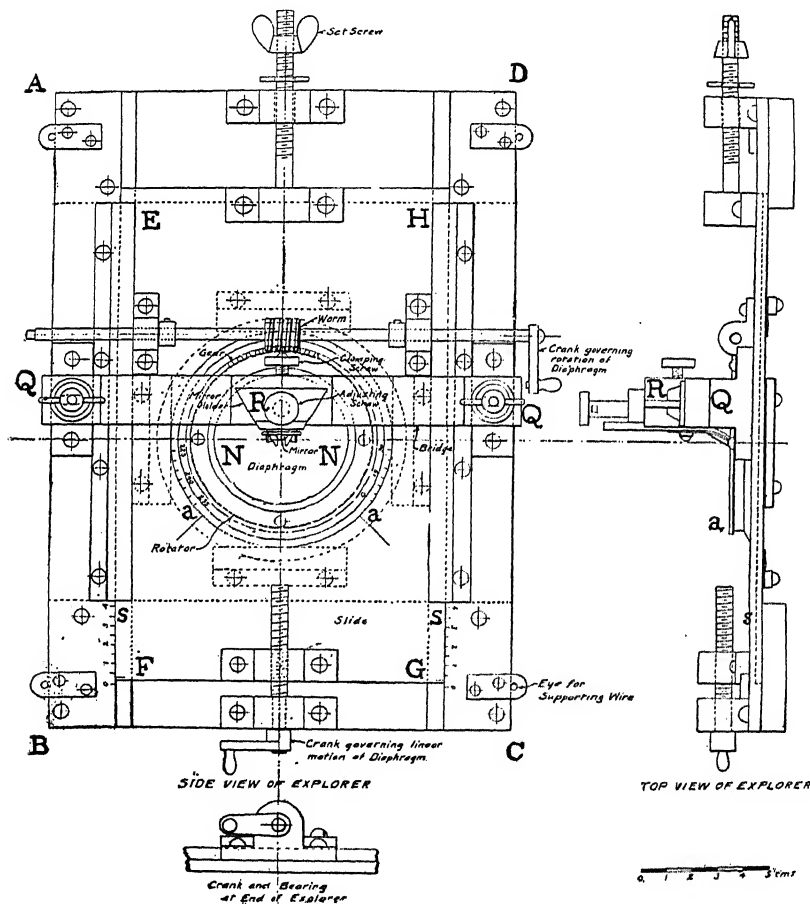


FIG. 7. Side view of explorer.

FIG. 8. Top view of explorer.

### Measurements of Diaphragm Vibration-Amplitude Distribution.

— In order to obtain information concerning the mode of motion of

receiver diaphragms under forced vibrations, an instrument for measuring the amplitude of displacement down to a tenth of a micron ( $10^{-4}$  mm.) was designed and built in 1914-15. It has been described as an *explorer* in relation to vibration amplitudes. The measurements, which occupied several months,\* were made by Dr. H. O. Taylor.

The explorer consists of a minute triangular mirror, elastically applied to the surface of a diaphragm, in such a manner that a beam of light reflected therefrom may be expanded into a luminous band of measurable length when that point on the diaphragm vibrates.

The explorer is illustrated to scale in Figs. 7, 8, and 9. A fairly massive rectangular brass frame *ABCD* holds a brass plate *EFGH*, which slides spring tight in grooves. The crank *K* con-

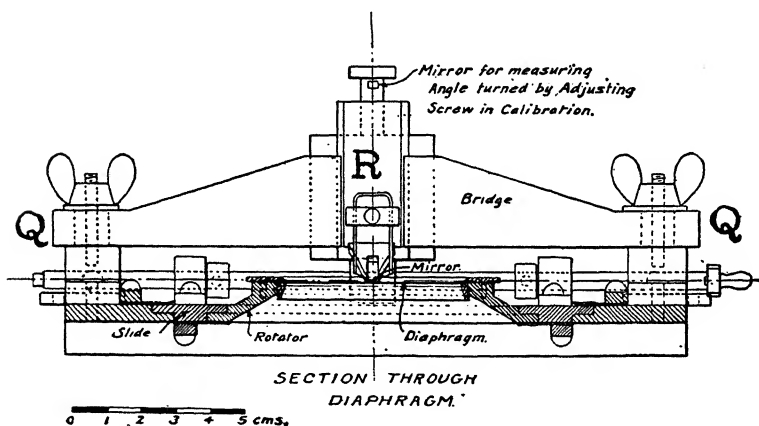


FIG. 9. Apparatus for exploring the vibration of diaphragms.

trols the sliding movement, with the aid of the set screw for arresting the motion. The extent of the plate's displacement in the slide can be read off on the scales ss. In the center of the plate *EFGH* is a circular frame *NN*, into which is clamped the diaphragm to be tested. The circular frame can be rotated in its own plane, by means of the crank shown.

A stout brass bridge *QQ* is fastened across the main frame *ABCD*. At the middle of this bridge is the mirror holder *R*,

\* Kennelly and Taylor, Bibliography 56.

shown in detail in Fig. 10. The mirror holder slides in a groove provided in the bridge, and can be clamped therein by the screw *S*. A fine-motion screw *M* is also provided, for adjusting the position of the mirror. One turn of *M* advances the mirror 0.8 mm. By means of an auxiliary mirror, fastened beneath the top of the screw *M*, the angle through which the screw is advanced may be measured, for calibrating the indications of the instrument. Adjustment can be made to a single degree of rotation of *M*; i.e., to  $0.8/360$  mm. = 2.2 microns or  $2.2 \mu$ , assuming that backlash is guarded against.

The construction is such that the tiny mirror is held at all times at the center of the main frame *ABCD*; while by means of the two crank adjustments, the diaphragm to be explored can be moved so as to bring any part of its surface beneath this mirror. With the aid of the scales of distance *ss*, and of angle *aa*, the position of the mirror with respect to the center of the diaphragm can be adjusted and read off in polar coordinates  $\rho$  and  $\beta$ . The motion in  $\rho$  can be adjusted to 0.1 mm. and the motion in  $\beta$  to  $1^\circ$  or less. The slide *EFGH* is held in position by stout flat springs on the main frame, so as to keep the motion of the slide confined to its own plane. A similar construction is used with the circular frame. It is important that the plane of the diaphragm shall not be disturbed when either crank is operated. The weight of the explorer is 4.6 kg.

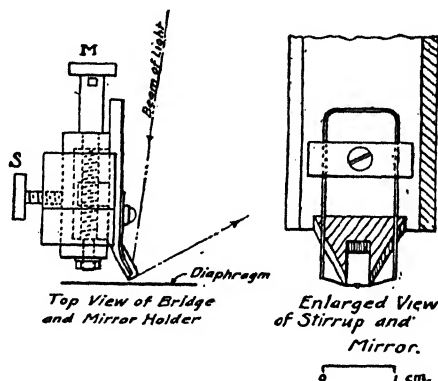


FIG. 10. Top view of bridge and mirror holder.  
Enlarged view of stirrup and mirror.

Figure 10 gives a magnified view of the exploring mirror *m* and its supports. The mirror is of silvered glass, 0.1 mm. thick,



and is equilaterally triangular in form, about 1 mm. in length of edge. One vertex of the mirror is applied to the surface of the diaphragm. The mirror is fastened with sealing wax across a thin phosphor bronze strip. This strip is approximately 3 mm. long between abutments, 0.02 mm. wide, and 0.013 mm. thick. The weight of the mirror, without varnish or sealing wax, is about 1 milligram. The tension of the strip in the stirrup is such as to make the natural frequency of the mirror's vibration about 2500  $\sim$ . It is important that the natural vibration frequency of the mirror should always exceed that of the diaphragm to which it is applied. These little mirrors are apt to break in service, so that they have to be renewed and recalibrated occasionally. The pressure exerted by the mirror point on the diaphragm was found to be approximately 200 dynes (0.2 gm. weight). A pressure of this order seems to be desirable, in order to secure a natural vibration frequency of 2500  $\sim$ . If, however, explorations are confined to lower diaphragm frequencies, the natural frequency of the mirror, and its pressure on the diaphragm, may be reduced accordingly.

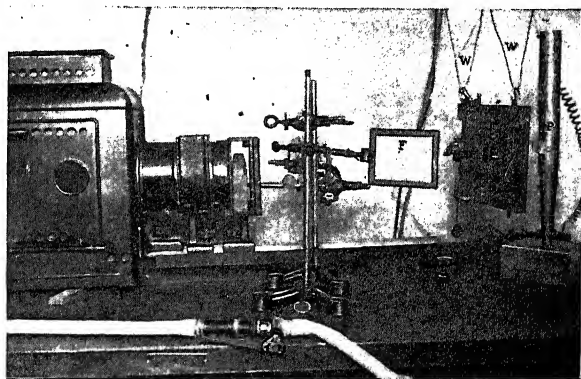


FIG. 11. Vibration explorer in position for observations.

The diaphragm to be explored was 5.4 cm. in diameter, in order to suit telephone receiver sizes, and was clamped tightly in the circular frame *NN* with a ring clamp, which has a clamping radius of 2.62 cm., when no auxiliary clamping rings are resorted to.

**Explorer Supports.** — The explorer is supported on wires *WW*, Fig. 11, from the ceiling of the testing room, in order to suppress

casual building vibrations of high frequency. A special testing-room was used for the purpose, consisting of a wooden sound-reducing booth, internally 274 cm.  $\times$  183 cm.  $\times$  214 cm. high, lined on the inside with hair felt 2.5 cm. thick, and surfaced with thin cotton cloth.

The mirror holder is advanced towards the diaphragm and clamped by the screw *s*. The mirror *m* is then carefully brought into contact with the diaphragm at the proper point, by means of the fine adjusting screw *M*.

Figure 11 is a photograph of the explorer and some of its adjacent optical accessories. The condensing and focusing lens of the stereopticon throws a narrow arc-light beam upon the exploring mirror, which reflects it on to the graduated translucent screen *F*. With the diaphragm at rest, the spot on this screen is a narrow, sharp, vertical luminous strip. When the diaphragm is set in vibration by sound waves from the organ pipe *P*, the mirror in contact with it vibrates synchronously, and the spot spreads into a luminous band, the limits of which are easily read on the graduated translucent scale. If the motions of the diaphragm and mirror are simple harmonic motions, the luminous band shows no discontinuities of intensity. If, however, there is a complex harmonic motion, the luminous band will show light and dark patches, either quiescent, or with beats. By means of the optical magnification of amplitude that can be effected with the apparatus, diaphragm vibrations of amplitude  $0.1 \mu$  ( $10^{-5}$  cm.), or less, can be observed; although the precision of measurement falls off considerably for amplitudes below  $0.5 \mu$  (half a micron).

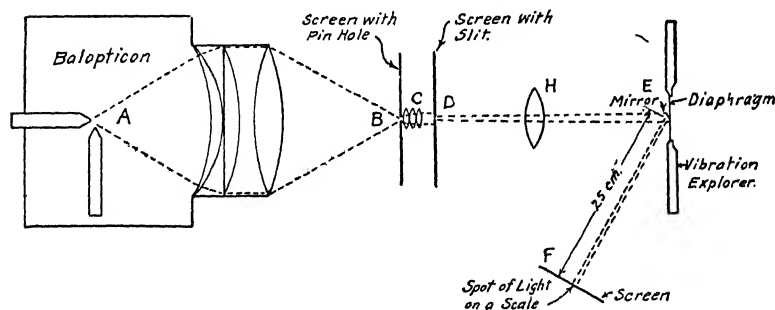


FIG. 12. Diagram of optical system used with vibration explorer.

**Explorer Optical System.** — In order to secure good measurements with the explorer, a good optical system is necessary for it. A satisfactory system is shown in Fig. 12. The stereopticon arc lamp *A* throws a powerful condensed beam of light on the pinhole *B* in a vertical brass screen. A set of small powerful collimating lenses *C* throws the nearly paralleled beam through the screen and slit *D*, as well as the focusing lens *H*, on the exploring mirror at *E*, whence it is reflected to the translucent screen *F*,

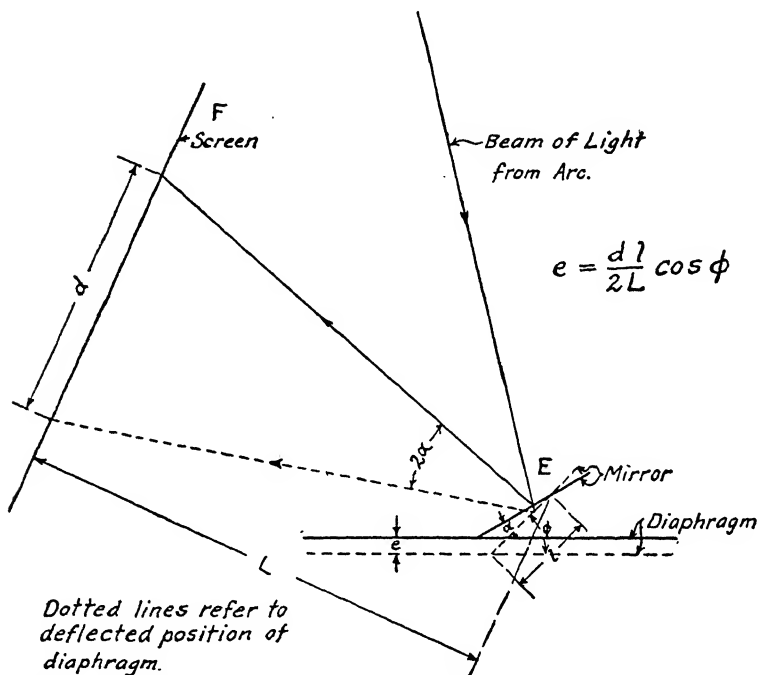


FIG. 13. Diagram showing action between mirror and diaphragm in explorer.

at a convenient distance, in this case 25 cm. An image of the slit in the screen *D* is then sharply focused at *F*. It is indicated geometrically in Fig. 13, that the double amplitude *e* of the diaphragm's displacement, is equal to the continued product of the observed double amplitude *d* of the luminous band, the ratio of *l* (the mirror's radius arm) to 2 *L* (the doubled mirror-screen distance), and the cosine of the angle  $\phi$  between the radius arm of the mirror and the plane of the diaphragm. In order to avoid frequent changes in  $\phi$ , it is desirable to keep the zero of the spot

of light as closely as possible constant at the center of the graduated scale  $F$ , and with it, the contacting angle plane of the mirror. The numerical expression

$$(16) \quad M = \frac{2L}{l \cos \phi}^*$$

may be called the *magnification factor* of the explorer. As ordinarily employed,  $2L = 50$  cm.,  $l = 0.05$  cm.,  $\phi = 45^\circ$ , approximately, or  $\cos \phi = 0.7$ ; so that  $M = 1400$  approximately, varying in different sets of measurements between 800 and 1500. In measurements with other modifications of the explorer, the magnification factor has been carried with advantage to 5000, but by increasing the distance  $L$ . There is a limit, however, to the advantage which may be secured in this way, owing to the reduction in the sharpness and intensity of the luminous band as  $L$  is increased. At  $L = 25$  cm. with the optical system described, the double amplitude could be read at each end to 0.1 mm. on the translucent scale  $F$ . A fine cross hair placed diametrically across the pinhole has also been found useful in reading off the double amplitude on the scale.

In determining the magnification factor for any series of measurements, it is not necessary to know  $l$  and  $\phi$  in equation (16). It is sufficient to advance the exploring mirror stirrup through a known small distance towards the quiescent diaphragm, by means of the fine-motion screw  $M$ , and observe the movement of the spot of light thereby produced on scale  $F$ . It is clearly a matter of indifference, so far as the movement of mirror  $m$  is concerned, whether the diaphragm moves up against a stationary stirrup, or the stirrup is moved down to the same extent against the stationary diaphragm. The displacement of the luminous spot will be the same. In this way, knowing the advance given by the screw  $M$ , the explorer becomes directly calibrated in position, for the particular values of  $l$  and  $\phi$  in use. In order to determine the advance of the screw  $M$  in such calibration tests, a little mirror is mounted on  $M$ . In other forms of explorer, this mirror is dispensed with, but a long indicator arm, radially attached to the fine-motion screw, moves over a graduated arc and enables the advance of the screw to be determined.

\* No unit is designated in equation (16), or in similar equations throughout the text, where the quantity expressed in the equation is dimensionless, i.e., a mere numerical ratio or a number; whether real or complex.

**Sources of Diaphragm Vibromotive Force.**— Two sources of diaphragm vmf. were employed in the tests: (1) acoustic, (2) electromagnetic.

(1) The acoustic vmfs. were produced from one of a series of small organ pipes, giving fairly simple musical tones, between  $C_2 = 128 \sim$  and  $C_6 = 2048 \sim$ . The organ pipe selected was mounted in a block on the table, at the back of the explorer, and supplied with air at constant pressure (about 18 cm. of water) from a pneumatic tank. The observer, after turning on the air to the organ pipe, observed the amplitude of the luminous band on the translucent screen  $F$ , Figs. 11 and 13, as the point of the exploring mirror was applied at successive positions on the diaphragm.

(2) The clamping ring of the diaphragm in the explorer was chosen of such dimensions that a standard telephone receiver could be substituted for it. In this case, a steel diaphragm had to be employed. The telephone was then operated by a feeble measured alternating current (2.0 milliamperes) obtained from a Vreeland mercury-arc oscillator, having its frequency steadily adjustable between the limits of  $425 \sim$  and  $2500 \sim$ .

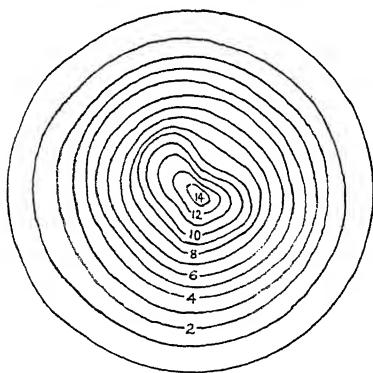


FIG. 14. Contour lines of vibration over diaphragm No. 1, at  $608 \sim$ .  
Vibration amplitudes in microns.

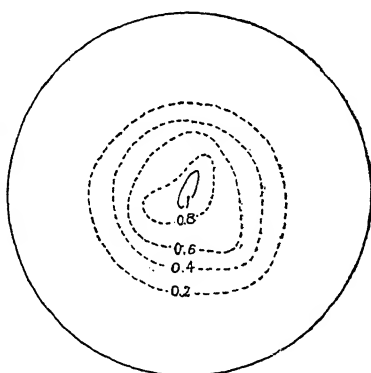


FIG. 15. Contour lines of vibration over diaphragm No. 2, at  $2100 \sim$ .  
Vibration amplitudes in microns.

**Exploration over Diaphragm No. 1.**— Diaphragm No. 1 was a telephone receiver diaphragm of steel, jappanned on one side. Its dimensions are given in Table IV. The diaphragm was clamped, around the boundary, between opposing circular knife-edges.

An organ pipe of  $D\#_4 = 608 \sim$ , was set up with its lip 5 cm. from the back of the diaphragm. An exploration was then made over the surface, at points differing by  $40^\circ$  in azimuth  $\beta$ , and at successive increments in radius  $r$  of about 3.5 mm. (7 steps in  $r$ , and 9 steps in  $\beta$ , or 63 observations in all). Table I sets forth these observations reduced to microns of amplitude, with a calibrated magnification factor of  $M = 1180$ .

TABLE I

VIBRATION AMPLITUDES OVER DIAPHRAGM NO. 1, AT FREQUENCY 608  $\sim$ , FOR NINE DIFFERENT AZIMUTHS  $\beta$ , AND SEVEN DIFFERENT RADIAL DISTANCES  $r$ . (Taylor)

RADIAL DISTANCE, $r$ — Cm.	VIBRATION AMPLITUDE OBSERVED WITH EXPLORER (MICRONS) AT DIFFERENT AZIMUTHS $\beta$ .								
	$0^\circ$ $\mu$	$40^\circ$ $\mu$	$80^\circ$ $\mu$	$120^\circ$ $\mu$	$160^\circ$ $\mu$	$200^\circ$ $\mu$	$240^\circ$ $\mu$	$280^\circ$ $\mu$	$320^\circ$ $\mu$
− 0.08	13.8	12.1	11.7	14.0	13.4	10.4	10.8	13.3	12.0
+ 0.31	12.7	10.9	11.3	12.3	12.7	9.7	10.6	12.6	11.6
+ 0.69	9.7	8.0	8.9	10.4	10.4	8.1	8.8	11.5	9.5
+ 1.06	6.6	5.9	6.4	6.8	7.0	6.2	6.4	7.1	6.8
+ 1.44	4.2	3.6	4.2	4.7	4.5	4.1	4.2	4.9	4.3
+ 1.82	2.5	2.2	2.1	2.5	2.5	2.3	2.4	2.5	2.4
+ 2.20	0.9	0.8	0.9	0.9	0.9	0.7	0.7	0.9	0.8
+ 2.54	0	0	0	0	0	0	0	0	0

It will be seen from this table that at any particular radius  $r$ , measured from the center of the diaphragm, the amplitudes of vibration displacement  $x$ , at varying azimuths  $\beta$ , are substantially equal. The irregularities, although small, seem however to be greater than can be accounted for by errors in observation, and are perhaps due to irregularities in the diaphragm. Figure 14 shows the contour lines of displacement amplitude in microns, the maximum amplitude being at or near the center, and amounting to  $14 \mu$ . Such amplitudes are larger than ordinarily obtain, and were specially reinforced in this case, in order to secure relatively large and easily measurable deflections. Figure 14 shows that the diaphragm vibrated in its fundamental or first mode, i.e., simple to-and-fro motion as a whole, without either nodal diameters or nodal circles. If other modes of motion are present, they are not noticeable on the scale of the diagram.

A similar exploration was made over the diaphragm, with acoustic vmf. from an organ pipe giving  $C_6 = 2050 \sim$ . Here the points of observation were in steps of about 3.5 mm. in  $r$ , and in steps of  $40^\circ$  in  $\beta$ , as before, with  $M = 1265$  (see Table II).

TABLE II  
VIBRATION AMPLITUDES OVER DIAPHRAGM No. 1, AT FREQUENCY 2,100 ~,  
FOR NINE DIFFERENT AZIMUTHS  $\beta$ , AND SEVEN DIFFERENT RADIAL  
DISTANCES  $r$ ., FIVE ONLY GIVING READABLE DEFLECTIONS (Taylor)

RADIAL DISTANCE, $r$ . CM.	VIBRATION AMPLITUDE OBSERVED, WITH EXPLORER, AT DIFFERENT AZIMUTHS $\beta$								
	0° $\mu$	40° $\mu$	80° $\mu$	120° $\mu$	160° $\mu$	200° $\mu$	240° $\mu$	280° $\mu$	320° $\mu$
- 0.08	0.70	0.95	0.95	0.95	0.87	1.02	0.95	0.87	0.95
+ 0.31	0.70	0.87	0.87	0.78	0.78	1.02	0.87	0.78	0.87
+ 0.69	0.62	0.78	0.78	0.62	0.62	0.78	0.62	0.62	0.78
+ 1.06	0.31	0.39	0.39	0.39	0.39	0.39	0.39	0.39	0.62
+ 1.44	0.16	0.16	0.16	0.08	0.08	0.08	0.08	0.08	0.23
+ 1.82	—	—	—	—	—	—	—	—	—
+ 2.20	—	—	—	—	—	—	—	—	—
+ 2.54	0	0	0	0	0	0	0	0	0

The vibration displacement contours for this case are given in Fig. 15. Here again, it is seen that, allowing for possible irregularities in the diaphragm, and for errors of observation, which are the more noticeable with the smaller amplitudes at the higher pitch, the mode of vibration is essentially fundamental, since there are no perceptible nodal circles or nodal diameters.

A series of explorations were then made at a number of acoustic pitches between 400 ~ and 1800 ~. The results are contained in Table III. They indicate the first or fundamental mode of vibration, throughout, within the limits of experimental error.

TABLE III  
SHOWING FUNDAMENTAL MODE OF VIBRATION MAINTAINED FOR A RANGE  
OF FREQUENCIES FROM 400 ~ TO 1,800 ~. (Taylor)  
*Amplitudes of Vibration in Microns ( $\mu$ ) along Radius of Diaphragm No. 1,  
Flat-Clamped.  $f_0 = 704$  ~.*

RADIAL DISTANCE, $r$ . CM.	FREQUENCY OF VIBRATION						
	400 ~ $\mu$	500 ~ $\mu$	750 ~ $\mu$	1,000 ~ $\mu$	1,250 ~ $\mu$	1,500 ~ $\mu$	1,800 ~ $\mu$
.04	.8	1.6	7.8	1.3	1.3	.9	.3
.29	.8	1.6	7.7	1.3	1.2	.9	.3
.54	.7	1.5	7.2	1.1	1.1	.8	.3
.79	.6	1.4	6.3	.9	.9	.6	.2
1.04	.5	1.3	5.3	.8	.8	.5	.2
1.29	.4	1.0	3.8	.5	.6	.3	.1
1.55	.2	.7	3.0	.3	.4	.2	+
1.79	.1	.4	1.9	.2	.2	.1	+
2.04	+	.3	1.2	.1	.1	+	—
2.30	—	.1	.8	—	+	—	—
2.65	0	0	0	0	0	0	0

Observations were also made at organ-pipe frequencies down to  $128 \sim$ . Explorations are difficult to make at such low frequencies on diaphragms of these properties and dimensions, because of the small amplitudes obtainable; so that the results lack precision, but so far as could be detected, the fundamental mode of vibration continued throughout.

In the case of this steel diaphragm, therefore, excited by acoustic vmfs., to frequencies as high as  $2050 \sim$ , the fundamental mode of vibration was the only one observed. This does not mean that the other modes of motion could not or did not exist; but merely that if they did exist, they were overshadowed by the preponderating first mode. Moreover, the uniformity of acoustic vmf. over the surface of the diaphragm may have favored the first mode of forced vibration. The effects of relatively very powerful vmfs. were not investigated.

The resonant frequency of this diaphragm, with flat clamping, was observed to be  $f_0 = 824 \sim$ , corresponding to  $\omega_0 = 5160$ . According to theory, the next overtone in the third mode would be at  $2.09 f_0$  or  $1720 \sim$ .

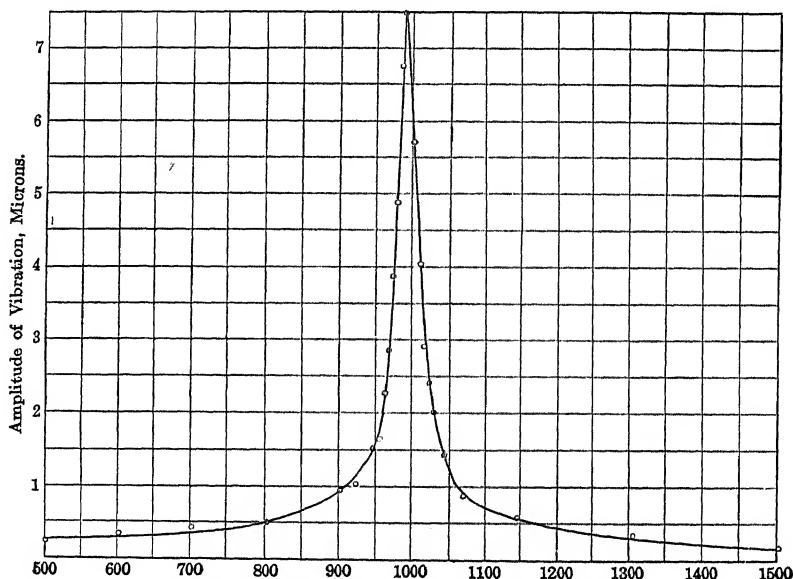


FIG. 16. Resonance curve of diaphragm No. 2.

The vibration-amplitude of the diaphragm was found to vary widely with the pitch of the acoustic vmf. At or near the natural



fundamental free-vibration frequency of the diaphragm, the amplitude of the vibratory response was a maximum. Either above or below this resonant frequency, the amplitude of vibration at the center, as shown by the explorer, fell off very markedly. The curve of relative amplitudes at different frequencies is given in Fig. 16, for diaphragm No. 2. It will be seen that when the impressed vmf. has a frequency remote from the resonant frequency  $f_0$ , in either direction, the amplitude becomes so small that the degree of precision obtainable near resonance cannot be maintained. The theory of this resonance curve is given in Chapter VI. It is shown that if we multiply the successive ordinates by  $\omega$ , the resulting values of vibrational velocity correspond to certain vector chords on a certain circle.

Figure 153, of Appendix I, page 305, gives the graph of the explored vibration amplitudes at successive radial distances from the center of diaphragm No. 1, for the impressed frequency of 896  $\sim$ . It will be seen that the circular dots fall off in amplitude smoothly from a maximum at or near the center ( $r = 0$ ), to zero at the flat-clamped edge ( $r = 2.62$  cm.). The heavy curve gives the computed relation according to Rayleigh's theory of free vibration. It appears, therefore, that the agreement between the distribution of observed forced vibration amplitudes, and computed free vibration amplitudes, is satisfactory.

Owing to the rapid change of amplitude with frequency in the neighborhood of resonance, it is desirable, when making explorations of amplitude over the surface, to select a frequency not too near resonance. The frequency near 950  $\sim$ , for instance, would be suitable for the case represented in Fig. 16.

**Explorations with Electromagnetic Vibromotive Forces.** — In order to ascertain the effects of exciting a steel diaphragm (No. 2), electromagnetically, a No. 144 Western Electric Bell receiver was screwed into the explorer behind the diaphragm, so as to obtain the ordinary air gap between the diaphragm and its poles. The cap or screw cover of the ordinary telephone receiver was here absent. An alternating current of 2 rms.\* milliamperes was supplied from a Vreeland oscillator, giving a close approximation to a pure sine wave, and in connection with a Rayleigh bridge (see Fig. 30), for the simultaneous measurement of both the resistance and the inductance of the telephone receiver, at 32

\* See footnote, p. 11.

successive frequencies between 429  $\sim$  and 2040  $\sim$ . Explorations were made at two frequencies; one at the resonant frequency of 992  $\sim$ , and the other slightly below this, or 974  $\sim$ .

The contour lines of amplitude in the latter case are presented in Fig. 17, where the outlines of the two magnetic poles are indicated in dotted lines. It will be seen that, while the mode of motion is still essentially fundamental, the amplitude is not a maximum at the center, as in the preceding acoustic cases. The maximum amplitude of  $2.0 \mu$  is reached in an elliptical loop embracing the pole at the top. Inside this loop, and immediately over the pole, the amplitude falls off to  $1.8 \mu$ . Over the lower pole in the Figure, the amplitude is about  $1.7 \mu$ , but there appears to be a slight diminution between the poles. If the geometric and magnetic conditions of the bipolar system were perfectly symmetric, these asymmetries in amplitude with respect to the two poles would presumably disappear.

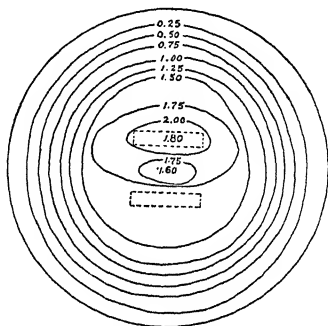


FIG. 17. Contour lines of vibration amplitude for diaphragm No. 2, electromagnetically excited at  $f = 974 \sim$ .

The curves of mean amplitude along a radius, against radial distance, are presented in Fig. 18. The curve *AAA* corresponds to that found at resonance. It shows that the amplitude is then far from being a maximum at the center of the diaphragm, owing to attractive forces being established over polar areas on each side of the center. The coefficient of equivalent mass for this curve, which will be explained in the next chapter, is over 0.5.

The curve *ABB* gives the corresponding distribution of mean azimuthal amplitude for the lower frequency 974  $\sim$ . The swelling of the amplitude over the poles is less marked in this case, and does not materially exceed that at the center. The equivalent-mass coefficient for this curve is 0.36, or about double that for the Rayleigh-Bessel curve, which is indicated by the broken line *ADD*. The curve *ACC* gives the distribution of mean amplitude in radial distance for another steel diaphragm (No. 3) in a bipolar receiver, at the resonant frequency of 1020  $\sim$ .

The curve *ABB* gives the corresponding distribution of mean azimuthal amplitude for the lower frequency 974  $\sim$ . The swelling of the amplitude over the poles is less marked in this case, and does not materially exceed that at the center. The equivalent-mass coefficient for this curve is 0.36, or about double that for the Rayleigh-Bessel curve, which is indicated by the broken line *ADD*. The curve *ACC* gives the distribution of mean amplitude in radial distance for another steel diaphragm (No. 3) in a bipolar receiver, at the resonant frequency of 1020  $\sim$ .

For both the steel diaphragms Nos. 2 and 3, a series of central amplitude measurements were made, with the explorer, at con-

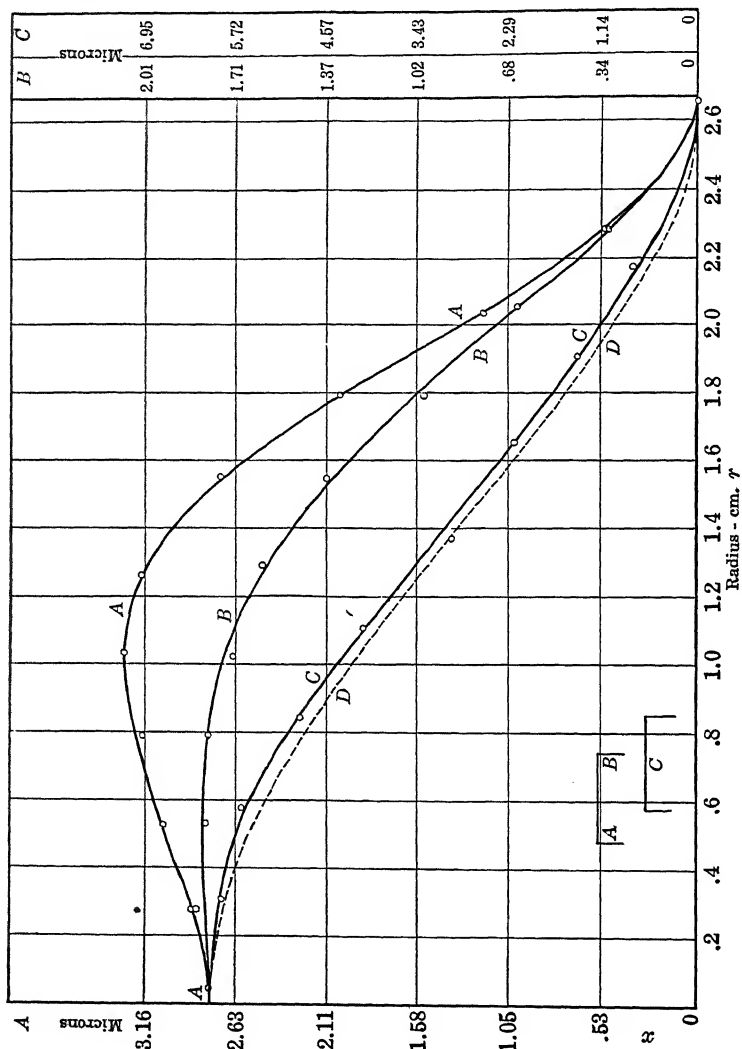


Fig. 18. Curves of vibration amplitudes of telephone receiver diaphragm along a radius.

stant a.c. strength, but adjustably varied frequency. These measurements will be referred to later in Chapter X. They were made simultaneously with the electric measurements of resistance and inductance in a Rayleigh bridge. In both cases, the ex-

plorer measurements of displacement satisfactorily checked the electrically deduced velocity-circle diagrams. The equivalent masses of the diaphragms computed from curves AAA and ACC in Fig. 18, agreed with those computed from the electric measurements within a few per cent.

**Temperature Effects on Exploration Measurements.** — It was found that changes of temperature in the air surrounding a diaphragm had a marked effect, both upon its resonant frequency, and upon its amplitude at any frequency. The curves representing  $x$  against  $r$  were apt to differ appreciably in outline from day to day. The degree of tightness of clamping also had a marked effect upon the measurements. In general, such disturbances, due to temperature and clamping, are likely to introduce tensions into the substance of the diaphragm, and to cause some of the characteristics of a vibrating membrane to be superposed upon those of a vibrating plate. It is, therefore, desirable that the clamping should be effected tightly, and that the measurements should then be made at constant temperature. Strictly speaking, the Rayleigh theory shows that there must be a difference in both the resonant frequency and in the distribution of amplitudes, if the diaphragm is clamped between opposed circular knife edges, instead of between circular flat rings at the boundary. The experiments have shown that flat-ring clamping is more likely to give consistent results than knife-edge clamping. These clamping difficulties are accentuated in thin glass diaphragms, for the boundary support of which a special technique had to be developed.

**Exploration of Thin Glass Diaphragms.** — From a number of thin glass diaphragms, one — No. 4 — was selected, on account of its uniformity in thickness (see Table IV). It was found very difficult to obtain uniform results with this in the explorer, owing to the above-mentioned troubles with the clamping. Finally, the glass diaphragm was cemented with water glass to a boundary ring of glass, and this was lightly supported between the clamping rings of the explorer. The diaphragm was then excited acoustically by organ pipes. The resonant pitch of the diaphragm was found to be 492  $\sim$ , in the fundamental mode. On raising the frequency, the mode of motion was found to change suddenly to the second, at 968  $\sim$ , with a single nodal diameter, the two halves of the diaphragm then vibrating harmonically in opposite

621. 386

N23

phases. This mode of motion continued until the frequency reached 1696 ~, when the mode changed to the third, the nodal diameter disappearing and giving place to a single nodal circle.

TABLE IV  
FLAT CIRCULAR DIAPHRAGMS

No.	MATERIAL	DIAMETER, CM.	THICKNESS* OVER JAPAN, CM.	MASS, GM.	NATURAL FRE- QUENCY ~
1	Steel japanned . .	5.4	0.038	5.615	824
2	Steel japanned . .	5.52	0.0399	5.979	992
3	Steel japanned . .	5.48	0.031	4.181	1020
4	Glass . . . . .	5.4	0.0108	0.6548	492

\*Thickness of japan 0.074 mm.

The ratios of the above three frequencies are 1 : 1.97 : 3.44; whereas, according to the Bessel-Function theory they should be 1 : 2.09 : 3.91. The discrepancies may readily be accounted for by imperfections in boundary support, or by temperature changes. Small changes in clamping were found to exercise a marked influence on these ratios.

**Conclusions concerning the Explorations of Amplitude.**— The results of the preceding tests with these diaphragms indicate that a receiver diaphragm vibrates, at least for by far the most part, in its first or fundamental mode, when excited either acoustically or electromagnetically within the limits of the relatively feeble vmfs. employed. That the other modes of motion which are theoretically possible may exist, is shown by the observations on thin glass diaphragms. (See also Appendix XIV.)

In acoustic excitation, the maximum displacement was found at the center, with substantially concentric circular contour lines, tapering off to zero at the clamping circle, in general accordance with the theoretical curve of free vibrations. In electromagnetic excitation, the maximum displacements were found over or around the poles, especially near resonance. So far as was observed under the action of a single feeble frequency, the first or fundamental mode of motion was observed. None of the observations yet secured on receivers operated by single-frequency alternating currents of one or two rms. milliamperes has indicated a departure from this mode.

Wide fields for further investigation of the motion of vibrating diaphragms lie (1) in steady-state conditions and (2) in transient conditions. In steady-state conditions, two or more simple impressed tones might be simultaneously impressed on the diaphragm, with the resultant motion explored and compared with theory. In transient conditions, sudden and brief tones might be impressed on the diaphragm, with the resultant motion explored and compared with theory.

In the working theory of telephonic transmission over electric conductors, the steady state is ordinarily assumed as the theoretical basis. It seems likely, however, that as our knowledge advances, the steady-state theory will need to be modified, in favor of transient theory, in order adequately to explain the phenomena of speech reproduction, especially with certain sounds. For such reasons, it would be advantageous to accumulate experimental knowledge concerning the transient as well as the steady vibrations of diaphragms.

**Possible Applications of Telephone-diaphragm Theory to Organ-pipe Standards.** — It has been pointed out in one of the papers\* here considered, that the motional circle-diagram of Chapter VII might be used for comparing the vmfs. of a set of organ pipes. In the simplest geometric condition, the standard vmf. on the diaphragm, which is proportional to the square root of the sound intensity at its surface,† would be observed in free space, with the orifice of the pipe facing the diaphragm at a definite distance, and with the diaphragm perpendicular to the line joining them. The pipes of different pitches would be so adjusted by wind pressure for standardization, that the central diaphragm amplitude multiplied by the impressed frequency, should lie on the circle diagram of the particular test diaphragm employed, assuming that the acoustic and dynamic conditions are held constant, and that the overtones produced by the pipes produce negligible effects.

\* Kennelly and Taylor, Bibliography 56, pp. 111-112.

† Barton, Bibliography 28.

## CHAPTER IV

### EQUIVALENT MASS OF A DIAPHRAGM VIBRATING IN ITS FUNDAMENTAL MODE

**Introduction.** — The vibration amplitude of a diaphragm, considered as a circular plate in its fundamental or first mode of motion, is a maximum at the center and diminishes symmetrically in all directions to zero at the clamped edge. We may consider that a simple harmonic vmf. is impressed at the center of the diaphragm, which will then execute simple harmonic vibrations, all parts having the same phase at the same instant.

If the total mass of the diaphragm within the clamping circle is  $M$  gm., each element of mass,  $dM$ , will have its own maximum cyclic velocity (depending on its radial distance  $r$ ) as it passes its normal position of rest. If  $\dot{w}_r$  be this velocity, corresponding to a maximum cyclic local displacement  $w_r$ , then the maximum cyclic kinetic energy of the element will be

$$(17) \quad dW = \frac{1}{2} \cdot dM \cdot \dot{w}_r^2 \quad \text{ergs.}$$

The total maximum cyclic kinetic energy  $W$  of the vibrating diaphragm will be the integral of  $dW$  over the entire surface within the clamp-ring. This integral can be evaluated, theoretically at least, if we know the shape of the curve of displacement  $w$  versus  $r$ , by exploration, over the surface.

**Central Equivalent Mass.** — The maximum cyclic velocity at the center of the diaphragm is  $\dot{w}_0$ . We may define the *central equivalent mass* of the diaphragm  $m_0$ , as the mass, which, vibrating with the central velocity, would have the same maximum cyclic kinetic energy as the whole diaphragm with its graded velocity distribution. Thus

$$(18) \quad \frac{1}{2} \cdot m_0 \cdot \dot{w}_0^2 = W = \frac{1}{2} \int \dot{w}_r^2 \cdot dM \quad \text{ergs,}$$

or

$$(19) \quad m_0 = \frac{1}{\dot{w}_0^2} \int \dot{w}_r^2 \cdot dM \quad \text{gm.}$$

when the integration is extended over the entire surface area. Since at any given frequency, the maximum-cyclic velocity is directly proportional to the maximum cyclic displacement, this equation may be written in the form

$$(20) \quad m_0 = \frac{1}{w_0^2} \int w_r^2 \cdot dM \quad \text{gm.}$$

where displacements are substituted for velocities.

If we can arrive at  $w_a^2$  the average square of the maximum cyclic displacement over the diaphragm as defined by the relation

$$(21) \quad w_a^2 M = \int w_r^2 \cdot dM \quad \text{gm.-cm.}^2$$

Then

$$(22) \quad m_0 = \frac{w_a^2}{w_0^2} M = \frac{\dot{w}_a^2}{\dot{w}_0^2} M \quad \text{gm.,}$$

and

$$(23) \quad \frac{m_0}{M} = \frac{w_a^2}{w_0^2} = \frac{\dot{w}_a^2}{\dot{w}_0^2}.$$

The ratio  $m_0/M$  may be called the *central equivalent-mass coefficient*. It is equal to the ratio of the average square of the velocity or displacement, to the square of the central velocity or displacement. It is evident that  $m_0/M$  must be less than unity. In Appendix II, on page 309, it is shown that in the case of a diaphragm executing forced vibrations of the same form as the free vibrations of a flat-clamped circular plate, according to the Rayleigh Bessel-Function theory, the value of  $m_0/M = 0.183$ , or the rms. displacement over the diaphragm is  $\sqrt{0.183} = 0.428$ , or 42.8 per cent of the central displacement. In the general and more complex case, however, the equivalent mass coefficient may vary from 0.15 to 0.5 or more.

**Polar Equivalent Mass.** — In a bipolar receiver, the distribution of displacements is likely not to be so simple as that considered above. The displacements, as we have seen in Fig. 18, may not have simple circular distribution. They may be as great, or even greater, over the poles than at the center. In such cases, the theory shows that the displacement and velocity over either pole is of greater importance than that at the center. If we denote these quantities by the symbols  $w_1$  and  $\dot{w}_1$ , respectively, and  $m_1$  the corresponding equivalent mass, which may be called the *polar equivalent mass*, then (18) becomes

$$(24) \quad \frac{1}{2} m_1 \dot{w}_1^2 = W = \frac{1}{2} \int \dot{w}_r^2 \cdot dM = \frac{1}{2} \cdot \dot{w}_a^2 \cdot M \quad \text{max. cy. ergs,}$$



or

$$(25) \quad m_1 = \frac{1}{\dot{w}_1^2} \int \dot{w}_r^2 \cdot dM = \frac{\dot{w}_a^2}{\dot{w}_1^2} M = \frac{w_a^2}{w_1^2} M = m_0 \frac{w_0^2}{w_1^2} \quad \text{gm.},$$

and

$$(26) \quad \frac{m_1}{M} = \frac{\dot{w}_a^2}{\dot{w}_1^2} = \frac{w_a^2}{w_1^2} = \frac{m_0}{M} \cdot \frac{w_0^2}{w_1^2}.$$

The ratio  $m_1/M$  may be called the *polar equivalent-mass coefficient*. It is evident from (26) that  $m_1/M$  is the ratio of the average squared displacement to the polar squared displacement. If the polar displacement happens to exceed the central displacement, then the polar equivalent-mass coefficient will be smaller than the central equivalent-mass coefficient.

A large number of polar equivalent-mass coefficients have been measured in the course of the researches on which this book is based. They have varied approximately from 0.15 to 0.5. That is, the average displacement square varied in different cases from 15 % to 50 % of the polar displacement square, or, the root-mean-square displacement has varied from 38 % to 70.7 % of the displacement over the poles. In the few cases where the curve of mean amplitude versus radius has been obtained by exploration, the electrically measured value of  $m_1/M$  has checked satisfactorily with that obtained from the curve, in the manner explained in Appendix II. As a rule, however, the average displacement over the surface is not known or measured mechanically. It can be inferred, however, from the mechanically measurable value of  $w_1$ , and the electrically measurable value of  $m_1/M$ , in the manner to be described in Chapter X, using (26) in the form

$$(27) \quad w_a = w_1 \sqrt{\frac{m_1}{M}} \quad \text{max. cy. cm.}$$

This result often supplies useful information concerning the character of the displacement distribution during a test.

**Effects of Loading a Diaphragm Symmetrically with a Central Mass.** — If we may assume that the relative distribution of displacement over the surface of a diaphragm, or the shape of its  $w, -r$  curve, is not altered by fastening a small known mass of say  $m'$  grams to the center of the diaphragm, then the central equivalent mass of the diaphragm should be increased from  $m_0$  to  $m_0 + m'$  grams by the change. Unfortunately, however, the application of the load is apt to change the curve of diaphragm

displacement, as found by exploration. This is shown in Fig. 19. Here  $E$  is the  $w - r$  curve, for an unloaded steel receiver dia-

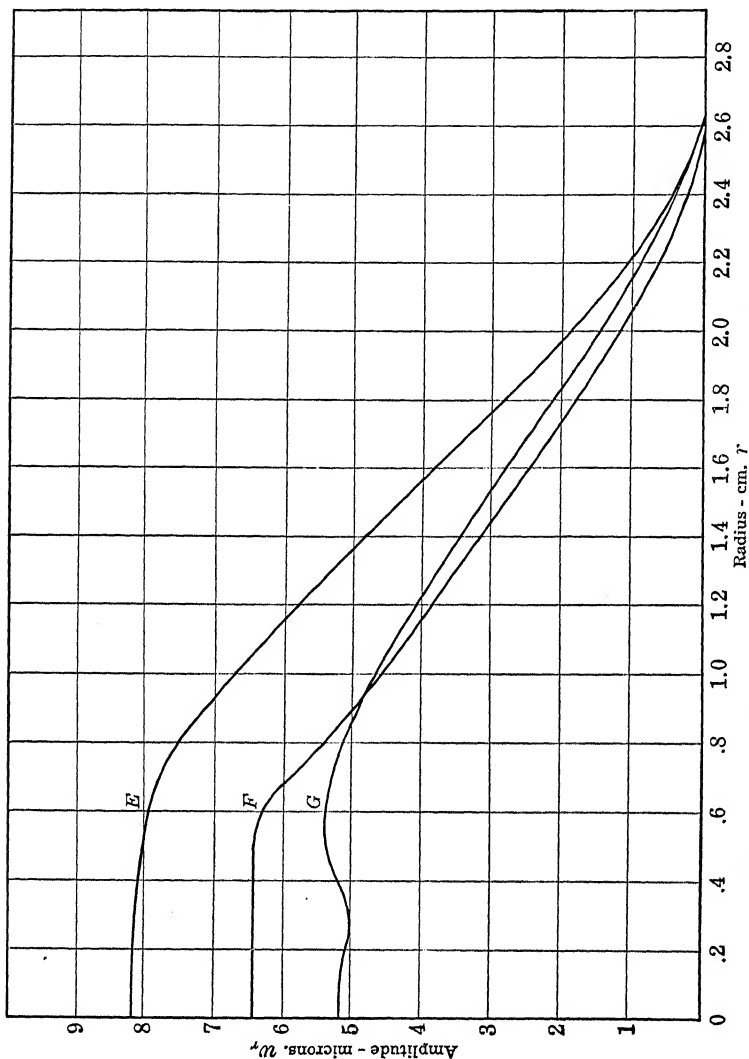


FIG. 19. Vibration Curves. Telephone diaphragm loaded at center.

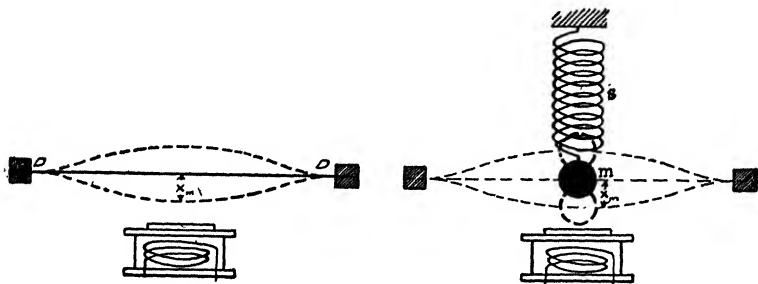
phragm excited acoustically and explored at  $904 \sim$ , its natural frequency being  $f_0 = 832 \sim$ . The corresponding curve  $F$  is for the same diaphragm loaded at the center by a small brass cylinder of  $0.536$  gm., explored at  $816 \sim$ , its new natural frequency being

$f_0' = 696 \sim$ . After increasing the load to 1.08 gm., the new exploration curve is shown at  $G$  ( $f = 660 \sim$ ,  $f_0'' = 616 \sim$ ). The shapes of these three curves being so different, it is evident that  $w_a/w_0$  the ratio of the rms. to the central displacement, and therefore the equivalent mass  $m_0$  will be different. Nevertheless, the smaller the loads applied to the diaphragm, the less the expected distortion, and the more nearly constant the central equivalent mass might be expected to remain. By applying two successive small loads, the electrical results with each will serve to indicate whether  $m_0$  remains constant, without the necessity of making an exploration over the surface.

## CHAPTER V

### EQUIVALENT SINGLE CENTRAL ELASTIC FORCE, OR STIFFNESS COEFFICIENT $s$ , OF A DIAPHRAGM

**Introduction.** — Just as the combined effect of all the distributed elements of mass over the surface of a diaphragm, vibrating in a given displacement curve, is equivalent to a single mass situated at the center, so the combined effect of all the distributed elastic forces over the surface is equivalent to a single elastic force  $s$  situated at the center. This equivalent single force will be the same, for the same displacement curve, whether the diaphragm is actuated by the single central pole of a monopolar receiver; or by the pair of symmetric poles of a bipolar receiver. The force is an elastically resisting force, and tends to restore the diaphragm to its normal position of rest, which is in the clamping plane with the permanent magnet removed, or in a symmetrically bowed surface of flexure, with the permanent magnet in place. We may properly assume that the displacements are always so small that the restoring force is directly proportional to the amount of the displacement. This force is expressed in dynes or megadynes per centimeter of displacement.



FIGS. 20-21. Diagrams illustrating a telephone-receiver diaphragm vibratory system, considered as replaced by its equivalent simple vibrator.

**Stiffness Coefficient.** — Figures 20 and 21 indicate diagrammatically a diaphragm vibrating distributed system and its equivalent concentrated vibrator, with its central equivalent

mass  $m$ , and its equivalent spring  $s$ . This dynamical substitution greatly simplifies the mathematical reasoning. The substitution is justified by experimental results.

Attempts have been made to measure this *stiffness coefficient*  $s$  by a direct mechanical method. One arrangement is shown in Fig. 22. Measurements of this kind appear to have been first carried out by Abraham\*; although the method used by him is not specified in the publication. The receiver  $T$  is mounted vertically, and the brass lever  $AB$ , fulcrumed at  $F$ , is maintained in equilibrium by means of the adjustable counterpoise  $C$ , when the weight is absent. A blunt point on the lower side of this lever is pressed down against the surface of the diaphragm, by

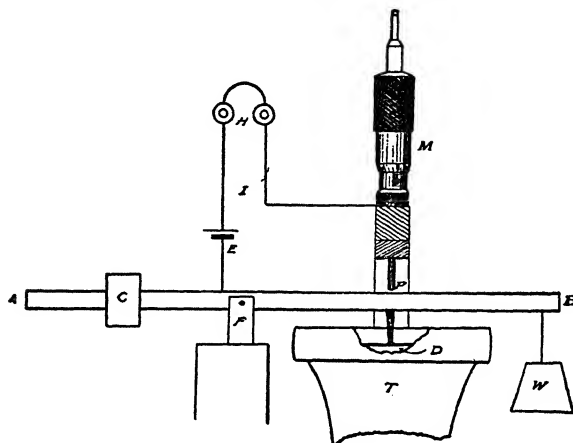


FIG. 22. Apparatus for diaphragm elasticity measurement.

the application of the known weight  $W$ . The force, in dynes, impressed downwards at the center of the diaphragm, is thus known. The displacement produced by this force is then measured, by means of a micrometer screw. The point  $P$  of the advanced micrometer screw-head  $M$ , comes into contact with the top of the lever  $AB$ , the moment of contact being determined electrically by the head telephones  $H$ , in the circuit  $I$ , of the voltaic cell  $E$ . Readings of the advance of point  $P$ , could be made on the micrometer head to  $10^{-3}$  inch ( $25 \mu$ ), and could be well estimated to  $10^{-4}$  inch ( $2.5 \mu$ ). Impressed forces were used in succession up to about 100 gm weight ( $10^6$  dynes).

\* Bibliography 24.

Figure 23 shows the results obtained, with ordinates as deflections in microns, and abscissas as impressed central forces in dynes. The different curves refer to diaphragms of different thickness.

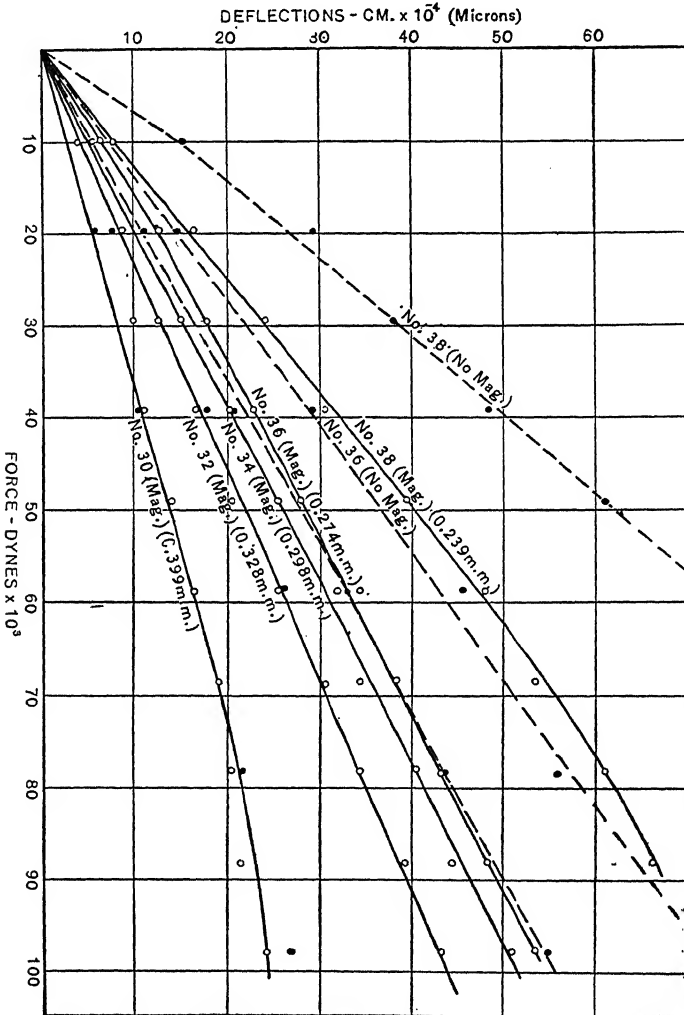


Fig. 23. Static force-deflection curves for different diaphragms, with and without permanent magnets. Heavy circles and dotted lines, without magnets.

every case, the clamping circle of the diaphragm in the receiver had a diameter of 5.0 cm. The full curves show the deflections with the permanent magnet in regular position. The dotted curves show the corresponding deflections with the permanent magnet removed.

It will be seen that the deflections obtained with varying impressed forces follow substantially straight-line laws, up to say 50 microns, a range of deflection considerably in excess of what these telephone diaphragms have to undergo ordinarily in practice. There is, however, a considerable difference between the deflection produced by a given impressed force when the permanent magnets were present, and when they were removed, the deflections being usually greater in the latter condition. The presence of the permanent magnet causes the diaphragm to be bowed down from the plane of the clamping circle, and subsequent deflections, due to impressed forces, occur from this distorted position of equilibrium.

TABLE V  
ELASTIC CONSTANTS OF DIAPHRAGM FROM STATIC DEFLECTION MEASUREMENTS (Affel)

SAMPLE No.	THICKNESS No.	CONDITION	THICKNESS OVER ALL	s IN MEGADYNES PER CM. DEFLECTION	
				WITH PERMANENT MAGNET IN PLACE	WITH PERMANENT MAGNET REMOVED
			mm.		
1	30	unjapanned	0.325	43.4	39.2
2	30	japanned	0.399	35.8	36.3
3	32	unjapanned	0.246	22.7	22.0
4	32	japanned	0.328	23.1	22.8
5	34	unjapanned	0.229	17.6	17.9
6	34	japanned	0.298	19.4	18.3
7	36	unjapanned	0.211	16.3	12.9
8	36	japanned	0.274	15.6	13.5
9	38	unjapanned	0.160	14.0	7.69
10	38	japanned	0.239	12.5	8.03

Table V gives the values of the stiffness coefficient  $s$  of the diaphragms, as determined from the force-deflection curves of Fig. 23. It should be noted that the sample diaphragm "japanned" was in each case a different sample from the diaphragm of the same thickness number "unjapanned." Consequently, it is not safe to assume that the difference in the Table between the values of  $s$  for a japanned and unjapanned diaphragm of the same thickness number is due merely to the effect of japan. Such differences are more likely to be due to accidental variations in the thickness or quality of the two diaphragms. The japan coating had an average thickness of 0.075 mm. (75  $\mu$ ), and does not

appear to have appreciably affected the observed values of  $s$ . Below the thickness of plate No. 34, (0.23 mm.), the values of  $s$ , with the magnet in place, are markedly greater than with the magnet removed.

The values of  $s$  in Table V indicate that  $s$  thus observed apparently increases a little faster than the square of the thickness of the unjapanned diaphragm. It must be noted, however, that no information was available as to how far the mechanical qualities of the steel differed in these different diaphragms.

Judging from measurements of the effective values of  $s$  obtained by other methods, the results by this static-deflection method are of the same order of magnitude; but they are unreliable, except as rough approximations. In the first place, the displacement curve of the diaphragm with the static deflections differs from that developed in the dynamic or vibratory state. In the second place, the static deflections are observed to increase very appreciably with the time of load application, especially with thin diaphragms. Consequently, the stiffness coefficient, as obtained statically, is likely to be less than that developed in rapid vibration.

Diaphragms numbers 2 and 6 in Table V were submitted to electromagnetic tests as described in Chapter X. In these tests their effective values of  $s$  were found to be respectively 77.6 and 36.7 megadynes per cm., values which are roughly twice as great as those given in the Table. It seems therefore that values of  $s$  obtained by static deflection are much less than those effectively developed with impressed vmfs.



# FORCED VIBRATIONS OF A RECEIVER DIAPHRAGM UNDER A SIMPLE IMPRESSED VIBROMOTIVE FORCE

**Introduction.** — We may now consider the mechanics of a receiver diaphragm subjected to a simple harmonic impressed vmf. The usual method of applying this vmf. is through an alternating

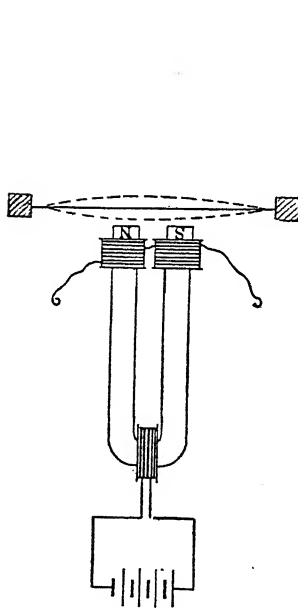


FIG. 24. Simplified magnetic circuit of bipolar receiver.

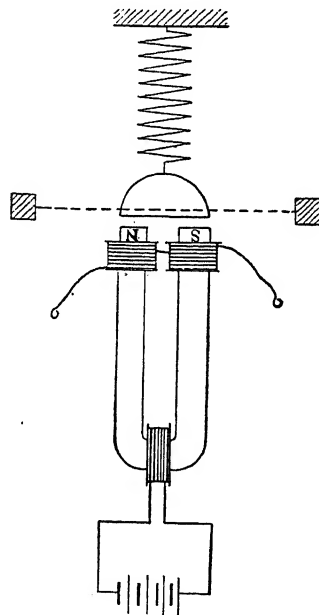


FIG. 25. Simplified mechanical system of bipolar receiver.

magnetomotive force in the magnetic circuit of a permanent magnet, acting on a thin ferrotype diaphragm, as is indicated in Fig. 24. The alternating magnetic pole is here assumed to be applied at or near the center of the diaphragm, in such a manner that a transverse alternating displacement  $x$  cm. is produced. (See Fig. 6.)

This displacement varies from zero at the clamping circle, to a maximum at or near the center; so that there is a distribution of vibration amplitude over the surface, and also a corresponding distribution of elastic restoring forces over the same area. This presents a relatively complicated dynamic system, and one that would, in most cases, be very difficult to analyze. Fortunately, however, the actual distributed system of total mass  $M$  may be resolved, for engineering purposes, into an equivalent concentrated system indicated in Fig. 25, where the equivalent single solid mass  $m$  executes a vibratory amplitude  $x_m$ , under the influence of the impressed vmf. below, and the single elastic force of a virtual spring  $s$ . This simple equivalent dynamic system has been found experimentally to be the counterpart of the actual distributed system of Fig. 24, so far as concerns the essential electromagnetic actions produced.

**Angular Velocity of Vibration.** — If a particle executes a simple vibration, or simple harmonic motion, about its position of rest  $o$ , Fig. 26, reaching the maximum displacements  $oa$  and  $oc$  alternately, and executing  $f$  complete cycles of vibration per second, an observer viewing the vibration from a distance might be unable to determine whether this particle was actually executing a linear to-and-fro vibration in the line  $ac$ , or whether it was executing a circular vibration in the path  $ABC$ . It is shown in textbooks on kinetics of a particle, that a simple rotation of the particle  $P$  with uniform tangential velocity in the circle  $ABC$ , about the center  $O$ , and with radius  $OP = x_m$ , would appear to the eye of a very distant observer in the plane of the orbit  $AOC$ , as though the particle executed the simple harmonic motion  $aoc$  in a straight line. That is, the position  $p$  of the particle in the simple vibratory motion, would be the orthogonal projection of the circularly

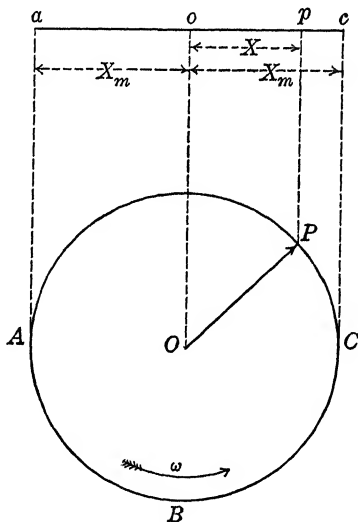


FIG. 26. Diagram of simple rectilinear vibration, and the corresponding path of circular vibration.

moving point  $P$  on the line  $ac$ , which is perpendicular to  $Oo$ . Consequently, to every straight-line path of simple vibration, there corresponds a circular path of uniform orbital rotation. The practical advantage of referring a rectilinear vibration to its corresponding circular orbit is that, whereas the particle  $p$  moves with different apparent velocities at different points in its line of vibration, stopping at  $a$  and  $c$  but moving fastest at  $o$ , the projecting particle  $P$  always moves in its circle with one and the same speed. The constant circular speed of  $P$  is just equal to the maximum apparent speed of  $p$ .

Since a complete revolution includes 360 degrees, or  $2\pi$  radians, of circular arc, it is evident that if the particle  $p$  executes  $f$  cycles of rectilinear vibration per second, the particle  $P$  executes  $360f$  degrees, or  $2\pi f$  radians, per second. The particle  $P$  therefore possesses a uniform angular velocity

$$(28) \quad \omega = 2\pi f \quad \text{radians per second.}$$

The particle  $p$ , although it moves in a straight line, may be said to possess the angular velocity  $\omega$ , in the sense that its equivalent circularly vibrating particle  $P$ , to which it is tied by projection, does possess this circular angular velocity.

The line of reasoning immediately preceding is likewise applicable to a simple alternating-current circuit. In the electric circuit, electricity may be considered as moving to and fro, or to be executing a simple harmonic motion, like the vibrating particle  $p$  of Fig. 26, with a frequency of  $f$  cycles per second. The angular velocity  $\omega = 2\pi f$  is then usually referred to as the angular velocity of the alternation.

This analogy between the angular velocity  $\omega$  of a simple alternating current, and the angular velocity  $\omega$  of a simple vibration, is but the first element of a whole series of remarkable and useful analogies between the alternating-electric circuit and vibratory mechanical systems. We shall find that

electric displacement $q$	corresponds to	mechanical displacement	$x$
" current $\dot{q} = i$	"	" velocity	$\dot{x}$
" resistance $r$	"	" resistance	$r$
" inductance $\mathcal{L}$	"	" mass	$m$
" elastance $s = \frac{1}{c}$	"	" stiffness	$s$
" impedance $z$	"	" impedance	$z$
" electromotive force $e$	"	" vibromotive force $f$	

(See also Table XVI, page 208.)

By means of these analogies, the student who is already familiar with the salient principles of the alternating-current circuit is readily able to understand the corresponding principles of a simple mechanical vibration system.

**Vibratory Displacement.** — In accordance with what has been stated in the foregoing chapters, we assume that when a small vmf. is impressed upon the diaphragm, the small vibratory displacement thereby produced is entirely in the first mode, so that the equivalent mass executes a simple harmonic displacement of the same frequency as the vmf., and of a small amplitude  $x_m$  maximum cyclic cm. This amplitude is assumed to occur equally over each pole. In practice, with a 75-ohm bipolar receiver, i.e., a bipolar receiver whose resistance to continuous currents is about 75 ohms, the maximum cyclic displacement to a current of 1 milliamper (rms.) in the coils is very small, if the frequency is remote from the resonant frequency, and is of the order  $0.1 \mu$  to  $1 \mu$ . At the resonant frequency, it is much greater, and ordinarily between  $1 \mu$  and  $10 \mu$ .

**Vibratory Velocity.** — It is shown in Appendix III that if a vibrating mass executes a maximum cyclic displacement of  $x_m$  cm. at a frequency of  $f$  cycles per second, or with an angular velocity of  $\omega = 2\pi f$  circular radians per second, the maximum cyclic velocity of the motion is  $\dot{x}_m = j\omega x_m$  cm. per second,\* or  $j\omega x_m$  kines.† The maximum cyclic vibratory velocity is thus  $\omega$  times the magnitude of the maximum cyclic displacement, and as is indicated by the coefficient  $j$ , is in leading quadrature to the phase of the displacement. When the displacement is zero, the velocity is at a cyclic maximum, and when the displacement is at a cyclic maximum, the velocity is zero. In practice, the ordinary 75-ohm bipolar receiver diaphragm, away from resonance, with 1 milliamper rms., has a maximum cyclic velocity of a small fraction of a kine, rising to a few kines at resonance.

The root-mean-square velocity is  $\dot{x}_m/\sqrt{2}$  or  $0.707 \dot{x}_m$ , in accordance with the well-known relations between the rms. and maximum cyclic values of any simple harmonic quantity. Similarly,

\* The symbol  $\dot{x}$  or "x-dot" may be regarded as an abbreviated form of  $dx/dt$ , the differential of  $x$  with respect to  $t$ , or the time rate of change in  $x$ . This is a well known method of writing a differential, originally due to Newton.

† The *kine*, as a short name for the unit velocity of 1 cm. per second, was recommended at a meeting of the British Association for the Advancement of Science.

the root-mean-square displacement would be  $x_m/\sqrt{2}$ . The arithmetic mean velocity or average velocity during any half cycle from zero through a maximum and back to zero, would be  $\dot{x}_m (2/\pi)$ , where  $\dot{x}_m$  is the maximum cyclic velocity. Thus, a diaphragm having a maximum cyclic displacement of  $x_m = 5.08$  microns over each pole, when excited by 1 milliampere rms. at the frequency of observed resonance  $f_0 = 1015 \sim$ , and consequent resonant angular velocity of  $\omega_0 = 6378$ , would develop a maximum cyclic vibrational velocity of 3.24 kines, which would be directed alternately from and towards the pole at successive alternations. The rms. displacement at resonance would be 3.59 microns per milliampere, and the rms. velocity 2.29 kines per milliampere. The average velocity during each alternation would be 2.06 kines per milliampere. Over any complete cycle, or whole number of cycles, the averaged algebraic velocity would be zero.

**Kinetic Energy.** — The equivalent mass of the diaphragm being  $m$  grams, and the maximum cyclic velocity of this mass being  $\dot{x}_m$ , the maximum cyclic kinetic energy of the diaphragm is

$$(29) \quad W_k = \frac{1}{2} m \dot{x}_m^2 \quad \text{ergs.}$$

This maximum kinetic energy will be attained at the instant when the diaphragm passes in either direction through its position of rest. It is clearly an essentially positive quantity. Thus, if the equivalent mass of the diaphragm were 0.902 gm., and the maximum cyclic velocity per milliampere 3.24 kines, the corresponding maximum cyclic kinetic energy per milliampere would be 4.73 ergs. This energy would be stored and released once in each alternation; or, since the resonant frequency was  $1015 \sim$ , it would be developed 2030 times per second.

**Elastic Restoring Force.** — We have already seen that the equivalent mass of the diaphragm is virtually acted upon by an elastic force of  $s$  dynes per cm. of displacement, which force tends to bring the diaphragm back to its position of rest, or zero displacement. Thus, if  $s = 36.7 \times 10^6$  dynes per cm., the maximum magnitude of this elastic force with a resonant maximum cyclic displacement  $x_m = 5.08 \mu = 5.08 \times 10^{-4}$  cm., would be  $36.7 \times 5.08 \times 10^2 = 1.865 \times 10^4$  dynes, or about 18.3 gms. weight. This force would be developed at maximum displacement, 2030 times per second under resonant frequency. The work which this force would do would be stored away in the diaphragm as elastic potential energy.

**Elastic Potential Energy.** — The average elastic force resisting displacement would be half the maximum force or  $-s x_m/2$  dynes. The work done by this force during the entire resonant displacement would be

$$(30) \quad W_e = -\frac{s x_m}{2} \times x_m = -\frac{s x_m^2}{2} = -\frac{s}{2} \left( \frac{\dot{x}_m}{j\omega_0} \right)^2 = \frac{s \dot{x}_m^2}{2 \omega_0^2} \quad \text{ergs.}$$

In the case considered, the receiver actuated by 1 milliampere at the resonant frequency of 1015  $\sim$ , would overcome an average force of  $0.933 \times 10^4$  dynes, over a maximum cyclic displacement of 5.08 microns, and would thus do work to the maximum cyclic value of  $5.08 \times 10^{-4} \times 0.933 \times 10^4 = 4.73$  ergs. This elastic potential energy is just equal to the maximum cyclic kinetic energy, and is developed at the instants when the kinetic energy is zero. It is easy to carry the analysis a step further, and to show that in the steady state of forced oscillations at the frequency of resonance, the mechanical energy in the diaphragm, being partly potential and partly kinetic, remains constant.

Although the maximum cyclic kinetic and potential energies are equal when the impressed steady frequency  $f$  is equal to  $f_0$ , the frequency of resonance, yet it is shown in Appendix III, that at any other single frequency, this equality does not hold, and the impressed force has to send energy cyclically into and out of the diaphragm in such a manner, and at such a phase, as will enable the energy balance to be maintained. At the frequency of resonance, the impressed force is not called upon, in the steady state, to supply either kinetic or potential energy to the system. It is entirely occupied in overcoming or balancing the opposing force of mechanical resistance. Under this condition, we may equate (29) and (30), the expressions for the two energies.

$$(31) \quad W_k = W_e = \frac{m}{2} \dot{x}_m^2 = \frac{s \dot{x}_m^2}{2 \omega_0^2} \quad \text{ergs,}$$

whence

$$(32) \quad \omega_0 = \sqrt{\frac{s}{m}} \quad \frac{\text{radians}}{\text{sec.}}$$

Or the angular velocity of resonance is numerically equal to the square root of the equivalent stiffness coefficient  $s$  after being divided by the equivalent mass of the diaphragm. The frequency of resonance immediately follows

$$(33) \quad f_0 = \frac{\omega_0}{2\pi} = \frac{1}{2\pi} \sqrt{\frac{s}{m}} \quad \frac{\text{cycles}}{\text{sec.}}$$

A definition of the condition of resonance in the forced vibration of a simply vibrating body is that condition in which the maximum cyclic kinetic and potential energies equate without any assistance from the impressed vmf.

**Mechanical Resistance.** — When a vibromotive force acting on a mass has set the latter in vibration, it has to overcome a force or set of forces resisting the motion. This force is called the force of mechanical resistance. It always acts in such a manner as to absorb mechanical energy from the vibratory system. A common form of mechanical resistance is frictional resistance, which absorbs and dissipates the mechanical energy in the form of heat. Frictional mechanical resistance is ordinarily a wasteful resistance; because it dissipates, as heat in the surrounding medium, the mechanical energy communicated to the system by the vibromotive source. Another form of mechanical resistance to the vibration of a mass is acoustic resistance, or the resistance to setting up sound waves in the surrounding medium, usually air. Acoustic resistance is a useful form of mechanical resistance in a telephone receiver. An ideally perfect telephone receiver diaphragm, considered as the armature of a sound-producing motor, would have all its mechanical resistance of the acoustic type and none of the frictional type.

Mechanical-resistance force of a telephone diaphragm is essentially a resistance to motion and varies with the velocity of vibration. It is found experimentally that the forces of mechanical resistance, whether frictional or acoustic, are directly proportional to the velocity, so that the square or higher powers of the velocity do not have to be considered. This is probably because the vibratory velocities involved in the motion of a receiver diaphragm are so small — only a few kins at most. If the velocities involved were greater, resistance terms including squares or higher powers of the velocity might be expected to present themselves, as they do in fact present themselves in the friction of surfaces moving rapidly through gases or liquids. It is fortunate that only the first power of the velocity has to be considered in dealing with telephone-receiver diaphragms, since the computations involved are thereby greatly simplified.

If the equivalent mass  $m$  of a diaphragm is vibrating with maximum cyclic velocity  $\dot{x}_m$  kins, the mechanic force of resistance is

$$(34) \quad f_m = -r\dot{x}_m \quad \text{max. cy. dynes } \angle,$$

where  $r$  is the coefficient of mechanical resistance to the motion. The negative sign indicates that the phase of this force is opposite to that of the velocity  $\dot{x}_m$ . Similarly, if we use the root-mean-square value  $\dot{x}_r$  of the velocity, the root-mean-square value of the force of resistance is

$$(35) \quad f_r = -r\dot{x}_r \quad \text{rms. dynes } \angle.$$

The resistance coefficient  $r$  includes several forms of frictional resistance, and the acoustic resistance of the air surrounding the diaphragm as well as that of the solid framework of the instrument. The unit of resistance coefficient  $r$  in the C. G. S. system, which we shall adhere to throughout, is the dyne per cm./sec. or the dyne per kine. The dimensions of  $r$  are  $MT^{-1}$ . The numerical value of  $r$  in an ordinary telephone receiver diaphragm commonly varies between 100 and 1000 dynes per kine.

Mechanical resistance  $r$  in a vibratory system bears a close analogy to electric resistance  $r$  in an alternating-current circuit. In a simple alternating-current circuit the electromotive force  $e_r$  of resistance is

$$(36) \quad e_r = -r\dot{q} = -ri \quad \text{rms. volts } \angle,$$

where  $i$  is the rms. current strength in amperes, and  $r$  is the coefficient of electric resistance, or simply the resistance of the circuit. The negative sign indicates that the phase of  $e_r$  is opposite to that of the current. Here  $r$  is ordinarily measured in ohms in electric engineering computations. If, however, we are dealing in the physical laboratory with experiments which have not become standard engineering processes, it is advantageous to adhere to the fundamental C. G. S. magnetic system, and to measure  $r$  in C. G. S. magnetic units,\* or abohms. For convenience of analogy, we may designate the C. G. S. unit of mechanical resistance as the "mechanical abohm." A mechanical resistance of  $r = 200$  say, may then be expressed either as 200 dynes per kine, or as 200 mechanical abohms.

**Mechanical Mass Reactance.** — Just as in a simple alternating-current circuit, an inductance of  $\mathcal{L}$  abhenries develops an electric reactance of  $j\mathcal{L}\omega$  abohms, where  $\dagger j = \sqrt{-1}$ , so in a steady vibratory system, a mass of  $m$  gm. develops a mechanical reactance

\* Many writers now use the prefix *ab* or *abs* before a unit in the practical system to designate the corresponding C. G. S. magnetic or absolute unit.

$\dagger$  Bedell and Crehore first introduced  $j$  as the symbol for  $\sqrt{-1}$  in electro-technical literature. Bibliography 8.



of  $j\omega$  mechanical abohms, or dynes per kine. In the electric circuit, the inductive reactance develops ccmf. of  $-j\omega L$ , rms. abvolts to a rms. current of  $i$ , abamperes; or a part of the impressed emf. equal to  $j\omega L$ , rms. abvolts must be used to overcome the inductive-reactance ccmf. In the mechanical system, the mass reactance likewise develops a ccmf. of  $-j\omega \dot{x}$ , rms. dynes to a rms. velocity of  $\dot{x}$ , kines; or a part of the impressed vmf. equal to  $j\omega \dot{x}$ , rms. kines must be used to overcome the mass-reactance vmf. In both cases the forces developed are nondissipative, i.e., they do work, but the work is alternately stored and released, or charged and discharged, without being permitted to leave the system, as distinguished from the forces of resistance, which do work on the motion for release or expulsion from the system.

**Mechanical Elastic Reactance.** — Just as in a simple alternating-current circuit, a capacitance of  $c$  abfarads or its reciprocal  $s = 1/c$  abdarafs, develops an electric reactance of  $-j(1/c\omega) = -j(s/\omega)$  abohms; so in a simple vibratory system, an elastance or stiffness coefficient  $s$  develops a mechanical reactance of  $-j(s/\omega)$  mechanical abohms or dynes per kine. In the electric circuit, the elastic reactance develops a ccmf. of  $+j(s\dot{i}/\omega)$  rms. abvolts to a rms. current  $i$ , abamperes; or a part of the impressed emf. equal to  $-j(s\dot{i}/\omega)$  rms. abvolts must be used to overcome this ccmf. In the mechanical system, the elastic reactance likewise develops a ccmf. of  $+j(s\dot{x}/\omega)$  rms. dynes to a rms. velocity of  $\dot{x}$ , kines; or a

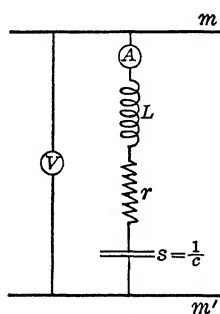


FIG. 27. Simple alternating current  $LRS$  branch circuit operated at constant voltage and varied frequency.

part of the impressed vmf. equal to  $-j(s\dot{x}/\omega)$  must be used to overcome this ccmf. In both cases, the forces developed are non-dissipative. They develop energies and activities that do not escape from the system.

**Electric Circuit Analogue of a Simple Vibratory System.** — A mass set into simple harmonic vibration by the application of a steady vmf. as in the simplified diaphragm system of Fig. 25, behaves like a simple alternating-current\* branch circuit containing a resistance, inductance and capacitance in series, as shown in Fig. 27. Here the impressed emf. between the mains  $mm'$ , corresponds to

\* In what follows the abbreviation a.-c. will be used for alternating-current.

the impressed vmf., the inductance  $L$  abhenries to the mass  $m$  gm., the resistance  $r$  abohms, to the resistance  $r$  mechanical abohms, and the electric elastance  $s$  abdarafs to the mechanic elastance  $s$  dynes per cm. The alternating current  $i$  in the electric system corresponds to the vibratory velocity  $\dot{x}$  in the mechanical system.

In all cases, the cvmfs. of mass reactance and elastance are in mutual phase opposition; so that the forces to which they give rise tend to cancel each other. At the frequency of resonance, they are in equilibrium, and cancel each other completely; i.e., in magnitude as well as in phase. Below the resonant frequency, the elastic reactance and its force exceed respectively the mass reactance and its force; whereas above the resonant frequency, the mass reactance and its force are in the ascendant. In all of these respects, the electric circuit displays close analogies.

**Mechanical Impedance to Velocity and its Analogue, Electric Impedance to Current.**—If we consider a single mass with its inertia as concentrated at the mass center, and with a single elastic restoring force, we have the simplest type of vibratory system. Such a system may be called a simple vibratory system. Figure 25 with its equivalent simplified diaphragm represents such a system. If a simple vmf., i.e., a vmf. of sinusoidal type and of a single frequency (devoid of harmonics) acts on a simple vibratory system, the opposition to motion consists of mechanical resistance and also of mechanical reactance in quadrature therewith. In other words the opposition consists of *mechanical impedance*. This is the complete analogue to what is found in the simple alternating-current circuit of Fig. 27. Referring to that figure, we have the vector relation

$$(37) \quad \text{Impedance of branch} = \text{Resistance} + j \times \text{Inductive Reactance} \\ - j \times \text{Elastic Reactance} \quad \text{electric abohms } \angle.*$$

Similarly in the simple vibratory system of Fig. 25.

$$(38) \quad \text{Impedance of system} = \text{Resistance} + j \times \text{Mass Reactance} \\ - j \times \text{Elastic Reactance} \quad \text{mechanical abohms } \angle.$$

In both cases, resistances are represented by ordinary positive real numbers, but reactances are represented by either positive or negative imaginary numbers; i.e., numbers measured along the *imaginary axis*. This will be well understood by students familiar

\* The sign  $\angle$  attached to a unit indicates that it is to be interpreted vectorially.

with the quantitative behavior of a. c. circuits. Such numbers are termed  $j$ -numbers, because the prefix  $j$ , as a symbol for  $\sqrt{-1}$ , should be attached to them.

Table VI presents the reactances in the case of a receiver diaphragm for which measurements showed the equivalent mass  $m$  to be 0.902 gm. and the equivalent elastic coefficient  $s$  to be  $36.7 \times 10^6$  dynes per cm.

TABLE VI  
REACTANCES OF RECEIVER DIAPHRAGM HAVING THE CONSTANTS  
 $m = 0.902$  GM.  $s = 36.7 \times 10^6$  DYNES/CM.

1	2	3	4	5
$f$	$\omega$	MASS REACTANCE $j m \omega$	ELASTIC REACTANCE $-j s / \omega$	TOTAL REACTANCE $j X$
$\sim$	RAD/SEC.	DYNES/KINE	DYNES/KINE	DYNES/KINE
0	0	$j 0$	$-j \infty$	$-j \infty$
200	1257	$j 1133$	$-j 29205$	$-j 28072$
400	2513	$j 2267$	$-j 14602$	$-j 12335$
600	3770	$j 3400$	$-j 9735$	$-j 6335$
800	5027	$j 4534$	$-j 7301$	$-j 2767$
900	5653	$j 5101$	$-j 6490$	$-j 1389$
992 $f_1$	6232 $\omega_1$	$j 5621$	$-j 5889$	$-j 268$
1000	6283	$j 5667$	$-j 5841$	$-j 174$
1002	6299	$j 5680$	$-j 5826$	$-j 146$
1015 $f_0$	6380 $\omega_0$	$j 5754$	$-j 5754$	0
1028	6461	$j 5827$	$-j 5681$	$+j 146$
1039 $f_2$	6529 $\omega_2$	$j 5889$	$-j 5621$	$+j 268$
1050	6597	$j 5951$	$-j 5563$	$+j 388$
1100	6912	$j 6234$	$-j 5310$	$+j 924$
1200	7540	$j 6801$	$-j 4868$	$+j 1933$
1400	8797	$j 7934$	$-j 4172$	$+j 3762$
1600	10053	$j 9068$	$-j 3651$	$+j 5417$
1800	11310	$j 10201$	$-j 3245$	$+j 6956$
2000	12566	$j 11335$	$-j 2921$	$+j 8414$
$\infty$	$\infty$	$j \infty$	$-j 0$	$+j \infty$

The first column contains the impressed frequency, advancing by steps of 200 cycles per second, except in the neighborhood of the resonant frequency  $f_0$ . Column 2 gives the corresponding angular velocities of the equivalent circular vibrations, in radians per second. Column 3 gives the mass reactances  $j m \omega$  at these angular velocities, increasing in direct proportion to the frequency. Column 4 gives the elastic reactance  $-j s / \omega$ . These vary inversely as the frequency. Column 5 gives the algebraic sum of these two reactances.

It will be seen that at a frequency very close to zero, the total reactance is elastic or of the type  $-j$ , and is indefinitely great. As the frequency increases, the total reactance diminishes in size, until at the resonant frequency  $f_0 = 1015 \sim$ , the total reactance vanishes. As the frequency advances beyond this point, the total reactance becomes increasingly large, and is of the massive type.

Table VI might also serve to show the reactances in a branch a. c. circuit like that of Fig. 26 having the constants

$$\begin{aligned} \mathcal{L} &= 0.902 \begin{cases} \text{abhenries} \\ \text{or henries} \end{cases} & s &= 36.7 \times 10^6 \begin{cases} \text{abdarafs} \\ \text{or darafs} \end{cases} \\ c &= 2.725 \times 10^{-8} \begin{cases} \text{abfarads} \\ \text{or farads} \end{cases} \end{aligned}$$

In the electric case, however, the reactances would come out in

$$j \begin{cases} \text{abohms} \\ \text{or ohms} \end{cases}.$$

By (40), the mechanical impedance of the receiver diaphragm here considered would be, at any of the frequencies appearing in Table VI, equal to the sum of the mechanical resistance  $r$  and the algebraic sum of the reactances at that frequency as given in the last column. The mechanical impedance  $z$  would therefore be

$$(39) \quad z = r + j \left( m\omega - \frac{s}{\omega} \right) \quad \text{mechanical abohms } \angle,$$

which corresponds precisely to the well known electric impedance of the branch circuit of Fig. 27; namely

$$(40) \quad z = r + j \left( \mathcal{L}\omega - \frac{s}{\omega} \right) \quad \text{electric abohms } \angle.$$

The mechanical impedance of the diaphragm at the frequencies already discussed, is presented in Table VII. In column 3 the mechanical impedances of the diaphragm are expressed in rectangular coordinates with a constant real term and a varying imaginary term. In column 4, these impedances are expressed in polar coordinates with varying sizes and slopes. Any rectangular complex quantity  $r + jx$  is convertible into a corresponding polar complex number  $\rho \angle \beta^\circ$  by the well known formulas:

$$(41) \quad \rho = \sqrt{r^2 + x^2} \quad \text{mechanical abohms,}$$

$$(42) \quad \tan \beta^\circ = \frac{x}{r}.$$

TABLE VII

IMPEDANCES AND ADMITTANCES OF RECEIVER DIAPHRAGM HAVING THE CONSTANTS  $m = 0.902$  GM.  $s = 36.7 \times 10^6$  DYNES/CM

$r = 268$  DYNES/KINE

1	2	3	4	5
$f$ ~	$\omega$ RAD. SEC.	IMPEDANCE $z$		ADMITTANCE $y$
		RECTANGULAR DYNES/KINE	POLAR DYNES/KINE	POLAR KINES/DYNE
		<i>real</i> <i>imag.</i>	<i>size</i> <i>slope</i>	$\times 10^{-3}$
0	0	$268 - j \infty$	$\infty \angle 90^\circ$	$0 \angle 90^\circ$
200	1257	$268 - j 28072$	$28073 \angle 89^\circ.27'$	$0.036 \angle 89^\circ.27'$
400	2513	$268 - j 12335$	$12338 \angle 88^\circ.45'$	$0.081 \angle 88^\circ.45'$
600	3770	$268 - j 6335$	$6341 \angle 87^\circ.34'$	$0.157 \angle 87^\circ.34'$
800	5027	$268 - j 2767$	$2780 \angle 84^\circ.29'$	$0.360 \angle 84^\circ.29'$
900	5653	$268 - j 1389$	$1565 \angle 79^\circ.4'$	$0.639 \angle 79^\circ.4'$
992 $f_1$	6232 $\omega_1$	$268 - j 268$	$379 \angle 45^\circ$	$2.638 \angle 45^\circ$
1000	6253	$268 - j 174$	$319.5 \angle 33^\circ$	$3.130 \angle 33^\circ$
1002	6299	$268 - j 146$	$305 \angle 28^\circ.36'$	$3.278 \angle 28^\circ.36'$
1015 $f_0$	6380 $\omega_0$	$268 - j 0$	$268 \angle 0^\circ$	$3.731 \angle 0^\circ$
1028	6461	$268 + j 146$	$305 \angle 28^\circ.36'$	$3.278 \angle 28^\circ.36'$
1039 $f_2$	6529 $\omega_2$	$268 + j 268$	$379 \angle 45^\circ$	$2.638 \angle 45^\circ$
1050	6597	$268 + j 388$	$473 \angle 55^\circ.24'$	$2.114 \angle 55^\circ.24'$
1100	6912	$268 + j 924$	$962 \angle 73^\circ.49'$	$1.039 \angle 73^\circ.49'$
1200	7540	$268 + j 1933$	$1952 \angle 82^\circ.7'$	$0.512 \angle 82^\circ.7'$
1400	8797	$268 + j 3762$	$3764 \angle 85^\circ.56'$	$0.265 \angle 85^\circ.56'$
1600	10053	$268 + j 5417$	$5424 \angle 87^\circ.10'$	$0.184 \angle 87^\circ.10'$
1800	11310	$268 + j 6956$	$6961 \angle 87^\circ.48'$	$0.144 \angle 87^\circ.48'$
2000	12566	$268 + j 8414$	$8418 \angle 88^\circ.10'$	$0.119 \angle 88^\circ.10'$
$\infty$	$\infty$	$268 + j \infty$	$\infty \angle 90^\circ$	$0 \angle 90^\circ$

A swifter method, however, is to find  $\beta^\circ$  by (42), and then if  $x$  is less than  $r$ , to find  $\rho$  by the relation

$$(43) \quad \rho = r \sec \beta^\circ \quad \text{mechanical abohms.}$$

If, however,  $x$  is numerically greater than  $r$ , it is better to use the equivalent formula

$$(44) \quad \rho = x \csc \beta^\circ \quad \text{mechanical abohms.}$$

On the other hand, a polar impedance  $\rho \angle \beta^\circ$  is convertible into the corresponding rectangular impedance by the usual formulas:

$$(45) \quad r = \rho \cos \beta^\circ \quad \text{mechanical abohms,}$$

$$(46) \quad x = \rho \sin \beta^\circ \quad \text{mechanical abohms.}$$

A mechanical aid for the rapid interconversion of rectangular and polar complex numbers has been developed by Fleming.\* A special slide-rule for performing the same operation with swiftness and ordinarily sufficient precision, has been worked out by Grinstead and Davis in England, and by the General Electric Co. in America.

Complex numbers are vitally important in the theory of vibratory mechanical systems and of alternating-current circuits. These numbers, introduced into electrotechnical literature in 1893,† are advantageously expressed in rectangular form for the purposes of addition and subtraction. They are advantageously expressed in polar form for the purposes of multiplication, division, involution, and evolution. In changing from either addition or subtraction to multiplication or division, or *vice versa*, it is usually well worth while to convert a complex quantity from one form to the other.

In Fig. 28 the impedance between the frequencies of 992 and 1100 ~ inclusive, are plotted in rectangular coordinates. Thus at 1028 ~, the impedance is  $OP' = OA + jAP'$ ;

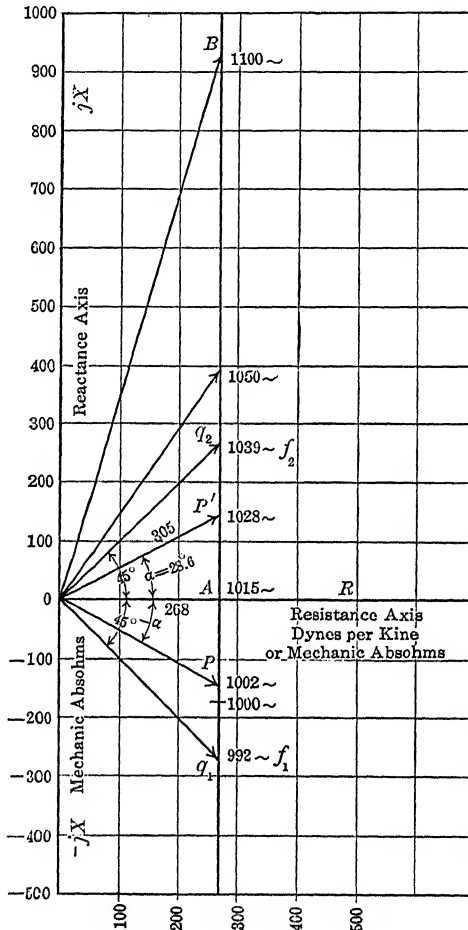


FIG. 28. Impedance of diaphragm to velocity, between  $f = 992 \sim$  and  $f = 1100 \sim$  of impressed frequency.  $r = 268$  dynes/kine.  $m = 0.902$  gm.  $s = 36.7 \times 10^6$  dynes/cm

\* Bibliography 49.

† Bibliography 9 and 9a.

where  $OA = 268$  and  $AP' = 146$ . In polar coordinates,  $OP' = 305 \angle 28^\circ.36'$ , where 305 is the size of the complex number, and  $+28^\circ.36'$  or  $28^\circ.6$  is its "slope."\*

It will be observed from Fig. 28 that the impedance of a simple vibratory system has a minimum size at the resonant frequency  $f_0$ , and this is equal to the mechanical resistance simply. This fact offers another method of defining the resonant frequency, i.e., the frequency at which the impedance to vibratory velocity is a minimum.

In Tables VI and VII as well as in Fig. 28, there are two frequencies,  $f_1$  and  $f_2$ , at which the magnitude of the total reactance is just equal to the magnitude of the resistance, or in this case 268 dynes per kine. These are called the lower and upper quadrantal frequencies respectively. In this case, the lower quadrantal frequency is  $992 \sim$ , and the upper  $1039 \sim$ . The two corresponding vector impedances,  $Oq_1$  and  $Oq_2$ , each makes an angle of  $45^\circ$  with the real axis  $OR$ . The vector  $Oq_1$  has a slope of  $-45^\circ$ ; while  $Oq_2$  has a slope of  $+45^\circ$ . The angle between them is thus one quadrant. The range of frequency comprised between these two quadrantal values is called the *quadrantal range*. The phenomena which accompany resonance are mainly displayed within this quadrantal range. Frequencies lying outside of this range may be regarded as being more or less remote from resonance.

**Vibratory Velocity and its Relations to Ohm's Law.** — Ohm announced in 1861 the remarkable law which bears his name and which states that the strength of electric current in a continuous-current circuit is equal to the quotient of the emf. by the resistance of the circuit. The extension of Ohm's law to alternating-current circuits by the use of complex numbers and plane-vector impedance was discovered† in 1893. The law, extended to simple a.-c. circuits, states that the current strength is the quotient of the emf. by the plane-vector impedance of the circuit; so that if  $I$  is the current strength,  $E$  the rms. emf., and  $Z$  the impedance

$$(47) \quad I = \frac{E}{Z} \quad \text{rms. amperes or abamperes } \angle.$$

The equation may be stated either in the practical or in the C. G. S. system; according to the units employed. The equation is a plane-vector equation, or employs complex numbers, as is indicated

\* Fleming, Bibliography 61, p. 11.

† Bibliography 9. See also a foreshadowing in Heaviside, Bibliography 7, Vol. II, p. 355.

by the  $\angle$  sign attached to the unit. If the slope of  $E$  is taken as zero, the magnitude of  $I$  will be the magnitude of  $E$  divided by the magnitude of  $Z$ ; while the slope of  $I$  will be equal to the slope of  $Z$  but of the opposite sign. Thus a simple a.-c. circuit has an emf. of 110 volts rms. taken as of standard phase or zero slope  $E = 110 \angle 0^\circ$ . If the total impedance of this circuit is  $10 \angle 60^\circ$  ohms (which in rectangular coordinates would be  $5 + j 8.66$  ohms), the current strength in the circuit would be  $110 \angle 0^\circ \div 10 \angle 60^\circ = 11 \angle 60^\circ$  amperes rms. That is, an ammeter in the circuit would indicate 11 amperes, and this current would lag  $60^\circ$  in phase behind the emf.

The alternating-current extension of Ohm's law applies immediately to a simple vibratory system, when velocity is substituted for current. The equation becomes either

$$(48) \quad \dot{x}_r = \frac{F_r}{z} = \frac{F_r}{r + j(m\omega - s/\omega)} \quad \text{rms. kines } \angle,$$

or

$$(49) \quad \dot{x}_m = \frac{F_m}{z} = \frac{F_m}{r + j(m\omega - s/\omega)} \quad \text{max. cy. kines } \angle,$$

according as we use in the numerator the rms. value  $F_r$  of the vibromotive force, or the maximum cyclic value  $F_m$ . In all cases of simple sinusoidal vmfs.,  $F_m = F_r \sqrt{2}$ ; so that it is a mere balance of advantages as to which should be used.

Thus, if a vmf. of 1765 maximum cyclic dynes, taken at standard phase, or as of zero slope, were applied to the diaphragm already considered at the frequency of 1100  $\sim$ , the impedance to motion of the system at this frequency is shown by Table VII to be  $268 + j 924 = 962 \angle 73^\circ.49'$  mechanical abohms. The vibratory velocity which will be developed in the steady state by the diaphragm, under these conditions, will be, by (49),  $\dot{x}_m = 1765 \angle 0^\circ \div 962 \angle 73^\circ.49' = 1.835 \angle 73^\circ.49'$  kines. Here we use the polar form of the impedance because division is involved. The diaphragm will attain a maximum cyclic velocity of 1.835 cm. per second. It will have this velocity at the instants when it passes its position of rest, midway between its full displacements on each side. The phase of this velocity will be  $73^\circ.49'$  behind the phase of the impressed vmf. In other words, the diaphragm would develop its maximum cyclic velocity about one-fifth of a cycle in time behind the maximum cyclic vmf. But a vmf. of 1765 maximum cyclic dynes is equivalent to a root-mean-square value





circumference of a circle having its center at  $c$  on the real axis  $OG$ . This circle passes through the origin  $O$ . This circular type of graph of plane-vector admittance to motion is characteristic of all simple vibratory systems. In other words, the vector graph of admittance of a simple vibratory system is a circle passing through the origin and centered on the real axis.

The reason for this remarkable geometric property of admittance in a simple vibratory system is due to the fact, proved by Möbius \* in 1855, that the plane-vector reciprocal of any circular graph is another circular graph. A straight-line graph is, however, only a limiting case of a circle, i.e., a circle of infinite radius. Therefore the reciprocal of any infinite straight-line graph must be a circle, and also a circle passing through the origin. But the vector graph of mechanical or electric impedance  $z$  was shown in connection with Fig. 28 to be an infinite straight line parallel to the imaginary axis, as the impressed frequency is varied in a simple system, all other conditions being held constant. Consequently the reciprocal of  $z$  or the admittance  $y$ , must have a circular graph centered on the real axis and passing through the origin. In a similar manner, it may be shown that the plane-vector graph of a.c. admittance in a simple *LRS* branch circuit like that of Fig. 27, as the impressed frequency is varied from zero to infinity, must be a circle centered on the real axis and passing through the origin.

As has been already pointed out, the admittance graph of Fig. 29 is also a velocity graph for unit vmf. and indeed for any vmf. taken at standard phase, if the scale of the diagram is suitably altered. Thus Fig. 29 informs us that at  $f = 1015 \sim$ , the maximum cyclic velocity of the diaphragm therein referred to will be  $3.731 \times 10^{-3} \angle 0^\circ$  kines per dyne maximum cyclic vmf. As the impressed frequency is increased from zero to  $f_0$ , keeping the magnitude of the vmf. constant, the vector velocity will advance from  $O$  through  $f_1$  to  $f_0$ , over the upper half of the circle, and then as the frequency is increased towards infinity, the velocity will move from  $f_0$  through  $f_2$  back to  $O$ , covering the lower half of the circle. At  $f_1$ , the lower numerical quadrantal frequency, the velocity graph would reach the top of the circle; while at  $f_2$ , the upper numerical quadrantal frequency, it would fall to the bottom of the circle. The quadrantal range of frequency would cover the outer half of the circle  $f_1 f_0 f_2$ .

\* Bibliography 1.

If the simple vibratory system had constants  $m$  and  $s$  other than those selected in this case, the admittance graph would be a similar circle, centered on  $OG$  and passing through  $O$ , but the distribution of frequencies over the circle would be different. The value of  $f_0$  depends, as we have seen in (33), only on the ratio of  $s$  to  $m$ . All systems having the same  $s/m$  have the same  $f_0$  at their diametral and resonant frequency. The diameter of the circle, however, keeping the scale unchanged, varies inversely as  $r$ , and the numerical values of  $f_1$  and  $f_2$  depend upon the value of  $r$ . In general, therefore, although every simple system has its own admittance circle, only systems identical in respect to  $m$ ,  $r$ , and  $s$  have the same circle.

The admittance circle throws a flood of light upon a number of seemingly obscure vibrational phenomena outside of the domain of ordinary telephone receivers. For example, a horizontal shaft, driven by a belt and pulley in a pair of slightly loose bearings, develops a characteristic vibrational behavior, if it is a little out of balance. If the want of balance is due, say, to a heavy spot near the shaft's surface and near one bearing, the centrifugal force of rotation will develop, through this lump, a rotary vmf. on the system. The system as a whole, in view of its dimensions and its geometric restraints, will possess an elastic coefficient  $s$ , a mass  $m$  and a frictional resistance  $r$ . The angular velocity of resonance (32) will be found at the value  $\sqrt{s/m}$ . Above this resonant angular velocity, the vibrational velocity will tend to diminish. This case is considered more fully in Appendix III.

When a reciprocating engine is mounted on or within a structural system, such as the hull of a steamship, the operation of the engine sets up a vmf. of the rotation frequency or of some associated frequency. All parts of the structural system are subjected to this vmf. If any member of the system which is able to vibrate independently, happens to have a ratio of  $\sqrt{s/m}$ , at or near the resonance value of the vmf., a relatively large vibrational velocity may be set up in that member. Occasionally, such fortuitous resonances give rise to dangerously large vibrations and vibrational velocities. In such cases, since the impressed engine frequency is not easily susceptible of being changed, the indicated procedure is to alter either the  $s$  or the  $m$  of the offending resonating member, (or both). These necessary changes can ordinarily be executed in a variety of ways, in which vibration specialists become expert.

## CHAPTER VII

### THE ELECTRIC IMPEDANCE OF TELEPHONE RECEIVERS, AND ITS MEASUREMENT

**Introduction.** — We have already seen that a telephone receiver is a particular type of reciprocating electromagnetic motor, adapted to receive alternating-current electric power from a circuit, convert it into magnetic power in its own magnetic circuit, and reconvert this into mechanical power at the diaphragm, for the production of acoustic power in the air over the diaphragm.

When we measure the impedance of the telephone receiver as a motor, we may do so with the reciprocating diaphragm element either in motion or at rest. This corresponds to measuring the impedance of an ordinary rotary a.-c. motor with its rotor either in motion, or clamped. The rotary motor is likely to vary greatly in its impedance between the free and the clamped conditions. The reciprocating telephone motor is also likely to vary considerably between these conditions. The impedance of the instrument with the diaphragm free is called the *free impedance*. With the diaphragm clamped or damped, the impedance is called the *damped impedance*. From measurements of the free and damped impedance of a receiver, many of its properties can be learned.

In order to obtain definitely comparable results, the free and damped impedance of a receiver should be measured at constant alternating-current strength, i.e., with the same rms. testing current in the coils of the instrument throughout both sets of measurements. The testing alternating current should be of telephonic strength, and should be as nearly sinusoidal as is practicable. If the current strength is too small, it will be difficult to secure adequate precision in the measurements. If it is too large, the magnetic flux through the poles of the instrument will be distorted, and will cease to be a constant permanent magnetic flux plus a small superposed sinusoidal variation. A suitable testing a.-c. mmf. to employ is usually about 3 gilberts rms.,

and such a mmf. may be developed in a common form of bipolar "75-ohm" receiver by a testing current through the instrument of 2 milliamperes rms. High-resistance instruments, with more numerous turns, should employ a correspondingly smaller testing current.

Although it might be possible to measure the impedance of a receiver in various ways, it is advisable to adopt and retain a simple and uniform method. Experience has shown that a Rayleigh bridge, or the Rayleigh modification of a Wheatstone bridge, furnishes a satisfactory means for making these tests. The general plan is very simple. The receiver to be tested is made the fourth arm of a bridge. The third or balancing arm contains both adjustable resistance and adjustable inductance in simple series. The other two arms, or ratio arms, are equal anti-inductive resistances, preferably of about the same magnitude as the size of the impedance developed in the receiver at or near the resonant frequency.

Figure 30 shows one set of connections that has been much used.

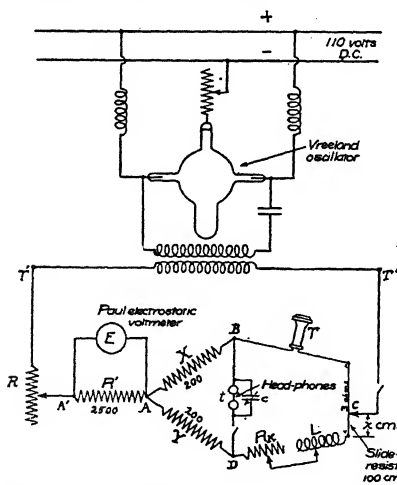


FIG. 30. Connection diagram for Rayleigh bridge and Vreeland oscillator. For  $X/Y=1$ ,  $R_T=R_L+R_K-3+0.06x$  ohms.

The bridge is  $ABCD$ . The ratio arms  $X$  and  $Y$  were each 200-ohm resistances, anti-inductively wound.  $R_K$  is the adjustable resistor or rheostat, reading to tenths of an ohm, and up to 1000 ohms.  $L$  is the adjustable inductor, reading easily to tenths of a millihenry, and up to 60 millihenries, for the ordinary type of tested receiver  $T$ . The a-c. galvanometer consists ordinarily of a pair of head telephones  $t$ , for detecting balance. The stabilizing resistance  $R$ , enables substantially constant current to be maintained through each arm of the bridge, when constant rms. voltage is maintained at the terminals of the static voltmeter  $E$  permanently connected across the terminals  $A'A$  of the resistance  $R'$ .

Ten volts is ordinarily maintained at this voltmeter, and  $R'$  is adjusted to 2500 ohms, in order to keep 2 milliamperes on each side of the bridge. In practice, the resistance  $R$  does not have to be kept closely adjusted, because, provided the testing current in the receiver is small, the receiver's impedance remains almost unchanged over a considerable range of the testing current strength.

The terminals  $T'T'$  are connected to the source of audio-frequency testing voltage. Both Vreeland oscillators and triode vacuum-tube oscillators have been used at different times. In either case, it is desirable that the impressed frequency shall be steady, accurately determinable, and free from parasitic frequencies or harmonics.

Another set of connections has also been employed, the only difference being that the alternating-current strength supplied to the bridge is measured by a thermocouple and associated millivoltmeter, instead of by a static voltmeter and associated resistance, as in Fig. 30. The choice between the two methods depends mainly upon the nature of the available measuring apparatus.

**Damping Devices.** — It is customary first to make a series of damped-impedance measurements, and then to follow these promptly with another series of free-impedance measurements; but the order of succession between the two is not important. It is necessary, however, to adopt a definite procedure for clamping or damping the diaphragm, when making the series of damped impedance measurements.

In the earliest group of measurements,\* the damping was effected by gently pressing a finger against the diaphragm of the receiver under test. This plan was effective, so far as concerns the arresting of vibration, but it was open to two objections. First the pressure of the finger flexed the diaphragm to some extent, and altered the airgap over the poles, thus altering the electromagnetic constants of the instrument during the test. Second, the application of the finger during the series of damped resistances was likely to raise the temperature of the diaphragm, and affect its behavior from a mechanical viewpoint.

In later groups of measurements, a more elaborate damping device was introduced, which was free from the preceding objections. It consisted of a massive brass cylinder  $C$ , Fig. 31, suspended in such a manner that little or no mechanical stress was

\* Kennelly and Pierce. Bibliography 40.

applied to the diaphragm, when the cylinder was temporarily fastened to the center of the latter. An axial projection or stem *A*, carried by the cylinder *C*, has a coating of carnauba wax on its face *K*, and a small electric heating coil, not shown in the figure, is applied to this stem. The tested receiver is held firmly on a suitably shaped wooden block *B*. The cylinder *C* is then moved into position, and clamped so that the wax-coated face of the stem rests lightly in contact with the center of the face of the diaphragm. A heating current is then sent through the coil from a storage battery or other independent source, so as to melt the wax on the face *K* of the stem, without disturbing the mechanical adjust-

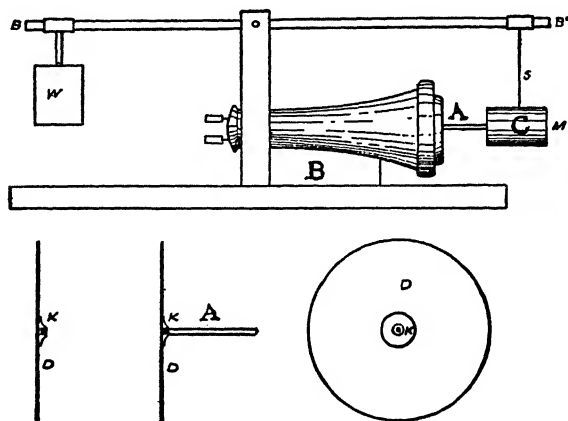


FIG. 31. Means for damping telephone diaphragm.

ments. If the procedure is successfully followed, the melted wax will adhere to the diaphragm at the center, so that when the heating current is cut off, the wax will set and connect the cylinder mechanically with the diaphragm. The large mass and inertia of the cylinder will then reduce the vibration of the diaphragm to an insignificantly small amount. After the series of damped impedances has been measured in this condition, the wax is again melted by current readmitted to the coil 1, and the cylinder withdrawn ready for the series of free impedances. Two precautions are necessary in the use of this damping device; namely, first to allow sufficient time for the diaphragm to cool down to normal temperature, after fastening on the cylinder; and second, to scrape off all the residual wax from the surface of the diaphragm after

the cylinder has been removed, lest the value of  $m$  should be affected appreciably.

Another plan\* for damping the diaphragm which calls for a little more manual skill, but which dispenses with the special mechanism of the plan just described, is to fasten a wax bridge or  $M$ , like that shown in Fig. 32. The bridge  $ABC$  is prepared in paraffine wax, or similar readily melted material. The pillars  $A$  and  $B$  are heated to softening, and applied to the telephone cap, leaving the central pillar  $C$  pressing lightly against the center of the diaphragm  $DD$ . A hot wire is then applied to the pillar  $C$ , so as to melt it to the point at which the pressure against the diaphragm is withdrawn. On cooling, the diaphragm will be held by the adherent wax pillar  $C$ , and will be prevented from vibrating to the testing currents used for obtaining the series of damped impedances.

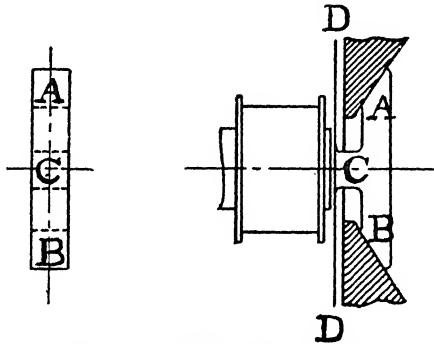


FIG. 32. Wax bridge damper.

Still another plan, which, though not so accurate, is very swift in application,\* is to make a shallow soft wooden plug that can be inserted adherently into the mouth of the telephone receiver, and yet not touch the diaphragm immediately under it. The diaphragm will now be mechanically free, but the thin film of air between its surface and the plug will have so large an acoustic resistance that the amplitude of its vibration will be relatively very small. For many purposes the amplitude may be regarded as practically nil. This approximate method of damping the diaphragm has been called *acoustic damping*.

One other plan is to dispense with the damping entirely, and to infer the approximate electrical conditions when damped from the observations made with the diaphragm free, in a manner to be described later (page 79).

**Series of Damped Impedances.**— With the diaphragm damped in one of the ways above suggested, the tested receiver is con-

\* Bibliography 87.



nected in the Rayleigh bridge of Fig. 30, and a balance is obtained both in resistance and inductance, at a suitable number of successively increased and measured frequencies, with the testing current substantially constant. With ordinary telephone receivers, which are resonant to a frequency in the neighborhood of 1000  $\sim$ , it is usually of little use to measure the impedance below 400  $\sim$  or above 1500  $\sim$ . The important measurements usually lie in the frequency range 900  $\sim$  to 1100  $\sim$ . A series of such measurements is recorded in columns 1, 4, and 7 of Table VIII.

Column 1 gives the frequency impressed by the source, which, in this case, was a Vreeland oscillator. Column 2 gives the corresponding angular velocity in radians per second, from formula (28). The apparent resistance  $R$  of the instrument, at each frequency, appears in column 4, and the apparent inductance  $\mathcal{L}$  in column 7. If we multiply  $\mathcal{L}$  in column 7 by the corresponding value of  $\omega$  in column 2, we obtain the apparent damped reactance  $X$  of the instrument at that frequency; since

$$(52) \quad X = \mathcal{L}\omega \quad \text{abohms or ohms.}$$

The measurements are naturally made in ohms, but in the computations, it is safer to adhere to the fundamental units of the C. G. S. system and to employ abohms. These damped reactances appear in column 8 of the Table, which shows that the damped resistance steadily increased from 124 ohms at 429  $\sim$  to 204 ohms at 1507  $\sim$ ; while the damped inductance diminished from 41.5 to 29.7 millihenries, but the damped reactance increased from 104.3 to 284.1 ohms. These changes in  $R$  and  $\mathcal{L}$  are partly attributable to hysteresis in the magnetic circuit of the receiver windings and partly attributable to systematic eddy currents or magnetic skin-effect in the steel cores, whereby the alternating magnetic flux diminishes in density towards their centers, and also falls off in magnitude and lags further in phase.

Figure 33 shows the plane-vector graph of the damped impedance. Resistances  $R$  from column 4 are plotted along the axis  $OR$ , and reactances  $X$  from column 8 are plotted along the axis  $OX$ . The origin of coordinates is not shown in the figure. The graph is the heavy curve  $ABCD$ . The frequencies at the different observations are marked on this graph. The graph would presumably be a straight line, if the magnetic skin-effect remained constant over the range of frequency represented. Actually, the graph is seen to bend slightly away from the  $OX$  axis, as the fre-

TABLE VIII

1	2	3	4	5	6	7	8	9	10	11	12
FREQ. C. P. S. $\omega$	ANG. VELOC. $\omega$	$E'$ RES. FREE OHMS	$R$ RES. DAMPED OHMS	$R' = R' - R$ MOTIONAL RES. OHMS	$E'$ INDUCTANCE FREE HENRIES	$E$ INDUCTANCE DAMPED HENRIES	$E_0$ REACTANCE DAMPED OHMS	$E' - E$ MOTIONAL INDUCTANCE HENRIES	$X^1$ MOTIONAL REACT. OHMS ( $E' - E$ )/ $\omega$	MAX. CYCLIC DISPLACE- MENTS MICRONS OBSERVED	MAX. CYCLIC VELOCITY KINES $\omega E$
429	2694	130	124	6	41.5	38.7	104.3	2.8	7.5	1.8	0.49
702	4410	153	145	8	36.6	35.7	157.4	0.9	4.0	1.6	0.70
804	5052	166	153	13	36.2	34.7	175.3	1.5	7.6	1.9	0.96
857	5385	174	157	17	36.3	34.2	184.2	2.1	11.3	2.6	1.40
897.4	5640	184	160	24	36.2	33.8	190.6	2.4	13.5	2.6	1.47
923.4	5801	193	162	31	36.3	33.6	194.9	2.7	15.7	2.85	1.65
945.6	5941	204	163	41	36.3	33.5	199.0	2.8	16.6	3.8	2.26
962	6046	218	164	54	36.0	33.4	201.9	2.6	15.7	4.56	2.76
974	6118	230	165	65	35.5	33.3	203.7	2.2	13.5	4.63	2.83
980	6156	241	166	75	35.0	33.2	204.4	1.8	11.1	5.07	3.12
987	6200	254	166	88	33.6	33.2	205.8	0.4	2.5	6.02	3.73
994	6245	270	167	103	31.0	33.1	206.7	-2.1	-13.1	6.97	4.35
1000	6283	283	167	116	27.0	33.1	208.0	-6.1	-38.3	8.23	5.17
1007	6328	278	168	110	21.5	33.0	208.9	-11.5	-72.8	9.18	5.81
1013.6	6370	261	168	93	17.2	33.0	210.2	-15.8	-100.6	10.1	6.43
1020.4	6412	224	168.5	55.5	14.2	32.9	211.0	-18.7	-119.9	10.45	6.70
1028	6461	191	170	21	14.5	32.8	211.9	-18.3	-118.2	9.38	6.06
1036	6508	164	170	-6	16.6	32.8	213.5	-16.2	-105.4	8.24	5.36
1043	6552	151	171	-20	19.4	32.7	214.3	-13.3	-87.1	7.60	4.98
1050	6597	148	171	-23	21.8	32.6	215.1	-10.8	-71.2	6.15	4.06
1066	6698	144	172	-28	25.0	32.5	217.7	-7.5	-50.2	4.75	3.18
1082	6798	148	173	-25	27.3	32.4	220.3	-5.1	-34.7	3.80	2.58
1108	6966	153	175	-22	28.7	32.2	224.3	-3.5	-24.4	2.22	1.55
1137	7145	159	177	-18	29.5	32.0	228.7	-2.5	-17.9	0.95	0.63
1190	7478	167	181	-14	30.3	31.7	237.1	-1.4	-10.5		
1306	8203	181	189	-8	30.5	31.0	254.3	-0.5	-4.1		
1507	9470	201	204	-3	29.7	30.0	284.1	-0.3	-2.8		

quency increases. At  $A = 429 \sim$ , the tangent makes a corresponding angle of about  $22^\circ.5$ . At  $O$ , near the resonant fre-

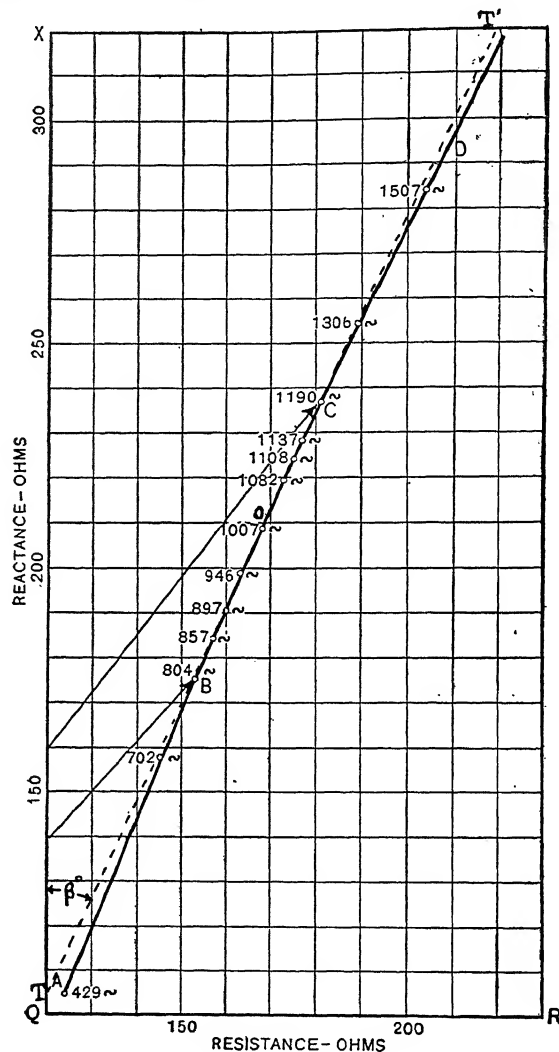


FIG. 33. Locus of vector damped impedance for tested receiver.

quency of  $1015 \sim$ , this angle between the broken-line tangent  $TOT'$  and  $OX$  is about  $25^\circ.3$ . This mean value of the angle, near resonance, is called the angle  $\beta$  for the receiver. At the time when

Fig. 33 was worked out and first published,\* the significance of this *reactance deviation angle* in the figure had not been recognized. As we shall see, it is an important characteristic. It represents the mean lag between the phase of the testing alternating current supplied to the coils of the instrument and the vector magnetic flux thereby produced and linked with the windings.

**Vector Diagram of Damped Impedance.** — Figure 34 is a vector diagram of these damped impedances at constant current but varied frequency. The length  $Oa$  is supposed to be the direct-current† resistance  $R_1$  of the instrument, or the resistance which would be observed at zero frequency if the magnetic skin-effect in the cores did not change. Owing to hysteresis and to the skin-effect, assumed constant, the magnetic flux lags behind the vector  $Oa$  by the angle  $\beta^\circ$ . The vector reactance  $\mathcal{X} = \mathcal{L}\omega$  is developed from  $a$  in a direction perpendicular to the flux, or in the direction  $ab$ , making an angle  $\beta$  with the  $OX$  axis. The imped-

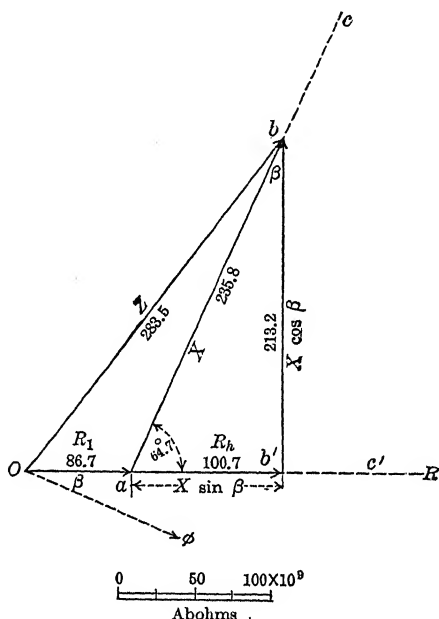


FIG. 34. Vector-impedance diagram — diaphragm damped.

ance of the instrument, as measured in the Rayleigh bridge, is the vector  $Z = Ob$ , having a real component  $R = R_1 + |\mathcal{X}| \sin \beta$ , and an imaginary component  $X = |\mathcal{X}| \cos \beta$ , where  $|\mathcal{X}|$  denotes the size of the vector  $\mathcal{X}$ . These are, respectively, the apparent resistance and the apparent reactance of the instrument. As the impressed frequency increases from zero upwards, the vector  $Z$ , with its origin fixed at  $O$ , moves along the straight line  $ab$  of vector reactance. This theory ignores the changes in skin-effect as the frequency

\* Bibliography 58.

† The abbreviation d.-c. will hereafter be used for "direct-current."

risers and is therefore imperfect, but the theory supplies a satisfactory first approximation for the ordinary receiver.

TABLE IX

FREQUENCY CYCLES PER SEC. $f$	ANGULAR VELOCITY RAD. PER SEC. $\omega$	MEASURED RESISTANCE ABOHMS AT 20 DEG. CENT. $R$	ACTIVE COM- PONENT OF INDUCTIVE RESISTANCE $R_R = \omega L_0$ $\times \sin \beta$	REACTIVE COMPONENT OF INDUC- TIVE RE- SISTANCE $X = \omega L_0$ $\times \cos \beta$	$R_1 = R - R_R$ ABOHMS
0	0	$86.7 \times 10^9$	$0 \times 10^9$	$0 \times 10^9$	$86.7 \times 10^9$
429	2694	124 "	41.9 "	89 "	82.1 "
702	4420	145 "	68.8 "	146 "	76.2 "
923.4	5801	162 "	90.5 "	191.5 "	71.5 "
*1015	6378	168.4 "	99.5 "	210.5 "	68.6 "
1306	8202	189 "	128 "	270.7 "	61 "
1507	9460	204 "	147.6 "	314.1 "	56.4 "

\*Resonant frequency.

Table IX indicates the amount of error involved in the case considered by the assumptions here made that the damped-im-

pedance graph  $ABCD$ , Fig. 34, is a straight line like  $abc$  in Fig. 34. The measured d.-c. resistance  $R_1$  of the instrument was 86.7 ohms, or  $86.7 \times 10^9$  abohms. It will be seen that, at 1507 ~, the inferred value of  $R_1$  has fallen to  $56.4 \times 10^9$  abohms, owing to the bending over of the vector-impedance curve. The discrepancy is much smaller, however, over the quadrantal range in frequency (991 ~ to 1040 ~).

**Vector Damped EMF Diagram.** — If we multiply each of the vectors in Fig. 34 by the real value of  $I$ , the rms. testing current strength through the instrument in abamperes (0.000204 ab-ampere or 2.04 milliamperes), we obtain the *EMF* vector

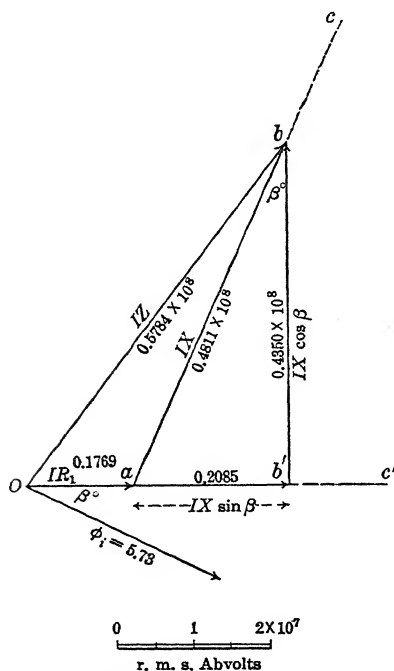


FIG. 35. Vector EMF diagram at  $f = 1028 \sim$  with diaphragm damped.

diagram of Fig. 35. Here  $IR_1$  is the vector part of the impressed emf. at receiver terminals, to overcome the d.-c. resistance, assumed as constant.  $I|\mathcal{X}|\sin\beta$  is the increase in apparent resistance emf., due to hysteresis and constant skin-effect. Similarly  $I\mathcal{X}$  is the vector part of the impressed terminal emf. overcoming the vector reactance.  $IZ$  is the vector impressed emf. which, with its origin fixed at  $O$ , moves along the line  $abc$  as the frequency is increased.

**Series of Free Impedances.** — If the damping device is removed from the tested receiver, a series of free impedances is measured with the instrument temperature as close to that in the damped series as may be practicable. It is desirable, although not essential, that the impressed frequencies used in the free series should be individually the same as those used in the damped series. Since, however, both the resistances and the inductances recorded in the free series are much more variable and seemingly erratic than in the damped series, it is important to make sure that a sufficient number of measurements are secured in the region of most rapid variation. For this purpose, it is convenient to plot the observations of  $R$  and  $\mathcal{L}$  against frequency on squared paper, as the series progresses, so as not to miss the maximum and minimum values. Occasionally, very small steps in frequency are desirable, near the resonant value, in order to deal with sharply resonant receivers. Table VIII gives the series of free resistances  $R''$ , and inductances  $\mathcal{L}''$  observed with the selected receiver, in columns 3 and 6 respectively. Multiplying each of the inductances by its respective angular velocity in column 2, the values of apparent reactance  $X''$  may be obtained.

If we proceed to plot the plane-vector locus of free impedances with change of frequency, we obtain the graph  $abPcd$  of Fig. 36. The origin of coordinates is here omitted, in order to save space. The graph has a loop, and this is characteristic of all receivers generally. It will be observed that at  $P$  there are two very distinct frequencies, which in this instrument develop identical impedances; namely, a frequency close to 600  $\sim$ , and the frequency 1050  $\sim$ . This dual value of frequency at some particular vector free impedance is a characteristic property of all telephone receivers.

In Fig. 37, the graphs of Figs. 35 and 36 are drawn side by side, and equifrequency points on them are connected by individual vectors. The light curve  $abc\dots hi$  is the vector locus of damped impedance from Fig. 35, and the heavy curve  $ABC\dots HI$  is the

corresponding vector locus of free impedance from Fig. 36. The successive vectors  $bB, cC, \dots hH, iI$ , connect a point of a definite

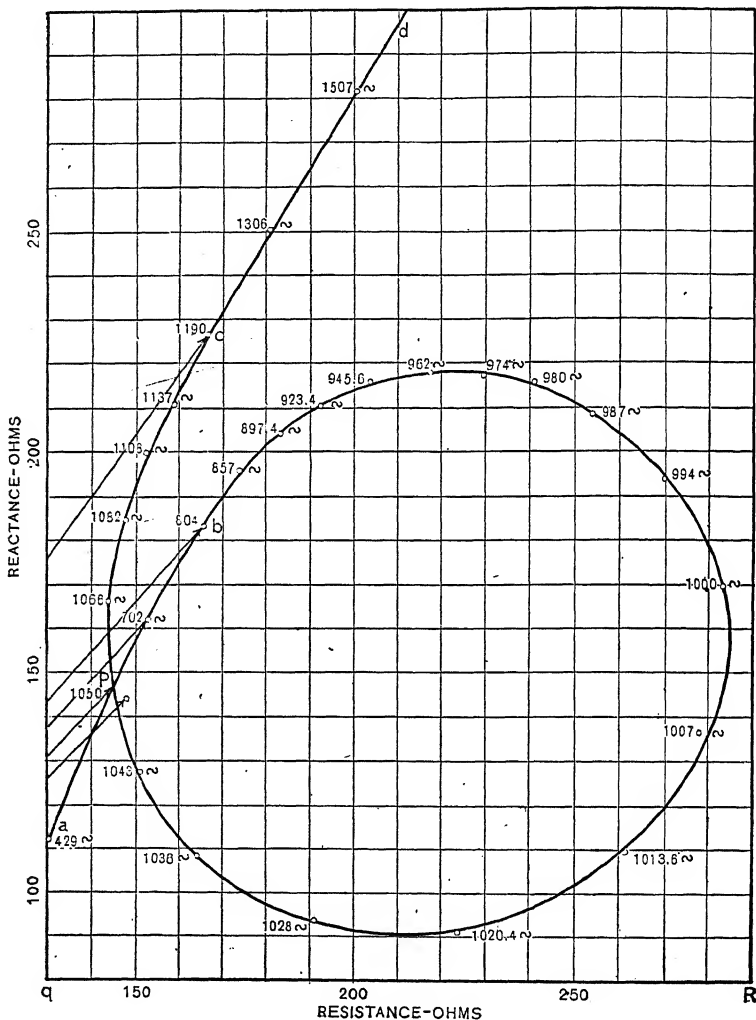


FIG. 36. Locus of vector free impedance, for the same receiver.

frequency on the damped curve with the point of the same frequency on the free curve. Thus, at 1028  $\sim$ , the connecting vector is  $fF$ , which has a size of 120 ohms, and a slope of approximately  $-80^\circ$  with the resistance axis.

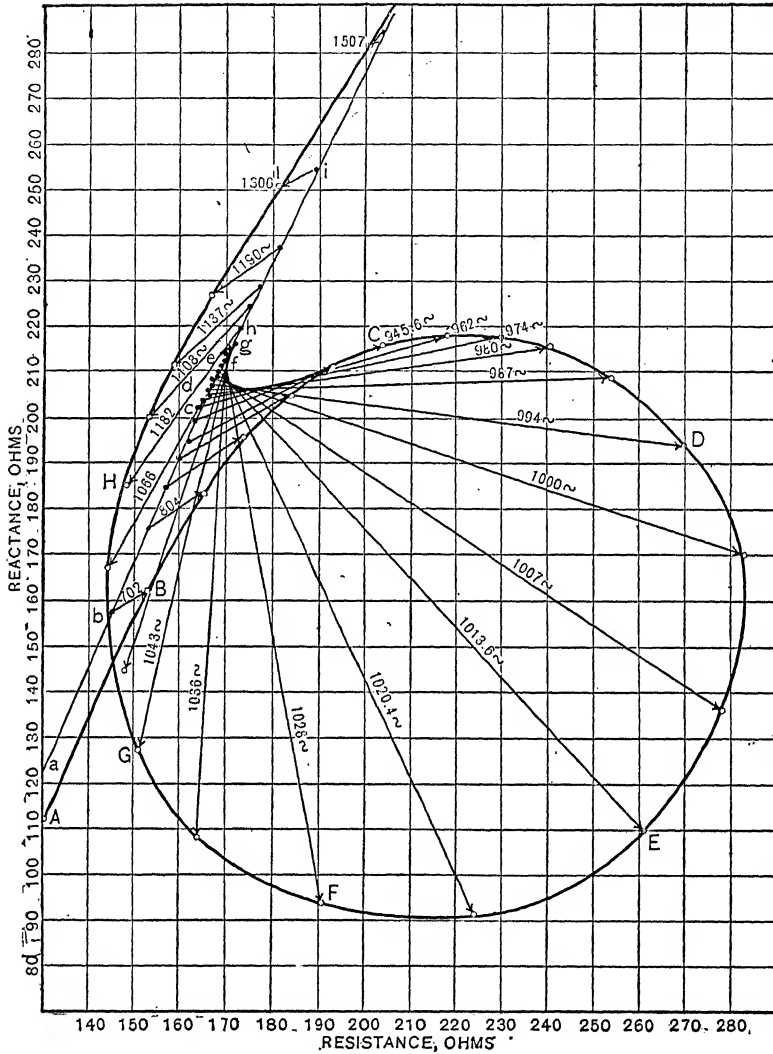


FIG. 37. Motional-impedance vectors at successive observed frequencies.

$$(53) \quad Z' = Z'' - Z \quad \text{ohms or abohms } \angle,$$

where  $Z$  is the damped impedance at a given frequency,  $Z''$  the free impedance at the same frequency, and  $Z'$  their vector differ-





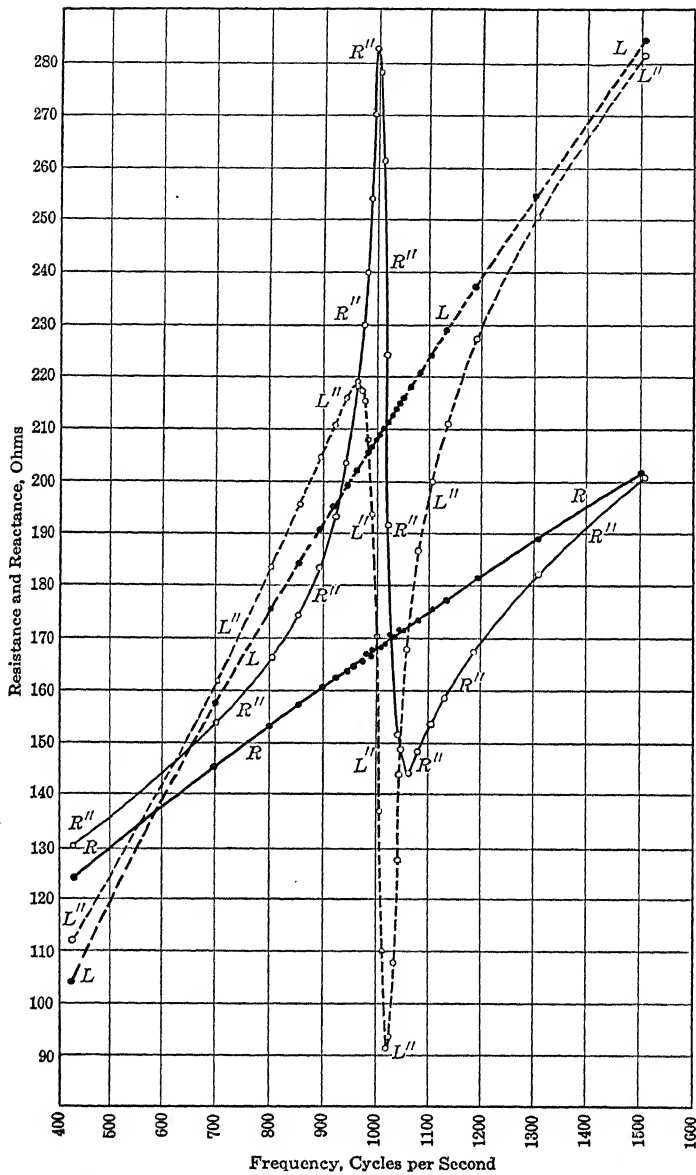


FIG. 39. Free and damped resistances and reactances of tested receiver at different impressed frequencies. Scalar diagram.

through the origin of coordinates, when the receiver is in normal operative condition in free air. The fact that the locus of motional impedance is a circle, at least to a first approximation, was discovered experimentally\* in 1912.

It is not actually necessary to go through all the steps of the process outlined above in order to derive the *motional-impedance circle* of a telephone receiver. It is sufficient to plot the damped and free values of resistance and reactance as numerical ordinates against impressed frequency as abscissas. We can then read off, at each selected frequency, the corresponding free and the damped apparent resistances  $R''$  and  $R$ , and likewise the free and the damped apparent reactances  $X''$  and  $X$ . Then at that frequency

$$(54) \quad Z' = R' + jX' = (R'' - R) + j(X'' - X)$$

ohms or abohms  $\angle$ .

It may even suffice to use this formula directly, with the entries in a table of observations, like Table VIII. Figure 39 presents a chart of the type referred to. It will be observed that both the free resistance and the free inductance execute sharp variations near the resonant frequency, but these variation peaks are not coincident.

Figure 40 presents a similar chart in which the sizes and slopes are given of the free and the damped impedances instead of their rectangular components. In this case, resonance occurs near to the sharp minimum in the slope of the free impedance.†

If we examine the motional-impedance circle of the reference instrument, Fig. 38, we may observe that the diameter  $OP$  of the circle is depressed below the resistance axis  $OR$ , by an angle  $2\beta$ . According to the approximate theory here discussed, this angle is just twice the angle  $\beta$  of lag of the vector alternating magnetic flux through the windings, behind the phase of the testing current. (See Figs. 33, 34, 35, 42 and 45.)

\* Bibliography 40.

† It has been suggested by the Engineering Department of the Western Electric Co. that the technique for producing the motional-impedance circle of a telephone receiver can be further simplified by taking two similar receivers, one damped and the other free, and connecting them on opposite sides of the same Rayleigh bridge (Fig. 30). The motional impedance would then be measured at once for each frequency, without having to take two successive series. This procedure requires, however, that the two selected instruments should be very nearly alike.

We may also notice that the frequency at the point  $P$  of the circle at which the diametral vector  $OP$  intersects it, is the *fre-*

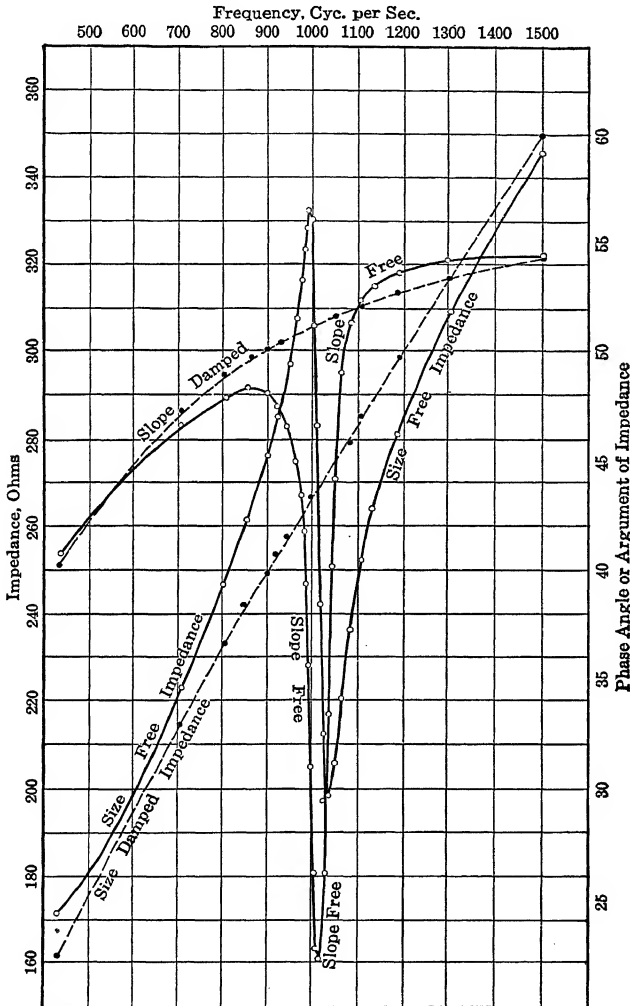


FIG. 40. Scalar diagram of free and damped impedance.

*quency  $f_0$  of apparent resonance* of the diaphragm in the presence of its constraints, i.e., with the particular type of clamping around its edge, with the particular air chambers above and below it, with the particular permanent magnetic field in which it vibrates, and

at its observed temperature. Strictly speaking, the temperature, pressure, and geometric constraints of the air in front of the instrument should also be included. It is found experimentally, and it is readily understood theoretically, that a change in any of these particulars may give rise to a change in the apparent resonant frequency value  $f_0$ , at the diametral point of the motional-impedance circle.

In view of the many variables which may affect the size, the depression angle, and the frequency distribution of a motional-impedance circle, it is not remarkable that different types of receiver should be found to possess different circles in these particulars. Roughly speaking, similar receivers of the same make have similar motional-impedance circles. It is seldom, however, that two instruments, of the same type and make, present identical motional-impedance circles within the limits of measurable variation. In fact, it is only by taking pains to insure constant mechanical, electric, and thermal conditions, that one and the same instrument can be made to reproduce closely the same circle at different times.

The curve of damped resistance, which we consider as a straight line in our first-approximation theory, appears in Fig. 39 as a curve gradually bending over towards the frequency axis. This curve has been found \* to be approximately quadratic, of the type

$$(55) \quad R = a + bf - cf^2 \quad \text{ohms,}$$

where  $a$ ,  $b$ , and  $c$  are ohmic constants, and  $f$  is the impressed frequency in cycles per second. In this case, the approximate equation between  $f = 400 \sim$  and  $f = 1500 \sim$  is

$$R = 90.76 + 0.0784f - 2.16 \times 10^{-6}f^2 \quad \text{ohms.}$$

It is evident that the formula is only empirical, because at  $f = 0$ , the resistance  $R$  is 90.76 ohms, whereas the actual resistance was 86.7 ohms.

Professor G. W. Pierce has also pointed out \* that the product of the damped resistance  $R$  and damped inductance  $\mathcal{L}$  remains approximately constant over a considerable range of frequency, the apparent resistance increasing and the apparent inductance decreasing as the frequency is raised. That is

$$(56) \quad R \mathcal{L} \cong \text{constant} \quad \text{ohms-henries.}$$

\* Bibliography 40.

In this instrument, the  $RE$  product was about 5.5. This relation appears to be maintained better, however, when the measurements are made at constant impressed terminal voltage, than at constant current strength.

**Motional-Impedance Data without the Measurement of Damped Impedances.** — An inspection of Figure 39 will show that in the case of such a standard type of receiver as is there referred to, we may approximately locate the curves  $RR$  and  $LL$ , of damped resistance and reactance respectively, by ignoring the differences between  $R$  and  $R''$ ,  $E$  and  $E''$ , at the highest and lowest frequencies of observation, and then drawing straight lines between the extreme points of  $R''$ , and likewise of  $E''$ . Thus, in Fig. 39, or in Table VIII, we find that the free resistance of this instrument at the lowest test-frequency (429  $\sim$ ) was 130 ohms, while at the highest test-frequency (1507  $\sim$ ) it was 201 ohms. If we join these two points on the diagram by a straight line, we should obtain a first approximation to the actual damped resistance curve  $RR$ . This approximation might suffice for many practical purposes, and would save the time and effort expended in measuring and plotting the damped resistance. Again we find in Fig. 39 that the free reactance at 429  $\sim$  was 111.8 ohms, and at 1507  $\sim$ , 281.3 ohms. If we also join these two points by a straight line, we obtain a first approximation to the curve  $LL$  of measured damped reactance. This plan of dispensing with damped measurements was devised by the research staff of the Western Electric Company. When the plan is used, it may be advantageous to commence the measurements of free resistance  $R''$  and inductance  $E''$  at a lower frequency than is shown in Fig. 39, say at 200  $\sim$ . This not only insures a closer agreement between the starting points of the  $RR''$  and  $EE''$  curves; but it also provides a greater range for guiding interpolation of frequencies over the straight lines of assumed damped resistance  $R$  and inductance  $E$ .

## THE VECTOR FORCE DIAGRAMS OF THE TELEPHONE RECEIVER

**Introduction.** — The analysis of the motional-impedance circle of a telephone receiver, taking into account the variation of eddy currents in the steel poles and in the diaphragm, with change of frequency, is a difficult problem. It becomes much simplified if we assume the eddy-current and magnetic skin-effect to retain a steady mean value over the range employed. We may therefore proceed on this assumption, and develop the vector force diagrams of the instrument, namely the diagrams of  $\text{mmf.}$ ,  $\text{vmf.}$ , and  $\text{emf.}$

The complete mathematical analysis of the dynamics of a telephone receiver was first worked out and published in 1907, by

Poincaré.\* As a piece of algebraic analysis, this was a remarkable achievement; but the results are expressed in very general form. On the other hand, the analysis detailed in this book is primarily experimental, having been developed step by step in practical procedure.

### Free Impedance Vector Diagram. —

Figure 41 is a vector diagram of the free impedance of the receiver considered as being measured to scale at the particular

frequency  $f = 1028 \sim$ . At this frequency, the damped impedance,

\* Bibliography 25 and 89.

according to Table VIII and Fig. 34, would be  $Z = Ob = Ob' + jb'b$ . The motional impedance is  $Z' = bh$ ; so that the free impedance is  $Z'' = Z + Z' = Oh$ . The broken circle  $bhO'$  is the motional-impedance circle. As the frequency is increased, the point  $b$  moves along the straight line  $ab$ , carrying with it the extending damped impedance  $Ob$  and the motional impedance  $Z'$  in the circle, which is also carried bodily along with  $b$ . The apparent resistance free, at  $1028 \sim$  is  $Oh'$ , and the apparent reactance is  $h'h$ . At all positions of the motional circle, the diameter  $bo'$  maintains its constant depression angle below  $bg$ , which is parallel to the resistance axis  $Oh'$ .

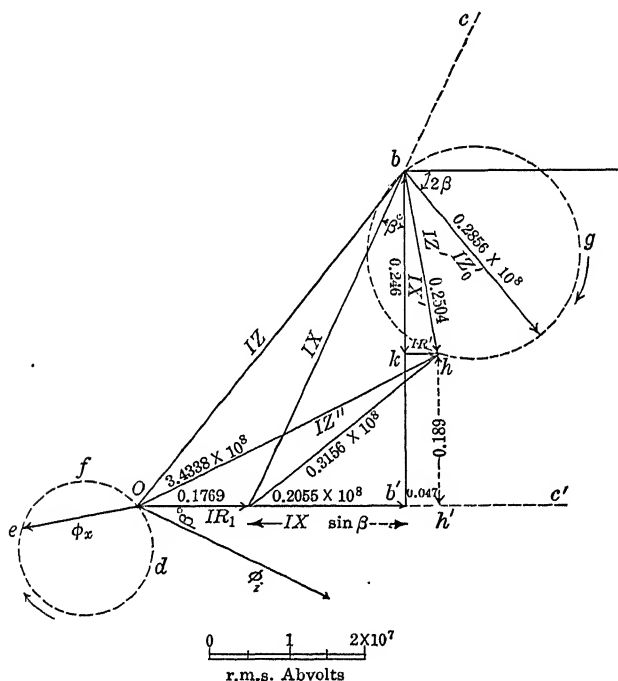


FIG. 42. Vector EMF Diagram at 1028 cycles per sec. — diaphragm free.

The reason for the circular locus  $bhO'$  of the motional impedance is found in the mechanical vibrational velocity, which, as has been pointed out in Chapter VI, develops a circular locus under constant vmf. and varied frequency. This will be considered in detail later.

If we multiply each of the vectors in Fig. 41 by  $I$ , the



magnitude of the rms. testing current through the instrument, we obtain a similar vector diagram of emfs. This is presented in Fig. 42, for the same frequency of  $1028 \sim$ . The vector  $IZ''$  represents the magnitude and phase of the emf. at terminals, free, taking  $Oc'$  as indicating standard current phase. The vector  $IZ' = bh$  is the motional emf., i.e., the part of the impressed emf. which is expended in overcoming a vector cemf. of  $hb$  due to the motion of the diaphragm. This cemf. may be regarded as due to the time rate of change of the *displacement flux*  $\phi_x$  which is linked with the windings and which occurs  $\beta^\circ$  in phase behind the diaphragm displacement, as will be shown later. The emf.  $bh$  is in leading quadrature with the displacement flux  $\phi_x = Oe$ , just as the emf.  $IX$  is in leading quadrature with the flux  $\phi_i$  set up by the testing current. The locus of  $\phi_x$  is the *displacement curve*  $def$ , and is approximately circular. As the frequency increases, the vector  $\phi_x$  pursues this locus  $def$  in the direction of the arrow, while the emf. thereby induced is the motional emf.  $bgh$  perpendicular to  $\phi_x$ .

**Vector Diagram of Magnetomotive Forces.** — When the receiver diaphragm is clamped, and damped impedances are measured, the only alternating magnetomotive force set up in the magnetic circuit of the instrument is that due to the testing current  $I$  passing around the cores. If  $N$  is the total number of turns in the winding, including both coils, and  $I$  is the rms. testing current strength in abamperes, the a.-c. mmf. set up will be, by (9),

$$(57) \quad \mathcal{F}_i = 4\pi NI \quad \text{rms. gilberts } \angle.$$

Thus, taking the testing current as  $2.04 \times 10^{-4}$  abampere and  $N = 1300$  turns or 650 on each pole,  $\mathcal{F}_i = 3.334$  rms. gilberts. This mmf. will be in cophase with the current  $I$ . It is represented to scale in Fig. 43. This alternating mmf. is superposed in the magnetic circuit upon the structural unidirectional mmf.  $\mathcal{F}_0$  of the horseshoe permanent magnet.

If now the diaphragm is freed, a new mmf. is developed in the magnetic circuit, as is indicated in Fig. 44 by the vector  $\mathcal{F}_x$ . This new mmf. is due to the cyclic change in the air gap effected by the vibration of the diaphragm. It is in phase with the alternating displacement of the diaphragm. We have not yet determined the phase of this displacement, so that we do not yet

assign the slope of  $\mathcal{F}_x$ ; but we can readily compute its size. The slope will be determined subsequently.

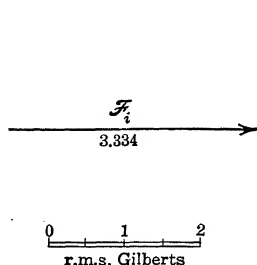


FIG. 43. Vector MMF. Diagram at constant current — diaphragm damped.

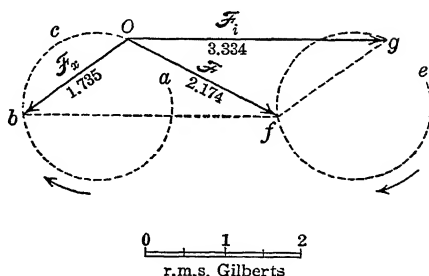


FIG. 44. Vector MMF. Diagram at constant current and 1028 cycles per sec. — diaphragm free.

The permanent magnetic flux  $\phi_0$  in the magnetic circuit of the coils is defined by formula (2). The reluctance in the circuit mainly resides in the air gaps between the poles and the steel diaphragm. If the diaphragm in its vibration advances towards the poles through a small displacement  $\delta x$  cm., the reluctance of the air gap over each pole will be changed by  $-\delta x/S$  oersteds, where  $S$  is the surface area of each pole in sq. cm., the polar flux being assumed to keep entirely within this area, without fringing at the edges. The total small change in reluctance due to the vibration of the diaphragm over both poles will thus be  $-2\delta x/S$  oersteds. But, differentiating (2), we have

$$(58) \quad \frac{\delta \phi_0}{\delta \mathcal{R}_0} = -\frac{\mathcal{F}}{\mathcal{R}_0^2} = -\frac{\phi_0}{\mathcal{R}_0} \quad \frac{\text{maxwells}}{\text{oersteds}},$$

or

$$(59) \quad \delta \phi_0 = -\phi_0 \frac{\delta \mathcal{R}_0}{\mathcal{R}_0} \quad \text{maxwells};$$

but it has just been pointed out that

$$(60) \quad \delta \mathcal{R}_0 = -\frac{2}{S} \delta x \quad \text{oersteds.}$$

Thus we find

$$(61) \quad \delta \phi_0 = \phi_0 \frac{2 \delta x}{S \mathcal{R}_0} = \mathcal{B}_0 \frac{2 \delta x}{\mathcal{R}_0} \quad \text{maxwells.}$$

The small change in magnetic flux  $\delta\phi$ , due to the vibratory displacement of the diaphragm, is such as would correspond to the action of a certain small mmf.  $\delta\mathcal{F}_0$  given by the relation

$$(62) \quad \frac{\delta\mathcal{F}_0}{\mathcal{R}_0} = \delta\phi_0 \quad \text{maxwells.}$$

Consequently, substituting (62) in (61), we find

$$(63) \quad \delta\mathcal{F}_0 = \mathcal{B}_0 \cdot 2 \delta x \quad \text{gilberts.}$$

If, then, we know the normal polar flux density  $\mathcal{B}_0$ , which we assume to be substantially unchanged by the small vibratory displacements of the diaphragm, a small maximum cyclic displacement  $x_m$  of the diaphragm will virtually generate a corresponding small mmf. of  $2 \mathcal{B}_0 x_m$  gilberts in the magnetic circuit. This mmf. will be in phase with the displacement. This is the vector mmf.  $\mathcal{F}_x$  in Fig. 44, except that the rms. displacement  $x$ , of the diaphragm is used instead of  $x_m$ , and we have

$$(64) \quad \mathcal{F}_x = 2 \mathcal{B}_0 x, \quad \text{rms. gilberts } \angle.$$

At the frequency of 1028  $\sim$ , the displacement of the diaphragm corresponds to  $Ob$ , Fig. 44, being in lagging quadrature to the vibratory velocity. We shall be able to assign this phase later. It suffices here to notice that as the impressed frequency varies from zero to infinity, all other conditions remaining constant, the vector displacement mmf.  $\mathcal{F}_x$  changes from  $Oa$ , through  $Ob$  and  $Oc$ , to zero at  $O$ . The locus  $abcO$  is a *displacement-admittance locus*; see Chapter XVIII. The resultant total mmf. in the magnetic circuit will be the vector sum of the testing-current mmf.,  $\mathcal{F}_i$ , Fig. 44, and the displacement  $\mathcal{F}_x$ . At 1028  $\sim$ , this vector sum will occupy the position  $Of$ . As the impressed frequency is varied from zero to infinity, the resultant vector mmf.  $f$  will change from  $Oe$ , through  $Of$ , to  $Og$ . It may be observed that, in this case, at frequencies below resonance, the size of the resultant mmf. will be greater than that due to  $\mathcal{F}_i$  alone; but that at frequencies above resonance the resultant will be less. At an indefinitely high frequency, the displacement mmf. vanishes, and  $\mathcal{F}_i$  is left in complete sway. At the frequency of 1028  $\sim$ , for which Fig. 44 is prepared, the mmf.  $Of$  is 2.174 gilberts, lagging  $28^\circ$  behind the 3.334 gilberts developed by  $\mathcal{F}_i$ .

**Vector Diagram of Magnetic Flux.** — Figure 45 is a simple vector diagram representing the rms. magnetic flux in the magnetic circuit of the coils due to the constant impressed mmf.  $\mathcal{F}_i$  with clamped diaphragm. In the selected instrument, this mmf. was

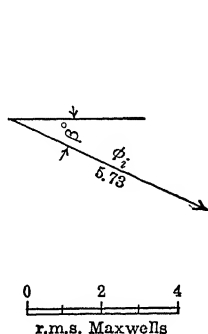


FIG. 45. Vector flux diagram at 1028 cycles per sec. — diaphragm damped.

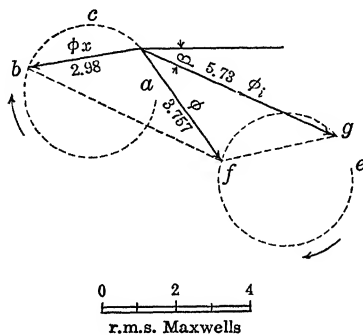


FIG. 46. Vector flux diagram at 1028 cycles per sec. — diaphragm free.

3.334 gilberts taken at standard phase or zero slope, and the reluctance is computed to have been  $\mathcal{R}_0 = 0.582 \angle \beta_0 = 0.582 \angle 25^\circ.3$  oersted. We take this vector reluctance as constant throughout the range of impressed frequency. The alternating magnetic flux  $\phi_i$  is thus

$$3.334 \angle 0^\circ \div 0.582 \angle 25^\circ.3 = 5.728 \angle 25^\circ.3 \quad \text{rms. maxwells,}$$

as shown to scale in the figure. By assumption, this magnetic flux remains constant at all frequencies, so long as the diaphragm is clamped; although, as we have already seen in the last Chapter, there is actually a small but distinct change in the value of  $\mathcal{R}_0$  as the frequency is varied.

Figure 46 is the corresponding flux vector diagram for the free condition of the diaphragm. Here we have to insert the additional flux  $\phi_x$  due to the added displacement mmf.  $\mathcal{F}_x$  of Fig. 45. We assume that the value of the reluctance  $\mathcal{R}$  to  $\mathcal{F}_x$  is the same both in magnitude and in slope as that offered to  $\mathcal{F}_i$ . This means that  $\phi_x$  will lag behind  $\mathcal{F}_x$  to the same extent that  $\phi_i$  lags behind  $\mathcal{F}_i$ , and also that the magnitude ratio of  $\phi_x/\phi_i$  is the same as the magnitude ratio  $\mathcal{F}_x/\mathcal{F}_i$ . Strictly speaking, this assumption can only be taken as a first approximation, because the seat of the mmf.  $\mathcal{F}_i$  is in the coils surrounding the poles, whereas





the storage needs of the vibratory mechanical system. The gross mechanical reactive power  $mh$  is  $-j\ 2445$  abwatts.

**Force Vector Diagram with Diaphragm Clamped.** — We have seen in Chapter II, formula (13), that the mechanical force  $F$  exerted on a bipolar telephone diaphragm is

$$(65) \quad F = F_0 + \frac{2\mathcal{B}_0NI_m}{\mathcal{R}_0} \quad \text{max. dynes.}$$

Here the first term  $F_0$  is the residual attractive pull on the diaphragm perpendicular to its normal plane when the testing current is withdrawn. This force flexes the diaphragm to a new quiescent or zero position, from which alternating displacements  $x$  are reckoned. The second term is the maximum cyclic alternating pull due to the maximum cyclic current  $I_m$  abamperes. If we substitute for the a.-c. reluctance of the magnetic circuit, its reciprocal  $\mathcal{P}$  the a.-c. permeance in oersteds<sup>-1</sup>, and use  $I$  the rms. value of current instead of the maximum cyclic value, the rms. alternating pull on the diaphragm becomes

$$(66) \quad f_t = (2\mathcal{B}_0N\mathcal{P}) I \quad \text{rms. dynes } \angle.$$

Since the reluctance  $\mathcal{R}$  may be considered as a plane-vector quantity, with a leading angle of  $\beta^\circ$ , the permeance  $\mathcal{P}$  becomes a plane-vector quantity, with the lagging angle of  $\beta^\circ$ . In the case considered,  $\mathcal{P} = 1.718 \angle 25^\circ.3$  oersteds<sup>-1</sup>. Formula (66) thus indicates that the phase of the alternating tractive force on the diaphragm lags the current by  $\beta^\circ$ . For convenience, the bracketed quantity in (66) is called the **vector force factor**, and is denoted by the symbol  $A$ . For a bipolar receiver

$$(67) \quad A = 2\mathcal{B}_0N\mathcal{P} \quad \text{rms. dynes/abampere } \angle.$$

The angle of  $A$  is  $\angle \beta^\circ$ . Consequently, we have, as a fundamental vector equation for a receiver with its diaphragm clamped,

$$(68) \quad f_t = AI \quad \text{rms. dynes } \angle.$$

It is evident that the force factor  $A$  is an important characteristic of a receiver. It increases directly with the intensity  $\mathcal{B}_0$  of the magnetic field in the air gaps, with the total number of turns  $N$ , and with the a.-c. permeance  $\mathcal{P}$  of the magnetic circuit. In the selected instrument,  $\mathcal{B}_0$  appears to be 1369 gaussses, and  $A = 6.12 \times 10^6 \angle 25^\circ.3$  rms. dynes per abampere.

Figure 49 indicates the vector force diagram of the selected receiver with its diaphragm clamped.  $OA$  is the standard phase of the testing alternating current of 2.04 milliamperes or  $I = 2.04 \times 10^{-4}$ . The rms. force on the diaphragm by (68) is  $1249 \angle 25.3^\circ$  dynes. This force is neutralized and balanced by an equal and opposite clamping force or elastic force  $f_c$  from the clamping constraints of the diaphragm, so that no motion is supposed to ensue.

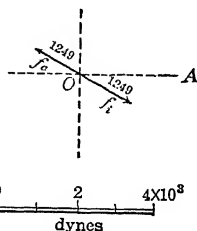


FIG. 49. Vector force diagram — diaphragm damped.

**Vector Force Diagram with Diaphragm Free. A Single Impressed V.M.F.** — When the diaphragm is freed, the clamping force  $f_c$  disappears, but in its place there appears a resultant

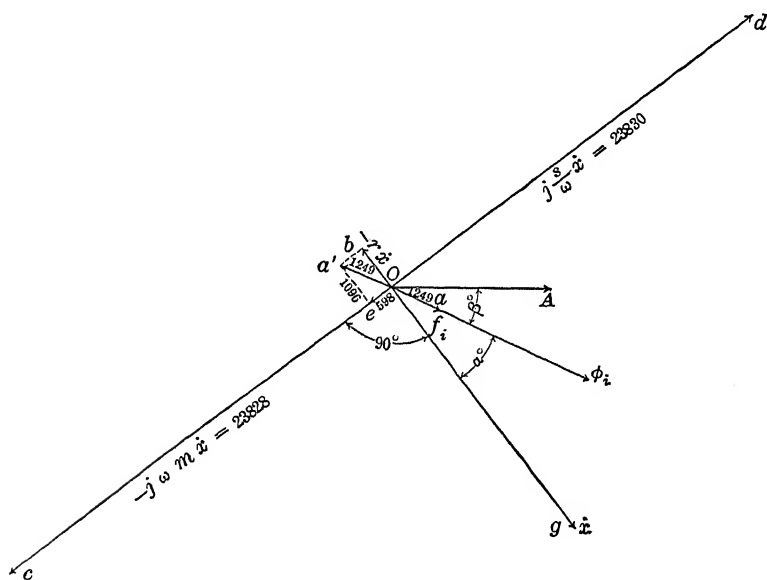


FIG. 50. Vector force diagram for the ideal case of a diaphragm free to vibrate under a single impressed V.M.F.  $f_i$  rms. dynes.

equilibrating force  $Oa'$ , Fig. 50, due to the motion which is set up. The reference phase  $OA$  is again taken as that of the testing current  $I$ . The flux  $\phi_i$ , due to the current, lags  $\beta^\circ$  behind  $OA$ . The



force  $f_i$  is in phase with this flux, and is represented in Fig. 50 by the vector  $Oa$ . Using formula (48), we have

$$(69) \quad \dot{x} = \frac{f_i}{r + j(m\omega - s/\omega)} \quad \text{rms. kines } \angle,$$

and

$$(70) \quad f_i - r\dot{x} - jm\omega\dot{x} + j\frac{s\dot{x}}{\omega} = 0 \quad \text{rms. dynes } \angle.$$

That is, the vector force  $Oa$  is balanced by a frictional force  $Ob = -r\dot{x} = -1096$  dynes, a lagging-quadrature reactive force  $oc = -jm\omega\dot{x} = -j23828$  dynes of inertia, and a leading-quadrature reactive force  $Od = +js\dot{x}/\omega = +j23830$  dynes of elastance. The resultant forces of friction, inertia and elastance is  $Oa'$ , equal and opposite to the impressed force  $f_i = Oa$ . The velocity  $\dot{x}$  has the phase  $Og$ , lagging  $\alpha^\circ$  behind  $f_i$  at this frequency.

**Force Vector Diagram with Two VMFs. acting on a free Diaphragm.** — We have thus far assumed that the diaphragm is acted on by a single vmf., namely the tractive force  $f_i$  produced by the testing current. When the diaphragm is set in vibration in the permanent field  $\mathcal{B}_0$ , however, there is a new alternating flux  $\phi_x$  set up, which we call the *displacement flux*, because it is proportional in magnitude to and also in phase with the diaphragm's displacement from the quiescent position. This flux superposes a new tractive force  $f_x$ . We have seen in formula (64) that the equivalent mmf. of the displacement flux is  $\mathcal{F}_x = (2\mathcal{B}_0)x$  vector rms. gilberts. This may be regarded as similar, by (9), to

$$(71) \quad \mathcal{F}_i = (4\pi N) I \quad \text{rms. gilberts } \angle,$$

so that a certain fictitious number of turns  $N'$  multiplied by unit rms. displacement  $x$ , would produce the same mmf. as unit rms. current in the actual turns  $N$ . That is

$$(72) \quad 4\pi N' = 2\mathcal{B}_0 \quad \text{equivalent turns,}$$

or

$$(73) \quad N' = \frac{\mathcal{B}_0}{2\pi} \quad \text{equivalent turns} \times \frac{\text{abampere}}{\text{cm.}}$$

If we consider the ratio

$$(74) \quad \frac{N'}{N} = p \quad \frac{\text{abampere}}{\text{cm.}},$$

which in the selected instrument was 0.168, we may observe that it is a characteristic ratio of the receiver. The displacement mmf. is now

$$(75) \quad \mathcal{F}_x = 4 \pi N' x \quad \text{rms. gilberts } \angle,$$

and the tractive force of displacement is

$$(76) \quad f_x = p A x = 2 p \mathcal{B}_0 N \mathcal{P} x \quad \text{rms. dynes } \angle.$$

It may be noted, in passing, that, just as in the case of a vector electromagnetic inductance,

$$(77) \quad \mathcal{L} = A/p = 4 \pi N^2 \mathcal{P} \quad \begin{array}{l} \text{abhenries } \angle \text{ or} \\ \text{ergs per abamp}^2 \angle, \end{array}$$

so

$$(78) \quad p A = 4 \pi (N')^2 \mathcal{P} \quad \frac{\text{rms. dynes}}{\text{cm.}} \angle,$$

and is a quantity bearing resemblance to an inductance. We have also

$$(79) \quad A = 4 \pi N N' \mathcal{P} \quad \frac{\text{rms. dynes}}{\text{abampere}} \angle,$$

so that in this sense, the force factor  $A$  bears resemblance to a mutual inductance.

There are two ways in which we may introduce the new vmf.  $f_x$  of displacement into the computation. We may add it vectorially to  $f_i$ , to form a resultant vmf.  $f$ , corresponding to  $\mathcal{F}$  in Fig. 44. This is the strictly logical method of procedure, as it restores the application of the single vmf. formula (48). The other way is to retain  $f_i$  as the sole vmf. in the system, but introduce the effect of  $f_x$  by way of a mechanical impedance. For practical purposes, the latter method is to be preferred as simpler.\* It corresponds to the ordinary method of dealing with the emf. of self-induction in a simple a.-c. circuit. Instead of vectorially combining the emf. of self-induction with the impressed emf. and then dividing by resistance to find the current, engineers prefer to consider the impressed emf. as acting alone, and then to introduce the effect of the self-induced emf. as a reactance.

The force  $f_x$  always lags behind the displacement  $x$  by the angle  $\beta^0$ , according to the relation

$$(80) \quad f_x = p A x = p A \frac{\dot{x}}{j\omega} = -j p A \frac{\dot{x}}{\omega} \quad \text{rms. dynes } \angle.$$

\* This method was suggested by Professor Nukiyama. Bibliography 75a and 79.



resistance  $r'$  of 68.8 dynes per kine, and an apparent component of elastance  $s'$  of  $0.928 \times 10^6$  dynes per cm. The system will now balance with 1096 dynes along the  $x$  axis and 24422 dynes in quadrature therewith. We must reapportion the values of  $r$  and  $s$ , however, to include the new increments in these values. The total resistance is

$$(81) \quad r'' = r + r' \quad \frac{\text{dynes}}{\text{kine}},$$

where  $r''$  is the *gross resistance* which the mechanical system appears to have, when assumed to act under the influence of  $f_i$  only. The quantity  $r'$  is the virtual resistance due to displacement, or the *displacement resistance*. It is defined by the relation

$$(82) \quad r' = \frac{p |A|}{\omega} \sin \beta \quad \frac{\text{dynes}}{\text{kine}},$$

where  $|A|$  represents that only the size  $Oe$  of the vector force factor  $A$  is to be taken; hence (82) is a scalar equation. The quantity  $r$  is the *net mechanical resistance* of the system, and is what would be evaluated by (50) and (69) if the resultant of  $f_i$  and  $f_x$  were used as a single vector force in the numerator.

Similarly in regard to elastic forces

$$(83) \quad s'' = s - s' \quad \frac{\text{dynes}}{\text{cm.}},$$

where  $s''$  is the *gross elastic coefficient* that the system appears to have when assumed to act under the influence of  $f_i$  only. The quantity  $s'$  is the virtual elastic coefficient due to displacement, or the *displacement elastic coefficient*. It is defined by the scalar relation

$$(84) \quad s' = p |A| \cos \beta \quad \frac{\text{dynes}}{\text{cm.}}.$$

The quantity  $s$  is the *net elastic coefficient* of the system, and is what would be evaluated by (48) and (69), if both the vmfs.  $f_i$  and  $f_x$  were combined into a single resultant in the numerator.

When, therefore, we consider, as is practically preferable, that the sole vmf. acting on the diaphragm is  $f_i$ , due to the testing current, we are virtually dealing with a gross resistance  $r''$ , a gross elastic coefficient  $s''$  and a net mass  $m$ , we have, according to (69),

$$(85) \quad x = \frac{f_i}{r'' + j(m\omega - s''/\omega)} = \frac{f_i}{z''} \quad \text{rms. kines } \angle,$$

where

$$(86) \quad z'' = r + j\left(m\omega - \frac{s}{\omega}\right) + j\frac{pA}{\omega} \quad \frac{\text{dynes}}{\text{kine}} \angle,$$

$$(87) \quad = (r' + r) + j\left\{m\omega - \frac{(s - s')}{\omega}\right\} \quad \frac{\text{dynes}}{\text{kine}} \angle,$$

$$(88) \quad = r'' + j(m\omega - s''/\omega) \quad \frac{\text{dynes}}{\text{kine}} \angle.$$

The gross elastic coefficient evaluated from (83) or (88) is always less than the true or net coefficient, by the constant quantity  $s'$ . In the selected instrument,  $s' = 0.928 \times 10^6$ , the net value  $s = 37.63 \times 10^6$ , and  $s''$  the gross value is  $36.7 \times 10^6$  dynes/cm. The effect of this is to make the apparent resonant angular velocity

$$(89) \quad \omega''_0 = \sqrt{\frac{s''}{m}} = \sqrt{\frac{s - s'}{m}} \quad \frac{\text{radians}}{\text{sec.}}$$

too low. In the case considered,  $\omega''_0 = 6378$ , ( $f''_0 = 1015 \sim$ ), and the diameter of the motional-impedance circle meets with this angular velocity. The angular velocity of resonance corrected for displacement would be  $s/m = 6459$  radians per second, or  $1028 \sim$ , which happens to be very near the frequency selected for reference in the vector diagrams. When, therefore, we speak of the resonant frequency of a receiver as obtained diametrically from its motional-impedance circle, or by vibration-amplitude measurements on its diaphragm, we mean its apparent or gross resonant frequency, under the modifying influence of vibration in the permanent magnetic field  $\mathcal{B}_0$ . If this influence could be neutralized, the resonance would appear at  $\sqrt{s/m}$ . With this reservation, it becomes unnecessary ordinarily to use  $\omega''_0$  and  $f''_0$  for designating apparent resonance, and we may employ  $\omega_0$  and  $f_0$  for representing these values, except when distinction must be made.

The gross frictional resistance  $r''$  is always greater than the net frictional resistance  $r$ . As is shown by formula (82), the virtual displacement resistance  $r'$  is not a constant quantity at all frequencies, because it is inversely proportional to  $\omega$ . This means that the action of the permanent magnetic field  $\mathcal{B}_0$  upon the diaphragm in vibration is to set up a distortion from the true circular graph of vibration velocity, and the corresponding true circular graph of motional impedance.

There are thus two disturbing influences which tend to distort the motional-impedance circle; namely the change in the vector

force factor  $A$ , as the impressed frequency changes, owing to variations in magnetic skin-effect, and the change in the virtual re-

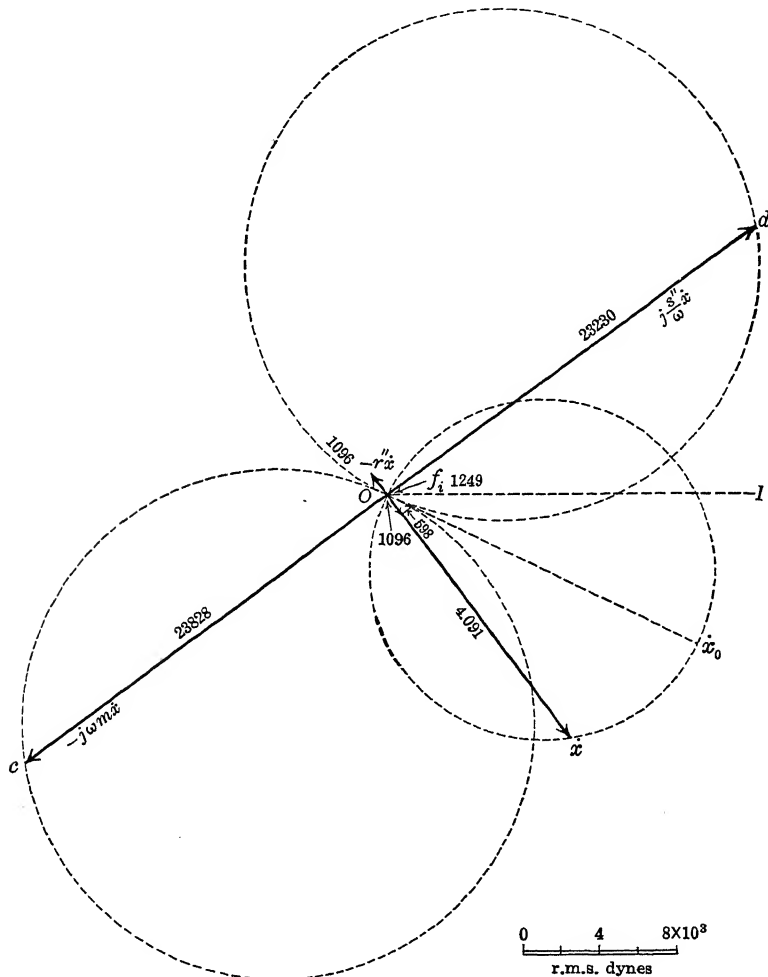


FIG. 52. Vector force diagram — complete — including magnetic force due to displacement.

distance  $r'$  of displacement with variations of frequency. In spite of these disturbances, the measured graphs of receiver motional impedances are usually remarkably close approximations to circles. It is often noticeable, however, that the circle drawn through them

does not pass accurately through the origin, as in the case of Fig. 38. It will be remembered that in a majority of receivers, the resonant half of the motional-impedance circle is covered within a range of 60 cycles per second in  $f$ ; so that the greater part of the circle has ordinarily been described before the frequency has changed sufficiently to bring the distortions into prominence.

Figure 52 is a force vector diagram giving the loci of the principal vectors.  $OI$  is the reference phase of testing current. The vector velocity  $\dot{x}$  travels over the dotted circle, if we neglect distortions. The diameter  $\dot{x}_0$  is the vibrational velocity at gross or apparent resonance. The reactive force of inertia  $Oc = -j\omega m\dot{x}$  is always in lagging quadrature to  $O\dot{x}$ , but its locus is only approximately circular. It is a *displacement-admittance curve*. Similarly, the reactive force of elasticity  $Od = js''\dot{x}/\omega$  is always in leading quadrature to  $O\dot{x}$ , but its locus is only approximately circular. It is a displacement admittance curve taken reversely.

The three vectors  $Oc$ ,  $Od$ , and  $O\dot{x}$  are thus rigidly connected in quadrature, and all move clockwise around their respective loci as the impressed frequency is increased.

**Mechanical Velocity Admittance.**—The *gross mechanical admittance* of the diaphragm is  $y''$  the reciprocal of its gross impedance to velocity, in (87). That is

$$(90) \quad y'' = \frac{1}{r'' + j(m\omega - s''/\omega)} \quad \frac{\text{kines}}{\text{dyne}} \angle,$$

neglecting variations in  $r''$  with frequency due to the virtual resistance  $r'$  of displacement, the locus of  $y''$  is a circle centered on the real axis and passing through the origin. The vibrational velocity  $\dot{x}$  is obtained by multiplying this gross admittance by the impressed vmf. of testing current.

$$(91) \quad \dot{x} = f_1 y'' = A I y'' \quad \text{rms. kines } \angle.$$

**Mechanical Displacement.**—The rms. displacement  $x$  is in lagging quadrature to the velocity  $\dot{x}$ , and is  $\omega$  times smaller or

$$(92) \quad x = \frac{\dot{x}}{j\omega} = -j \frac{\dot{x}}{\omega} = -j \frac{f_1 y''}{\omega} = -j \frac{A I y''}{\omega} \quad \text{rms. cm.}$$

The size of the actual maximum cyclic displacement of the diaphragm at any impressed angular velocity  $\omega$  is then

$$(93) \quad x_m = |x| \sqrt{2} \quad \text{max. cyclic cm.}$$

Figure 53 is a vector gross-velocity diagram taken in accordance with (91). If we neglect distortion due to  $r'$ , it is a circle passing through the origin and having the slope of  $A$  for its diameter  $Ob$ , provided that we take  $Oa$ , the reference phase of current, as of zero slope. That is,  $Ob$  is the velocity  $\dot{x}$  at gross resonance, lagging  $\beta^\circ$  behind the testing current, but in phase with the vmf.  $f_t$ . At the selected frequency of 1028  $\sim$ , which happens to be very near net resonance, the velocity is  $\dot{x} = 4.091 \angle 28^\circ.6$ , i.e.,  $Oc$  lagging  $\alpha = 28^\circ.6$  behind  $f_t$ , owing to unbalance between the reactances  $m\omega$  and  $s''/\omega$  in (88). As the impressed frequency is varied, the vector velocity  $\dot{x}$  moves over the circle in the direction  $abc$ , commencing at the origin with  $f = 0$ , and ending again at the origin with  $f = \infty$ .

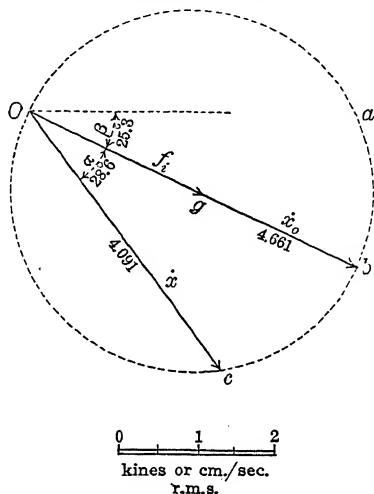


FIG. 53. Vector rms. velocity diagram — diaphragm free — constant VMF. and varied frequency.

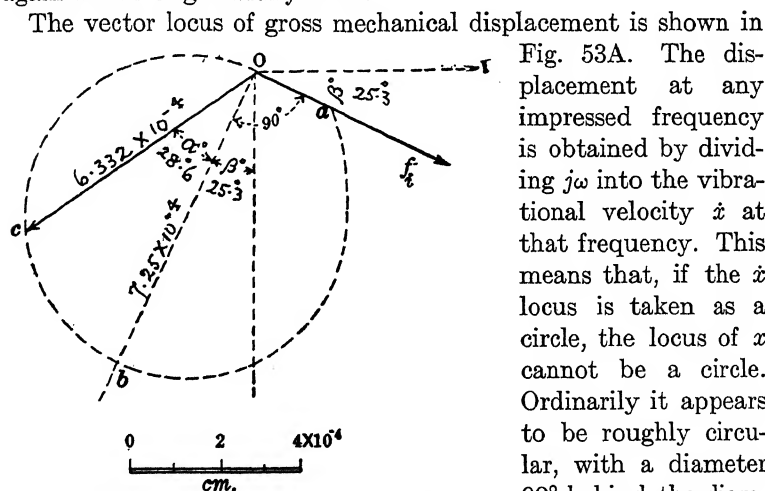


FIG. 53A. Vector rms. displacement diagram — diaphragm free.

Fig. 53A. The displacement at any impressed frequency is obtained by dividing  $j\omega$  into the vibrational velocity  $\dot{x}$  at that frequency. This means that, if the  $\dot{x}$  locus is taken as a circle, the locus of  $x$  cannot be a circle. Ordinarily it appears to be roughly circular, with a diameter  $90^\circ$  behind the diameter of the velocity



$\dot{x}$ . Strictly speaking, the locus is a *displacement-admittance locus*, *abc*, Fig. 53A, which will be discussed in Chapter XVIII. At  $f = 1028 \sim$ , the rms. displacement is  $Oc = 6.332 \mu$ ,  $143^\circ.9$  behind the phase of the testing current, in accordance with (92).

**Vector Motional Electromotive Force.**— We have already seen that the displacement flux  $\phi_x$  lags  $\beta^\circ$  behind the virtual mmf. of displacement  $\mathcal{F}_x$ . This flux is obtained by multiplying  $\mathcal{F}_x$  by the vector permeance  $\mathcal{P}$ . Thus from (75) we have

$$(94) \quad \phi_x = \mathcal{F}_x \mathcal{P} = 4 \pi N' x \mathcal{P} = \frac{pAx}{N'} \quad \text{maxwells } \angle.$$

The emf. produced in the receiver coils by the cyclic variation of this flux is

$$(95) \quad e_x = -N \dot{\phi}_x = -jN\omega \phi_x \quad \text{abvolts } \angle.$$

The emf. expended in overcoming this emf. is the motional impedance drop  $IZ'$  or

$$(96) \quad IZ' = -e_x = jN\omega \phi_x = j\omega pAx \frac{N}{N'} = j\omega Ax \quad \text{abvolts } \angle \\ = A\dot{x} = A^2 y'' I \quad \text{abvolts } \angle,$$

from which

$$(97) \quad Z' = \frac{A\dot{x}}{I} = A^2 y'' = \frac{A^2}{z''} \quad \text{abohms } \angle.$$

That is, the motional-impedance drop  $IZ'$  is  $A$  times the velocity  $\dot{x}$ , and is in quadrature to the displacement flux  $\phi_x$ . Moreover, since  $\dot{x}$  has a circular locus, it follows that  $IZ'$  and  $Z'$  both have circular loci. Referring to Fig. 42, the vector emf. diagram, we may observe that  $IZ'$  is in leading quadrature to  $\phi_x$ , and is caused by the time variation of  $\phi_x$ . The vector reactance drop  $I\mathcal{X}$  is similarly in leading quadrature to  $\phi_i$  and the total free impedance drop  $IZ''$  to the resultant flux  $\phi = \phi_i + \phi_x$ .

It is also evident from (97) that, at gross resonance,  $z''$  being reduced to  $r''$

$$(98) \quad Z'_0 = \frac{A^2}{r''} \quad \text{abohms } \angle,$$

and the slope of this diametral motional impedance is the same as that of  $A^2$  or  $-2\beta^\circ$ .

## CHAPTER IX

### THE ANALYSIS OF THE MOTIONAL-IMPEDANCE CIRCLE

**Introduction.** — In this chapter we shall consider the deductions that may be drawn from the motional-impedance circle of a telephone receiver, as observed according to such a technique as has been described in Chapter VII. For this purpose, we may here consider Fig. 38.

Having plotted a suitable number of motional impedances, we draw through them, by trial, the best empirical circle  $OCDEFGH$ . Through  $o$  the center of this circle, we draw the diameter  $OoP$  and we measure its magnitude  $Z'_o$  in ohms or ab-ohms. In this case,  $Z'_o$  is 140 ohms. The frequency at the diametral point  $P$  is the gross resonance frequency or frequency of apparent mechanical resonance  $f_o$ . In this case,  $f_o = 1015 \sim$  and  $\omega_o = 6378$ . At this frequency, the mechanical reactance  $m\omega_o$  and  $s''/\omega$  are equal, whence formula (89) is obtained.

Through the center  $o$ , we draw the quadrantal diameter  $QoQ'$ , perpendicular to the principal diameter  $OoP$ . The points  $Q$  and  $Q'$  are called the *quadrantal points* of the circle. The frequencies at these points are called the *quadrantal frequencies*, and are denoted by  $f_1$  and  $f_2$ . In this case,  $f_1 = 991 \sim$  and  $f_2 = 1039.5 \sim$ . The corresponding *quadrantal angular velocities* are  $\omega_1 = 6227$  and  $\omega_2 = 6532$  radians per second. It is generally taken that  $f_1$  is the lower-quadrantal and  $f_2$  the higher-quadrantal frequency for numerical reasons, in spite of the fact that, in the circle,  $f_1$  is ordinarily raised above  $f_2$ . At these quadrantal frequencies, the apparent mechanical reactance is numerically equal to the mechanical resistance  $r''$ .

**Frequency Relations between Impedances or Admittances of Equal Opposite Slopes.** — Referring to the mechanical-impedance diagram of Fig. 28, if we select any pair of frequencies such as at  $P$  and  $P'$ , at equal reactance distances below and above  $A$ , a simple relation connects these frequencies with the resonant frequency  $f_o$  at  $A$ . Thus at  $OP$ ,  $f = 1002 \sim$ , and  $AP = -146$ . At  $OP'$ ,

$f = 1028 \sim$ , and  $AP' = +146$ . Let  $\omega_{11}$  be the angular velocity at  $P'$  and  $\omega_1$  the angular velocity at  $P$ . The mass reactance is in excess at  $P'$ , and the elastic reactance is in excess at  $P$ . Consequently we have

$$(99) \quad m\omega_{11} - \frac{s}{\omega_{11}} = \frac{s}{\omega_1} - m\omega_1 \quad \frac{\text{dynes}}{\text{kine}},$$

or

$$(100) \quad \omega_{11} - \frac{s}{m\omega_{11}} = \frac{s}{m\omega_1} - \omega_1 \quad \frac{\text{rad.}}{\text{sec.}},$$

whence, by (32),

$$(101) \quad \omega_{11} - \frac{\omega_0^2}{\omega_{11}} = \frac{\omega_0^2}{\omega_1} - \omega_1 \quad \frac{\text{rad.}}{\text{sec.}},$$

$$(102) \quad \omega_1\omega_{11}^2 - \omega_1\omega_0^2 = \omega_{11}\omega_0^2 - \omega_1^2\omega_{11} \quad \left(\frac{\text{rad.}}{\text{sec.}}\right)^3,$$

$$(103) \quad \omega_0^2 (\omega_1 + \omega_{11}) = \omega_1\omega_2 (\omega_1 + \omega_{11}) \quad \left(\frac{\text{rad.}}{\text{sec.}}\right)^3,$$

$$(104) \quad \omega_0^2 = \omega_1\omega_{11} \quad \left(\frac{\text{rad.}}{\text{sec.}}\right)^2.$$

From this, it follows that the resonant angular velocity  $\omega_0$  is the geometric mean of any such pair of reactively equidistant angular velocities  $\omega_1$  and  $\omega_{11}$ . But any such pair of reactively equidistant angular velocities have equal and opposite slopes. In the case considered, these angles are  $+28^\circ.6$  and  $-28^\circ.6$ , respectively. Hence any pair of impedances having equal sizes and equal and opposite slopes, have frequencies defined by (104). The same relation must also hold for admittances. Consequently, in any vibrational-velocity circle, such as that of Fig. 29, any pair of vectors which, like  $OP$  and  $OP'$ , have equal and opposite slopes with respect to the diameter, have frequencies whose root product is equal to the diametral resonant frequency  $f_0$ . That is, they conform to (104).

It follows that in any motional-impedance circle, such as that of Fig. 38, if we know by observation the frequency at a point making a certain vector angular distance with the diameter  $OP$ , we can compute by (104) the frequency at a vector point the same angular distance on the other side of the diameter, assuming that the resonant frequency  $f_0$  is known.

The quadrantal frequencies make a particular case under this proposition, and for any motional-impedance circle

$$(105) \quad f_1 f_2 = f_0^2 \quad \left( \frac{\text{cycles}}{\text{sec.}} \right)^2,$$

or

$$(106) \quad \omega_1 \omega_2 = \omega_0^2 \quad \left( \frac{\text{rad.}}{\text{sec.}} \right)^2.$$

**The Damping Constant  $\Delta$  of a Diaphragm.** — If we consider any point  $P$  on the circle (Fig. 38) whose vector  $OP$  makes an angle  $\alpha$  with the diameter  $OP$ , then we have, with reference to the mechanical impedance at this velocity, see Fig. 28,

$$(107) \quad m\omega - \frac{s''}{r''} = \tan \alpha,$$

or

$$(108) \quad \omega - \frac{s''}{m\omega} = \frac{r''}{m} \tan \alpha \quad \frac{\text{rad.}}{\text{sec.}},$$

$$(109) \quad \omega - \frac{\omega_0^2}{\omega} = 2 \left( \frac{r''}{2m} \right) \tan \alpha \quad \frac{\text{rad.}}{\text{sec.}}.$$

The quantity  $r/(2m)$  is called the **damping constant**, and is denoted by  $\Delta$ . The quantity  $r''/(2m)$  is here the gross or apparent damping constant. Hence

$$(110) \quad \Delta = \frac{\omega^2 - \omega_0^2}{2\omega \tan \alpha} \quad \frac{\text{rad.}}{\text{sec.}}$$

We can always evaluate  $\Delta$ , if we know  $\omega_0$ , and the slope  $\alpha$  at which one other angular velocity  $\omega$  is found. In the case of the lower-quadrantal angular velocity at  $\omega_1 = 6227$  at  $OQ$ ,  $\alpha = -45^\circ$  and  $\tan \alpha = -1$ , for  $oq_1$  Fig. 28, so that

$$(111) \quad \Delta = \frac{\omega_1^2 - \omega_0^2}{-2\omega_1} = \frac{\omega_0^2 - \omega_1^2}{2\omega_1} \quad \frac{\text{rad.}}{\text{sec.}}$$

Again, at the upper-quadrantal angular velocity  $\omega_2 = 6532$  at  $OQ$ ,  $\alpha = 45^\circ$  and  $\tan \alpha = +1$ , for  $oq_2$  Fig. 28, so that

$$(112) \quad \Delta = \frac{\omega_2^2 - \omega_0^2}{2\omega_2} \quad \frac{\text{rad.}}{\text{sec.}}$$

Adding (110) and (111) together and canceling, we obtain

$$(113) \quad \Delta = \frac{\omega_2 - \omega_1}{2} = \pi (f_2 - f_1) = \frac{r''}{2m} \quad \frac{\text{rad.}}{\text{sec.}}$$

It is shown in Appendix IV that the damping constant  $\Delta$  indicates the rate of decay of free vibrations of a system. If the diaphragm over the poles is displaced arbitrarily to a distance  $x$  cm. from its normal quiescent position, and is then allowed to return automatically to that position, ordinarily by decaying oscillations, the displacement amplitude  $x_t$  remaining at time  $t$  seconds is

$$(114) \quad x_t = x\epsilon^{-\Delta t} \quad \text{cm.},$$

where  $\epsilon = 2.718\cdots$ , the Napierian base. In the case considered,  $\Delta = 152$ . The time required for the amplitude to fall to  $1/\epsilon$ th of its initial value is the *epsilon time interval*

$$(115) \quad t_\epsilon = \frac{1}{\Delta} \quad \text{seconds.}$$

In this case,  $t_\epsilon = 6.58 \times 10^{-3}$  or 6.58 milliseconds. A receiver diaphragm of large  $\Delta$  is heavily damped, and falls to  $1/\epsilon$ th amplitude in a relatively small interval of time.

In the discussion of the exponential decay of free vibrations, as in (114), it appears that  $\Delta$  may be regarded as a hyperbolic angular velocity, and its unit may be taken as a hyperbolic radian per second. (See Appendix IV.)

**Vector Reactance Angle  $\beta^\circ$ .**—The depression angle  $ROP$  (Fig. 38) of the motional-impedance diameter, has already been shown to be twice the angle  $\beta$  of the departure of damped vector reactance  $\mathcal{X}$  (Fig. 34) from the vertical or  $OX$  axis. This is according to the provisional theory here presented, and involves the assumptions that the magnetic skin-effect is constant over the working range of impressed frequency, and also that the lag  $\beta_2$  of displacement flux,  $\phi_2$  behind  $\mathcal{F}_x$  is the same as the lag  $\beta_1$  of the current flux  $\phi_i$  behind  $\mathcal{F}_i$ . In all cases, the diametral depression angle is  $\beta_1^\circ + \beta_2^\circ$ , and we regard them provisionally as each equal to  $\beta^\circ$ . Experiments have shown (Bibliography 60) that this is only correct to a first approximation, which is ordinarily sufficiently close for many practical purposes. In the case considered, the depression angle is  $50^\circ.6$ , making  $\beta = 25^\circ.3$ .

**Motional-Power Diagram.**—If we multiply the vector motional-impedance circle diagram, Fig. 38, to abohm scale, by  $I^2$ , the square of the rms. testing current magnitude, we shall reproduce the same as a vector power diagram, to a scale of abwatts or ergs per second. Thus, in the case considered, the diametral impedance  $OP$ , Fig. 38, is  $140 \times 10^9$  abohms, and  $I^2 = 4.162 \times 10^{-8}$ . The

product is 5827 abwatts = 582.7 microwatts. This is the power along the diameter  $Op$ , Fig. 54. The axes  $OR$  and  $OX$  of the impedance diagram, Fig. 38, are repeated in the power diagram of Fig. 54, and may be called, respectively, the active and the re-

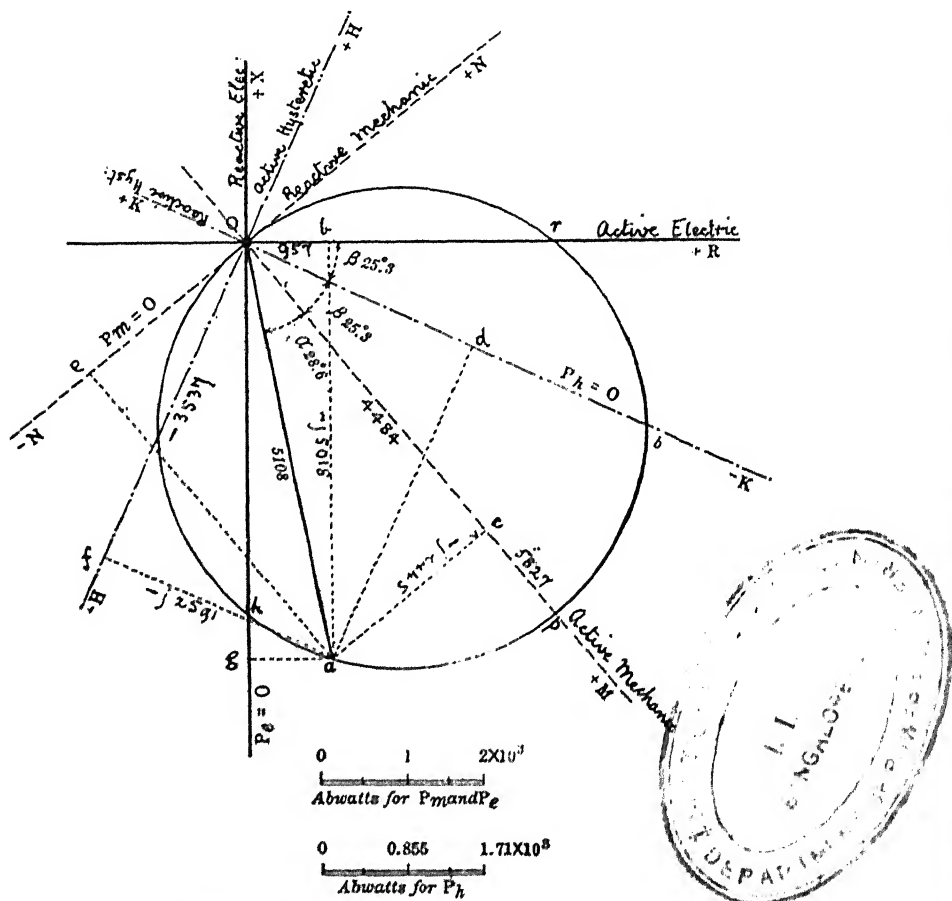


FIG. 54. Vector diagram of motional power.

active electric-power axes. Power measured along  $OR$  is both the average and the maximum cyclic active or dissipated power, supplied by the circuit. Power measured along  $O + X$  is the maximum cyclic reactive or conserved power, also supplied by the electric circuit. At the vector  $Oh$  in the diagram, no active power will be supplied from the circuit, but reactive power to the extent

of  $-jOh$  abwatts will be thus supplied. On the other hand, at the vector  $Or$  in the circle, Fig. 54, no reactive power will be supplied by the circuit, but active power to the extent  $Or$  abwatts will be thus supplied. At the vector  $Oa$ , 957 active abwatts and  $-j 5018$  reactive abwatts are supplied by the circuit.

The vector electric power of the motional-power circle is denoted by the symbol  $P_e$  and has active and reactive components  $P_{ea}$  and  $P_{er}$ ; thus

$$(116) \quad P_e = P_{ea} + jP_{er} = I^2(R' + jX') = I^2Z' \quad \text{abwatts } \angle.$$

Thus, at the frequency  $1028 \sim$  in the selected instrument, at vector  $Oa$ , Fig. 54,  $P_e = 5108 \angle 79^\circ.2 = 957 - j 5018$  abwatts.

We now add a new pair of coordinate power axes to the diagram; namely  $OM$  along the diameter, and  $ON$  perpendicular to the diameter. These may be called, respectively, the active and the reactive *gross-mechanical-power axes*. Powers measured along and parallel to  $OM$ , are active mechanical powers dissipated in overcoming  $r''$ , the gross mechanical resistance to motion. Powers measured along and parallel to  $O + N$  are reactive mechanical powers, cyclically exchanged between the elasticity and the inertia of the vibratory system. The maximum mechanical power which can be delivered to the diaphragm for dissipation and liberation will be  $P''_{mo} = I^2R'_0 = 5827$  abwatts, at resonance. At the vector position  $Oa$ , the gross active mechanical output is  $Oc = 4484$  abwatts, and the gross mechanical reactive power is  $ca = -j 2445$  abwatts. The gross mechanical output may also be expressed in the form

$$(117) \quad P''_m = \dot{x}^2 \{ r'' + j (m\omega - s''/\omega) \} = \dot{x}^2 z'' \quad \text{abwatts } \angle.$$

Thus, at the frequency of  $1028 \sim$  in the selected instrument, the mechanical-power vector is  $Oa = 5108 \angle 28^\circ.6$ . In rectangular coordinates, this is  $4484 - j 2445$ . At this frequency,  $\dot{x}$  has been shown to be  $4.091 \angle 28^\circ.6$  rms. kines, and  $\dot{x}^2 = 16.74 \angle 57^\circ.2$ . With  $r'' = 268$ ,  $m = 0.902$ ,  $s'' = 36.7 \times 10^6$  and  $\omega = 6460$ , we have by (117)  $z'' = 268 + j 146 = 305.2 \angle 28^\circ.6$ , so that  $P''_m = 4484 - j 2445 = 5108 \angle 28^\circ.6$  abwatts.

It will be clear that at the diametral frequency  $f_0$  of gross resonance, the mechanical power will be a maximum, and will be all active. That is, there will be no reactive mechanical component.

Finally, a third set of coordinate axes may be added to the diagram, namely, the active and the reactive *hysteretic-power axes*. The reactive hysteretic axis is  $O + K$ , which is the bisector of the depression angle  $ROM$  taken in the reverse direction. The active hysteretic axis is  $O + H$ . Powers measured along and parallel to  $O + H$  are active powers contributed for dissipation or liberation, by saving in hysteretic loss. Powers measured along and parallel to  $O + K$  are reactive powers contributed for cyclic storage and from the same source, i.e., change in magnetic-hysteretic power when the diaphragm is changed from the clamped to the free condition. The scale of the hysteretic power is, however, not the same as the scale of the electric and the mechanical power. Unit length of vector hysteretic power represents  $2 \sin \beta$  unit length value of electric or mechanical power. Thus with  $\beta = 25^\circ.3$ ,  $2 \sin \beta = 0.855$ , and this change in scale is indicated below Fig. 54.

At the frequency corresponding to the vector  $Ob$ , there can be no active hysteretic power. Any hysteretic power is all reactive. Vector hysteretic power in the motional-power circle is denoted by the symbol  $P_h$ , thus

$$(118) \quad P_h (2 \sin \beta) = (P_{ha} + jP_{hr}) 2 \sin \beta \quad \text{abwatts } \angle,$$

where  $P_{ha}$  and  $P_{hr}$  are the active and the reactive vector components on the diagram, as measured to the electric scale.

At any frequency and corresponding vector position in the power circle, the vector motional power may be expressed in electric, mechanical, and hysteretic coordinates. We then have the vector relation

$$(119) \quad P''_m = P_e - P_h \cdot 2 \sin \beta \quad \text{abwatts } \angle.$$

That is, the vector mechanical power, as read off in its coordinates, is equal to the vector sum of the electric power and the hysteretic power, each read in its own coordinates. Thus at  $Oa$ , corresponding to  $1028 \sim$ ,  $P''_m = 5108 \angle 28^\circ.6 = 4484 - j 2445$  abwatts,

$$P_e = 5108 \angle 79.2 = 957 - j 5018,$$

$$P_h = 5108 \times 0.855 = 4369 \angle 143^\circ.9 = -3537 - j 2591.$$

The gross active mechanical output of the diaphragm  $P''_{ma}$  is 4484 abwatts. Of this, 957 is  $P_{ea}$ , contributed by the electric circuit as  $I^2 R'$ , where  $R'$  is the motional resistance in Fig. 38 at this vector  $Oa$ , and  $-(-3537) = +3537$  is contributed by reduction of



hysteretic loss in the magnetic circuit, when changing from clamped to free diaphragm. Actually,  $3537 + 957 = 4494$ , or 10 abwatts in excess, due to geometric inaccuracy.

Similarly, the gross reactive mechanical power of the diaphragm at this frequency is  $-j 2445$  abwatts. Of this,  $-j 5018$  is contributed electrically by the circuit as  $-j I^2 X'$ ,  $X'$  being the motional reactance in abohms, and  $-(-j 2591) = +j 2591$  abwatts are contributed hysteretically. Here again  $-j 5018 + j 2591 = -j 2427$ , which does not, however, agree precisely with  $-j 2445$ , owing to geometric errors in the diagram.

It also follows from (119) that

$$P''_{ma} = P_{ea} - P_{ha} 2 \sin \beta \quad \text{active abwatts,}$$

and

$$(120) \quad P''_{mr} = P_{er} - P_{hr} 2 \sin \beta \quad \text{reactive abwatts.}$$

Of the gross active mechanical power,

$$(121) \quad P''_{ma} = \dot{x}^2 r'' = \dot{x}^2 (r + r') \quad \text{abwatts,}$$

a portion  $\dot{x}^2 r'$ , or 1152 abwatts, is dissipated in displacement; i.e., in electric and magnetic diaphragm losses due to hysteresis and eddy currents, owing to its vibrating in the permanent magnetic field  $\mathcal{B}_0$ . The remainder or net output  $\dot{x}^2 r = 3332$  abwatts, is put into active alternating mechanical power or vibratory power of the diaphragm. Most of this power is expended in internal mechanical frictions, and only a lesser part is delivered to the surrounding air as acoustic power or sound.

The diaphragm, in regard to power, may be compared with an alternating-current motor driving a lathe through belt and shafting. The gross active power  $\dot{x}^2 r''$  corresponds to the gross mechanical power of the motor rotor. The displacement active-power  $\dot{x}^2 r'$  corresponds to the internal frictions of the rotor. The net active power  $\dot{x}^2 r$  corresponds to the output of the motor at its pulley. Beyond the pulley, there are belt and shafting losses before we arrive at the useful power given to the lathe. So beyond the active mechanical output  $\dot{x}^2 r$  there are the friction losses of the diaphragm before we arrive at the useful acoustic power given to the air. The mechanical efficiency of the diaphragm or the motor at the resonant frequency  $f_0$  is

$$(122) \quad \eta'_0 = \frac{r}{r''} = \frac{r}{r + r'}.$$

In the case considered, this mechanical efficiency is 0.74

Proceeding in the manner indicated above, the gross active power delivered by the diaphragm can be measured from the motional-impedance circle, taken to power scale, in terms of the electric and hysteretic components. Commencing with a low frequency, the electric power supply increases up to a point near  $b$ , Fig. 54, where the projection perpendicularly on the  $OR$  axis is a maximum. The hysteretic supply is negative; or the magnetic circuit absorbs more active power than it yields, up to the point  $b$  where  $P_{ha} = 0$ . At this point, all of the mechanical power comes from the circuit as  $I^2R'$ , or at  $Ob$

$$(123) \quad \dot{x}^2 r'' = I^2 R' \quad \text{abwatts.}$$

Beyond the frequency of  $b$ , the hysteretic active-power changes from negative to positive; or the magnetic circuit absorbs less power with free than with damped diaphragm. This is because the total magnetic flux  $\phi$ , Fig. 47, has become smaller than  $\phi_i$  due to the testing current alone. The reduced alternating flux entails a reduced hysteretic loss, and the saving is available for giving active power to the diaphragm.

At the diameter  $Op$ , the resonant point, the mechanic output is a maximum. At  $Oh$  on the  $X$  axis, the active electric power vanishes, and the mechanical output is supported entirely by hysteretic power, i.e., by the saving in hysteretic loss when free over the loss in the damped condition. At higher frequencies than this, the hysteretic power not only supplies the mechanical output  $P''_{ma}$ , but also restores active power to the circuit.

The vector equation (119) expresses, in algebraic terms, a particular proposition concerning power in the motional-power circle. There is, however, an interesting general proposition of the same type, which states that a planevector at a given slope  $\sphericalangle \alpha^\circ$  is vectorially equal to a vector of the same magnitude at a slope of  $\sphericalangle (2\beta^\circ + \alpha^\circ)$  diminished by a vector of  $2 \sin \beta$  times the same magnitude at a slope of  $\sphericalangle (90^\circ + \alpha + \beta)$ . This proposition is presented in Appendix X.

The gross efficiency  $\eta''_0$  of the receiver at the resonant frequency is the ratio of the gross active mechanical power  $\dot{x}_0^2 r''$  of  $I^2 R'_0$  to the active electric input  $I^2 R''$ .  $R'_0 = |Z'_0|$  the size of the diametral impedance. We have therefore

$$(124) \quad \eta''_0 = \frac{I^2 R'_0}{I^2 R''} = \frac{R'_0}{R''} = \frac{|Z'_0|}{R''}.$$

The net efficiency  $\eta_0$  at the resonant frequency will be the product of the gross efficiency and the mechanical efficiency  $\eta'_0$ , that is

$$(125) \quad \eta_0 = \eta''_0 \frac{r}{r''} = \eta''_0 \eta'_0.$$

In the instrument considered, the gross efficiency  $\eta''_0$  was  $140/257.3 = 0.544$ , the mechanical efficiency  $\eta'_0 = 0.74$ , and the net efficiency  $\eta_0 = 0.40$ , all taken at the resonant frequency  $f_0$ . In the free-impedance diagram of Fig. 41, the gross efficiency at resonance is the ratio of the size of the diameter  $bo'$  to the size of the horizontal vector  $oo'$ . The gross efficiency can therefore always be obtained from the free-impedance diagram. The net efficiency cannot be determined, however, without knowing the mechanical efficiency, or the ratio of  $r/r''$ . This calls for additional measurements, as described in Chapter X. It should also be remembered that a receiver, in ordinary use, is pressed against the ear of the listener, and is therefore in an intermediate condition between free and damped. Consequently, the gross efficiency of a receiver in the ordinary service condition is less than when free.

Although the power analysis of a receiver, deduced as above described from the motional-impedance circle, is satisfactory from a practical standpoint, yet it is in a certain sense a fictitious procedure. When we invoke the aid of hysteretic power to explain why a receiver behaves as a motor over that part of the motional-impedance circle where its motional resistance is negative (from  $k$  to  $b$ , Fig. 41), we are setting up a convenient fiction. The receiver cannot actually save active power when free over what it consumed when damped, and liberate the saving in motion. It is proper, therefore, to analyze the actual conditions more strictly, even though we do not employ the strict analysis in practical applications.

**Power in a Magnetic Circuit.** — It is well known that when, in a simple a.-c. circuit, an rms. emf.  $E$  abvolts in the

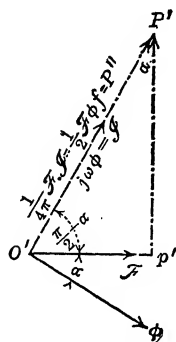


FIG. 55. Vector diagrams of power in electric and magnetic circuits.

standard-phase direction  $OE$ , Fig. 55, propels a rms. current of  $I$  abamperes in the phase direction  $OI$ , the emf. exerts power on the current which may be represented by the vector  $OP = EI$  abwatts drawn in the direction  $OI$ . The real part of this vector  $Op$  is the active power  $= EI \cos \alpha$  abwatts, and is the average rate of expelling energy from the circuit, as well as the maximum cyclic rate of active power development. The imaginary component  $pP$  is the reactive power  $EI \sin \alpha$  abwatts, and is the maximum cyclic rate of shifting energy from one part of the circuit to another.

In a similar manner, if a magnetic circuit has a rms. mmf.  $\mathcal{F}$  gilberts applied to it, it may be kept in the standard-phase direction  $O\mathcal{F}$ . The rms. magnetic flux  $\phi$  thereby produced, lags by an angle  $\alpha^\circ$ . The magnetic current is the time rate of change of this flux, which being assumed as sinusoidal, is

$$(127) \quad \mathcal{I} = \frac{\delta \phi}{\delta t} = \dot{\phi} = j\omega \phi \quad \frac{\text{maxwells}}{\text{second}} \angle.$$

This is a vector  $\omega$  times the magnitude of  $\phi$  and advanced  $90^\circ$  ahead of  $\phi$ . The power exerted by the mmf.  $\mathcal{F}$  on the magnetic current  $\phi$  is a vector in the direction of  $\mathcal{I}$  and is

$$(128) \quad P'' = \frac{\mathcal{F} \dot{\phi}}{4\pi} = j \frac{\mathcal{F} \omega \phi}{4\pi} = j \frac{f \mathcal{F} \phi}{2} = jNI\omega \phi \quad \text{abwatts } \angle.$$

This vector is represented as  $O'P'$  in Fig. 55. Its real component is  $O'p' = (f\mathcal{F}\phi \sin \alpha)/2$  abwatts, and is the active power expended in expelling energy from the magnetic circuit. In a simple magnetic circuit with only a primary winding, the expulsion occurs as heat in hysteresis and eddy currents. The imaginary component  $p'P'$  is  $(f\mathcal{F}\phi \cos \alpha)/2$  abwatts and is reactive power engaged in supplying energy to the magnetic circuit to the amount of  $\mathcal{B}^2/8\pi\mu$  ergs per cu. cm., where  $\mathcal{B}$  is the local instantaneous flux density, and  $\mu$  the local permeability.

In Fig. 56, following the above procedure,  $O\mathcal{F}_i$  is the standard phase direction of the mmf.  $\mathcal{F}_i$  in the telephone receiver, and  $O\phi_i$  the phase direction of the magnetic flux, lagging  $\beta^\circ$  behind  $\mathcal{F}_i$ .  $Oa$ , in

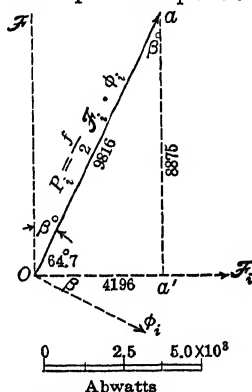


FIG. 56. Vector power delivered to magnetic circuit at 1028 cycles per sec. Diaphragm damped.

leading quadrature to  $O\phi_i$ , is the vector power delivered to the magnetic circuit with the diaphragm damped. At the reference frequency  $f = 1028 \sim$ , this power is 9816 abwatts or 981.6 microwatts. Of this power  $Oa' = 4196$  are consumed thermally in the magnetic circuit, and  $a'a = 8875$  abwatts are utilized in storing and releasing magnetic energy.

Figure 57 indicates the corresponding vector power relations when two mmfs.  $\mathcal{F}_i$  and  $\mathcal{F}_x$  are simultaneously impressed on the magnetic circuit. At the reference frequency  $1028 \sim$ , the resultant mmf. is  $O\mathcal{F}$ , 2.174 gilberts, lagging  $27^\circ.9$  behind  $\mathcal{F}_i$  (see Fig. 44). The displacement mmf. is  $O\mathcal{F}_x$ , 1.735 gilberts,  $143^\circ.9$  behind  $\mathcal{F}_i$ . The resultant flux  $O\phi$ , lags  $\beta$  or  $25^\circ.3$  behind  $O\mathcal{F}$ . The magnetic current is  $O\mathcal{I}$ ,  $90^\circ$  ahead of  $O\phi$ , or  $64^\circ.7$  ahead of  $O\mathcal{F}$ . The product  $j\phi\omega$  is  $24260 \angle 64^\circ.7$  maxwells per second.

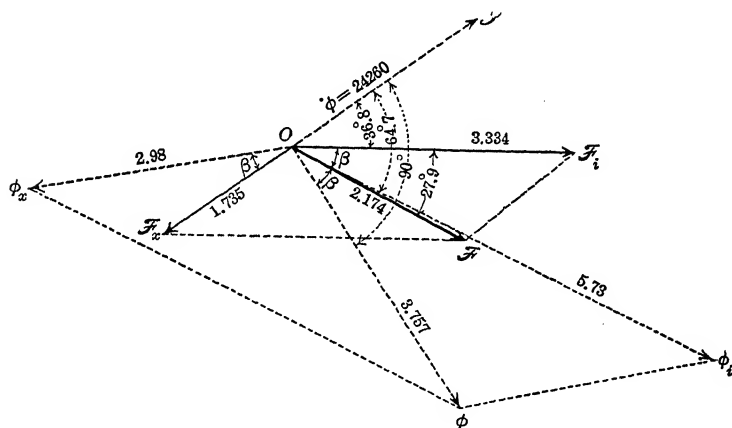


FIG. 57. Vector diagram of rms. MMFs, fluxes and resultant currents in magnetic circuit — diaphragm free.

We now have a diagram closely resembling that pertaining to a simple alternating-current circuit connecting an alternator with a synchronous motor, and supplying a current  $I$  to it through a total impedance  $Z$ . The mmfs.  $\mathcal{F}_i$ ,  $\mathcal{F}_x$ , and  $\mathcal{F}$  correspond respectively to the emfs. of the alternator  $E$ , the motor  $e$ , and of the circuit, where  $E + e = IZ$ . The magnetic current  $O\mathcal{I}$  corresponds to the electric-circuit current. In the electric circuit, the vector generator input is  $EI$ , the motor vector output is  $eI$ , and the power expended in the circuit is  $I^2Z = (E + e)I$ . So in this case, the vector magnetic-circuit power input is  $P''_i = \mathcal{F}_i f \phi / 2 = 6438 \angle 36^\circ.8$  ab-

watts, or  $Ob$ , Fig. 58, the vector magnetic-circuit output is  $P_m = -\mathcal{F}_x f \phi / 2 = 3349 \angle 0^\circ.7$  abwatts or  $Oa$ , Fig. 58, and the power expended in the magnetic circuit is  $P'' = \mathcal{F} f \phi / 2 = 4199 \angle 64^\circ.7$ . Here  $P_m$  is net mechanical power defined by the formula

$$(128) \quad P_m = \dot{x}^2 z = \dot{x}^2 \{ r + j(m\omega - s/\omega) \} \quad \text{abwatts } \angle,$$

and  $P''$  is power employed in sending the magnetic flux through the magnetic circuit, according to the relation

$$(129) \quad P'' = \frac{\mathcal{F} \dot{\phi}}{4 \pi} \quad \text{abwatts } \angle.$$

$$(130) \quad = j \phi^2 \mathcal{R} \frac{f}{2} \quad \text{abwatts } \angle.$$

Of this power, 1800 abwatts are consumed thermally, and 3797 abwatts are utilized for storage. The square of the rms. velocity,  $\dot{x}^2$ , being 16.74 at  $f = 1028 \sim$ , and the net mechanical resistance  $r$  being 199 dynes per kine, the net active mechanical power  $P_{ma}$  is 3332 abwatts, which is in satisfactory agreement with  $Oa'$ , Fig. 58.

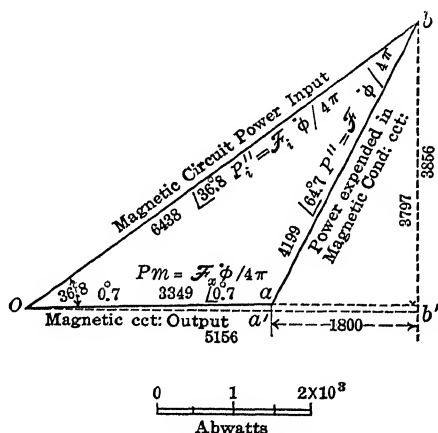


FIG. 58. Vector diagram of magnetic-circuit power — diaphragm free.

Figure 58 therefore presents the formal relations of magnetic-circuit power in the system at the assigned frequency. The motional power is obtained from the vectors of Figs. 54 and 56 through the relation

$$(131) \quad P'_e = P''_e - P_t \quad \text{abwatts } \angle,$$

or the electric vector power  $Oa$  of the motional-power circle

(Fig. 54) is obtained by subtracting the damped magnetic-circuit power  $P_t$  (Fig. 56), from the free magnetic-circuit input power  $P''_i$  (Fig. 58). The vector diagram is given in Fig. 59. The result is—  
 (132)  $P'_e = 5108 \angle 79^\circ.2 = 957 - j 5018$  abwatts  $\angle$   
 which is in conformity with  $Oa$ , Fig. 54.

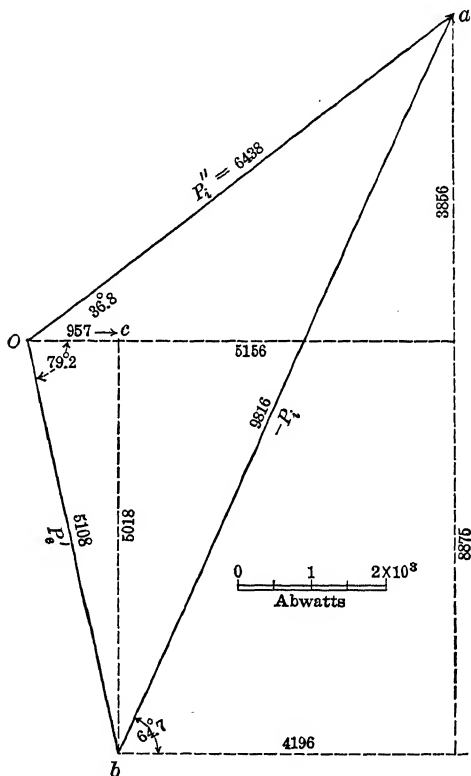


FIG. 59. Vector diagram of motional power in magnetic circuit — diaphragm free.

Figure 60 is a scalar diagram of the various powers described above, given as ordinates against impressed frequency as abscissas.  $P''_{ma}$  is the gross mechanical active power expended as  $\dot{x}^2 r''$ , and reaching a maximum of 5827 abwatts at  $f_0$ .  $P_{ma}$  is the net mechanical active power expended as  $\dot{x}^2 r$  and reaching a maximum of 4323 abwatts, also at  $f_0$ .  $P'_{ra}$  is the displacement power  $\dot{x}^2 r'$  and is the difference between the above, or 1504 abwatts at  $f_0$ .  $P'_{ea}$  is the active electric power of the motional circle, reaching a

maximum of 4800 abwatts at a frequency a little above 1000~, and falling to zero at about 1030 ~.  $P_{ha}$  is the hysteretic active power, which supplies  $P''_{ma}$  when the electric power fails, since the saving of active damped power in the magnetic circuit when the diaphragm is freed is  $-P_{ha}$ .

**Summary of Data determinable from the Motional-Impedance Circle.** — Summing up the analysis of this chapter, it may be stated that the normal motional-impedance diagram of a telephone receiver is a circle through the origin of coordinates. Motional-impedance circles of different receivers differ in three particulars; namely, (a) in their diametral impedance  $Z'_0$ . The sizes  $R'_0$  of these diametral impedances have been found to vary from about 1 ohm in a low-resistance imperfect receiver, to over 4000 ohms, in a high-resistance sensitive instrument. (b) In the depression angle  $2\beta$  of the circle diameter. This depression angle has been found to vary from  $20^\circ$  to  $120^\circ$ , approximately, in different instruments. (c) In the distribution of frequencies around the circle, upon which depend the value of the damping constant  $\Delta$  and of the resonance sharpness  $\Lambda$  of the diaphragm.

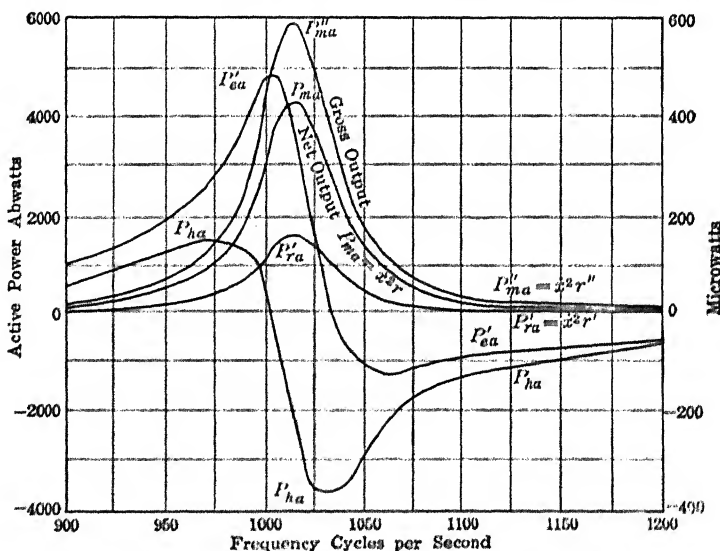


FIG. 60. Magnetic-circuit motional-power distribution at different frequencies.  $P''_{ma}$ , gross mechanical active output;  $P'_{ea}$ , active electric power increases;  $P_{ha}$ , change of active hysteretic power;  $P'_{ra}$ , active mechanical power expended against  $r'$  in displacement;  $P_{ma}$ , net mechanical output free.  $P''_{ma} = P'_{ea} - P_{ha} = P'_{ra} + P_{ma}$



From a measurement of the d.-c. resistance  $R_1$  of a telephone receiver, and its motional-impedance circle at a known testing-current strength, various constants of the instrument can be evaluated, as set forth in Table IX A. There are fifteen entries

TABLE IX A

CONSTANTS OF A TELEPHONE RECEIVER. DETERMINABLE FROM ITS  
MOTIONAL-IMPEDANCE CIRCLE

SYMBOL	NAME OF CONSTANT	UNIT	DEFINING EQUATION IN TEXT
$R_1$	Direct-current resistance	ohms or abohms	—
$R'_0 =  Z'_0 $	Diametral resistance of circle	ohms or abohms	124
$R'_0/R_1$	Motional-resistance ratio	numeric	124
$2\beta$	Depression angle of circle diameter	degrees	—
$\beta$	Lag angle of magnetic flux	degrees	Fig. 45
$f_0$	Frequency of apparent resonance	cycles/sec.	33, 89
$\omega_0$	Angular vel. apparent resonance	radians/sec.	32, 89
$\Delta$	Damping constant of diaphragm	hyps/sec	113
$\Lambda_s$	Resonance sharpness to sustained a.c.	numeric	205
$\Lambda_0$	Resonance sharpness to decaying oscillations	numeric	207
$t_\epsilon$	Time of decay in amplitude to $1/\epsilon$	seconds	115
$P''_m$	Gross vector mechanical-power output	abwatts	117, 119
$P_e$	Electric vector power input to diaphragm	abwatts	116, 119
$P_h$	Hysteretic vector power input to diaphragm	abwatts	118, 119
$\eta''_0$	Gross efficiency of diaphragm at resonance	numeric	124

in the list and it is remarkable that so much information concerning the electrical and mechanical conditions of a telephone receiver should be obtainable by so simple a procedure. The fundamental constants  $A$ ,  $m$ ,  $r$  and  $s$  are not however found in the Table and means for their determination are reserved for the next Chapter.

## CHAPTER X

### METHODS FOR DETERMINING THE FUNDAMENTAL CONSTANTS OF A RECEIVER

**Introduction.** — As has been shown in the last chapter, there are various quantitative properties or constants of a telephone receiver which can be evaluated from its motional-impedance circle. The four fundamental constants of a receiver from a dynamical standpoint are  $A$ ,  $m$ ,  $r''$  and  $s''$ , as already defined. The data obtainable from the motional impedance in relation to these four constants may be repeated here for closer examination

$$(133) \quad \omega_0 = \sqrt{s''/m} \quad \text{rad. per sec.}$$

$$(134) \quad \Delta = r''/(2m) \quad \text{hyp. per sec.}$$

$$(135) \quad Z'_0 = A^2/r'' \quad \text{abohms } \angle.$$

These three equations are inadequate to furnish the values for the four unknown fundamental constants  $A$ ,  $m$ ,  $r''$ , and  $s''$ ; so that a fourth independent relation must be supplied from some other measurement or test. A number of different methods have been either suggested or tried for providing the fourth equation;\* but only two have been found to give satisfactory results, namely:

(1) By loading the diaphragm with a known mass at its center and repeating the motional-impedance test in this condition.

(2) By measuring the amplitude of maximum cyclic displacement over the poles, at the frequency of resonance.

Method (2) is the one here advocated, as method (1) has not been found to give uniformly reliable results.

**Method (1) of Loading the Diaphragm.** — If, after the motional-impedance circle of a receiver has been measured in the usual way, the diaphragm is loaded by fastening a small concentrated mass of  $m'$  gm. to the center with wax, and the motional-impedance circle is then measured afresh, formula (133) becomes

$$(136) \quad \omega_{01} = \sqrt{\frac{s''}{m + m'}} \quad \text{rad. per sec.,}$$

\* Kennelly and Affel, Bibliography 58.

on the assumption that the addition of the load  $m'$  has not appreciably altered the distribution of amplitudes over the surface of the vibrating diaphragm; so that the equivalent mass  $m$  of the diaphragm remains the same in the loaded and unloaded states. This assumption cannot always be justified, as the load tends to alter the mass factor. The smaller the load, the less the disturbance in  $m$  is likely to be;\* but with very small loads the formulas become insensitive and liable to error. From (133) and (136), we find

$$(137) \quad m = \frac{\omega_{01}^2 m'}{\omega_0^2 - \omega_{01}^2} \quad \text{gm.}$$

The value of  $m$  thus derived, being introduced into (133), gives  $s''$ , and introduced into (134) gives  $r''$ . Finally, the latter value of  $r''$  used in (135) gives  $A$ .

A series of measurements made in this manner on a standard bipolar type of receiver using loads from 0.98 to 2.998 gm. are reported in one of the papers† already published on this subject. As the results were not very satisfactory, they are not repeated here. It seems quite likely, however, that by keeping to small loads not exceeding 0.5 gm. say, a suitable technique could be developed with this method.

**Method (2) of Measuring the Amplitude at Resonance.** — Using formula (96) we have at the resonant frequency

$$(138) \quad IZ'_0 = A\dot{x}_0 = j\omega_0 A x_0 \quad \text{abvolts } \angle$$

or

$$(139) \quad A = \frac{IZ'_0}{\dot{x}_0} = \frac{IZ'_0}{j\omega_0 x_0} = \frac{I_m Z'_0}{j\omega_0 x_{m0}} = \left| \frac{I_m Z'_0}{\omega_0 x_{m0}} \right| \angle \beta^\circ \quad \frac{\text{abvolts}}{\text{kine}} \angle,$$

here  $Z'_0$  is the vector diametral motional impedance at resonance,  $x_0$  is the rms. amplitude of the diaphragm over either pole at resonance,  $I_m = \sqrt{2} I$  the maximum cyclic current at standard phase or zero slope and  $x_{m0} = \sqrt{2} x_0$  the maximum cyclic amplitude at resonance. The rms. resonant velocity  $\dot{x}_{m0}$  is taken as lagging  $\beta^\circ$  behind  $I$ , the measured rms. testing current; so that the slope of  $A$  is  $-\beta^\circ$ . If we can measure  $\dot{x}_{m0}$ , we can, after obtaining  $Z'_0$  and  $\omega_0$  from the motional-impedance circle, determine

\* Dr. R. L. Jones has reported having obtained satisfactory results with this method of loading in cases where the total added mass  $m$  did not exceed 0.3 gm.

† Bibliography 58, pages 438-442.

the value of the vector force factor  $A$ , expressed either in abvolts per kine, or in dynes per abampere. Then from (98), we have

$$(140) \quad r'' = \frac{A^2}{Z'_0} = \frac{I_m^2 R'_0}{x_{m0}^2 \omega_0^2} \quad \text{dynes per kine.}$$

This gives the gross mechanical resistance of the diaphragm to motion, in terms of the force factor  $A$  and the diametral vector motional impedance  $Z'_0$ . Since the slopes of  $A^2$  and  $Z'_0$  are each equal to  $-2\beta^\circ$ , their ratio is the real quantity  $r''$ .

Next using (113) and (134), after finding  $\Delta$  from the motional-impedance circle, we have

$$(141) \quad m = \frac{r''}{2\Delta} \quad \text{gm.}$$

Finally, by (89) or (133), having identified  $\omega_0$  from the diametral angular velocity of the motional-impedance circle, we find

$$(142) \quad s'' = m\omega_0^2 \quad \frac{\text{dynes}}{\text{cm.}}$$

The four last equations completely determine the four fundamental dynamic constants of the receiver.

We may now proceed to evaluate the subsidiary constants  $\mathcal{L}$ ,  $p$ ,  $N'$ ,  $r'$ ,  $r$ ,  $s$  and  $\mathcal{B}_0$ . We first ascertain the total number of turns  $N$  in the winding of the receiver. Then, from the damped-impedance diagram Fig. 34, we draw in the vector reactance  $\mathcal{X}$ , making an angle  $\beta$  with the  $OX$  axis. The angle  $\beta$  can be found from the graph of the damped impedance, Fig. 33, using the slope of the tangent at resonance; or better still, by taking half the depression angle  $ROP$  of the motional-impedance diameter Fig. 38. This gives the mean vector inductance  $\mathcal{L}$  from the relation

$$(143) \quad \mathcal{L} = \frac{\mathcal{X}}{\omega} \quad \text{abhenries } \angle.$$

It must be remembered that this relation is only true to a first approximation, owing to the secondary effects of frequency change on the magnetic circuit, and that, as shown by comparing Tables VIII and IX, there will be some discrepancies between the observed values of impedance and those computed from  $\mathcal{X}$  and Fig. 35. We then have, by (77),

$$(144) \quad p = \frac{A}{\mathcal{L}} \quad \frac{\text{abamperes}}{\text{cm.}}$$

Since  $A$  and  $\mathcal{L}$  have the same slope,  $p$  will be a real quantity. The equivalent number of turns  $N'$  from (74) is

$$(145) \quad N' = pN.$$

We can then use (82) to find  $r'$ , the virtual resistance to displacement at resonance:

$$(146) \quad r' = \frac{p |A| \sin \beta}{\omega_0} \quad \frac{\text{dynes}}{\text{kine}}.$$

Since only real quantities appear on the right hand of this equation  $r'$  is also a real quantity.

Neglecting changes in  $r'$  due to change in  $\omega$ , we then have, from (81),

$$(147) \quad r = r'' - r' \quad \frac{\text{dynes}}{\text{kine}}.$$

The virtual stiffness coefficient of displacement  $s'$  may now be found from (83); and using this value, we find

$$(148) \quad s = s'' + s' \quad \frac{\text{dynes}}{\text{cm}}.$$

The normal permanent magnetic flux density in the air gaps is found from (73) and (74)

$$(149) \quad \mathcal{B}_0 = 2 \pi p N \quad \text{gausses.}$$

**The Amplitude Measurer.** — One amplitude measurer, i.e., the amplitude explorer of Figs. 7, 8, and 9, has already been described. This instrument, however, is not only needlessly elaborate for the purpose of finding the amplitude over the poles, but also has the disadvantage of requiring the cap to be removed from the diaphragm under test. A simpler and more convenient form of optical amplitude measurer is shown in Figs. 61 and 62.

Strictly speaking, the amplitude of diaphragm vibration should be measured over one or both of the poles; but in practice it is convenient and practicable to measure the amplitude at or near the center of the diaphragm in the middle of the cap opening. The error involved is probably small.

A minute triangular mirror  $M$ , Fig. 61, of thin silvered glass, about 1 mm. in length of edge, is fastened by shellac or hard wax, at about its geometric center, to a little phosphor-bronze strip, about 4 mm. long. The strip is soldered at each end to the elastic prongs of a brass fork, as shown. This strip should be fixed with

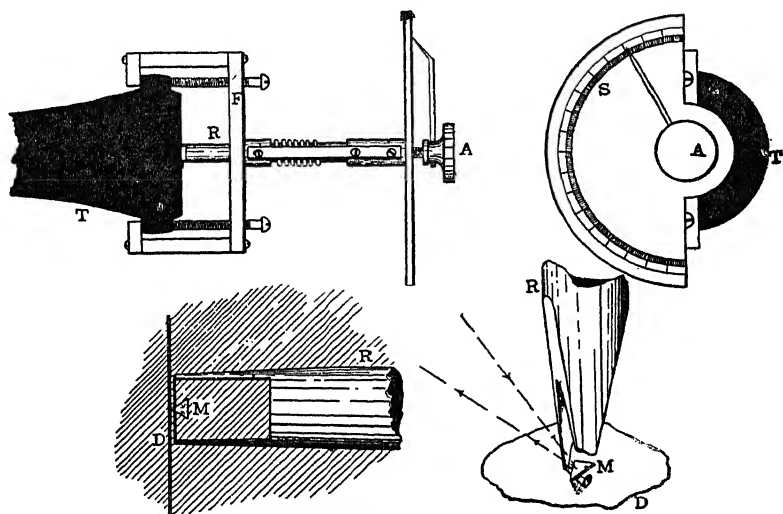


FIG. 61. Amplitude measurer.

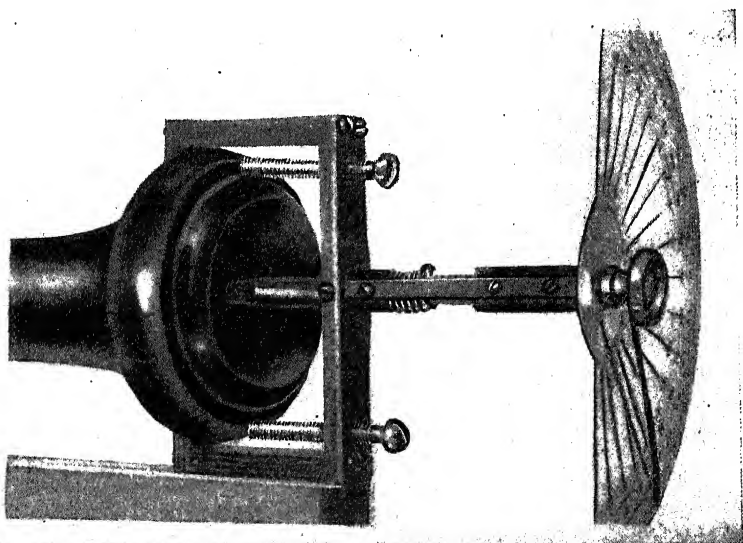


FIG. 62. Photographic view of amplitude measurer applied to a telephone receiver.

sufficient tension to make sure that the mirror fastened thereon will have a suitably high natural frequency of vibration, so that it will keep in contact with the vibrating diaphragm to which it is applied. If the strip is too slack, the triangular mirror will not keep in contact with the rapidly vibrating diaphragm, and partake of all its up and down motions. The brass fork  $R$  is supported in a frame on a bridge  $F$  fastened securely to the receiver cap. A fine-thread screw  $A$ , working in the collar, against the pressure of the spiral spring shown, enables the fork  $R$  to be advanced or withdrawn, without twisting, through a short distance perpendicularly to the surface of the diaphragm. The milled-head screw  $A$  carries a pointer, over the surface of a stationary graduated semi-circular scale  $S$ . By giving to the screw an observed number of degrees of twist, the distance of advance of the fork and stirrup can be readily found, from the pitch of the screw. In the instrument shown, the screw has 24 threads to the inch; so that one turn = 1.06 mm. The position of the pointer on the scale  $S$  can be read easily to  $1'20''$  and estimated to  $1/10^\circ$ . A half degree advances the fork and strip  $1.06/720 = 1.47 \mu$ , and an estimated tenth degree =  $0.29 \mu$ ; so that the advance of the strip carrying the mirror can be estimated to a fraction of a micron.

One of the triangular points of the mirror  $M$  is brought into contact with the diaphragm, in such a manner that the phosphor-bronze strip is thereby twisted at its center, through an angle of say  $45^\circ$ . This twist supplies a suitable couple of forces to the mirror, so that it will tend to keep in contact with the diaphragm. The exact angle of contact fortunately does not need to be known; nor does the geometry of the strip and mirror come into the analysis, provided that the strip is suitably taut.

**Technique for Measuring the Amplitude at Resonance.** — The amplitude-measurer frame is fastened to the receiver in the general manner indicated in Fig. 62, but not specifically as there shown. As was found by unfortunate experience, and as will be described in Chapter XII, it is objectionable to have the clamping pressure of the frame brought on to the cap at two opposite screw feet, as is indicated in Fig. 62. It is important that the clamping pressure should be distributed around the cap by the insertion of a pair of brass clamping rings, one below and the other above the edge of the cover. The clamping screws then press these rings together, and the rings distribute the pressure around the cover.

The receiver with clamped amplitude-measurer is now supported fairly rigidly on one side, as in Fig. 62, so that a beam of light from an arc lamp may fall on the little mirror  $M$ , and be reflected thence to a graduated scale at a distance of not less than 1 meter. The path of the beam is indicated in broken lines in Fig. 61. It is convenient to mount the entire apparatus in a sound-reducing chamber with padded walls, and to keep this chamber darkened during the measurements. The reflected beam of light is then brought to the center of the graduated scale, after the mirror  $M$  has been advanced by the screw  $A$  into suitable contact with the diaphragm  $D$ . The adjusted and measured alternating testing current is then admitted to the coils of the instrument, and the diaphragm is allowed to vibrate under its influence; this causes the reflected beam of light to expand into a luminous band on the graduated scale. The distant edges of this band can be made distinct by attending to the optical system. With (say) 2 milliamperes passed through a receiver of the 75-ohm type, the band is likely to be very small, even with a magnification factor of 10,000, except near resonance, when it rapidly widens. By careful adjustment, the frequency of the testing current is varied until the band of light reaches its maximum length, which is then recorded. Half this length is taken as the resonant luminous amplitude.

The testing current is now cut off, and the spot of light is brought to rest on the graduated scale. The instrument has now to be calibrated. This is done by successively advancing the screw through a few short distances, as measured by the position of the pointer  $P$ . This causes the spot of light on the scale to be displaced by corresponding successive shifts. A calibration curve is then plotted between spot displacements on the scale, versus advances of the screw  $A$ . It is clear that the deflection of the spot of light on the scale is due to the relative motion of the toe of the mirror  $M$  on the diaphragm and the phosphor-bronze strip which holds it. When the alternating current is brought to resonance, the diaphragm moves the toe of the mirror cyclically through the distance  $x_m$  cm. and produces a certain measured luminous deflection, the phosphor-bronze strip and fork  $F$  being kept fixed. In the calibration test, the screw is advanced in a succession of displacements  $x_c$  cm. with the diaphragm kept fixed, and a series of measured luminous deflections is secured. Thus the resonant value of  $x_m$  can be evaluated against the calibrated displacement  $x_c$ .



The pressures exerted by the toe of the mirror  $M$  on the diaphragm are ordinarily less than 100 dynes at maximum cyclic displacement. This pressure adds to the gross frictional resistance  $r''$ , and tends slightly to reduce the amplitude of vibration. Consequently, the amplitude is likely to be a little less, for a given testing-current strength, with the amplitude-measurer applied, than with the diaphragm free. This source of error can be eliminated, however, by repeating an electric measurement of the motional impedance at resonance, after the amplitude-measurer has been applied. If the vibration amplitude is reduced (say) 5 per cent by the pressure of the mirror; then the diametral motional impedance  $Z'_0$  will also be reduced 5 per cent. The proper correction for  $x_{m0}$  freed, can be obtained in this manner without repeating the whole series of free-impedance tests.

The strip usually stands well up to its duty for some time; but the test is severe on the little exploring mirrors. They are apt to break in service, especially during the a.-c. applications. It is desirable to have additional mirrors in reserve.

#### Experimental Comparisons of Velocity and Motional Impedance.

— We have already seen in formula (96) that the motional impedance at any impressed frequency is directly connected with the vibrational velocity by the relation

$$(150) \quad Z' = \frac{A}{I} \cdot \dot{x} = j\omega \frac{A}{I} \cdot x \quad \text{abohms } \angle$$

$$(151) \quad = \frac{A}{I_m} \cdot \dot{x}_m = j\omega \frac{A}{I_m} \cdot x_m \quad \text{abohms } \angle.$$

This means that the size of the motional impedance at any impressed frequency is directly proportional to the velocity, and also to  $\omega$  times the maximum cyclic displacement  $x_m$ . If, therefore, we observe  $x_m$  as well as  $Z'$ , in a series of free and damped impedances, and if our theory is correct, when we plot the scalar  $\omega x_m$ , or inferred maximum cyclic velocity, against frequency, we should obtain the same curve as that found by plotting the size of  $Z'$  against frequency. This has been done satisfactorily with two different receivers. One set of results is indicated in Fig. 63. Here the upper curve is the graph of the observed motional-impedance size, at different frequencies between 400  $\sim$  and 1500  $\sim$ , for a particular bipolar receiver described as  $B$ . The lower curve joining the black dots is the graph of the inferred corresponding velocities  $\omega x_m$  from measurements of  $x_m$ . The little white circles

on or near this curve indicate what the graph should be if the proportionality to the motional impedance by formula (151) were strictly maintained. The agreement is seen to be satisfactory.

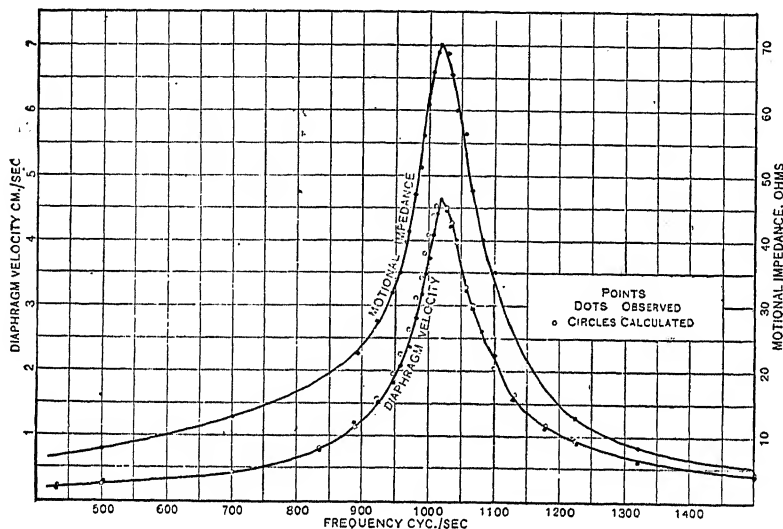


Fig. 63. Resonance curves of diaphragm velocity and motional impedance, for receiver B.

The same results are also indicated in the motional-impedance diagram of receiver B in Fig. 64. Here the vector motional impedances  $Z'$  are shown at or near the circular locus. The corresponding inferred velocities  $\omega x_m$  are also shown lying on a smaller circular locus. The phases of these velocities were not observed in this case, but are taken, for comparison, as coincident with the phases of  $Z'$ , the corresponding motional impedance. Actually (151) shows that the phase of  $\dot{x}_m$  should lie  $\beta^\circ$  ahead of  $Z'$ .

Table X gives the particulars for four different receivers, A, B, C, and D, analyzed at about the same time by the same observer (Mr. Affel) with the motional-impedance method. Of these, A and B were tested in two different ways, namely, by the technique described in this chapter, measuring the polar amplitude  $x_{m0}$  at resonance, and also by finding the amplitude distribution over the diaphragm at resonance, with the explorer described in connection with Figs. 7, 8, and 9. The equivalent mass  $m$  and the corresponding equivalent mass factor  $m/M$  was thus obtainable in two different ways. As shown in Table X, the agreement between them is to 8 per

TABLE X  
DATA SECURED ON PARTICULAR RECEIVERS (Affel)

RECEIVER NUMBER	A	B	C	D
TYPE	BELL BIP.	BELL BIP.	BELL BIP.	WATCH CASE BIP.
<i>Data</i>				
Area of each Pole cm. $\times$ cm. . . . .	1.14 $\times$ 0.199	1.40 $\times$ 0.225	1.14 $\times$ 0.199	1.15 $\times$ 0.18
Distance separating poles cm. . . . .	0.686	0.85	0.686	1.10
External diam. of diaph. cm. . . . .	5.52	5.40	5.52	5.57
Diameter of clamping circle cm. . . . .	5.00	4.94	5.00	4.95
Thickness of diaphragm over japan cm. . . . .	0.0399	0.031	0.031	0.0244
Wt. of diaphragm, gm. . . . .	5.979	4.181	4.397	3.365
Direct-current Resistance of coils, ohms at 20° C. . . . .	87.1	73.0	86.7	1079
<i>Test Data</i>				
Temperature of Test Deg. C. . . . .	26.7°	27.8°	20°	20°
Current through Rec. abamps. <i>rms.</i> <i>I</i> . . . . .	0.000 202	0.000 200	0.000 204	0.000 116
Resonant Freq. of Rec. cyc./sec. <i>f</i> <sub>0</sub> . . . . .	993	1020.4	1015	898.5
Resonant Ang. Vel. rad/sec. $\omega_0$ . . . . .	6240	6412	6378	5646
Motional-Impedance Circle diameter ab-ohms. <i>R'</i> <sub>0</sub> . . . . .	80.2 $\times 10^9$	70 $\times 10^9$	140 $\times 10^9$	367 $\times 10^9$
Max. Amplitude of Resonance cm. $\times 10^{-4}$ (Microns). <i>x</i> <sub>m</sub> . . . . .	7.53	7.19	10.35	6.64
Velocity of Diaph. at Resonance cm./sec. (max. cyclic). $\dot{x}_m$ . . . . .	4.70	4.62	6.6	3.75
Decrement per sec. $\Delta$ (Mean) . . . . .	61.2	236	149	356
<i>Calculated Data</i>				
Equivalent Mass of Diaph. <i>m</i> , (gms.) . . . . .	2.41	0.557	0.902	0.986
Equivalent Mass Factor . . . . .	0.49	0.17	0.245	0.387
Equivalent Mass Factor by Exploration Method . . . . .	0.53	0.18		
Equivalent Elasticity, <i>s'</i> , dynes per cm. . . . .	94.0 $\times 10^6$	22.9 $\times 10^6$	36.7 $\times 10^6$	31.44 $\times 10^6$
Equivalent Diaph. Resistance <i>r''</i> , dynes per kine . . . . .	295	262.3	268	702
Force Factor, $ A $ , dynes per abampere . . . . .	4.87 $\times 10^6$	4.28 $\times 10^6$	6.12 $\times 10^6$	16.05 $\times 10^6$
Mean Angle of Lag $\beta$ degrees . . . . .	29.7	37.3	25.3	37.0

cent in the case of *A*, and to 6 per cent in the case of *B*, which may be considered satisfactory. In both cases, the mass factor by ex-

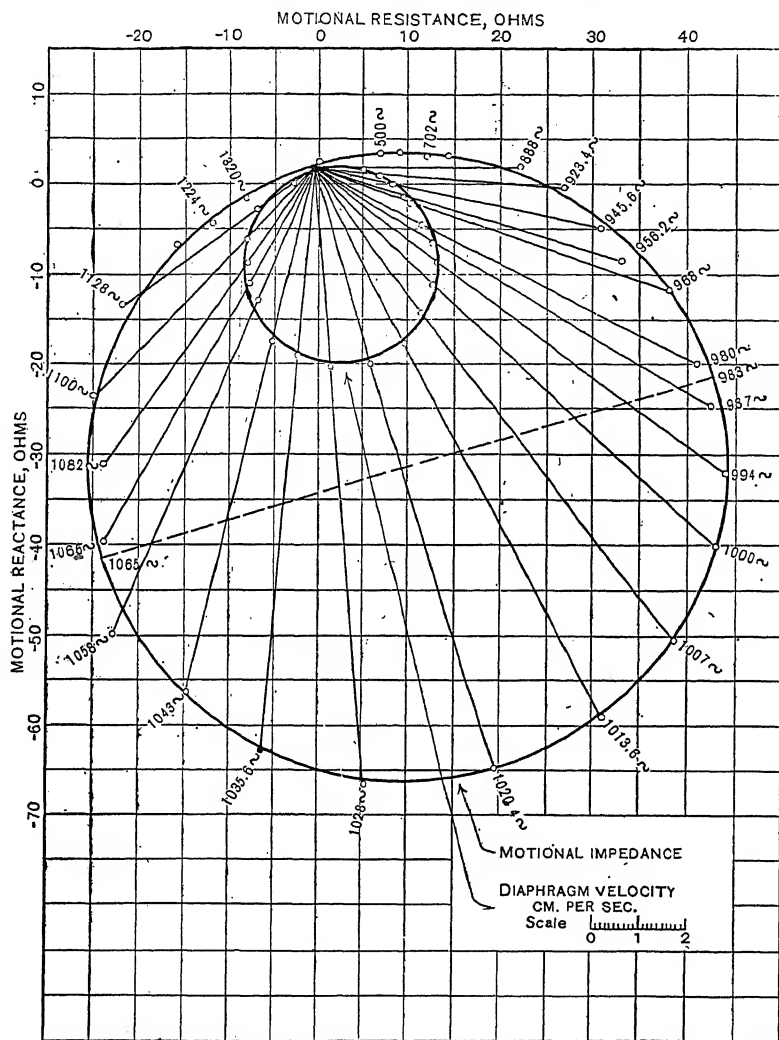


FIG. 64. Motional impedance and maximum cyclic velocity, receiver *B*.

ploration of amplitudes was the greater. In measuring small amplitudes near the edge of the diaphragm by the optical method, there is often a tendency to overestimate them, and so to raise the apparent average amplitude square and equivalent mass. Of the

two, the motional-impedance and single polar-amplitude method is probably the more reliable. The instrument designated as *C* in Table X is the one which has had its behavior more fully analyzed in this and preceding chapters, in connection with Figs. 33 to 64. The computed data for this instrument are recorded in Table XI, which is, in the case of *C*, an extension of Table X.

TABLE XI

## COLLECTED NUMERICAL DATA CONCERNING THE ANALYZED RECEIVER

*Mechanical Data*

Dimensions of each polar surface, cm. $\times$ cm. . . . .	$1.14 \times 0.199$
Area of each polar surface, $S$ sq. cm. . . . .	0.227
Distance separating poles, cm. . . . .	0.686
Diameter of diaphragm, cm. . . . .	5.52
Diameter of clamping circle, cm. . . . .	5.0
Thickness of diaphragm over japan, cm. . . . .	0.031
Gross weight of diaphragm, gm. . . . .	4.40
Net weight of diaphragm (within clamping circle), $M$ gm. . . . .	3.68
Approx. number of turns, including both spools, $N$ . . . . .	1300
Length of mean flux path in perm. magnet, excluding pole pieces, $L$ cm. . . . .	18.5

*Electrical Test Data*

D. C. resistance at 20° C., $R_1$ abohms . . . . .	$86.7 \times 10^9$
Vector inductance at resonant frequency, $\mathcal{L}_0$ abhenries $\angle$ . . . . .	$3.65 \times 10^7 \angle 25^\circ.3$
Testing current in receiver winding, $I$ rms. abamperes . . . . .	$2.04 \times 10^{-4}$
Frequency of apparent resonance, $f_0$ cycles per sec. . . . .	1015
Angular vel. of " " $\omega_0$ radians per sec. . . . .	6378
Size of motional impedance circle diameter, $R'_0$ abohms . . . . .	$140 \times 10^9$
Slope of " " " " $2\beta$ degrees . . . . .	$-50^\circ.6$
Slope of permeance at resonance, $\beta$ degrees . . . . .	$-25^\circ.3$
Max. cyc. vibration amplitude at resonance, $x_{m0}$ c.m. . . . .	$10.35 \times 10^{-4}$
Effective " " " " $x_3$ rms. cm. . . . .	$7.32 \times 10^{-4}$
Max. cyc. velocity of diaph. center at resonance, $\dot{x}_{m0}$ kins . . . . .	6.6
Effective " " " " $\dot{x}_0$ " " " " . . . . .	4.66
Quadrantal frequencies, $f_1, f_2$ cycles per sec. . . . .	991, 1039.5
Quadrantal ang. velocities, $\omega_1, \omega_2$ radians per sec. . . . .	6227, 6532
Damping factor of diaphragm, $\Delta$ hyps. per sec. . . . .	149
Resonant Sharpness $\Delta_0 = \omega_0 / \Delta$ numeric . . . . .	42.8

*Computed Electromagnetic Data*

Vector force factor, $A$ dynes per abampere $\angle$ , or abvolts per kine $\angle$ . . . . .	$6.12 \times 10^6 \angle 25^\circ.3$
Equivalent polar mass, $m_1$ gm. . . . .	0.902
Mass factor, $m_1/M$ numeric . . . . .	0.245
Gross elastic coefficient of diaphragm, $s$ " dynes per cm. . . . .	$36.7 \times 10^6$
Virtual " " " displacement, $s'$ " " " " . . . . .	$0.928 \times 10^6$
Net " " " diaphragm, $s$ " " " " . . . . .	$37.63 \times 10^6$
Gross mechanical resistance of diaphragm, $r$ " dynes per kine . . . . .	268
Virtual " " " displacement, $r'$ " " " " . . . . .	68.8
Net " " " diaphragm, $r$ " " " " . . . . .	199
Equivalent No. of turns per cm. of displacement, $N'$ gilberts per cm. . . . .	218
Ratio of numbers of turns, $p = N'/N$ abamperes per cm. . . . .	0.168
Equivalent mmf. of permanent magnet, $\mathcal{F}_0$ gilberts . . . . .	181
Total useful polar flux, $\phi_0$ maxwells per pole . . . . .	311
Average useful polar flux density, $\mathcal{B}_0$ gaussess . . . . .	1369

Equivalent magnetic reluctance of entrefers, $\mathcal{R}_0$ oersteds	0.582 $\angle$ 25°.3
Equivalent magnetic permeance, $\mathcal{P}_0$ (oersteds) <sup>-1</sup>	1.718 $\angle$ 25°.3
Effective mmf. of testing current $I$ , $\mathcal{F}_i$ rms. gilberts	3.334 $\angle$ 0°
Effective flux in mag. cet. due to current $I$ , $\phi_i$ rms. maxwells	5.73 $\angle$ 25°.3
Effective flux density in entrefers due to current $I$ , $\mathcal{B}_i$ rms. gaussses	2.50 $\angle$ 25°.3
Tractive force on diaphragm due to current $I$ , $F_i$ dynes vmf. rms.	1249 $\angle$ 25°.3
Gross efficiency of receiver at resonance, $\eta'' = R'_0/R'' = 140/257.3$ , numeric	0.544
Mechanical efficiency of diaphragm at resonance, $\eta'_0 = r/r''$ numeric	0.74
Net efficiency of receiver at resonance, $\eta_0 = \eta'_0 \cdot \eta''_0$ numeric	0.40

TABLE XI A

DATA COMPUTED FOR THE FREQUENCY OF 1028  $\sim$  WITH THE TESTING CURRENT OF 2.04 MILLIAMPERES.  $\omega = 6458$

Effective mmf. due to testing current, $\mathcal{F}_i$ rms. gilberts $\angle$	3.334 $\angle$ 0°
Effective mmf. due to displacement, $\mathcal{F}_x$ rms. gilberts $\angle$	1.735 $\angle$ 143°.9
Effective resultant mmf. vector, $\mathcal{F} = \mathcal{F}_i + \mathcal{F}_x$ rms. gilberts $\angle$	2.174 $\angle$ 27°.9
Effective flux in magnetic circuit due to current $I$ , $\phi_i$ rms. maxwells $\angle$	5.73 $\angle$ 25°.3
Effective flux in magnetic circuit due to displacement, $\phi_x$ rms. maxwells $\angle$	2.98 $\angle$ 169°.2
Effective resultant flux vector in mag. circuit, $\phi = \phi_i + \phi_x$ rms. maxwells $\angle$	3.757 $\angle$ 53°.2
Effective resultant magnetic current, $\mathcal{I} = \phi$ rms. maxwells per sec. $\angle$	24260 $\angle$ 64°.7
Gross mechanical impedance of diaphragm, $z'' = r'' + jx''$ dynes per kine $\angle$	$268 + j146 = 305.2 \angle 28°.6$
Net mechanical impedance of diaphragm, $z = r + jx$ dynes per kine $\angle$	$199 + j2.5 = 199 \angle 0°.7$
Effective diaphragm velocity, $\dot{x}$ rms. kines	$4.091 \times 10^{-4}$
Mean square of diaphragm velocity, $\dot{x}^2$ kines <sup>2</sup>	16.74
Net mechanical output, $P_m = \mathcal{F}_x \cdot \phi / 4\pi = \dot{x}^2 z$ abwatts $\angle$	$3349 + j40 = 3349 \angle 0°.7$
Power expended in magnetic circuit, diaphragm free, $P'' = \mathcal{F} \cdot \phi / 4\pi$ abwatts $\angle$	$1795 + j3797 = 4199 \angle 64°.7$
Magnetic-circuit power input, diaphragm free, $P''_i = \mathcal{F}_i \cdot \phi / 4\pi$ abwatts $\angle$	$5156 + j3856 = 6438 \angle 36°.8$
Magnetic-circuit power input, diaphragm damped, $P_i = \mathcal{F}_i \cdot \phi_i / 4\pi$ abwatts $\angle$	$4196 + j8875 = 9816 \angle 64°.7$
Electric power of motional-power circle, $P_e$ abwatts $\angle$	$957 - j5018 = 5108 \angle 79°.2$
Hysteretic power of motional-power circle, $P_h$ 2 sin $\beta$ abwatts $\angle$	$= 0.855 \times 5108 \angle 143°.9$
Gross mechanical output motional-power circle, $F_m'' = P_e - P_h$ 2 sin $\beta = \dot{x}^2 z''$	$4484 - j2445 = 5108 \angle 28°.6$

*With reference to other windings of same useful volume but different resistance*

Motional-impedance Ratio $Z'_0/R_i$ , numeric $\angle$	1.62 $\angle$ 50°.6
Unit-resistance force factor $A/\sqrt{R_i}$ , dynes $\times$ abohms <sup>1/2</sup> /abvolts $\angle$	20.8 $\angle$ 25°.3

**Effect of Size of Wire in Receiver Winding on Receiver Constants.** — If the coils of a given telephone receiver are allotted a fixed volume or winding space, we may consider the effects produced by filling this winding space with different sizes of insulated wire. If the ratio of bare to insulated wire diameters is variable, the matter becomes very complicated. The matter is greatly simplified, however, if we make the assumptions — which are justifiable as first approximations over a certain range of wire sizes — that the ratio of bare to insulated wire diameters remains constant, and that the unfilled space in the winding also remains constant. Under these assumptions, the volume and weight of copper in the winding space will remain unchanged; although the size of wire, number of turns, and d.-c. resistance of the winding may be suitably varied.

Under these conditions, if we reduce the wire diameter one-half, the total number of turns  $N$  will be quadrupled, and the d.-c. resistance  $R_1$ , at constant temperature, will be increased sixteen fold. If we neglect changes in electric skin-effect, or a.-c. density, over the cross-section of the wire, as the diameter is changed, the a.-c. resistances of the winding will be also increased sixteen fold. The effect, with constant current  $I$ , will be to increase

$$N, A, \mathcal{F}_t, \dot{x}, x \text{ and } \phi_t,$$

each four times, leaving

$$\mathcal{F}_0, \mathcal{B}, \mathcal{P}, \mathcal{P}, r, r', r'', s, s', s'', m, \text{ and } \beta$$

unchanged. The quantities

$$\mathcal{L}, \mathcal{L}, \mathcal{X}, Z, Z'_0, P_e, \text{ and } P_m$$

will all be increased sixteen times (neglecting variations in  $r'$ ) or in direct proportion to the d.-c. resistance. Consequently, the ratio of net active mechanical power output  $\dot{x}^2 r$  to the d.-c. power-loss  $I^2 R_1$  will remain substantially unchanged for all values of  $R_1$  within the range for which the assumption of constant copper in the winding space holds true. On this theory, changing the winding of a receiver, other things remaining the same, increases both the gross and net mechanical output in proportion to the resistance, for a fixed exciting-current strength  $I$ ; but for a given amount of  $I^2 R_1$  d.-c. power-loss in the winding, these outputs remain substantially constant.

**Impedance Ratio and Efficiencies.** — Since  $Z'_0$ , the maximum or diametral value of the vector motional-impedance increases,

according to this theory, directly with the d.-c. resistance of the winding, the motional-impedance ratio (at resonance)  $Z'_0/R_1$  should be constant. This motional-impedance ratio is an important characteristic of a receiver. For receivers of the same resistance, since we have, by (139),

$$(152) \quad \dot{x}_0 = \frac{I}{A} \cdot Z'_0 \quad \text{kines } \angle,$$

the resonant vibratory velocity that can be imparted to the diaphragm over the poles is proportional to the resonant values of the motional impedance for constant excitation. It follows that where maximum velocity at a single and resonant frequency is desired, the size of the diametral motional impedance is a criterion of the sensibility of the receiver. With receivers of different resistance, the ratio of  $R'_0/R_1$ , or motional-resistance ratio, is to a first approximation, a comparative criterion of the same kind. In making the tests, the testing-current should be preferably inversely as the square root of the d.-c. resistance, i.e., by assumptions given above, inversely as the number of turns in the windings. This will keep the a.-c. mmf.  $\mathcal{F}_i$  the same in instruments of the same construction but of different windings, and will keep the a.-c. density in the wire the same. In the case of receiver *C*, the motional-impedance ratio was  $140 \simeq 50^\circ.6 \div 86.7 \angle 0^\circ = 1.62 \simeq 50^\circ.6$ .

The force factor, as we have seen, increases as the square root of the resistance in instruments of the same construction that differ only in size of wire. In such instruments, the force factor may be divided by the square root of the d.-c. resistance, in order to bring it to a comparative basis, namely, the force factor for unit resistance, or the force factor in an ideal instrument that had one abohm of d.-c. resistance. In the case of instrument *C*, this unit-resistance force factor would be

$$\begin{aligned} 6.12 \times 10^6 \simeq 25^\circ.3 \div \sqrt{86.7 \times 10^9 \angle 0^\circ} \\ = 6.12 \times 10^6 \simeq 25^\circ.3 \div 2.945 \times 10^5 \angle 0^\circ \\ = 20.8 \simeq 25^\circ.3 \end{aligned}$$

Similarly, from (149), the ratio  $p$  in a given instrument should vary inversely as the square root of the d.-c. resistance, or inversely as the number of turns in the winding. The equivalent number of turns  $N'$  should, by (145), be independent of the size of wire in the winding. The displacement resistance  $r'$ , by (82), should be



unaffected by the size of wire according to our theory. Consequently the mechanical efficiency at resonance,

$$\eta'_0 = \frac{r}{r''},$$

should be likewise unaffected. By the same reasoning, neither the gross efficiency at resonance,

$$\eta''_0 = \frac{R'_0}{R_1},$$

nor the net efficiency,  $\eta_0 = \eta'_0 \eta''_0$ , should be affected, to a first approximation, by changing the size of wire.

It may be observed from Fig. 48 that the gross efficiency at resonance tends to be increased by an increase in the lag angle  $\beta^\circ$ , other quantities remaining constant. The value of  $\beta^\circ$  is commonly in the neighborhood of  $30^\circ$ ; but it has been found to exceed  $54^\circ$  in at least one case. Cases have been reported in which the gross efficiency at resonance exceeds 1.0. The net efficiency cannot, of course, reach 1.0, even at resonance, and it usually falls off rapidly, as the resonant frequency is departed from. The motional-impedance circle, as we have already seen, always indicates apparent gross or resonance  $f_0''$ , as affected by the displacement force  $f_x$ , and gives a gross efficiency  $\eta_0''$ . The net values can only be found by reduction.

**Amplitude Measurer for Increased Precision.** — Figure 65 gives a plan, side elevation, and end elevation of an amplitude measurer of greater sensitiveness and precision than that obtainable with the instrument already described in connection with Figs. 61 and 62.

A light rectangular brass frame  $FF, F'F'$ , is pivoted on a vertical axis through steel points  $pp$ . A brass strap  $QQ$ , fastened across the frame, supports the brass stirrup by the clamp screw  $B$ . The tension on the phosphor-bronze strip  $rr$  (6.7 mm. long, 0.28 mm. wide, and 0.02 mm. thick) is capable of being adjusted by the screw  $C$ . This strip carries the triangular mirror  $m$ , about 0.7 mm. in length of edge, 0.15 mm. thick, and weighing about 0.7 mg. The receiver to be tested is not shown in Fig. 65, but screws  $W$  are indicated for securing the receiver on to the base, with its axis horizontal. The tip of the mirror  $m$  is presented to the diaphragm near the center and over a pole. It is brought into contact with the diaphragm by the use of the screw  $A$ , with 19 threads per cm. The index arm  $P$  moves over a circular scale, partly indicated in the side elevation, and divided to single degrees.

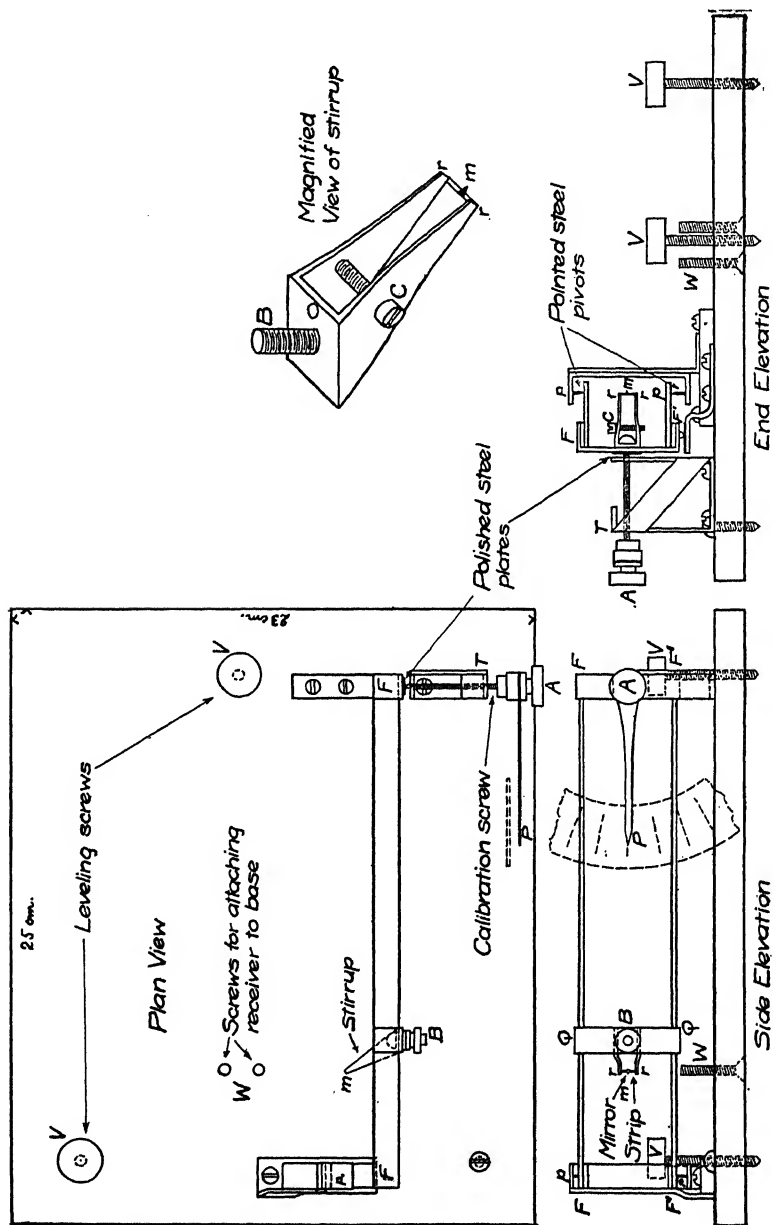
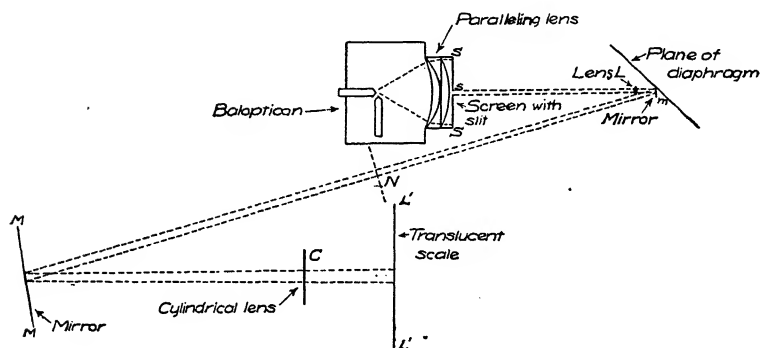


FIG. 65. Amplitude measurer for increased precision.

The optical system used with this improved amplitude measurer is seen in Fig. 66. It differs from that already described in connection with Fig. 12, by having a cylindrical lens  $C$  in the path of the reflected beam, near to the translucent scale  $L'L'$ , so as to collect the light into a relatively narrow line on that scale. When using the full optical system, a magnification factor of 25000 was obtainable; so that 1 micron range of diaphragm vibration produced 25 mm. length of luminous band on the scale  $L'L'$ . For less sensitive measurements, an opaque scale was inserted at  $N$ , reducing the magnification factor about three times.



Distance from slit to mirror  $m = 111.5$  cm.  
 Distance from mirror to scale  $= 57.5$  cm.  
 Distance from lens  $L$  (focal length 89.4 cm.) to mirror  $m = 5.8$  cm.  
 Distance from cylindrical lens  $C$  to scale  $= 59$  cm.  
 Cylindrical lens  $C$ : focal length 50.8 cm, length 20.4 cm, face 2.54 cm.  
 Width of slits 0.1 cm.  
 Distance from mirror  $m$  to scale  $N = 159$  cm.

FIG. 66. Optical system used with amplitude measurer.

**Summary.**— It has already been pointed out at the end of the last chapter, that there are various constants of a telephone receiver which can be determined directly from its motional-impedance circle, when the testing-current strength and the d.-c. resistance of the instrument are known. A list of those constants has been given in Table IX A on page 114. If, in addition, the maximum cyclic-vibration amplitude of the receiver diaphragm over one of the magnetic poles, at the frequency of apparent resonance,  $x_{m0}$ , is measured, also the total mass  $M$  of the diaphragm within the clamping circle, and the total number of turns  $N$  in the winding, the following additional constants of the instrument can be evaluated.

TABLE XI B

CONSTANTS OF A TELEPHONE RECEIVER OBTAINABLE FROM AMPLITUDE VIBRATION MEASUREMENTS AT RESONANCE IN ADDITION TO THE MOTIONAL-IMPEDANCE CIRCLE

SYMBOL	NAME OF CONSTANT	UNIT	DEFINING EQUATION IN TEXT
$A$	Vector force factor	{ abvolts/kine $\angle$ or dynes/abampere $\angle$	139
$r''$	Gross mechanical resistance of diaphragm	dynes/kine	140
$m$	Equivalent mass of diaphragm	gm.	141
$s''$	Gross elastic coefficient of diaphragm	dynes/cm.	142
$\mathcal{L}$	Mean vector inductance of winding	abhenries $\angle$	143
$p$	Displacement current turns ratio	abamperes/cm	144
$N'$	Equivalent displacement turns	numeric	145
$r'$	Mechanical resistance to displacement	dynes/kine	146
$r$	Net mechanical resistance of diaphragm	dynes/kine	147
$s$	Net elastic coefficient of diaphragm	dynes/cm	148
$\mathcal{B}_0$	Permanent mag. flux density in air gaps	gausses	149
$\mathcal{P}$	Vector permeance of mag. cct.	oersteds <sup>-1</sup>	77
$m/M$	Polar equivalent mass coefficient	numeric	26
$A/\sqrt{R_1}$	Unit resistance force factor	dynes abohms <sup>1/2</sup> / abvolts $\angle$	—

**Particular Case of Determining the Intrinsic Constants of a Receiver, from Measurements of  $\omega_0$ ,  $\Delta$ ,  $Z'_0$ ,  $x_{m0}$  and  $I_m$ .**—We may take the case of Bell receiver Type C, of Tables X and XI, pages 124 and 126, with the following observed data:— $\omega_0 = 6378$ ,  $\Delta = 149$ ,  $Z'_0 = 140 \times 10^9 \angle 50^\circ.6$ ,  $x_{m0} = 10.35 \times 10^{-4}$ , and  $I_m = 2.884 \times 10^{-4}$ . Then, by (139),

$$A = \frac{2.884 \times 10^{-4} \times 140 \times 10^9}{6378 \times 10.35 \times 10^{-4}} \angle 25^\circ.3 = 6.12 \times 10^6 \angle 25^\circ.3$$

By (140),

$$r'' = \frac{6.12^2 \times 10^{12}}{140 \times 10^9} = 268.$$

Next, by (141),

$$m = \frac{268}{2 \times 149} = 0.902$$

Finally, by (142),

$$s'' = 0.902 \times 6378^2 = 36.7 \times 10^6.$$

These values are found in the Tables.

## CHAPTER XI

### INFLUENCES THAT AFFECT THE CONSTANTS OF A RECEIVER

**Introduction.** — Among the influences which notably affect the constants of a telephone receiver are (1) the clamping of the cap or cover, (2) the temperature, (3) the air-chamber and the air within it.

**Variations in the Clamping of the Cap.** — Tests of receivers, made before and after a removal and replacement of the cap, were found, at times, to differ considerably. This led to an investigation of the influence of screwing on the cap with differing degrees of tightness. The caps were of the same molded composite material as the receiver cases. A lever-clamping device was designed and constructed, as shown in Fig. 67. It consists of a brass rod

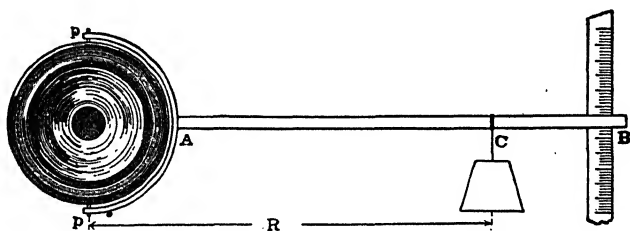


FIG. 67. Method of applying cap torque.

$AB$ , with a known sliding weight applied at a measured horizontal distance  $R$ . The rod terminates in a brass fork containing notches, which engage with pins  $PP$  screwed into the cover. The receiver is clamped by its case or shell in a horizontal position. The cap is then screwed on slackly, and the final screwing up is completed under the measured torque. The instrument is then tested for motional impedance under these conditions. The torque applied in each instance is expressed in gram-perpendicular-meters; i.e., in grams weight acting vertically at a horizontal radius arm of one meter. (See page 207.)

The effects of varying the screwing-on torque upon the motional-impedance circle are indicated in Fig. 68. The particular instru-

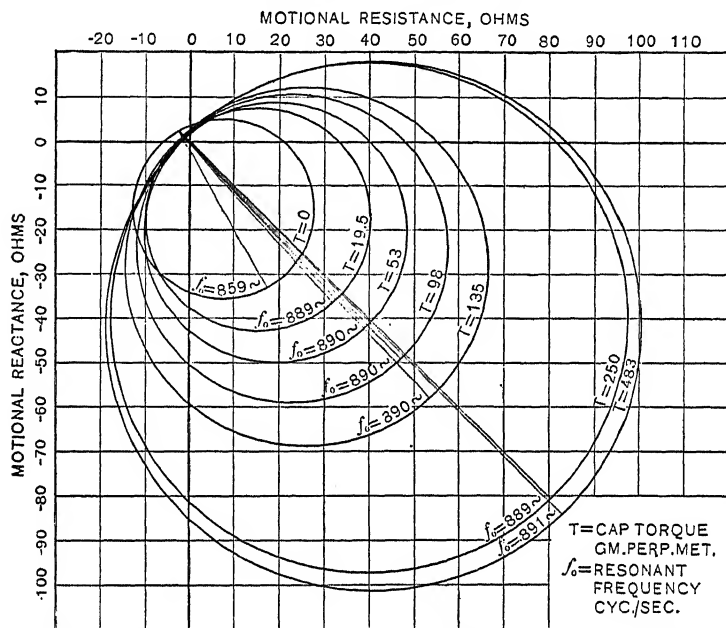


FIG. 68. Motional-impedance circles with different cap adjustments.

ment used in these tests was that designated as *B* in Table X, but with a different diaphragm from that employed in the tests of Table X. It will be seen that with zero torque, i.e., with the cap merely laid horizontally on the diaphragm, but not screwed, the motional-impedance circle has the smallest diameter, and is nested within the others. The resonant frequency of the diaphragm was 859 ~. As the screwing-on torque

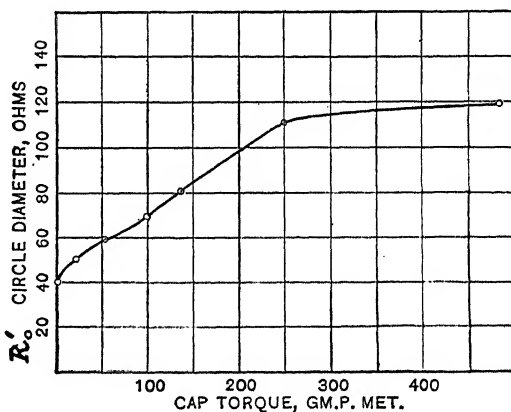


FIG. 69. Curve showing relation between motional-impedance circle diameter and cap torque.

was increased, the diameter  $R'_0$  of the motional-impedance circle (Fig. 69) is seen to increase, in nearly simple proportion, until a torque of 250 gm.-perp.-meters is attained. Beyond this torque, there is very little effect on the circle diameter. After the torque reached 250 gm.-p.-m., no appreciable effect is visible on the resonant frequency of this instrument. The size of  $Z'_0$ , the diametral motional impedance, is plotted in Fig. 69 against the screw-torque.

At the time these torque tests were made, the method of amplitude measurement had not been developed. Hence an exact determination of all four constants  $A$ ,  $m$ ,  $r''$ , and  $s''$  throughout this series is not possible. If, however, we assume that the equivalent mass  $m$ , and gross stiffness coefficient  $s''$  remained constant, since their ratio  $f_0^2$  remained constant, the only variables would have been  $A$  and  $r''$ , which are plotted in Fig. 70 against cap-torque.

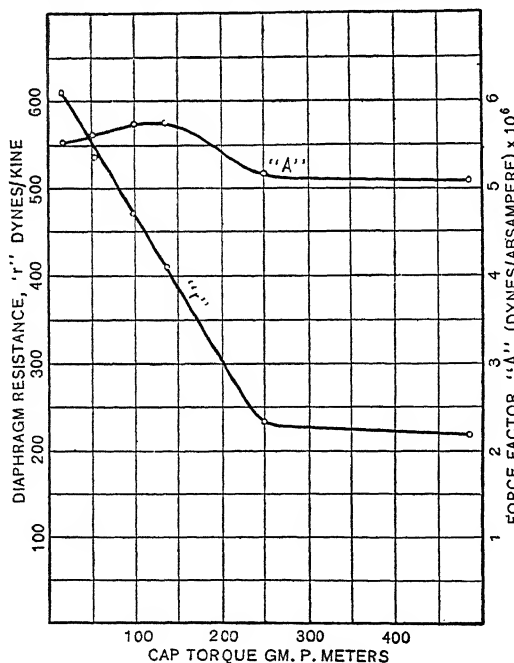


FIG. 70. Curves showing values of  $A$  and  $r''$  for different cap torques.

little reduction beyond this torque. It is supposed that this reduction occurred in the virtual displacement resistance  $r'$  rather than in the mechanical resistance  $r$ .

It will be seen that the value of the force factor  $A$  remained nearly unchanged throughout the series, varying only between 5.75 and 5.1 megadynes per abampere. The gross mechanical resistance  $r''$  of the diaphragm diminishes, however, considerably, and nearly in a straight line, from 600 dynes per kine at 20 gm.-p.-m., to 230 dynes per kine at 250 gm.-p.-m., with but

It was found that a noticeable effect of screwing on the cap tightly was to increase the air gap between the diaphragm and the poles. It is easy to understand that the permanent magnetic flux flexes the diaphragm towards the poles, when the diaphragm is laid on the lower clamping ring. The application of cap pressure, under the influence of screwing-on torque to the upper clamping ring, tends to flatten the diaphragm and to diminish the flexure, thus somewhat increasing the polar air gaps.

The increase in air gap accompanying increase in torque was measured, up to a certain point in the earlier part of the torque range, by the device shown in Fig. 71. Here the micrometer-head depth-gauge *D* is applied to the upper surface of the diaphragm from a temporary brass frame *FF* attached to the shell at *SS*.

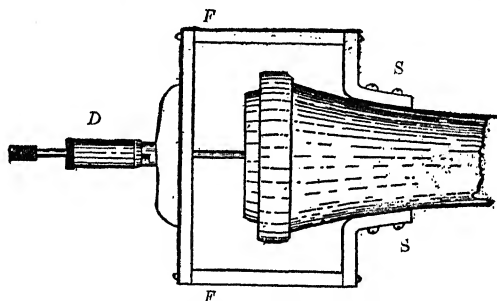


Fig. 71. Method of air gap measurement.

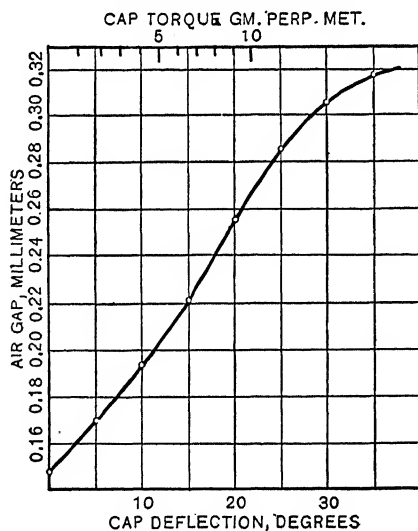


Fig. 72. Curve showing relation between air gap in receiver *B* and the cap adjustment.

As circular degrees of twist were given to the cap, the depth gauge showed that the center of the diaphragm moved slightly away from the poles. The precision of the method was not sufficient to enable the test to be carried over the whole range of screwing-on torque. The results are indicated in Fig. 72. They show that the air gap increased by 0.17 mm. as the torque increased from 0 to about 16 gm.-p.-m.; and roughly in simple proportion as far as 14 gm.-p.-m.

It seems reasonable to suppose that the virtual



displacement resistance  $r'$  might be increased when the polar air gap was reduced. At all events, the screw-on tests with this receiver indicate that the tightness of clamping may have a marked influence on its characteristic behavior and constants. It is desirable that a receiver should be tested with its cap screwed on tightly. In this instrument, the greatest  $Z'_0$  and resonant sensitiveness were attained with the greatest clamping torque and pressure tried.

**Effect of Variations in Temperature.** — In order to ascertain the influence of temperature upon the characteristics of a receiver, a large electric oven was used, in which the receiver was placed at a conveniently controlled temperature. A number of motional-impedance circles were observed, at oven temperatures from 16° C. to 50° C., all other conditions being maintained constant. It was found that two effects were produced with rise of temperature, namely:

(1) A reduction in resonant frequency, amounting to about 2.5 cycles per second, per degree C. rise.

(2) A slight reduction in circle diameter, which, however, was not always noticed.

TABLE XII  
TEMPERATURE EFFECT ON RECEIVER CHARACTERISTICS

	SERIES A		SERIES B			SERIES C		
Condition of Cap Adjustment	Tight	Tight	Loose	Loose	Loose	Tight	Tight	Tight
Temperature deg. C. . . . .	19°·3	47°·0	16°·0	46°·0	31°·5	51°·0	36°·0	22°·0
Resonant Frequency cyc/sec. $f_0$ . . . . .	886·7	834·9	827	742	788	817·3	852·5	867·5
Resonant Ang. Vel. rad/sec. $\omega_0$	5575	5248	5200	4666	4956	5140	5360	5450
Motional Impedance circle diam. ohms $R'_0$ .	88·2	72·0	52·0	48·0	45·5	70·5	70·0	71·0

The results obtained are given in Table XII. They are given in the sequence of observation.

The reasons for the effects of temperature on the receiver characteristics indicated above have not been analyzed. They might be attributed to temperature changes in the mechanical elasticity constants of the diaphragm, or to expansional effects in the structure, or to both causes.

It is evident, therefore, that the influence of temperature on a telephone receiver's characteristics may be very appreciable. Care should be taken to maintain the temperature of the instrument constant during any set of observations. With this object in view, it was customary to conduct the tests with the instrument inside the large closed oven, but with the heat shut off.

**Effects of Variations in Air-chamber between Diaphragm and Cap.** — In order to ascertain the influence of the air-chamber over the diaphragm of the ordinary receiver, a special cap was used, in which the air-chamber could be varied by altering the position of a friction-tight cylindrical plug, of the same diameter as the clamping circle. Motional-impedance circles were observed under these conditions, with the results given in the following table.

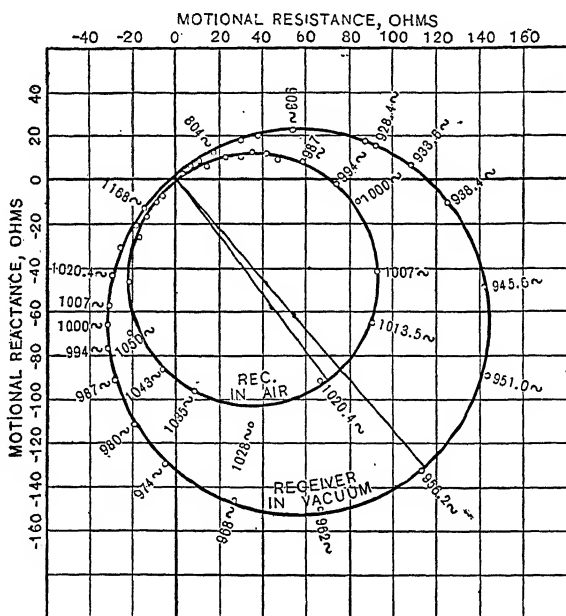
TABLE XIII

MOTIONAL-IMPEDANCE CIRCLES WITH CHANGES IN CAP AIR-CHAMBER

AIR-CHAMBER THICKNESS	CIRCLE-DIAMETER OHMS	RESONANT FREQUENCY CYCLES PER SEC.
Normal, 0.5 mm.	139	872
Large, 5 mm.	150	892
Infinite, Plug Removed	155	927

The effect of a shallow air-chamber over the diaphragm, as compared with an open diaphragm, was to lower the resonant frequency slightly, and to reduce the circle diameter. The effects upon the four fundamental constants of the instrument were not analyzed. The effect was evidently to alter somewhat the ratio of  $s/m$  and to increase the value of  $r''$ . That is to say, the gross resistance  $r''$ , with open diaphragm, was apparently increased about 10 per cent, when the ordinary shallow air-chamber was provided with the narrow central circular orifice. This does not necessarily mean, however, that the amplitude at the center was less with the cover on than with the cover withdrawn. It would be interesting to make further investigations along this line.

**Effects of the Atmosphere and Atmospheric Pressure.**—In order to ascertain the influence of the ordinary atmospheric pressure upon the characteristics of a receiver diaphragm, the bipolar receiver *C* was suspended in the glass bell jar of an air pump, the two wires to the receiver being carried through a seal at the top of the jar. One motional-impedance circle was then obtained with full atmospheric pressure in the ordinary way, and another after the pressure had been reduced by the pump to about 1 cm.



the same in both tests, the results of Table XIV are found. The removal of air pressure apparently reduced  $s$  from  $37 \times 10^6$  to  $32.5 \times 10^6$ . The force factor  $A$  being the same in both tests, the gross resistance  $r''$  fell from 317.5 in air to 216.5 in vacuo, a reduction of 101, or 31.8 per cent. It is supposed that nearly all of this change occurred in the net resistance  $r$ , and that but little change occurred in the virtual displacement resistance  $r'$ .

TABLE XIV  
THE EFFECT OF THE ATMOSPHERIC PRESSURE ON RECEIVER CHARACTERISTICS  
Receiver C. (Affel)

Condition of Receiver	In Vacuo	In Air
Temperature, deg. Cent. . . . .	18.5°	18.5°
Current, abamperes. rms. $I$ . . . . .	0.000 05	0.000 05
Resonant Frequency, cyc/sec. $f_0$ . . . . .	956	1020
Resonant Ang. Velocity, rad/sec. $\omega_0$ . . . . .	6007	6409
Impedance Circle Diam. ohms $R'_0$ . . . . .	177	116
Decrement per sec. $\Delta$ . . . . .	120	176
Equivalent mass gm. $m$ . . . . .	0.902	0.902
Equivalent Elasticity, dynes/cm. $s''$ . . . . .	$32.5 \times 10^6$	$37.0 \times 10^6$
Equivalent Resistance, dynes/kine. $r''$ . . . . .	216.5	317.5
Resistance due to Air, dynes/kine. . . . .	101	
= 31.8% of total resistance		

If all of the change occurred in  $r$ , it would appear that the mechanical output into acoustic power was 101  $\hat{x}^2$  abwatts. Part of this would be delivered to the air chamber below the diaphragm, and only the remainder to the air above the diaphragm. The subject of the share of mechanical output  $\hat{x}^2 r$  that takes the acoustic form requires further investigation.

At frequencies near resonance, the Rayleigh bridge balance becomes in this test very sensitive to variations of atmospheric pressure within the air-pump bell jar. From an examination of the balance at these frequencies, it was easy to ascertain, without consulting the air-pressure gauge, whether air was leaking into the exhausted bell jar. It seems likely, therefore, that variations of barometric pressure, within the normal range, might produce perceptible changes in the free impedance of the receiver near resonance. In other words, a motional-impedance circle should, for precision, be accompanied by a record of not only the ambient atmospheric temperature, but also the atmospheric pressure. In this case, there was an average change of not far from one ohm, (0.81 ohm.) of diametral motional impedance, for each centimeter of change in mercury column of barometric pressure.

## CHAPTER XII

### SECONDARY DISTORTIONS OF MOTIONAL-IMPEDANCE CIRCLES

**Introduction.** — In finding the motional-impedance circles of receivers, it happens occasionally that internal loops or internal circles present themselves as distortions of the diagram. The engineering research department of the Western Electric Company seems first to have discovered such cases, in 1913. They were first noticed in the laboratories of the Massachusetts Institute of Technology, in 1915. Distorted diagrams of this sort appear in Figs. 75 to 84.

At first, these distorted circle diagrams presented themselves in but a small percentage of the motional-impedance diagrams investigated. They were looked upon as curiosities of unknown origin, and were set aside as unguessed riddles. This was before the method of amplitude measurement described in Chapter X had been devised.

Later, in the researches described by this book, these parasitic loops began to present themselves more frequently. At one period, more diagrams were developed with internal loops than without them. It became necessary to study them as a pathology of the normal motional-impedance circle. For a long time, these parasitic abnormalities baffled inquiry, but finally their origin was brought to light. It was found possible to produce them artificially, at will. Although a large field for further investigation lies here unexplored, it is now fairly well established that these parasitic loops in the circle are due to the presence of secondary vibrational systems, mechanically connected to, and forming a part of, the primary diaphragm system. The secondary system, whatever may be its geometric and physical nature, has its own  $r$ ,  $m$ , and  $s$ , and therefore its own  $\omega_0$ ,  $\hat{x}_0$ , and  $x_{m0}$ . It receives its vibrational energy from the primary system, and since the motional impedance of the primary system is measured, the diagram indicates the modifications which are superposed thereon by the

secondary system. Ordinarily, these secondary superposed modifications are very small, except in the vicinity of secondary resonance. An outline theory will be presented in this Chapter, based on the experimental facts of these internal loop distortions. This

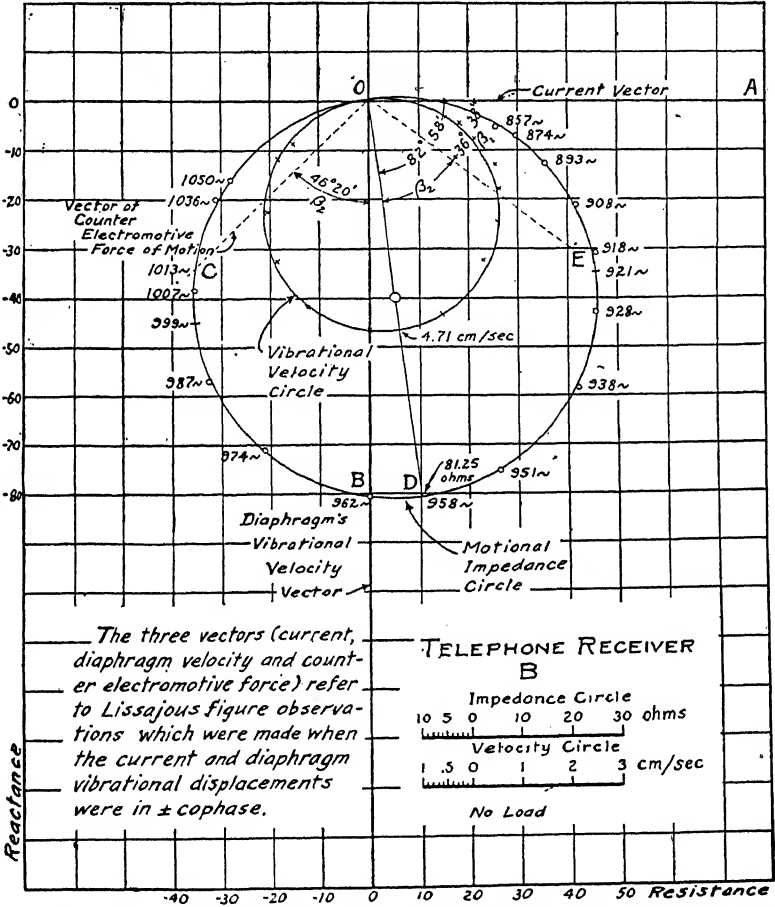


Fig. 74. Undistorted circles of motional impedance and velocity.

theory is closely connected with the theory of coupled circuits, with which students of electricity are already familiar. Much remains to be done, however, both experimentally and analytically, before the theory can be regarded as completely established.

Figure 74 is a motional-impedance graph *OEDBC* from measurements taken by Dr. Taylor on receiver *B*, of Table X, already

mentioned, some months after the measurements in Table X were made. The diaphragm used in connection with Fig. 74 was not the same as that specified in Table X. The inner circle in Fig. 74 is a vibrational velocity circle of  $\dot{x}$ , deduced from measurements of the central amplitude of the diaphragm, with the aid of the amplitude-measurer of Fig. 62. As has already been pointed out, the maximum cyclic velocity locus is a circle, like the motional impedance, although these two quantities  $\dot{x}$  and  $Z'$  are, as we have seen, dephased by  $\beta^\circ$ .

It will be noticed that the motional-impedance graph *OEDBC*, Fig. 74, is a smooth circle, all the observation points falling nicely upon its circumference. Nevertheless, there is reason to believe that this graph actually contains a small inner loop distortion, between the origin *O* and the lowest indicated frequency of  $857 \sim$ . No measurements were made in this instance below  $857 \sim$ , and had they been made, it is probable that the expected distortion loop would have been almost too small to notice, without careful search for it.

When the diaphragm of receiver *B*, as used in the test of Fig. 74, was loaded at its center by fastening to it a small copper washer, about 1 cm. in diameter and weighing 0.73 gm., a repetition of the test gave the motional-impedance graph shown in Fig. 75, the data from which are as follows:

$$Z'_0 = 92.5 \angle 76^\circ.6, \quad f_0 = 794.5 \sim, \quad \Delta = 141, \quad A = 7.18 \times 10^6 \angle 38^\circ.3, \\ m = 1.95, \quad r'' = 551, \quad s'' = 48.6 \times 10^6.$$

The graph shows two internal loops or abnormalities, one a little loop near  $691.9 \sim$ , well defined, however, by numerous observations, and the other a larger loop near  $789.5 \sim$ . The latter proved to be a casual and evanescent visitor. Since it did not appear in the subsequent tests to be described forthwith, it may be left out of consideration here. It suffices, therefore, to notice that the loop at  $691.9 \sim$  had an inwardly projecting radial length of about 2.5 ohms, and occurs in the circle at an arc distance of about  $30^\circ$  from the origin *O*. The load on the diaphragm has reduced its resonant frequency from  $958 \sim$  in Fig. 74, to  $794.5 \sim$  in Fig. 75.

The central load on the diaphragm was next increased from 0.73 to 0.975 gm. This had the effect of bringing the resonant frequency down to  $699.4 \sim$ , or close to the frequency at which the abnormality of Fig. 75 appeared ( $691.9 \sim$ ). The result of a new

motional-impedance graph under these conditions is shown in Fig. 76. The distortion loop is now central at  $697.2 \sim$ , and has a radial length of 42.5 ohms on the motional-impedance scale. It is evident that when the diaphragm is brought nearly into resonance

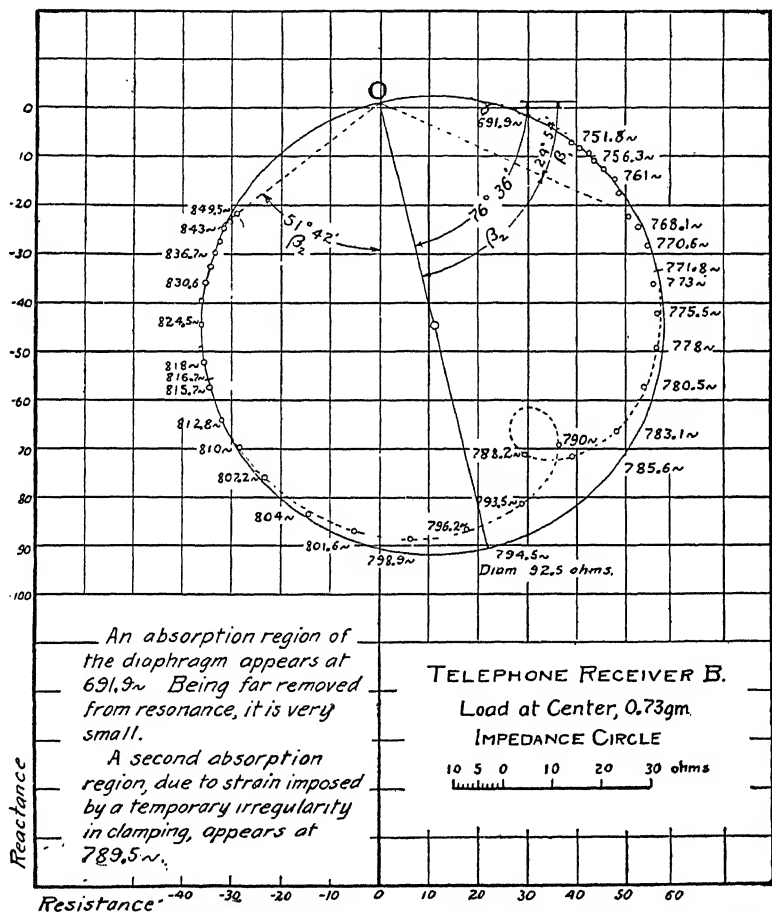


FIG. 75. Distorted motional-impedance circle. Small distortion, rising on the right.

with the frequency of the distortion loop, the magnitude of the distortion loop is greatly enlarged, and it is brought into a nearly diametral position. By drawing in the circumference of the circle, as it would appear in the absence of distortion, and marking on it the computed positions of the various observed frequencies, it is



seen that the chords, or vector differences, between the distorted and undistorted points of the same frequency, give rise to the roughly circular, or lily-pad locus  $a' b' c' d' \dots h'$ , when referred to the origin  $O$ . This showed that, at least to a first approxima-

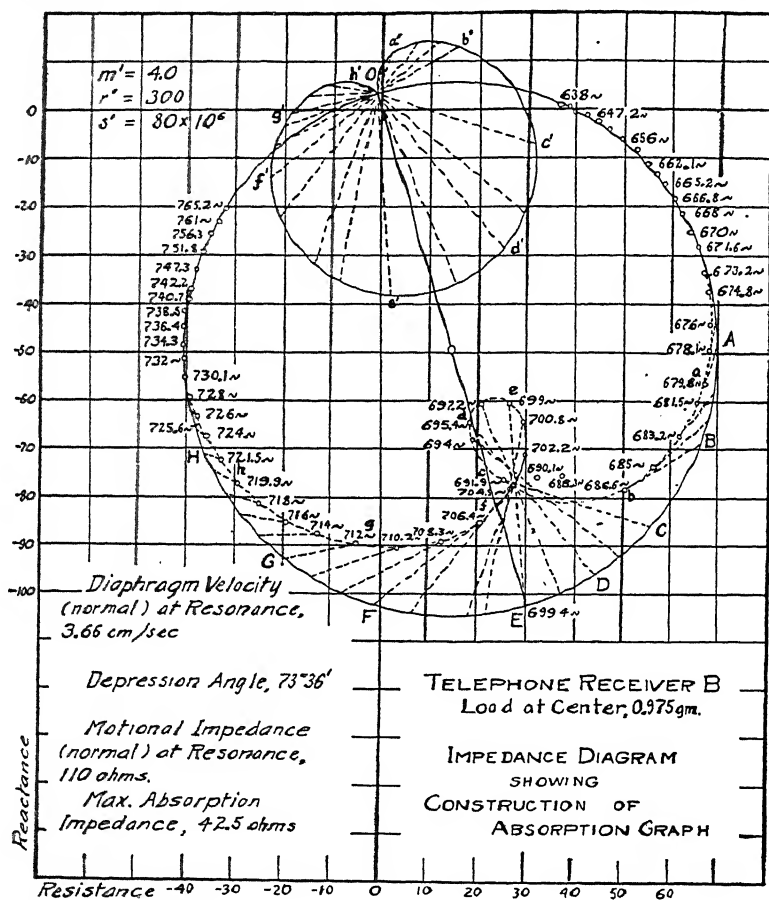


FIG. 76. Distorted motional-impedance circle. Distortion nearly central on main diameter.

tion, the distortion consists of a negative or absorption circle, of the same general character as the main motional-impedance circle, but which is swept over by the radius vector much more rapidly. The hypothetical constants  $A$ ,  $m$ ,  $r$ , and  $s$  of this absorption circle were capable of being roughly determined. These conclusions

were supported by various other distorted motional-impedance graphs not shown here.

By still further increasing the load at the center of the diaphragm to 1.3 gm., and thus bringing the resonant frequency  $f_0$

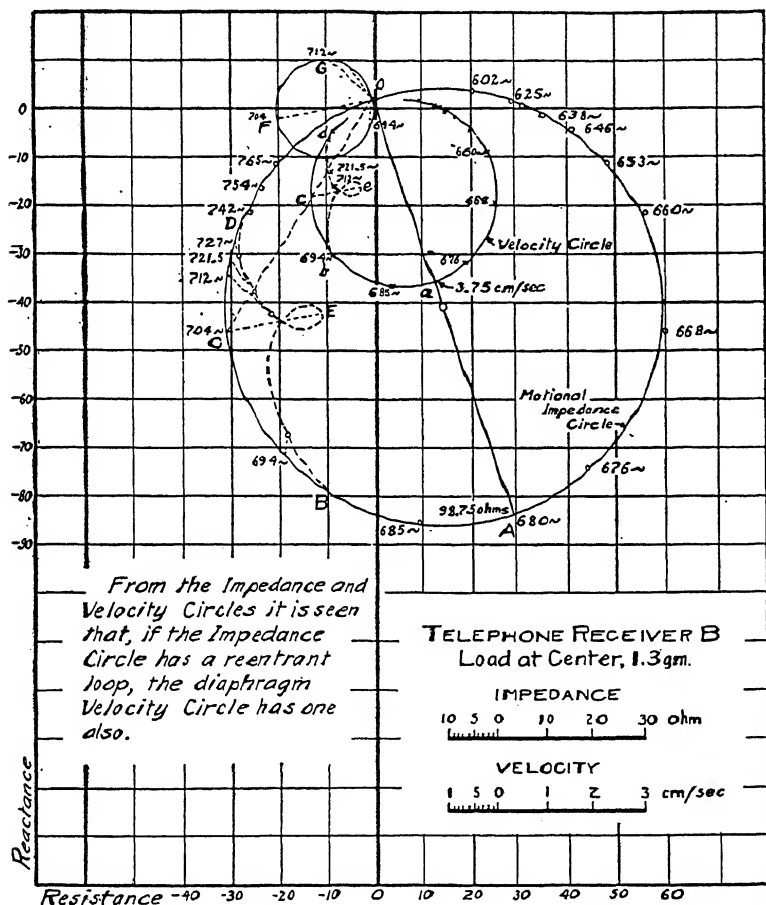


Fig. 77. Distorted impedance and velocity circles. Distortion loop setting in the left.

down to 680 ~, or below that of the distortion loop, the next test, represented in Fig. 77, showed that the distortion loop, central at 704 ~, has moved over to the left-hand side of the diameter  $OA$ , and has diminished in radial length to about  $OF = EC = 17$  ohms. The central amplitudes  $x_m$  of diaphragm vibration were

also measured in this instance, and from them the inner circle of vibrational velocity  $Oabcd$  has been deduced. This also shows the same distortion at  $c$ . The corresponding distortional motional-impedance graph of vector differences  $OFG$  is indicated. It is approximately circular. It may be noticed that the angle  $FOC$  is roughly equal to the angle  $COA$ , or that the vector  $OC$ , at which the distortion is central, approximately bisects the angle  $AOF$ , between the diameters of the main and absorption circles.

Finally, the load at the center of the diaphragm was slightly lowered (to 1.2 gm.). This brought the resonant frequency a little nearer to the distortion frequency. The loop  $CE$ , Fig. 78, is now a little larger,  $OF = CE = 21.5$  ohms, and it is brought back a little nearer to the main diameter  $OA$ . Incidentally, a small new and transient distortion makes its appearance at  $H$ .

This series of tests, and others like them, show that one and the same distortional disturbance in a motional-impedance circle, resident near  $700 \sim$ , was made to appear, by suitable adjustments of the main diaphragm resonant frequency  $f_0$ , first as a small loop on the upper right-hand side, then as a greatly magnified loop at or near the main diameter, and finally as a small loop on the upper left-hand side. The absorption graphs are roughly circular, and the vector to the undistorted position of the distortion frequency approximately bisects the angle between the diameters of the two circles.

After a time it was noticed that whenever the distortion near  $700 \sim$  manifested itself in the motional-impedance diaphragm, the amplitude measurer of Fig. 62 was mounted on the instrument, ready for use in determining the central amplitude  $x_m$ . This led to the suspicion that the two clamping screws  $SS$ , in the brass frame  $F$ , might be responsible for the abnormality. On actual trial, the removal of the screws  $SS$  was found to remove the distortion, which could be revived by the reapplication of the screw pressure. It thus became evident that the application of diametral clamping pressure to the composition cap of the receiver warped it slightly, and interfered with the uniformity of boundary vibration around the clamping circle. It is supposed that the diaphragm, under the diametral clamping, develops a secondary vibrational system, having its resonance at or near  $700 \sim$ , although the mechanism by which this hypothetical secondary system is developed has not been explained.

According to this view, it should only be necessary to attach to a properly clamped receiver diaphragm a secondary vibrational system, with its own  $r$ ,  $m$ , and  $s$ , to simulate the localized distortional behavior of an irregularly clamped diaphragm.

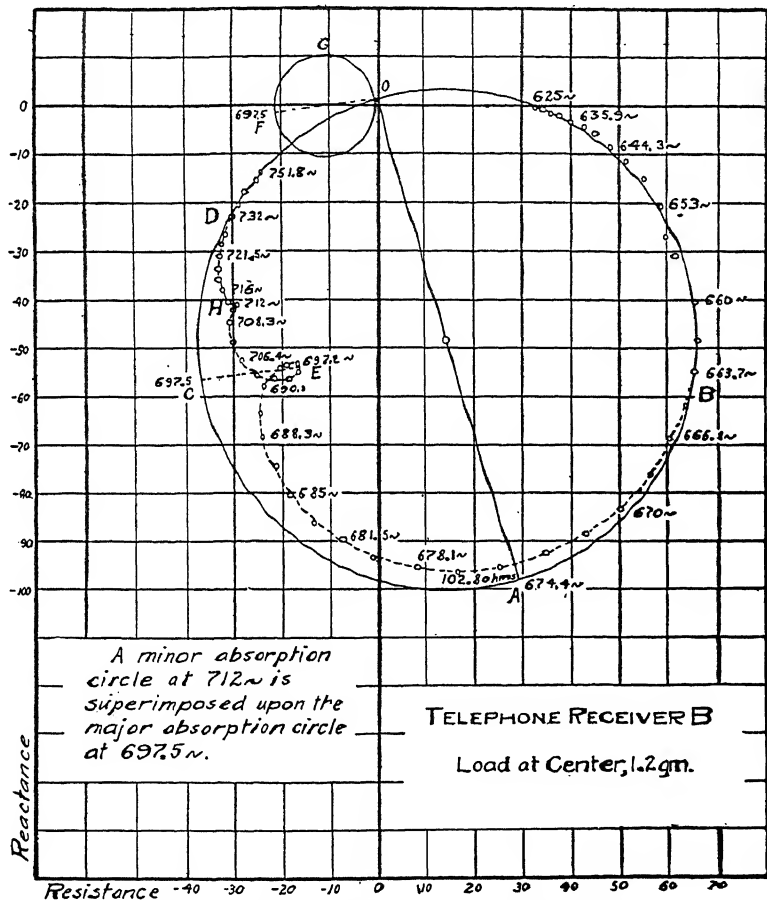


FIG. 78. Doubly distorted motional-impedance circle.

With this object in view, a small piece of bent hard copper strip was fastened by sealing wax to the center of the diaphragm of the same receiver, as shown to scale in Fig. 79. The weight of this spring was 0.6 gm. in all, of which the freely projecting portion weighed only 0.2 gm. The free frequency of this spring, when

mounted on the diaphragm, was adjusted, by trial, to approximately  $750 \sim$ , which is nearly the same as the resonant frequency  $f_0$  of the diaphragm thus loaded. Figure 80 shows the motional-impedance diagram of the receiver ( $B$ ), with the diaphragm and spring load. It will be seen to consist of a large reëntrant loop almost forming a pair of linked circles. From  $O$  to  $660 \sim$ , and

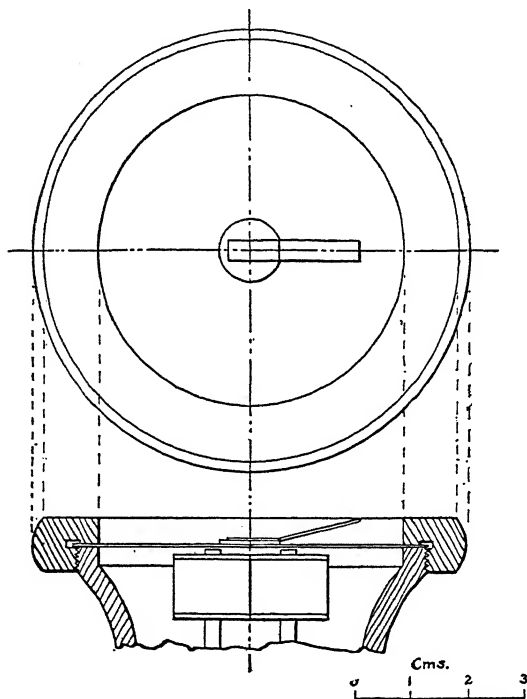


FIG. 79. Plan and longitudinal section of the test receiver with secondary vibrational system attached to center of diaphragm.

from  $866 \sim$  back to  $O$ , the diagram corresponds very closely to a single circle, which is  $ODAC$ , the supposed undistorted circle. At  $753 \sim$ , the actual amplitude  $OB$  is only about 4 per cent of the inferred undistorted diameter  $OA$ . The receiver in this test was practically quiet at  $753 \sim$ , but gave one loud tone in the neighborhood of  $675 \sim$ , and another loud tone in the neighborhood of  $840 \sim$ . It is evident that, in this case, the parasitic distortion is so great that the form of the motional-impedance diagram is completely changed. There are now two maximum motional

impedances, one near  $676 \sim$  and the other near  $840 \sim$ . Nearly midway between these, the motional impedance almost vanishes at  $OB$ .

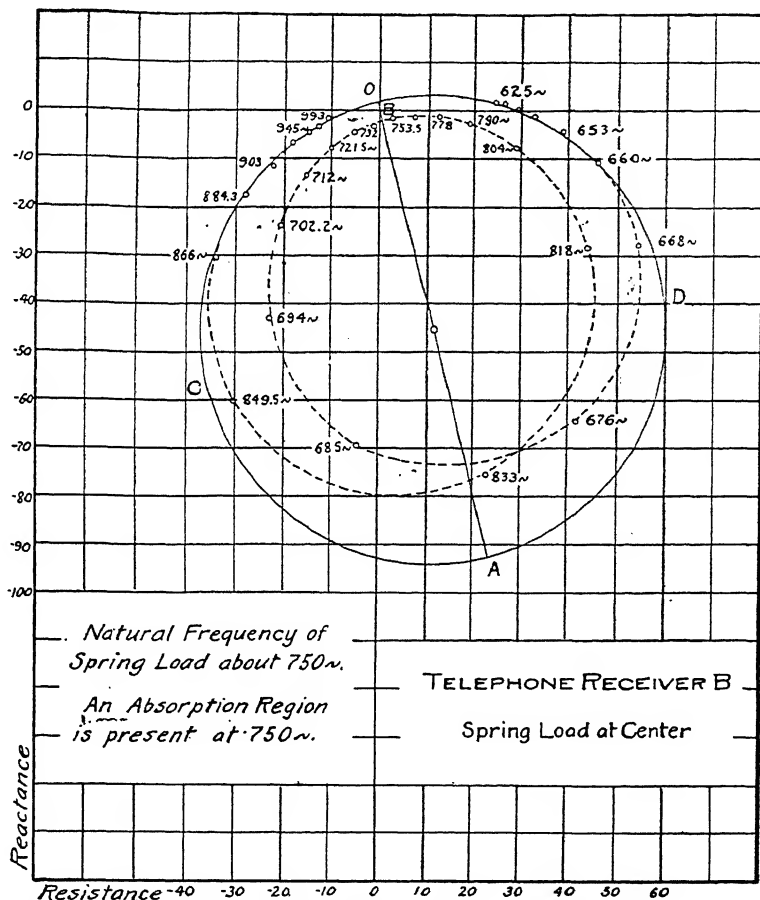


FIG. 80. Distorted motional-impedance diagram. Large distortion loop.

The amplitudes of vibration of the spring-loaded diaphragm of Fig. 79, as deduced from the motional-impedance diagram, Fig. 80, are represented as ordinates, in microns, against frequencies as abscissas, in Fig. 81. It will be seen that the amplitude almost vanishes at  $753 \sim$ , which is approximately the resonant frequency

of the undistorted circle  $ODAC$ , Fig. 80. The broken line  $ABCDE$ , Fig. 81, is the inferred maximum cyclic-amplitude curve of the undistorted diagram, and the double-humped heavy curve is the distorted amplitude curve. The peak at the lower frequency of apparent resonance  $678 \sim$ , is higher than the peak at the higher frequency  $838 \sim$ .

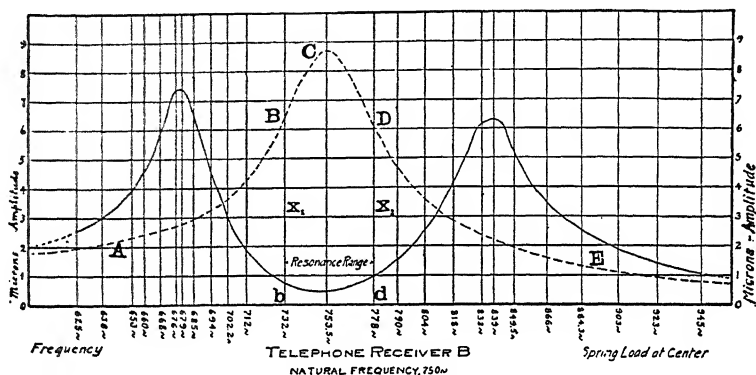


FIG. 81. Relative vibration amplitudes of diaphragm with spring attached.

This peculiar property of a tuned spring-loaded diaphragm to be silent at a selected frequency, but to sound loudly at a relatively small departure from that frequency on either side, may have useful applications.

The natural frequency of the spring load was then altered to about  $913 \sim$ , leaving the natural frequency  $f_0$  of the diaphragm at  $712 \sim$ , a little below its preceding value. The effect of this change on the motional impedance diagram is shown in Fig. 82. Here the distortion loop is reduced in diameter nearly one half, and it has moved to the upper left-hand side of the diagram. At  $712 \sim$ , the resonant frequency of the diaphragm, there is no appreciable disturbance due to the presence of the secondary system. The distortion is confined, for practical purposes, to that portion of the diagram which lies between  $753.5 \sim$  and  $968 \sim$ .

By lowering a little more the resonant frequency  $f_0$  of the diaphragm to  $698 \sim$ , leaving the secondary system unchanged, the distortion loop was brought still higher on the left-hand side and its diameter further reduced.

It is evident that, in order to develop an internal secondary loop,

the secondary vibrational system must be free and independent of the primary, depending only on the latter for its supply of power. Thus, on several occasions, a receiver diaphragm has been coupled to a second and parallel diaphragm, by a rigid aluminum

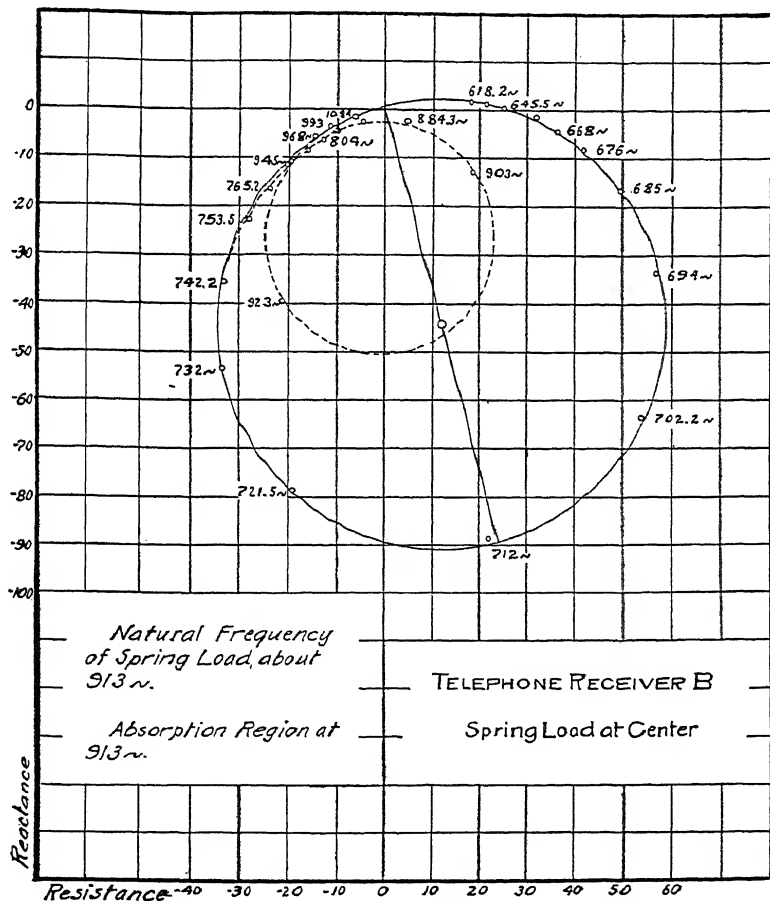


FIG. 82. Distorted impedance circle. Spring load out of tune with diaphragm.

bar, say 6 cm. long and 2 mm. in diameter, connecting their centers. The former diaphragm was clamped in the tested receiver, and the latter in, say, the vibration explorer. Under these conditions, the double-diaphragm combination gave an undistorted motional-impedance circle, corresponding to the  $m$ ,  $r$ , and  $s$



of the composite system. It appears then that when two or more diaphragms, suitably clamped and supported, are rigidly connected at their centers, they have only one degree of freedom, and will be

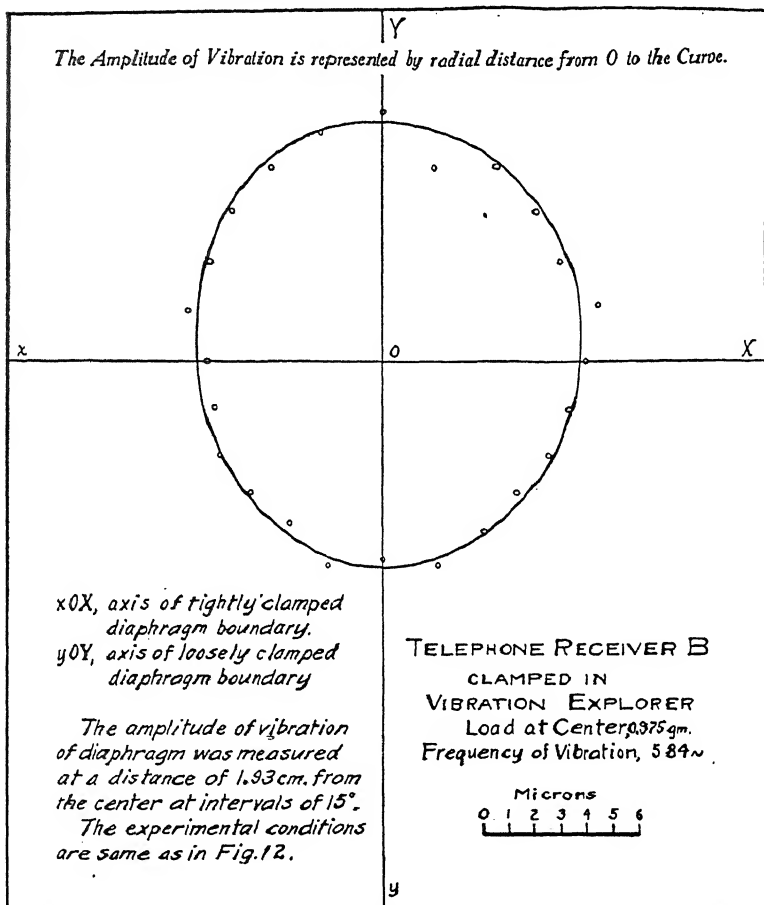


FIG. 83. Amplitudes of vibration around imperfectly clamped diaphragm.

unable of themselves to produce a distorted motional-impedance circle.

In order to ascertain what change in the distribution of vibrational amplitudes might occur in a diaphragm clamped tightly across one diameter, and only loosely over the rest of its circumference, the same receiver *B* was mounted in the vibration explorer

of Figs. 7, 8, and 9. These figures indicate that the diaphragm is there supported under a metallic clamping ring, which is attached to the main frame by four machine screws. Two of these screws, diametrically opposite to each other, were removed, leaving the diaphragm clamped under opposite points only, thus simulating the effects of the clamping screws *S, S*, Fig. 62. The diaphragm had a central load of 0.975 gm., and its resonant frequency was approximately 584  $\sim$ . The impressed frequency was held at this value with an a.-c. testing-current strength of 2.26 milliamperes through the instrument. The amplitude of vibration was then measured at 24 angularly equidistant points, 15° apart, on a circle 3.86 cm. in diameter, concentric with the clamping ring, whose diameter was 5.24 cm. The results obtained are shown geometrically in Fig. 83. Here the axis of the tightly clamped boundary is horizontal with the lines of text, and the axis of the loosely clamped boundary is vertical. It will be seen that the average amplitude on the loose axis was about 9 microns; whereas on the tight axis it was about 7.6 microns, so that the amplitude was about 18 per cent greater on the loose axis, with intermediate values in the intervening directions. This again indicates the importance of securing uniformly tight clamping around the boundary of a telephone-receiver diaphragm, in order to secure a uniform radial distribution of vibration.

The motional-impedance diagram for this case is given in Fig. 84. No localized distortion loop is visible, but there is a general shrinkage of impedance, and therefore also of diaphragm velocity, over a considerable range of the diagram (559  $\sim$  to 618  $\sim$ ). No distortion loop was obtained at any time in the tests with the vibration explorer of Figs. 7, 8, and 9. For some reason, the conditions in its use did not favor the development of a secondary free vibration system, perhaps because the cap or cover was metallic, and not of composition material.

**Summary.** — Summing up the experimental facts, therefore, two kinds of distortion, due to abnormal vibration, were found in the tests and development of motional-impedance circles. Both were due to imperfections in the clamping of the diaphragm. One is due to an asymmetry of clamping, without the development of a secondary free vibrational system. This gave rise to a flattened motional-impedance diagram, without internal loops. The other, also due to asymmetric clamping, happened to develop in

some way a secondary free vibrational system. This gave rise to internal loops and a roughly circular secondary absorption diagram.

**Torsional-Pendulum Model for Illustrating Motional-Velocity Phenomena.** — A psychological obstacle to the use of the motional-

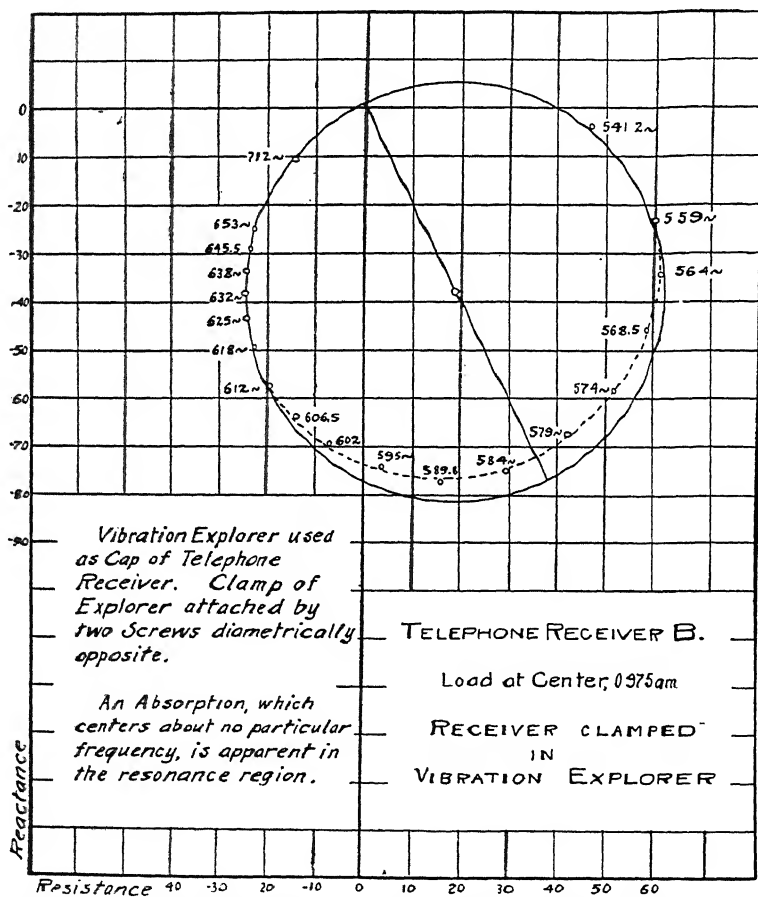


FIG. 84. Distorted impedance circle of imperfectly clamped diaphragm, with unlocalized distortion.

velocity circle conceptions is their abstract quality, and their remoteness from concrete apprehension. Thus, in the case of the telephone receiver, its motional-velocity circle is obtained through the medium of the motional-impedance circle, as determined from electrical measurements. It is therefore a great advantage to be

able to construct a motional-velocity circle from direct observations on a simple dynamical model.

A useful and very simple dynamical model for illustrating the conditions of diaphragm vibration and the resulting motional-impedance circle has been designed and constructed by Dr. Taylor. It is indicated in Fig. 85. It consists of a hollow brass cylinder  $K_0$  which, in the particular model used, has a mass of 1215 gm., a radius of gyration of 2.48 cm., and a moment of inertia of 7470 gm.-cm<sup>2</sup>. This is suspended by a brass wire of diameter 0.76 mm.

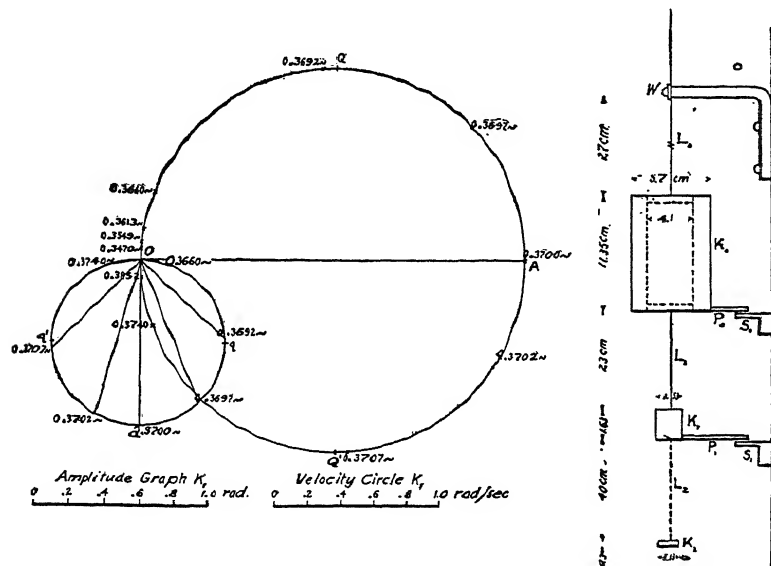


FIG. 85. Multiple coupled torsion pendulum model, with its velocity and amplitude graphs.

of a length adjustable, by means of a clamping screw  $W$ , between 10 and 40 cm., with a corresponding oscillation frequency range of 0.6 to 0.3  $\sim$ . The logarithmic decrement being very small, it oscillates about the suspension-wire axis with but little diminution of amplitude for several minutes. In the model used, the time constant  $\tau_0$ , or the time of fall to  $1/e$ th amplitude, is 216 seconds. This driving cylinder takes the place of the a.-c. generator in the case of the telephone. The smaller solid brass cylinder  $K_1$  has a mass of 26.8 gm. and a moment of inertia of 8.4 gm.-cm<sup>2</sup>. It is suspended from the driving cylinder by a smaller wire of copper whose length is usually kept constant at 23 cm., and whose diame-

ter is 0.13 mm. This driven cylinder corresponds to the telephone diaphragm, and performs oscillations of the period impressed on it by  $K_0$ . The driving cylinder  $K_0$  is so much larger than the driven cylinder  $K_1$ , that the reaction of the latter is insignificant. With  $K_0$  and  $K_1$  in action, the principal dynamic phenomena of the telephone diaphragm, and its velocity circle, can be observed, the frequency impressed by  $K_0$  being adjusted by successive steps through a considerable range, by shortening up the main suspension wire  $L_0$ . As the impressed frequency overtakes and passes the natural frequency of  $K_1$ , with its suspension  $L_1$ , the phenomena in the vicinity of resonance are reproduced. The  $K_1$  system has its  $m$ ,  $r$ , and  $s$ , substantially in the same manner as the systems described in this and other Chapters.

**Technique of Model.** — In operating the model, the cylinder  $K_0$  is first set by hand, in torsional oscillation about the suspension-wire axis, with the lowest frequency of longest suspension  $L_0$ , and with as little side swing as possible. The initial angular amplitude of  $K_0$  may be made  $90^\circ$  or more. After a few oscillations, the coupled pendulum system settles down to a substantially steady state, the oscillations of  $K_1$  having the same frequency as those of  $K_0$ . The oscillations are allowed to subside naturally under the damping constant ( $\Delta = 0.00462$  hypos per second) until a convenient standard amplitude is reached, as is indicated by a pointer  $P_0$ , upon a suitably supported angular scale  $S_0$ . When this happens, the eye of the observer at  $O$  can observe also the angular amplitude of  $K_1$ , as well as the angular phase-difference of the two elongations at  $P_0S_0$  and  $P_1S_1$ . The decay of amplitude is so slow that these conditions repeat themselves very closely for several oscillations above and below the standard amplitude of  $K_0$ , so that the observations can be repeated at several successive oscillations to obtain an average.

The oscillation frequency of  $K_0$  is then increased in small successive steps, by shortening up the suspension  $L_0$ , and the observations mentioned above are repeated at each step. The amplitude of oscillation of  $K_1$  increases rapidly as resonance is approached. In the model used, the resonant sharpness is  $\Lambda_0 = 503$ , but this can be controlled at will, by applying any motional resistance to  $K_1$  which is substantially proportional to the velocity. Figure 85 gives the angular-amplitude and angular-velocity circles for the model. It is seen that the semicircular range of resonant frequency,

as computed from the circle diagram, is between  $0.3692 \sim$  at  $f_1$  and  $0.3707 \sim$  at  $f_2$ . For impressed frequencies below this range, the oscillation of  $K_1$  comes nearly into cophase with  $K_0$ . On the other hand, at impressed frequencies above this range, the amplitude of  $K_1$  comes nearly into opposite phase with  $K_0$ . At resonance, the oscillation of  $K_1$  is in quadrature with the amplitude of  $K_0$ ; or the angular velocity of  $K_1$  will be in cophase  $OA$  with the vector torsional torque or vibromotive torque (vmt.) exerted by the wire on  $K_1$ . This vmt. is proportional to the angular displacement between the ends of  $L_1$ , and the observations obtained must be corrected to constant maximum cyclic vmt.

A student working with the model in the manner described above, can acquire a concrete conception of a motional-velocity circle, based upon direct observations of oscillations executed so leisurely that they are easily observed directly by the eye, without the use of reflecting mirrors or of electric apparatus. Moreover, the oscillations are sufficiently large to be perceived directly by a large class. When  $K_1$  oscillates in air, the motional resistance  $r$  seems to increase somewhat with the amplitude. When  $K_1$  was allowed to oscillate in water, the motional resistance was found to be more nearly constant.

When it is desired to study the phenomena of absorption, a secondary torsion pendulum  $L_2K_2$  is attached to  $K_1$ . It is then convenient to adjust the natural frequency of the secondary pendulum  $K_2$  into approximate coincidence with that of  $K_1$ . Under these conditions, the phenomena of absorption, at or near resonance, can be observed readily. It has been possible in this manner to check the causes and essential characteristics of telephone-diaphragm absorption.

**The Absorption Loop in the Motional-Impedance Circle.** — The following theory was originated on a purely empirical basis to meet the peculiarities of absorption loops, like those of Figs. 74 to 78. At a later stage, it became evident that the theory resembled that of inductively coupled a.-c. circuits. In the form first published\* the apparent resistance of the secondary circuit at resonance,  $r_a$  or  $(\mu\omega)^2/r_2$ , was replaced by  $r_2$ , the secondary resistance, which was an unnecessary limitation. As was pointed out by Professor Mori,† it is advantageous to introduce the mutual inductance  $\mu$ . It is not clear, however, what mechanical condition

\* Bibliography 60.

† Bibliography 86.

determines the value of  $\mu$ , and further investigation should be directed to this and other points.

**Electrical Theory of Coupled a.-c. Circuits.** — A simple primary  $r_1, \mathcal{L}_1, s_1$  branch, Fig. 86, is connected across a pair of a.-c. mains supplied with constant voltage, but of varied frequency. A simple secondary circuit  $r_2, \mathcal{L}_2, s_2$  is linked with the branch through a mutual inductance  $\mu$ .

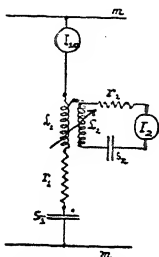


FIG. 86.  $\mathcal{LRS}$  branch across constant potential mains with associated secondary circuit.

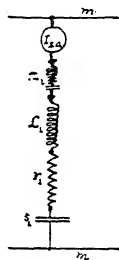


FIG 86 A.  $\mathcal{LRS}$  branch with additional impedance  $z_a$  to replace secondary circuit.

It has long been known\* that, under these conditions, the primary circuit behaves as though the secondary circuit were removed, and a new impedance  $z_a$  were inserted in the branch, as shown in Fig. 86 A. We may call this the *virtual absorption impedance* of the secondary circuit, as developed in the primary circuit. This impedance is

$$(153) \quad z_a = -\frac{(\mu j\omega)^2}{z_2} = \frac{\mu^2 \omega^2}{z_2} \quad \text{ohms or abohms } \angle,$$

where  $\omega$  is the impressed angular velocity on the mains in radians per second,  $\mu$  is the mutual inductance in henries or abhenries, and  $z_2$  is the impedance of the secondary circuit considered separately, in vector ohms or abohms, according to the system of units employed; moreover

$$(154) \quad z_2 = r_2 + j(\mathcal{L}_2\omega - s_2/\omega) \quad \text{ohms or abohms } \angle.$$

The current in the primary circuit if the secondary circuit is removed or  $\mu = 0$  is

$$(155) \quad I_1 = \frac{E}{z_1} = \frac{E}{r_1 + j(\mathcal{L}_1\omega - s_1/\omega)} \quad \text{amp. or abamp } \angle.$$

\* Bibliography 11.

With the secondary circuit restored, the primary current is

$$(156) \quad I_{1a} = \frac{E}{z_1 + z_a} = \frac{E}{z_{1a}} = \frac{E - E_a}{z_1} \\ = I_1 - I_a \quad \text{amp. or abamp. } \angle,$$

where  $E_a$  is the *absorption emf.* in the primary circuit due to the presence of the secondary circuit.  $I_a$  is the virtual current in the primary due to the presence of the secondary circuit. From the above it follows that

$$(157) \quad E_a = I_{1a} z_a \quad \text{volts or abvolts } \angle,$$

and

$$(158) \quad I_a = \frac{E_a}{z_1} = I_{1a} \frac{z_a}{z_1} \quad \text{amp. or abamp } \angle.$$

The current in the secondary circuit is also

$$(159) \quad -I_2 = j \frac{\mu \omega I_{1a}}{z_2} = j \frac{\mu \omega E}{z_{1a} z_2} \quad \text{amp. or abamp } \angle.$$

### Corresponding Mechanical Theory of Coupled Systems.—

Turning now to the mechanically coupled system of Fig. 79, let the secondary spring vibration system have constants  $r_2$ ,  $m_2$ , and  $s_2$ ; while those of the primary diaphragm, considered alone, have constants  $r_1$ ,  $m_1$ , and  $s_1$ . Let the system have a *mutual mass*  $\mu$  gm., corresponding to the mutual inductance  $\mu$  henries of the electric case; then the absorption effect of the secondary system on the primary may be regarded as equivalent to an absorption impedance like that of (153):

$$(160) \quad z_a = \frac{\mu^2 \omega^2}{z_2} \quad \text{mechanical abohms } \angle,$$

and the vibratory velocity of the primary system at constant impressed vmf. but varied frequency will be like (155), when  $\mu = 0$ :

$$(161) \quad \dot{x}_1 = \frac{F}{z_1} = \frac{F}{r_1 + j(m_1 \omega - s_1/\omega)} \quad \text{rms. kines } \angle;$$

and when  $\mu$  is no longer zero,

$$(162) \quad \dot{x}_{1a} = \frac{F}{z_1 + z_a} = \frac{F}{z_{1a}} = \frac{F - F_a}{z_1} = \dot{x}_1 - \dot{x}_a \\ = \dot{x}_1 \left( \frac{z_1}{z_1 + z_a} \right) = \dot{x}_1 \left( \frac{z_1}{z_{1a}} \right) = \dot{x}_1 \left( 1 - \frac{z_a}{z_{1a}} \right) \quad \text{rms. kines } \angle,$$

where  $F_a$  is the *absorption vmf.*,  $\dot{x}_{1a}$  is the velocity of the primary system in the presence of absorption,  $z_{1a}$  is the *virtual impedance*



of the primary system,  $\dot{x}_a$  is the *virtual vibratory velocity of absorption*. The vibratory velocity of the secondary system is like  
159 :

$$(163) \quad \dot{x}_2 = -\frac{j\mu\omega \dot{x}_{1a}}{z_2} = -\frac{j\mu\omega F}{z_{1a}z_2} = \frac{F_2}{z_2} \quad \text{kines } \angle.$$

The virtual vibratory velocity of absorption  $\dot{x}_a$  is, following (162),

$$(164) \quad \begin{aligned} \dot{x}_a &= \dot{x}_1 - \dot{x}_{1a} = \dot{x}_1 \left(1 - \frac{z_1}{z_{1a}}\right) = \dot{x}_1 \left(\frac{z_a}{z_{1a}}\right) = \dot{x}_1 \left(\frac{z_a}{z_1 + z_a}\right) \\ &= \dot{x}_{1a} \left(\frac{z_a}{z_1}\right) = \frac{F_a}{z_1} \quad \text{kines } \angle, \end{aligned}$$

and the virtual absorption vmf. is like (157)

$$(165) \quad F_a = \dot{x}_{1a} z_a = \dot{x}_a z_1 \quad \text{dynes } \angle.$$

Formula (162) shows that the distorted velocity  $\dot{x}_{1a}$  is equal to the undistorted velocity  $\dot{x}_1$  multiplied by the vector ratio  $z_1/(z_1 + z_a)$ . It is evident from (160) that  $z_a$  tends to be large at the frequency of secondary resonance:

$$(166) \quad \omega_{r2} = 2\pi f_{r2} = \sqrt{s_2/m_2} \quad \frac{\text{radians}}{\text{sec.}}$$

At this frequency  $z_2 = r_2$ , and

$$(167) \quad r_a = \frac{\mu^2 \omega_{r2}^2}{r_2} \quad \text{mechanical abohms.}$$

If this also happens to be the primary resonant frequency,  $z_1 = r_1$  and by (164),

$$(168) \quad \frac{\dot{x}_{1a}}{\dot{x}_{10}} = \frac{r_1}{r_1 + r_a},$$

or, the distorted velocity at joint resonance will be in phase with the undistorted resonant velocity, but will be reduced in the proportion  $r_1/(r_1 + r_a)$ , where  $r_a$  is the apparent resistance of the secondary circuit at secondary resonance or  $(\mu\omega)^2/r_2$ . If  $r_a$  is large in proportion to  $r_1$ , this will be a small fraction, or the vector velocity will be diametral to the undistorted velocity circle, but will be greatly reduced. This is the condition of Fig. 80. If  $r_a = pr$ ; then the reduction ratio of (168) becomes  $1/(p + 1)$ . In Fig. 80,  $p$  is over 20; or the mechanical resistance of the second-

ary system is over 20 times that of the primary. At co-resonance, the secondary velocity becomes, by (163),

$$\begin{aligned}
 (169) \quad -\dot{x}_2 &= \frac{j\mu\omega}{r_2} \cdot \frac{F}{r_1 + r_a} = \frac{j\mu\omega}{r_2} \cdot \dot{x}_{10} \cdot \frac{r_1}{r_1 + r_a} \\
 &= \frac{j\mu\omega}{r_2} \cdot \dot{x}_{10} \cdot \frac{1}{p + 1} \quad \text{kines } \angle.
 \end{aligned}$$

This means that the secondary velocity will be in lagging quadrature to the undistorted primary velocity and may be large in comparison with it, if  $\mu\omega/r_2$  is large by comparison with  $p + 1$ .

If the resonant frequency of the secondary circuit  $f_{\omega_2}$  is remote from  $f_{\omega_1}$ , that of the primary, the secondary velocity can never become large, because in (163), when  $\omega = \omega_{\omega_2}$  and  $z_2$  reaches its minimum size at  $r_2$ ,  $z_{1a}$  remains large, on account of the large mechanical reactance in the unresonant primary system. At secondary resonance, however, the value of  $\dot{x}_a$  is, by (164), equal to the undistorted primary velocity  $\dot{x}_1$  at that frequency multiplied by the vector ratio  $z_a/(z_1 + z_a)$ . This will usually be a small ratio; because  $z_1$  will be large in the primary unresonant circuit. The slope of  $\dot{x}_a/\dot{x}_1$  at  $f_{\omega_2}$  will be the slope of  $z_a/(z_1 + z_a)$ . But  $z_a$  is then a real quantity  $r_a$ , so that  $\dot{x}_a$  will lag behind  $\dot{x}_1$  the undistorted velocity, a little more than the slope of  $z_1$  at that frequency; i.e., a little more than the undistorted velocity lags behind the resonant diametral value. This means that in Fig. 78, for example,  $OF = \dot{x}_a$  should lag behind  $OC = \dot{x}_1$  a little more than  $OC$  lags behind  $OA = \dot{x}_{10}$ . In fact, in Fig. 78,  $FOC = 52^\circ$  and  $COA = 49^\circ$  approximately. This is the theory of the approximate equality of those angles already discussed.

The theory thus explains, by (164), why a distortion loop becomes so much smaller as it departs from the primary resonant frequency.

Figure 87 is a computed case of distortion for the particular case where  $F = 3000$  dynes rms.,  $m_1 = 2.5$  gm.,  $r_1 = 800$  dynes per kine,  $s_1 = 50 \times 10^6$  dynes per cm.,  $m_2 = 4$  gm.,  $r_2 = 300$  dynes per kine, and  $s_2 = 80 \times 10^6$  dynes per cm. Also  $\mu = 0.0671$  gm. Here the angular velocity  $\omega_0 = 4472$  radians per second, gives resonance to both primary and secondary systems. At this frequency the undistorted velocity would be  $\dot{x}_1 = OE = 3.75$  kines rms. at zero slope, or in phase with the impressed vmf. The primary absorption velocity  $\dot{x}_a$ , at resonance is  $Oe' = 1.023$  kines and  $\dot{x}_{1a}$  the distorted primary velocity is  $Oe = 2.727$  kines. As the im-

pressed angular velocity is varied from 4350 to 4700 radians per second, the primary absorption velocity changes from  $Oa'$  through  $Oc'$  to  $Oh'$ . These vectors subtracted from  $OA$ ,  $OE$ ,  $OH$  in the undistorted circle give rise to the looped path  $a...e...h$ . At any

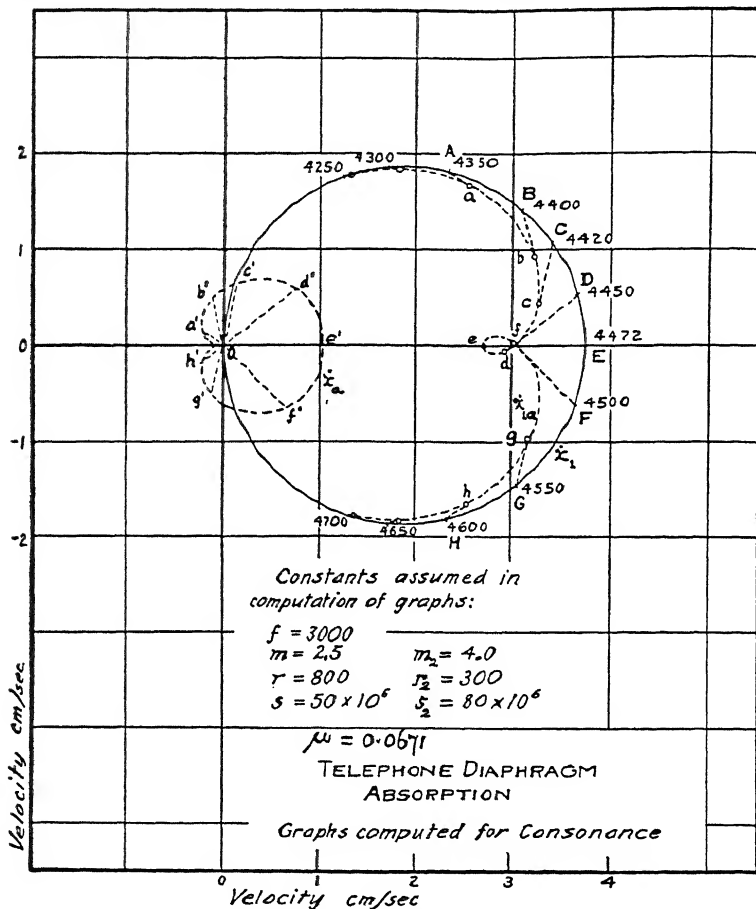


Fig. 87. Computed distorted velocity circle.

point such as  $C$ , we have  $OC - Oc' = Oc$ , corresponding to  $\dot{x}_1 - \dot{x}_a = \dot{x}_{1a}$  by (162). This looped graph of primary velocity in the presence of absorption, would correspond to the graph of the primary current in the electric system of Fig. 86 with the corresponding electric constants.

Figure 88 gives the computed graphs for the same pair of mechanical systems as in Fig. 87; but with  $\mu$  increased to 0.25. Here the circle  $OAB \dots GH$  is the undistorted primary velocity circle of  $\dot{x}_1$  with the secondary system prevented from responding. The internal dotted and looped curve at  $ab \dots gh$ , shows  $\dot{x}_{1a}$ , the primary distorted velocity, which should be reduplicated to the proper

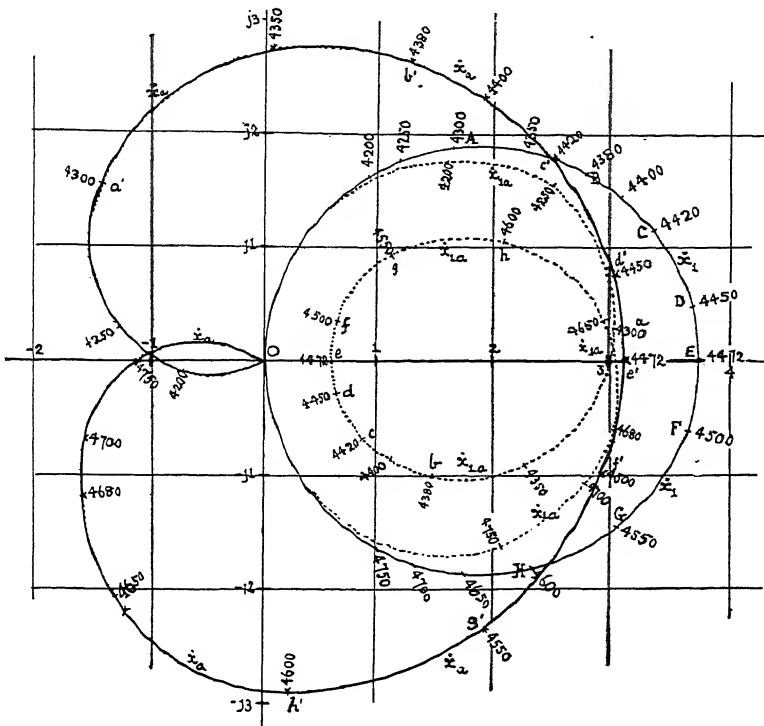


FIG. 88. Vector graphs of  $\dot{x}_1$ ,  $\dot{x}_a$ , and  $\dot{x}_{1a}$  for the same system as Fig. 87, but with  $\mu = 0.25$ .

scale in the measured motional impedance. The heavy curve  $a'b' \dots g'h'$  of primary absorption velocity,  $\dot{x}_a$  is also given.

Comparing Figs. 87 and 88, it will be noticed that when  $\mu$  is small compared with  $\sqrt{m_1 m_2}$ , i.e., when the coupling between the primary and secondary systems is loose, the graph of  $\dot{x}_{1a}$ , the distorted primary velocity, tends to become a pure circle of undistorted velocity  $\dot{x}_1$ , with a small superposed internal loop at  $f_{02}$ . The graph of absorption velocity  $\dot{x}_a$  is also a small nearly circular

loop at the origin. As the coupling becomes closer, the distorted velocity approaches the condition of Fig. 86 with a double internal loop; while the graph of  $\dot{x}_a$  is of lily-pad shape somewhat asymmetric, and with the edges overlapping on the left-hand side of the origin. This family of  $\dot{x}_{1a}$  lily-pad graphs, of the types  $abc \dots gh$ , represented in Figs. 87 and 88, and algebraically defined in (162), may be described as absorption graphs of *coupled-system primary velocity*, or current.

Further investigation is needed for a direct method of evaluating the mutual mass  $\mu$  and for determining the constants of the secondary system.

## CHAPTER XIII

### ACOUSTIC IMPEDANCE

In preceding Chapters we have discussed the mechanical impedance of vibratory systems in general, and of telephone-receiver diaphragms in particular. In this Chapter we shall consider that portion of the mechanical impedance which is caused by the medium — ordinarily air — in which the diaphragm vibrates, and which we may call *acoustic impedance*.\* It is the energy expended in overcoming this impedance which manifests itself in acoustic phenomena.

Let a small thin rigid disk, or circular diaphragm  $AB$ , Fig. 89, fitting without edge friction into a smooth cylindrical tube  $TT$ ,  $T'T'$ , be actuated, through the axial rod, by a simple vmf.  $F$  rms. dynes, directed along the axis of the tube. The effect of this vmf., neglecting friction of the air on the walls of the tube, will be to set up an alternating velocity  $\dot{x}$  cm. per second, in the air or other fluid contained in the tube. The maximum cyclic amplitude of vibration  $\dot{x}_m$  is supposed to be very small. The fluid filling the tube on each side of the disk may be compressible, as in the ordinary case of an air tube. The maximum cyclic velocity  $\dot{x}_m$  of the fluid in contact with the disk must be the same as that of the disk itself. In the assumed case of a rigid disk, this velocity would have the same magnitude and phase — or size and slope — at all parts of its surface. The magnitude and the phase of this velocity, for a given impressed vmf., will depend upon the impedance to vibration of the column of fluid on the total surface of the disk. This impedance to vibrational velocity, of the fluid in a tube at a driving section, may be called the *acoustic impedance* of the fluid at each of the two surfaces of the disk.

\* When the measurements described in this Chapter were made and first published (1917, Bibliography 87), it was supposed that the expression *acoustic impedance*, here defined, was new. The expression acoustic impedance, however, already had been used by Prof. A. G. Webster and published by him in 1919 (Bibliography 82a).

Acoustic impedance is the plane vector sum of *acoustic resistance* and *acoustic reactance*. In a frictionless fluid, acoustic resistance absorbs and dissipates the energy imparted by the vmf. Acoustic reactance cyclically stores and releases, without dissipation, the energy of acoustic vibration. Acoustic impedance is thus a particular form of mechanical impedance. If a diaphragm is thrown into vibrational velocity by an impressed vmf. and is in contact with a fluid on either or both of its surfaces, the mechanical impedance of the diaphragm will be partly composed of acoustic impedance.

Referring to the simple rigid and frictionless diaphragm of Fig.

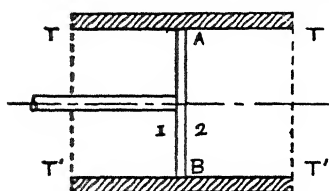


Fig. 89. Diagram of longitudinal section of an acoustic tube with vibrating disk.

89, assumed as of negligible mass, the mechanical impedance which it develops to velocity may be entirely acoustic. If we denote the acoustic impedance on the sides 1 and 2 of the disk as  $z_1$  and  $z_2$  respectively, with their sum equal to  $z$ ; then the vector rms. vibrational velocity of vibration

at the disk will be

$$(170) \quad \dot{x} = \frac{F}{z_1 + z_2} = \frac{F}{z} \quad \text{rms. kins } \angle,$$

or

$$(171) \quad z_1 + z_2 = z = \frac{F}{\dot{x}} \quad \begin{array}{l} \text{acoustic abohms } \angle \\ \text{or dynes per kine } \angle. \end{array}$$

If the two sides of the disk are entirely symmetric with respect to the tube and the vmf., then  $z_1$  and  $z_2$  will be identical vector impedances. In any case, their sum  $z$  will be a single definite vector impedance.

**Acoustic-Impedance Density.**—The acoustic impedance  $z$  will manifestly increase as the cross-sectional area of the tube is increased. Neglecting friction at the walls of the tube, the increase will be in direct proportion to the area. If  $S$  be the cross-sectional area of the tube in sq. cm., then the acoustic impedance per sq. cm. or *acoustic-impedance density*  $\mathfrak{z}$  will be  $z/S$  vector acoustic ab ohms per sq. cm. Or if we employ a vibromotive pressure intensity  $p = F/S$  to actuate the disk; then,  $p$  being taken as of standard phase or without slope,

$$(172) \quad \dot{x} = \frac{p}{\mathfrak{z}} = \frac{p}{\mathfrak{z}_1 + \mathfrak{z}_2} \quad \text{rms. kins } \angle,$$

or

$$(173) \quad \mathfrak{z} = \mathfrak{z}_1 + \mathfrak{z}_2 = \frac{p}{\dot{x}} \quad \frac{\text{acoustic abohms}}{\text{sq. cm.}} \angle.$$

The dimensions of acoustic impedance, like those of mechanical impedance, are  $MT^{-1}$ , or mass per unit time (force divided by velocity). The dimensions of acoustic-impedance density are  $ML^{-2}T^{-1}$ , or  $MT^{-1}/L^2$ .

As thus far defined, acoustic impedance involves the existence of a diaphragm filling the cross-section of a fluid-containing tube. Although this is perhaps the easiest conception of the matter, the limitations are unnecessary. Acoustic impedance may be conceived of as occurring at an imaginary surface of equal velocities, such as the cross-section of an air tube in the absence of a diaphragm. Moreover, acoustic impedance is not necessarily confined to a section of fluid in a tube. It may occur in a region of any shape.

#### Acoustic Impedance over the Surface of a Flexible Diaphragm.

— We have hitherto assumed that the velocity  $\dot{x}$  was the same at all parts of the vibrating disk or diaphragm. In any actual flexible diaphragm, however, such as a telephone-receiver diaphragm, the vibrational displacement  $x$ , and the velocity  $\dot{x}$ , will be different at different distances from the center of the disk. If we take any elementary area  $dS$  of the surface of the disk, at which the velocity is  $\dot{x}$  rms. kines, the power of this motion is

$$(174) \quad dP = \dot{x}^2 \cdot \mathfrak{z} \cdot dS \quad \text{abwatts } \angle,$$

where  $\dot{x}$  is taken at standard phase or zero slope. Of this power, the real component is dissipated, and the imaginary part conserved. The total power delivered to the diaphragm will be

$$(175) \quad P = \int_0^S \dot{x}^2 \cdot \mathfrak{z} \cdot dS = \mathfrak{z} \int_0^S \dot{x}^2 \cdot dS \quad \text{abwatts } \angle,$$

where the integration is carried over both sides of the diaphragm, and the impedance density is assumed as uniform. If we define the scalar mean square velocity as

$$(176) \quad \underline{\dot{x}^2} = \frac{1}{S} \int_0^S \dot{x}^2 \cdot dS \quad \text{kines}^2,$$

the power  $P$  may be expressed as

$$(177) \quad P = \underline{\dot{x}^2} \mathfrak{z} S = \underline{\dot{x}^2} \mathfrak{z} \quad \text{abwatts } \angle,$$



Under these conditions, the acoustic impedance of the tube at the disk, including both of its sides, will be

$$(178) \quad z = \frac{F}{\dot{x}} \quad \text{acoustic abohms } \angle.$$

The mean square ratio  $(\dot{x}/\dot{x}_0)^2 = (x/x_0)^2$  of the average to the maximum central velocity or amplitude, has already been defined as the mass factor  $m/M$  of the diaphragm. The acoustic power of the diaphragm will then be

$$(179) \quad P = \dot{x}^2 z = \frac{m}{M} \dot{x}_0^2 z = \frac{m}{M} \dot{x}_0^2 S \quad \text{abwatts } \angle,$$

or will be equal to the apparent power  $\dot{x}_0^2 z$  multiplied by the mass factor of the diaphragm. If the actual displacement  $x_1$  over a pole is observed, and the polar mass factor measured, the corresponding total power will be  $\dot{x}_1^2 z$  ( $m_1/M$ ).

**Relations between Acoustic Impedance and Electric Motional Impedance.** — We have already seen by formula (97) in relation to the motional impedance  $Z'$  of a telephone receiver, that

$$(180) \quad Z' = \frac{A\dot{x}}{I} = \frac{A^2}{z'}, \quad \text{electric abohms } \angle,$$

where  $A$  is the vector force-factor of the instrument,  $\dot{x}$  the vector rms. velocity of the diaphragm over a pole in kines,  $I$  the vector rms. testing current in abamperes and  $z''$  the gross vector mechanical impedance. Consequently, the gross mechanical impedance is

$$(181) \quad z'' = \frac{A^2}{Z'} = A^2 Y' \quad \text{mechanical abohms } \angle.$$

At apparent resonance, the motional impedance acquires the diametral value  $Z'_0$ , with the same slope  $-2\beta^\circ$ , as  $A$ ; so that  $z''$  reduces to a real quantity, the gross mechanical resistance of the diaphragm. At any impressed frequency, however, we can find the total mechanical impedance of the diaphragm from (181), if we know the value of  $A$ , and we can find the motional impedance  $Z'$ , or its reciprocal, the motional admittance  $Y'$  at that frequency.

It has also been shown in Chapter X that the total gross mechanical impedance  $z''$  of the diaphragm is made up of (1) the virtual mechanical impedance of displacement in the magnetic field, (2) the net mechanical impedance of the diaphragm, and (3) the acoustic impedance behind as well as (4) in front of the

diaphragm. If we denote these components by  $z_v$ ,  $z$ ,  $z_1$ , and  $z_2$  respectively, we have:

$$(182) \quad z'' = z_v + z + z_1 + z_2 \quad \text{mechanical abohms } \angle,$$

or the gross total mechanical impedance is the vector sum of these four components, two of which are acoustic.

The virtual mechanical impedance of displacement varies with the impressed frequency by (82) and (83)

$$(183) \quad z_v = \frac{jpA}{\omega} = r' + \frac{js'}{\omega} = \frac{p|A|}{\omega} \sin \beta - \frac{jp|A|}{\omega} \cos \beta$$

$$= r' + jx' \quad \text{mechanical abohms } \angle.$$

The mechanical resistance  $r'$  is usually taken as constant to a first approximation, and the elastic reactance  $s'/\omega$  is inversely proportional to the impressed frequency.

The net mechanical impedance of the diaphragm is

$$(184) \quad z = r + j(m\omega - s/\omega) = r + jx \quad \text{mechanical abohms } \angle.$$

The acoustic impedance in the air-chamber behind the diaphragm is

$$(185) \quad z_1 = r_1 + jx_1 \quad \text{mechanical abohms } \angle,$$

where  $r_1$  is the acoustic resistance of the chamber, and  $jx_1$  its acoustic reactance. Similarly, the acoustic impedance of the air in front of the diaphragm will be

$$(186) \quad z_2 = r_2 + jx_2 \quad \text{mechanical abohms } \angle;$$

$x_1$  and  $x_2$  are functions of the frequency of the same general type as  $x$ . The resistance  $r_1$  and  $r_2$  are assumed to be constant and unaffected by the frequency, for a given environment. The total gross mechanical impedance is thus

$$(187) \quad z'' = r'' + jx'' = (r' + r + r_1 + r_2) + j(x' + x + x_1 + x_2) \quad \text{mechanical abohms } \angle.$$

**Method of Evaluating the Acoustic Impedance  $z_2$ .** — There are two methods available for evaluating  $z_2$ , the acoustic impedance of the air in front of the receiver diaphragm:

(1) By measuring the motional impedance  $Z'$  of the receiver at constant impressed current strength  $I$  and at constant impressed angular velocity  $\omega$ , but with adjusted acoustic load. Under these conditions  $z$ ,  $z_v$ , and  $z_1$  will all remain constant; but since  $z_2$  is altered, the gross vector sum  $z''$  is altered correspondingly.

This causes the motional impedance  $Z'$  of the instrument to be changed in a measurable manner. From the electrically measured changes in  $Z'$ , the changes in  $z''$  and therefore in  $z_2$ , are determined.

(2) By keeping the acoustic load  $z_2$  constant as well as  $I$ , but by varying the impressed value of  $\omega$ . This will involve changes in the gross mechanical impedance  $z''$  that can be determined from corresponding measurements of the motional impedance, using the technique described in relation to Figs. 30 and 31. The variations in  $z_r$ ,  $z$  and  $z_1$  caused by variation of  $\omega$  must then be allowed for, from independent information as to their behavior. The change in  $z_2$  can then be evaluated.

Method (1) is the simpler. It gives measured values of acoustic impedance at constant frequency and varied load. Method (2), or some equivalent, is necessary when we have to measure the change in acoustic impedance under varied impressed frequency.

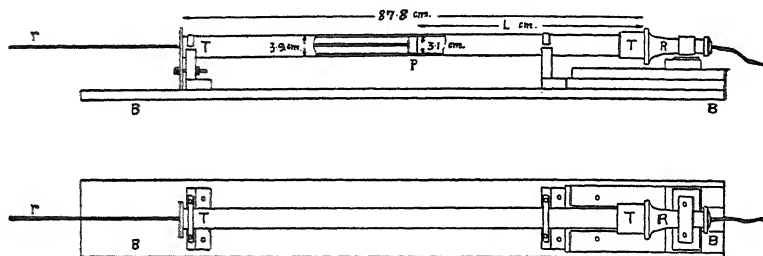


FIG. 90. Side elevation and plan of acoustic tube conductor.

**Application of Method (1) to the Measurement of the Acoustic Impedance of the Air Column in a Tube of Varied Length.** — A straight smooth fiber tube 87.8 cm. long, of 3.1 cm. internal diameter, and 3.9 cm. external diameter, was supported horizontally, by metallic strips packed with felt, over a wooden base  $BB$ , Fig. 90. The tube  $TT$  was brought into contact with the cover of a regular form of bipolar telephone receiver  $R$ , as is shown in detail by Fig. 91. The axis of the tube was in line with the axis of the receiver. A hard rubber piston  $PP$  slides freely in the tube, and can be set at any desired position within it, by means of the projecting brass rod  $r$ . The telephone receiver  $R$  is clamped, by means of a metallic strip, on a wooden pedestal rising from the base  $BB$ . The composition cap or cover of the receiver had its

opening enlarged, as is seen in Fig. 91, in order to connect more easily with the tube *TT*.

The electric impedance of the receiver was measured in the Rayleigh bridge of Fig. 30. The current in the receiver was kept constant at 1.5 milliamperes in some tests, and at 2 milliamperes in others. The current detector in the bridge wire was a pair of medium-resistance head telephones.

A single series of damped impedances served for the evaluation of the motional impedance of the instrument under any conditions of free impedance at the same temperature. Figure 92 shows the

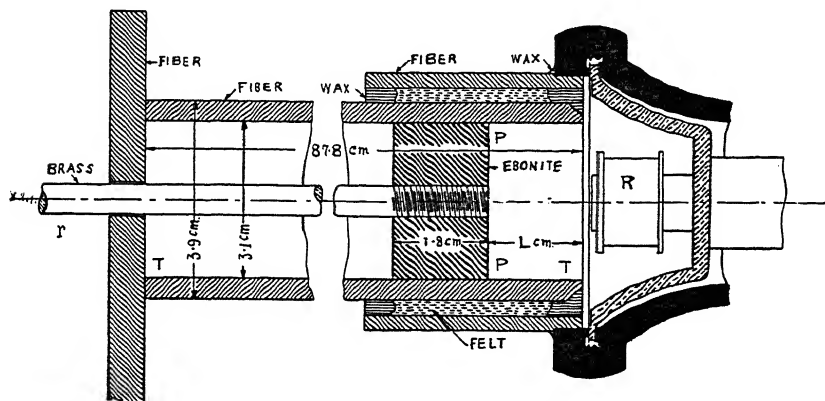


Fig. 91. Longitudinal section of air tube and details of telephone receiver fastenings to the same.

motional-impedance circle of the instrument at  $20^{\circ}$  C. It will be seen that  $f_0 = 930.6 \sim$ ,  $f_1 = 912 \sim$ ,  $f_2 = 953 \sim$ ; so that  $\Delta = 41\pi = 129$ . The diametral impedance is  $Z'_0 = 158 \angle 55^{\circ}.6$  ohms; so that  $\beta = -27^{\circ}.8$ . The d-c. resistance of the instrument at this temperature was 86.4 ohms., so that its motional-impedance ratio was  $Z'_0/R_1 = 1.83 \angle 55^{\circ}.6$ . The vector force-factor  $A$  was  $5.138 \times 10^6 \angle 27^{\circ}.8$ .

**Variations of Free Resistance and Reactance with Load.** — The receiver having been connected to the fiber tube as shown in Figs. 90 and 91, its resistance and inductance were measured in the same Rayleigh bridge, as the length of air column in front of the diaphragm was varied from 0 to 64 cm. by altering successively the distance between the piston *P* and the beginning of the tube, holding the frequency at  $f = 921 \sim$ , and  $I = 1.575$  milliamperes

rms. The results obtained are indicated in Fig. 93. It will be seen that both the apparent resistance  $R''$  and the apparent reactance  $X''$  go through regular fluctuations resembling damped sinuoids, as the length of air column is increased. The values of

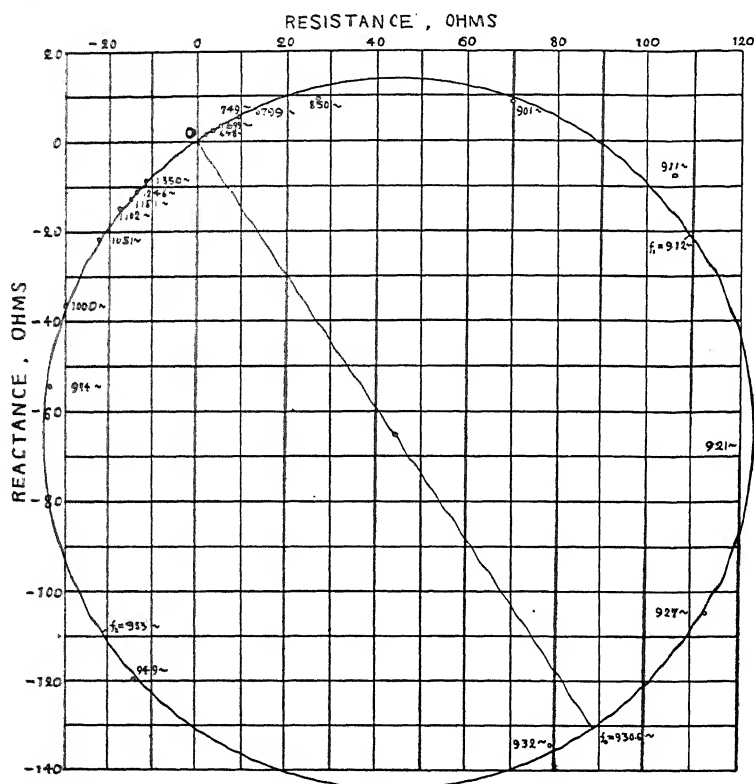


Fig. 92. Motional impedance circle of telephone receiver used with the tube.

damped resistance and reactance for the same temperature ( $20^{\circ}\text{C.}$ ) are indicated in the figure at  $R_d$  and  $X_d$ , respectively.

If we plot the simultaneous motional resistances  $R'' - R'$  and reactances  $X'' - X'$  of Fig. 93 vectorially, we obtain the motional-impedance diagram of Fig. 94. It will be seen that it consists of a spiral succession of roughly circular loops becoming smaller as the length of air column is increased. Since the impressed frequency was here constant throughout, the changes in the motional impe-

dance of this receiver are entirely attributable to changes in the acoustic impedance  $z_2$  as the air column length is varied.

The numbers marked on the spiral of Fig. 94 are the air-column lengths in cm. It will be seen that at  $L = 0$  cm., with the piston within 1.5 mm. of the diaphragm, the motional impedance was  $12.5 \angle 75.4$  ohms. This value was nearly repeated at  $L = 19$  cm. At  $L = 10$  cm., however, the motional impedance had increased to  $142.8 \angle 42.1$  ohms. The spiral curve has a pitch of 18.7 cm., which corresponds to half a wave length of sound in the air of the

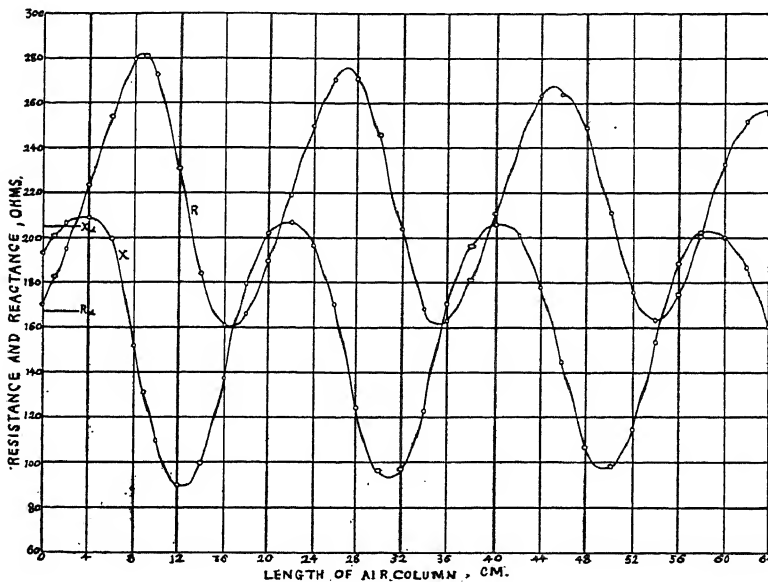


FIG. 93. Curves of apparent resistance and reactance of receiver when attached to air column of successively varied length (Kurokawa).

tube at  $921 \sim$ , for, since the velocity of sound in air is 34,430 cm. per sec. at  $20^\circ \text{C.}$ , the wave length,  $\lambda = 34,430/921 = 37.38$  cm.

It is evident from the preceding, that in order to secure consistent results in such measurements, the frequency must be carefully maintained constant. A small change in impressed frequency may affect the wave length very appreciably, and so distort the diagram of motional impedance. The measurements are very sensitive to small acoustic changes. The frequency selected should be near to the resonant frequency  $f_0$ . If the frequency used is remote from apparent resonance, the mechanical reactance of the

diaphragm will be so large that changes in the acoustic impedance  $z_2$  will not alter the total gross mechanical impedance  $z''$  materially, and so will not make appreciable changes in the electric motional impedance  $Z'$ . If, however, the system is tested at a steady frequency near to apparent resonance, the reactance of the system will be small, and small changes in  $z_2$  may be expected to produce relatively large observable changes in  $Z'$ .

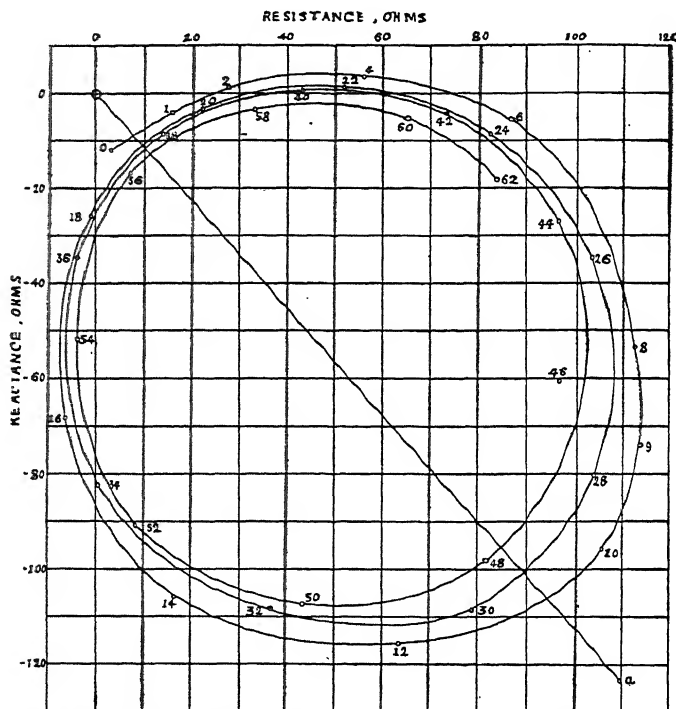


Fig. 94. Motional impedance diagram of receiver at constant impressed frequency (921 ~) with varying length of attached air column.

**Technique for Converting Motional Impedance into Mechanical Impedance.** — In order to utilize the motional-impedance diagram of Fig. 94 for deriving the acoustic impedance  $z_2$  in front of the diaphragm, we may use (181) and obtain the graph of motional admittance  $Y'$ . This means that we must find the reciprocal graph to that of Fig. 94. At each vector position on the curve, we use the reciprocal of the size with the negative slope, in accord-

ance with (50). In this way we construct a *motional-admittance curve*, also a spiral in this case. Multiplying this motional-admittance graph by the vector  $A^2 = 26.4 \times 10^{12} \angle 55.6^\circ$ , by suitably altering the scale of sizes and rotating it bodily clockwise through  $55.6^\circ$ , we obtain the graph of gross mechanical impedance in Fig. 95. This is also a contracting spiral. The heavy curve connects points of observation, while the broken curve refers to a computed graph to be discussed later. Thus in Fig. 94, the vector

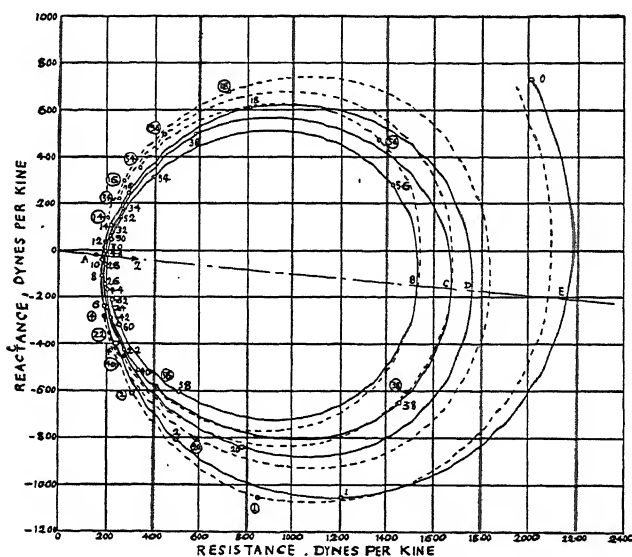


FIG. 95. Graph of total mechanic impedance on receiver diaphragm obtained by inverting the graph of Fig. 94, and multiplying by  $A^2$ . Heavy curve connects observation values. The dotted curve represents the computed values.

0 - 18 measures  $Z' = 26 \times 10^9 \angle 92.6^\circ$  electric abohms. The reciprocal is  $Y' = 0.03846 \times 10^{-9} \angle 92.6^\circ$  abmhms. Multiplying by  $A^2$ , we obtain  $1.015 \times 10^3 \angle 37^\circ$  mechanical abohms, or dynes per kine. The axis of the spiral is the broken line *OABCDE*.

The operation of inverting a motional-impedance diagram into a motional-admittance diagram is somewhat tedious. It would be advantageous to avoid this step if possible, by measuring the motional admittance in the first instance directly, instead of the motional impedance. As yet, however, no technique for measure-



ment of motional admittance has been worked out satisfactorily. Such a motional-admittance graph would be a total mechanical-impedance graph to a suitably altered scale, after being rotated through the angle  $2\beta^\circ$ .

Analysis of Fig. 95 indicates that the impedance  $OA$  mechanical abohms is the total internal mechanical impedance ( $z_r + z + z_1$ ) at this frequency. In other words, if the acoustic impedance  $z_2$  in front of the diaphragm could be completely removed, the total mechanical impedance remaining in and behind the diaphragm would be the vector impedance  $OA$ . This would correspond to a vector motional impedance  $Oa = 165 \angle 48^\circ.1$  in Fig. 94. Hence  $Oa$  is the inferred motional impedance for the case of removal of all acoustic load from the front of the diaphragm. Consequently, if we transfer the coordinate axes parallel to themselves from the origin  $O$  to the point  $A$ , Fig. 95, we obtain the corresponding graph of pure acoustic impedance  $z_2$ . The spiral locus  $0, 1, 2, 4, \dots 62$  is then the spiral of vector acoustic impedance of the tube acoustic conductor with its distant end sealed at distances of  $0, 1, 2, 4, \dots 62$  cm. from the diaphragm, or more strictly, from a plane  $1.5$  mm. in front of the diaphragm, where the tube may be considered as beginning.

The spiral acoustic impedance of Fig. 95, taken with the origin of coordinates at  $A$ , conforms fairly well with the expression (see Appendix IX).

$$(188) \quad z_0 \tanh \delta_A \quad \begin{array}{l} \text{acoustic abohms} \\ \text{or dynes per kine } \angle, \end{array}$$

where  $z_0$  is the *surge impedance* of the tube; or the acoustic impedance offered to this frequency by an indefinitely great length of the tube, and  $\delta_A$  is the *position angle* at the sending end  $A$  of the tube, as its length is varied. The deduced value of  $z_0$  is  $187 \angle 5^\circ.2$ ; or  $AZ$  in Fig. 95. This point  $Z$  is thus the inferred inner terminus of the spiral  $EDCB$ , if the tube were prolonged indefinitely. The hyperbolic angle  $\delta_A$  appears to be, in hyperbolic radians:

$$(189) \quad \delta_A = \left\{ L(0.000\,706 + j\underline{0.107}) + (0.0974 + j\underline{0.97}) \right\} \text{ hyps } \angle, \\ = (0.000\,706\,L + 0.0974) + j(\underline{0.107}\,L + \underline{0.97})$$

the length of the air column being  $L$  in cm. and the underscored numbers being in quadrants of arc. This expression is borrowed

from the theory of long a.-c. line conductors.\* Following that theory, the linear hyperbolic angle of the tube is  $\alpha = 0.000706 + j 0.107$  hyps. per cm. The amplitude of vibration  $x$  on such a tube of great length, would fall to  $1/\epsilon^{\alpha l}$  in a distance of  $1/0.000706 = 1416$  cm. The per-unit loss of amplitude in 1 cm. is 0.000706. The loss of phase in 1 cm. is 0.107 quadrant or  $9^{\circ}.63$ . The acoustic wave length is  $4/0.107 = 37.38$  cm. The apparent group velocity of the acoustic waves is  $v = 4 \times 921/0.107 = 34\,430$  cm. per sec. If the tube were completely sealed by a perfectly sound-reflecting piston, it would correspond acoustically to an electric a.-c. conductor, freed, or perfectly insulated, at its far end, and the position angle  $\delta_A$  of the home end  $A$  would be increased by  $\pi/2$  circular radians, or 1.0 quadrant. In this case, the piston, which is neither tightly fitting nor perfectly reflecting, appears to add a circular or imaginary hyperbolic angle of 0.97 quadrant, and in conjunction with imperfection or acoustic resistance at the  $A$  junction between telephone and tube it adds a real hyperbolic component of 0.0974 hyps., equivalent to 138 cm. of tube.

The dotted spiral in Fig. 95 indicates the computed locus according to (188). The agreement between the heavy spiral of observations and the dotted spiral of formula (188) is seen to be fairly satisfactory. At the time when the observations were made, the above theory of analogy between an acoustic-tube conductor and an electric-line conductor had not been reached. It has been pointed out, however, by Fleming † and Fitzgerald ‡, and also more recently by Brille § and Drysdale ||, that an analogy exists between sound waves along air tubes and electric waves along conducting lines.

According to this analogy, therefore, the plugged tube of varied length offered an acoustic impedance similar to the electric impedance of a uniform alternating-current line of varied length, put to ground in each case at the distant end, through a certain leak or high resistance. At each quarter wave of tube lengthening, the impedance of the tube crosses the axis of  $z_0$  and reaches alternately a high and low value. Thus at  $C$ , where  $L = 37.7$  cm., the

\* Bibliography 38 and 71.

† Bibliography 13.

‡ Bibliography 61.

§ Bibliography 85a.

|| Bibliography 85a.

acoustic impedance  $AC$  is a maximum and, according to (188),

$$\begin{aligned}
 (190) \quad z_{37.7} &= 187 \sphericalangle 5^\circ.2 \times \\
 &\quad \tanh \left\{ (0.0266 + j \underline{4.03}) + (0.0974 + j \underline{0.97}) \right\} \\
 &= 187 \sphericalangle 5^\circ.2 \tanh (0.124 + j \underline{5}) \\
 &= 187 \sphericalangle 5^\circ.2 \operatorname{ctnh} 0.124 \\
 &= 187 \sphericalangle 5^\circ.2 \times 8.106 = 1517 \sphericalangle 5^\circ.2
 \end{aligned}$$

acoustic abohms  $\angle$ .

The quarter wave length being 37.4 cm., the acoustic impedance should be a maximum at  $L = 0.30, 19.0, 37.7$ , and 56.4 cm., and should fall on the axis of  $z_0$  at  $E, D, C$  and  $B$  respectively, while it should be a minimum at  $L = 9.65, 28.35$ , and 47.05 cm. At these points the acoustic impedance should also lie on the same axis but nearer to  $A$ . All of these requirements are seen to be moderately well met in the diagram of Fig. 95.

It is thus possible, by making purely electrical measurements of the motional impedance of a telephone receiver, to arrive at the corresponding variations in acoustic impedance, when the acoustic load is varied, at constant impressed frequency. In the case of an air tube of varied length, the acoustic impedance appears to follow substantially the same quantitative behavior as the electric impedance of an alternating-current line of correspondingly varied length. A large field for electro-acoustic investigation lies open in this direction. An outline theory of acoustic wave transmission along a tube under certain assumptions is offered in Appendix IX, following the indications just mentioned.

In the case of a uniform electric line, we can always determine the position angle  $\delta_A$  and the surge impedance  $z_0$ , by successively grounding and freeing the line at the distant end, and measuring the corresponding impedances  $Z_r$  and  $Z_o$  at the home end  $A$ . The ratio of these two vector impedances is  $\tanh^2 \delta_A$  and their product is  $z_0^2$ . In the case of a tube or acoustic line, we can approximately free the line, by plugging the tube with a smooth hard plug, which is designed as a good sound reflector; but no means are available for "grounding" the acoustic line. With the tube wide open at the distant end, there is still an appreciable acoustic impedance at and beyond the open end. If the tube opens into a room or walled space, this terminal acoustic impedance will, in general, possess some reactance due to reflections from the walls; but if the tube

terminates in the open air, the *terminal acoustic impedance* is likely to have only a small reactive component or slope. If the amount of the terminal impedance  $\sigma$  of a tube opening out of doors could be accurately and easily ascertained from the geometry of the tube, it would be readily possible to compute  $\delta_A$  and  $z_0$  from the acoustic impedance  $Z_f$  with the distant end freed, and  $Z_\sigma$  with the distant end open to the free air. Until  $\sigma$  can be satisfactorily predetermined, it will be necessary to find  $\delta_A$  and  $z_0$  by indirect methods, and to determine  $\sigma$  from the differences between  $Z_f$  and  $Z_\sigma$ . Such investigations might lead to satisfactory experimental determination of  $\sigma$ , the open-end terminal impedance of a tube of given material and dimensions.

**Effects of Different Apertures at the Far End of the Tube on the Acoustic Impedance at the Sending End.**—Figure 96 shows several motional-impedance diagrams for the case of a fixed length (87.8 cm.) of the same air tube, each diagram being taken at a constant impressed frequency, and with different successive sizes of circular aperture in the plug or closure, at the distant end of the tube. The tube was closed with a flat slab of fiber 0.62 cm. thick. Circular holes marked Nos. 1, 2, 3, and 4 on the diagram were cut in different parts of this slab, with the following diameters: No. 1, 0.6 cm.; No. 2, 0.95 cm.; No. 3, 1.3 cm.; No. 4, 1.6 cm. and No. 5, full tube aperture (3.1 cm.); i.e., with slab removed. No. 0 represents the case of a complete closure of the tube by the unpierced slab.

The origin of all the diagrams is at  $K$ , Fig. 96. At the constant frequency of 850  $\sim$ , the successive motional impedances of the receiver attached to the tube, with successive terminal orifices 0-5 are  $K 0$ ,  $K 1$ , ...  $K 5$ . The ends of these vectors are connected by the freely drawn curve  $AA$ . Repeating the motional-impedance measurements at the successive steady frequencies of 901, 921, 949 and 1000  $\sim$ , the corresponding vector loci with different terminal apertures are marked on the curves  $BB$ ,  $CC$ ,  $DD$ , and  $EE$ .

It is evident that the motional-impedance variations, due to varying the distant-end orifice of the tube, are greatest on the long curves  $CC$  and  $DD$ , apparently because the frequencies pertaining to them (921 and 949  $\sim$  respectively) lie nearest to the resonant frequency of the receiver, when loaded with the tube under these conditions. For sensitiveness in the measurement of tube terminal

effects in the receiver, the frequency of  $850 \sim$  was manifestly too low, and that of  $1000 \sim$  too high. Figure 96 thus indicates the importance of selecting the best frequency for measurements of this nature.

The total mechanical impedances  $z''$  at the receiver diaphragm in the various measurements recorded in Fig. 96, are presented in

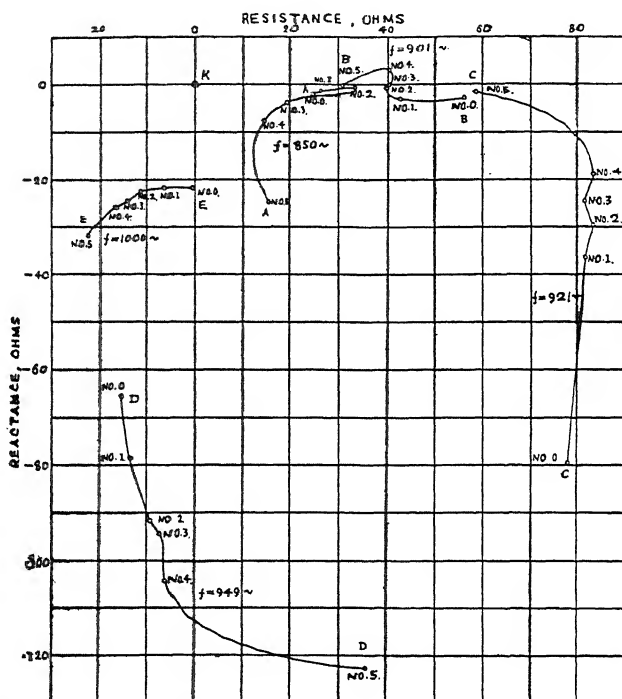


FIG. 96. Motional impedance of receiver at constant impressed frequencies, attached to air-tube of constant length (87.8 cm.) with apertures of different diameters at far end (Kurokawa).

the *mechanical-impedance diagrams* of Fig. 97, after inversion and multiplication by  $A^2$ , as already explained. These impedances are vectors expressible in mechanical resistance and reactance, as dynes per kine, or mechanical abohms, as may be preferred. Their origin is at  $k$ . The vector graph  $AA$  of Fig. 96 becomes converted into the vector graph  $aa$  of Fig. 97,  $BB$  into  $bb$ , and so on.

It will be observed that the most sensitive graphs  $CC$  and  $DD$  of Fig. 96, give rise to graphs  $cc$  and  $dd$  in Fig. 97, revealing

only small changes in total mechanical resistance; but relatively large changes in mechanical reactance, with change of tube aperture. On the other hand, *ee* at 1000  $\sim$  includes more change in mechanical resistance (230 to 980 dynes per kine) than in mechanical reactance (*j* 630 to *j* 920 dynes per kine). This indicates that the changes in acoustic load, effected by altering the tube aperture at the distant end, may preponderate in mechanical resistance, or in mechanical reactance, depending upon the impressed frequency, and on the system of stationary sound waves thereby set up in the tube.

Another set of measurements was made with the same telephone receiver and fiber tube, plugged at certain tube lengths, but with a row of holes, like those of a flute, bored in the tube wall. The diameter of each hole was 6.5 mm., and their distance apart, between centers, 4 cm. Removable plugs were inserted in these holes. The motional impedance of the receiver was found to be sensitively affected by the position of the particular plug removed. The results, although interesting, have not been analyzed, and are therefore not presented here in quantitative detail. Theoretically, they pertain to the domain of casual leaks in an a.-c. line conductor. They indicate, however, that the acoustic impedance of the air column in a perforated tubular musical instrument, such as a flute, undergoes marked variations when the instrument is manipulated, as in playing. Such changes of acoustic impedance might be measured in the manner described, with respect to a telephone receiver diaphragm as the source of sound.

**Motional and Acoustic Impedances of a Telephone Receiver pressed against the Ear.** — When a telephone receiver is freely exposed to the air in a large room, the total mechanical impedance

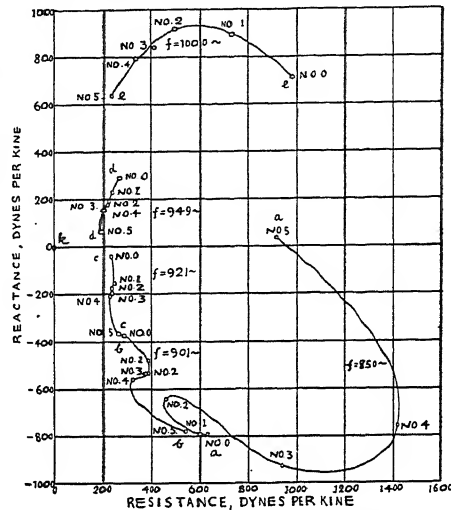


FIG. 97. Total mechanical impedance at receiver diaphragm by inversion from Fig. 96, and multiplying by  $A^2$ .

on its diaphragm is the total internal impedance ( $z_0 + z + z_1$ ) plus the external impedance  $z_2$  of the air in front of the diaphragm, including the cushion under the cap. The ordinary motional-impedance circle of the instrument is measured under these conditions. When, however, the receiver is pressed against the ear, the external acoustic impedance  $z_2$  is that of the air in the ear cavity, as well as under the cap of the instrument. The free and the motional impedances of the instrument under these conditions approximate to those actually presented in the ordinary telephonic use of the device as a receiver of speech, or when the receiver is under "ear acoustic load."

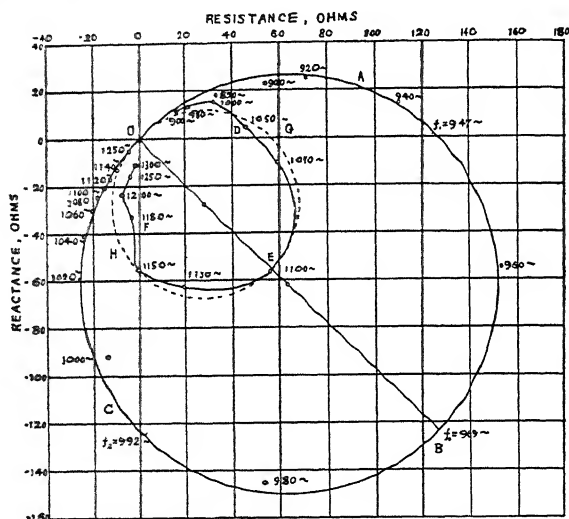


FIG. 98. Motional impedance graphs of receiver in free air of room, and pressed against listener's ear.

Figure 98 gives the motional-impedance circle  $OABC$  of the particular receiver used in these ear tests and which was similar to but not identical with that used in the tube tests above described. The frequency of apparent resonance  $f_0$  in free air was  $969 \sim$ , when the diametral motional impedance was  $Z'_0 = 177 \angle 44^\circ.2$  ohms. This receiver, when held against the ear of a listener, as in the ordinary conversational use of the instrument, gave rise to the smaller graph  $ODEF$ , which departs very clearly from the circular form. The exact shape of this graph  $ODEF$  is not considered of importance, however, because, if the instrument was placed against the ear,

with less or more pressure, or if it was centered differently on the ear, or if some other ear was selected, the shape of the graph would probably be altered appreciably. To a first approximation, however, the graph *ODEF* may be regarded as an approach to the dotted circular motional impedance *OGEH*, which may be described as the *motional circle of reference*, with the instrument applied to the ear. It may be observed that the diameter of this circle of approximation is  $78.5 \angle 44^\circ$  ohms. The diameter *OE* has, therefore, substantially the same slope as the free-air motional impedance diameter *OB*, but has been reduced in length somewhat more than 50 per cent. The frequency of apparent resonance has also been changed from  $969 \sim$  to  $1100 \sim$ , by applying the receiver cap to the ear.

**Mechanical-Impedance Graph corresponding to Motional-Impedance Circle.**

Figure 99 gives the corresponding mechanical-impedance graphs for this receiver and ear, obtained from Fig. 96 by the operations of inversion and multiplication by the vector  $A^2$ , as already described. The straight line *abc*, parallel to the reactance axis, corresponds to the motional-impedance circle *OABC* of Fig. 96, taken in the free air of a room. This means that the total mechanical impedance of the receiver free to the room, was a constant mechanical resistance  $r'' = r_e + r + r_1 + r_2$  of 149 dynes per kine, plus or minus a mechanical reactance depending on the impressed

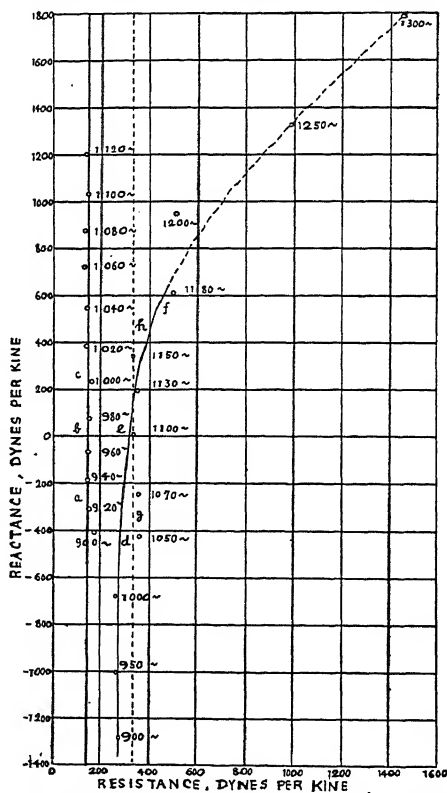


Fig. 99. Mechanical impedance of receiver in free air of room, and when pressed against listener's ear.



frequency. At  $f_0 = 969 \sim$ , the frequency of apparent resonance, the mechanical reactance disappears, leaving the resistance of 149 dynes per kine as the residual mechanical impedance of resonance.

It is important to observe that any motional-impedance circle of a telephone receiver, assumed to pass regularly through the origin of coordinates, corresponds to such a straight-line locus of total mechanical impedance parallel to the reactance axis, no matter what the depression angle ( $2\beta^\circ$ ) of the motional-impedance diameter may be. The application of the vector factor  $A^2$ , in formula (181), cancels out the diametral depression. In other words, all motional-impedance circles of telephone receivers correspond to, and are convertible into, rectilinear mechanical-impedance graphs of constant mechanical resistance, neglecting those influences, described in Chapter XI, which are known to distort the motional-impedance graph from the purely circular form. From an electric viewpoint, therefore, the motional-impedance circle, like that of Fig. 98, is the primary geometric property of a telephone receiver; but from a mechanical viewpoint, the primary geometric property is the rectilinear locus, like that of Fig. 99.

If the motional-impedance circle of approximation  $OGEH$  in Fig. 98, is accepted for this receiver applied to the listener's ear; then the dotted straight line  $geh$  of Fig. 99 would represent the corresponding mechanical-impedance graph, where the mechanical resistance is 335 dynes per kine, and zero reactance is found near  $1100 \sim$ . The curved line  $def$  corresponds more nearly to the actually recorded motional-impedance graph  $ODEF$ , Fig. 98. The particular shape of this curved graph  $def$  may not, however, be relied upon, for the reasons already given.

Figure 99 indicates, therefore, that at least to a first approximation, the acoustic resistance of the listener's ear in this measurement was 186 dynes per kine. At higher frequencies, this resistance appears to increase. There is room, however, for much further research in this direction.

Experiments were also made with an artificial ear\* composed of paraffin wax, and in form modeled closely after an anatomical model of a human ear. A motional-impedance graph made for

\*It is believed that an "artificial ear," consisting of a flat slab of some suitable substance selected experimentally, on which a receiver is laid face down, had been used in the telephone laboratories of the Western Electric Co., at New York, before the tests here presented were made.

the same telephone receiver, applied to this artificial ear, agreed fairly well in form with the graph for the actual ear *ODEF*, Fig. 98. The corresponding approximate circle of reference had a diameter of  $98 \angle 44^\circ$  ohms; or was somewhat larger than the circle *OGEH* of Fig. 98, corresponding to a somewhat lower mechanical resistance. It may be noted, however, that a receiver, when applied to a model ear in a solid substance like paraffin wax, does not fit to it as closely as when applied to the human ear. The imperfect fit would tend to lower the acoustic resistance by offering acoustic leakage.

With the receiver applied face downwards upon a flat slab of glass, the motional-impedance diagram was a closed curve through the origin, roughly circular in form. The approximating circle of reference had a diameter and a depression angle about the same as when the measurement was made with the receiver open to the air of the room. The frequency of apparent resonance was, however, raised to 1090  $\sim$ .

**Application of Variable Acoustic Air Column to the Tuning of Telephone Receivers, for increasing their Sensibility.** — If a telephone receiver is to be applied, not for the best reproduction of speech, but for producing as loud a sound as possible in the listener's ear with a very feeble exciting current, it should be brought into its most sensitive condition, by bringing about agreement between the impressed frequency and the frequency  $f_0$  of apparent resonance in the instrument. Figure 63, which is fairly typical of the ordinary receiver, indicates how much depends on the tuning of the diaphragm to the received frequency. That figure shows that the amplitude of vibration produced at a frequency 10 per cent below that of resonance was only 37.8 per cent of the resonant amplitude. Since the intensity of sound is taken as proportional to the square of the amplitude,\* a ten per cent departure from resonance gives in this instrument an intensity of  $(0.378)^2 = 0.143$ , or only one-seventh that obtained at resonance.

When the impressed frequency is under control, it is therefore desirable to employ a sharply resonant telephone receiver, as an a.-c. galvanometer, and to adjust the frequency by trial into accordance with  $f_0$  for the instrument, when the latter is pressed against the observer's ear. In many cases, however, the test frequency is fixed unadjustably. It then becomes desirable to

\* Lamb, Bibliography 35.

effect the same result by bringing  $f_0$  for the instrument, by trial, into agreement with the test frequency.

By reference to Figs. 93 and 94, it will be seen that for the given impressed frequency of 921  $\sim$  on the receiver connected to the fiber tube, a variation in the length of the tube by a quarter wave length, or 9.4 cm., altered the motional impedance from a maximum to a minimum, or *vice versa*, and also altered the maximum cyclic velocity of the diaphragm in the ratio of more than 8 to 1. The maximum cyclic amplitude must therefore have been altered in the same ratio; so that the intensity of the sound emitted by the diaphragm in its immediate vicinity would be increased in the ratio of more than 64 to 1. From this it will be evident that when such a tube of adjustable length is inserted between the telephone cover and the listener's ear, as by the insertion of an ear tube in the plug *P*, Fig. 90, the loudness of the sound emitted by the receiver, under steady excitation, can be adjusted by altering the

tube length. In other words, the tube length can be tuned to maximum sensitiveness at the ear. Observations made in this way have shown that this method of tuning is applicable at least over a certain range of impressed frequency. Thus, if the impressed frequency is 900  $\sim$ , and the receiver on the observer's ear has an apparent resonant frequency of 1000  $\sim$ , an inserted adjustable tube may make it possible to lower the resonant frequency to 900  $\sim$ . There is a good opportunity for further work in the convenient application of this principle to specified service conditions.

**Application of the Motional-impedance Method to the Measurement of Added Mechanical Resistance in Fluids.**—We have already referred in the last chapter to some effects of changes in atmospheric density upon the mechanical impedance at the diaphragm of a telephone receiver. The

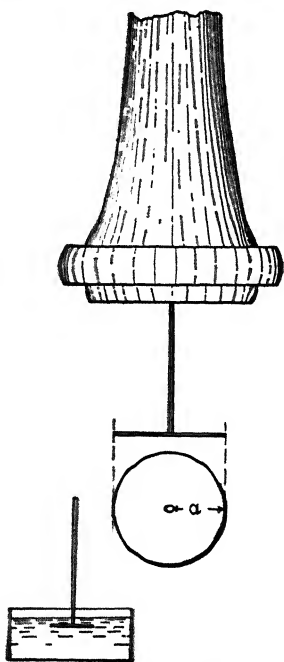


FIG. 100. Apparatus for measurements of mechanical vibratory resistance.

results obtained led to some tests for ascertaining the mechanical resistance offered by small circular aluminum vanes of various diameters fastened by a small metallic tie-rod to the center of the diaphragm, as shown in Fig. 100. The small vane was in each case held at its center, coaxial with the diaphragm, and with its plane parallel to that of the diaphragm. In changing from one size of vane to another, the mass of the tie-rod was so altered as to maintain the resonant frequency of the loaded diaphragm substantially unchanged, and, therefore, also the total equivalent mass. The results are given in Table XV.

TABLE XV  
TABLE OF VANE MECHANICAL RESISTANCE TO VIBRATION (Affel)

TEST NO.	ADDED MASS OF VANE & ROD. GMS.	RESONANT FREQUENCY CYC./SEC. $f_0$	VANE AREA SQ. CM. ON ONE SURFACE	IMPEDANCE CIRCLE DIAM. OHMS. $Z_0$	DECREMENT PER SEC. $\Delta$	EQUIVALENT TOTAL MECHANICAL RES. $r$ . DYNES/KINE	EXTRA RES.
1	3.00	704	0	26.5	157	1370	—
2	3.11	689	5	21.2	167	1490	120
3	3.18	685	10	17.0	173	1570	200

It would appear from the results in the table, as far as they go, that the extra mechanical resistance of a circular disk vibrating perpendicularly to its plane in ordinary atmospheric surroundings, was about 20 dynes per kine for each sq. cm. of disk area ( $\pi a^2$ ).

A few similar measurements, made with circular disk vanes immersed in water instead of in air, gave results of roughly 500 dynes per kine, per sq. cm. of disk area, or some 25 times the mechanical resistance in air. In this case it was found that the water not only added mechanical resistance, but also an appreciable extra mass (about 0.5 gm. per sq. cm. of disk area) to the vibrating system.

These measurements are cited, not as giving definite values, but as indicating directions in which the motional-impedance methods may be applied to research on the behavior of vibrating systems.

**On Applications of the Motional-impedance Method to Architectural Acoustics.** — When the free impedance of a telephone receiver is measured with the axis of the instrument horizontal, and with its cover facing a wall of the room at not too great a distance, it is found that, near the frequency of apparent resonance,

the electric impedance of the instrument is affected by its distance from the wall. Holding the frequency steady, this impedance is found to vary if the instrument is moved nearer to, or further from, the wall which it faces. This means that the acoustic impedance, at the diaphragm, of the air in front of the instrument, is affected by the distance from the wall, in relation to the wave length of the emitted sound. The amount of variation of electric impedance, or the sensibility of the measurement to small mechanical displacements, depends upon the sharpness of resonance of the diaphragm. It seems likely that this method of measurement is capable of being applied to architectural acoustics, for example, in determining the sound-reflection coefficient of draperies. For such purposes a telephone receiver should be selected with a small gross mechanical resistance in its diaphragm, and with a small damping constant  $\Delta$ , i.e., with a large sharpness of resonance. Such an instrument would have a relatively large motional-impedance circle, and a small change of impressed frequency would carry the vector over the entire resonant range, or from one quadrantal point, through resonance over to the other. Relatively feeble reflected sound waves falling on the diaphragm would thus appreciably affect the motional impedance and enable the corresponding acoustic-impedance variation to be measured.

This effect of reflected sound waves on the motional impedance was first noticed and described in measurements made and published in 1912.\* It was found at that time that with a sharply resonant telephone receiver lying on the testing table, not only the bridge balance, but also the emitted sound, were affected by walking about the room in front of the instrument. These effects were most noticeable in the case of an experimental bipolar receiver having an unusually low value of  $\Delta$ ; i.e., about 20, and a resonant sharpness  $\Delta_0$  of approximately 323. This instrument had its diaphragm clamped between metallic circles, instead of the usual circles of molded insulating material. Its motional-impedance ratio  $Z'_0/R_1$  was, however, only  $0.436 \angle 26^\circ.5$  which does not speak highly for its sensitiveness to current flow at resonance. The acoustic changes in its electric impedance were, nevertheless, of such a nature as to suggest that by using a similarly sharply resonant receiver of good design, still larger acoustic reflection effects could be secured.

\* Bibliography 40.

## INFLUENCE OF THE DIMENSIONS OF THE DIAPHRAGM UPON ITS CONSTANTS

**Introduction.** — It was shown by Lord Rayleigh\* that the natural or free-vibration frequency  $f_f$ , of a circular plate diaphragm, such as is used in a telephone receiver, is directly proportional to the thickness, and inversely proportional to the area of the plate within the clamping circle. This is on the assumption that the material of the plate remains uniform and homogeneous; and that all other conditions remain constant. The resonant frequency to forced vibrations,  $f_0$ , of such a plate is only very slightly above the free-vibration frequency  $f_f'$  under ordinary conditions, and the two may be regarded, for practical purposes, as identical. Consequently, we should expect that in one and the same telephone receiver, using the same clamping circle and clamping conditions, the resonant frequency  $f_0$  should increase directly with the thickness of the plate. The elastic constant  $s$  may be expected to follow the equation

$$(191) \quad s = k_s \frac{b^3}{a^2} \quad \frac{\text{dynes}}{\text{cm.}},$$

where  $b$  is the thickness of the plate in centimeters,  $a$  is its clamp radius, and  $k_s$  is an elasticity constant of the material clamp, affected by the kind of clamping.

The equivalent mass  $m$  should also follow the equation

$$(192) \quad m = k_m b a^2 \quad \text{gm.}$$

where  $k_m$  is a density constant of the material (gm/cc.), affected also by the mass ratio  $m/M$ . On these premises

$$(192) \quad \omega_0^2 = \frac{s}{m} = \frac{k_s}{k_m} \cdot \frac{b^2}{a^4} \quad \left( \frac{\text{rad.}}{\text{sec.}} \right)^2,$$

and

$$(193) \quad \omega_0 = k_{sm} \cdot \frac{b}{a^2} \quad \left( \frac{\text{rad.}}{\text{sec.}} \right),$$

\* Bibliography 12, Vol. I, p. 367 (1894).

where the constant

$$(194) \quad k_{em} = \sqrt{\frac{k_s}{k_m}} \left( \frac{\text{ergs.}}{\text{gm.}} \right)^{\frac{1}{2}}.$$

Some experiments in this direction were made at the Massachusetts Institute of Technology, and at Harvard University, by Mr. C. H. Calder, in a graduation thesis, during 1915, the work being directed by the author, with the aid of Mr. H. A. Affel. Tests were made on the effect of changing the thickness of a telephone diaphragm upon the characteristics of the instrument. It would have been very desirable to have determined the effects upon all four fundamental constants  $A$ ,  $m$ ,  $r$ , and  $s$ ; but at that time the technique for determining these separately had not been completed. The tests were therefore confined to determining the motional-impedance circle with each thickness of diaphragm successively.

The same receiver and cap was used throughout the series of tests, and was of a standard make. It had a d.-c. resistance of approximately one hundred ohms at 20° C. The inner diameter of the clamping circle was 5 cm. The tests were made by obtaining the motional-impedance circle of the instrument, over a range of impressed frequency from 400 to 1500 cycles per second, as furnished by a Vreeland oscillator. The different diaphragms were obtained through the courtesy of the Western Electric Co. They were of standard ferro-type steel, in pairs of each thickness, one of the pair being japanned and the other unjapanned. They were all of the same diameter, and of approximately the same quality of metal. They varied in metallic thickness from 0.14 mm. to 0.325 mm., in five steps; viz., 0.14, 0.16, 0.21, 0.23 and 0.325 mm.

The results obtained with the japanned and unjapanned specimens of the same metallic thickness differed slightly, but not in any recognized systematic way; so that, in what follows, the mean of the two results for each thickness has been taken. When introducing a new diaphragm into the receiver, care was taken to maintain the conditions as nearly uniform as possible, and the cap was screwed on, in each instance, with substantially the same measured torque.

The results are summarized graphically in the accompanying curve sheet, Fig. 101.

Referring first to the curve  $ABC$  of natural frequency, it will be observed that as the thickness of the diaphragm was increased

from 0.14 mm. to 0.325 mm., the natural or resonant frequency  $f_0$  varied from  $A$ , at 970  $\sim$ , through  $B$  at 900  $\sim$ , to  $C$  at 1175  $\sim$ .

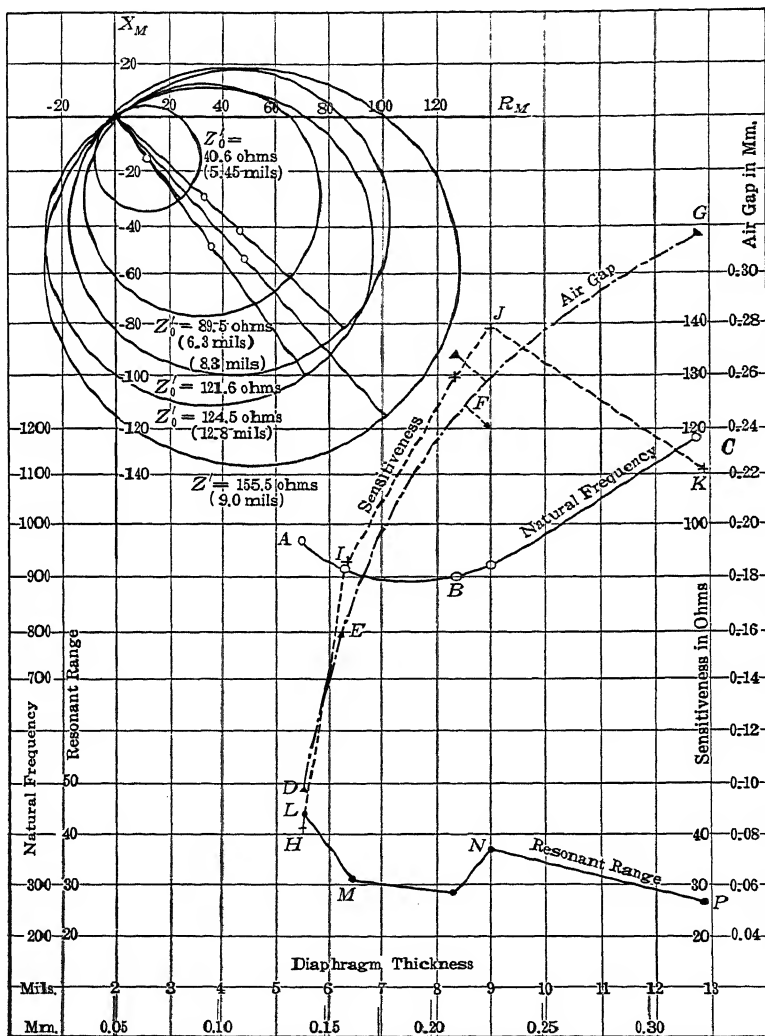


FIG. 101. Effects of changes in diaphragm thickness on instrument characteristics.

If this frequency had been simply proportional to the thickness, in accordance with (193), this curve should have been a straight line from the origin through some such point as  $B$ .



A reason for the departure from the simple straight-line law is found in the curve *DEFG* of air-gap thickness, which varied from 0.1 mm., with the thinnest diaphragm, to nearly 0.32 mm. with the thickest. These air gaps were measured by means of a depth gauge, after the diaphragms were set in place. It is evident that the thin diaphragms were bowed in, toward the center, by the magnetic attraction of the permanent poles. This inward bending not only distorts the diaphragm, and alters the magnetic-circuit conditions; but it also tends to make them behave partly like a stretched membrane, rather than wholly as a simple plate. The curve *ABC* indicates, however, a tendency to follow a simple straight-line law through the origin, towards the thicker diaphragms, which suffer the least bending and have the largest air gaps.

The graph *HIJK* shows the "sensitiveness" of the receiver with the various successive diaphragms. The ordinates are taken equal to the diametric sizes  $R'_0$  of the respective motional-impedance circles. These circles are reproduced to scale in the left-hand top corner of the figure, for the japanned diaphragms only. It will be seen that for the thinnest diaphragm, the maximum diametric impedance  $Z'_0$  is 40.6 ohms; while for the thickest diaphragm, it was 124.5 ohms. The largest circle and greatest  $Z'_0$  (155.5 ohms), is found at the intermediate thickness of 9 mils or 0.23 mm. This indicates that the greatest sensitiveness, within the range of diaphragm thickness explored, was at this particular intermediate stage.

The reciprocals of these diametric impedances would be proportional to the respective gross mechanical resistances  $r''$ , assuming that the force factor  $A$  remained constant throughout the series. The gross mechanical resistance includes the acoustic resistance, the internal frictional resistance, and the displacement resistance due to losses of energy from vibrations in the permanent magnetic field. The relations to diaphragm thickness of these components are complicated. They need much more investigation to be rendered simple.

Finally, the broken line *LMNP* represents the successive observed "resonant ranges" of the instrument, in cycles per second, as taken from the motional circles. This resonant range is directly proportional to  $\Delta = r''/(2m)$ , the damping constant. Theoretically,\* the resonant range should be inversely proportional to the

\*H. O. Taylor, Bibliography 69.

thickness, if the gross resistance  $r''$  remained constant. Actually, with  $r''$  variable, no such simple relation can be expected. The graph indicates, however, on the whole, a diminution in resonant range and in  $\Delta$ , as the thickness increases.

In a general way, therefore, the increase of thickness tends to increase the resonant sharpness  $\Delta$  of the diaphragm. (See Chapter XVII.)

It may be observed that the depression angles ( $2\beta$ ) of the diameters in the various motional-impedance circles lie fairly close together, and do not depart far from  $45^\circ$  throughout the series, which included the measurement of more than fifty motional-impedance circles. Only five of these appear in Fig. 101.

It may be inferred from these results that within the range of thicknesses explored (0.14 to 0.33 mm.) the theoretical relations in regard to  $f_0$  and  $\Delta$  are only very roughly verified, owing to secondary disturbances, especially those associated with change in air gap. It would be desirable to repeat the series of tests over a wider range in thicknesses, analyzing for  $A$ ,  $m$ ,  $r$ , and  $s$  throughout, with some compensatory adjustment to maintain nearly uniform air-gap lengths in all cases.

## CHAPTER XV

### OSCILLOGRAPHS

**Types of Oscillograph.** — An *oscillograph* is an instrument, originally developed by Blondel,\* for recording photographically the wave form of an electric current or impulse. For many purposes of investigation or analysis, the oscillograph has become an indispensable instrument in the electrical-engineering laboratory.

There are two kinds of oscillographs, namely,

- (1) Electromechanical oscillographs, in which the electric current to be studied acts magnetically or otherwise, upon a mechanical vibratory system, whose motion is photographically recorded.
- (2) Cathode-ray oscillographs, in which the electric current to be studied acts magnetically or otherwise upon a beam of cathode rays impinging on a fluorescent screen. The motion of the fluorescent patch on the screen is recorded photographically. These are generally known at present as Braun tubes.

Oscillographs of the second type have the advantage of being for all practical purposes inertialess, and therefore free from errors of inertia. For the study of very high frequencies, such as are encountered in radio-communication, these cathode-ray oscillographs are essential. On the other hand, the operation and technique of cathode-ray oscillographs are not nearly so simple and convenient as those of electromechanical oscillographs. The latter are in practically universal use for audio frequencies, i.e., frequencies up to but excluding the fourth order ( $10^4 \sim$ ).

Oscillographs of the first type are divisible into three classes:

- (a) Electromagnetic oscillographs with bifilar vibrators.
- (b) Electromagnetic oscillographs with unifilar vibrators.
- (c) Electrothermal oscillographs.

Class (a) is the one used in the vast majority of cases, and is the one specially considered in this book. Class (b) was the one

\* Bibliography 20.

first developed. Class (c) employs the thermal expansion of a fine wire carrying the current under analysis to deflect the mechanical vibratory system.

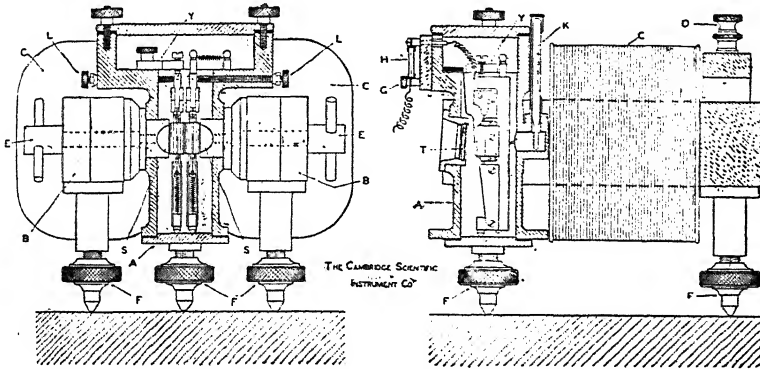


FIG. 102. Sections of Duddell double-oscillograph galvanometer through oil bath, showing both vibrators in position. *SS* polepieces of electromagnet *C*. *T* plano-convex window, *K* oil-bath thermometer.

Figure 102 illustrates a well known British form of oscillograph as developed by Duddell, and made by the Cambridge Instrument

Company. Figure 103 illustrates a well-known American form of the same electro-magnetic bifilar class, made by the General Electric Company. The fundamental principle of operation is the same for both. One or more bifilar vibrators are supported in a powerful steady magnetic field. The vibrators consist of a pair of thin strong parallel wires or strips of non-magnetic metal, supported under tension over insulating projections, in such a manner

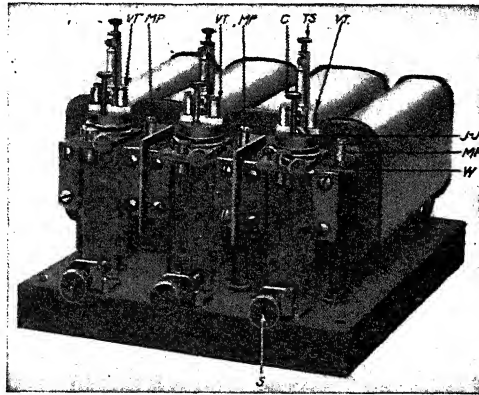


FIG. 103. General Electric Company's triple oscillograph galvanometer. *TS*, tension screw. *C*, clamping screw. *W*, screw for horizontal adjustments. *S*, screw for vertical adjustments. *JJ'*, tinned lips. *VT*, vibrator terminals. *MP*, field-magnet terminal posts.

that the electric current to be studied passes up one strip and down the other. The two strips are almost always arranged to lie in a vertical plane parallel to the direction of the steady magnetic field. A tiny mirror is fastened across the two strips.

Figure 104 illustrates a bifilar vibrator, and indicates the nature of the suspension. *AB* and *CD* are the two wires or thin strips, usually of phosphor bronze or tungsten, stretched over grooves in insulating projections. At one end, the loop of the strip passes over an insulating pulley carried by a lever, the tension of which can be adjusted by a spring. The free ends of the strip are fastened tightly to insulated terminals. The small mirror is at *m*, bridging the strips centrally and symmetrically. The mirror *m* acts as a rigid mechanical connecting piece between the strips, and also as an optical indicator to the central deflection of the system from the normal plane *ABCD*. The mirror is designed to give a minute but sufficiently large and clear beam of reflected light, from a special luminous source, for photographing its motion. It must add as small a mass and

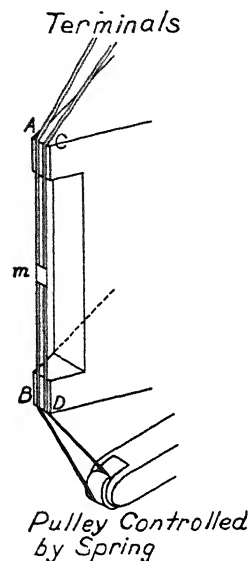


FIG. 104. Oscillograph vibrator.

moment of inertia to the suspension as is practicable, and must not connect the two strips electrically. The proper fulfillment of these conditions calls for considerable mechanical skill in construction.

When an alternating electric current is sent through the vibrator, one of the strips tends to move in the magnetic field towards, and the other away from, the observer. This puts a torque upon the system. The phase of the torque will be the same as the phase of the current at any instant, in the absence of magnetic material in the vibrator.

The suspension is ordinarily arranged to be supported in a non-magnetic tank of oil, or other damping liquid. A glass window in the oil tank allows the registering beam of light to enter and leave the face of the immersed mirror. Polepieces are often placed in the sides of the tank to carry the powerful magnetising flux with as little unnecessary magnetic reluctance as possible.

**Oscillograms.**—An oscillogram is a photographic record obtained by an oscillograph. As ordinarily obtained from the photographic fixing bath, an oscillogram shows a black line traced by the moving beam of light over the photographic film which has been rendered transparent by the process. This negative picture is the oscillogram, as usually inspected and filed away. The positive print, for subjection to analysis, shows a white line traced on a black background.

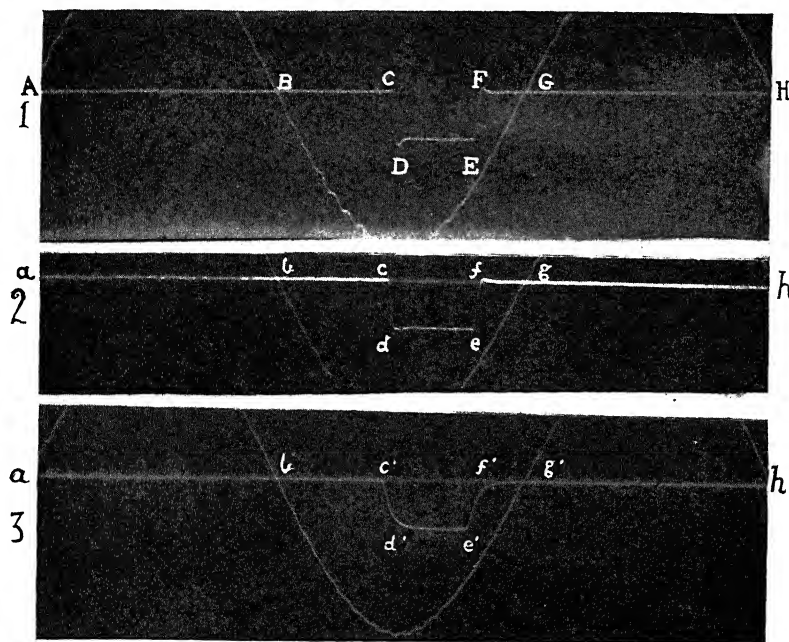


FIG. 105. Oscillograms of a rectangular current-wave impulse, lasting 0.0029 second, as recorded with a vibrator of successively varied damping and bluntness.

Oscillograms from an electromagnetic standpoint are of two kinds, namely:

- (1) Transient oscillograms,
- (2) Steady-state or steady oscillograms.

A transient oscillogram is a record of a transient movement of the vibrator, such as corresponds to the passage of a transient electric impulse through the vibrator. Such an oscillogram is indicated in Fig. 105. The impulse here recorded is a sudden single

impulse unprecedented by similar cyclic impulses. The wavy line crossing the zero at *A*, *B*, *G* and *H*, Fig. 105, is the trace of a current having a frequency of approximately  $60 \sim$ , so that the distance *BG* represents a lapse of  $1/120 = 0.00825$  second. The ripples on the wave line indicate the presence of a relatively high-frequency "tooth harmonic" in the otherwise nearly sinusoidal wave of time-marking alternating current.

A simple commutator, rotated by a small synchronous a.-c. motor, caused another vibrator tracing the zero line *ABGH* to deflect, by closing its circuit on a storage battery through a high resistance of entirely negligible inductance. The current wave impulse was therefore very nearly of rectangular form, both at making and breaking. The duration of the commutator contact and also of the current-wave impulse is seen to have been approximately one-third of a semicycle, and to have lasted 0.0029 second, or nearly 3 milliseconds. The trace produced at *CDEF* is that of the very nearly rectangular current wave, as recorded by the particular oscillographic vibrator used, which was immersed in light oil. It will be observed that the vibrator was less than critically damped; or its bluntness (see page 217) was less than unity. The precise value of  $B_0$  was not measured.

In the oscillogram No. 2, at *abgh*, Fig. 105, the vibrator was more heavily damped, being immersed in a more viscous medium oil. It will be observed that the recorded impulse *cdef* is more nearly rectangular than before; but there is a trace of overthrow or residual oscillation at *f*. The bluntness  $B_0$  is greater than in oscillogram No. 1, but remains less than unity.

In oscillogram No. 3, at *ab'g'h*, Fig. 105, the vibrator is still more heavily damped, being immersed in castor oil. Here it will be seen that the vibrator was *ultrapariodic*, or  $B_0$  was greater than unity. The recorded impulse departs considerably from the rectangular wave form.

In Fig. 105, the same substantially rectangular type of current wave impulse is recorded in three distinctly different forms, owing to the mechanical properties and inertia of the vibrator in the three cases, respectively. It is shown, in Appendix V, that no simple mechanical vibrator can be expected to record a rectangular wave impulse correctly, as a rectangular wave. It can only do so within a certain degree of approximation, depending on its free angular vibration velocity  $\omega$ , and its oscillatory bluntness  $B_0$ .

A steady oscillogram is one in which the vibration recorded is periodic and to which the suspension has been subjected for such a number of cycles that its motion is completely cyclical. A typical steady-state oscillogram is any alternating-current or alternating-voltage wave in the steady state, such as is represented in Fig. 106, where  $E$  is a nearly sinusoidal wave of impressed emf., and  $I$  is the lagging current thereby established in a star group of transformers. In this oscillogram, time is to be read from right to left, or in the opposite sense to that ordinarily employed. At the starting point on the right, the emf.  $E$  is passing through zero towards the negative values; but the current  $I$  does not pass through zero until about  $20^\circ$  later in the emf. cycle.

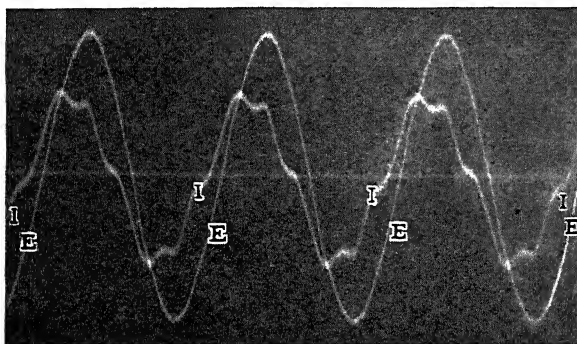


FIG. 106. Rectangular coordinate oscillogram.  $E$ , impressed emf. at  $60 \sim$  with small ripple at tooth frequency.  $I$ , lagging current, supplied to group of transformers in star connection with triple-frequency harmonic removed and with a strong fifth-frequency harmonic.

Both transient and steady oscillograms obtained from mechanical vibrators are subject to errors of inertia. The motion, as photographed, does not correspond completely to the impulse, owing to the inertia of the moving system. The error is liable to be considerable in transient oscillograms, especially if the recorded impulses are swift and sudden. It is also likely to be considerable in steady oscillograms of high-frequency waves. The error is commonly small in steady oscillograms of ordinary power frequencies, if the harmonics are few, and of relatively low orders.

It is proposed to consider, in this and the following chapter, the nature and extent of the errors in steady oscillograms, as well



as the procedure for determining them. Incidentally, however, these considerations will be applicable in part to transient oscillograms.

**Oscillogram Coordinates.** — Oscillograms may be prepared and presented to either (1) rectangular coordinates; or (2) polar coordinates. In the rectangular coordinate system, which is the system in more general use, the horizontal axis parallel to the length of the photographic film is the time axis, and is ordinarily read from left to right in the direction of increasing time. The quadrature component is that of wave amplitude, and is ordinarily read as positive above the time axis, and negative beneath.

In the polar coordinate system, the slope or angle increases directly with time, and is usually read in the counter-clockwise direction with increasing time. The size or length of the radius vector, measures the instantaneous amplitude. Figure 107 is an example of a *polar oscillogram*. Figures 105 and 106 are *rectangular oscillograms*.

In the ordinary rectangular oscillogram, the uniform peripheral time movement of the recording film is commonly provided by a small auxiliary rotating motor. It is important that its velocity should be uniform during the photographic exposure; since small deviations in uniformity may give rise to serious apparent distortions of wave form. An oscillogram is in a certain sense a test of the uniform angular velocity of the auxiliary driving motor. A sprocket-chain drive with a lumpy link, or a string drive with a lumpy knot, may be responsible for distortions in the oscillogram secured through their use.

In the polar oscillogram, the uniform rotation with time is also ordinarily provided by an auxiliary rotating motor, concerning the behavior of which similar remarks apply.

Figure 107 is a circular-zero polar oscillogram of emf. and of current, as produced by a Chubb rotary oscillograph. The circle OOOO is the zero line for emf. The closed curve  $E_0 E E_2 E_3$ , intersecting this zero-circle at diametrically opposite points, is the photographic trace of one cycle of the emf. wave, which in this case was nearly sinusoidal. At any point on this emf. wave, the radial distance from the zero circle to this point measures the emf. at that instant, counting radial distances outwards from the center as positive. At  $E_0$  and  $E_2$ , the emf. passed through zero. At  $E$ , it reached a positive maximum, and at  $E_3$  a negative maximum.

The zero line for the current wave is the outer circle  $O'O'O'$ . The closed curve  $I_0 I_1 I_2 I_3$ , intersecting this circle at diametrically opposite points, is the current wave. The phase lag, or time-phase displacement, between the zeros of emf. and current is  $57^\circ$ . The current passes through zero at  $I_0$  and  $I_2$ . It reaches a positive maximum at  $I_p$ , near to the descending zero instant of the emf. It also reaches a negative maximum at  $I_m$ , near to the ascending zero of the emf.

The emf. and current were supplied in this case to a large 60 ~ transformer (4166 Kva), at a frequency of 25 ~. The effective emf. was 5560 volts rms., and the effective current 7.2 amperes. It will be seen that an advantage in favor of the polar oscillogram is that a phase displacement is presented as an angle.

Each wave on such a circular-zero polar oscillogram is arranged to be copied on a metallic sheet or template. The outer edge of the template, when properly cut, coincides with the photographic curve of the wave on the oscillogram. The template is then mounted on a Chubb analyzer, and the values of the successive Fourier components in the wave (see Appendix XIII), are then obtained by the aid of a mechanical process. By applying a small driving motor to the analyzer, the procedure has been made almost entirely automatic.

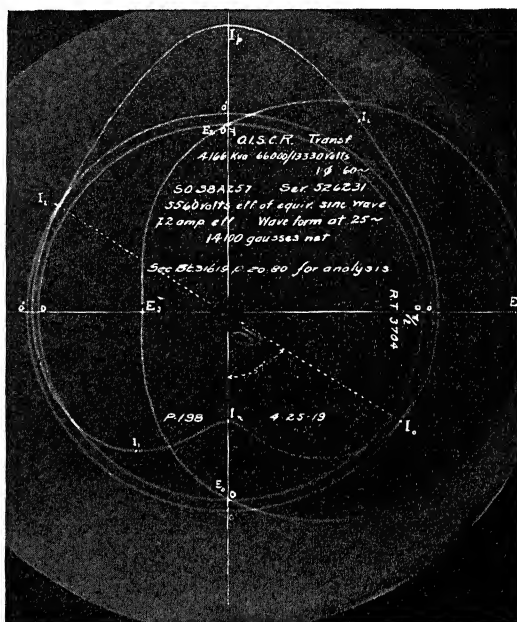


FIG. 107. Circular zero polar oscillogram of voltage and current supplied to a large transformer, operating at a flux density of 14.1 kilogausses maximum cyclic  $B$ .

In the case of Fig. 107, the harmonic analysis of the voltage wave is given as:

ORDER OF HARMONIC	A SINE	B COSINE	C RESULTANT
1	+ 100	- 1.1	100.0
3	0	0	0
5	+ 0.8	+ 0.8	1.1
7	0	+ 0.4	0.4
9	0	0	0
11	0	+ 0.3	0.3

The values in column C are in percentages of the equivalent sine-wave amplitude. It will be seen that the third and ninth frequency harmonics are absent, while the largest harmonic present up to the 11th inclusive had a resultant amplitude of only 1.1 per cent.

The exciting current wave supplied to the transformer has the following analysis given for it.

ORDER OF HARMONIC	A SINE	B COSINE	C RESULTANT
1	+ 1.11	- 6.74	6.82
3	+ 0.156	- 3.56	3.56
5	+ 0.086	- 1.17	1.17
7	+ 0.056	- 0.28	0.28
9	0	- 0.128	0.128

The resultant amplitude values in column C are expressed in maximum cyclic gilberts-per-cm. of average magnetizing force around the magnetic circuit of the transformer. It will be seen that there is a third-frequency harmonic having an amplitude of more than 50 per cent of that of the fundamental.

The polar oscillogram has one inherent advantage, that if the rotation can be made exactly synchronous with the alternating current to be studied, several overlapping cycles can be recorded by repetition over the same path. If the motions are all uniform, these repetitions will substantially coincide, and thus furnish a test of reliability in this respect. The rectilinear oscillogram does not so readily offer a test of repetitive uniformity, unless driven by a synchronous motor. On the other hand, where transients or progressive changes in the wave are under consideration, the

rectilinear oscillogram has advantages in keeping the successive waves separated. Most persons more readily comprehend an oscillogram in the rectilinear than in the polar form, and some persons even prefer to convert a polar oscillogram into rectangular form, in order to analyze it.

The polar form of oscillograph facilitates the evaluation of the root-mean-square of a complex harmonic wave; because, as is well known,\* the area of a polar oscillogram is directly proportional to the root-mean-square value of the wave therein recorded, no matter how many harmonic ripples may be present in it.

**Correction Data for Marking upon Oscillograms.**— Every oscillogram that is intended for careful analysis should be accompanied by the necessary data from which to obtain, if necessary, the corrections for inertia. We shall see that there are two necessary and sufficient data for this purpose; namely (1) the resonant frequency  $f_0$  of the vibrator, and (2) its bluntness  $B_0$ . These two data, or their equivalents, will always furnish the material for correcting the indication of any steady oscillogram, at any assigned frequency under examination. It may be advantageous to record also the temperature of the damping fluid at the time of observation.

\* D. C. Jackson, *Alternating Currents and Alternating-Current Machinery*, The Macmillan Co., 1913, page 15.

## ANGULAR VELOCITY OF A ROTATIONAL VIBRATING SYSTEM

**Introduction.** — In Chapter VI, consideration was given to the rectilinear vibration velocity steadily set up in a simple vibratory system having a single degree of rectilinear freedom, under an impressed vmf.

In this Chapter, it is proposed to consider the cyclic angular velocity which may be steadily set up in a corresponding simple vibratory system, having a single degree of rotary freedom about an axis, under an impressed alternating vibromotive force, which is also applied about that axis, and which is therefore an alternating vibromotive twist or *vibromotive torque* (vmt.). There is a close analogy between the two cases. So close is the analogy, indeed, that it is often sufficient for the trained mathematician to have the new problem enunciated to him and he will immediately reinterpret the rectilinear-motion equations of the first case, into the corresponding angular-motion equations of the second case, and apply them accordingly. However, the dynamical difference between the two cases is sufficiently great to make a rediscussion of the problem either necessary or desirable for the student of electrical engineering.

A force acting about a rotation axis is called a "couple" in mechanics, and is also called a "torque." A torque is defined, in reference to any given axis, by a force acting perpendicularly to a radius arm of stated length. In the fundamental C. G. S. system, which we shall use throughout, a torque is expressed in dynes force, acting perpendicularly to a radius arm of stated length in cm., the arm being supposed to project perpendicularly from the axis. Thus a torque is expressed in dyne-cm. A torque of 5000 dynes-cm. would be such as would be developed either by 5000 dynes acting perpendicularly to the axis and to a lever arm 1 cm. long, itself perpendicular to the axis; or by 1000 dynes similarly acting on a lever arm 5 cm. long, or by a force of  $f$  dynes acting on an arm of  $a$  cm. length, provided that  $fa = 5000$ .

There is the objection to the unit dyne-cm. as representing torque, that it conflicts with the dyne-cm. or erg, which is the unit of work. It is well known that a torque does no work, unless it moves through an angle. If  $\beta$  is the angle in circular radians through which the torque  $\tau'$  moves, about the axis to which it is applied, the work done is

$$(194a) \quad w = \tau' \beta \quad \text{ergs or torque-radians.}$$

In order, therefore, to avoid the ambiguity raised by such a double meaning of the term dyne-centimeter, we shall use the term dyne-perpendicular-centimeter, abbreviated dyne-p.-cm., to signify a torque of one dyne acting at a radius arm of one cm.

**Rotational Velocity.** — Just as a rectilinear force, applied to a simple rectilinear-vibration system, tends to set up rectilinear velocity therein; so a torque, applied to a simple rotation-vibration system, tends to set up rotational velocity therein. An alternating vibromotive torque tends to set up alternating angular velocity. The law is the same in each case, and corresponds to that of alternating current in the simple  $\mathcal{E}RS$  branch circuit of Fig. 27. With reference to the schedule on page 44, we have, in addition, the following:

Angular velocity is expressed in circular radians per second, and is denoted by the symbol  $d\theta/dt$  abbreviated to  $\dot{\theta}$ , where  $\theta$  is the angle or rotational displacement, in radians of  $57^\circ.296$  each. The maximum cyclic value of alternating angular velocity is denoted by the symbol  $\dot{\theta}_m$ . The root mean square of an alternating angular velocity of any single frequency is  $\dot{\theta}_m/\sqrt{2}$ , or  $0.707 \dot{\theta}_m$ , following the analogy of simple alternating rectilinear vibrations or of simple alternating electric currents.

The angular displacement of the optical beam in an oscillograph is, by a well-known law of optics, double the actual angular displacement of the vibrator mirror. In our theory, it is the mirror and not the reflected beam whose angular displacement and velocity are considered. Mirror displacements at maximum cyclic value are commonly of the order 0.015 radian or 1.5 cm. at a range of 1 meter. Angular velocities are expressed by the relation already found in the rectilinear case (see page 45)

$$(194b) \quad \dot{\theta}_m = j\omega \theta_m \quad \frac{\text{rad}}{\text{sec.}}$$

TABLE XVI  
COMPARISON BETWEEN THE ESSENTIAL QUANTITIES IN THE ELECTRIC, RECTILINEAR MECHANICAL,  
AND ROTATIONAL MECHANICAL VIBRATION SYSTEMS

ELECTRIC			MECHANICAL			
			RECTILINEAR		ROTATIONAL	
Electromotive force	$E$	Abvolts	Vibromotive force	$F$	Vibromotive torque	$F$
Electric current	$I$	Abamperes	Mechanical velocity	$\dot{x}$	Angular velocity	$\dot{\theta}$
Electric quantity	$q$	Abcoulombs	Mechanical displacement	$x$	Angular displacement	$\theta$
Electric resistance	$r$	Abohms	Mechanical resistance	$r$	Moment of resistance	$r$
Electric inductance	$\mathcal{L}$	Abhenries	Mechanical mass	$m$	Moment of inertia	$m$
Electric elastance	$s$	Abdarafs	Mechanical elastance	$s$	Moment of elastance	$s$
Electric ind. reactance	$\mathcal{L}\omega$	Abohms	Mechanical mass reactance	$m\omega$	Moment of mass reactance	$m\omega$
Electric elas. reactance	$s/\omega$	Abohms	Mechanical elas. reactance	$s/\omega$	Moment of elas. reactance	$s/\omega$
Electric cur. impedance	$z$	Abohms $\angle$	Mechanical vel. impedance	$z$	Moment of vel. impedance	$z$
Electric displ. impedance	$z'$	Abvolts $\angle$ Abcoulomb	Mechanical displ. impedance	$z'$	Moment of displ. impedance	$z'$
						Dynes Kines Cm. Dynes Kine Gm. Dynes Cm. Dynes Kine Dynes Kine Dynes Kine Dynes Kine Abvolts Abcoulomb
						Dyne-p-cm. Radians Sec. Cir. radians Dyne-p-cm. Rad/Sec. Gm-cm. <sup>2</sup> Dyne-p-cm. Radian Dyne-p-cm. Radian/Sec. Dyne-p-cm. Radian/Sec. Dyne-p-cm. Radian/Sec. Dyne-p-cm. Radian

**Moment of Inertia.** — As is fully explained in textbooks on dynamics, the moment of inertia of a simple vibratory system is the integral

$$(194c) \quad \mathbf{m} = \int a^2 \cdot dm_0 = \underline{a^2} m_0 \quad \text{gm.-cm.}^2,$$

where  $dm_0$  is the mass of each element of volume in the system, and  $a$  is its radial distance from the axis of rotation. In the C. G. S. system, the integral will be expressible in gm.-cm.<sup>2</sup>. If this integral be expressed as  $\underline{a^2} m_0$ , where  $m_0$  is the total mass of the rotating system, the quantity  $\underline{a^2}$  is the mean square of all the radii entering into the integral, and  $\underline{a}$ , the root-mean-square radius, is called the *radius of gyration*. The actual system therefore behaves as though its mass were concentrated into a uniform ring of very thin wire lying in the plane of angular rotation, the ring having its center on the axis of rotation, and a radius equal to the radius of gyration  $\underline{a}$ .

It is difficult to compute with precision the moment of inertia of a bifilar oscillograph vibrator as actually used, if only for the reason that when the vibrator is immersed in liquid, its effective mass  $m_0$  is found, by experiment, to be greater than the mass of the vibrator itself. It is evident that a layer of the liquid attaches itself to the vibrator in rotation, and serves to increase the virtual mass. It would be interesting to investigate this subject, in order to ascertain the thickness of the virtual liquid attachment film, and how this is affected by the nature of the liquid and the geometry of the immersed vibrator system. The motional impedance of the system would enable such determinations to be made.

A common value of  $\mathbf{m}$  in oscillograph vibrators immersed in damping liquid seems to be about  $10^{-7}$  gm.-cm.<sup>2</sup>.

**Kinetic Energy of Angular Velocity.** — The maximum cyclic kinetic energy of rotation in a vibrating system is

$$(194d) \quad W_k = \frac{1}{2} \mathbf{m} \dot{\theta}^2 \quad \text{ergs,}$$

which corresponds precisely to the corresponding formula (29) for a rectilinear system. The average kinetic energy throughout a cycle is half the maximum cyclic value.

Thus a vibrator mirror executing vibrations of 0.015 radian maximum cyclic displacement, at a pure frequency of 60 ~, would have a maximum cyclic angular velocity of  $0.015 \times 60 \times 2 \pi = 5.66$  rad./sec. With a moment of inertia of  $10^{-7}$  gm.-cm.<sup>2</sup>, the



maximum cyclic kinetic energy would be  $5.66^2 \times 10^{-7} \div 2 = 1.60 \times 10^{-6}$  ergs or 1.6 microergs. The average kinetic energy would be 0.8 microergs.

**Elastic Restoring Torque and Potential Energy.** — It is generally assumed, and apparently with satisfactory justification, that the elastic torque which opposes vibratory displacement and tends to restore the system to its normal zero position of repose is, for the small range of vibratory displacement employed, directly proportional to the displacement. In a bifilar vibrator, this torque increases with the distance between the centers of the two strips and also with their tension. It is reckoned in dyne-p.-cm. per radian of displacement, on the understanding that the actual displacement shall not exceed a few centiradians, or a few degrees. A common value of the restoring torque, which we may denote by  $s$ , in an oscillograph vibrator, appears to be of the order 100 dyne-p.-cm. per radian; so that a maximum cyclic mirror displacement of 0.015 radian would develop a corresponding maximum cyclic restoring torque of say 1.5 dyne-p.-cm. Following the analogy of the rectilinear case in (30) the average cyclic torque would be half the maximum, and the work done in displacement would be

$$(195) \quad W_e = -\frac{s\theta_m}{2} \cdot \theta_m = -\frac{s}{2} \theta_m^2 = -\frac{s}{2} \left( \frac{\dot{\theta}_m}{j\omega} \right)^2 = \frac{s}{2} \frac{\dot{\theta}_m^2}{\omega^2} \quad \text{ergs.}$$

In the case considered, the work done would be  $1.5 \times 0.015/2 = 0.0113$  erg. This is the maximum cyclic elastic potential energy stored in the system. Under forced vibrations, the kinetic and potential cyclic energies are independent, except at the resonant frequency  $f_0$ , when the two become exactly equal. In this condition, the energy in the vibration system remains constant during the steady state. What the system lacks in kinetic energy, it acquires in potential energy, and reciprocally, so that the vibromotive torque does not have to furnish any energy cyclically to the system. At other impressed frequencies, the vibromotive torque is called upon to furnish energy cyclically to the system for storage, either in unsatisfied kinetic or elastic needs. This is in addition to the active energy which is continually dissipated in friction.

**Resonance.** — Following the analogy of (31), we equate the elastic and kinetic energies at resonance

$$(196) \quad W_k = W_e = \frac{m}{2} \dot{\theta}_m^2 = \frac{s}{2} \frac{\dot{\theta}_m^2}{\omega_0^2} \quad \text{ergs,}$$

and

$$(197) \quad \omega_0 = 2 \pi f_0 = \sqrt{\frac{s}{m}} \quad \frac{\text{radians}}{\text{sec.}}$$

Thus an oscillograph having  $s = 10^2$  and  $m = 4 \times 10^{-7}$ , would have  $\omega_0 = \sqrt{2.5 \times 10^8} = 15811$ , and  $f_0 = 2517 \sim$ .

The resonant frequency or angular velocity is of first importance in the oscillograph theory. It may be defined in various ways, such as those that follow:

Under gradually increased frequency of constant impressed sinusoidal torque:

- (1) The resonant frequency is the frequency at which the maximum cyclic potential and kinetic energies are equal.
- (2) The maximum cyclic potential and kinetic powers are equal.
- (3) The total internal energy remains constant.
- (4) The mechanical impedance is a minimum.
- (5) The maximum cyclic angular velocity becomes a maximum.
- (6) The maximum cyclic angular velocity comes into cophase with the torque.
- (7) The power expended in dissipation becomes a maximum.

All of the above definitions will be evident, by analogy, to students familiar with the properties of simple alternating-current circuits.

**Resistance Torque.** — When an impressed alternating torque acts upon a vibratory system, it has to overcome an opposing torque of resistance, expressible in dynes-p.-cm. This torque is assumed to be simply proportional at any instant to the angular velocity of the system. It is well known that the friction between a liquid and the surface of a solid body immersed therein, such as the submerged surface of a boat in water, is not simply proportional to the ordinary velocity, but is more nearly proportional to the square of the velocity. For the relatively very small peripheral velocities of an oscillograph vibrator, in its damping liquid, the friction appears to be simply proportional to the first power of the velocity (see Appendix XII). This fortunately keeps the principal formulas of the oscillograph from becoming complicated, and maintains the analogy of Ohm's law. It also involves the consequence that the power dissipated by a vibrator in overcoming the frictional torque is directly proportional to the square of the angular velocity.

If  $r$  is the resistance torque coefficient in dynes-p.-cm., per

radian-per-second or per unit of angular velocity, the maximum cyclic resistance torque is, following (34)

$$(198) \quad f_m = -\mathbf{r} \dot{\theta}_m \quad \text{max. cyc. dynes-p.-cm. } \angle.$$

The resistance coefficient  $\mathbf{r}$  is a real quantity. If  $\dot{\theta}_m$  is regarded as a complex quantity, having a phase or slope as well as a size; then the torque  $f_m$  will have the same slope. The negative sign indicates that the resistance torque opposes the motion. Similarly, if we use  $\dot{\theta}$  as the rms. value of angular velocity

$$(199) \quad f_r = -\mathbf{r} \dot{\theta} \quad \text{rms. dynes-p.-cm. } \angle.$$

If  $\mathbf{r} = 10^{-3}$  in an oscillograph, and  $\dot{\theta}_m = 20$  rad./sec.,  $f_m = 0.02$  maximum cyclic dyne-p.-cm.

**Inertia Reactance and its Torque.**—Following the rectilinear analogy, a vibrator system having a moment of inertia  $\mathbf{m}$ , develops a mass reactance of  $j\mathbf{m}\omega$  dynes-p.-cm./(radian-per-sec.) where  $\omega$  is the angular velocity of the impressed frequency. As in the rectilinear case, a maximum cyclic angular velocity of  $\dot{\theta}_m$  radians per sec. develops a mass reactive torque of  $-j\mathbf{m}\omega\dot{\theta}_m$  dynes-p.-cm.

**Elastic Reactance and its Torque.**—Referring to the rectilinear analogy, a vibrator system having an elastic torque coefficient  $\mathbf{s}$  develops an elastic reactance of  $-j\mathbf{s}/\omega$  dynes-p.-cm./(radian-per-sec.), and a maximum cyclic angular velocity developed by the vibrator gives rise to a maximum cyclic elastic torque of  $j\frac{\mathbf{s}}{\omega}\dot{\theta}_m$  dynes-p.-cm. for the impressed torque to overcome.

**Impedance to Angular Velocity, and the Corresponding Torque.**—Continuing the analogy to the rectilinear case and to a branch alternating-current circuit, like that of Fig. 27, a vibrator system will develop a mechanical impedance to angular velocity:

$$(200) \quad \mathbf{z} = \mathbf{r} + j(\mathbf{m}\omega - \mathbf{s}/\omega) \quad \frac{\text{dynes-p.-cm.}}{\text{radians per sec.}} \angle.$$

The mass reactance is essentially a  $+j$  quantity, and the elastic reactance an essentially  $-j$  quantity, by definition and convention.

For values of  $\omega$  less than the resonant value  $\omega_0$ , the  $j$  term in (200) is essentially negative; while for values of  $\omega$  greater than  $\omega_0$ , the  $j$  term is essentially positive. At the resonant value  $\omega_0$ , the imaginary term disappears and the impedance degenerates to simple mechanical resistance.

It is convenient to introduce a symbol  $u$  for the ratio of impressed frequency to resonant frequency, and to call it the *frequency ratio*. That is

$$(201) \quad u = \frac{f}{f_0} = \frac{\omega}{\omega_0}.$$

Consequently, when  $u < 1$ ,  $\mathbf{z}$  in (200) has a negative slope  
when  $u > 1$ ,  $\mathbf{z}$  “ ” has a positive slope  
when  $u = 1$ ,  $\mathbf{z}$  “ ” has zero slope.

Following what has been shown in Table VI and Fig. 28, for a rectilinear case, Fig. 108 represents the impedance graph to angular velocity of a vibrator having the following constants:  $\mathbf{r} = 10^{-2}$ ,  $\mathbf{m} = 5 \times 10^{-7}$ ,  $\mathbf{s} = 2 \times 10^2$ ,  $\omega_0 = 20,000$ . This graph might equally represent the corresponding rectilinear vibratory case with  $m = 5 \times 10^{-7}$ ; or it might represent the impedance to current in an a.-c. branch circuit having, say, the constant  $r = 10^3$  ohms,  $\mathcal{L} = 5 \times 10^{-2}$  henries,  $s = 2 \times 10^6$  darafs,  $\omega_0 = 20,000$ .

In the vibrator case, unit length on the diagram would then represent  $10^{-2}$  mechanical ohms or dyne-p.-cm./ (radian per sec). In the electric case, unit length would represent 100 ohms.

Figure 108 is drawn in terms of the frequency ratio  $u$ . The vector impedance is presented between the limits of  $u = 0.2$  and  $u = 5$ . The lower and upper quadrantal values are at  $OB$  and  $OE$ , for  $u_1 = 0.618$  and  $u_2 = 1.618$  respectively, corresponding to  $\omega_1 = 12361$  and  $\omega_2 = 32361$  radians per second. The quadrantal range in this case is thus from 0.618 to 1.618 in  $u$ .

**Vector Angular Velocity Admittance.** — Following the rectilinear-vibration analogy al-

ready developed in connection with formula (50) and Fig. 29,

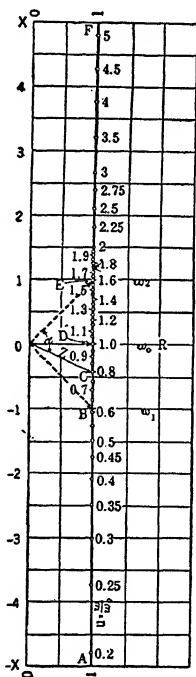


FIG. 108.

Retilinear graph of impedance to current for cases of

$$\left\{ \begin{array}{l} r = 10^2, \quad f = 5 \times 10^{-3}, \quad s = 2 \times 10^6 \\ r = 10^{-2}, \quad m = 5 \times 10^{-7}, \quad s = 2 \times 10^2 \end{array} \right\}$$

In the electric case, unit length =  $10^2$  ohms.

In the electric case, unit length =  $10^9$  ohms.  
In the mechanical case, unit length =  $10^{-2}$  mechanical abohms  
or dynes-p.-cm. per radian per sec.

the admittance to angular velocity in a simple rotational system is  $\mathbf{y}$ , the vector reciprocal of the impedance  $\mathbf{z}$ , and has a circular locus passing through the origin and centered on the conductance axis. Figure 109 is such an admittance graph for the impedance diagram of Fig. 108. The graph is marked off in terms of the frequency ratio  $u$ , and the value  $u = 1$  always appears opposite the diameter.  $Y_1$  and  $Y_2$  are the lower and upper quadrantal points, with frequency ratios  $u_1$  and  $u_2$ . At any impressed frequency,  $\omega = u\omega_0$ .

$$(202) \quad \mathbf{y} = \frac{1}{\mathbf{z}} = \frac{1}{r + j(\mathbf{m}\omega - \mathbf{s}/\omega)} = \mathbf{g} + j\mathbf{b}$$

mechanical abmhos, or  $\frac{\text{radians/sec.}}{\text{dynes-p.-cm.}} \angle,$

where  $\mathbf{g}$  is the *mechanical conductance* and  $\mathbf{b}$  the *mechanical susceptance* to impressed angular velocity.

At any two opposite points in the circle having the slopes  $+\alpha$  and  $-\alpha$  respectively, with frequency ratios,  $u_1, u_{11}$ , the relation holds, following (104).

$$(203) \quad u_1 u_{11} = 1.$$

The pair of ratios  $u_1$  and  $u_2$  are a particular case included under (203).

It may be noted, in comparing impedance and admittance graphs, like those of Figs. 108 and 109, that frequencies or frequency ratios advance counterclockwise in Fig. 108; but clockwise in Fig. 109. Moreover, any positive vector slope  $\alpha$  in Fig. 109 corresponds to a negative slope in Fig. 108.

**Vector Angular-Velocity Circular Locus.** — Corresponding to what has been already considered in connection with rectilinear vibration and Fig. 29, any circular-admittance graph for an angular vibration system may also be regarded as a graph of angular velocity in that system under varied frequency with any given constant vmt. Thus, if, in the equation,

$$(204) \quad \dot{\theta}_m = \frac{\mathbf{F}_m}{\mathbf{z}} = \mathbf{F}_m \mathbf{y} \quad \text{max. cyc.} \frac{\text{radians}}{\text{sec.}} \angle,$$

we have only to assign unit size and zero slope to  $\mathbf{F}_m$  in order to obtain numerical identity between the values of the maximum cyclic angular velocity and the vector admittance  $\mathbf{y}$ . Whatever size the impressed torque  $\mathbf{F}_m$  may have, so long as its slope is taken as zero, the graph of  $\mathbf{y}$  can still be regarded as the graph of  $\dot{\theta}_m$ , to a suitably altered scale of linear dimensions.

We may therefore infer that when a constant maximum cyclic torque is steadily impressed upon any simple vibrator system, with successively increasing frequency, the maximum cyclic

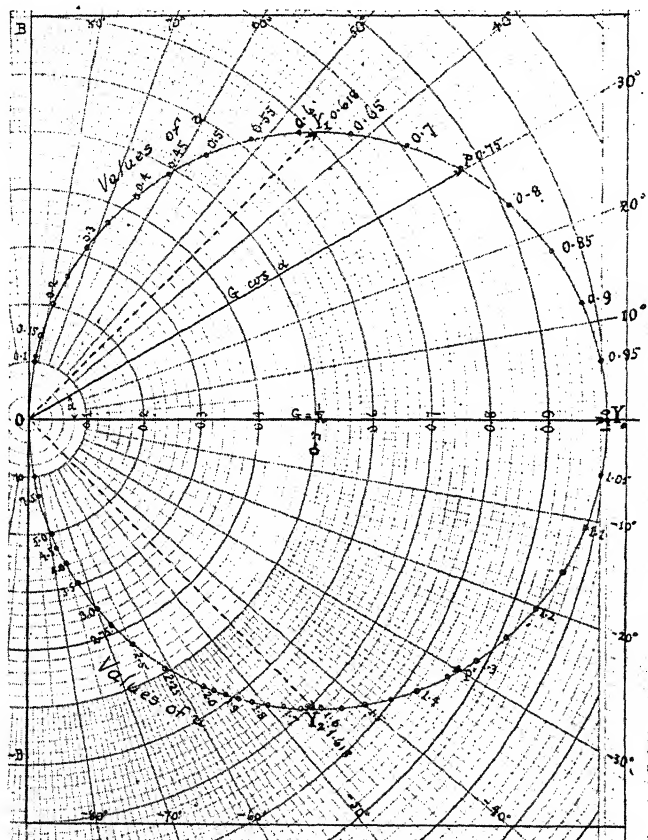


FIG. 109. Circular graph of admittance to current or to velocity for cases of

$$\left\{ \begin{array}{l} r = 10^2, \quad \mathcal{L} = 5 \times 10^{-3}, \quad s = 2 \times 10^6 \end{array} \right\} \omega_0 = 20,000, \Delta = 10,000$$

$$\left\{ \begin{array}{l} r = 10^{-2}, \quad m = 5 \times 10^{-7}, \quad s = 2 \times 10^2 \end{array} \right\} B_0 = 0.5$$

In the electric case, unit length represents  $10^{-2}$  mho.

In the mechanical case, unit length represents  $10^2$  mechanical abmhos or radians per sec. per unit vmt.

angular velocity thereby developed will follow the circular-admittance graph of the system. At a very low impressed frequency, the velocity generated will be very small, and in leading quadrature with the vmt. That is, the maximum cyclic angular velocity

generated will be at the instants when the torque is passing through zero. As the impressed frequency is increased, the corresponding angular velocity will increase according to the chord of the admittance circle, and come more nearly into phase. At resonance, when  $u = 1$ , the maximum cyclic generated angular velocity will be a maximum, will have a size of  $\mathbf{F}_m/\mathbf{r} = \mathbf{F}_m \cdot \mathbf{g}$  radians per second, and will be completely in phase with the vmt. As  $u$  is further increased, the velocity will fall off and lag in phase, until at a very high value of  $u$ ,  $\dot{\theta}_m$  will be very small and in lagging quadrature with  $\mathbf{F}_m$ .

At the quadrantal frequencies  $f_1$  and  $f_2$ , as particular cases, the size of the generated angular velocity will be 0.707 or  $2^{-1/2}$  of that at resonance, and will be in *semiquadrature* to the impressed vmt.

Thus, in Fig. 109, interpreted electrically at  $10^{-2}$  mho per unit of length, with impressed frequency  $\omega = 10,000$  radians per second or  $u = 0.5$ ,  $y = 0.555 \times 10^{-2} \angle 56^\circ.3$ ; so that 1 volt maximum cyclic emf. at this frequency and at standard phase, applied to the  $\mathcal{E}RS$  branch circuit of Fig. 27 of the constants chosen above, would establish a current of  $0.555 \times 10^{-2} \angle 56.3$  maximum cyclic amperes, or 5.55 maximum cyclic milliamperes, leading the emf. by  $56^\circ.3$ . If, however, the mechanical application of Fig. 109 is considered, with 100 mechanical abmhohs to the unit of length, one maximum cyclic dyne-p.-cm. applied to the vibrator at  $\omega = 10,000$  or  $u = 0.5$ , would establish a maximum cyclic angular velocity of  $\dot{\theta}_m = 55.5 \angle 56^\circ.3$  radians per sec. As the vibrator mirror crossed the zero point of its scale, it would be moving with the angular velocity of 55.5 radians per second or 3180 degrees per second, and the zero would be crossed  $56^\circ.3$  ahead in phase of the impressed vmt.

## CHAPTER XVII

### BLUNTNESS AND SHARPNESS OF RESONANCE IN A VIBRATOR

A sharply resonant electric or mechanical system is one in which the maximum of the curve of current or velocity (rectilinear or angular) with respect to impressed frequency, is sharp and steep. On the contrary, such a system is bluntly resonant when the same maximum is slight and gradual. For example, curve *I* of Fig. 127 represents a case of sharp resonance; while curve *III* of the same figure represents a case of blunt resonance.

**Sharpness of Resonance.** — The term “sharpness of resonance” requires, however, to be quantitatively defined, and this may be done in various ways. It has been defined as the ratio of either the mass reactance or the elastic reactance at resonance to the resistance of the circuit or system. In a simple  $\mathcal{E}RS$  branch circuit, like that of Fig. 27, this would also be the ratio of the resonant condenser voltage to the voltage across the mains. If we denote the sharpness of resonance thus defined by the symbol  $\Lambda_s$ , we have the following relations:

$$(205) \quad \Lambda_s = \frac{\mathcal{E}\omega_0}{r} = \frac{m\omega_0}{r} = \frac{\omega_0}{2\Delta} = \omega_0\tau_s = \frac{\pi f_0}{\Delta} = \frac{f_0}{\left(\frac{\Delta}{\pi}\right)} = \frac{s}{r\omega_0} = \frac{z_0}{r}$$

$$= \frac{1}{cr\omega_0} = \frac{\omega_0}{\omega_2 - \omega_1} = \frac{f_0}{f_2 - f_1} = \frac{1}{u_2 - u_1} = \frac{\Lambda_0}{2}$$

where  $\tau_s = m/r = \mathcal{E}/r$  is the time constant of a system containing negligible elastance; i.e., only mass and resistance. A unidirectional current from which the supporting emf. is suddenly withdrawn in such a circuit falls to  $1/e$ th in a time equal to  $\tau_s$  seconds. This value of resonant sharpness has been employed by several writers.\* Sharpness of resonance was defined by Dr. R. L. Jones, in 1914,† as the diminution in the resonant kinetic energy per unit of mistuning, which leads to  $\Lambda_s$ , as in (205). In discussing oscillographs, however, there is an advantage in using a different definition, which gives a numerical value twice as great. We may

\* Bibliography 50, 56, 78.

† Bibliography 50.



define the sharpness as the size ratio of the vector change in current or velocity at resonance to any small change in the impressed frequency ratio  $u$ . If the velocity at resonance ( $u = 1$ ) is  $\dot{x}_0$ , then a small change of frequency ratio  $du$  will involve a departure from resonance and produce a change  $d\dot{x}$  in the velocity, so that calling  $\Lambda_0$  the sharpness of resonance thus defined

$$(206) \quad \frac{d\dot{x}}{d\omega} = \frac{d\dot{x}}{\dot{x}_0} = \frac{d\dot{x}}{\dot{x}_0} = -j \frac{\omega_0}{\Delta} = -j \Lambda_0.$$

Thus, if  $u$  be increased from 1.0 to 1.01, or by 1 per cent, and the vector change in the current is  $-j10$  per cent; then the sharpness of resonance  $\Lambda_0 = 10$ . In the case of Fig. 108,  $\Lambda_0 = 2$ . The relations of  $\Lambda_0$  are, if  $\rho = r/2$  and  $z_0 = \sqrt{\mathcal{E}/c}$ ,

$$(207) \quad \Lambda_0 = \frac{\mathcal{E}\omega_0}{\rho} = \frac{m\omega_0}{\rho} = \frac{2m}{r} \omega_0 = \frac{\omega_0}{\Delta} = \omega_0\tau_0 = \frac{2\pi f_0}{\Delta} = \frac{2}{u_2 - u_1} \\ = \frac{f_0}{\left(\frac{\Delta}{2\pi}\right)} = \frac{1}{\frac{r}{c_2}\omega_0} = \frac{\omega_0}{\left(\frac{\omega_2 - \omega_1}{2}\right)} = \frac{f_0}{\left(\frac{f_2 - f_1}{2}\right)} = \frac{z_0}{\rho} = 2\Lambda_s$$

where  $\tau_0 = 1/\Delta$  is the *oscillatory time constant*, or the time in which the system, if allowed to oscillate freely, will allow its oscillations decay to  $1/e$ th. Several important formulas relating to oscillographs (241) to (248), are simplified by the use of the *oscillatory sharpness*  $\Lambda_0$  instead of the *sustained* or *steady-state sharpness*  $\Lambda_s$ ; but, in particular, there is the advantage that in a critically damped vibrator, we shall see that  $\Lambda_0 = 1$  and its reciprocal, the oscillatory bluntness is  $B_0 = 1$ ; whereas,  $\Lambda_s = 0.5$  and  $B_s = 2$ , relations that are more awkward to remember. We shall, therefore, incline to the use of the oscillatory sharpness  $\Lambda_0$ ; but for the benefit of those who have already familiarized themselves with  $\Lambda_s$ , or who may prefer that definition, reference to  $\Lambda_s$  will be retained.

Resonant sharpness ( $\Lambda_0$ ) in designedly resonant electric circuits is commonly of the first order ( $10^1$ ) and occasionally exceeds the second order ( $10^2$ ). In vibrators, the magnitudes encountered are of similar orders. In air-damped vibration galvanometers, a resonant sharpness as high as the third order ( $1000$ ) may be met

**Bluntness of Resonance.** — When the sharpness of resonance of a vibrating system or circuit falls below unity, it is often convenient to use the reciprocal quantity *bluntness of resonance*, and to denote the same by  $B_0$  or  $B_s$ . We shall give preference to  $B_0$ .

$$(208) \quad B_0 = \frac{1}{\Lambda_0} = \frac{\Delta}{\omega_0} = \frac{1}{\omega_0 \tau_0} = \frac{\omega_2 - \omega_1}{2 \omega_0} = \frac{u_2 - u_1}{2} = \frac{f_2 - f_1}{2 f_0} = \frac{\rho}{z_0} \\ = \frac{\rho}{\mathcal{L} \omega_0} = \frac{\rho}{\sqrt{\mathcal{L} S}} = \frac{cr \omega_0}{2} = \frac{r}{2 m \omega_0} = \frac{r}{2 \sqrt{ms}} = \frac{B_s}{2}$$

$$(209) \quad B_s = \frac{1}{\Lambda_s} = \frac{2\Delta}{\omega_0} = \frac{1}{\omega_0 \tau_s} = \frac{\omega_2 - \omega_1}{\omega_0} = u_2 - u_1 = \frac{f_2 - f_1}{f_0} = \frac{r}{z_0} \\ = \frac{r}{\mathcal{L} \omega_0} = \frac{r}{\sqrt{\mathcal{L} S}} = cr \omega_0 = \frac{r}{m \omega_0} = \frac{r}{\sqrt{ms}} = 2 B_0.$$

There is no limit to the bluntness of resonance that a system or circuit may possess, if its resistance is made large enough. Oscillograph vibrators immersed in castor oil may have a bluntness  $B_0$  exceeding 1.2.

Sharpness and bluntness are important quantities in oscillograph theory. If we say that an oscillograph has a bluntness  $B_0 = 0.5$ , we infer that the mechanical resistance to motion is just half that which would be necessary to make its free oscillations critically aperiodic; or just deadbeat. Such a case is illustrated in Figs. 108 and 109; where the quadrantal range in  $u$  is 1.0. In all cases, the bluntness by (208) is half the quadrantal range of  $u$ , or the mean deviation of  $u$  between 1 and the quadrantal value.

A sharply resonant system or circuit is therefore one in which  $\Lambda_0$  is a relatively large number. A bluntly resonant system is one in which  $B_0$  is a relatively large number. The intermediate case, where  $\Lambda_0 = B_0 = 1$  is an *aperiodic* or critically damped system.

**Rapidity of Change in Phase Angle  $\alpha$ , of  $I$ ,  $\dot{x}$ , or  $\dot{\theta}$ , with respect to  $\omega$ .** — In sharply resonant systems, a relatively small change in the impressed angular velocity will involve a relatively large change in the phase angle or slope  $\alpha$  of current  $I$ , rectilinear velocity  $\dot{x}$ , or angular velocity  $\dot{\theta}$ , near resonance, as may be seen by an inspection of Fig. 108. This follows at once from our definition of resonant sharpness. In cases of very sharp resonance, or small damping, a change of a few radians per second in  $\omega$ , near to  $\omega_0$ , may carry the vector of  $I$ ,  $\dot{x}$  or  $\dot{\theta}$  around the entire quad-

rantal range of slope (from  $\alpha = +45^\circ$  to  $\alpha = -45^\circ$ ). On the other hand, in bluntly resonant systems, it may require a relatively large change in  $\omega$  to carry the vector over the same range. In the neighborhood of the resonant impressed angular velocity  $\omega_0$ , we may notice that

$$(210) \quad -\frac{d\alpha}{d\omega} = \frac{1}{\Delta} = \tau_0 = \frac{m}{\left(\frac{r}{2}\right)} = \frac{\mathcal{L}}{\left(\frac{r}{2}\right)} = \frac{\mathcal{L}}{\rho} \quad \text{seconds,}$$

so that the slope  $\alpha$  changes near resonance by  $-\tau_0$  radians per single radian per second in  $\omega$ . It is seen from (210) that the damping constant  $\Delta$  is a measure of the slowness of change in  $\alpha$  with change of  $\omega$ . A large value of resistance, especially if accompanied by a small mass or inductance, gives rise to a large damping constant  $\Delta$  and a slowly changing  $d\alpha/d\omega$ .

The quadrantal range in  $\alpha$  from  $\alpha_1$  to  $\alpha_2$  is  $-90^\circ$  or  $-\pi/2$  radians (see Fig. 108). The accompanying change in impressed angular velocity is  $\omega_2 - \omega_1 = 2\Delta = 2/\tau_0$ . Consequently, the average rate of change in slope  $\alpha$  with respect to  $\omega$  over the whole quadrantal range is

$$(211) \quad \frac{\alpha_2 - \alpha_1}{\omega_2 - \omega_1} = -\frac{\frac{\pi}{2}}{\frac{2}{\tau_0}} = -\frac{\pi}{4} \tau_0 = -\frac{\pi}{4} \cdot \frac{1}{\Delta} = -0.7854 \tau_0 \quad \text{seconds,}$$

or the average rate of change in  $\alpha$  with respect to  $\omega$  over the whole resonant range is 78.5 per cent of what it is at resonance, where the rate reaches its maximum. Above and below the quadrantal frequencies, at which the reactive factor

$$(212) \quad \frac{m\omega - s/\omega}{r} = \pm 1$$

the rate of change in  $\alpha$  with respect to  $\omega$  falls off. At large reactive factors, it changes approximately as the inverse square of the reactive factor.

## CHAPTER XVIII

### DISPLACEMENT IMPEDANCE AND ADMITTANCE

In the rectilinear vibration system of the telephone receiver, as well as in the alternating-current electric circuit, the vibrational velocity  $\dot{x}$  and the current  $I$  are ordinarily the principal subjects of interest. The vibrational displacement  $x$  and the electric quantity  $q$  are usually of subsidiary importance. In the cases of the oscillograph and vibration galvanometer, however, the vibrational angular velocity is of small practical concern; while the maximum cyclic displacement is a principal consideration. It is, therefore, necessary to pay particular attention to the coordinate displacements  $q$ ,  $x$ , and  $\theta$ , in the three cases.

**Displacement-impedance Parabolas.** — It is shown in Appendix III that the impedance to electric displacement, or quantity, offered by a simple a.-c.  $\mathcal{E}RS$  branch circuit is

$$(213) \quad z' = j\omega \left\{ r + j(\mathcal{E}\omega - s/\omega) \right\} = (s - \mathcal{E}\omega^2) + jr\omega \quad \frac{\text{volts}}{\text{coulomb}} \angle,$$

and similarly in a simple mechanical vibratory system with either rectilinear or rotational freedom,

$$(214) \quad z' = j\omega \left\{ r + j(m\omega - s/\omega) \right\} = (s - m\omega^2) + jr\omega \quad \frac{\text{dyne-p.-cm.}}{\text{radian}} \angle,$$

$$(215) \quad = s \left\{ (1 - u^2) + j2B_0u \right\} = s \left\{ (1 - u^2) + jB_s u \right\} \quad \frac{\text{dyne-p.-cm.}}{\text{radian}} \angle.$$

These equations are characteristic of a simple parabola:

$$(216) \quad Y^2 = pX,$$

where the origin of the coordinates  $X$  and  $Y$  is taken at the vertex  $A$  of the curve  $ABCD$ , Fig. 110, at a distance  $OA = s$  from the vector origin  $O$  of the equation (214).  $X$  is reckoned positively from  $A$  towards  $O$ , along the axis of reals. The value of the parameter  $p$  in (216) is

$$(217) \quad p = 2 B_0 \sqrt{s} = B_s \sqrt{s}.$$

The ordinate  $OC$  drawn through the vector origin  $O$  has a length  $r\omega_0$ . The point  $C$  in which it cuts the curve corresponds to the resonant angular velocity  $\omega_0$ , or to a frequency ratio of  $u = 1$ . The curve at  $C$  is inclined to the axis  $AO$  at an angle whose tangent is  $B_0$ . The tangent of the angle  $CAO$  is numerically equal to  $2B_0 = B_s$ , or twice the oscillatory bluntness of system. That is, the ordinate through  $O$  is twice the bluntness  $B_0$ , if  $OA = 1$ .

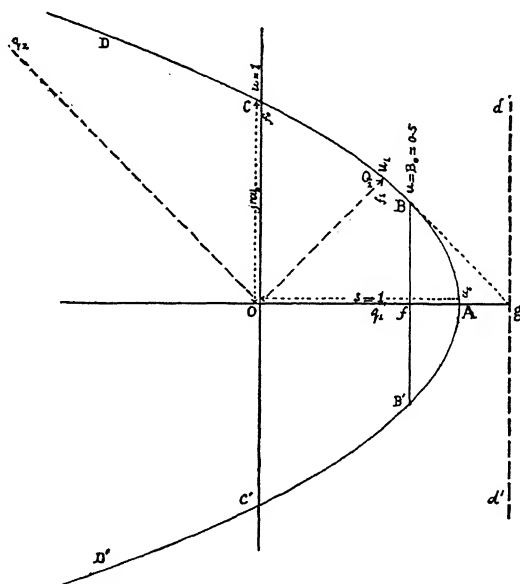


FIG. 110. Displacement-impedance parabola. Case of  $B_0 = 0.5$ .

At a very low frequency  $f_s$ , the vector displacement impedance is  $OA = s$ . At the lower-quadrantal frequency  $f_1$ , it is  $OQ_1$ , whose slope is  $45^\circ$ . At resonance  $f_0$ , it is the perpendicular vector  $OC = jr\omega_0$ . At the upper-quadrantal frequency  $f_2$ , it is a vector along  $Oq_2$  to the point where this meets the curve. This vector has a slope  $135^\circ$ . At very high frequencies, the vector attains great size and approaches  $180^\circ$  in slope.

In any parabola having its axis on the axis of abscissas, the focus  $f$  lies at the foot of the ordinate through that point on the curve where the tangent is equally inclined to ordinates and abscissas, or makes an angle of  $45^\circ$  with the base. The ratio of

the focal abscissa  $Af$  to the distance  $AO$  of the vertex  $A$  from the vector origin  $O$  is

$$(218) \quad \frac{Af}{AO} = \frac{1}{\Lambda_0^2} = B_0^2,$$

or, taking  $AO$  as of unit length,  $Af$  is the square of the bluntness. The ratio of the ordinate through  $f$  (termed geometrically the semi-latus-rectum) to the distance  $AO$  is

$$(219) \quad \frac{fB}{AO} = 2 B_0^2$$

or with  $AO$  taken as unity,  $fB = 2 Af = 2 B_0^2$ . Moreover, the value of  $u$  on the curve at the point  $B$  is just equal to  $B_0$ .

The ordinate  $d'gd$  is the directrix of the curve; so that

$$(220) \quad Ag = Af = \frac{B_0}{2} \sqrt{s}.$$

It will be evident from a consideration of (214) and (217) that in general, different electric or mechanical vibratory systems, with different values of  $m$ ,  $r$ , and  $s$ , will have different displacement-impedance graphs; but they will all be simple parabolas of the type (216). There are various ways in which a series of such parabolas may be depicted or graphically presented;

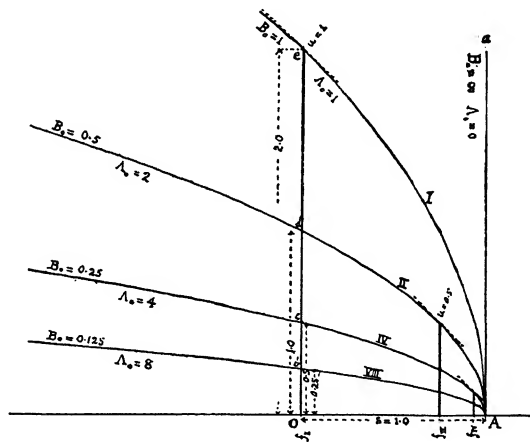


FIG. 111. Family of displacement-impedance parabolas, all drawn with  $s = 1$ .

but a convenient way for our purposes is to bring them all to a common horizontal abscissa  $OA$ , that is, to consider  $s$  as the standard of reference throughout. This also makes the displacement at zero frequency the standard of reference. We then obtain the infinitely numerous family of coaxial parabolas, a few of which are indicated in Fig. 111. Here it is evident that each parabola is de-

finned by the resonant bluntness  $B_0$  (or by the sharpness  $\Lambda_0 = 1/B_0$ ) of the system it represents. A system of blunt resonance has a blunt parabola and a system of sharp resonance a sharp parabola. In the limiting case of  $B_0 = \infty$  or  $\Lambda_0 = 0$ , the parabola cannot be distinguished near the vertex  $A$  from the  $Y$  axis  $A\alpha$ . In the opposite limiting case of  $B_0 = 0$  or  $\Lambda_0 = \infty$ , the parabola collapses into a straight line and coincides with the  $X$  axis  $AO$ . In all the members of the family, the vector lies on the  $j$  axis at resonance ( $u = 1$ ), and the size of this vector is  $B_s$  or  $2 B_0$ , taking  $OA$  as unit size.

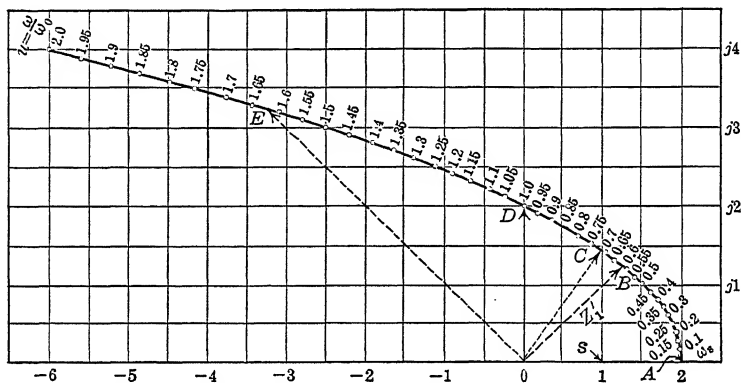


FIG. 112. Graph of vector impedance to electric or mechanical displacement for cases of

$$\begin{cases} r = 10^2, & \mathcal{L} = 5 \times 10^{-3}, & s = 2 \times 10^6 \\ r = 10^{-2}, & m = 5 \times 10^{-7}, & s = 2 \times 10^2 \\ \omega_0 = 20,000, & \Delta = 10,000, & B_0 = 0.5 \end{cases}$$

In the electric case, unit length represents  $10^6$  volts per coulomb. In the mechanical case, unit length represents  $10^2$  dynes-p.-cm. per radian.

The particular system already referred to in connection with Figs. 108 and 109, for which  $B_0 = 0.5$ , has its displacement-impedance parabola presented in Fig. 112. At  $\omega = 0$  or  $u = 0$ , representing an indefinitely low impressed frequency, the impedance is the vector  $OA = 200$  dynes-p.-cm. per radian, a real quantity. Unit maximum cyclic vmt. applied to this system under such conditions would develop a maximum cyclic displacement of  $\pm 1/200$  radian, at each elongation, in phase with the torque. As the impressed frequency is increased, the vector increases in slope; but at first diminishes in size. At the lower-quadrantal frequency, with  $u = 0.618$ , the vector has reached the broken

line  $OB$ , at a slope  $45^\circ$ . At the resonant frequency ( $\omega_0 = 20,000$  or  $u = 1$ ) the vector assumes the quadrature position of  $OD$  or is a pure imaginary. This is a characteristic property in every system. At the higher-quadrantal frequency, the vector has reached the position  $OE$  at a slope  $135^\circ$ , or  $90^\circ$  beyond  $OB$ . At very high impressed frequencies, the vector attains great size and tends to the slope  $180^\circ$ .

On considering (213) and (214), it will be evident that the displacement-impedance graph of Fig. 112 may be obtained from the velocity-impedance graph of Fig. 108, by rotating the latter positively or counterclockwise through one quadrant, and then multiplying the size of the vector at each point by the instantaneous value of  $\omega$ .

The displacement impedance has minimum size, not at  $D$ , the point of resonance, but at the point  $C$ , where the tangent is perpendicular to the radius vector.

It will be seen that the displacement-impedance graph is the upper half of a complete parabola; or is a semiparabola, extending from the vertex  $A$  through  $D$  to infinity as the frequency is increased from zero to infinity. It has been pointed out by Professor F. S. Dellenbaugh,\* however, that the curve is really a complete parabola with a lower, as well as an upper, half. The lower half belongs to cases where the resistance is negative, i.e., where a force  $\dot{x}r$  is introduced into the system equal to the opposing frictional force  $-\dot{x}r$  assumed above. Such cases are generator cases, where alternating motive power is applied to the system internally in lieu of being absorbed dissipatively. The lower half of the displacement-impedance parabola is thus actually the generator half, and the upper half, with which we are here mainly concerned, is the motor half.

Taking the electric case, the maximum cyclic quantity of electricity  $q_m$  accumulated in the network condenser of Fig. 27 is

$$(221) \quad q_m = \frac{E_m}{z'} \quad \text{max. cyc. coulombs } \angle.$$

Since the potential difference at the terminals of a condenser is directly proportional to the quantity of electricity or charge it contains, the maximum cyclic voltage on the condenser will be

$$(222) \quad E_{cm} = \frac{q_m}{c} = q_m s = \frac{E_m s}{z'} \quad \text{max. cyc. volts } \angle,$$

\* Bibliography 79, discussion.



or the condenser voltage is to  $E_m$  as is the constant condenser impedance  $s$  to the total branch impedance  $z'$ .

Similarly in the oscillograph case, the maximum cyclic angular displacement of the vibrator mirror will be

$$(223) \quad \theta_m = \frac{F_m}{z'} \quad \text{max. cyc. radians } \angle.$$

**Displacement Admittance.** — The reciprocal of displacement impedance, or *displacement admittance*  $y'$  is of still greater interest and practical importance from the oscillographic viewpoint. From (214), considering the mechanical case:

$$\begin{aligned} (224) \quad y' &= \frac{1}{z'} = \frac{1}{(s - m\omega^2) + j r \omega} = \frac{1}{m(\omega_0^2 - \omega^2) + j r \omega} \\ &= \frac{1}{m\{(\omega_0^2 - \omega^2) + j 2 \Delta \omega\}} = \frac{1}{s\{(1 - u^2) + j 2 B_0 u\}} \\ &= \frac{1}{m\omega_0^2\{(1 - u^2) + j 2 B_0 u\}} = \frac{y}{j\omega} = \frac{-jy}{\omega} \quad \frac{\text{radians}}{\text{dynes-p.-cm.}} \angle. \end{aligned}$$

The last expression shows that the displacement admittance  $y'$  is obtainable from the velocity admittance  $y$ , by operating thereon with  $-j/\omega$ ; that is, by clockwise rotation through a quadrant and at the same time dividing the size by  $\omega$ .

The following particular cases of (224) are worth noting:

$$(225) \quad \text{At } \omega = 0, y' = y'_s = \frac{1}{s} \angle 0^\circ = c \angle 0^\circ \quad \frac{\text{radians}}{\text{dyne-p.-cm.}} \angle.$$

$$(226) \quad \omega = \omega_1, y' = y'_1 = \frac{1}{\sqrt{2} r \omega_1} \angle 45^\circ \quad \frac{\text{radians}}{\text{dyne-p.-cm.}} \angle.$$

$$\begin{aligned} (227) \quad \omega = \omega_0, y' = y'_0 &= -j \frac{1}{r \omega_0} \\ &= \frac{1}{r \omega_0} \angle 90^\circ = \frac{g}{\omega_0} \angle 90^\circ \quad \frac{\text{radians}}{\text{dyne-p.-cm.}} \angle. \end{aligned}$$

$$(228) \quad \omega = \omega_2, y' = y'_2 = \frac{1}{\sqrt{2} r \omega_2} \angle 135^\circ \quad \frac{\text{radians}}{\text{dyne-p.-cm.}} \angle.$$

$$(229) \quad \omega = \infty, y' = y'_\infty = 0 \angle 180^\circ \quad \frac{\text{radians}}{\text{dyne-p.-cm.}} \angle.$$

These particular values of the displacement admittance are  $y'_s$ ,  $y'_1$ ,  $y'_0$ ,  $y'_2$  and  $y'_\infty$ . They may be called respectively the initial, lower-quadrantal, resonant, upper-quadrantal and ultimate values. The resonant value is always a  $-j$  quantity.

**Displacement-admittance Graph.** — Referring to (224) and to Fig. 113, it will be seen that if we draw the circular graph  $ABCD$  of velocity admittance  $y$ , and at any value of  $\omega$  or  $u\omega_0$ , such as  $\omega = 10,000$ , ( $u = 0.5$ ), draw the vector  $OP$  of size  $0.555 \times 10^2$

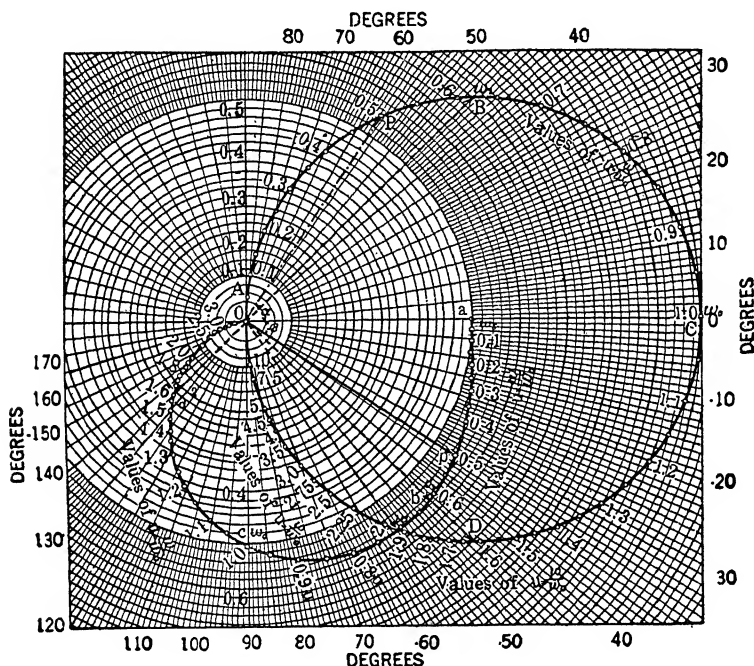


Fig. 113. Graph of displacement admittance for cases of

$$\begin{cases} r = 10^2, & \mathcal{L} = 5 \times 10^{-3}, & s = 2 \times 10^6 \\ r = 10^{-2}, & m = 5 \times 10^{-7}, & s = 2 \times 10^2 \end{cases}$$

$$\omega_0 = 20,000, \Delta = 10,000, B_0 = 0.5$$

For Circle  $A B C D$   $\begin{cases} \text{In the electric case, unit length} = 10^{-2} \text{ Mho.} \\ \text{In the mechanical case, unit length} = 10^2 \text{ Mechanical abmhos, or } 10^2 \left( \frac{\text{Radians}}{\text{Sec.}} \right) \text{ per unit vmt.} \end{cases}$

For Graph  $a b c d$   $\begin{cases} \text{In the electric case, unit length} = 10^{-6} \text{ coulomb per volt.} \\ \text{In the mechanical case, unit length} = 10^{-2} \text{ radian per unit vmt.} \end{cases}$

rad. per sec./ (dynes-p.-cm.) at slope  $\alpha = 56^\circ.3$ , we may then draw perpendicularly thereto the vector  $Op$ , and dividing 55.5 by  $\omega$ , obtain, to a correspondingly altered scale, the displacement admittance  $5.55 \times 10^{-3}$  radian/(dyne-p.-cm.), at a slope  $\beta = -33^\circ.7$ . This means that if unit maximum cyclic vmt., or 1 dyne-

p.-cm. be applied to the vibrator of this case, at  $\omega = 10,000$ , the maximum cyclic displacement of the mirror will be  $5.55 \times 10^{-3}$  radians =  $0.32^\circ$ . This elongation or maximum cyclic angular displacement would occur  $33^\circ.7$  in phase behind the corresponding elongation in torque or exciting current.

Proceeding in this manner, we might draw in the entire displacement-admittance graph  $apbcdO$ , Fig. 113. At or near zero frequency, denoted by  $\omega_s$ , the displacement admittance would be the vector  $Oa$ , in phase with the exciting current. At the lower-quadrantal frequency  $\omega_1$ , it would be the vector  $Ob$ . At the upper-quadrantal frequency  $\omega_2$ , it would be  $Od$ . At resonance, or  $\omega_0$ , it would be  $Oc$ , in lagging quadrature with the exciting current in the vibrator.

The maximum admittance would occur at  $\omega_d$ , in this case at  $u = 0.707$ , or  $\omega = 14,140$ . This vector will vary in position or slope with different values of the bluntness  $B_0$ . It may be noted that the maximum admittance never occurs at resonance; although in sharply resonant vibrators, it will lie very close to resonance.

If we consider Fig. 113 in terms of its electric representation, the scale being  $10^{-2}$  mho per unit length, then at  $\omega = 10,000$ , and  $\omega = 0.5$ , the electric displacement would be  $0.555 \times 10^{-6} \angle 33^\circ.7$  coulombs per maximum cyclic volt on the  $\mathcal{E}RS$  branch terminals.

It is also easy to show that the displacement-admittance graph  $abcd$ , Fig. 113, is obtainable by direct vector reciprocals, or by inversion, from the displacement-impedance parabolic graph  $ABCD$ , Fig. 112. In other words, a displacement-admittance graph is always the vector inverse of a certain parabola. It may therefore be described as an *inverse parabola*; but it is more definitely termed\* a *displacement-admittance curve*.

The shape of these inverse parabolas depends only upon the bluntness of resonance in the system to which they refer. A family of bluntly resonant inverse parabolas appear in Fig. 116. A family of sharply resonant graphs appear in Fig. 117. An intermediate family appears in Fig. 115. The value of  $\mathbf{y}'_s$  is kept constant throughout these series as a common basis of reference.

**Electric or Mechanical Displacement.** — Since

$$(230) \quad q_m = E_m y' \quad \text{max. cyc. coulombs } \angle$$

or

$$(231) \quad \theta_m = F_m y' \quad \text{max. cyc. radians } \angle,$$

\* Bibliography 79.

it is evident that a graph of displacement admittance  $\mathbf{y}'$  is also a graph of maximum cyclic displacement at unit impressed maximum cyclic torque, and can be used with any impressed torque by a suitable change in scale of dimensions. Thus, taking Fig. 113, at resonant frequency; i.e.,  $u = 1$ ,  $\omega_0 = 20,000$ , or  $f_0 = 3183 \sim$ , an impressed vmt. of say 10 maximum cyclic dynes-p.-cm. would produce a maximum cyclic mirror displacement of  $\theta_m = 0.05 \angle 90^\circ$  radian  $= 2^\circ.87$ , in lagging quadrature to the excitation. A beam of light, reflected by the mirror, would be cyclically deflected to twice this angle or  $\pm 5^\circ.74$  at elongation, on each side of the zero, owing to the doubling optical reflecting property of mirrors. It may be noted that, at resonance, ( $u = 1$ ), the displacement is always  $90^\circ$  in phase behind the impressed torque, or exciting current in the vibrator, for any and all values of  $B_0$ .

**Formulas for Oscillographic Displacement Admittance.** — Remarking that the slope  $\beta^\circ$  of the displacement admittance  $\mathbf{y}'$  is always negative, lying between the values  $-0^\circ$  and  $-180^\circ$ , we have

$$(232) \quad \omega = \sqrt{\omega_0^2 + \Delta^2 \operatorname{ctn}^2 \beta} + \Delta \operatorname{ctn} \beta \\ = \omega_0 \left\{ \sqrt{1 + B_0^2 \operatorname{ctn}^2 \beta} + B_0 \operatorname{ctn} \beta \right\} \frac{\text{radians}}{\text{sec.}},$$

or

$$(233) \quad u = \frac{\omega}{\omega_0} = \sqrt{1 + B_0^2 \operatorname{ctn}^2 \beta} + B_0 \operatorname{ctn} \beta.$$

The polar scalar equation of displacement admittance is

$$(234) \quad |\mathbf{y}'| = -\frac{\sin \beta}{r\omega} = \frac{-\sin \beta}{r\omega_0 \{ \sqrt{1 + B_0^2 \operatorname{ctn}^2 \beta} + B_0 \operatorname{ctn} \beta \}} \\ \frac{\text{mirror radian}}{\text{vmt.}}$$

$$(235) \quad = \frac{-\sin \beta}{2 B_0 s \{ \sqrt{1 + B_0^2 \operatorname{ctn}^2 \beta} + B_0 \operatorname{ctn} \beta \}} \frac{\text{mirror radians}}{\text{vmt.}}$$

The corresponding polar vector equation is

$$(236) \quad \mathbf{y}' = -\frac{\sin \beta^\circ}{r\omega} \angle -\beta^\circ = \frac{-\sin \beta^\circ \angle \beta^\circ}{2 B_0 s \{ \sqrt{1 + B_0^2 \operatorname{ctn}^2 \beta} + B_0 \operatorname{ctn} \beta \}} \\ = -\frac{\sin \beta^\circ \angle \beta^\circ}{2 B_0 s u} = -\frac{\sin \beta^\circ \angle \beta^\circ}{B_s s u} \frac{\text{mirror radians}}{\text{vmt.}} \angle.$$

The slope  $\beta^\circ$  pertaining to any assigned value of  $\omega$  is

$$(237) \quad \beta^\circ = \tan^{-1} \left( \frac{2 \Delta \omega}{\omega^2 - \omega_0^2} \right) \quad \text{degrees}$$

$$= \tan^{-1} \left( \frac{2 B_0 u}{u^2 - 1} \right) = \tan^{-1} \left( \frac{B_s u}{u^2 - 1} \right) \quad \text{degrees}$$

$$(238) \quad = \tan^{-1} \left( \frac{2 B_0}{u - u^{-1}} \right) = \tan^{-1} \left( \frac{B_s}{u - u^{-1}} \right) \quad \text{degrees.}$$

In the testing of oscillographs, their calibration is ordinarily conducted at a relatively low frequency, say  $60 \sim$ , which for practical purposes, in the case of a vibrator, may be regarded as of the same effect as zero frequency, or  $\omega_s$ . By (225), the displacement admittance at  $\omega_s$  is  $1/s$  or  $c$ , at zero slope. It is then desired to find what ratio the admittance will bear, at any impressed angular velocity  $\omega$  (or its ratio  $u$ ), to that at the calibration frequency  $\omega_s$ . From (236) and (225) we obtain

$$(239) \quad D = \frac{y'}{y'_s} = \frac{-\sin \beta^\circ \angle -\beta^\circ}{2 B_0 u} = \frac{-\sin \beta^\circ \angle \beta^\circ}{B_s u}$$

$$= \frac{-\sin \beta^\circ \angle \beta^\circ}{2 B_0 \{\sqrt{1 + B_0^2 \cot^2 \beta^\circ} + B_0 \cot \beta^\circ\}}.$$

This is an important formula. It gives the polar vector *deviation factor*  $D$  for any oscillograph at any impressed  $\omega$ , when the values of  $\omega_0$  and  $B_0$  are known for the instrument. Thus, in the case represented by Fig. 113, where  $\omega_0 = 20,000$ , and  $B_0 = 0.5$ , if the instrument is calibrated at  $60 \sim = \omega_s$ , it may be required to know what will be the deviation factor  $D$  at  $\omega = 5000$ , or  $u = 0.25$ .

$$\text{Here by (237) } \beta^\circ = \tan^{-1} \left( \frac{0.25}{-0.9375} \right) = \tan^{-1}(-0.2667) = -14^\circ 56'.$$

$$\text{Then by (239) } D = \frac{y'}{y'_s} = \frac{-\sin(-14^\circ 56') \angle 14^\circ 56'}{2 \times 0.5 \times 0.25}$$

$$= \frac{0.2577}{0.25} \angle 14^\circ 56' = 1.031 \angle 14^\circ 56'.$$

This means that the maximum cyclic displacement produced at  $796 \sim$  or  $5000$  radians per second, will be 3.1 per cent greater than that produced by the same torque at  $60 \sim$ , and will lag  $14^\circ 56'$  of its own phase behind the impressed torque. The *correction factor*  $C$  will be

$$(240) \quad C = \frac{1}{D}$$

TABLE XVII  
PRINCIPAL IMPRESSED ANGULAR VELOCITIES OF A VIBRATORY SYSTEM

Angular Velocity radians/sec.	Displacement Admittance Mirror radians/dyne-p.-cm.
1. Initial, (near zero), $\omega_s$	$y_s' = 1/s \angle 0^\circ = c \angle 0^\circ$ (241)
2. Lower quadrantal, $\omega_1 = \sqrt{\omega_0^2 + \Delta^2} - \Delta = \omega_0 \{ \sqrt{1 + B_0^2} - B_0 \}$	$y_1' = \frac{1}{r\omega_1\sqrt{2}} \angle 45^\circ = \frac{g}{\omega_1\sqrt{2}} \angle 45^\circ$ (242)
3. Max. admittant, $\omega_d = \sqrt{\omega_0^2 - 2\Delta^2} = \omega_0 \sqrt{1 - 2B_0^2}$	$y_d' = \frac{1}{r\omega_d} \angle \tan^{-1}(\omega_d/\Delta)$ (243)
4. Free vibrational, $\omega_f = \sqrt{\omega_0^2 - \Delta^2} = \omega_0 \sqrt{1 - B_0^2}$	$y_f' = \frac{1}{r\sqrt{\omega_f^2 + (\Delta/2)^2}} \angle \tan^{-1} \frac{\omega_f}{(\Delta/2)}$ (244)
5. Resonant, $\omega_0 = \sqrt{\omega_0^2 - 0} = \omega_0 \sqrt{1}$	$y_0' = \frac{1}{r\omega_0} \angle 90^\circ = \frac{-jg}{\omega_0}$ (245)
6. Midquadrantal, $\omega_{12} = \sqrt{\omega_0^2 + \Delta^2} = \omega_0 \sqrt{1 + B_0^2}$	$y_{12}' = \frac{1}{r\sqrt{\omega_{12}^2 + 5\Delta^2/4}} \angle \tan^{-1} \left\{ \frac{-\omega_{12}}{(\Delta/2)} \right\}$ (246)
7. Higher quadrantal, $\omega_2 = \sqrt{\omega_0^2 + \Delta^2} + \Delta = \omega_0 \{ \sqrt{1 + B_0^2} + B_0 \}$	$y_2' = \frac{1}{r\omega_2\sqrt{2}} \angle 135^\circ = \frac{g}{\omega_2\sqrt{2}} \angle 135^\circ$ (247)
8. Duplicate initial, $\omega_{s2} = \omega_d \sqrt{2} = \omega_0 \sqrt{2(1 - 2B_0^2)}$	$y_{s2}' = c \angle \tan^{-1} \left( \frac{-2\Delta\omega_{s2}}{\omega_d^2 - 2\Delta^2} \right)$ (248)

the reciprocal of the deviation factor, or in this case  $0.969 \angle 14^\circ 56'$  at  $796 \sim$ . The frequency  $796 \sim$  would be 13 times  $61.23$ , or would be thirteenth harmonic of a fundamental  $61.23 \sim$ . The recorded wave of this frequency on the oscillogram of an instrument having these characteristics would have to be reduced in amplitude by the factor  $0.969$ , and its phase should be advanced by nearly  $15^\circ$  of its own cycle, in order to represent the record obtainable from an ideal oscillograph devoid of inertia.

Table XVII, containing a series of important displacement frequencies, on page 231, may be convenient for reference.

Of the eight given important angular velocities, Nos. 1, 2, 5 and 7 are always presented, at the successive negative slopes  $0^\circ$ ,  $45^\circ$ ,  $90^\circ$  and  $135^\circ$ . No. 3, the *maximum admittant value* of  $\omega$ , is always found when  $B_0 < 1$ , or  $\Lambda_0 > 1$ , i.e., for vibrators in which there is oscillation. For values of  $B_0$  equal to or greater than unity, which we may call blunt cases,  $\omega_z$  has no independent existence, because the greatest admittance is then found at  $\omega = \omega_s = 0$ . In other words, the displacements then always diminish at frequencies exceeding the low calibration frequency  $\omega_s$ . Angular velocity No. 4,  $\omega_r$ , is always presented when  $B_0 < 1$ ; but in blunt cases, the system is too heavily damped to admit of free vibration. Number 6, the midquadrantal frequency, is always presented; but its phase position depends upon the value of  $B_0$ . It is midway between  $\omega_1$  and  $\omega_2$  in angular velocity, but not midway between them in phase. Number 8, the upper angular velocity at which the displacement has the same size as at the initial value  $\omega_s$ , is not found when  $B_0 > 0.707$ . In sharply resonant systems, it is always presented, but its phase position or slope varies with  $B_0$ .

Figure 114 is a displacement-admittance graph showing all of the eight angular velocities of Table XVII for the particular case of  $\omega_0 = 25000$ , or  $f_0 = 3979 \sim$  and  $B_0 = 0.225$ . Here  $\mathbf{y}_s'$  is taken as 1, corresponding to an oscillographic standard calibration at or near zero frequency. We find  $\mathbf{y}_1'$ ,  $\mathbf{y}_0'$  and  $\mathbf{y}_2'$ , all at their definite respective slopes  $-45^\circ$ ,  $-90^\circ$ , and  $-135^\circ$ , with the corresponding sizes 1.9642, 2.222, and 1.2571, at the frequencies 3182, 3979, and 4973  $\sim$ . Thus at the impressed frequency 3182  $\sim$  on a vibrator of such constants, a given exciting alternating current has a deviation factor  $D = 1.964 \angle 45^\circ$ , or would produce 96.4 per cent more deflection than at  $60 \sim$ ; and this deflection would be in lagging semiquadrature to the current.





with  $u$ , the ratio of the impressed frequency  $f$  to the resonant frequency  $f_0$  of the vibrator. The curves of  $u$  are given in Fig. 115 by steps of 0.1 from  $u = 0.1$  to  $u = 2.0$ . The intersection of the  $u$  line with the  $B$  line marks the vector deviation factor  $D$ . Thus a vibrator of  $B_0 = 0.5$ , at  $u = 0.8$ , has a deviation factor  $1.15 \angle 66^\circ$ . That is to say, it will over-indicate 15 per cent at this frequency by comparison with its indications at  $60^\circ$ , and the wave will lag a little more than one-fifth of its own wave length.

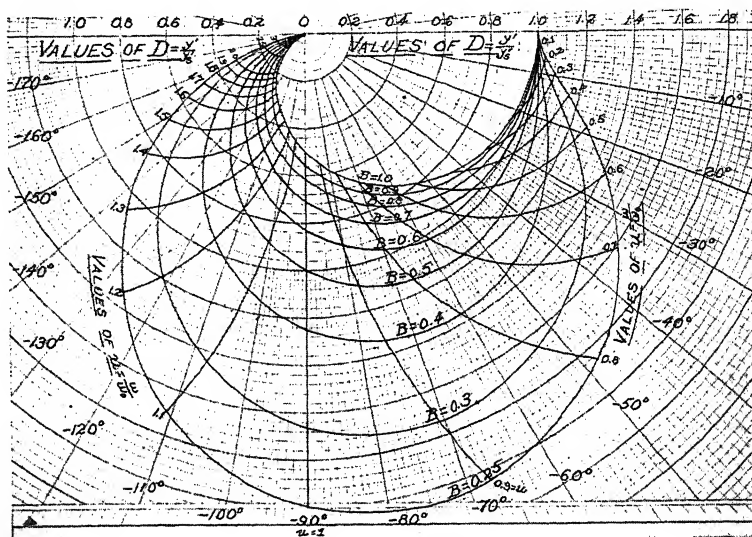


FIG. 115. Plane-vector chart of the deviation factor  $D$  for any oscillograph whose bluntness lies between  $B_0 = 0.25$  and  $B_0 = 1.0$ , and whose resonant frequency is given. Example: If  $B_0 = 0.6$ , and  $u = 0.3$ , then  $D = 1.022 \angle 21.6^\circ$ .

Figure 116 is a similar vector chart for finding  $D$  by inspection when  $B_0$  lies between 1.0 and  $\infty$ . There is actually little change in the form of the curve after  $B_0$  exceeds 4. The limiting curve at  $B_0 = \infty$  is a semicircle of unit diameter on the real axis.

Figure 117 is a similar chart for finding  $D$  when  $B_0$  lies between 0.25 and 0.05 inclusive. As  $B_0$  diminishes, the curve of  $D$  rapidly approximates to a circle of diameter  $1/(2B_0) = \Delta_0/2$ , or of radius  $1/(4B_0) = \Delta_0/4$ . The center of the circle is displaced approximately 0.25 unit to the right of the axis  $Ob$ . At  $B_0 = 0$ , this circle would have an infinite diameter.

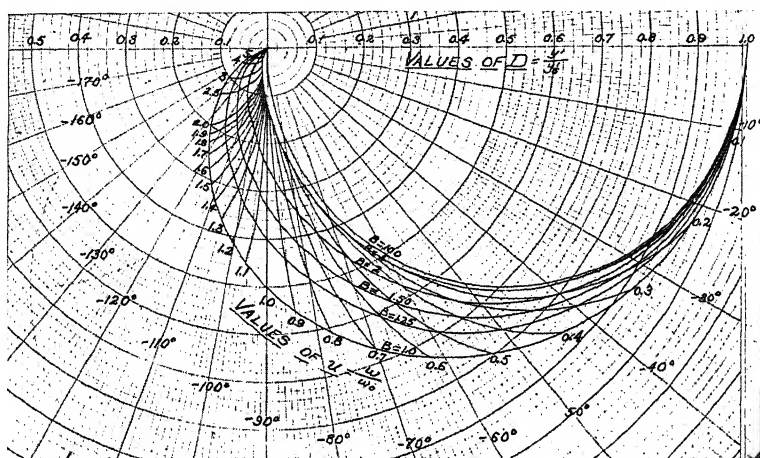


FIG. 116. Plane-vector chart of deviation factor  $D = y'/y_s'$  for any oscillator whose bluntness lies between  $B_0 = 1$  and  $B_0 = \infty$ , and whose resonant frequency is given. Example: If  $u = 0.5$  and  $B_0 = 2.0$ ,  $D = 0.468 \angle 69.4^\circ$ .

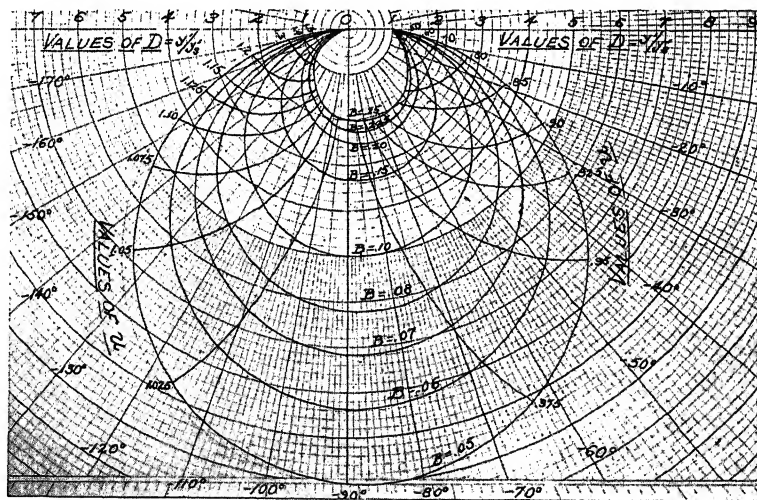


FIG. 117. Plane-vector chart of the deviation factor  $D = y'/y_s'$  for any oscillator whose bluntness lies between 0.05 and 0.25, and whose resonant frequency is given. Example: If  $u = 0.9$ , and  $B_0 = 0.08$ ,  $D = 4.17 \angle 37.1^\circ$ .

As may be seen, therefore, in Figs. 114, 115, and 116, as  $B_0$  increases from 0 to  $\infty$ , the graph of  $\mathbf{y}'$  or  $D$  changes from a unit semicircle based on the  $g'$  axis to an indefinitely great circle diametered close to the  $b'$  axis. See formula (202).

**Constants of an Oscillograph Vibrator.** — From an inspection of (238) and (239), it is evident that the deviation factor  $D$ , or its reciprocal  $C$ , can be either computed or determined by graphical inspection of the vector charts, if we can ascertain the two essential constants of the instrument  $\omega_0$  and  $\Delta$ , or what is equivalent thereto,  $\omega_0$  and  $B_0$ , or  $f_0$  and  $B_0$ . The tests of an oscillograph thus direct themselves towards a determination of these two constants. If, however, we require to find not merely the deviation factor  $D$ , but also the fundamental constants  $A$ ,  $m$ ,  $r$ , and  $s$  of the instrument, then, as we shall see in another chapter, an additional test is necessary.

If we divide (245) by (241), we find:

$$(249) \quad \mathbf{y}_s' / \mathbf{y}_0' = j2 B_0 = 2 B_0 \angle 90^\circ = B_s \angle 90^\circ.$$

If, therefore, we can (1) identify the resonant frequency  $f_0$  of a vibrator, and (2) compare the calibration of the vibrator at this frequency with that at zero frequency, we shall have,

$$(250) \quad \left| \frac{\mathbf{y}_s'}{\mathbf{y}_0'} \right| = 2 B_0 = B_s,$$

or

$$(251) \quad \left| \frac{\mathbf{y}_0'}{\mathbf{y}_s'} \right| = \frac{\Delta_0}{2} = \Delta_s.$$

*The bluntness  $B_0$  of the vibrator will then be half the ratio of the maximum cyclic displacement at zero frequency to the maximum cyclic displacement at resonant frequency, equal current excitations and impressed torques being used in each test. If the vibrator is sharp, the same fact may be expressed by saying that the sharpness  $\Delta_0$  will be twice the ratio of the electric current needed to produce the same maximum cyclic displacement or deflection at zero frequency, as will produce it at resonant frequency.*

An alternative formula is

$$(252) \quad \Delta = \frac{\omega_0}{j2} \cdot \frac{\mathbf{y}_s'}{\mathbf{y}_0'} = \pi f_0 \cdot \frac{\mathbf{y}_s'}{\mathbf{y}_0'} \angle 90^\circ \quad \frac{\text{hypos}}{\text{sec.}} \angle.$$

All that is necessary, therefore, for finding the deviation factor  $D$ , or its reciprocal  $C$ , of a vibrator at any impressed frequency, is to identify the resonant frequency  $f_0$ , and then compare its calibration at that frequency with that at  $f_s$ , a very low frequency.

## CHAPTER XIX

### OSCILLOGRAPHMETERS

**Oscillographmeters.**—An *oscillographmeter* is a device for measuring the constants of an oscillographic vibrator, and particularly for measuring the resonant frequency  $f_0$ . A form of oscillographmeter is illustrated in Figs. 118, 119, and 120. This device consists of a small and portable auxiliary vibrator, using a permanent magnet to supply the working magnetic flux, and air damping, so as to secure great sharpness of resonance.

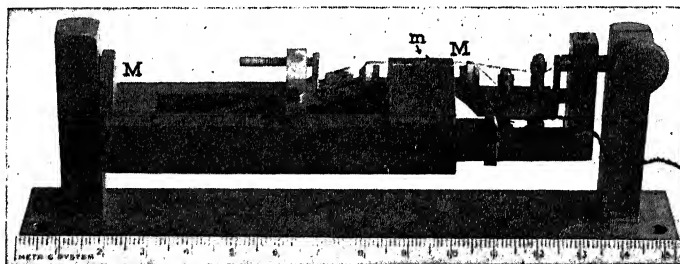


FIG. 118. Oscillographmeter or auxiliary vibrator. Length of mirror 2.3 mm. Breadth 0.9 mm.

The characteristic property of a vibrating system at resonance is that the phase of displacement is exactly in lagging quadrature to that of impressed torque; or, in an oscillograph, to that of the exciting alternating current. We can therefore determine the resonant frequency if we can ascertain at what impressed a.-c. excitation frequency the displacement of the vibrator mirror is just out of step with the excitation, or lags  $90^\circ$  behind it.

If we place in the same alternating electric circuit as the tested vibrator, an auxiliary vibrator of sharp resonance, the latter will have a displacement admittance substantially either in cophase with the exciting current; or in opposite phase thereto, except in the immediate vicinity of its own resonant frequency. In other words, it will not produce a displacement differing sensibly in

phase from the exciting current (direct cophase or opposition phase) except close to its own resonance. It will describe its vector displacement graph in a range of only a few cycles of impressed frequency. If, therefore, the tested vibrator and the auxiliary vibrator are actuated by the same alternating current, we may be sure that, provided the resonant frequency of the tested vibrator is not close to that of the auxiliary vibrator, the former will have at its resonance  $90^\circ$  phase displacement, while the latter will have sensibly  $0^\circ$  phase displacement. In other words, the

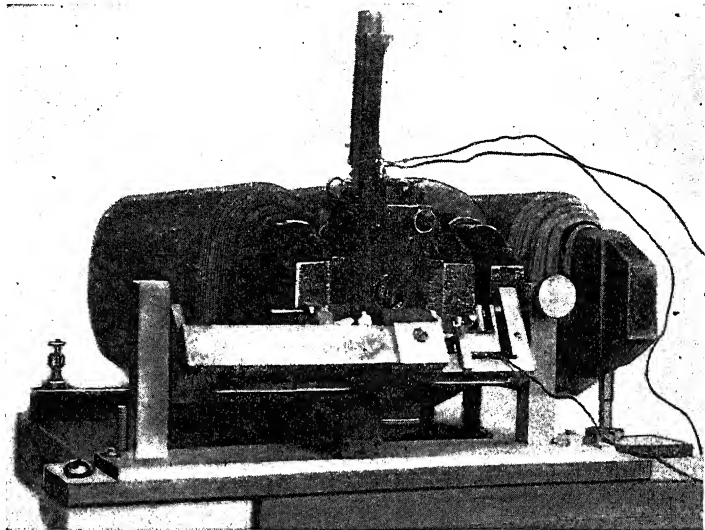


FIG. 119. Oscillogrometer applied to an oscillograph for test of latter.

two vibrating mirrors will be out of phase almost  $90^\circ$ , or in the quadrature relation. The quadrature relation, when produced, can be detected by the optical method of Lissajous, i.e., by allowing a beam of light to be reflected from one mirror on to the other, and thence on to a screen. The spot of light will then execute a figure or series of figures known as Lissajous\* figures. The particular figure formed at quadrature phase relation can be recognized with a certain degree of precision, depending upon the optical conditions, and serves to identify the condition of resonance in the tested vibrator.

\* Bibliography 2.

Figures 118 and 119 are photographic views of an oscillograph-meter or auxiliary vibrator constructed for the author by Mr. H. G. Crane.\* Figure 120 is a sectional diagram through the plane of the reflected beam of light at quiescence.

In Fig. 118, the little mirror *m* is supported on a bifilar strip suspension, between the poles of the permanent magnet *MM*. The breadth of this mirror should be as small as is practicable, but the length parallel to the suspension must be sufficiently great to keep the beam of light, received from the tested mirror, from running off at either end. In the instrument shown, the breadth of mirror *m* was approximately 0.9 mm. and the length 2.3 mm. The permanent magnet and its suspension may either be cradled on a horizontal axis between two brass end pillars as shown; or it may be supported at an adjustable height on a single central pillar. The vibrator suspension is also cradled in its supports for convenience of optical adjustment.

Figure 119 shows the auxiliary vibrator mounted in position in front of the oscillograph to be tested. The axes of the two vibrators are set mutually perpendicular. The tested vibrator is nearly always constructed with a vertical axis; so that the auxiliary vibrator must take up a horizontal axis.

Figure 120 indicates that the auxiliary mirror *A* must be supported close to the tested mirror *O*. The distance *OA* may conveniently be made from 11 to 14 mm. This requires that the auxiliary permanent magnet must be supported in close proximity to the electro-magnet poles of the tested instrument. The mounting must therefore be mechanically firm and rigid. It is important that the permanent magnet should not become demagnetized by resting in close proximity to the more powerful electro-magnet.

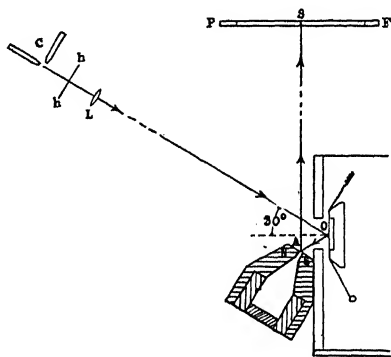


FIG. 120. Optical system of oscillograph-meter *A* and the tested oscillograph *O*. Length of *A* mirror 2.3 mm., width 0.9 mm.

The optical arrangement is such that, as shown by Fig. 120, a

\* Bibliography 62.

small but powerful arc-light beam, traversing a small hole in the screen  $hh$ , passes, with the aid of the lens  $L$ , to the tested mirror  $O$ , at a depression angle approximately  $30^\circ$ . It is thence reflected at  $30^\circ$  on to the auxiliary mirror  $A$ . The plane of this mirror is inclined about  $30^\circ$  with the horizontal, so that its normal makes an angle of about  $30^\circ$  with the beam it receives. Thence the beam will be reflected vertically upwards on to a translucent screen  $FF$  of squared paper, conveniently divided to square millimeters. The spot of light  $S$  should form on this screen, with the aid of the focusing lens  $L$ , an optical image of the small hole in the opaque screen  $hh$ . The distance  $AS$  is unimportant, but may conveniently be made 50 cm.

**Lissajous Figures.** — If the oscillograph and auxiliary vibrator are operated from the same source of adjustable frequency, they will both vibrate or execute forced vibrations of that frequency. Because their vibration axes are set mutually perpendicular, the vibratory path of the beam of light on the paper plane  $FF$ , perpendicular to the beam  $AS$ , will be a Lissajous figure. This figure, in the case of two such cofrequent simple vibrations, will always be an ellipse, including the straight line and the circle as limiting cases.

If the maximum cyclic displacements of the two mirrors are cophasal, the permanent optical figure executed by the spot  $S$  on the paper sheet  $FF$  will be a straight line. If they are not cophasal, the figure will broaden into an ellipse. When the phase difference amounts to the maximum value of quadrature, the ellipse will include its maximum area, assuming that the maximum cyclic displacements are constant, the two perpendicular axes of the ellipse being each parallel to the two component angular displacements. The ellipse will become a circle at quadrature phase-displacement, if the two are equal.

Figure 121 illustrates the development of the Lissajous figures for the particular case in which the auxiliary vibrator amplitude is half the tested vibrator amplitude, on the assumption that these amplitudes remain constant. Referring to the upper series  $A, B, C, D, E$ , the two mirrors start at  $A$  in cophase, the oscillograph in  $A_0$  being directed vertically to  $O$ , and the auxiliary mirror  $A_a$  being directed horizontally to  $O$ . The two then virtually rotate their vectors in synchronism through successive 8 points of their circumferences. The path of the doubly reflected beam is then the

straight line  $O4$ , with its center at 2 or 6. This path is described with a resultant simple harmonic motion.

At  $B$  in Fig. 121, the auxiliary vibrator  $B_a$  is represented as retaining standard phase, while the oscillograph vibrator  $B_o$  has lost  $45^\circ$  in phase. The resultant path of the beam is the ellipse  $B$ . Again, at  $C$ , the oscillograph vibrator  $C_o$  has lost  $90^\circ$  in displacement phase or has its displacement in quadrature with the auxiliary  $C_a$ . This represents the ordinary condition at resonance in  $C_o$ . The beam now executes the upright ellipse  $C$ . At  $D$  the oscillograph  $D_o$  has fallen  $135^\circ$  behind standard phase. The ellipse  $D$  now inclines backwards. Finally, at  $E$ , the oscillograph has lost  $180^\circ$ , or has come into reverse phase with  $E_a$ . The resultant path is a straight line  $E$  with backward slope.

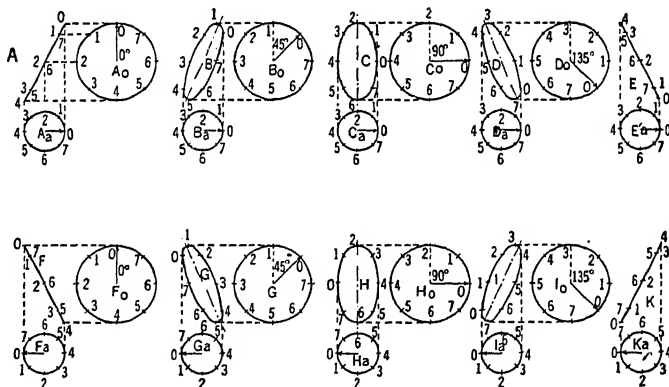


FIG. 121. Lissajous figures with components in the ratio of 2 to 1 and various phase differences.

The  $F G H I K$  series in Fig. 121 show what occurs with original phase opposition at  $F$  instead of the cophase at  $A$ , the other conditions remaining unchanged. It will be observed that in this case also the ellipse  $H$  is vertical when the oscillograph loses  $90^\circ$  in phase. Consequently, whether the auxiliary is working below its own resonant frequency and in phase with its excitation, as in  $A B C D E$ , or above its own resonant frequency and in opposite phase to its excitation, as in  $F G H I K$ , the ellipse will stand vertical at  $C$  or at  $H$ , when the tested oscillograph mirror falls  $90^\circ$  behind its excitation phase, as will necessarily happen at its resonant frequency  $f_0$ .



It generally happens that the amplitude of the auxiliary vibrator is less than that of the tested oscillograph vibrator, so that the conditions indicated in Fig. 121 are fairly representative of an actual test. There are two reasons why the auxiliary amplitude should be the smaller. First, the magnetic field of the auxiliary vibrator with its permanent magnet is much weaker than that of the oscillograph with its more powerful electromagnet. The amplitude of vibratory displacement of a vibrator, other things being equal, is proportional to the intensity of its ambient magnetic field. Second, the auxiliary vibrator is required to be operated away from its resonant frequency, and this entails a relatively small deflection. In making the test, it is usually necessary to carry the exciting alternating current in the auxiliary vibrator much higher than in the tested oscillograph, and sometimes to carry it to the safe carrying capacity of the auxiliary vibrator, without overheating or overexpansion of its strips. This limit has usually been in the neighborhood of 250 milliamperes rms., but the current can be made much stronger than this without any permanent injury to the auxiliary vibrator.

In making the test of the oscillograph in this way, we must first ascertain that the resonant frequency of the auxiliary vibrator is not near to that of the oscillograph. This is done by making a preliminary short series of impressed frequency observations with the Lissajous figure arrangement, but with each vibrator only operated at a time. Under these conditions, the reflected beam will execute only one component vibration, and by observing the amplitude of this vibration, we can readily make a rough estimate of the frequency  $f_d$  of maximum displacement, near which the resonant frequency will lie very closely in the air damped auxiliary vibrator, and not very far off in the ordinary liquid damped oscillograph. If the maximum admittant frequency  $f_d$  should happen to be nearly alike in the two vibrators, the auxiliary must have its mechanical tension either raised or lowered, as may be found more desirable, so as to throw its resonant frequency further away from that of the oscillograph. Beyond this requirement, the various constants of the auxiliary vibrator, such as  $\omega_0$ ,  $B_0$ ,  $A$ ,  $m$ ,  $r$ , and  $s$ , are of no concern. It is sufficient only that its  $B_0$  shall be small, and that its  $\omega_0$  shall not be close to the  $\omega_0$  of the tested oscillograph.

## CHAPTER XX

### OSCILLOGRAPH TESTS

It is proposed, in this Chapter, to consider the technique of testing oscillographs by the use of an auxiliary vibrator, and also to discuss some of the results thus obtained.

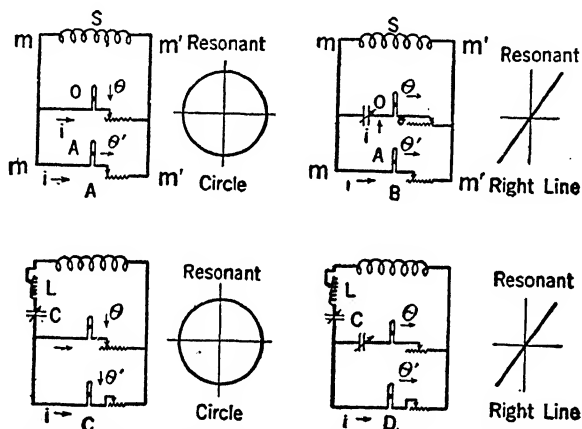


FIG. 122. Methods of testing oscillograph vibrators by means of oscillograph-meter.

**Electric Connections for the Test.** — The electric connections for measuring the resonant frequency  $f_0$  of an oscillograph, by means of the oscillograph-meter described in the last Chapter, are indicated in different forms by Fig. 122, at A, B, C, and D. In each case  $S$  is the source, or secondary coil, of the adjustable-frequency oscillator which supplies the testing current. Either a Vreeland oscillator\* or a triode vacuum-tube oscillator may be used. The source  $S$  supplies both the tested oscillograph  $O$ , and the auxiliary vibrator  $A$ , in parallel, from the same mains  $mm'$ . Each vibrator has its own adjustable non-inductive resistance, so that the phase of the current supplied to each should be the same within all desired limits of precision. The two impressed

\* Bibliography 27.

vmts. will therefore be cophasal. The phase of the displacement of mirror *O* will be in lagging quadrature to the vmt. at its resonant frequency  $f_0$ , as is indicated by the small arrow on the right hand of *O* in the figure. The phase of the displacement of mirror *A* will be very nearly in agreement with the vmt. at this frequency, if its resonance is remote. Under these conditions, the Lissajous figures obtained on the screen *FF* of Fig. 121 will be a circle at resonance  $f_0$  if the two vibratory components are equal, as is indicated by the circle at the right hand side of *A*. If the two components are unequal, and that of oscillograph *O* is the greater, we have seen in the last chapter that the Lissajous figure will be an upright ellipse. In the one case, the criterion for the attainment of resonance in *O* will be the equality of perpendicular diameters in the circle, and in the other, the verticality of the resonant ellipse *C* or *H*, Fig. 121.

If the optical adjustment of the Lissajous system is fine, so that the beam of reflected light is sharp and thin, it may be more easy to observe the existence of the thin cophase straight line *A*, *E*, *F*, or *K* in Fig. 121, than the roundness of a resonant circle, or the verticality of a resonant ellipse. This is a matter of personal choice with the observer. If he prefers the straight line or collapsed ellipse of Fig. 122*B* as a criterion, then the connections in that figure may be used. Here, the resistance in one of the two vibrator circuits, *O* as shown, is replaced by a nearly resistanceless adjustable condenser. This has the effect of advancing the phase of the exciting current in that branch by  $90^\circ$ ; so that the two impressed vmts. will be in quadrature throughout the frequency range. If the two vibrator displacement-admittance slopes are cophasal, the Lissajous figure will then be either a circle, or an upright ellipse. At displacement-admittance slope quadrature, combined with vmt. quadrature, the two mirror displacements will come into phase — either cophase or opposition phase — and the Lissajous figure at resonance in *O* will be the straight line of Fig. 122*B*.

It was found that when a Vreeland oscillator was used as the source of impressed frequency, difficulties arose owing to small parasitic harmonics or impurities in the derived current wave form, which produced false resonances and erroneous results in the behavior of the sharply resonant air-damped auxiliary vibrator. These false resonances did not occur when the vibrator was im-

mersed in a damping liquid. Much trouble was experienced in the first few months of research with this method of testing, from such parasitic resonances. They were obviated, however, by electrically tuning the main circuit to the test frequency, as indicated in Figs. 122*C* and *D*, where the adjustable inductor  $L$  and adjustable condenser  $C$ , inserted in series with the secondary coil  $S$ , serve to weed out impurities in the a.-c. waves by opposing a relatively large reactance to all but the test frequency. If this plan is used, care must be taken to make the proper tuning adjustment in  $L$  and  $C$  at each change of impressed frequency. With the ordinary connections of a pliotron or triode vacuum-tube oscillator, this parasitic resonance difficulty was not experienced, and the simpler connections of Fig. 121*A* or *B* could be used.

**Technique of Test.** — The oscillograph vibrator to be tested must be used on a base which permits of mounting the oscillograph-meter securely in front of it. This usually means removing the oscillograph from its photographic case. The oscillographmeter is then mounted in the proper position as indicated in Figs. 119 and 120, with the electromagnet of the oscillograph unexcited. The mounting is made sufficiently rigid to withstand safely the magnetic pull on the oscillographmeter when the electromagnet of the oscillograph is excited. The scale  $FF$ , Fig. 120, and the optical system are then adjusted until a sharp spot of light is produced at  $S$  with a shading tube laid over the scale  $FF$ . The electric connections are then made, and the deflections produced by  $O$  and  $A$  separately are roughly tried out to make sure that the resonances are sufficiently remote, as has been described in the last Chapter. The type of resonant Lissajous figure — ellipse or straight line — is selected in accordance with Fig. 122*A* or *B*, respectively. Most observers prefer an upright ellipse, the ratio of major to minor diameters in which is between 2 and 3.

The two vibrators are then set in operation, and the test frequency on both is raised to the point at which the Lissajous figure on the screen denotes displacement quadrature and resonance in the oscillograph. The temperature of the latter is noted.

Having identified the resonant frequency  $f_0$ , or corresponding resonant angular velocity  $\omega_0$ , of the tested oscillograph vibrator, the latter is then tested for its "specific deflection," or calibration, both at a low frequency  $f$ , and at the frequency of resonance  $f_0$  just determined.

**Specific Deflection.** — The specific deflection of an oscillographic vibrator may be defined as the size of maximum cyclic deflection per unit rms. exciting current. It may be denoted by the symbol  $\theta'$  and is expressed in mirror radians per rms. abampere in the theory, or in arbitrary scale divisions per rms. ampere in practical service. If we observe the maximum cyclic angular displacement  $\theta_{ms}$  in mirror radians produced at a low frequency of say  $f_s = 60 \sim$ , then

$$(253) \quad \theta_s' = \left| \frac{\theta_{ms}}{I_s} \right| \frac{\text{max. cyc. mirror radians}}{\text{rms. abampere}}$$

is the specific deflection of the oscillograph at this frequency, where  $I_s$  is the rms. current strength in abamperes through the vibrator. Similarly, the resonant specific deflection is

$$(254) \quad \theta_0' = \left| \frac{\theta_{m0}}{I_0} \right| \frac{\text{max. cyc. mirror radians}}{\text{rms. abampere}}.$$

The measurement of  $\theta_s$  and  $\theta_0$  determine the resonant bluntness of the oscillograph, as already described, according to the relation (250)

$$(255) \quad B_0 = \frac{1}{2} \left| \frac{y_s'}{y_0'} \right| = \frac{1}{2} \frac{\theta_s'}{\theta_0'}.$$

It is evident that since only the ratio of  $\theta_s'/\theta_0'$  is required for establishing the bluntness  $B_0$ , the two specific deflections may be measured in any uniform scale, without a determination of the respective radian angular displacements.

From (236) we may find that if  $\theta'$  is the specific deflection of the oscillograph at any impressed frequency ratio  $u$ , the deviation factor is:

$$(256) \quad D = \frac{1 - u_s^2 + j 2 B_0 u_s}{1 - u^2 + j 2 B_0 u} = \frac{1 - u_s^2 + j B_s u_s}{1 - u^2 + j B_s u}.$$

Since  $u_s = f_s/f_0$  is usually a negligibly small real number (with say  $f_s$  at  $60 \sim$  and  $f_0$  at  $2400 \sim$ ,  $u_s = 0.025$ ) we may write this equation without serious error as follows:

$$(257) \quad D = \frac{1}{(1 - u^2) + j 2 B_0 u} = \frac{1}{(1 - u^2) + j B_s u},$$

or

$$(257a) \quad C = \frac{1}{D} = (1 - u^2) + j 2 B_0 u = (1 - u^2) + j B_s u,$$

which agrees with (239) at resonance, when  $u = u_0 = 1$ .

If we seek only the size of the deviation ratio, and ignore its slope, we have

$$(258) \quad |D| = \frac{\theta'}{\theta_s'} = \frac{1}{\sqrt{1 + 2u^2(2B_0^2 - 1) + u^4}},$$

an equation which is free from complex quantities. The correcting factor is then

$$(259) \quad |C| = \frac{1}{|D|} = \frac{\theta_s'}{\theta'} = \sqrt{1 + 2u^2(2B_0^2 - 1) + u^4}.$$

When making specific-deflection tests with the optical arrangement of Fig. 120, it has been found advantageous to insert a fine cross-hair into the beam at the screen  $hh$ , on the lens  $L$ , or at such a point as will enable a sharp image of the hair to be formed in the quiescent spot  $S$ , on the graduated paper scale  $FF$ . Since the spot of light, when making a simple vibration, comes regularly to rest at each elongation, the two extreme positions of the hair can be detected easily by carefully examining the band of light drawn out by vibration on the scale. When, however, Lissajous figures are being examined, the cross-hair is withdrawn.

Specific deflections may be measured conveniently by taking the full length from end to end, between hair-line images of the band of light on the scale  $FF$ . When measuring angular displacements of the vibrator in radians, however, it must be remembered that not only is the amplitude of deflection half the total luminous scale distance, but also the mirror angular displacement is half the angular displacement of the reflected beam. In other words, the maximum cyclic angular displacement of the mirror is one-fourth of the full luminous length of the scale from elongation to elongation, divided by the perpendicular distance of the scale from the mirror, which is assumed to be relatively large.

When measuring specific deflections of the tested oscillograph, with the auxiliary vibrator in position, as in Fig. 120, it should be remembered that magnetic leakage from the oscillograph electromagnet poles through the magnet of the auxiliary vibrator may perceptibly weaken the field in which the oscillograph vibrator works. This should not affect the measurement of  $f_0$ , but it may affect the specific deflection. If both  $\theta_0'$  and  $\theta_s'$  are measured with the auxiliary vibrator in place, their ratio may not be affected by this source of error; but if one is measured with the auxiliary vibrator in place, and the other with it removed, the ratio entering into the value of  $B_0$  may be distinctly affected.

**Observation of Quadrantal Frequencies by means of Lissajous Figures.** — Instead of determining  $B_0$  by the ratio of the specific deflections  $\theta_s'/\theta_0'$ , it is possible, after finding  $\omega_0$ , to find  $\Delta$ , and hence  $B_0 = \Delta/\omega_0$ , by identifying optically one, or preferably both, of the quadrantal angular velocities  $\omega_1$  and  $\omega_2$ . The electric connections for this are indicated in Fig. 123. The plan is to introduce such equal resistance and reactance into the auxiliary branch circuit  $A$ , at the test frequency, as shall cause the exciting current and the vmt. in the auxiliary vibrator to differ in phase from that in the oscillograph by  $45^\circ$ , and so to enable a quadrantal frequency to be identified optically from a Lissajous diagram. After observing  $\omega_0$  and say  $\omega_1$  in this way, we can compute  $\omega_2$  by (106). Again, if we observe all three angular velocities  $\omega_0$ ,  $\omega_1$ , and  $\omega_2$ , they should check by (106). We may then find  $\Delta$  by (113) and thence  $B_0$  by (208).

This method of determining  $B_0$  dispenses with the measurement of specific deflections. On the other hand, it is apt to be less precise than the specific-deflection method; because  $\Delta$  is found as the difference of two identified frequencies. With sharp vibrators, these two quadrantal frequencies lie close together, and their difference is thus subject to relatively considerable observation error. In complete and thorough tests of an oscillograph, however, it may be well to identify optically all three values  $\omega_0$ ,  $\omega_1$ , and  $\omega_2$ , besides measuring the specific deflections  $\theta_0'$  and  $\theta_s'$ , so as to secure mutual checks.

**Alternative Measurement of  $\Delta$  and  $\omega_0$ .** — Another method of measuring  $\Delta$  and  $\omega_0$ , without using an oscillographmeter, when the vibrator is sharp, is to make an oscillogram of a series of naturally decaying oscillations of the mirror with the vibrator circuit interrupted, impressing on the same record a wave of known fairly high frequency from the movement of a second vibrator separately excited. See Fig. 140. The rate of decay in amplitude is

$$(260) \quad \theta_t = \theta_i e^{-\Delta t} \quad \text{max. cyc. radians,}$$

where  $\theta_i$  is the initial displacement at time  $t = 0$  and  $\theta_t$  is the displacement after  $t$  seconds have elapsed. Hence

$$(261) \quad \Delta = (1/t) \log_h (\theta_i/\theta_t) \quad \text{hyp. per. sec.}$$

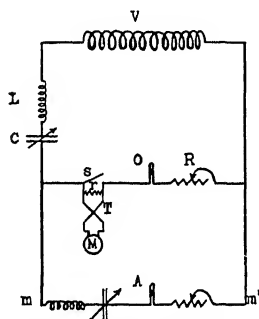


FIG. 123. Electrical connections for the measurement of quadrantal frequencies.

The frequency of vibration as determined from the oscillogram, with the aid of the waves of known frequency, is  $f_f \sim$ . This will be a little less than the resonance frequency  $f_0$ , the correction being obtainable through (244). This method can be applied with fair success to sharp vibrators. It cannot be applied ordinarily when  $B_0$  is greater than 0.2. This means that in ordinary liquid-damped oscillographs the method is unsatisfactory.

It might be supposed that since a calibration or specific deflection is desired near to zero frequency, a continuous-current calibration would suffice. It has been found, however, that the specific deflections  $\theta_s'$  obtained with continuous currents is considerably in excess of that measured with a low-frequency alternating current, apparently because the elastic system of the vibrator has a greater opportunity to stretch under a steady impressed torque than under alternating torques. In other words, the elastic constant  $s$  is essentially a vibratory property.

Although fairly satisfactory results have been obtained in the tests of oscillographs by the use of the oscillographmeter as above described, there is abundant opportunity for further work in this method, directed towards improvement in the design, construction, mounting, and manipulation of the oscillographmeter.



## TESTS OF OSCILLOGRAPHS

It is proposed to present in this Chapter some of the results obtained in the testing of oscillographs by oscillographmeters.

**Tests of the Air-damped Auxiliary Vibrator, of high Resonant Sharpness.**—The air-damped auxiliary vibrator is a typical example of an oscillograph of very sharp resonance or very small bluntness, and is of interest on that account. Figure 124 shows a curve of observed specific deflection  $\theta'$  versus impressed frequency  $f$ , taken on one of the oscillographmeters used in the tests. The observations are plotted to two different scales, in ratio of 10:1, to facilitate the interpretation of the graph. The graph to the enlarged scale runs far off the top of the diagram, at and near resonance. The small circles represent the individual observations of specific deflection, in mirror radians per rms. abampere; while the curves show the theoretical graphs as obtained by the formulas (257) and (258) and (239), from tests made by the oscillographmeter method described in the last Chapter. It will be seen that the agreement between the observations and the curve is very satisfactory.

The three principal frequencies of this auxiliary vibrator are  $f_1 = 2511 \sim$ ,  $f_0 = 2514.5 \sim$  and  $f_2 = 2518 \sim$ . The resonant range is thus 7 cycles per second. The corresponding angular velocities are  $\omega_1 = 15777$ ,  $\omega_0 = 15799$ ,  $\omega_2 = 15821$ . The damping constant  $\Delta$  is thus  $(15821 - 15777)/2 = 22$ . The oscillatory sharpness  $\Lambda_0$  is  $15799/22 = 718$ , and its reciprocal, the bluntness  $B_0$ , is 0.00139. This means that the maximum cyclic displacement at resonance is 359 times as great as at very low frequency, which agrees with the ratio of  $\theta'_0/\theta'_s$ , so far as can be read from the curves in Fig. 124. The angular velocities  $\omega_r$  and  $\omega_d$ , of free vibration and maximum displacement, by (244) and (243), are indistinguishable from  $\omega_0$ , within the limits of engineering laboratory measurements. All three frequencies  $f_0$ ,  $f_r$ , and  $f_d$  are in this case inseparable, except from the standpoints of mathematics, physics, and

philosophy. It is also evident that, provided the resonant frequency of this vibrator is slightly avoided, the phase departure of the mirror from zero or  $180^\circ$  in the vmt. will be small. The deviations can be found from (238) in any given case, if necessary.

It may be noted that any asymmetry in the construction of an air-damped vibrator, such as unequal dimensions, or unequal tensions in the two strips composing it, is likely to give rise to plural resonance in the behavior of the instrument. The curve of

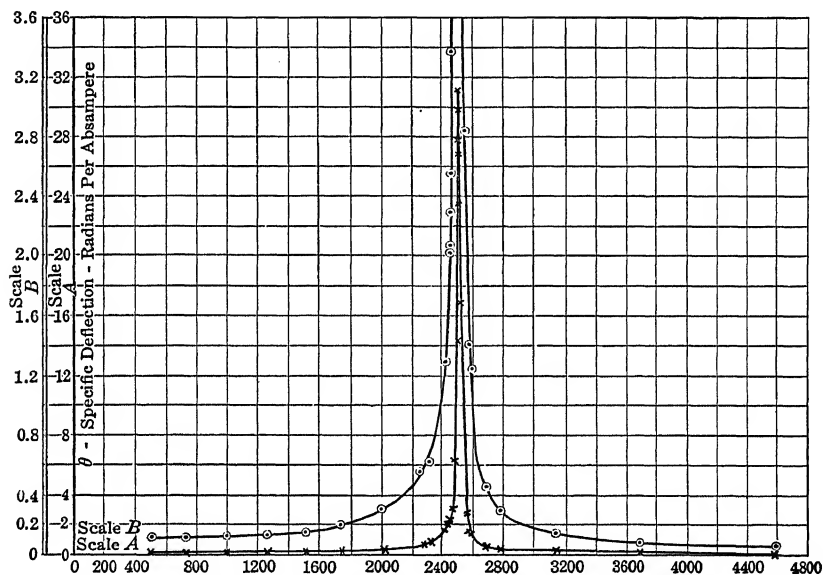


FIG. 124. Specific deflection vs. frequency for the auxiliary vibrator A-1.  
Temp. =  $22.5^\circ$  C.,  $\Delta = 22$  hys./sec.,  $\omega_0 = 15799$ ,  $\Delta_0 = 718$ .

$\theta'$  versus  $f$ , such as curve A in Fig. 124, may reveal two or more separate peaks, and the Lissajous figures will likewise go through two or more sets of ellipses. A number of such cases have been observed. A good air-damped oscillographic vibrator requires good mechanical workmanship, to secure the requisite geometric and dynamic symmetry. When the vibrator is immersed in a damping liquid, these plural resonances often disappear, so that a vibrator which is apparently of normal behavior when liquid-damped, may behave abnormally after drying and when operated in air.

### Liquid-damped Oscillographs of Moderate Resonant Bluntness.

— A fairly typical and commercial form of oscillograph has its specific-deflection behavior at various frequencies displayed in Fig. 125. The curve is drawn to the theoretical behavior from oscillographmeter measurements of  $f_0$  and  $B_0$ . The small crosses represent the observed specific deflections, as the impressed frequency was varied from 500 ~ to 4900 ~. The agreement between the observations and the curve is fairly satisfactory. This vibrator is damped by a specially prepared liquid, supplied with the instrument. The principal frequencies of  $f_1 = 2620$  ~,  $f_0 = 3300$  ~ and  $f_2 = 4070$  ~, were observed by Lissajous figures. The corresponding angular velocities are  $\omega_1 = 16460$ ,  $\omega_0 = 20740$ ,

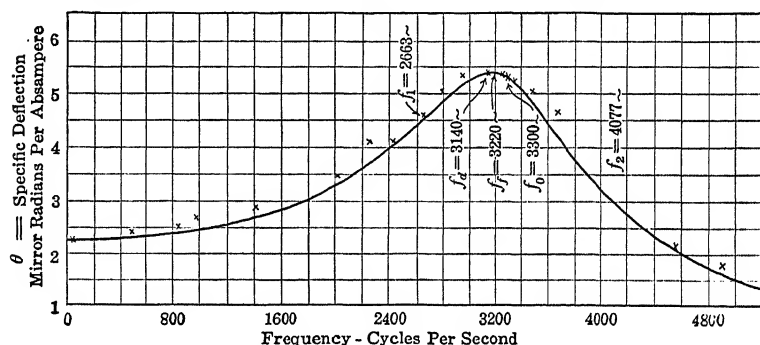


FIG. 125. Specific deflection vs. frequency. Oscillograph vibrator in light damping liquid.  $\Delta = 4450$  hysps per second.  $B_0 = 0.214$ .

and  $\omega_2 = 25573$ . The quadrantal frequencies as computed from  $f_0$  and  $B_0$  are 2663 ~ and 4077 ~ with angular velocities 16732 and 25617. The damping factor  $\Delta$  is thus 4443 and the bluntness  $B_0 = 4443/20740 = 0.214$ . The specific deflection  $\theta_0'$  observed at resonance was 4.35 mirror radians per rms. abampere, and  $\theta_s$  at 60 ~ was also observed to be 1.25. The ratio  $\theta_s'/\theta_0' = 0.42$ , from which the bluntness  $B_0 = 0.21$ . In this instrument the free-vibration frequency  $f_f$  by (244) is 3220 ~, and the frequency of maximum-displacement admittance  $f_a$ , by (243), is 160 ~ below  $j_0$  or 3140 ~, when the specific deflection was found to be 5.4, or about 1 per cent more than at resonance.

The deviation factor of this oscillograph at 1000 ~ is  $1.09 \simeq 8^\circ$  by (239). It would overindicate waves of that frequency by 9 per cent with respect to waves of 60 ~, and would record them  $8^\circ$  of their cycle behind the true position ( $\beta = -8^\circ$ ).

**Assymetry of Specific-deflection and Frequency Curve with Respect to the Maximum Ordinate.** — It may also be observed that any curve of  $\theta'$  versus  $f$ , such as that in Fig. 125, always rises to a maximum ordinate at  $f_d$ , unless  $B_0$  exceeds unity. The curve is asymmetric with respect to that ordinate, being steeper on the high-frequency side. It is shown, however, in Appendix XI, that if the specific deflections as ordinates are plotted against  $f^2$  as abscissas, the resulting curve will be symmetric about the maximum ordinate, as far as  $f_{s2}$ , the duplicate initial frequency; i.e., as far as symmetry can be carried. Consequently, if the curve of  $\theta'$  versus  $f^2$  is plotted from observations over the range  $f = 0$  to  $f = f_d$ , it can be extended, by symmetry, from  $f = f_d$  to  $f = f_{s2}$ , without making observations over that range.

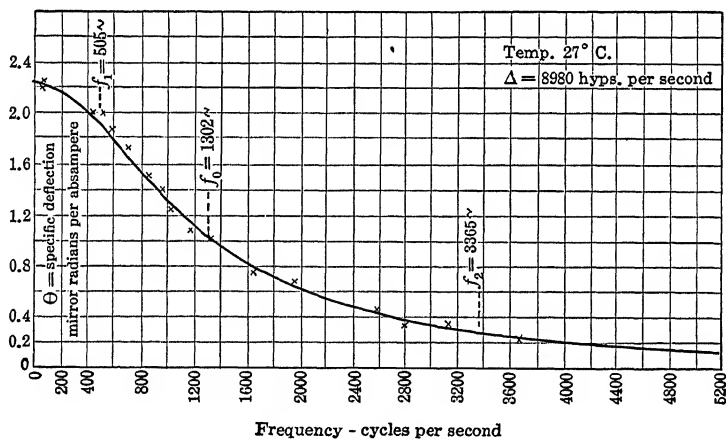


FIG. 126. Specific deflection vs. frequency. Oscillograph vibrator 0-6 in castor oil. Temp. 27° C.  $\Delta = 8980$  hyps./sec.  $B_0 = 1.1$ .

**Tests of an Oscillograph with large Resonant Bluntness.** — Figure 126 illustrates the behavior of an oscillograph with a bluntness  $B_0 = 1.1$ , obtained by the use of castor oil as the damping liquid. It will be noticed that the resonant frequency  $f_0 = 1302 \sim$  occurs about halfway down the curve.

**Effects of Changing the Damping Liquid on the Behavior of an Oscillograph.** — Figure 127 gives the curves of specific deflection  $\theta'$  versus impressed frequency  $f_1$  for a vibrator in four successive damping fluids; viz., air, glycoline, mineral oil, and castor oil. The results are summarized in Table XVIII.

TABLE XVIII

CONSTANTS OF AN OSCILLOGRAPHIC VIBRATOR IN DIFFERENT DAMPING FLUIDS (Hunter)

CURVE	DAMPING FLUID	$f_0$ Cycles Sec.	$\omega_0$ Rad. Sec.	$B_0$ NUM- ERIC	$f_1$ Cycles Sec.	$f_2$ Cycles Sec.	$\Delta$ Hyps. Sec.	$f_d$ Cycles Sec.	RESON- NANT RANGE Cycles Sec.
I	Air	4,110	25,820	0.024	4,013	4,207	609	4,110	194
II	Glycoline	1,891	11,880	0.26	1,523	2,513	3,100	1,827	490
III	Mineral Oil	1,614	10,140	0.43	1,060	2,460	4,400	1,272	1,400
IV	Castor Oil	1,302	8,180	1.1	505	3,365	8,980	0	2,860

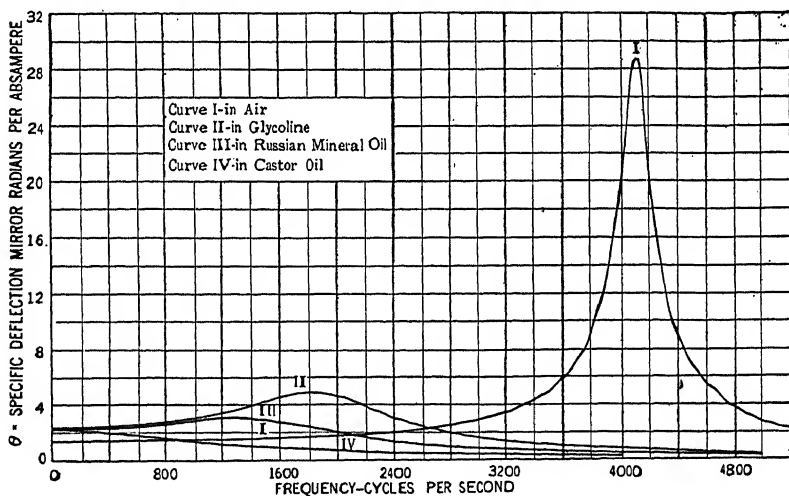


FIG. 127. Specific deflection vs. frequency. Oscillograph vibrator 0-6. Temp. 26.5° C. under different damping conditions.

Whereas in air, the vibrator had a bluntness of  $B_0 = 0.024$ , or a sharpness of  $\Delta_0 = 41.7$ , the bluntness was increased in castor oil to 1.1 ( $\Delta_0 = 0.9$ ). The effect was also to change the resonant frequency  $f_0$  from 4110 ~ in air, to 1302 ~ in castor oil.

In case III with mineral-oil damping, the resistance  $r$  of the vibrator was 0.43 of that which would render the motion aperiodic. In case IV, however, with castor-oil damping, the resistance is ten per cent greater than that required for aperiodicity. The case is therefore one of overdamping or ultraperiodicity. It is developed in greater detail in Fig. 126. The curve is drawn from the formulas already given, and the crosses indicate the observations. It

will be seen that  $f_d = 0$ , and by (243) is imaginary. At resonance, the specific deflection is only about half that at zero frequency.

It may be noted that in Fig. 127, the value of  $\theta_s'$  is substantially the same for all of the damping fluids except air. The deflection is less with air than with liquid damping. This is not due to resistance  $r$ . According to theory, the resistance plays no part in determining the specific deflection at zero frequency. Everything depends upon the elastic yield  $c = 1/s$ , by (241). It might be supposed that air would be more yielding than oils; but according to the results shown in Fig. 127, which have been substantiated in an independent series, the reverse condition presents itself. The matter warrants further investigation.

According to these indications, the specific deflection of an oscillograph in a heavily damping liquid like castor oil, at a very low frequency, is substantially the same as in a lightly damping liquid like glycolin. The differences in these cases are found at the higher frequencies. If  $B_0$  is less than unity, there will always be some increase in specific deflection when the frequency is raised. With very light damping, the increase will be marked, especially near resonance. With damping near to unit bluntness, the increase will be small and the specific deflection will soon decrease.

**Best Values of Bluntness in an Oscillograph.** — From a considerable number of oscillograph tests, of which Figs. 124 to 127 are fairly typical, and from an examination of displacement-admittance charts Figs. 115 to 117, it appears that there is no precise value of  $B_0$  which an oscillograph should possess, in order to have minimum deviation factor, or minimum change in specific deflection with change of impressed frequency. Figure 115 indicates, however, that near  $B_0 = 0.6$ , the specific deflection remains nearly constant from  $u = 0$  to  $u = 0.75$ , the maximum increase being only 4 per cent over this range. This is, therefore, in general, a good value of  $B_0$  to secure. If, however, a greater range of impressed frequency is to be employed than is available up to 75 per cent of the resonant value, it may be better to use  $B_0 = 0.5$  or less.

**Measurements Necessary for Evaluating the Fundamental Constants  $A$ ,  $m$ ,  $r$  and  $s$ .** — In order to evaluate the fundamental constants of an oscillograph, an additional independent datum is needed, over and above the information necessary for determining  $\omega_0$  and  $\Delta$ , or  $f_0$  and  $B_0$ . Such a datum is supplied by the measure-

ment of the motional impedance of the vibrator under working conditions.

**Damped, Free, and Motional Impedance of an Oscillograph.** —

The nature and construction of the ordinary bifilar oscillograph-vibrator is such that its inductance is extremely small, and its reactance is negligible by comparison with its resistance at the highest frequencies which are likely to be used. Moreover, provided the temperature of the damping fluid remains constant, the resistance of the vibrator remains substantially unchanged at all frequencies. The vector impedance graph of an oscillograph vibrator, when either damped, or free, but removed from its permanent magnetic field, may be regarded as the simple straight line  $OA$ , Fig. 128, of pure resistance at all frequencies. If, now, the

vibrator be freed, and restored to the normal magnetic field of its operating electromagnet, the vector graph of free impedance is the circular path  $A'B'C'D'$ , Fig. 128, where the resistance  $OA'$  is equal to the damped resistance  $OA$ . At resonant frequency

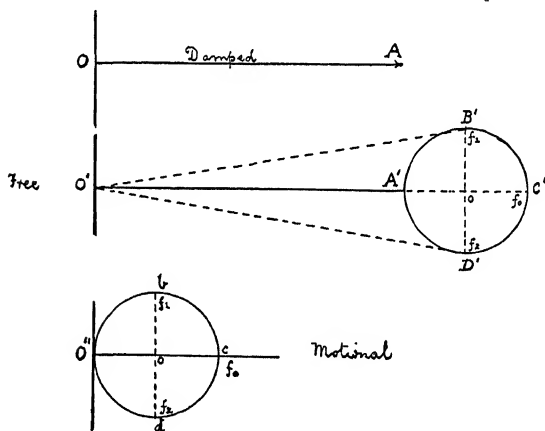


FIG. 128. Damped, free, and motional-impedance diagrams of an oscillograph or of a vibration galvanometer.

$f_0$ , or  $u = 1$ , the free impedance is  $OC'$ , a pure resistance. At the lower quadrantal frequency  $f_1$ , where  $u = u_1$ , the free impedance is  $Z'' = O'B' = O'o + j\omega B'$ ; or there is an apparent reactance of  $j\omega B'$  ohms, due to the vibration of the mechanical system in the magnetic field. At the upper quadrantal frequency  $f_2$ , where  $u = u_2$ , the free impedance is  $Z'' = O'D' = Oo - j\omega D'$ ; or the reactance is negative, as though the instrument contained a condenser in series with its vibrator. At either a very low or a very high frequency, the free impedance will be  $OA'$ , the same as when the vibrator was damped.

Subtracting the damped from the free impedance at each frequency, we obtain the motional-impedance circle  $O''bcd$ , Fig. 128, which is the same circle as  $A'B'C'D'$ , transferred to the origin of coordinates. The diameter of this circle is the pure resistance  $Z'_0 = O''c$  ohms, or abohms. The motional impedance at the lower quadrantal frequency  $f_1$ , of frequency ratio  $u_1$ , is  $Z' = O''b$  ohms, a semi-imaginary quantity, or impedance of  $45^\circ$  slope. At the upper quadrantal frequency, the impedance is  $Z' = O''d$ , another semi-imaginary quantity. The resonant bluntness of the vibrator can be read from this circle directly. To a first approximation it is

$$(262) \quad B_0 = u_2 - 1.$$

The precise value, by (208), is

$$(263) \quad B_0 = \frac{u_2 - u_1}{2}.$$

The motional-impedance circle of an oscillograph therefore differs from that of a telephone receiver in two respects; namely,

- (1) The diameter of the circle coincides with the resistance axis, or has no slope.
- (2) The diameter of the circle is very small compared with that of the ordinary telephone, if both are drawn to the same scale.

Thus the motional impedance of a telephone receiver  $Z'_0$  at apparent resonance is commonly about 100 ohms in size, for an instrument of  $R_1 = 75$  ohms d.-c. resistance; whereas the resonant motional impedance  $Z'_0 = R'_0$  of an ordinary liquid-damped oscillograph vibrator, may only be about 0.025 ohm. Air-damped oscillographs have larger motional impedances. Nevertheless, the resonant motional impedance must have a real value, however small; because there could be no motional or mechanical power dissipated in the vibrator unless through the establishment of a motional impedance. The low value of  $R'_0$  in an oscillograph calls, however, for a special technique in its measurement, such as will be presently described.

**Motional Power.** — The power expended in and by an oscillograph vibrator is closely associated with its motional-impedance circle, and follows the same general theory as that already discussed in Chapter IX, with reference to the telephone receiver.



Let *Obcd*, Fig. 129, be the motional-impedance circle of the vibrator

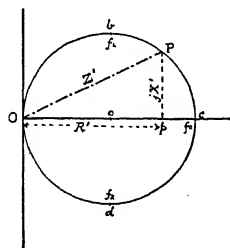


FIG. 129. Vector power in an oscillograph, as related to the motional-impedance circle.

to a scale of abohms. Let  $I$  be the rms. alternating-current strength steadily supplied to the vibrator in abamperes; then the power expended by this current in the vibrator at any vector position  $P$ , where  $OP = Z'$  abohms  $\angle$ , is, for zero slope in  $I$ ,

$$(264) \quad P_e = I^2 Z' \quad \text{abwatts } \angle.$$

The active component  $P_{ea} = I^2 R' = Op$  abwatts, read off to power scale, will be dissipated as heat in friction overcome by the motion, and will be power expended from the system. The reactive component

$P_{er} = jI^2 X' = pP$  abwatts, will be power cyclically stored and released. Following the reasoning of (117)

$$(265) \quad \dot{\theta}^2 \mathbf{z} = I^2 Z' = \dot{\theta}^2 \left\{ \mathbf{r} + j(\mathbf{m}\omega - \mathbf{s}/\omega) \right\} \quad \text{abwatts } \angle,$$

where  $\dot{\theta}$  is the rms. angular velocity of the mirror in radians per sec., and  $\mathbf{z}$  is the mechanical-impedance torque in dynes-p.-cm. per (radian/sec.). Consequently,

$$(266) \quad I^2 R' = \dot{\theta}^2 \mathbf{r} \quad \text{abwatts}$$

$$(267) \quad I^2 X' = \dot{\theta}^2 (\mathbf{m}\omega - \mathbf{s}/\omega) \quad \text{abwatts,}$$

or the active electric power is equal to the active mechanical power, and the reactive electric power to the reactive mechanical power. In other words, all of the mechanical power in the motional-impedance circle comes directly from the electric circuit.

**Steps for the Evaluation of  $\mathbf{A}$ ,  $\mathbf{m}$ ,  $\mathbf{r}$  and  $\mathbf{s}$ .** — Assuming that we already know  $\omega_0$  and  $\Delta$  for an oscillograph, from such measurements as were described in the last Chapter, and that we have also determined the resonant motional resistance  $R_0'$ , we find, following the reasoning of (139),

$$(268) \quad \mathbf{A} = \frac{I_m R_0'}{j\theta_{m_0} \omega_0} = \frac{R_0'}{\theta'_{m_0} \omega_0} \quad \frac{\text{dynes-p.-cm.}}{\text{abampere}},$$

where  $\theta'_{m_0} = \theta_{m_0}/I_m$ , is the scalar resonant specific deflection in maximum cyclic mirror radians per *maximum cyclic* abampere. This is the torque factor of the instrument, having the nature of a vector without slope, or a real quantity in the case of an oscillo-

graph. The maximum cyclic torque established by a maximum cyclic current of  $I_m$  absamperes will then be  $\mathbf{A}I_m$  dyne-p.-cm.

Again, following (140) the resistance-torque coefficient is

$$(269) \quad \mathbf{r} = \frac{\mathbf{A}^2}{R_0'} = \frac{\mathbf{A}}{\theta'_m \omega_0} = \frac{R_0'}{\theta'^2_m \omega_0^2} \quad \frac{\text{dyne-p.-cm.}}{\text{mirror radians per sec.}}$$

In the telephone-receiver case, the mechanical resistance evaluated in this way was a gross resistance modified by the displacement of the diaphragm in the magnetic field. This displacement energy is dissipated in the diaphragm by hysteresis and eddy currents. In the oscillograph case, the mechanical resistance may be considered as the net value  $\mathbf{r}$ .

Again following (141), we have

$$(270) \quad \mathbf{m} = \frac{\mathbf{r}}{2\Delta} \quad \text{gm.-cm.}^2 \text{ or } \frac{\text{dyne-p.-cm.}}{(\text{mirror radian/sec.})^2}$$

This is the apparent moment of inertia of the vibrating system, in its damping fluid.

Finally, following (142), we find

$$(271) \quad \mathbf{s} = \mathbf{m}\omega_0^2 \quad \frac{\text{dyne-p.-cm.}}{\text{mirror radian}}$$

This is the net elastic torque per unit of angular displacement. Thus all four fundamental constants can be deduced readily from measurements of  $f_0$ ,  $B_0$ , and  $R_0'$ .

An analysis of the constants of several oscillographic vibrators is given in Table XIX, on page 260.

It will be observed that in this particular set of vibrators, the torque factor  $\mathbf{A}$  varied from 119 to 255 dyne-p.-cm. per abampere —

The moment of inertia  $\mathbf{m}$  from  $9.85 \times 10^{-3}$  to  $51.15 \times 10^{-3}$  gm.-cm.<sup>2</sup>,

the resistance factor  $\mathbf{r}$  from  $0.705 \times 10^{-3}$  to  $3.124 \times 10^{-3}$   $\frac{\text{dyne-p.-cm.}}{(\text{rad./sec.})}$

the elastance factor  $\mathbf{s}$  from 18.2 to 175.3  $\frac{\text{dyne-p.-cm.}}{\text{m. radian.}}$

**Technique for Measuring the Motional Impedance of an Oscillograph.** — A convenient form of slidewire Wheatstone bridge is shown in Fig. 130, for the purpose of measuring the small resonant motional resistance  $R_0'$  of a liquid-damped oscillograph.

TABLE XIX  
DATA FOR SOME OSCILLOGRAPH VIBRATORS TESTED (Hunter)

VIBRATOR DAMPING FLUID	V <sub>1</sub> GLYCOLINE	V <sub>2</sub> GLYCOLINE	V <sub>3</sub> GLYCERINE	V <sub>4</sub> GLYCOLINE	V <sub>5</sub> GLYCOLINE	V <sub>6</sub> GLYCOLINE
Span, cm. . . . .	.....	1.26	1.26	1.18	1.25	1.25
Strip { width, cm. . . . .	.....	0.0350	0.0350	0.0350	0.0372	0.0372
Strip { thickness, cm. . . . .	.....	0.0025	0.0025	0.0025	0.0028	0.0028
Strip spacing, center to center, cm. . . . .	.....	0.055	0.055	0.056	0.052	0.052
Mirror { length, cm. . . . .	.....	0.150	0.150	0.130	0.180	0.180
Mirror { width, cm. . . . .	.....	0.065	0.065	0.080	0.060	0.060
Mirror { thickness, cm. . . . .	.....	0.014	0.014	0.014	0.014	0.014
Strip tension, kilodynes per strip . . . . .	.....	51.5	51.5	74.5	39.1	96.0
Air gap of vibrator well in cm. . . . .	.....	0.28	0.28	0.23	0.15	0.15
D.-c. resistance, ohms . . . . .	1.591	0.725	0.725	0.670	1.610	1.610
A.-c. resistance at the resonant freq., ohms . . . . .	1.650	0.753	0.745	0.733	1.739	1.739
$f_0$ , ~ . . . . .	2280	2366	1707	2950	2170	2760
$f_1$ , ~ . . . . .	1862	2010	1246	2520	1670	2240
$f_2$ , ~ . . . . .	2790	2780	2340	3480	2815	3390
$\omega_0$ , rad/sec. . . . .	14,320	14,840	10,720	18,520	13,630	17,320
$\omega_1$ , rad/sec. . . . .	11,680	12,620	7,825	15,730	10,480	14,050
$\omega_2$ , rad/sec. . . . .	17,520	17,460	14,705	21,840	17,650	21,300
$R'_0$ , abohms. . . . .	$0.032 \times 10^9$	$0.0219 \times 10^9$	$0.0054 \times 10^9$	$0.02085 \times 10^9$	$0.0201 \times 10^9$	$0.030 \times 10^9$
$\theta'_m$ , rad/abamp. . . . .	9.15	8.55	2.62	4.41	12.4	8.38
$\Delta$ , hyp. rad/sec. . . . .	2920	2420	3440	3055	3580	3655
$A$ , dyne-p.-cm./abamp. . . . .	244.4	173.0	102.5	255.0	119.0	207.0
$r$ , dyne-p.-cm./rad. per sec. . . . .	$1.865 \times 10^{-3}$	$1.364 \times 10^{-3}$	$6.85 \times 10^{-3}$	$3.124 \times 10^{-3}$	$0.705 \times 10^{-3}$	$1.428 \times 10^{-3}$
$m$ , gm.-cm. <sup>2</sup> . . . . .	$31.94 \times 10^{-8}$	$28.3 \times 10^{-8}$	$99.6 \times 10^{-8}$	$51.15 \times 10^{-8}$	$9.85 \times 10^{-8}$	$19.56 \times 10^{-8}$
$s$ , dyne-p.-cm./rad. . . . .	65.5	62.1	114.5	175.3	18.2	58.6
$B_0$ . . . . .	0.203	0.1295	0.320	0.1645	0.262	0.211

TABLE XX  
OSCILLOGRAPHIC RESULTS (Hunter and Prior)

VIBRATOR			DAMPING FLUID	TEMP. DEG. CENT.	FROM OBSERVATIONS OF $f_0$ , $\theta_0$ AND $\theta_s$							FROM LISSAJOUS FIGURES		$\omega_0$	$B_0$
					$\Delta$	$f_0$ ~	$f_d$ ~	$f_r$ ~	$f_1$ ~	$f_2$ ~	$f_1$ ~	$f_2$ ~	$f_1$ ~		
1	2	3	4	5	6	7	8	9	10	11	12	13			
0-1	Castor Oil	27.5	5,750	1,486	721	1,170	827	2,657	813	2,570	9,388	0.615			
0-3	Air	22.5	1,010	3,235	3,220	3,228	3,079	3,401	3,100	3,420	20,320	0.050			
0-4	Air	27	1,430	2,985	2,970	2,978	2,767	3,223	2,760	3,215	18,755	0.096			
0-5	Air	28.5	823	2,880	2,875	2,878	2,751	3,013	2,760	3,000	18,095	0.0455			
0-5	Castor Oil	28	5,700	1,151	Imag.	707	561	2,375	513.5	2,475	7,230	0.79			
0-6	Air	25	609	4,110	4,110	4,110	4,013	4,207	4,010	4,240	25,830	0.0286			
0-6	Glycoline	26	3,100	1,957	1,827	1,891	1,523	2,513	1,464	2,645	12,300	0.252			
0-6	Russian Min'l Oil	28	4,400	1,614	1,272	1,451	1,060	2,460	993	....	10,140	0.434			
0-6	Castor Oil	27	8,980	1,302	Imag.	Imag.	505	3,365	517	....	8,180	1.10			
0-7	Air	26	92	2,635	2,335	2,635	2,620	2,650	2,615	2,650	16,560	0.0055			
0-7	Glycoline	27	1,320	1,674	1,650	1,662	1,475	1,895	1,444	1,957	10,520	0.125			
0-7	Russian Min'l Oil	25	3,000	1,614	1,460	1,540	1,202	2,158	1,246	2,133	10,140	0.288			
0-7	Castor Oil	27	6,240	1,196	Imag.	665	560	2,544	555	2,520	7,515	0.83			
0-8	Air	27	1,620	4,210	4,195	4,203	3,962	4,468	3,830	4,570	26,460	0.0613			
0-8	Russian Min'l Oil	26	4,150	2,010	1,780	1,900	1,455	2,775	1,404	2,755	12,630	0.33			
0-8	Glycoline	27	3,142	2,323	2,215	2,270	1,880	2,880	1,932	2,820	14,600	0.215			
0-8	Castor Oil	27	12,400	1,674	Imag.	Imag.	615	4,565	634	....	10,520	1.18			
G	Light Damping Liquid	....	4,450	3,300	3,140	3,220	2,663	4,077	2,620	4,070	20,740	0.2146			

Two equal anti-inductive resistances  $A$  and  $B$  have one ohm each.

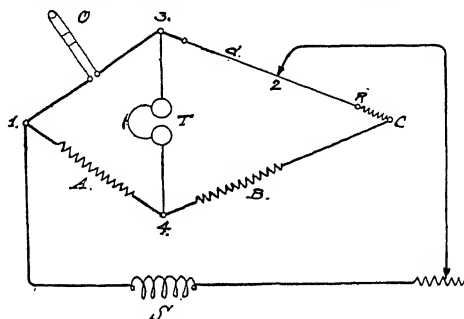


FIG. 130. Slide-wire bridge, for measuring the motional impedance of an oscillograph vibrator  $O$ .

The oscillator  $S$ , supplying the adjustable impressed frequency, is brought to slider 2 and junction 1, or a small transformer may be inserted between these terminals and the oscillator, so as to obtain ample testing-current strength. The slider 2 can be set to a fraction of a millimeter, on a scale, over the manganin slidewire, which has a linear resistance not exceeding 0.01 ohm per cm. A pair of low-impedance head-telephones  $T$ , enable the observer to obtain a resistance balance on the oscillographic vibrator  $O$ . An extraneous resistance  $R$  connects the end of the slidewire to the junction  $C$ . A zero balance is first obtained at the resonant frequency after this has been ascertained, and then at any frequency well removed from resonance, or at the same frequency with the vibrator withdrawn from its electromagnetic field. The change in the setting of the slider thus produced, enables the observer to evaluate the resonant motional resistance  $R_0'$  by well-known arithmetic procedure.

If the vibrator has sharp resonance, care must be taken to make the measurement precisely at  $f_0$ . Measurements very near to this frequency above and below should be made to check.

Table XX, on page 261, contains the results of a number of tests on different vibrators to determine their correction constants  $\omega_0$  and  $B_0$ , using the oscillographmeter.

**Analysis and Correction of Oscillograms.**—If a steady-state alternating-current oscillogram be analyzed into its Fourier components, by any of the methods employed for that purpose, then, assuming, as is usual, that only odd harmonics are present, we obtain from the analysis the ordinary series of uncorrected terms:

$$(272) \quad A_1 \sin \omega t + A_3 \sin 3 \omega t + A_5 \sin 5 \omega t + \dots \\ + B_1 \cos \omega t + B_3 \cos 3 \omega t + B_5 \cos 5 \omega t + \dots \quad \text{inst. amp.}$$

This pair of series may be combined, as is well known, into a single series:

$$(273) \quad A_1' \sin (\omega t + \alpha_1^\circ) + A_3' \sin (3 \omega t + \alpha_3^\circ) \\ + A_5' \sin (5 \omega t + \alpha_5^\circ) + \dots \quad \text{inst. amp.}$$

where

$$(274) \quad \tan \alpha_k^\circ = \frac{B_k}{A_k}$$

and

$$(275) \quad A_k' = \sqrt{A_k^2 + B_k^2} \quad \text{amp.}$$

If now the oscillographic vibrator with which the record was made had a resonant angular velocity  $\omega_0$ , then the angular velocities  $\omega$ ,  $3 \omega$ ,  $5 \omega$ , etc. in (273) may be written as  $u_1 \omega_0$ ,  $u_3 \omega_0 = 3 u_1 \omega_0$ ,  $u_5 \omega_0 = 5 u_1 \omega_0$ , etc., respectively; so that (273) becomes

$$(276) \quad A_1' \sin (u_1 \omega_0 t + \alpha_1^\circ) + A_3' \sin (u_3 \omega_0 t + \alpha_3^\circ) \\ + A_5' \sin (u_5 \omega_0 t + \alpha_5^\circ) + \dots \quad \text{inst. amp.}$$

For the bluntness  $B_0$  of the vibrator, the correction factor  $C$  becomes known by (257) at each and all of the frequency ratios  $u_1$ ,  $u_3$ ,  $u_5$ , etc. These correction factors may be written  $c_1 \angle \beta_1^\circ$ ,  $c_3 \angle \beta_3^\circ$ ,  $c_5 \angle \beta_5^\circ$ , etc., where  $c_k$  is the size of the correction factor and  $\beta_k^\circ$  its slope. Approximate values of  $c_k$  and  $\beta_k^\circ$  can be obtained from an inspection of  $D_k \dots$  in Figs. 115-117. The Fourier series of the oscillogram corrected for inertia in the vibrator will then be

$$(277) \quad c_1 A_1' \sin (\omega t + \alpha_1^\circ + \beta_1^\circ) + c_3 A_3' \sin (3 \omega t + \alpha_3^\circ + \beta_3^\circ) \\ + c_5 A_5' \sin (5 \omega t + \alpha_5^\circ + \beta_5^\circ) + \dots \quad \text{inst. amp.}$$

The correction factors ordinarily differ but little from  $1.0 \angle 0^\circ$  at low frequencies. The numerical value of  $C$  may be either greater or less than unity, depending on the particular values of  $B_0$  and  $u$  employed. The slope always advances the phase of the harmonic to which it is applied.

Thus, supposing an oscillograph having a resonant frequency of  $f_0 = 3000 \sim$ , and a bluntness  $B_0$  of 0.5 was employed to record a steady emf. wave on an a.-c. circuit of fundamental frequency  $100 \sim$ , and that the Fourier analysis of the wave gave for the ninth-frequency harmonic of  $900 \sim$ , the values  $A_9 = 20$  and  $B_9 = 15$ . Then  $A_9' = 25 \sin (2 \pi \times 900 t + 36^\circ 52')$ . For this frequency  $u_9 = 0.3$ , and by (257 a) or the charts,  $C_9 = 0.9497$ ,  $\beta_9 = 18^\circ 15'$ . The corrected harmonic thus becomes

$0.9497 \times 25 \sin(900 \times 2\pi t + 55^\circ 07') = 23.74 \sin(900 \times 2\pi t + 55^\circ 7')$ . The apparent amplitude has thus to be reduced by 5 per cent, and the apparent phase advanced by  $18^\circ 15'$ .

In Appendix XIII a pair of schedules for harmonic analysis are offered for the analysis of rectangular-coordinate oscillograms. One relates to the ordinary alternating-current case, with odd harmonics only, up to the eleventh frequency inclusive. For schedules evaluating more numerous harmonics, the reader may be referred to special papers on the subject.\*

It may be noted that a vector correction-factor chart of  $C$ , corresponding to the vector deviation-factor charts of  $D$  in Figs. 114, 115 and 116, would contain a family of coaxial parabolas like Fig. 111. It was considered, however, that the deviation-factor charts of Figs. 114 and 116 would be of greater interest and value, as showing the deflection behavior of an oscillograph with a known bluntness  $B_0$ , than correction-factor charts.

As an example of the application of formulas (268) to (271) for evaluating the intrinsic constants of an oscillograph, from measurements of  $\omega_0$ ,  $\Delta$ ,  $\theta'_{m_0}$  and  $R'_0$ , we may take the case of vibrator  $V_1$ , Table XIX, page 260. Here,  $\omega_0 = 14,320$ ,  $\Delta = 2920$ ,  $\theta'_{m_0} = 9.15$  and  $R'_0 = 0.032 \times 10^9$ . Then by (268),

$$A = \frac{0.032 \times 10^9}{9.15 \times 14320} = 244.4$$

From (269) we have

$$r = \frac{244.4^2}{0.032 \times 10^9} = 1.865 \times 10^{-3}.$$

Next, from (270), we obtain

$$m = \frac{1.865 \times 10^{-3}}{2 \times 2920} = 3.194 \times 10^{-7},$$

and finally, from (271), we find

$$s = 3.194 \times 10^{-7} \times 14320^2 = 65.5$$

These values are stated in the Table. Their slopes are all zero.

\* Bibliography 88, which contains an extensive list of papers on harmonic analysis.

## CHAPTER XXII

### VIBRATION GALVANOMETERS

A vibration galvanometer is an alternating-current measuring instrument in which a vibrating system is adapted to give a large sustained oscillatory displacement, when tuned to the frequency of the current to be measured. In order to magnify the

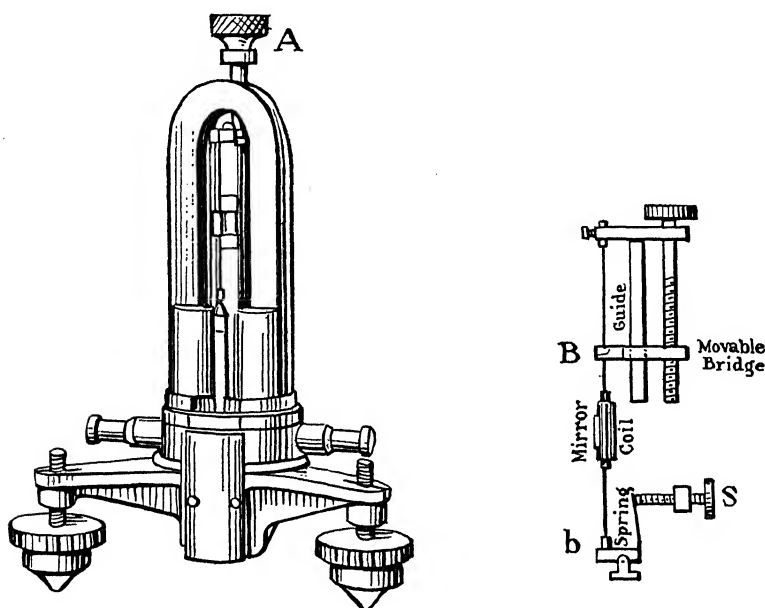


FIG. 131. Unifilar vibration galvanometer, Leeds and Northrup Co.

specific oscillatory displacement, in mirror radians per abampere, the mechanical resistance moment  $r$  is reduced as far as practicable, which means that the instrument is sharply resonant. A relatively small change in impressed frequency is therefore likely to reduce very appreciably the specific deflection of a sensitive vibrating galvanometer.



Vibration galvanometers are of several types. The three following are prominent, depending on the nature of the vibration system:

- (1) Unifilar vibration galvanometers,
- (2) Bifilar vibration galvanometers,
- (3) Reed vibration galvanometers.

(1) Unifilar vibration instruments, originally developed by Blondel, employ a single-wire vibrating system. In some, as in the Drysdale-Tinsley galvanometer of Fig. 132, this wire carries no current, and merely supports a small crossbar permanent-magnetic needle and a little reflecting mirror.

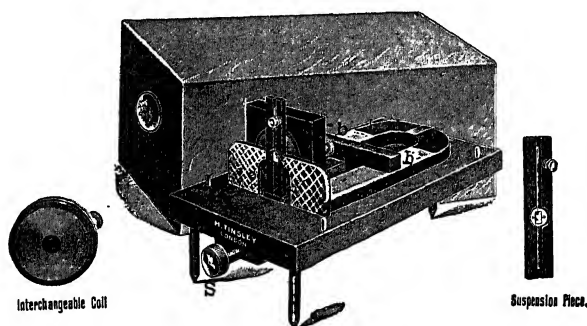


FIG. 132. Tinsley unifilar vibration galvanometer, with adjustable magnetic field.

The tuning of the vibrator to the test frequency may be effected by adjusting the intensity of the magnetic field in which the needle swings. In others, such as that shown in Fig. 131, the wire carries the current into a special narrow coil of the D'Arsonval type.

(2) Bifilar instruments as developed by Duddell, and which are of the same nature as the oscillograph of Figs. 102, 103, and 104, except that they have no damping liquid, the length of their vibrating segments is made adjustable for tuning, and the tension on the strips is also made adjustable. These instruments can be made serviceable for frequencies from 25 ~ to 1000 ~.

(3) Reed instruments as developed at the Bureau of Standards,\* of the type shown in Fig. 133. A thin steel wire or reed, which carries no current, is supported in a permanent magnetic field, in such a manner that a little a.-c. electromagnet sets it in resonant

\* Agnew, Bibliography 85.

vibration. The reed, being polished, serves as its own mirror, and a very small amplitude of vibratory motion can be detected with the aid of a microscope. Different sizes of reed can be used for different frequencies, the tuning of each being effected, over a certain range, by adjusting the intensity of the magnetic field.

**Principle of Operation of Vibration Galvanometers.** — As is shown in Appendix III, if a vibrating system having one degree of freedom, contains energy that is free to exchange between the elastic or potential, and the kinetic forms, and obeys the three postulates contained in the fundamental differential equation (363), then a simple harmonic steadily impressed vmt. will set up simple harmonic vibrations in the system,

according to equations (364) and (365), and as already considered in relation to oscillographs. Under these conditions, the working theory of the vibration galvanometer becomes the same as the working theory of the oscillograph. There is, however, the important difference in detail, that whereas oscillographs are ordinarily operated at frequencies that are kept remote from resonance, vibration galvanometers are ordinarily operated at frequencies as close as possible to the resonant frequency, by tuning the vibrator to resonance. Moreover, the resonant sharpness of an oscillograph galvanometer is usually near unity; whereas that of a vibration galvanometer may even reach 1000. A vibration galvanometer is therefore a type of oscillograph galvanometer which has small damping, and which can be tuned to resonance over a suitable range of frequency.

**Working Constants of a Vibration Galvanometer.** — The principal working constants of a vibration galvanometer may be determined from (1) the measured d.-c. resistance of the instrument under working conditions, (2) the curve of observed deflec-

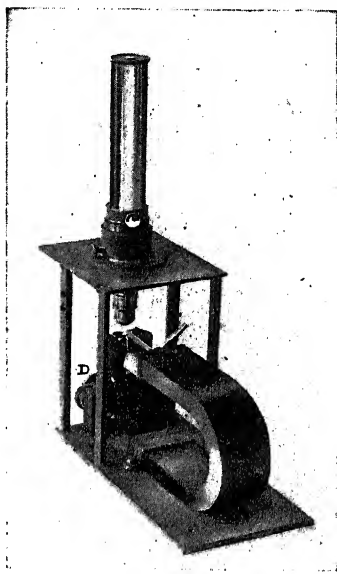


FIG. 133. Agnew reed vibration galvanometer.

tion amplitudes under constant alternating testing current at varied frequency near resonance, and (3) the curve of observed deflection amplitudes under constant alternating impressed terminal voltage at varied frequency, near resonance.

In accordance with the terminology and symbols employed in preceding chapters, these constants may be stated as follow:

(1) The d.-c. resistance  $R_1$ , under working conditions of adjustment and temperature. In practical use, it is expressed in ohms, but in theoretical discussion, the abohm is sometimes a preferred unit.

(2) The *specific deflection* or *current sensitivity*  $\theta' = \theta/I$  at resonant frequency. In practical use, this is commonly expressed in millimeters of scale double amplitude, at 1 meter range, per rms. microampere of testing current. In theoretical discussion, the mirror-radian per rms. ab-ampere has advantage. The unit 1 mm. double amplitude at 1 meter is a deflection of  $1/4000$  mirror radian maximum cyclic displacement.

(3) The *emf. sensitivity*, or deflection per micro-volt, at resonant frequency. In practical use, this is commonly expressed in mm. of scale double amplitude at 1 meter range, per terminal rms. microvolt.

(4) The *resonant range*. This is frequently defined, in practical use, as the percentage change in resonant frequency which will reduce the resonant deflection to one half, either (a) for constant rms. current strength; or (b), for constant rms. terminal voltage. In theoretical discussion, we have used the term as the change in frequency ratio  $u_2 - u_1$ , required to pass from one quadrantal frequency to the other. In order clearly to distinguish between these definitions, the former may be described as the *resonant range to half deflection*, and the latter as the *quadrantal resonant range*.

(5) The *sensitivity to current, or to emf. of triple resonant frequency*, with the instrument tuned to the fundamental frequency, is often a useful criterion; since it is practically advantageous, in most cases, to have a large sensitivity at the resonant frequency, associated with a small sensitivity at the triple-frequency harmonic. This property of a large response to a feeble resonant-frequency current, together with a relatively very small response to currents of other frequencies, is a great advantage in a vibration galvanometer.

**Fundamental Constants of a Vibration Galvanometer.** — In addition to the working constants, which are useful in the ordinary use of a vibration galvanometer, there are the same intrinsic constants that pertain to an oscillograph galvanometer; namely

**A, m, r and s;** besides  $\omega_0$ ,  $\Delta$ , and their ratio  $\Lambda_0$ . There is also the motional resistance  $R_0'$  at resonant frequency. These quantities have already been defined in Chapters XVII and XVIII.

**Vibrational Frequencies.** — In the oscillograph vibrator, under the amount of damping commonly found to be advantageous, there are often, as we have seen, very appreciable differences between the resonant frequency  $f_0$ , the free vibrational frequency  $f_f$ , and the maximum admittant frequency  $f_a$ . It is to this latter frequency that a vibration galvanometer is theoretically tuned; because the maximum deflection is thereat obtainable. In the ordinary vibration galvanometer, however, the damping is designedly reduced to a point at which these three frequencies are practically rendered identical. Thus referring to Table XVII and formulas (243) to (245), if the sharpness  $\Lambda_0$  is say not less than 100, and the bluntness  $B_0$ , therefore not more than 0.01, the maximum admittant frequency will very nearly be  $(1 - 0.0001)$ , or only 1 per myriad less than the resonant frequency; so that in all such cases, we may safely ignore the difference between the maximum admittant frequency of tuning  $f_a$  and the resonant frequency  $f_0$ . Moreover, even the quadrantal frequencies usually lie very close to the resonant frequency. With a bluntness of 0.01, they would be very nearly 1 per cent above and below the resonant frequency. The principal difficulty in testing the behavior of sharply resonant vibration galvanometers is to hold the impressed frequency sufficiently nearly steady for constant-frequency tests, or to adjust it through sufficiently small gradations, for variable-frequency tests. A very small accidental variation in frequency may interfere seriously with the deflectional behavior of the instrument.

**Methods of Tuning to the Impressed Frequency.** — Since  $\omega_0 = \sqrt{s/m}$ , it is evident that the resonant frequency of a vibrator can only be tuned by altering either **s** or **m**. In general, it is the resilient moment **s** which is adjusted, leaving the moment of inertia **m** substantially constant.

In unifilar instruments with constant magnetic field, as of the Leeds and Northrup type, Fig. 131, the resilient moment **s** may be varied by raising and lowering the movable bridge *B*, and thus altering the total length of the suspension *Bb*. Lowering the bridge, with the aid of screw *A*, increases **s** and  $\omega_0$ . The screw *S* also supplies a fine adjustment, by altering the tension on the

suspension. Increase of tension tends to increase  $s$ , but it may also, in some cases, diminish  $m$  slightly.

In unifilar instruments with adjustable magnetic field and suspended magnet, as of the Drysdale-Tinsley type, Fig. 132, the resilient moment  $s$  is derived partly from the mechanical torsion of the suspending wire, in this case of constant length, and partly from the magnetic restoring torque on the suspended needle. In this case, the magnetic field is adjustable, varied by altering the position of the steel bar  $bb$ , with the aid of the screw  $S$ . The bar  $bb$  acts as a magnetic shunt to the air-gap in which the needle swings, so that bringing the bar forward weakens the magnetic control on the needle and lowers  $\omega_0$ .

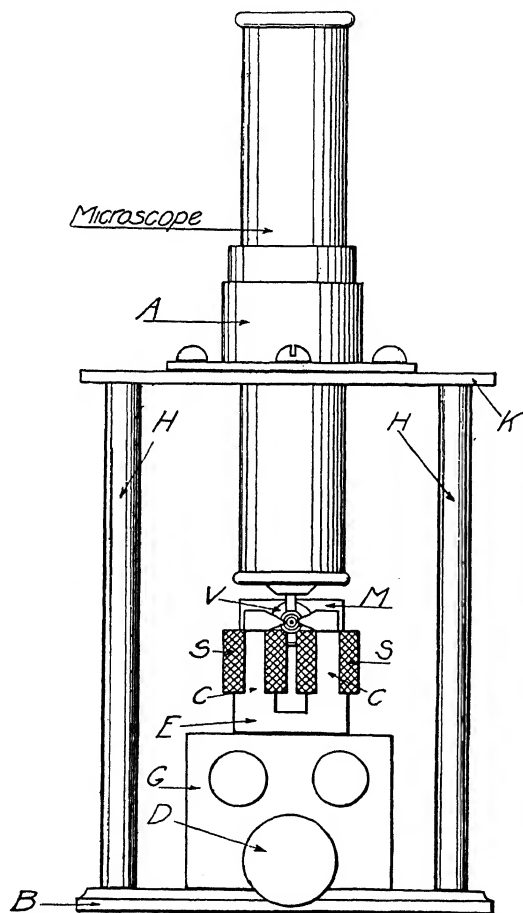


FIG. 134. Vertical section of reed vibration galvanometer through electromagnet.

*E* laminæ. *H* pillars.  
*S* winding. *D* adjusting screw.  
*B* base. *G* terminals.

in construction to the instrument shown in Fig. 102, but with air damping, the length of the bifilar suspension is altered by a bridge

above and another below the poles, under the control of a single screw; while the tension on the bifilar suspension is altered by a screw and spring, for fine adjustment.

In reed instruments of the Agnew type, Figs. 133 and 134, the steel vibrating reed is permanently magnetized. The resilient moment  $s$  is supplied not only by the elasticity of the reed; but also by the magnetic field in which it vibrates. The magnetic component can be adjusted, over a certain range, by altering the geometric relations between poles and reed under control of the screw  $D$ , Figs. 133, 134.

A difficulty which presents itself in the practical adjustment and manipulation of vibration galvanometers is keeping the vibrators in resonance. If the impressed frequency of the testing current were absolutely fixed, a single tuning of the instrument to resonance at that frequency would suffice theoretically for the duration of an ordinary series of tests. In sharply tuned instruments, however, a change of 1 per mil in the impressed frequency may cut down the specific deflection nearly one half. In other words, the current sensitiveness depends so much upon the maintenance of resonance, that small changes occurring in the impressed frequency call for immediate corresponding changes in the adjustment of  $s$ , to ascertain that the vibratory deflection produced is a maximum.

Such frequent changes of mechanical adjustment are time-consuming and inconvenient. A useful device for adjusting  $s$  electromagnetically has been worked out at the Bureau of Standards, and is indicated in Figs. 135 and 136. The tension on the suspension is partly gravitational (10 to 15 gm. weight), and partly electromagnetic (up to 50 or even to 100 gm. weight). By adjusting the continuous-current strength

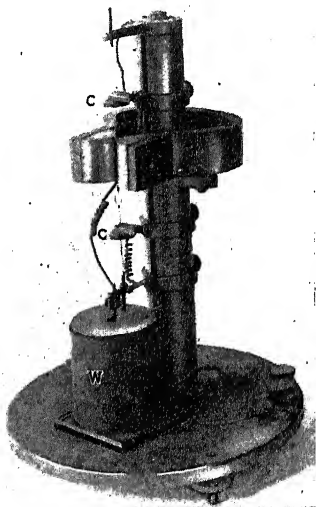


FIG. 135. Unifilar vibration galvanometer with electromagnetic adjustment of tension.

in the solenoid *W*, with the aid of a rheostat under the observer's hand, the resonant frequency of the vibrating system can be altered over a suitable range (2 or 3 cycles per second in a 60 ~ instrument) very speedily, and without agitating the mirror; so that the maximum deflection can be found at any moment with very little delay. Coarse adjustment of the frequency can be made by varying the distance between the clamps *CC*, which

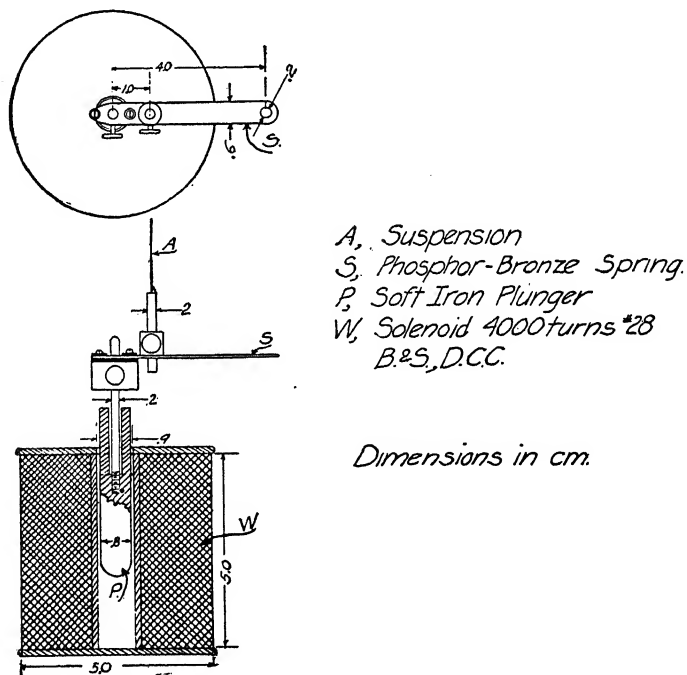


FIG. 136. Details of Silsbee electromagnetic tension adjustment.

press against the suspension strips above and below the coil. When wound for a low resistance (about one ohm), such an instrument has a voltage sensitivity of 0.2 mm. double amplitude at 1 meter, per microvolt at terminals, and at 60 ~. A change of 1 per cent in frequency decreases this to about one half.

**Elimination of Mechanical Vibratory Disturbance.** — When a vibration galvanometer has been tuned to resonance with a standard impressed frequency, such as 60 ~, it is rendered peculiarly sensitive to mechanical vibratory disturbances of that

frequency, or even of some integral submultiple of the same. Thus, if the alternator supplying this frequency is in the same building as the galvanometer, the engine driving the alternator is likely to produce a tremor in the floors and walls, of a frequency to which the vibrator will respond. In some instances, it is found impossible to use a vibration galvanometer on a wall of the building containing the generator, or a synchronous motor, owing to the vibratory disturbance of the mirror in the absence of any current through the instrument. In particular cases, a satisfactory degree of quiescence in the suspension can be obtained by supporting the instrument on a thick layer of felt, or other nonconductor of vibration. In other cases, more elaborate precautions are necessary.

Figure 137 shows an arrangement found serviceable at the Bureau of Standards. A massive block *B* is supported on a simple wooden platform, which is carried at corners by four stout spiral springs, fastened to a frame of metallic piping. The vibration galvanometer or galvanometers rest on a board *bbb*, which is separated from the block *B* by a thick layer of felt. If any accident should happen to the suspending springs, the wooden platform will descend to rest on supports

*pp*. The mass *m*, and resilient coefficient *s*, of the suspended block and instruments, are such that the resonant frequency of the system is far below the testing frequency to which the galvanometers are tuned. Consequently, the amplitude of vibration produced in block *B* by building tremors of testing frequency, or of its congeners, is very small. This is a great convenience in the practical use of such instruments.

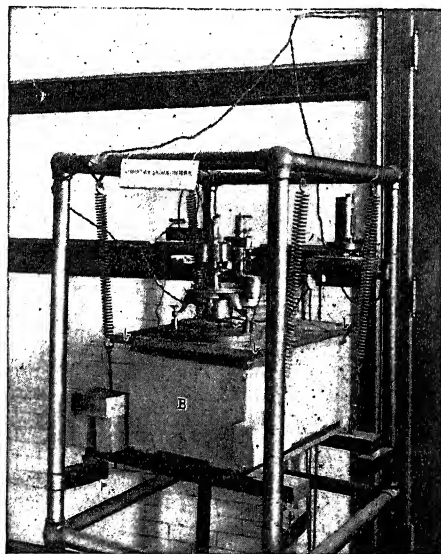


FIG. 137. Anti-shake suspension system for vibration galvanometers.



**Motional Impedance and Velocity Circles of a Vibration Galvanometer.** — Just as in the case of oscillographs, already discussed in Chapter XXI, every vibration galvanometer has a circular graph of angular velocity, and of motional impedance, when subjected, without change of mechanical adjustment, to varied impressed frequency. Figure 138 shows the motional-impedance circle  $OBRA$ , found by Dr. Taylor for a Duddell bifilar vibration galvanometer, which was left tuned to  $1000 \sim$ . It will be seen that the resistance of the instrument, which had

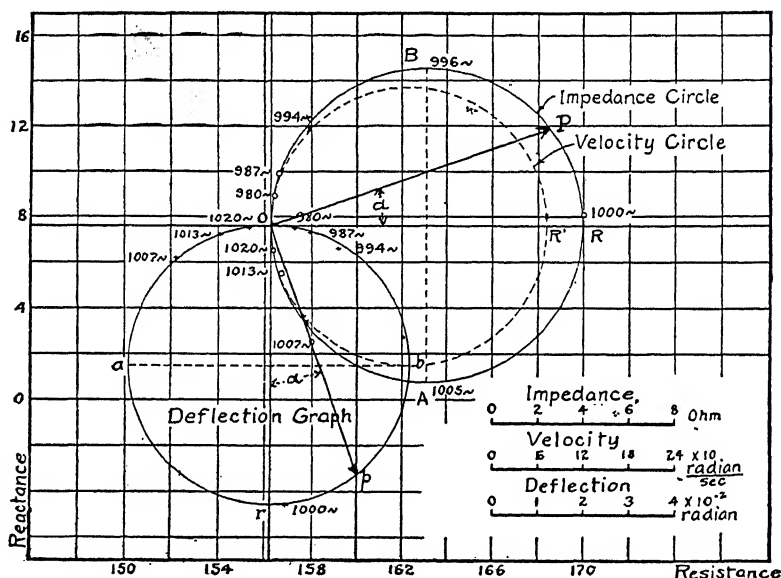


FIG. 138. Motional-impedance, velocity, and deflectional circles for Duddell vibration galvanometer.

two fine wires but no coil, was 156.2 ohms at rest. At  $1000.5 \sim$  its resistance was a maximum, at 170 ohms; so that its motional impedance at resonance was  $R_0' = 13.8$  ohms or  $13.8 \times 10^9$  abohms. At the lower quadrantal frequency  $f_1 = 996 \sim$ , the impedance of the instrument was  $163.1 + j 6.9$  ohms, and at the upper quadrantal frequency  $f_2 = 1005 \sim$ , it was  $163.1 - j 6.9$  ohms. The quadrantal range of resonance was thus  $9 \sim$ . Outside the frequency limits  $980 \sim - 1020 \sim$  the vibratory response was very small. The impedance measurements indicated in the figure were obtained with a Rayleigh bridge.

With the motional-impedance circle, there is associated a circle  $ObR'$  of vibratory angular velocity  $\dot{\theta}$ , indicated in dotted line. The motional-impedance circle may itself be interpreted as a circle of angular velocity, to a suitable scale. Thus, at resonance, the maximum cyclic angular velocity of the mirror was 384 radians per second, in phase with the alternating current and vmf. This velocity would be developed at the instant when the mirror was passing, in either direction, through its central and zero position. The vector velocity at other frequencies might be read off the circle, by the lengths and slopes of chords, from the origin  $O$ . The characteristics of the vibration galvanometer referred to in Fig. 138 for the frequency of  $1000 \sim$  are detailed in Table XXI.

TABLE XXI

PARTICULARS CONCERNING DUDELL HIGH-FREQUENCY VIBRATION GALVANOMETER TUNED TO BE RESONANT TO  $1000.5 \sim$

Resistance at rest  $R_1$  156.2 ohms at  $20^\circ \text{ C.} = 156.2 \times 10^9 \text{ abohms.}$   
 Motional resonant res. at  $1000.5 \sim R_0' = 13.8 \text{ ohms} = 13.8 \times 10^9 \text{ abohms.}$   
 Max. cyclic resonant deflection 0.0611 mirror radians  $\pm$  at  $5.5 \times 10^{-5} \text{ abamperes rms.} = 7.778 \times 10^{-5} \text{ max. cy. abamperes.}$   
 Specific resonant deflection  $\theta' = 1.111 \times 10^3 \text{ mirror radians/abampere rms.}$   
 Current sensitivity 0.444 mm. at 1 m., for  $1 \mu \text{ amp.,}$  at  $1000.5 \sim$ .  
 $\omega_d = 6286.2, \omega_f = 6286.27, \omega_0 = 6286.33 \text{ rad./sec.}$   
 $f_d = 1000.48 \sim, f_f = 1000.49 \sim, f_0 = 1000.5 \sim$ .  
 Quadrantal frequencies  $f_1 = 996.0 \sim, f_2 = 1005.0 \sim$ .  
 Range of resonance  $9 \sim$ , or 0.009 in  $u$ .  $\theta'_{mo} = 785.6 \text{ m. rad./max. cy. abamp.}$   
 $\Delta = 9.0 \times \pi = 28.27 \text{ hypos./sec.}$   $\tau_0 = 1/\Delta = 0.0354 \text{ sec.}$   
 $\Lambda_0 = \frac{\omega_0}{\Delta} = 222.3$   $B_0 = \frac{\Delta}{\omega_0} = 0.0045 = \text{oscillatory bluntness of resonance.}$   
 $A = 2795 \text{ dyne-p.-cm./abampere} = \text{torque factor.}$   
 $m = 1.0008 \times 10^{-5} \text{ gm.-cm.}^2 \text{ or dyne-p.-cm./radian per sec.}^2 = \text{moment of inertia.}$   
 $r = 5.659 \times 10^{-4} \text{ dyne-p.-cm./rad. per sec.} = \text{moment of resistance.}$   
 $s = 395.5 \text{ dyne-p.-cm./radian} = \text{moment of elastance.}$   
 Max. cy. torque at  $5.5 \times 10^{-5} \text{ rms. abamp.}$  0.2174 dynes-p.-cm.  
 Max. cy. ang. velocity at  $5.5 \times 10^{-5} \text{ rms. abamp.} = \dot{\theta} = 384.1 \text{ rad./sec.}$

**Vibratory Displacement or Deflection Graph.** — We have already seen that the deflection graph of an oscillographic galvanometer, when liquid-damped, is a curve like  $apbc$ , Fig. 113, differing materially from a circle. When, however, the damping is very small, as in the case of a vibration galvanometer operated in air, the curves of Fig. 117 show that the deflection graph closely approximates to a circle. The deflection graph, in the case represented by Fig. 138, is seen to be very nearly a circle  $obra$ . At the resonant frequency of  $1000.5 \sim$ , the deflection is  $Or = 0.0611$

mirror radians, on each side of zero, or 0.1222 optical-beam radians on each side of zero, or 0.2444 optical-beam radians of double amplitude, with a current of  $5.5 \times 10^{-5}$  abampere, or 550 microamperes. The maximum specific deflection was therefore

$$\frac{0.0611}{5.5 \times 10^{-5}} = 1.11 \times 10^3 \text{ mirror radians per rms. abampere,}$$

corresponding to a current sensitivity of  $0.444 \times 10^{-3}$  beam radians of double amplitude, per rms. microampere, or 0.444 scale mm. at 1 m. The phase of this maximum deflection is seen to be  $90^\circ$  behind the phase of the alternating current, or impressed vmt. We may thus take the motional-impedance circle  $OARB$  of any ordinary vibration galvanometer, and by rotating it about  $O$  clockwise through  $90^\circ$ , into a position like that of  $Oab$ , interpret it to be a correspondingly altered scale of deflection, either in mirror radians per rms. absampere, or scale double amplitude in mm. at 1 meter, per rms. microampere. At and below  $980 \sim$ , the deflections in Fig. 138 are nearly in phase with the vmt.; while at and above  $1020 \sim$ , they are nearly in opposition to it.

**Influence of Frequency on Maximum Deflection.**—If a vibration galvanometer can be tuned over a wide range of frequency, its current sensitivity, or specific deflection at resonance, is lower as the testing-current frequency is increased. The maximum cyclic angular velocity  $\dot{\theta}_m$ , produced by a maximum cyclic current strength  $I_m$  abamperes will be, by (204),

$$(278) \quad \dot{\theta}_m = \frac{F_m}{z} = \frac{AI_m}{z} \quad \frac{\text{mirror radians}}{\text{sec.}} \angle$$

which at resonance becomes

$$(279) \quad \dot{\theta}_{m_0} = \frac{AI_m}{r} \quad \frac{\text{mirror radians}}{\text{sec.}} \angle.$$

The maximum cyclic deflection produced at resonance will also be by (227) and (231)

$$(280) \quad \theta_{m_0} = \frac{AI_m}{j\omega_0 r} \quad \text{mirror radians } \angle.$$

Consequently, if the torque factor  $A$  remains constant as the frequency is increased, and if the mechanical resistance moment  $r$  also remains independent of the frequency; then, as the frequency is increased, and the vibrator is retuned to maintain resonance, the mirror radians of resonant deflection produced by

a fixed current strength will be inversely as the impressed frequency. Under these conditions, if an instrument had a current sensibility of say 60 mm. per meter and per microampere at 60  $\sim$ , it might be expected to have about 20 mm. per meter and per microampere when retuned to the triple-frequency harmonic of 180  $\sim$ .

If, however, the instrument is kept tuned to the fundamental frequency, its deflectional response to any other frequency, such as the triple harmonic, can be computed readily if its oscillatory sharpness  $\Lambda_0$  is known. Let  $u$  be the frequency ratio of the harmonic to the resonant frequency. In the case of an instrument tuned to resonance with a fundamental frequency, the successive harmonics will have  $u = 3, 5, 7$ , etc. Then, by (234), the size of the displacement admittance of the vibrator at resonance is

$$(281) \quad |y'_0| = \frac{1}{r\omega_0} \frac{\text{mirror radians}}{\text{vmt.}}$$

Again, the size of the displacement admittance of the vibrator in the same mechanical adjustment to the  $u$ th harmonic of angular velocity  $u\omega_0$ , will be

$$(282) \quad |y'_u| = - \frac{\sin \beta}{ru\omega_0} \frac{\text{mirror radians}}{\text{vmt.}}$$

The ratio of displacement admittance at the  $u$ th harmonic to that at the fundamental ( $u = 1$ ), to which the vibrator is tuned, may be called the displacement ratio for the  $u$ th harmonic, and will be:

$$(283) \quad \left| \frac{y'_u}{y'_0} \right| = - \frac{\sin \beta}{u}$$

The lag angle  $\beta$  will always be nearly  $180^\circ$ , and  $\sin \beta$  will therefore be very nearly equal to  $-\tan \beta$ ; so that by (238)

$$(284) \quad -\sin \beta = \frac{2 B_0 u}{u^2 - 1} = \frac{B_s u}{u^2 - 1}.$$

Hence

$$(285) \quad \left| \frac{y'_u}{y'_0} \right| = \frac{2 B_0}{u^2 - 1} = \frac{2}{\Lambda_0 (u^2 - 1)} = \frac{1}{\Lambda_s (u^2 - 1)}.$$

Thus the displacement ratio for the 3d harmonic will be  $2 B_0/8 = B_0/4$ , and for the 5th harmonic  $2 B_0/24 = B_0/12$ . The ratios for the harmonics of the 3d, 5th, 7th, 9th, etc., frequency will thus be  $B_0/4$  divided by 1, 3, 6 or the series  $(1 + 2 + 3 + 4 + \dots)$  of the integral numbers. We may always expect the 5th-frequency

harmonic to have one-third the displacement admittance of the 3d frequency harmonic, and the 7th-frequency harmonic one-sixth, and so on.

Conversely, if the specific deflection, or the current sensibility, is measured first with the instrument tuned to a fundamental frequency, and then, without altering this tuning, with a  $u$ th harmonic frequency, the ratio of these specific deflections can be used to evaluate  $B_0$  or  $\Lambda_0$ . Thus, if this ratio for a triple harmonic frequency is found to be say 0.0020, then, by (285), the oscillatory bluntness is four times this ratio; or  $B_0 = 0.0080$  and  $\Lambda_0 = 125$ .

**Electromotive Force Generated in a Vibration Galvanometer.** — The motion of the vibrator in its magnetic field sets up an emf.  $e_m$  abvolts  $\angle$ , which acts in opposition to the emf. impressed at its terminals, or is a cemf., such as would be generated by the motion of a synchronous reciprating motor. Its value is

$$(286) \quad e_m = \mathbf{A} \dot{\theta}_m = \frac{\mathbf{A} \mathbf{F}_m}{\mathbf{z}} = \frac{\mathbf{A}^2 I_m}{\mathbf{z}} = I_m Z' \quad \text{max. cy. abvolts } \angle.$$

That is, the cemf.  $e_m$  is the vector drop of potential in the motional impedance  $Z'$  of the instrument. At resonance, this becomes

$$(287) \quad e_{m_0} = \mathbf{A} \dot{\theta}_{m_0} = \frac{\mathbf{A} \mathbf{F}_m}{\mathbf{r}} = \frac{\mathbf{A}^2 I_m}{\mathbf{r}} = I_m R'_0 \quad \text{max. cy. abvolts,}$$

and is then in direct phase opposition to the current in its coil.

**Power Absorbed by Vibrator at Constant Current.** — The vector power  $P'_m$  abwatts absorbed from the a.-c. circuit and expended mechanically by the vibrator is

$$(288) \quad P'_m = I^2 Z' = \dot{\theta}^2 \mathbf{z} \quad \text{abwatts } \angle,$$

where  $I$  is the current in rms. abamperes. The real component is active, or dissipated power, and the imaginary component reactive power, cyclically stored and released. When the vibrator is tuned to resonance with the alternating current,  $\mathbf{z}$  becomes  $\mathbf{r}$ , and  $Z'$  becomes  $R'_0$ ; so that

$$(289) \quad P'_{m_0} = I^2 R'_0 = \dot{\theta}_0^2 \mathbf{r} = \frac{\dot{\theta}_0^2 m_0}{2} \mathbf{r} \quad \text{abwatts,}$$

all of which is active. In the case represented in Fig. 138,  $P'_{m_0}$   
 $= (5.5 \times 10^{-5})^2 \times 13.8 \times 10^9 = \frac{(384.1)^2}{2} \times 5.659 \times 10^{-4}$   
 $= 41.75 \text{ abwatts.}$

**Power Absorbed by Vibrator at Constant Impressed Terminal Voltage.** — If a vibration galvanometer is connected across a constant impressed alternating emf., of  $E$  rms. vector abvolts; then if  $R_1$  is the resistance of the galvanometer with the vibrator at rest, the vector current through the instrument will be

$$(290) \quad I = \frac{E}{R_1 + Z'} = \frac{E - e}{R_1} \quad \text{abamperes } \angle.$$

Here the  $E$  may be taken as of standard phase, or zero slope. The vector mechanical power expended in the vibrator will be  $P = I^2 Z'$  abwatts, with  $I$  taken as at standard phase. At resonance,  $Z' = R_0'$ , and

$$(291) \quad P_{m_0} = I^2 R_0' = \frac{E^2 R_0'}{(R_1 + R_0')^2} \quad \text{abwatts.}$$

This power will be a maximum when the motional resonant resistance  $R_0'$ , assumed as variable, is equal to the resistance  $R_1$  of the instrument with the vibrator at rest. The mechanical power will then be equal to the power expended electrically in heating the coil. There is therefore an advantage in adjusting the torque factor **A** of a constant-voltage vibration galvanometer to the value at which

$$(292) \quad \frac{\mathbf{A}^2}{\mathbf{r}} = R_0' = R_1 \quad \text{abohms.}$$

If the motional resistance  $R_0'$  is less than the coil resistance  $R_1$ , there will be an advantage in raising the torque factor **A** or diminishing the damping moment **r**; whereas, if the motional resistance exceeds the coil resistance, it is desirable to diminish the magnetic field, or to increase the damping. This was pointed out by Dr. Wenner in 1909.\* In most vibration galvanometers, the motional resonant resistance is less than the resistance at rest. It is not ordinarily either easy or convenient to change  $R_0'$  in a working vibrational galvanometer; so that the preference for equality between  $R_0'$  and  $R_1$  in an instrument operated at constant terminal voltage, affects the design rather than the manipulation of such instruments.

**Measurement of the Motional Impedance of a Vibration Galvanometer.** — If the vibration galvanometer is of the high-resistance type (say over 100 ohms at rest), the electric connections of Fig. 30 may be employed. If the instrument is of the low-resistance type

\* Bibliography 33.

(say under 10 ohms at rest), the electric connections of Fig. 130 are preferable. For instruments of intermediate resistance (10 to 100 ohms), either set of connections may be made applicable. In any case, the source of testing alternating currents, to be satisfactory, must be very steady in frequency, and also capable of frequency adjustments over very small measured steps. An oscillator either of the Vreeland, or of the pleiotron type, can be made serviceable in this respect.

The resistance and inductance of the vibration galvanometer can be measured in the Rayleigh bridge,\* of Fig. 30, at successive steps of increased frequency in the neighborhood of that to which its vibrator has been tuned and left set. In the slidewire bridge of Fig. 130, only changes in the resistance component of motional impedance  $Z'$  can be read. In this case, the impressed frequency is adjusted until at  $f_0$ , the maximum resistance in the instrument  $R_1 + R_0'$  is reached.

In high-resistance instruments there is ordinarily no difficulty in determining the quadrantal frequencies  $f_1$  and  $f_2$ , at which the resistance component of  $Z' = R_0'/2$ , and the inductance of the instrument reaches a maximum value in either direction. In low-resistance instruments it may be difficult to determine these quadrantal frequencies with precision.

**Measurement of the Damping Constant  $\Delta$  of a Vibration Galvanometer.** — There are at least three ways of determining the damping constant  $\Delta$ ; namely,

- (1) From a motional-impedance circle.
- (2) From a curve of relative vibrational displacement  $\theta_m$  versus frequency ratio  $u$ , in the neighborhood of resonance.
- (3) From the photographic record of a vibrational decay curve, i.e., displacement amplitude  $\theta_m$  versus time  $t$ .

(1) From a motional-impedance circle, like that in Fig. 138, the quadrantal frequencies  $f_1$  and  $f_2$  can be found, either by experimental determination, using formula (113) or by computation from some particular frequencies at observed points on the circle, using formula (110).

(2) From a curve of relative vibrational displacement, we can obtain  $B_0$ , and then knowing  $\omega_0$ , the resonant angular velocity, we obtain  $\Delta = B_0\omega_0$ , by (208). In this case, we measure the double deflection or optical-band breadth on the scale of the vibration galvanometer at constant testing-current strength, for gradually

\* Bibliography 12, page 449.

varied frequency in the neighborhood of resonance. The curve of displacement  $\theta_m$  versus frequency  $f$ , is asymmetric with respect to the maximum ordinate, unless, as is explained in Appendix XI, the abscissas are taken as  $f^2$ , i.e., as the squares of the impressed frequency. Nevertheless, when the resonant sharpness  $\Lambda_0$  exceeds 100, as in the ordinary vibration galvanometer, the curve  $\theta_m$  versus  $f$  is very nearly symmetric about the maximum ordinate, for some distance on each side. For such vibrators, the displacement graph *Oarb*, Fig. 138, becomes very nearly a circle. The deflection *Op* is then *Or* cos  $\alpha$ , where  $\alpha$  is the angle between *Op* and *Or*, and also equal to the angle between the corresponding vectors *Op* and *OR*, in the impedance circle. As was shown in formula (107),

$$(293) \quad \tan \alpha = \frac{\mathbf{m}\omega - \mathbf{s}/\omega}{\mathbf{r}} = \frac{u - \frac{1}{u}}{2 B_0}.$$

Within the range of resonance, the frequency ratio  $u$  of a sharply resonant vibrator differs but little from unity; so that

$$(294) \quad u = 1 \pm \delta,$$

where  $\delta$  is a small numerical deviation. Formula (293) thus becomes

$$(295) \quad \tan \alpha = \pm \frac{2\delta}{2 B_0} = \pm \frac{\delta}{B_0}.$$

At the quadrantal points *a*, *b*, Fig. 138,  $\alpha = \pm 45^\circ$ , and  $\tan \alpha \pm 1$ , so that  $\delta = B_0$ , or the departure of  $u$  from unity at the quadrantal points is just numerically equal to the oscillatory bluntness  $B_0$ . Moreover, the size of the deflection being proportional to the chord *Op*, Fig. 138, we have for sharply resonant vibrators,

$$(296) \quad |\theta_m| = |\theta_{m0}| \cos \alpha = |\theta_{m0}| \frac{B_0}{\sqrt{B_0^2 + \delta^2}} \quad \text{mirror radians.}$$

or

$$(297) \quad \nu' = \left| \frac{\theta_m}{\theta_{m0}} \right| = \frac{B_0}{\sqrt{B_0^2 + \delta^2}} = \frac{1}{\sqrt{1 + \left( \frac{\delta}{B_0} \right)^2}}.$$

This shows that the deflection ratio at the quadrantal frequencies is 0.707. Figure 139 gives the graph of the deflection ratio  $|\theta_m/\theta_{m0}|$  as ordinates, versus frequency ratio  $u$  as abscissas,\* by (297) for

\* It will be seen from an examination of Appendix XI (Figs. 203–207), that the deflection ratio  $\nu'$  of a sharply resonant vibration galvanometer follows the same rules as the velocity ratio or current ratio  $\nu$ , see (566) to (567d), since the displacement curve becomes very nearly circular, and is a reproduction of the velocity circle with change of scale and  $90^\circ$  of rotation.



the case of  $B_0 = 0.0045$ , corresponding to the instrument referred to in Fig. 138. At  $u_2 = 1.0045$ , and also at  $u_1 = 1 - 0.0045 = 0.9955$ , the deflection has fallen to 70.7 per cent of the maximum resonant value. Any curve of deflections versus frequency, thus enables us to read off its bluntness  $B_0$ , by observing the values of  $u$ , at which the deflection falls to 70.7 per cent of the maximum.

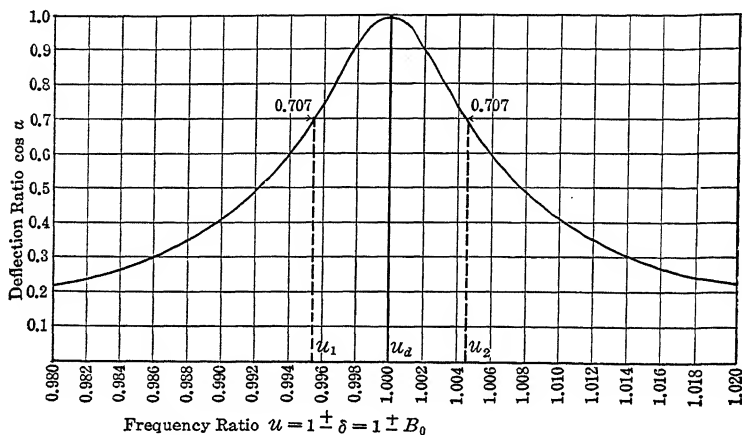


FIG. 139. Curve of deflection ratios ( $\cos \alpha$ ) for various frequency ratios  $u$ , in the case of a vibrator of sharp resonance  $\Lambda_0 = 222$ ,  $B_0 = 0.0045$ .

(3) From a photographic decay curve, like that of Fig. 140, we can approximate to  $\Delta$ , by the use of formulas (260) and (261); in the case of Fig. 140, the frequency of oscillation is  $f_0 = f_f = 60.8 \sim$ , and  $\Delta = 1.07$  hyps./sec., approximately; hence, knowing  $\omega_0 = 385$  rad./sec., we find  $B_0 = 1.07/385 = 0.00277$ , or  $\Lambda_0 = 360$  for the particular low-resistance instrument from which Fig. 140 was secured.

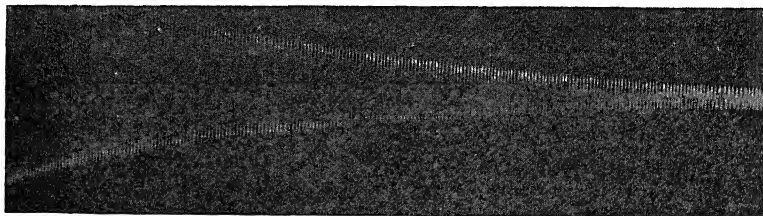


FIG. 140. Photographic record of damped oscillations executed by the vibrator of a vibration galvanometer.  $f_0 = 60.8 \sim$ .

It would be a useful investigation to secure a set of comparative observations for  $\Delta$ , on one or more vibration galvanometers, by all three of the above-mentioned methods, with a view to finding how closely they might agree, and which gives the best results.

An attempt was made\* to ascertain how the constant  $\Delta$  varied, for successive tuned adjustments, to different values of  $\omega_0$ , in the case of the bifilar instrument referred to in Fig. 138. It was found, however, that the results were inconsistent. The inconsistency was traced to slight differences of tension between the two wires forming the bifilar vibrating system. Any such departure from symmetry in the tension of the two wires sets up a tendency to unifilar as well as to bifilar vibrational characteristics. A decay curve, of the type shown in Fig. 140, then reveals irregularities. All bifilar vibrational suspensions that have to be altered in length for tuning, are subject to this source of possible complication.

**Determination of all Four Intrinsic Constants,  $\mathbf{A}$ ,  $\mathbf{m}$ ,  $\mathbf{r}$  and  $\mathbf{s}$ .** — Having ascertained the resonant angular velocity  $\omega_0$ , to which the instrument is tuned, the damping constant  $\Delta$ , the motional resistance  $R_0'$  at resonance and the maximum deflection at resonance  $\theta_{m_0}$ , produced by a measured maximum cyclic current  $I_m$ , the four intrinsic constants are immediately obtainable. From (286), at resonance,

$$(298) \quad \mathbf{A}\dot{\theta}_{m_0} = I_m R_0' \quad \text{abvolts,}$$

$I_m$  being taken in abamperes,  $R_0'$  in abohms, and  $\dot{\theta}_{m_0}$  in mirror radians per sec.

Hence, by (268),

$$(299) \quad \mathbf{A} = \frac{I_m R_0'}{\dot{\theta}_{m_0}} = \frac{I_m R_0'}{\omega_0 \theta_{m_0}} = \frac{R_0'}{\omega_0 \theta'_{m_0}} \quad \frac{\text{dyne-p.-cm.}}{\text{abampere}},$$

where  $\theta_{m_0}$  is the maximum cyclic angular deflection, in mirror radians on either side of the zero and  $\theta'_{m_0}$ , a scalar, is  $\theta_{m_0}/I_m$ . In the telephone receiver,  $\mathbf{A}$  is a complex quantity, owing to the magnetic properties of the steel vibrating diaphragm. In the ordinary vibration galvanometer, as also in the ordinary oscillograph, where such magnetic lag phenomena are absent from the vibrator, the constant  $\mathbf{A}$  is a real quality, or has no slope.

From (287) at resonance,

$$(300) \quad \theta_{m_0} = \frac{\mathbf{A} I_m}{\omega_0 \mathbf{r}} \quad \text{max. cy. mirror radians.}$$

\* Bibliography 60.

and, following (140) and (269),

$$(301) \quad \mathbf{r} = \frac{\mathbf{A}I_m}{\omega_0\theta_{m_0}} = \frac{\mathbf{A}}{\theta'_{m_0}\omega_0} = \frac{I_m^2 R_0'}{\omega_0^2 \theta'^2_{m_0}} = \frac{R_0'}{\omega_0^2 \theta'^2_{m_0}} \quad \frac{\text{dyne-p.-cm.}}{\text{rad. per sec.}}$$

again by (134),

$$(302) \quad \mathbf{m} = \frac{\mathbf{r}}{2\Delta} = \frac{I_m^2 R_0'}{2\Delta\omega_0^2 \theta'^2_{m_0}} = \frac{R_0'}{2\Delta\omega_0^2 \theta'^2_{m_0}} \quad \text{gm.-cm.}^2,$$

and finally by (32),

$$(303) \quad \mathbf{s} = \mathbf{m}\omega_0^2 = \frac{I_m^2 R_0'}{2\Delta\theta'^2_{m_0}} = \frac{R_0'}{2\Delta\theta'^2_{m_0}} \quad \frac{\text{dyne-p.-cm.}}{\text{radian}}.$$

This set of equations for evaluating the intrinsic constants was presented\* in 1916. Another set of equations for obtaining the same intrinsic constants in terms of the resistance at rest, and the observed instrument sensibilities, was given by Dr. Wenner† in 1910.

**EMF. Sensitivity of a Vibration Galvanometer.**—If the resistance of a vibration galvanometer remained equal to its direct-current or quiescent value  $R_1$  abohms at all frequencies, then the emf. sensitivity of the instrument, or maximum cyclic deflection per abvolt of impressed terminal emf., would be exactly  $R_1$  times less than its current sensitivity  $\theta$ , in mirror radians per abampere. Moreover, the curve of maximum cyclic deflection versus frequency, near resonance, at constant terminal voltage, would be the same as that at constant a.-c. strength, like the curve in Fig. 139. Actually, however, we have already noted that the impedance of a vibration galvanometer, at any given frequency and under a definitely fixed tuning adjustment of its vibrator, is

$$(304) \quad Z'' = R_1 + Z' \quad \text{abohms } \angle,$$

as in Fig. 128 *b*, where  $Z'$  is the motional impedance. The maximum cyclic deflection  $\theta_m$ , in mirror radians produced by an impressed terminal emf. of  $E$  rms. abvolts, will be

$$(305) \quad \theta_m = I\theta' = \frac{E\theta'}{R_1 + Z'} \quad \text{max. cy. mirror radians } \angle,$$

where  $\theta'$  is the specific deflection in mirror radians per rms. abampere.

Thus

$$(306) \quad \frac{\theta_m}{E} = \frac{\theta'}{R_1 + Z'} = \frac{\theta'}{Z''} \quad \frac{\text{max. cy. mirror radians}}{\text{rms. abvolts}} \angle.$$

\* Bibliography 58.

† Bibliography 33.

At precise resonance, when  $Z' = R_0'$ , the resonant motional resistance, and

$$(307) \quad \frac{\theta_m}{E} = \frac{\theta'}{R_1 + R_0'} \quad \frac{\text{max. cy. mirror radians.}}{\text{rms. abvolts}}$$

At frequencies slightly above or below resonance, the reduction in the size of  $Z''$  tends to increase the current through the instrument, and to compensate for the reduction in the specific deflection with change of frequency. Consequently, the curve of specific deflection versus frequency, under constant terminal emf., is ordinarily much flatter than that obtained under constant current strength. Indeed, if  $R_1 = 0$ , or the impedance of the instrument were practically all motional, then it is easily seen that the deflection of a sharply resonant vibration galvanometer, under constant terminal emf., would be constant over a wide range of impressed frequency, and there would be no peak at resonance.

If an inductive impedance  $R + jX$ , such as that of low resistance reactor, is inserted in series with the vibration galvanometer, its total impedance will be  $R + R_1 + jX + Z'$  abohms  $\angle$ .

If this impedance be laid off on a vector diagram, it will be seen that when the motional reactance is changing from zero to negative maximum, i.e., between  $f_0$  and  $f_2$ , the size of the total impedance is also falling much faster than when the motional reactance is changing from a positive maximum to zero (between  $f_1$  and  $f_0$ ). The current through the instrument will therefore be appreciably greater near  $f_2$  than  $f_1$ . This will cause the maximum deflection under varied frequency to occur nearer  $f_2$  than  $f_1$ , or on the  $f_2$  side of the true resonant frequency  $f_0$ . In other words, the apparent resonant maximum deflection will be displaced towards the upper quadrantal frequency, under constant terminal voltage. This phenomenon was described by Wenner\* in 1910. If a suitable condenser were inserted in the circuit of the instrument, instead of a reactor, the shift of apparent resonance should be reversed and take place towards  $f_1$ .

**Use of an Instrument Transformer with a Vibration Galvanometer.** — If a low-resistance vibration galvanometer must be used in a high-impedance network, under conditions where a high-resistance instrument would be more suitable and sensitive, it may be advantageous to use a small reducing voltage transformer between the network and the instrument, so as to increase the flow

\* Bibliography 33.

of current through the latter, thereby increasing its apparent sensitivity. Similarly a high-resistance instrument may be used in a low-impedance network by using a transformer of opposite turns-ratio. If the instrument has  $n$  times too much or too little resistance for best service in a network, the turns-ratio of the transformer windings should be approximately  $\sqrt{n}$ . The advantage accruing from the use of a transformer in such a case is always offset to some extent by power losses in the transformer.

**Effects of Exhausting the Air from the Case Containing a Vibration Galvanometer.** — The effect of removing the air from the chamber in which the vibrator swings is to reduce the mechanical resistance torque  $\mathbf{r}$ , to a degree depending on the form of the vibrating system. It therefore tends to increase the resonant sharpness  $\Delta_0$  of the instrument. If the moment of inertia  $\mathbf{m}$  were strictly confined to the solid elements of the vibratory system, no effect of changing the air pressure on the resonant frequency  $\sqrt{s/\mathbf{m}}$  should be expected. Actually, however, as was shown by Wenner in 1910, an incidental effect of exhausting the air from the instrument case was to raise the resonant frequency  $f_0$  slightly (about 0.8 per cent in the case he cited). This he showed might be accounted for by supposing that a certain thickness of air adheres to the vibrating system, and thus increases its moment of inertia. It would be interesting to measure in this way the apparent thickness of this air layer, on vibrators of simple form, and to study the influence of temperature upon it.

**Example of the Evaluation of the Intrinsic Constants  $\mathbf{A}$ ,  $\mathbf{m}$ ,  $\mathbf{r}$ , and  $\mathbf{s}$ .** — We may take the case, presented in Table XXI, page 275, of a vibration galvanometer with the following measured constants:— $\omega_0 = 6286.3$ ,  $\Delta = 28.27$ ,  $\theta'_{m_0} = 785.6$  and  $R_0' = 13.8 \times 10^9$ . Then by (299),

$$\mathbf{A} = \frac{13.8 \times 10^9}{6286.3 \times 785.6} = 2795.$$

By (301),

$$\mathbf{r} = \frac{2795}{785.6 \times 6286.3} = 5.659 \times 10^{-4}.$$

Next, by (302),

$$\mathbf{m} = \frac{5.659 \times 10^{-4}}{2 \times 28.27} = 1.0008 \times 10^{-5}.$$

Finally, by (303),

$$\mathbf{s} = 1.0008 \times 10^{-5} \times 6286.3^2 = 395.5$$

These values appear in Table XXI. They all have zero slope.

## CHAPTER XXIII

### THE HUMMING TELEPHONE

The fact that a telephone receiver held, either in contact with, or close to, the face of its electrically associated transmitter, may cause the production of a hum or singing tone, appears to have been first discovered by Professor D. E. Hughes\* in 1883. It was rediscovered† by A. S. Hibbard in 1890, and was to some extent examined experimentally by F. Gill‡ in 1901. The subject was investigated by Professor Walter L. Upson, with the author, in 1908.§ A joint paper was published|| on *The Humming Telephone* in that year. The present Chapter is mainly based on the last named paper.

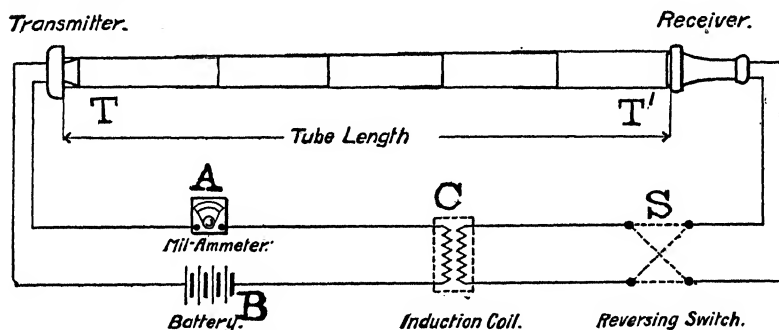


FIG. 141. Diagram of humming telephone connections.

The humming phenomenon can be evoked in various ways. A typical set of suitable connections is, however, shown in Fig. 141. Here the telephone receiver  $T'$  is coupled mechanically with the transmitter  $T$ , through the acoustic tube of adjustable length. It is also electrically coupled with the same transmitter through an ordinary telephone induction coil  $C$ , a reversing switch  $S$  and a voltaic battery  $B$ . In practice, the connecting air tube is often unnecessary, and it may suffice to lift a telephone receiver from its hook and hold it facing its associated carbon microphone transmitter, in order to produce a loud hum.

\* Bibliography 3.

† Bibliography 5.

‡ Bibliography 17.

§ Bibliography 29.

|| Bibliography 30.

The details of the apparatus employed as in Fig. 141, are set forth in the above mentioned joint paper of 1908, and need not be repeated here.

**Effects of Shortening the Air-Tube.** — Commencing with the connections of Fig. 141, a battery of 8.6 volts, and a tube length of 267 cm., as indicated in Fig. 142 on the scale of abscissas, a loud steady note between  $G''$  and  $A''$  ( $850 \sim$ ) was sustained in the telephone. The pitch of this note is shown at  $P$  on the upper zig-zag line  $I$ . The current strength, on the d.-c. milliammeter  $A$ , Fig.

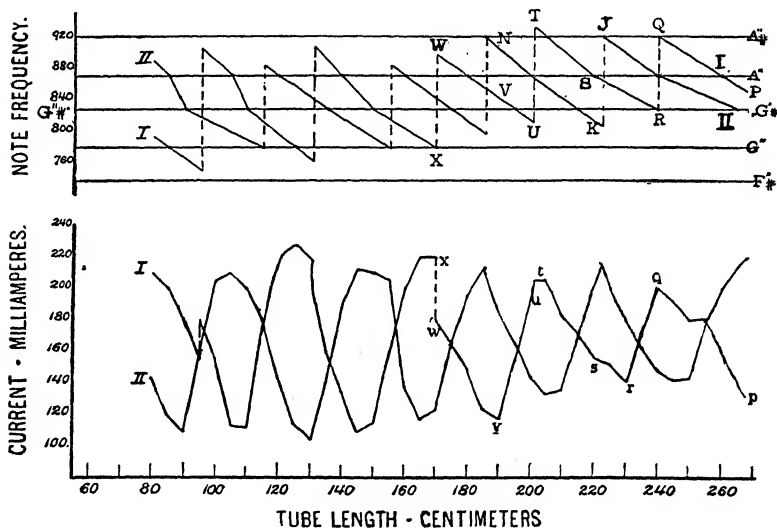


FIG. 142. Effect of shortening tube, and of reversing receiver connections. Curves  $I$  for one connection of the reversing switch and Curves  $II$  for the other.

141, as shown at  $p$  on the lower zig-zag line  $I$ , Fig. 142, was 130 milliamperes. When the telescopic tube was gradually shortened, the pitch of the note steadily rose, until it reached  $Q$ , at  $A''$  ( $920 \sim$ ), with 240 cm. of tube-length, and a primary current strength  $q$  of 200 mas. The intensity of the note near  $920 \sim$  was ordinarily somewhat weaker than when near  $825 \sim$ . On continuing to shorten the tube, the pitch suddenly broke from  $Q$ , at  $920 \sim$ , to  $R$  at  $825 \sim$ . Pushing in the tube further, the pitch would again climb steadily to  $T$ , at 201 cm., with a new maximum of current. Beyond this point, the pitch would break suddenly to  $U$  at  $810 \sim$ . Again it would climb to  $W$ , at 170 cm., and suddenly collapse to  $X$ .

Continuing in this manner, the pitch would alternately "rise" to local maximum and break suddenly to a local minimum along the pitch zig-zag *I*. At the breaks of pitch, the current would sometimes break to a lower value, as at *t*, *u*; or break to an upper value, as at *w*, *x* or vary suddenly in rate of change, without discontinuity in magnitude, as at *q*. Repeating the experiment, the zig-zag lines of pitch and of current would be repeated, not exactly but substantially, the variations being due not merely to observational error, but also to small variations in the behavior of the carbon microphone transmitter.

The zig-zag pitch line *PQRST* of curve *I* is seen to be somewhat irregular. The slants are by no means regularly parallel. The breaks *QTW* are neither regularly elevated, nor regularly spaced. The only substantial regularity is in the spacing along the mean pitch line *G''* of 825  $\sim$ . The intersections of the ascending branches with this line lie approximately 40 cm. apart, at 110, 150, 190, 230, and 270 cm. of tube length, or in accordance with the series  $30 + 40m$  cm., where *m* is a positive integer. It may be observed that for this frequency of 825  $\sim$ , the wave length in air is close to  $33000/825 = 40$  cm., so that these intersections occur substantially at successive wave lengths.

Curve *II*, *JKN*, shows the changes in pitch with diminishing tube length, when the terminals of the receiver were reversed, at the reversing switch *S*, of Fig. 141. This zig-zag pitch line also crosses the mean frequency of 825  $\sim$ , at points approximately 40 cms. apart, which lie about midway between the corresponding crossings of curve *I*.

The lower curves, *pqrs*, etc., in Fig. 142, indicate the changes of rms. current flowing from the voltaic source through the milliammeter in the transmitter circuit. In general, this current strength reached a local minimum at or near tube lengths giving the mean pitch of 825  $\sim$ . The current flowing reached a local maximum, near the lengths where the pitch changed abruptly.

Figure 143 shows what took place in regard to the emitted pitch, and the current taken by the transmitter, when the tube was shortened gradually from 60 cm. to about 1 cm., at which proximity the receiver cap came into contact with the transmitter face (cone removed). Curve *I* crosses the mean pitch line of 825  $\sim$ , at 30 cm. of tube length, and then goes up to a high note above 1300  $\sim$ , where it breaks without reestablishment at any reduced length up



to contact. Curve *II* crosses the mean pitch line at 50 cm., and again at 10 cm., rising to about 860 ~, when the receiver and

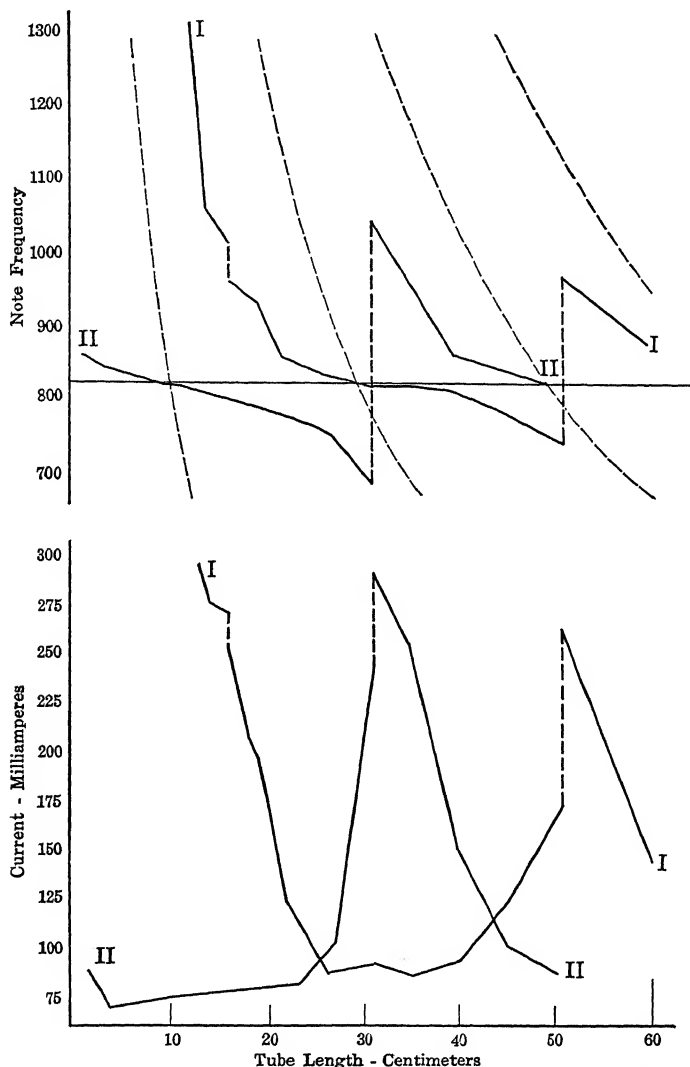


FIG. 143. Humming note frequencies and primary current strengths with short tubes. Tube progressively shortened.

transmitter came into contact. This means that with one connection of the receiver (*II*), there would be a hum emitted at con-

tact, or at any tube length up to the indicated limit of 60 cm.; while for the reversed connection (*I*), no hum would be emitted until the tube-length separation was over 10 cm. This means that in practical service, a receiver will often hum when brought into facing contact with its associated transmitter, in one connection of its terminals; whereas it will refuse to hum in the reversed connection.

The broken lines in the upper part of Fig. 143 indicate the points of  $1/4$  and  $3/4$  wave length, in the air-tube distance at the frequencies within the diagram. Thus, at 825  $\sim$ , the first quarter wave would lie at 10 cm. separation, the three-quarter wave at 30 cm., and the five-quarter wave at 50 cm. At 1000  $\sim$ , these distances would be 8.25, 24.75, and 41.25 cm. respectively. It is

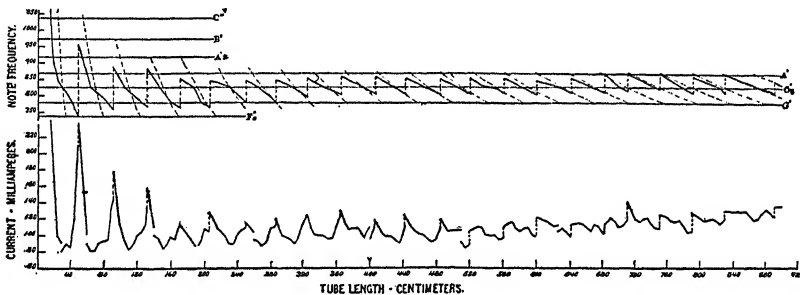


FIG. 144. Frequency and primary-current curves for tube-lengths up to 920 cms. Steadily reduced in length, 8.6 volts in primary circuit

clear from Figs. 142 and 143, that curve *I* crosses the mean pitch line at 30, 70, 110... ( $30 + 40m$ ) cm.; while curve *II* crosses it at 10, 50, 90, ... ( $10 + 40m$ ) cm.

The telescoping air-tube was extended in one set of measurements to more than 9 meters of total length. The changes in emitted pitch, and in transmitter current, over this length, as the tube was steadily shortened, are shown in Fig. 144. Near the full tube length of 9 m, the tone emitted was relatively feeble, and the range of its pitch increases, before breaking to a lower pitch, was relatively small. This zig-zag corresponds to curve *I* in Figs. 142 and 143. The pitch broke 22 times in succession, as the length was reduced from 800 to 50 cm. or on the average once every 38 cm. At short distances (within 40 cm.), the range in pitch frequency was from 740 to 1060  $\sim$ , or through 320  $\sim$ . At the full distance of 9 meters, this range fell to 75  $\sim$ . The apparent cur-

rent strength, by d.-c. milliammeter, was usually near a local minimum at the points where the mean pitch of  $825 \sim$  was produced, and reached a local maximum at or near points where the pitch broke.

**Effects of Lengthening the Air-tube.** — The curves of pitch and of current strength in the transmitter, when the air tube was steadily lengthened, were of the same general character as those of Figs. 142–144, in which the tube was steadily shortened. There were, however, certain characteristic differences in detail. Although the zig-zag pitch curve crossed the mean frequency line of  $825 \sim$ , at very nearly the same points as before, yet the points of break in pitch, when extending the tube, were not the same as when compressing the tube. In the former case, the pitch would fall to a lower value before breaking, and when it broke, it would not start again at so high a value as in the other series.

**Effects of Alternating Lengthening and Shortening the Air-tube.** — The above mentioned peculiar tendency of the pitch to break at one set of distances with decreasing, and at another with increasing, tube lengths, led to observation of the conditions occurring in a humming cycle, with a cyclic compression and extension of the tube. Such a cycle is illustrated in Fig. 145. Commencing at *O*, with 110 cm. of tube length, on the mean frequency of  $825 \sim$ , if we shorten or compress the tube to 90.5 cm., we reach *P* at  $900 \sim$ , near *A''*#. The note then breaks to *Q* at  $780 \sim$ . Increasing the tube length back to 95 cm., we reach *R* at  $770 \sim$ . The note then breaks upwards to *S* at  $880 \sim$ . This humming cycle *PQRS*, could be repeated indefinitely, with a considerable degree of precision as to pitch and tube length; although with only a more moderate degree of precision as regards primary-current strength. Similarly, the cycle *TUVW*, of 10.5 cm. amplitude in length, and  $100 \sim$  in pitch, might be repeated indefinitely. The amplitudes and areas of these humming cycles vary, however, at different breaking points in the tube length.

**Purity of the Humming Tone Emitted.** — With the greater tube lengths, shortly before the break of pitch occurred, there was frequently noted an appearance of the new tone in advance. As the breaking point was approached, the dying tone waned, while the new tone waxed. At the break, the old tone, already faint, would suddenly cease. Consequently, before breaking, both the

old and new tones might be recognized, forming a sort of combination tone. With the shorter tube lengths, which involved a

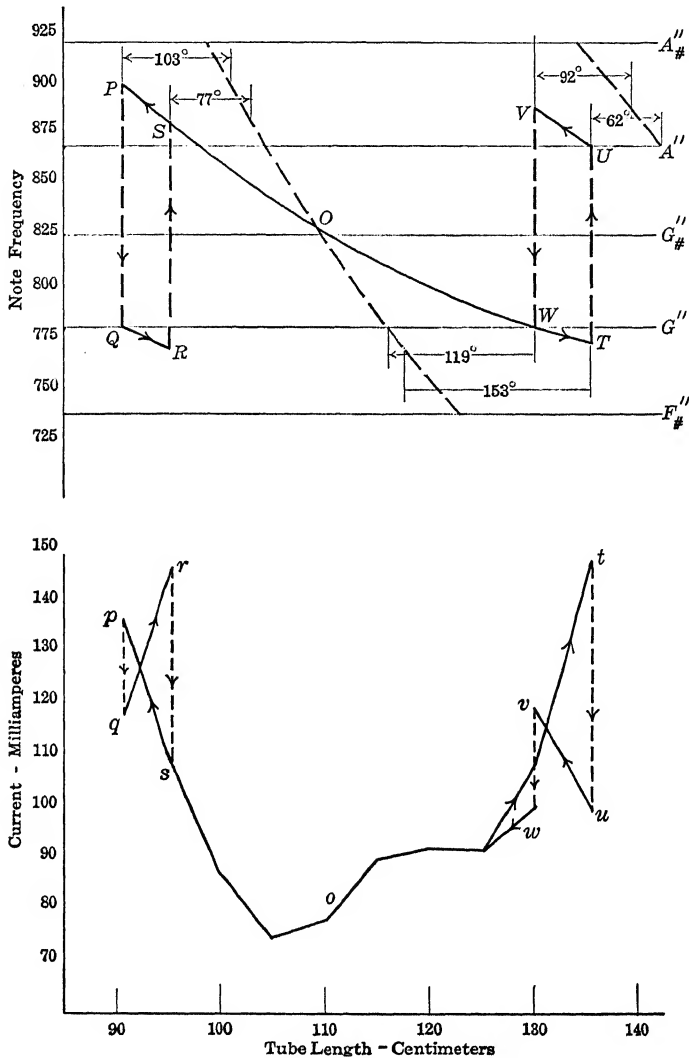


FIG. 145. Humming cycles with cyclic changes in tube-length.

greater jump of frequency at the breaks, these combination tones were rarely heard, and the old note would break suddenly into the new note, without any suggestion of a trill.

Irregularities in the fitting of the telescoping tube sections, or in other acoustic connections, were found to be productive of superposed notes. Although occasionally such plural tones or superposed tones could be discerned, yet, as a general rule, the emitted note was clear and flute-like in quality.

**Effects of Mechanical Changes in the Diaphragm of the Receiver.**

— Altering the resonant frequency of the receiver diaphragm, either by applying a load at the center, or by altering the dimensions of the diaphragm, had a very marked influence on the pitch of the emitted hum. It was found that the mean pitch agreed closely with the resonant frequency of the diaphragm. Weakening the receiver electromagnetically, without altering the mechanical constants of the diaphragm, had very little effect on the pitch of the emitted hum, but affected the range over which the pitch could be altered without breaking, when the tube length was changed. With a very weak receiver, the hum could only be set up when the tube length was close to a mean-frequency point. A small change in tube length either way would then cause the hum to disappear.

**Effects of Mechanical Changes in the Transmitter.** — Altering the load carried at the center of the diaphragm in the carbon-microphone transmitter did not appreciably alter the points of tube length at which the mean frequency hum of the receiver diaphragm was emitted. Such variations of load affected, however, the pitch and the tube lengths at breaks in the tone. This shows that *it is the resonant pitch of the receiver diaphragm which determines the normal mean frequency of the emitted tone.* The transmitter only determines, in conjunction with other factors, the limits of pitch above or below the mean frequency, at which the tone will break and recommence.

**Effects of Electrical Changes in the Humming-telephone System.** — Inserting resistance in either the primary (transmitter) or secondary (receiver) circuit of Fig. 141, weakened the emitted tone and finally caused it to disappear. The value of the extra resistance which, in either case, brought about extinction of the tone, was called the *extinguishing resistance* in the primary, or secondary circuit, respectively. Just before extinction, the pitch of the emitted tone was always close to the mean frequency, or resonant frequency, of the receiver (in most of the tests 825 ~). The amount of either primary or secondary extinguishing resist-

ance, keeping the battery voltage, receiver and tube length constant, was found to depend on the quality of the transmitter. Normal transmitters permitted of a normal extinguishing resistance in their circuits. Defective transmitters were accompanied by abnormal extinguishing resistances. This method of determining the amount of extinguishing resistance in a given humming system, therefore, lends itself to the testing of transmitters within certain limits. A number of such tests are detailed in the original paper mentioned above.

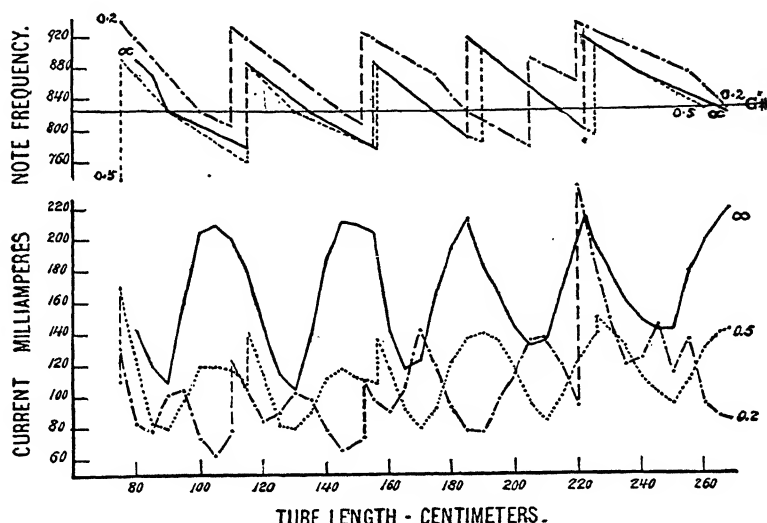


FIG. 146. Frequencies and primary current strengths for different condensers in secondary circuit.

**Change of Battery EMF.**—It was found that between the limits of 6.5 and 10.5 volts in the terminal emf. of the storage battery *B* (Fig. 141), such change of emf. produced very little noticeable effect in the humming system.

**Condenser in the Secondary Circuit.**—A condenser inserted in the secondary circuit was found to be capable of producing a marked influence upon the tube lengths at which the mean tone was produced. A series of observations are indicated in Fig. 146. Here the tube length was reduced steadily from 270 cm. to 75 cm., with 8.6 volts in the primary circuit. Three sets of curves are shown, for 0.2  $\mu f.$  (microfarad), 0.5  $\mu f.$ , and  $\infty \mu f.$  (condenser shorted) respectively. Referring to the pitch lines, it will be seen

that there is not much difference between the cases of  $\infty$  and  $0.5 \mu f$ . The ascending branches of the zig-zags cut the mean-frequency line of  $825 \sim$ , at 90, 132.5, 175, and 210 cm., or fairly in conformity with the series  $(10 + 40 \text{ m.}) \text{ cm.}$ , as in curve *II*, of Fig. 142. With  $0.2 \mu f$ ., however, the intersections occur at 100, 145, and 185 cm., or more nearly in conformity with the series  $(22 + 40 \text{ m.}) \text{ cm.}$ ; that is, at points 12 cm. further along the tube. Moreover, the breaks occur at higher frequencies, by about  $40 \sim$ . In other words, this condenser produced a change of phase approximately equal and opposite to the phase lag in 12 cm. of tube at  $825 \sim$  ( $12/40$ ths of a cycle, or  $108^\circ$ ).

**Conclusions.** — As is described in greater detail in the original paper, or as here above described in abstract, a receiver connected acoustically with a transmitter and a d.-c. source of electric energy, tends to emit a humming note, of the same frequency as that to which its diaphragm is resonant. In the tests described, this mean frequency was emitted at tube lengths of  $(1/4 + m) \left( \frac{v}{f_0} \right) \text{ cm.}$ , for one connection, and at  $(3/4 + m) \left( \frac{v}{f_0} \right) \text{ cm.}$ , for the other connection of the receiver, where  $v = 33000 \text{ cm./sec.}$ , the velocity of sound in air, and  $f_0$  is the resonant frequency of the receiver diaphragm,  $m$  being any integer. As the tube length was slightly reduced from such a mean-frequency point, the pitch rose to a certain extent, and then broke. Under feebly reinforcing conditions, it broke permanently until close to the next point in the series of mean-frequency lengths. Under strongly reinforcing conditions, it broke to a note below the mean-frequency pitch.

**Outline Theory of Humming-telephone Action.** — The humming telephone is a particular case of a system of reinforced and sustained oscillations. Examples of such systems are (1) the ordinary clock or watch, in which a source of unidirectional power (a clockspring or a slowly falling clockweight) maintains a pendulum or vibrator in sustained oscillation; (2) the ordinary electric bell, in which a voltaic source of unidirectional power maintains a hammer in sustained vibration; (3) the ordinary electrically-driven tuning fork; (4) the electric oscillator of the triode vacuum-tube type, in which a source of unidirectional current maintains an oscillation circuit in activity.

The case of reinforced and sustained oscillation is discussed in

Appendix VI. It needs only to be pointed out at this point that a vibrator having a resonant angular velocity  $\omega_0 = \sqrt{s/m}$ , can be sustained indefinitely in action, if an alternating force which may be called a *reinforce*, having the same frequency as the vibrator; i.e., in synchronism with the vibrator, is applied to the system in cophase with the vibratory velocity  $\dot{x}$ , and therefore in opposite phase to the damping force  $-r\dot{x}$ .

Figure 147 is a vector diagram of reinforced oscillation. The

force  $OF$  represents the elastic restoring force, opposed to the mechanical displacement  $x$ , which displacement is directed along  $OE$ . The value of the elastic force  $OF$ , at resonance, is  $js\dot{x}/\omega_0$  dynes, in a rectilinear vibrator, or  $js\dot{\theta}/\omega_0$  dyne-p.-cm. torque in a rotary vibrator. We shall retain the rectilinear notation throughout, on the understanding that the rotary notation may be substituted in appropriate cases. The vibratory velocity  $\dot{x}$  will be directed

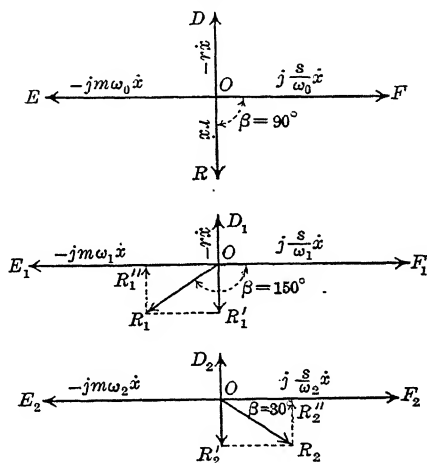


FIG. 147. Diagrams indicating reinforced oscillation and the effects of the phase of reinforcement.

along  $OR$ , in lagging quadrature to  $OF$ . The force  $OE$  is the inertia force of the system, and has the value  $-jm\omega_0\dot{x}$ . At resonance,  $OE$  and  $OF$  are equal, opposite, and in equilibrium. The force  $OD = -r\dot{x}$  is the damping force, opposed to the velocity, and tending to bring the system to rest. If now a reinforce  $OR$  is introduced and applied to the system, equal, opposite, and in equilibrium to the damping force, the system will remain in sustained oscillation. If the four vectors  $OD$ ,  $OE$ ,  $OF$ , and  $OR$  rotate positively or counterclockwise about  $O$ , with uniform angular velocity  $\omega_0$ , their instantaneous projections upon a properly directed reference axis, in the rotation plane passing through  $O$ , will indicate the instantaneous values of these respective forces. The size of  $OR$ , or the magnitude of the applied reinforce, determines the amplitude  $|\dot{x}|$  of the sustained velocity; since  $OR = r\dot{x}$ ,



a weak reinforce produces a correspondingly weak sustained vibration.

If the reinforce  $OR$ , instead of being applied at the proper and appropriate cophase with the velocity  $\dot{x}$ , and  $90^\circ$  lagging behind  $OF$ , should be applied say at  $OR_1$ , lagging  $150^\circ$  behind  $OF$ , and  $60^\circ$  behind the phase of  $\dot{x}$ ; then this reinforce may be resolved into two components, a reactive component  $OR_1''$ , along  $OE_1$ , and an active component  $OR_1'$  along  $OD$ , reversed. This disturbs the reactive equilibrium which previously existed, at resonance, between the elastic force  $OF$  and the inertia force  $OE$ . With the aid of  $OR_1''$ , the reactive force of inertia is virtually increased, as though the mass  $m$  of the system were suddenly increased. In order to restore equilibrium, the angular velocity of the system must fall to a value say  $\omega_1$  radians per second, which is lower than  $\omega_0$ ; but need not be the quadrantal value. This will increase  $OF_1$ , since  $\omega_1$  appears there in the denominator. The system will now remain in sustained oscillation, with the new angular velocity  $\omega_1$  of new apparent resonance, and with the reinforce  $OR_1'$ , at the proper phase position, opposite to  $OD_1$ . Introducing the extra lag of phase in the reinforce has, therefore, two effects. It lowers the angular velocity, or frequency of the sustained oscillation, and it reduces the magnitude of the active component  $OR_1'$ , available for overcoming resistance. The vibrations will be lowered in frequency, and will be weakened in amplitude. As the lag angle  $\beta$  is increased, towards  $180^\circ$ , the pitch of vibration is continually lowered, and the amplitude reduced. When  $B$  reaches  $180^\circ$ , the active component of reinforce vanishes, and the oscillations cannot be sustained.

If now the reinforce is applied at say  $OR_2$ , and at a lag of less than  $90^\circ$  behind  $OF_2$ , the reinforce is resolved into a virtual elastic reactive force  $OR_2''$ , and an active driving force  $OR_2'$ . The system has its elastance artificially increased, and resonance will now occur at a new frequency. The system will now find a new angular velocity  $\omega_2$ , greater than  $\omega_0$ , at which equilibrium between  $-j m \omega_0 \dot{x}$ , and  $(j s \dot{x} / \omega_2 + OR_2'')$  will be restored. The pitch will rise, and the amplitude will fall to that determined by  $OR_2'$ .

On this reasoning, reinforced sustained oscillation can only occur when  $OR$  is applied with a lag angle  $\beta$  between the limits  $0^\circ$  and  $180^\circ$ . It will be most effective when  $\beta = 90^\circ$ , in which case the reinforce will maintain the original resonant angular

velocity  $\omega_0$ . At other values of the lag angle  $\beta$ , the angular velocity will be changed.

When the receiver diaphragm is connected acoustically with its transmitter, in such a manner that the reinforce current in the receiver circuit sets up a reinforce pull on the diaphragm in cophase with its velocity  $\dot{x}$ , ( $90^\circ$  ahead of the displacement  $x$ , or  $90^\circ$  behind the elastic force  $OF$ ), then the hum should be most powerful, and its pitch should be the same as the resonant pitch of the diaphragm. If the acoustic tube length is such that the reinforce pull on the diaphragm is not at this proper phase, the action reinforce component will be reduced, and the pitch will also be altered. If the acoustic wave length were kept constant, then we should expect to find alternate half-wave lengths of tube in which reinforcement could occur, interspersed with half-waves in which no reinforcement could occur. Actually, however, with any change in pitch, there is a corresponding change in wave length, and in phase relations, so that when the acoustic tube is shortened say, below the point of mean-frequency maximum action, the pitch rises regularly, and the amplitude diminishes to perhaps  $\beta = 20^\circ$ , but before it is completely extinguished, a lower pitch is generally found, ready to give a louder hum at some large lag angle  $\beta$ , perhaps  $160^\circ$ .

The results obtained and given in the paper of 1908, are in fairly satisfactory agreement with the above outline of theory. There remain, however, a number of details to be cleared up. An adequate expression for the relations involved would include a quantitative knowledge of the change in resistance of the carbon transmitter with change of vibratory amplitude for its diaphragm. At that time, the motional-impedance circle of the telephone receiver had not been found out; so that there were several gaps in the theory of the humming system. On the assumption, however, that the maximum cyclic amplitude of vibration of the

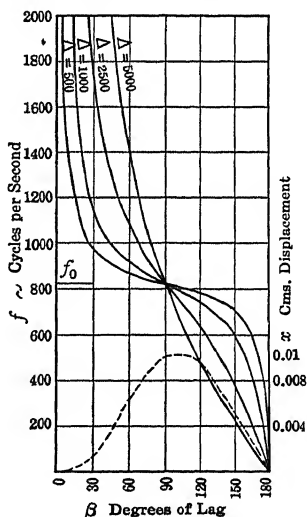


FIG. 148. Reinforced frequency in relation to the phase of the reinforcement.

receiver diaphragm under the most favorable reinforce conditions was  $10\mu$ , and that the reinforce on that diaphragm received through the action of the transmitter, varied as the square root of the amplitude, the frequency curves of Fig. 148 have been worked out for different assumed values of  $\Delta$ , the damping constant of the receiver. Of these, the curve for  $\Delta = 500$ , is that which would probably most nearly represent the conditions of

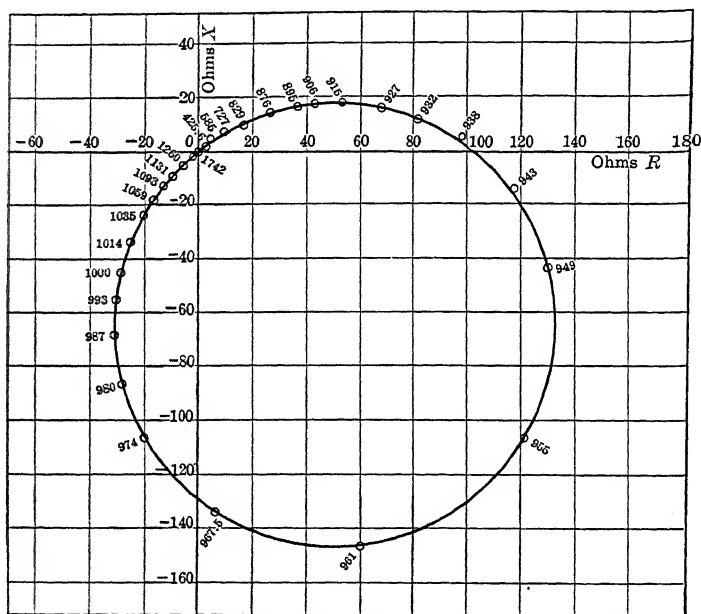


FIG. 149. Motional-impedance circle of the receiver used in receiver-transmitter tests.

the instrument used. This theoretical curve resembles fairly well the curve *I* of observed frequencies in Fig. 143, between 50 and 80 cm. of tube length.

The subject of the humming telephone was again taken up and studied experimentally by Professor H. Mori, in 1918, using motional-impedance methods. The receiver was a bipolar instrument of the Western Electric Company, type 143, of the 75-ohm d.-c. winding. It was acoustically coupled to a solid-back carbon transmitter of the Western Electric Company, type No. 329, having a quiescent d.-c. resistance of about 25 ohms. The instruments were similar in all substantial respects to those

used in Professor Upson's research of 1908, described above. The acoustic coupling between the receiver and transmitter was a telescoping tube of smooth fiber, 1.6 cm. in internal diameter, and of various lengths up to 227 cm. The measurements were made (1) by finding the motional-impedance circle of the receiver alone, and (2) by connecting the receiver and transmitter together in simple series, and measuring the motional impedance of the combination. It should then be possible to analyze the electric

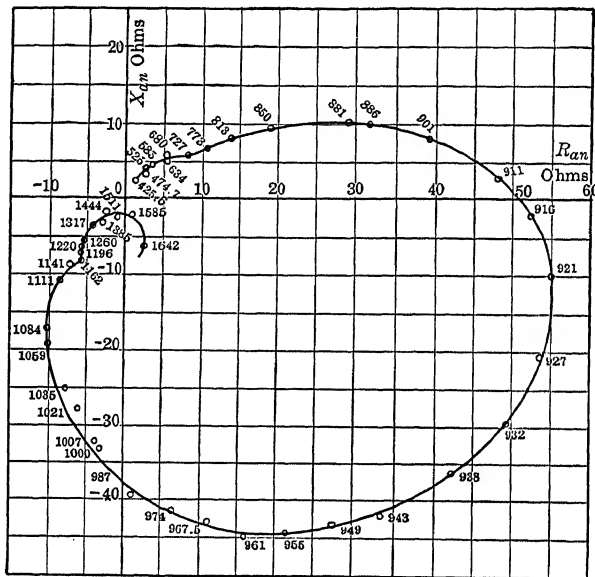


FIG. 150. Motional-impedance graph of receiver and transmitter in simple series, with 8 cm. of acoustic tube between them. Testing current 2.2. milliamperes.

and mechanical properties of the transmitter microphone and diaphragm from these data.

Figure 149 is a motional-impedance circle of the receiver alone. It has a diameter  $Z'_0$  of 164 ohms, dipping at an angle of  $2\beta = 51^\circ$ . The resonant frequency  $f_0$  is  $958 \sim$ , and the damping constant  $\Delta = 90$ .

Figure 150 shows the motional-impedance diagram, for the same receiver, when tested in series with the acoustically coupled transmitter, the length of the coupling air tube being 8 cm. It will be seen that the circle has been flattened, or distorted into elliptic

form, and there are two other distortions. One is between 425.6  $\sim$  and 727  $\sim$ . The other is between 1162  $\sim$  and 1642  $\sim$ . In this case, the coupling air tube was so short that there was very little opportunity to develop the proper relation of reinforce. Figure 151 shows, however, the corresponding motional-impedance graph obtained when the coupling air tube was 227 cm. long. The successive resonances occur approximately at the following impressed frequencies:—565, 634, 700, 760, 837, 901, 958, 1007, 1070, 1145, and 1220  $\sim$ . The average difference of frequency between suc-

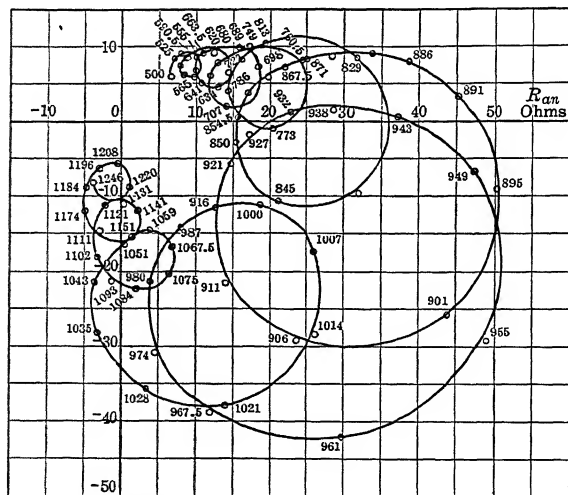


FIG. 151. Motional-impedance graph of receiver and transmitter in simple series, with 227 cm. of acoustic tube between them. Testing current 2.2 milliamperes.

cessive resonances, in this series, is 65.5  $\sim$ . The principal resonance occurs at or near 958  $\sim$ , the resonant frequency of the receiver diaphragm. The other resonances occur at the frequencies which can produce the most favorable phases of reinforce, under the electrical and mechanical couplings of the system. A number of motional-impedance diagrams were secured by Professor Mori, of which only those in Figs. 149–151 are here presented. The data have not yet been properly analyzed in detail. A large field for further investigation, both experimental and analytical, lies open in this direction. Under favorable circumstances, it should lead to the analysis of the intrinsic constants of the transmitter diaphragm, for which the data are still lacking.

## APPENDIX I

### APPLICATION OF BESSEL FUNCTIONS TO THE ELEMENTARY THEORY OF PLATE VIBRATION

We assume a uniform flat circular diaphragm uniformly clamped, at radius  $a$  cm., in such a manner that the displacement is always zero at the clamping circle, and also that there is neither bending nor slope of the plate at this circle. Required the free pitch of the plate in its fundamental mode, and also the law of ascending pitches in its third mode, the second mode being absent. (See Chapter III.)

The formula for the instantaneous amplitude of free vibration in a flat plate in Rayleigh's "Theory of Sound," Vol. I, page 352, is

$$(308) \quad w_{nr} = P \{ J_n(kr) + \lambda J_n(ikr) \} \cos(n\theta + \alpha_n) \cos(\omega t + \beta) \quad \text{cm.}$$

where  $n$  = number of nodal diameters (numeric)

$w_{nr}$  = instantaneous displacement at a point on the plate, whose central polar coordinates are  $r$  cm.,  $\theta$  radians (cm.)

$P$  = constant of amplitude-magnitude (cm.)

$$(309) \quad k = \sqrt{\omega}/c, \text{ a constant of the material (cm.}^{-1}\text{)}$$

$c$  = a constant of the material defined by

$$(310) \quad c = \sqrt[4]{\frac{qb^2}{12\rho(1-\sigma^2)}} \quad \frac{\text{cm}}{\sqrt{\text{sec.}}}$$

$q$  = Young's modulus for the plate material (dyne/cm.<sup>2</sup>)

$\rho$  = density of the plate material (gm./cm.<sup>3</sup>)

$\sigma$  = Poisson's ratio for the plate material (numeric)

$b$  = thickness of plate (cm.)

$\lambda$  = a boundary-condition constant (numeric)

$J_n$  = a Bessel's Function of the  $n$ th order (numeric)

$i = \sqrt{-1}$

$\alpha_n$  = a phase-angle measured around the plate (radians)

$f$  = frequency of free vibration (cycles/sec.)

$\omega = 2\pi f$  = angular velocity of free vibration (radians/sec.)

$t$  = time elapsed from a given epoch (seconds)

$\beta$  = a timephase determined by the epoch (radians)

$a$  = radius of clamping circle (cm.)

If the second mode of motion is absent, there will be no nodal diameters, and subscript  $n = 0$ . Consequently (308) reduces to

$$(311) \quad w_r = P \{ J_0(kr) + \lambda J_0(ikr) \} \cos(\omega t + \beta) \quad \text{cm.}$$

Following Rayleigh's demonstration, we have for the case under consideration,  $w_r = 0$  at  $r = a$ , and also  $dw_r/dr = 0$  at  $r = a$ .

Hence

$$(312) \quad 0 = P \{J_0(ka) + \lambda J_0(ika)\} \cos(\omega t + \beta) \quad \text{cm.}$$

or

$$(313) \quad \lambda = \frac{-J_0(ka)}{J_0(ika)}.$$

Again, differentiating (311) with respect to  $r$ , for  $r = a$ , where  $dw/dr$  vanishes, we have

$$(314) \quad \frac{1}{k} \frac{dw_r}{dr} = J_0'(ka) + i\lambda J_0'(ika) = 0,$$

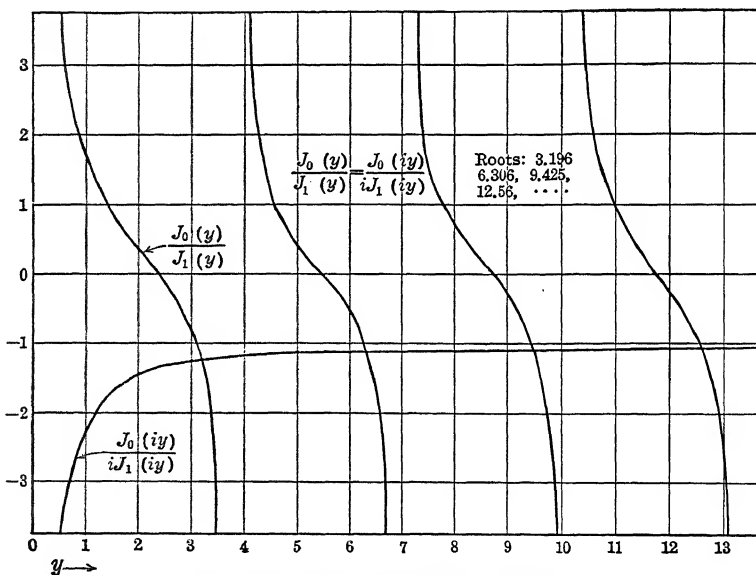


FIG. 152. Graph of a Bessel's equation.

or

$$(315) \quad \lambda = \frac{-J_0'(ka)}{iJ_0'(ika)}.$$

Combining (313) and (315)

$$(316) \quad \frac{J_0(ka)}{J_0(ika)} = \frac{J_0'(ka)}{iJ_0'(ika)} = \frac{J_1(ka)}{iJ_1(ika)}.$$

Hence

$$(317) \quad \frac{J_0(ka)}{J_1(ka)} = \frac{J_0(ika)}{iJ_1(ika)}.$$

This last equation, involving Bessel's functions of  $ka$ , of the first and zeroth orders, must be satisfied for free vibrations. It can be satisfied by graphical solution, as in Fig. 152. Here, the abscissas are of  $y = ka$ ,

and the ordinates give the corresponding numerical values of  $\frac{J_0(iy)}{iJ_1(iy)}$ , in the rising curve. The four upright curves follow the numerical values of  $\frac{J_0(y)}{J_1(y)}$ . At each of the four intersections of the rising with the upright curves, the abscissa is a root of equation (317), such as corresponds to a possible vibration frequency. These roots occur at the numerics  $y = 3.196, 6.306, 9.425, \text{ and } 12.56$ . There is no limit to the number of such increasing possible roots. The lowest root  $ka = 3.196$ , corresponds

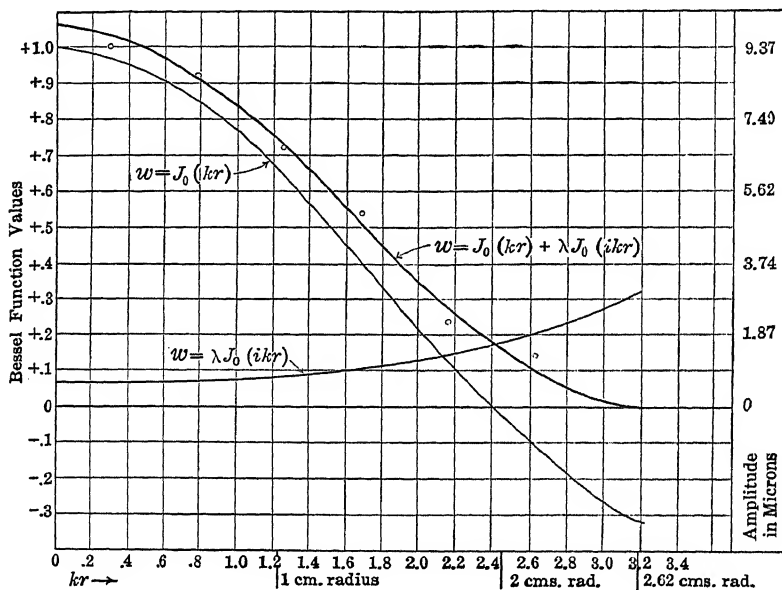


FIG. 153. Curves of vibration of telephone diaphragm. Amplitudes along a radius.

to the fundamental mode, with no nodal circles. Substituting this root in (313), we obtain from tables

$$(318) \quad \lambda = \frac{-J_0(3.196)}{J_0(i3.196)} = -\frac{-0.3197}{5.730} = +0.05571$$

Reëntering (311) with this value of  $\lambda$ , we have for the fundamental mode of vibration of such a circular plate:

$$(319) \quad w_{rm} = P\{J_0(kr) + 0.05571 J_0(ikr)\} \quad \text{max. cy. cm.}$$

In Fig. 153, the abscissas are drawn to two different scales: namely the upper for  $kr$ ,  $k = 1.21 \text{ cm}^{-1}$ , for the particular case where  $a = 2.62 \text{ cm.}$  ( $ka = 3.196$ ), and the lower for  $r$  in cm.



The upper faint curve follows  $J_0(kr)$ , as taken from Bessel Function Tables, and the lower faint curve follows  $0.05571 J_0(ikr)$ . The heavy curve is the sum of these two curves, and represents the amplitude of displacement of points along any radius of the plate, when freely vibrating in its fundamental or first mode, taking 1.056 as the maximum or central amplitude. The small circles, lying near to the heavy curve, indicate a series of observed amplitudes to the right-hand scale, in the forced vibration of a receiver diaphragm as detailed in Chapter III, page 26. The observations show that the amplitudes of acoustically forced vibrations over the surface of the diaphragm, substantially agreed with the theoretical amplitude distribution of free vibrations for a corresponding circular plate, according to the Rayleigh formula.

## APPENDIX II

### OUTLINE THEORY OF EQUIVALENT MASS OF A DIAPHRAGM

Let  $M$  = the mass of a uniform circular diaphragm within the circle of the clamping ring of radius  $a$  cm. (gm.)

$\rho$  = superficial density of the diaphragm (gm./cm.<sup>2</sup>)

$w_0$  = maximum cyclic vibration amplitude at the center of the diaphragm (cm.  $\angle$ )

$w_r$  = maximum cyclic vibration amplitude at the radius  $r$  cm. of the diaphragm (cm.  $\angle$ )

$\dot{w}_0$  = maximum cyclic vibration velocity at the center of the diaphragm (cm./sec.  $\angle$ )

$\ddot{w}$  = maximum cyclic vibration acceleration at the center of the diaphragm (cm./sec.<sup>2</sup>  $\angle$ )

$W$  = maximum cyclic kinetic energy of vibration of the diaphragm (maximum cyclic ergs)

It is assumed that the diaphragm is vibrating in its first fundamental mode, and that all of its parts have the same phase. Moreover, the frequency of vibration is single; so that all parts possess a simple harmonic motion.

The maximum cyclic kinetic energy of an element of the diaphragm of surface area  $ds$  sq. cm., having a maximum cyclic velocity  $\dot{w}_r$ , is

$$(320) \quad dW = \frac{1}{2} (\rho \cdot ds) \dot{w}_r^2 \quad \text{max. cy. ergs.}$$

The total maximum cyclic kinetic energy of the diaphragm will be the integral of this value over the surface, or

$$(321) \quad W = \int_0^a \frac{1}{2} \rho \cdot 2\pi r \cdot \dot{w}_r^2 \cdot dr = \pi \rho \int_0^a \dot{w}_r^2 \cdot r \cdot dr \quad \text{max. cy. ergs.}$$

If we assume that the displacement distribution is symmetric with respect to the center, where it is a maximum we may write

$$(322) \quad W = \frac{1}{2} m_0 \dot{w}_0^2 \quad \text{max. cy. ergs,}$$

where  $m_0$  is the equivalent mass of the diaphragm with respect to the velocity at the center, or the mass which, vibrating with the velocity at the center, would have the same kinetic energy as the whole diaphragm with its actual graded velocity distribution.

Hence, by (321) and (322)

$$(323) \quad m_0 = \frac{2\pi\rho}{\dot{w}_0^2} \int_0^a \dot{w}_r^2 \cdot r \cdot dr = \frac{2\pi\rho}{\dot{w}_0^2} \int_0^a w_r^2 \cdot r \cdot dr \quad \text{gms.}$$

In a monopolar receiver, the central equivalent mass  $m_0$  would be of essential practical interest. In a bipolar receiver, however, the theory attaches mainly to the actions over the poles, where also the displacement and velocity may be as great, or even greater, than at the center. If  $w_1$ , and  $\dot{w}_1$  be the observed maximum cyclic displacement and velocity of the diaphragm, over one of the poles, and  $m_1$  the equivalent mass with respect to the velocity over the poles, i.e. the *polar equivalent mass*, then

$$(324) \quad W = \frac{1}{2} m_1 \dot{w}_1^2 \quad \text{max. cy. ergs,}$$

whence as before

$$(325) \quad m_1 = \frac{2\pi\rho}{\dot{w}_1^2} \int_0^a \dot{w}_r^2 \cdot r \cdot dr = \frac{2\pi\rho}{w_1^2} \int_0^a w_r^2 \cdot r \cdot dr \quad \text{gm.}$$

and

$$(326) \quad m_1 = m_0 \frac{\dot{w}_0^2}{\dot{w}_1^2} = m_0 \frac{w_0^2}{w_1^2} \quad \text{gm.}$$

Thus the polar equivalent mass is to the central equivalent mass, as the squares of the displacements at the center and poles respectively.

In the electrical measurements of the equivalent mass of the diaphragm in a bipolar instrument, it is the polar equivalent mass which is theoretically evaluated.

**Central Equivalent Mass on the Assumption that the Vibrational Displacements follow the Rayleigh Bessel-Function Distribution of Free Plate Vibration.** — We have seen in Appendix I, equation (311), that in the theory of free vibrations of a uniform circular plate, flat-clamped at the edge

$$(327) \quad w_{rm} = P \{ J_0(kr) + \lambda J_0(ikr) \} \quad \text{max. cy. cm.,}$$

also, at the center,

$$(328) \quad w_0 = P \{ J_0(0) + \lambda J_0(i0) \} = P(1 + \lambda) \quad \text{max. cy. cm.}$$

Thus

$$(329) \quad \frac{w_{rm}}{w_0} = \frac{J_0(kr) + \lambda J_0(ikr)}{1 + \lambda}$$

and by (323)

$$(330) \quad m_0 = \frac{2\pi\rho}{(1+\lambda)^2} \left\{ \int_0^a \{ J_0(kr) + \lambda J_0(ikr) \}^2 r \cdot dr \right. \quad \text{gm.}$$

$$(331) \quad = \frac{2\pi\rho}{(1+\lambda)^2} \left[ \int_0^a J_0^2(kr) r \cdot dr + \int_0^a \lambda^2 J_0^2(ikr) r \cdot dr \right. \\ \left. + \int_0^a 2\lambda J_0(kr) \cdot J_0(ikr) r \cdot dr \right] \quad \text{gm.}$$

$$(332) \quad = \frac{2\pi\rho}{(1+\lambda)^2} \left[ \frac{a^2}{2} \{ J_0^2(ka) + J_1^2(ka) \} + \frac{\lambda^2 a^2}{2} \{ J_0^2(ika) + J_1^2(ika) \} \right. \\ \left. + \frac{2\lambda a}{k^2 - i^2 k^2} \{ k J_0(ika) J_1(ka) - ik J_0(ka) J_1(ika) \} \right] \quad \text{gm.}$$

But  $M = \pi \rho a^2$ , is the total vibrating mass; so that

$$(333) \quad \frac{m_0}{M} = \frac{1}{(1 + \lambda)^2} \left[ \left\{ J_0^2(ka) + J_1^2(ka) \right\} + \lambda^2 \left\{ J_0^2(ika) + J_1^2(ika) \right\} \right. \\ \left. + \frac{2\lambda}{ak} \left\{ J_0(ika)J_1(ka) - iJ_0(ka)J_1(ika) \right\} \right].$$

Using the ratios equated in (316) this reduces to

$$(334) \quad \frac{m_0}{M} = \frac{1}{(1 + \lambda)^2} \cdot 2 J_0^2(ka),$$

$$(335) \quad = \frac{1}{(1.05571)^2} \cdot 2 J_0^2(3.196) = \frac{0.20378}{1.1145} = 0.18285,$$

or to three significant digits, the *equivalent central mass coefficient* of such a plate is 0.183.

If we know the shape of the displacement curve,  $w$ , versus  $r$ , for the diaphragm, from exploration measurements, we can compute the equivalent central mass coefficient  $m_0/M$  of the diaphragm, on the assumption that the distribution of displacement is uniform about the center, or independent of the azimuth, by a method of quadratures, as follows:

Draw the  $w$ , curve as in Fig. 154. Divide the line of abscissas into an integral number  $n$  of annular rings of equal area and successively diminish-

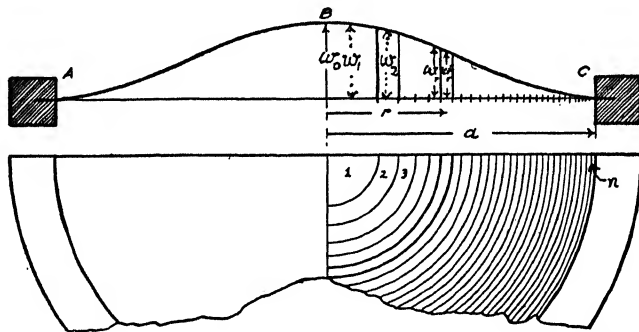


FIG. 154. Illustrating method of diaphragm equivalent mass determination from exploration data.

ing width, each ring will therefore have a mass of  $M/n$  gm. Find the middle ordinate  $w_r$  at the mid radius of each ring, which will be the mean displacement at that ring. Find its square. Let the successive squares of these displacements be  $w_1^2, w_2^2, w_3^2, \dots, w_n^2$ ; then

$$(336) \quad \frac{m_0 w_0^2}{2} = \frac{1}{2} \frac{M}{n} \left\{ w_1^2 + w_2^2 + w_3^2 + \dots + w_n^2 \right\} \quad \text{max. cy. ergs.}$$

or

$$(337) \quad \frac{m_0}{M} = \frac{1}{n} \frac{\sum (w^2)}{w_0^2}$$

This process was actually carried out on the curve of Fig. 153, before the integration of (331) and (332) had been derived, and as is shown in the original \* paper, the value of the equivalent central mass coefficient from 50 concentric annuli was just 0.183, which indicates that for the case of this diaphragm acoustically set into forced vibration, the distribution of amplitudes over its surface conformed closely with the Rayleigh Bessel-function theory of free plate vibration.

\* Kennelly — Taylor Paper, Bibliography 56, page 133. The writers were indebted to Dr. Geo. A. Campbell for an indication as to how the mathematical integral could be derived.

## APPENDIX III

### ELEMENTARY THEORY OF A SIMPLE VIBRATOR, WITH ESPECIAL REFERENCE TO A TELEPHONE-RECEIVER DIAPHRAGM

**Forced Vibrations.** — The rectilinear vibration of a vibrator of one degree of freedom, upon which a simple harmonic vibromotive force is steadily impressed, is perhaps most easily presented by considering the case of a particle of mass  $m$  grams rotating uniformly in a circular orbit.

In Fig. 155, a particle  $P$ , is assumed to describe the circular orbit  $PQ$ , about center  $O$ , with uniform angular velocity  $\omega$  of its radius vector  $OP$ . The particle is to be acted upon by an "elastic force," or elastic restoring force, always directed towards the center  $O$ , and proportional to the particle's distance from the center. This distance is the constant radius  $x_m$  cm. If the particle occupies the position  $P$  at the instant  $t = 0$ , then its radius vector, or displacement vector  $OP$ , at any subsequent elapsed time  $t$  seconds, will be

$$(338) \quad x = x_m \epsilon^{j\omega t} \quad \text{inst. cm } \angle.$$

The position  $OP$  in Fig. A represents the displacement at times  $t = 0, 1/f, 2/f, 3/f$ , etc., where  $f$  is the frequency of rotation in cycles per second.

At any moment when the particle is at  $P$ , its velocity is tangentially directed from  $P$  to  $P'$ . Calling this velocity  $\dot{x}$ , we have from (338)

$$(339) \quad \dot{x} = j\omega \cdot x_m \epsilon^{j\omega t} = j\omega x \quad \text{inst. cm/sec. or kins } \angle.$$

At the same moment, the acceleration of the particle will be directed along the tangent  $QQ'$ , taken from the point  $Q$ , advanced  $90^\circ$  in phase beyond  $P$ . Calling this acceleration  $\ddot{x}$ , we have from (339)

$$(340) \quad \ddot{x} = (j\omega)^2 \cdot x_m \epsilon^{j\omega t} = j\omega \cdot \dot{x} = -\omega^2 x \quad \text{inst. kins/sec. } \angle.$$

This is a constant vector acceleration of the particle, or the steady rate of change of its velocity in space. In addition to the elastic force, we may assume that the particle is subjected to a frictional retarding force, proportional to its velocity  $\dot{x}$ , and directed at each instant oppositely to  $\dot{x}$ . We may express this retarding force as  $-r\dot{x}$  dynes  $\angle$ . The minus sign here indicates the essential opposition between the frictional retard-

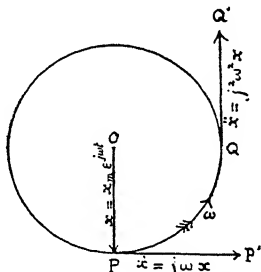


FIG. 155. Vector diagram of vibromotive forces. General case.

ing force and the instantaneous velocity. At the moment seized by Fig. 155, since the velocity is in the direction  $PP'$ , the frictional force will be in the direction  $P'P$ .

According to Newtonian dynamics, the constant vector acceleration will be opposed by a force of inertia, equal in size to  $m\ddot{x}$  dynes, and directed at each instant opposite to  $\ddot{x}$ . Its plane-vector value will therefore be  $-m\ddot{x}$  dynes  $\angle$ . In Fig. 155, the instantaneous acceleration being along  $QQ'$ , the inertia force resisting acceleration will be directed at that instant along  $Q'Q$ .

The three forces of elastance, resistance, and inertia will not of themselves maintain a steady state of equilibrium. The particle, under these

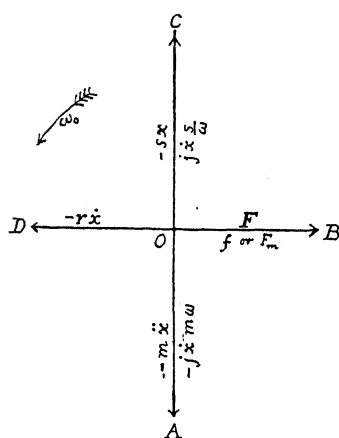


FIG. 156. Vector diagram of vibromotive forces. Resonance.

$OP$ ,  $OC$  will be in the direction  $-x$ . Its size will be  $-sx$  dynes, to a suitably chosen geometric scale.

The force of inertia, being opposed to acceleration, will have the direction  $Q'Q$ , Fig. 155, or  $OA$ , Fig. 156. Since  $\ddot{x}$  has the direction  $QQ'$ ,  $OA$  will have the direction  $-\ddot{x}$ . Its size will be  $-|m\ddot{x}|$ .

These two forces of elastance and inertia will always be directly opposite to each other, at all positions of  $P$  in its orbit. The two vectors  $OC$  and  $OA$  are always in the same straight line through  $O$ , but, as we shall see, their relative sizes depend upon  $\omega$ .

The retarding force of friction, being opposite to the velocity  $\dot{x}$ , will have the direction  $P'P$ , or  $OD$ , Fig. 156. This has direction  $-\dot{x}$ , and its size is  $-|r\dot{x}|$ . The direction of the velocity  $\dot{x}$  will be  $OB$  on the diagram.

It is convenient to keep the  $\dot{x}$  direction  $OB$ , as standard, or as the phase of reference. The frictional force  $OD$  is always diametrically opposite to this, or in the standard phase reversed.

three forces alone, would come to rest at  $O$ , as we shall see later. If, however, a rotating force of  $f$  dynes is impressed on the particle, equilibrium may be steadily maintained. The vector size and the position of this force in the plane of the orbit, in order that steady equilibrium may be maintained, depend upon the value of the angular velocity  $\omega$ .

Figures 156, 157, and 158 are vector diagrams of the forces acting on the particle at an instant when the particle occupies the position  $P$  in Fig. 155. It is evident that the elastic force will then be in the direction  $PO$ , Fig. 155, or  $OC$ , Fig. 156. Since  $x$ , according to (338), is measured in the direction

From (339) we have the vector relation

$$(341) \quad x = \frac{1}{j\omega} (\dot{x}) = -j \frac{\dot{x}}{\omega} \quad \text{inst. cm. } \angle.$$

This means that the displacement  $x$  is always in  $-j$  phase relation to the velocity, is in lagging quadrature thereto, or has the direction  $OA$  with reference to  $OB$  as  $\dot{x}$ . Consequently, the elastic force  $-sx$  or  $OC$ , being opposite to  $OA$ , is always in leading quadrature to  $\dot{x}$  and  $OB$ .

Again, from (340),  $\ddot{x}$  being in  $+j$  phase relation to  $\dot{x}$ , or along  $OC$ , the inertia force opposed to it will be in  $-j$  phase relation to  $\dot{x}$  and  $OB$ , or along  $OA$ .

Consequently, the three vectors  $OC$ ,  $OD$ , and  $OA$ , respectively, of elastance, friction, and inertia, maintaining their fixed phase relations at all times, rotate, together with the force  $OB$ , about the fixed reference point  $O$ , Fig. 156, at the angular velocity  $\omega$  of the orbit in Fig. 155. The reference point  $O$  may be supposed to coincide with the particle at all times and to travel with it.

In a circular orbit, and with circular oscillation, such as occurs with the circular pendulum, the vector forces would rotate about the axis  $O$  of system Fig. 155, as by rotation of the diagram in Fig. 156. In a rectilinear path, and with rectilinear vibration, such as occurs in a telephone diaphragm with its simplest mode, the diagram of Fig. 156 may be regarded as a stationary-vector diagram, the vectors indicating relative phases only. We may, however, also regard it as a rotary-vector diagram, if in rotation about center  $O$ , with angular velocity  $\omega$ , we take instantaneous projections of the several vectors upon the reference axis  $OB$ . These instantaneous projections along  $OB$  will represent the corresponding momentary values of the respective forces in the rectilinear vibration system.

**Case of Resonant Angular Velocity.** — If we assign to  $\omega$  the particular value

$$(342) \quad \omega_0 = \sqrt{\frac{s}{m}} \quad \frac{\text{rad.}}{\text{sec.}},$$

so that  $m\omega_0 = s/\omega_0 = \sqrt{ms}$ , we have, in terms of the corresponding velocity  $\dot{x}$ ,

$$(343) \quad x = -j\dot{x} \sqrt{\frac{m}{s}} \quad \text{inst. cm. } \angle,$$

and

$$(344) \quad \ddot{x} = j\dot{x} \sqrt{\frac{s}{m}} \quad \frac{\text{inst. kines}}{\text{sec } \angle},$$

so that the elastic force  $OC$  is

$$(345) \quad -sx = +j\dot{x} \sqrt{ms} = +j\dot{x} \frac{s}{\omega_0} \quad \text{inst. dynes } \angle,$$

and the inertia force  $OA$

$$(346) \quad -m\ddot{x} = -j\dot{x} \sqrt{ms} = -j\dot{x}m\omega_0 \quad \text{inst. dynes } \angle.$$



At this particular angular velocity of orbital rotation, which is called the resonant angular velocity, the elastic and inertia forces, always diametrically opposed, exactly equate, or maintain equilibrium. This leaves the frictional force  $OD = -r\dot{x}$ , as the only unbalanced force acting on the system. In order, therefore, to maintain the system in equilibrium as a whole, a vector force  $OB = -OD$ , Fig. 156, must be applied opposite to the frictional force. Its magnitude will be

$$(347) \quad f = r\dot{x} \quad \text{inst. dynes } \angle,$$

or

$$(348) \quad \dot{x} = \frac{f}{r} \quad \text{inst. kines } \angle.$$

This means that, at the resonant angular velocity  $\omega_0$ , as determined from (342), the force  $f$  which will maintain the system in equilibrium is equal and opposite to the frictional force, and will be entirely expended in overcoming friction. The velocity then obeys an Ohm's law equation (348).

In rotational vibration with a circular orbit, the velocity  $\dot{x}$  as expressed by (348) will be constant in size, its direction in the orbital plane varying, however, from moment to moment. The force  $f$  would have to be maintained in the tangential position, or in leading quadrature to the displacement. In rectilinear vibration, with a straight-line orbit, the velocity  $\dot{x}$ , as expressed by (348), will be a maximum cyclic velocity, or the maximum projection of  $\dot{x}$  on the  $OB$  axis, i.e., when  $\dot{x}$  is in phase momentarily with  $OB$ . The direction of  $\dot{x}$  will not rotate. It will always lie in the axis  $OB$  of its rectilinear orbit, but it will vary in magnitude from moment to moment, following the instantaneous projections on  $OB$  of a vector  $\dot{x}$ , rotating about  $O$ , Fig. 156, with uniform angular velocity  $\omega$ . Each of the forces  $OB$ ,  $OD$ ,  $OC$  and  $OA$  then becomes a simple harmonic force, i.e., varies as  $\sin \omega t$ .

If we impress a constant tangential rotary force  $f$  on the rotating particle  $P$ , Fig. 155, with the resonant angular velocity  $\omega_0$  peculiar to the system, then, after the system has had time to settle down to the steady state, the velocity  $\dot{x}$  of the system will become the constant Ohm's law quantity (348), and the diagram of Fig. 156 will be established as a rotary vector diagram, with  $OB$  in equilibrium with  $OD$ , and  $OA$  with  $OC$ . If, on the other hand, we impress a maximum cyclic alternating vibromotive force on a rectilinearly vibrating particle with the resonant angular velocity  $\omega$ , then after the system has become steady, the maximum cyclic velocity will follow the Ohm's law relation of (348), and the diagram, Fig. 156, will be established as a projection rotary-vector diagram.

Any such vibratory-vector force diagram as that of Fig. 156 therefore may be regarded in any of the three following ways:

- (1) As a pure rotary diagram for a simple circular vibratory case, with the four forces maintaining fixed magnitudes, but varying their directions progressively in space.



abundant reactive force of elastance. The resultant vector force  $F_1$  lags behind the velocity  $\dot{x}$  of the particle in its orbit by the angle  $\alpha_1$ , whose tangent is  $F_r/F_a$ . We have the planevector relation, amended from (347)

$$(351) \quad f - sx - r\dot{x} - m\ddot{x} = 0 \quad \text{inst. dynes } \angle,$$

or

$$(352) \quad f + j\dot{x}s/\omega - r\dot{x} - j\dot{x}m\omega = 0 \quad \text{inst. dynes } \angle,$$

whence

$$(353) \quad f = \dot{x} \{ r + j(m\omega - s/\omega) \} \quad \text{inst. dynes } \angle,$$

and

$$(354) \quad \dot{x} = \frac{f}{r + j(m\omega - s/\omega)} = \frac{f}{z} \quad \text{inst. kines.}$$

In the last equation,  $z$  is the impedance to the velocity, or

$$(355) \quad z = r + j(m\omega - s/\omega) \quad \frac{\text{dynes}}{\text{kine}}, \text{ or mech. abohms } \angle;$$

also

$$(356) \quad \dot{x}_m = \frac{F_m}{r + j(m\omega - s/\omega)} = \frac{F_m}{z} \quad \text{max. cy. kines } \angle,$$

where  $F_m$  is the maximum cyclic value of  $f$  in the case of rectilinear vibration, and  $\dot{x}_m$  the corresponding maximum cyclic value of the velocity  $\dot{x}$ .

We may substitute the rms. values  $F_r$  and  $\dot{x}_r$  for the maximum cyclic values  $F_m$  and  $\dot{x}_m$  in (356), where  $\dot{x}_m = \dot{x}_r\sqrt{2}$ , and  $F_m = F_r\sqrt{2}$ .

These equations express the Ohm's law relation extended to include the alternating-motion case.

It may be noted that all of the vibrational phenomena here considered have their complete analogies in the alternating-current  $\mathcal{E}RS$  branch-circuit case (Fig. 27), when inductance  $\mathcal{L}$  is substituted for mass  $m$ , elastance  $s$  for  $s$ , resistance  $r$  for  $r$ , and emf.  $E$  for vmf.  $F$ . This correspondence between the electric and mechanical systems is helpful to follow.

If, instead of beginning with a sub-resonant angular velocity  $\omega_1$  and ascertaining what force  $F_1$  will keep the system in equilibrium, we begin by impressing a force  $F_1$  with the same angular velocity  $\omega_1$  on the system, then after the steady state has been attained, the velocity  $\dot{x}$  will become established in accordance with (354). If we take  $OF_1$ , Fig. 157, as the reference phase, or as the axis of  $X$ , then the velocity  $\dot{x}$  will lie along  $OB_1$ , leading in phase by  $\alpha_1$ , and all the other quantities will take their corresponding vector relations.

In a case of circular vibration, the impressed force would have to be maintained at an angle  $\alpha_1$  behind the instantaneous tangent, or the active component  $F_a$  would lie along the tangent  $PP'$ , while the reactive component  $F_r$  would lie along  $OP$ , to keep the superabundant elastic force in check. In a case of rectilinear vibration, the impressed force would have its maximum cyclic value  $F_m$  equal to  $f$  in the circular case, but retarded in phase by  $\alpha_1$  behind the axis of reference  $OB_1$ , which we have taken as parallel to the straight path of vibration.



between the maximum value  $F_m^2/r = \dot{x}_m^2 r$  and zero. The average value of the power will be

$$(359) \quad P = \frac{1}{2} \frac{F_r^2}{r} = \frac{1}{2} \dot{x}_m^2 r = \frac{F_r^2}{r} = \dot{x}_r^2 r \quad \text{abwatts,}$$

where  $F_r$  is the scalar rms. value of  $F$ , and  $\dot{x}_r$  is the rms. value of  $\dot{x}$  during the cycle. Consequently, the power in a resonant vibratory case is always the square of the rms. velocity multiplied by the resistance  $r$  of the medium. The energy is dissipated in the medium as heat.

In the case of sub-resonant angular velocity, Fig. 157, with circular vibration, the reactive component  $F_r$  of the impressed force  $F$ , being in quadrature to the velocity  $\dot{x}$ , exerts no power. It is merely engaged in maintaining the superabundant reactive component of elasticity in static equilibrium. On the other hand, the active component  $F_a$  exerts power, and does work just as in the resonant case. The energy expended by  $F_r$  is zero at all times in the steady state, while that expended by  $F_a$  corresponds to the active power and to the elapsed time. In the rectilinear case, however, the reactive component  $F_r$  expends energy or delivers power to the system in one part of the cycle and restores energy or absorbs power from the system in the remainder of the cycle, the total reactive energy being zero during one complete cycle of the steady state. The active component  $F_a$  delivers power and dissipates energy from the system into the frictional medium just as in the resonant case, except that, instead of being uniform at all times, the active power delivery varies alternately between a maximum and zero.

The maximum rate of active power delivery is

$$(360) \quad P_{am} = \frac{F_a^2}{r} = \dot{x}_m^2 r = \omega^2 r x_m^2 \quad \text{abwatts.}$$

The maximum rate of reactive power delivery is

$$(361) \quad P_{rm} = F_r^2/x = \dot{x}_m^2 x = \omega^2 x x_m^2 \quad \text{abwatts,}$$

where the mechanical reactance is

$$(362) \quad x = m\omega - s/\omega \quad \text{mech. abohms.}$$

Active power is thus engaged in sending energy out of the system into the medium. It is always positive or plus. Its average value in the cycle is half the maximum value  $P_{am}$ . Reactive power is zero in the circular case, and alternately plus and minus in the cycle. It is engaged during the one interval in storing energy in the system, and in the other interval in reabsorbing this stored energy.

Although the power and energy relations of a vibrational system are not vectorially directional, in the same sense as the forces, displacements, and velocities, there are great systematic advantages in considering power and cyclic energy as plane-vector quantities. The vector

power  $P$  then contains, as its real part, the active or dissipatory component  $P_a$ , while its imaginary part is the reactive component  $P_r$ , which is the internal activity of the system and which is conserved. Thus (362a)

$$P = P_a + jP_r \quad \text{abwatts } \angle;$$

see formulas (116), (117), (128), (177), (179), (264) and (265).

**Steady-State Vector Diagrams of Forced Vibrations at Constant Impressed Frequency.**—A simple and convenient method for following the quantitative relations in a simple single-frequency forced-vibration *mrs* system, is to prepare a set of schedule vector diagrams, like those which are correspondingly applicable to a simple *ERS* a.-c. system.\* Such a set of diagrams is presented in Fig. 158a, for the case of a simple vibrator having the following constants: Mechanical impedance  $z = 80 + j60 = 100 \angle 36^\circ 52' 11''$  vector mech. abohms, see triangle *ABC*. The vibromotive force  $F = 1000$  dynes rms., or 1414 max. cy. dynes, at an impressed angular velocity  $\omega = 1000$  rad. per sec., corresponding to an impressed frequency of  $f = 159.1 \sim$ . The velocity  $\dot{x}$ , set up by  $F$  in the system, will be  $10 \angle 36^\circ 52' 11''$  kines rms., see triangle *def*, or 10 kines, lagging by this phase behind the impressed vmf. *of*. The mechanical activity or power in the system will be either  $8000 - j6000$  or  $8000 + j6000$  abwatts (triangles *ghk* or *GHK*), according as this power is referred to *of* or *OV*, as standard phase. The maximum cyclic energy is likewise either  $4 - j3$  or  $4 + j3$  ergs, according to the standard of phase selected.

In the case of Fig. 158a, the system has preponderating inertia reactance, with the slopes of  $F$  and  $z$  positive. If, however, the reactance should be negative, the slopes of the triangles  $z$  and  $F$  would be negative, while those of  $y$  and  $\dot{x}$  would become positive.

**Complete Solution including a Transient Initial Velocity.**—Equations (353) and (354) express the dynamic solution of a case of simple circular or simple rectilinear vibration under an impressed vector force  $F$  in the steady state, or the steady-state solution of the differential equation

$$(363) \quad f = |F| e^{j\omega t} = sx + r\dot{x} + m\ddot{x} \quad \text{dynes } \angle.$$

The complete solution of this equation in terms of the velocity  $\dot{x}$  is

$$(364) \quad \dot{x} = \frac{|F| e^{j\omega t}}{r + j(m\omega - s/\omega)} + \dot{x}_t e^{-t\omega_0 \gamma} \quad \text{kines } \angle$$

$$(365) \quad = \frac{F}{z} + \dot{x}_t e^{-t(\Delta - j\omega_p)} = \frac{F}{z} + \dot{x}_t e^{-t(\Delta - j\omega_0 \sqrt{1 - B_0^2})} \quad \text{kines } \angle,$$

where  $\dot{x}_t$  is a certain vector initial velocity at  $t = 0$ , or an arbitrary velocity constant. The time  $t$  is chosen from the proper epoch. Here  $B_0 = \Delta/\omega_0$  is the oscillatory bluntness of the system.

\* Bibliography 34 and 71, page 126.

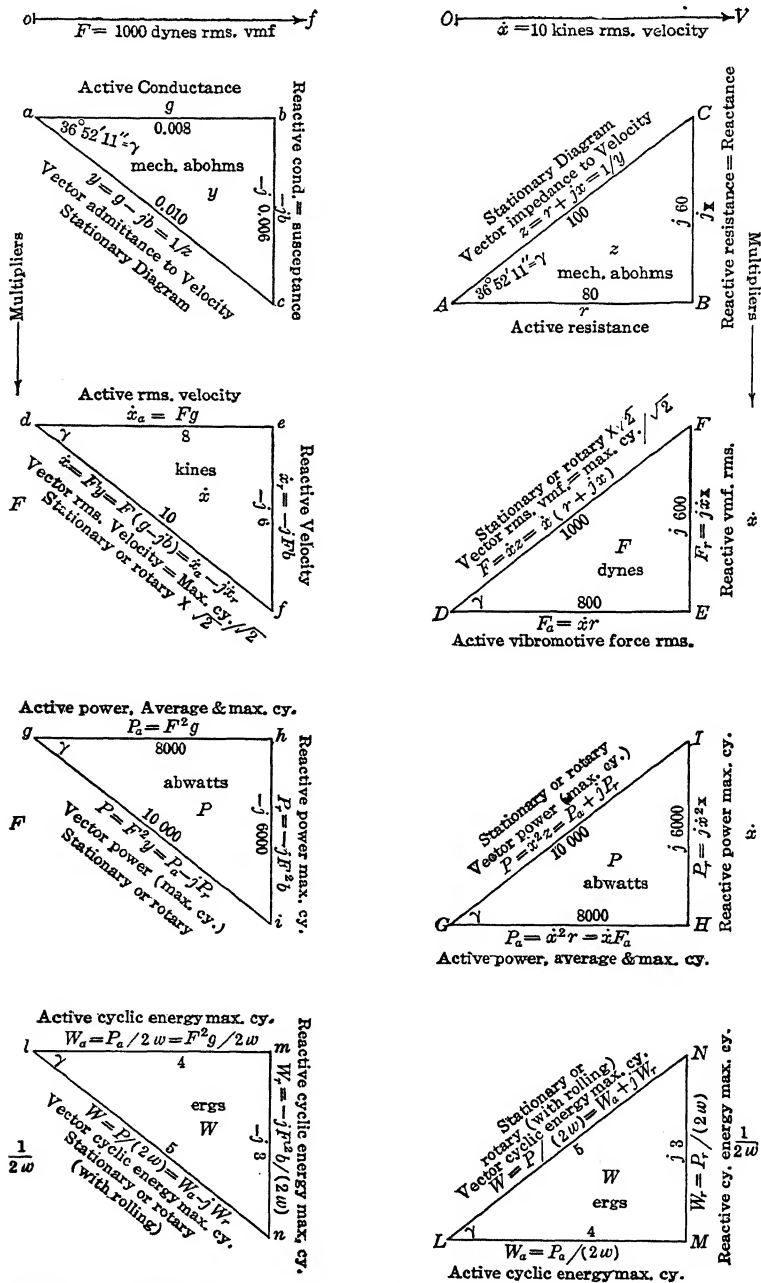


FIG. 158a. Vector diagrams for forced vibrations in a simple *mrs* mechanical system under constant impressed frequency.

The first term in (365) expresses the steady-state solution, as already found in (354). The second is a transient term, and expresses a temporary or evanescent condition which rapidly dies away. The second term differs from the first, not only in its temporary character, but also in possessing a different angular velocity, i.e., the angular velocity  $\omega_0 \nless \gamma$  of free vibration, and which is independent of the impressed angular velocity  $\omega$ . The free angular velocity  $\omega_0 \nless \gamma$  is a complex quantity, and will be considered in Appendix IV.

The quantity  $\dot{x}_i$  in (364) is an initial vector velocity satisfying the dynamic conditions of a suddenly impressed change in vmf. For example, if the vmf. is suddenly applied to a system previously at rest, then at the instant of application, it is evident that the initial velocity  $\dot{x} = 0$ , because the velocity cannot instantly and discontinuously change from zero to a finite value. Consequently  $\dot{x}_i$  must be equal and opposite to the velocity  $F/z$  which should pertain to the steady state at the instant of application. The case is considered further in Appendix IV.

**Dynamic Illustration in the Case of an Unbalanced Shaft.** — The foregoing principles receive illustration in the well known dynamical case of an unbalanced shaft. Figure 159 represents at  $SS_1$  a steel shaft in longitudinal section through the axis. It is mounted in bearings  $BB$ , and carries a symmetric pulley  $P$ , by which it may be belt driven in either direction of rotation, at adjustable speeds. At the lower part of the figure is an enlarged cross-section of the shaft with a vector diagram of forces.

We may suppose that the shaft is so formed and constituted that it may be considered as perfectly symmetric about its axis, except for a single excessive mass  $m'$ , situated at a certain radial distance  $a$  from the axis. When the shaft is rotated at a uniform angular velocity  $\omega$  radians per second, this unbalanced mass  $m'$  develops a force  $F$  along its own radius, of  $m'a\omega^2$  dynes. This force will tend to throw the mass of the

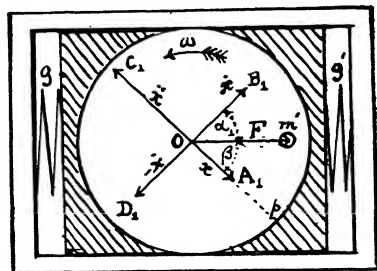
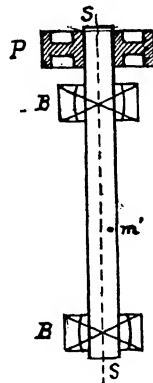


FIG. 159. Unbalanced rotating shaft and its vector diagram.



shaft at any moment in the instantaneous direction of the radius  $Om'$ .

If the bearings are supposed to be set up tightly in the vertical direction, but to admit of a certain small amount of elastic play in the horizontal plane, then the geometric constraints may be regarded as equivalent to those in the lower part of the figure, where the stiff springs  $gg'$  resist the lateral motion of the shaft with an elastic coefficient  $s$  dynes per cm. of displacement. The displacement produced in a direction perpendicular to the axis of the springs  $gg'$  is negligible, because the elastic forces in the perpendicular direction are much greater. Under these conditions, the centrifugal force  $F$  will set up a horizontal vibromotive force on the shaft, whose maximum size is equal to  $m'\omega^2$ , and whose phase is that of the radius  $Om'$ .

The resonant angular velocity of rotation will be  $\omega_0 = \sqrt{s/m}$  where  $m$  is the effective mass of the shaft entering into vibration. Unless  $s$  is unusually small, by reason of weak equivalent springs  $gg'$ , in the bearings, this angular velocity is likely to be high. If the shaft is driven by a belt at an angular velocity  $\omega$ , in the direction of the arrow, we may assume at the outset that this is a sub-resonant angular velocity, and the vector diagram of Fig. 157 will apply to it. We may therefore take the force  $F = OF_1$ , Fig. 157, as horizontal, or at standard phase, and correspondingly draw in the lines  $OA_1$ ,  $OB_1$ ,  $OC_1$ , and  $OD_1$  on Fig. 159, noting that the angle  $\alpha_1$  with which the vibration velocity  $\dot{x}$  leads the force, is at present unknown. This angle  $\alpha_1$  will be  $90^\circ$  at a very small angular velocity, and will fall to zero when  $\omega = \omega_0$ .

With the shaft rotating steadily at angular velocity  $\omega$ , the vmf. of the unbalanced mass will produce a horizontal vibratory displacement  $x$  in the bearings, and also a horizontal vibratory velocity  $\dot{x}$ . The shaft will throb in its bearings with a total amplitude of displacement of  $2x_m$  cm., where  $x_m$  is the maximum cyclic value. The vector direction of the velocity  $\dot{x}$  will be along  $OB_1$ , with the frictional retarding force along  $OD_1$ . The vector direction of the displacement  $x$  will be along  $OA_1$  as also will be the vector force of inertia. Opposite to  $OA_1$  will be  $OC_1$ , the vector direction of the elastic force opposing displacement. The two directions  $A_1OC_1$  and  $B_1OD_1$  will always be mutually perpendicular, but their joint relations with the unbalanced force  $OF$  depend upon  $\omega$ , being such that

$$(366) \quad \tan \alpha_1 = \frac{m\omega - s/\omega}{r}.$$

None of the quantities  $m$ ,  $r$  and  $s$  is likely to be known under the conditions of the test. All we know is that the maximum cyclic displacement of the shaft will lag behind the unbalanced force by some angle  $\beta = 90^\circ - \alpha_1$ , which is zero at a vanishingly low angular velocity  $\omega$ , but increases to  $90^\circ$  at resonance.

If now a piece of chalk, or a lead pencil, is presented carefully towards the shaft near  $m'$  in the horizontal plane, the pencil will first touch the surface of the shaft, at the instants of maximum cyclic displacement, in the direction from which the pencil approaches. At these instants, the shaft will present the surface line through  $p$ , to the horizontal pencil, because that will be the phase position of maximum cyclic displacement with respect to the unbalanced mass  $m'$ . Consequently, if the pencil is carefully presented in the horizontal plane to the rotating shaft, until it just touches, and is then withdrawn, the shaft will receive a pencil mark at a point on its surface  $\beta^\circ$  behind the radius  $Om'$  of unbalanced mass. With the shaft brought to rest, the pencil mark should be perceptible, but the angle  $\beta^\circ$  is still unknown.

If now the pulley  $P$  is driven in the opposite direction, as may be done by crossing the belt, which should be quite smooth and free from irregularities, the same angular velocity  $\omega$  imparted to the shaft in the opposite direction will give rise to a reversed vector diagram, such as would be seen by regarding Fig. 159 in a horizontal mirror, with the plane of the page vertical. At the correct speed, the pencil brought up to the shaft as before, will give a mark at the point of maximum cyclic displacement  $p$ , which will lag by the same angle  $\beta^\circ$  behind  $Om'$ , but will lie oppositely on the oppositely rotating shaft. When the shaft is brought to rest, the two pencil marks should subtend at the axis an angle of  $2\beta^\circ$ , and midway between them should be the radius  $Om'$  of unbalanced mass. A counterpoise of the proper amount should then be applied opposite to this midpoint, in order to reduce the shaft to the balanced condition.

If the impressed angular velocity  $\omega$  happened to be super-resonant instead of sub-resonant, the only change in the effect produced from this standpoint would be an angle  $\beta^\circ$  greater than  $90^\circ$ . The arc  $2\beta^\circ$  would be greater than  $180^\circ$  but the middle of the arc should still coincide with the radius of unbalanced mass  $Om'$ . In practice, cases present themselves where it is uncertain whether  $m'$  lies at one end or the other of a diameter through  $Om'$ . In such cases, marks with chalks of different colors made at successive measured velocities  $\omega$ , may remove the uncertainty.

Theoretically, it would be possible to find the radius  $Om'$  of unbalance by increasing the impressed angular velocity to the resonant value, when the pencil-mark radius would be in lagging quadrature to  $Om'$ . Resonance in such cases is supposed to be detected by the maximum vibratory throb. Actually, however, maximum vibration may not coincide with the resonant angular velocity, partly because of the fact that maximum displacement does not occur at  $\omega_0$ , partly because the force  $F$  increases with  $\omega$ , thus tending to produce a greater throb somewhat above resonance, and partly due to secondary mechanical reactions, such as the bending of the shaft under the impressed unbalanced forces. The

test by reversed velocities is therefore more reliable, as a rule, than the test by resonance in one and the same direction of rotation.

In practice, the dynamical conditions are apt to be more complex than those above discussed, because very frequently the unbalanced masses, instead of being single, as here assumed, are multiple. However, the single unbalanced-mass case can easily be experimented with in the laboratory, and is introduced here for the purpose of illustration.

# ANGULAR VELOCITIES OF A SIMPLE MECHANICAL OR ELECTRIC SYSTEM

**Periodic Case.** — It has been pointed out in connection with formula (364) that when a simple mechanical system of constants  $m$ ,  $r$ , and  $s$  (or a simple electric system of corresponding constants  $\mathcal{L}$ ,  $r$ , and  $s$ ) is subjected to any sudden change in impressed vmf., a transient velocity (or current) is set up in the system, according to the expression

$$(367) \quad \dot{x} = \dot{x}_i \epsilon^{-i\omega_0 \nabla \gamma} = \frac{\dot{x}_i}{\epsilon^{i\omega_0 \nabla \gamma}} \quad \text{kines } \angle.$$

Here the exponent of the Napierian base  $\epsilon$  is the product of the elapsed time  $t$  sec. and the resonant angular velocity  $\omega_0$ , at a certain slope  $\nabla \gamma$ , which, as we shall see, depends on the  $m$ ,  $r$ , and  $s$  constants of the system. The quantity  $-\omega_0 \nabla \gamma$  is therefore a complex angular velocity, having a real component  $-\omega_0 \cos \gamma$ , and an imaginary component  $+j\omega_0 \sin \gamma$ . Such complex angular velocities present themselves in the study of free oscillations. They may therefore be examined advantageously at the outset.

**Simple Velocity of a Particle in a Circular Orbit.** — If a radius vector  $OP$ , Fig. 160, of unit length and centered at  $O$ , rotates in the  $XOY$  plane with uniform angular velocity  $\omega$  radians per second, in the positive direction  $ABC$  as viewed from  $Z$  and as indicated by the arrows, then the displacement position of the radius vector, and of its free extremity  $P$ , at any time  $t$  seconds from the start is defined by:

$$(368) \quad x = 1 \cdot \epsilon^{j\omega t} \quad \text{cm. } \angle.$$

At the initial time  $t = 0$ , the initial position of the radius vector may be taken as  $OA$ , and the circular angle  $\omega t$  radians, described in time  $t$ , will then be measured from this initial line  $OY$ , in the positive direction, or counter clockwise about  $OZ$ .

The magnitude of the angular velocity  $\omega$  may be marked off along the axis  $OZ$ , in the positive direction, as shown. If the angular velocity

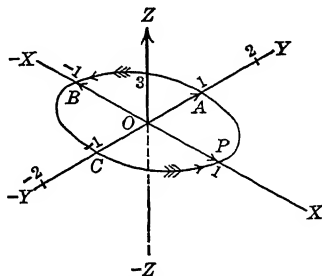
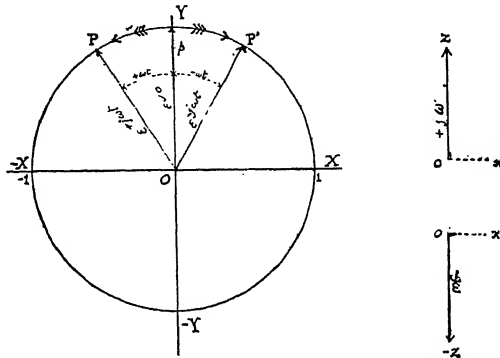


FIG. 160. Uniform circular angular velocity  $\omega$  in  $XOY$  plane about axis  $OZ$ .

should be  $-\omega$ , or negative, the motion of the radius vector would be clockwise in the  $XY$  plane, and its magnitude would be indicated in the  $-OZ$  direction.



FIGS. 161 and 162. Rotary and stationary vector diagrams of circular angular velocity.

If the motion, instead of being circular, and corresponding to simple circular vibration, should be simply harmonic, or corresponding to simple rectilinear vibration, then the orthogonal projection of the circularly moving particle  $P$  on a straight line of reference in the  $XY$  plane would represent the motion. In Fig. 161, if the initial reference line is the axis  $+OY$ , then the projection  $p$  on this line of the point  $P$ , when the latter is moving according to equation (368), will correspond to the cosinusoid

$$(369) \quad x = 1 \cdot \cos \omega t \quad \text{cm.}$$

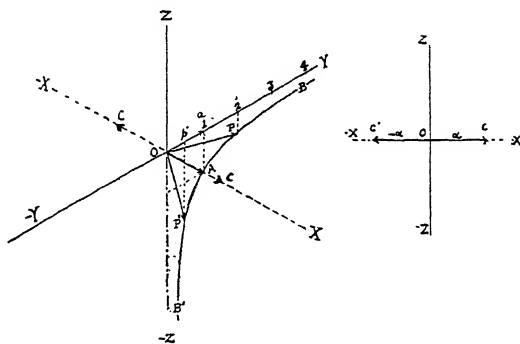
If, however, while  $P$  starts from  $OY$  at  $t = 0$ , we take instantaneous projections upon  $OX$ , considering  $-OX$  as the positive direction, the projection will move according to the sinusoid

$$(369) \quad x = 1 \cdot \sin \omega t \quad \text{cm.}$$

Figure 161 is thus a rotary-vector projection diagram, or the so-called "crank diagram," applying to a simple rectilinear vibration. We may, however, represent the angular velocity in a stationary-vector diagram by the line  $oz$  for  $+j\omega$ , and by  $o - z$  for  $-j\omega$ , Fig. 162. Here  $ox$  is a reference line in the  $XY$  plane, along the  $X$  axis, and  $oz$  is measured to a suitable scale of angular velocity along the  $OZ$  axis; so that with reference to  $OX$ ,  $oz$  is a  $j$  quantity.

**Significance of the Sign of  $j\omega$ .**—In the case of a simple circular vibration, the direction of rotation is distinctive, and the proper sign of  $\omega$ , as  $+j\omega$  or  $-j\omega$ , must be conserved. In the ordinary case, however, of a simple rectilinear vibration, the direction of rotation may have

no significance, if the projection axis is suitably selected. Thus, in Fig. 161, if starting from  $OY$  at  $t = 0$ , two unit vectors begin to rotate in opposite directions, after any time  $t$  seconds, one will have described the angle  $YOP = +\omega t$  radians, and the other the angle  $YOP' = -\omega t$  radians. The projection of either of these points  $P$  and  $P'$  on the  $OY$  reference axis will be the same, at  $p$ . So far as the cosinusoid (369) is concerned, it is therefore a matter of indifference as to which direction of rotation is used. Either of the two stationary vectors  $+j\omega$  or  $-j\omega$  would represent the motion. In the case of the sinusoid (370), the reference projection axis would be  $-OX$  in the one case, and  $OX$  in the other; but the result would be otherwise the same. At most, therefore, the difference between  $+j\omega$  and  $-j\omega$  as angular velocities, would be a phase difference in the simple harmonic projected motion. If then in a discussion of rectilinear vibration, we meet with an algebraic expression  $e^{\pm j\omega t}$ , where the sign of the exponent is indeterminate, we may interpret it as corresponding to a simple harmonic motion, or rectilinear vibration, of circular angular velocity  $\omega$  radians per second, the sign adopted being either insignificant, or selected to suit the phase of some other circumstance.



FIGS. 163 and 164. Hyperbolic angular velocities and their projections  $e^{\alpha t}$  or  $e^{-\alpha t}$  with corresponding stationary vector diagram.

**Real Angular Velocities.** — Just as the expression  $e^{j\omega t}$  may be interpreted as representing a circular angular velocity  $\omega$ , or an imaginary angular velocity  $j\omega$ ; so the expression  $e^{\alpha t}$  may be interpreted as representing a hyperbolic angular velocity  $\alpha$ , or a real angular velocity  $+\alpha$ . This interpretation may be illustrated as in Fig. 163, where a rectangular hyperbola  $BAB'$  is drawn in the  $YOZ$  plane, with its vertex  $A$  at coordinates  $Y = +1$ , and  $Z = -1$ . If a vector centered at origin  $O$  and initially at  $OA$  moves along this hyperbola in the positive direction  $AB$ , at a uniform hyperbolic angular velocity,  $\alpha$  hyperbolic radians (hyps.) per second, it will describe equal areas in equal times, and its perpendicular projection at any time  $t$  seconds on the axis  $OY$ , will measure  $e^{\alpha t}$  units of

length. Thus in Fig. 163, at time  $t = 0$ , the projection of the initial vector  $OA$  is  $Oa = 1 = \epsilon^0$ . After a time  $t$ , such that  $\alpha t = 0.693$  hyperbolic radians, the radius vector has advanced to the position  $OP$ , and its projection will be  $Op = 2 = \epsilon^{0.693}$ .

If, on the other hand, the hyperbolic angular velocity is reversed, the radius vector initially at  $OA$ , will move in the clockwise or negative direction towards  $B'$ , describing equal areas in equal times. After any elapsed time  $t$ , the radius vector having reached  $OP'$  say, its projected position will be  $Op'$  along the axis  $OY$ , and  $Op' = \epsilon^{-\alpha t} = 0.5$ , with  $-\alpha t = -0.693$ , the enclosed sector area  $AOP'$  being 0.693 units of area.

Consequently, just as the projection of a uniform imaginary or circular angular velocity  $j\omega$ , upon a coordinate axis, traces a simple harmonic motion of the type  $\cos \omega t$ : so the projection of a uniform real hyperbolic angular velocity  $\alpha$ , upon a coordinate axis, traces either a simple damped motion or an expanding motion, of the type  $\epsilon^{-\alpha t}$  or  $\epsilon^{+\alpha t}$ , respectively.

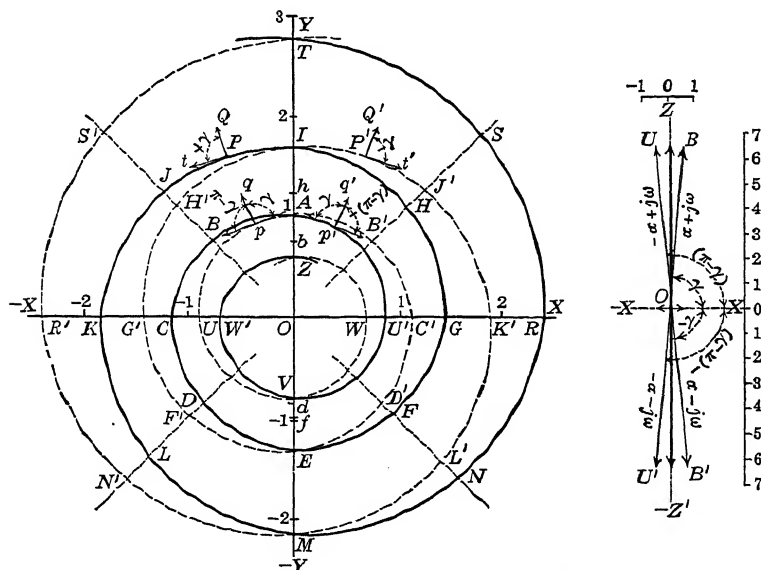
The magnitude of the hyperbolic angular velocity  $\alpha$  may be marked conveniently as  $OC$ , along the axis  $OX$  of positive rotation in the hyperbola. If the angular velocity  $\alpha$  should be negative, the axis of rotation in the hyperbola is reversed, and falls along  $O - X$ ; so that the magnitude of the velocity is correspondingly  $OC'$ .

The hyperbola, radius vector, and plane  $YOZ$ , Fig. 163, form a rotary-vector diagram for the case of a simple damped motion having the real angular velocity of  $-\alpha$  hyps. per sec. This diagram is the analogue of the circle radius vector and plane  $XOY$ , Fig. 161, for the case of a simple undamped harmonic motion having the imaginary angular velocity  $\pm j\omega$  circular radians per second.

In Fig. 164, we have the corresponding stationary vector diagram. For a positive real angular velocity  $+\alpha$ , we draw  $oc$  of  $\alpha$  units length along the  $OX$  axis. For a negative velocity  $-\alpha$ , we draw  $oc'$  of  $\alpha$  units length along  $-OX$ .

**Complex Angular Velocity, or Combined Damped and Harmonic Vibration.** — If we combine a simple circular angular motion  $\epsilon^{\pm j\omega t}$ , like that of Figs. 161 and 162, with a simple hyperbolic angular motion  $\epsilon^{\pm \alpha t}$ , like that of Figs. 163 and 164, we obtain a combined hyperbolic and circular angular motion, of the type  $\epsilon^{(\pm \alpha \pm j\omega)}$ , or  $e^{nt}$ , where  $n$  is a complex angular velocity, having both real and imaginary components. This case is represented in Fig. 165, where the unit vector  $OA$ , coinciding with the  $OY$  axis at time  $t = 0$ , begins to revolve in the  $XY$  plane, either clockwise or counter-clockwise, according as the circular angular velocity is  $-j\omega$  or  $+j\omega$  radians per second. At the same time, the rotation of the vector  $OA$  of Fig. 163, in a hyperbola occupying the  $YOZ$  plane with angular velocity  $\alpha$  hyps. per sec. causes the projected radius to expand at the rate  $e^{\alpha t}$ . This increase is supposed to be communicated at each moment to the radius vector  $OP$  rotating in the  $XOY$  plane. The resulting motion is an

expanding spiral, which is known geometrically either as a hyperbolic spiral, or an equiangular spiral. Thus, with  $\alpha = +0.5$ , and  $\omega = 2\pi = 6.283$ , the radius vector with positive  $\omega$  will pursue the path  $ABCDEFGHI$ , during one second of time. After one complete revolution in the  $XOY$  plane, the radius vector has increased from  $OA$  to  $OI$ , or from  $e^0$  to  $e^{0.5} = 1.649$ . If, on the other hand, the circular angular velocity is  $-j\omega$ , or negative, the corresponding path will be  $A'B'C'D'E' \dots R'S'T'$ . In either case, the projected positions on the  $OY$  axis at successive eighths of a second will be  $A, b, O, d, E, f, O, h, I$ . This rectilinear motion may be described as an expanded cosinusoid  $e^{\alpha t} \cdot \cos \omega t$ . It is evident that the cosinusoid will be the same, whichever direction of rotation may be selected in  $\omega$ .



FIGS. 165 and 166. Rotary and stationary vector diagrams of a complex angular velocity  $(\pm \alpha \pm j\omega)$ .

If the hyperbolic angular velocity  $\alpha$  is negative, the projection of the hyperbolic radius vector will shrink with time according to the expression  $e^{-\alpha t}$ . This shrinkage being communicated to the rotating vector in the  $XY$  plane, we obtain the contracting spirals  $AUVWZ$ , or  $AU'VW'Z$ , according as  $\omega$  is positive or negative. These curves are also equiangular spirals, and are the inward continuations of the expanding spirals already described for the expanding case. The projected motion of the radius vector on the  $OY$  axis will be a damped cosinusoid  $e^{-\alpha t} \cdot \cos \omega t$ . Consequently, although the sign of  $j\omega$  does not affect the cosinusoidal motion, the sign of  $\alpha$  changes the motion from an expanding cosinusoid to a con-



tracting or damped cosinusoid. In one second, for the case selected in Fig. 165, the circular angle  $\omega t$  described will be  $2\pi$  radians, or one revolution in the  $XY$  plane; while the hyperbolic angle as described will be 0.5 hyp. in the  $YZ$  plane. The vector will have passed from  $OA = 1.0$  to  $OZ = 0.6065$ . It will thus have lost 39.4 per cent of its amplitude in one cycle, and each successive cycle will be attended by a similar loss of 39.4 per cent of what remains.

**Stationary-Vector Diagram of Complex Angular Velocity.** — Figure 165, based upon associated rotations in the  $XY$  and  $YZ$  planes, may be regarded as a rotary-vector diagram for a complex angular velocity. The projection of the spirally rotating point upon a properly selected axis gives the required expanding or contracting harmonic motion. The corresponding stationary vector diagram appears in Fig. 166, where  $OB = \alpha + j\omega$ ,  $OB' = \alpha - j\omega$ ,  $OU = -\alpha + j\omega$ , and  $OU' = -\alpha - j\omega$ . Here the real component of hyperbolic angular velocity is taken along the  $OX$  axis, as in Fig. 164, and the imaginary component  $j\omega$  of circular angular velocity along the  $OZ$  axis, as in Fig. 162.

It may be observed that, in each case, the slope of the stationary vector in Fig. 166 is the same as the slope which the advancing tangent to the corresponding spiral in Fig. 165 makes with the radius vector as reference line. Thus  $OB$ , Fig. 166, makes a slope of  $\gamma$  degrees or radians with  $OX$ . The curve of  $\alpha + j\omega$  in Fig. 165 is the heavy expanding spiral  $ABCD \dots$ . At any point  $P$  on this spiral, the advancing tangent  $Pt$  has the same slope  $\gamma$ , with respect to the instantaneous radius vector  $OPQ$ . Similarly  $OB'$ , Fig. 166, has a slope of  $-\gamma$ , which is the same as the tangent  $P't'$  has with respect to  $OP'Q'$ . In other words, the slope of the vector angular velocity, in the stationary-vector diagram, is the same as the slope of the equiangular spiral in the corresponding rotary-vector diagram.

**Conjugate Pairs of Complex Angular Velocities.** — From the foregoing, it will be seen that the conjugate pair of angular velocities  $\alpha \pm j\omega$ , when referring to a simple vibrating system with one degree of freedom (rectilinear or angular) jointly define an expanding vibration. The sign of the imaginary is indifferent, if the projection axis is properly selected. Expanding vibrations relate to reinforced oscillations, and rarely present themselves in cases of free vibration. The conjugate pair  $-\alpha \pm j\omega$  jointly define a contracting vibration, or damped harmonic motion. The projected motion of  $e^{(-\alpha \pm j\omega)t}$  is  $e^{-\alpha t} \cdot \cos(\omega t + \beta)$ , where  $\beta$  is some phase angle appropriate to the projection axis. Damped vibrations of this kind very frequently present themselves in the study of free electric or mechanical vibrations.

Since

$$(370) \quad e^{-(\alpha \pm j\omega)t} = \frac{1}{e^{(\alpha \pm j\omega)t}}$$

it follows that a damped or contracting harmonic vibration is the vector

reciprocal of an expanding harmonic vibration of the same components  $\alpha$  and  $\pm j\omega$ . On the rotary diagram, both pertain to the same equiangular spiral, traversed respectively in opposite directions. In the stationary diagram, the vectors have equal sizes and opposite slopes. Reversing the sign of a complex angular velocity reverses the direction of both real and imaginary components. The reversal of the imaginary component may have no effect upon the projected motion; but the reversal of the real component changes the motion from expansion to contraction, or *vice versa*.

#### Application of Complex Angular Velocities to Transient Vibrations. —

Returning to equation (364) we see that the transient term is

$$(371) \quad \dot{x} = \dot{x}_t \cdot e^{-i\omega_0 \nabla \gamma} \\ = \dot{x}_t e^{i\omega_0 \angle (\pi - \gamma)} \quad \text{kines } \angle.$$

The angular velocity  $\omega_0 \angle (\pi - \gamma)$  is a complex quantity of size  $\omega_0 = \sqrt{s/m}$ , the resonant value, and of slope  $(\pi - \gamma)$  whose cosine is

$$(372) \quad \cos(\pi - \gamma) = \cos - (\pi - \gamma) \\ = -\cos \gamma = -\frac{\Delta}{\omega_0} = -B_0,$$

or

$$(373) \quad \cos \gamma = \frac{\Delta}{\omega_0} = B_0.$$

This is represented in Fig. 167 by the plane-vector  $OU$ . The conjugate value is  $OU' = \omega_0 \nabla (\pi - \gamma)$  hyps. per second.

$OV = \Delta = \frac{r}{2m}$  is called the damping

constant of the system. It will be seen that vectorially,

$$(374) \quad \omega_0 \nabla (\pi - \gamma) = -\Delta - j\omega_f \quad \frac{\text{hyps.}}{\text{sec.}} \angle,$$

or

$$(375) \quad 1 \nabla (\pi - \gamma) = -B_0 - ju_f,$$

whence

$$(376) \quad \omega_f = \sqrt{\omega_0^2 - \Delta^2} = \omega_0 \sqrt{1 - B_0^2} = \omega_0 \sin \gamma \quad \frac{\text{rad.}}{\text{sec.}},$$

and

$$(377) \quad u_f = \sqrt{1 - B_0^2} = \sin \gamma,$$

Consequently, to find the circular angular velocity  $\omega_f$  of free vibration, geometrically, draw (Fig. 167) the circle  $Z - X - Z$ , with radius  $\omega_0$ . Along  $O - X$  mark off  $OV$ , the numerical value of  $\Delta = r/(2m)$ , the damping constant. The ordinate through  $V$  which meets the circle in  $U$  or  $U'$

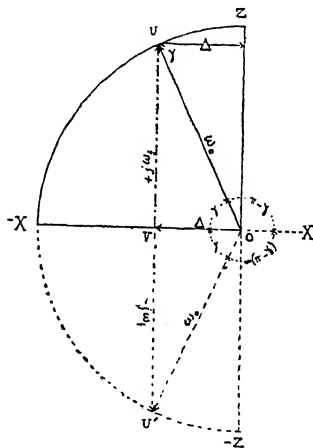


FIG. 167. Stationary vector diagram of free angular velocity. Damped.

is the required free angular velocity  $\omega_f$ , in circular radians per second. Either of the two conjugate values  $\pm j\omega_f$  may be used, with the proper selection of phase.

**Undamped Vibration.** — In the ideal case of a vibratory system without resistance, energy losses, or damping,  $\Delta = 0$ , and  $\omega_f = \omega_0$ . The vector diagram becomes that of Fig. 168, where the angular velocity is a pure  $j$  quantity,  $ou$  or  $ou'$ , equal to the resonant angular velocity  $\omega_0$ . The slope  $\gamma$  is then  $\pm \pi/2$  radians, or  $\pm 90^\circ$ . This case is considered particularly in Appendix VI.

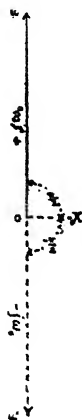


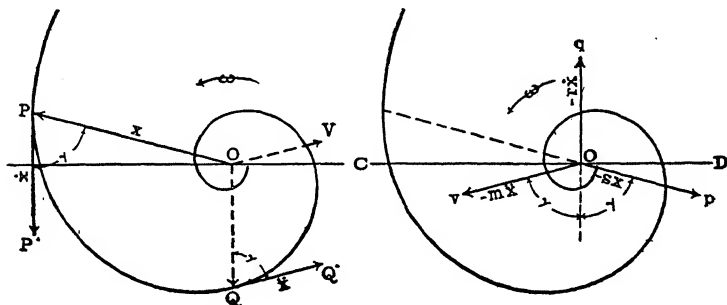
FIG. 168. Undamped. Stationary-vector diagram of freeangular velocity.

**Aperiodic Case.** — As the damping increases, the real component  $\Delta$ , Fig. 167, increases and  $\omega_f$  diminishes, the vector  $OV$  rotating counterclockwise towards  $O - X$ . When  $\Delta = \omega_0$ , or  $B_0 = 1$ ,  $\omega_f = 0$ , and there ceases to be any circular angular velocity, or to-and-fro vibration. The angular velocity may be regarded as wholly hyperbolic. This may be called the aperiodic case. It is the case of unit bluntness of resonance  $B_0 = 1$ , or of unit sharpness  $\Lambda_0 = 1$ . It is usual to regard any non-periodic vibration as aperiodic, i.e., to consider as aperiodic any case whose sharpness  $\Lambda_0$  of resonance does not exceed unity. There are, however, as we shall see, certain advantages in restricting the term aperiodic to the case  $\Lambda_0 = B_0 = 1$ .

Although all kinds of free vibration present themselves in practice, from cases where  $B_0$  is very small, to cases where  $B_0$  approaches unity, yet, in order to develop the properties of free vibration,  $B_0$  must be small compared with unity, or the damping must be small. Otherwise, the vibrations may disappear so quickly as to leave little evidence of their existence. In general, a freely vibrating system is one in which  $B_0$  is not greater than say  $\pi/100$ , or 0.031, the logh. decrement  $\delta$  not greater than 0.2,  $\gamma$  not less than  $88^\circ$ , and  $u_f$  not less than 0.9995. If the free frequency is not over 99 per cent of the resonant frequency, the damping is so great that only a very few cycles of vibration can ordinarily be distinguished on the record.

**Vector Diagram of Damped Vibrations.** — In Fig. 169, let a particle at  $P$ , of mass  $m$  gm., be attracted centripetally towards  $O$ , with an elastic force varying directly as the size of the displacement  $x$ , and be subjected to a frictional retarding force opposite to the instantaneous velocity  $\dot{x}$ , as well as to an inertia force opposite to the acceleration  $\ddot{x}$ . Then, because there is no impressed force to give energy to the particle, energy will continually be absorbed from it, and the orbit of the particle will dwindle, until finally the particle will fall to rest at  $O$ . This means that

the orbit, instead of being a circle, will be an equiangular spiral, in which the tangent  $PP'$  at any orbital position  $P$ , makes an angle  $\gamma$ , less than  $90^\circ$ , with the reversed radius vector  $PO$ . The instantaneous acceleration will be directed along the tangent  $QQ'$  of the spiral, at the point  $Q$ ,  $(180^\circ - \gamma)$  in advance of  $P$ . The centripetal force will thus be directed along  $PO$ , the frictional force along  $P'P$ , or parallel to  $QO$ , and the inertia force along  $Q'Q$ , or parallel to  $VO$ .



FIGS. 169 and 170. Loci of damped oscillatory displacement, velocity and acceleration force.

These force vector relations are indicated in Fig. 170, where  $Op$  is the centripetal force  $-sx$  dynes,  $Oq$  is the frictional force  $-r\dot{x}$ , and  $Ov$  the inertia force  $-m\ddot{x}$ ,  $x$  being the instantaneous displacement in cm.

$$(378) \quad x = x_t e^{(-\Delta + j\omega')t} \quad \text{cm. } \angle,$$

where  $\omega' = \omega_f$  is the free angular velocity of the particle about  $O$  in radians per second, and  $x_t$  is a properly selected initial plane-vector displacement at  $t = 0$ .

Hence

$$(379) \quad r\dot{x} = r(-\Delta + j\omega')x_t e^{(-\Delta + j\omega')t} = r(-\Delta + j\omega')x \quad \text{dynes } \angle,$$

and

$$(380) \quad m\ddot{x} = m(-\Delta + j\omega')^2 x_t e^{(-\Delta + j\omega')t} = m(-\Delta + j\omega')^2 x \quad \text{dynes } \angle.$$

For equilibrium we require that

$$(381) \quad -sx - r\dot{x} - m\ddot{x} = 0 \quad \text{dynes } \angle,$$

or

$$(382) \quad -s - r(-\Delta + j\omega') - m(-\Delta + j\omega')^2 = 0 \quad \frac{\text{dynes}}{\text{cm.}} \angle,$$

whence

$$(383) \quad \omega' = \sqrt{\omega_0^2 - \Delta^2} = \omega_0 \sqrt{1 - B_0^2} = \omega_0 \sin \gamma = \omega_f \quad \frac{\text{radians}}{\text{sec.}},$$

where

$$(384) \quad \cos \gamma = \frac{\Delta}{\omega_0} = B_0,$$

and  $\omega' = \omega_f$ , is the free angular velocity of rotation. Each of the vector quantities  $x$ ,  $\dot{x}$  and  $\ddot{x}$ , pursues an equiangular spiral around center  $O$ , or may be considered to pursue a circular path with uniform angular velocity  $\omega' = \omega_f$ , subject to an independently applied damping coefficient  $\epsilon^{-\Delta t}$ .

In the case of simple rectilinear vibrations, the projections of the spiral motion may be taken on a reference axis such as  $COD$ , Fig. 170. The initial vector velocity  $\dot{x}_i$  must be such as meets the physical conditions of the system at the moment of the application of the impressed vmf. After the application, the vibratory motion will be the sum of the two terms in (364), or the sum of the projections of the respective vectors in Figs. 158 and 170, the former rotating at the impressed angular velocity  $\omega$ , and the latter at free angular velocity  $\omega'$  or  $\omega_f$ . The latter motion, however, speedily expires by damping, leaving the former in the steady state, uninterfered with.

**Complete Solution in Terms of Displacement.** — Equation (364) gives the solution of the differential equation (363) in terms of velocity  $\dot{x}$ . We may however integrate for the solution in terms of displacement  $x$ .

$$(385) \quad x = \left( \frac{1}{j\omega} \right) \frac{F}{z} + x_i \epsilon^{-i\omega_f \gamma} \quad \text{cm. } \angle,$$

$$(386) \quad = \frac{F}{z} + x_i \epsilon^{-i\omega_0 \gamma} \quad \text{cm. } \angle.$$

Here  $x_i$  is an initial vector displacement chosen to meet the initial conditions.

**Generalized Complex Angular Velocities.** — An alternative method of finding the frequency of an electric or mechanical vibrating system is by the method of generalized angular velocities.

Any complex angular velocity of the type  $(\pm \Delta \pm j\omega)$  may be denoted by the symbol  $n$ . Thus

$$(387) \quad \epsilon^{(\pm \Delta \pm j\omega)t} = e^{nt}$$

where  $n$  is a complex number or plane-vector quantity. A mass of  $m$  grams, actuated by such an angular velocity, develops a vector oscillatory mass impedance of  $mn$  mechanical abohms  $\angle$ , or dynes per kine  $\angle$ . In an electric system, the corresponding vector oscillatory impedance is  $\epsilon n$  ohms  $\angle$  or abohms  $\angle$ . The proposition applies either (1) to expanding or contracting spiral vibration, (2) expanding or contracting rectilinear vibration, or (3) to expanding or contracting rotary vibration.

Similarly, the oscillatory elastic impedance of the system is  $s/n$  mechanical abohms  $\angle$ , corresponding to  $s/n = 1/(cn)$  ohms  $\angle$  or abohms  $\angle$  in the electric case. The oscillatory impedance of a resistance  $r$  remains simply  $r$ .

When  $n$  is a pure imaginary quantity  $j\omega$ , with  $\Delta = 0$ , corresponding to steady forced vibration, the oscillatory mass impedance  $mn$  becomes  $j\omega$ , and the oscillatory elastic impedance  $s/n$  becomes  $-js/\omega$ . These

are pure  $j$  quantities, which have already been discussed in dealing with the steady state. When, however,  $n$  is a complex quantity, with a real component  $\Delta$ , both the oscillatory mass impedance and the oscillatory elastic impedance cease to be pure  $j$  quantities, and are general complex quantities.

Thus, if we consider a vibratory system having the following constants  $s = 250,000$ ,  $m = 0.1$ ,  $r = 200$ ,  $B_0 = 0.632$ , its oscillatory mass impedance to a sustained angular velocity  $j\omega = j1581.14$ , would be  $jm\omega = j158.114$  mechanical abohms, and its oscillatory elastic impedance  $-js/\omega = -j158.114$ . These are simple  $j$  quantities, or ordinary mechanical reactances. At this particular frequency, they are equal and opposite, so that this is the resonant angular velocity  $\omega_0$  of the system. If, however, the angular velocity, instead of being a pure sustained circular or  $j$  quantity, contains a real or hyperbolic term, so that  $n = -1581.14 \angle 50^\circ 46' 6'' = -1000 + j1224.75$  hyps. per sec., then the oscillatory mass reactance  $mn = -158.114 \angle 50^\circ 46' 6'' = -100 + j122.475$  mech. abohms, and the oscillatory elastic impedance  $s/n = -158.114 \angle 50^\circ 46' 6'' = -100 - j122.475$  mech. abohms.

In any free oscillation, the angular velocity  $n$  is such that the total oscillatory impedance automatically reduces itself to zero. In this case

$$(388) \quad mn + \frac{s}{n} + r = 0 \quad \begin{array}{l} \text{mechanical} \\ \text{electric} \end{array} \left\{ \begin{array}{l} \text{abohms } \angle, \\ \end{array} \right.$$

whence

$$(389) \quad n = -\frac{r}{2m} \pm j\sqrt{\frac{s}{m} - \left(\frac{r}{2m}\right)^2} \quad \frac{\text{hyps.}}{\text{sec.}} \angle,$$

$$(390) \quad = -\Delta \pm j\sqrt{\omega_0^2 - \Delta^2} = -\Delta \pm j\omega_0 \sqrt{1 - B_0^2} \quad \frac{\text{hyps.}}{\text{sec.}} \angle,$$

$$(391) \quad = -\Delta \pm j\omega' = -\Delta \pm j\omega_f = -\omega_0 \angle \pm \gamma \quad \frac{\text{hyps.}}{\text{sec.}} \angle.$$

This represents a damped harmonic vibration with a hyperbolic angular velocity of  $-\Delta$ , and a circular angular velocity of  $\omega_f$ . The sign of  $j\omega_f$  is indifferent, for reasons already discussed.

Generalized angular velocities are of great service in dealing with vibration systems.\*

\* The application of generalized angular velocities to electrical and mechanical impedances, powers, etc., was pointed out by the author in 1915, Bibliography 59. For earlier references in the same direction, see, however, Heaviside, 1887, Bibl. 7, p. 373, Campbell, 1911, Bibl. 37a, Eccles, 1912, Bibl. 42 and Fleming, 1915, Bibl. 57b; also Bush, 1916, Bibl. 66a.

## FREE DAMPED VIBRATIONS OF A SIMPLE MECHANICAL OR ELECTRIC SYSTEM. PERIODIC VIBRATION

The quantitative relations affecting damped vibrations in mechanical systems are completely analogous to those which occur in electric systems. Therefore the two sets of phenomena may be studied advantageously together. There is an extensive literature on the subject, both in mechanics and in electrodynamics. The subject is usually treated algebraically with the aid of differential equations. For engineering purposes, the simplest method of treatment is perhaps with the aid of vector diagrams. These vector diagrams have their counterparts in the theory of sustained oscillations \* or alternating currents. (See Fig. 158a.) There are ten such diagrams, as presented in Fig. 171, in two series of five each; namely the  $\omega, y, \dot{x}_1, P_1, W_1$  series, and the  $\omega^{-1}, z, F_1, P_1, W_1$  series.

The problems to be dealt with ordinarily present themselves in one of the following forms. A free vibrational system has its resonant angular velocity  $\omega_0$  and its damping constant  $\Delta$  given. Its free vibration is started at time  $t = 0$ , either kinetically energized with a known initial  $\left\{ \begin{array}{l} \text{velocity } \dot{x}_1 \\ \text{current } I_1 \end{array} \right\}$ , or potentially energized with a suddenly impressed known  $\left\{ \begin{array}{l} VMF \\ EMF \end{array} \right\}$ , or with some known combination of these two kinds of energization. A transient decaying series of oscillations is thus set up. It is required to determine the state of the system at any time  $t$ , during the existence of the transient.

**Transient with Given Initial Velocity or Current.** — We may first consider the kinetically energized case of a system of known  $\omega_0$  and  $\Delta$ , starting at  $t = 0$  with a known initial velocity. In a mechanical case, this corresponds to oscillations started from rest by a sudden impulse, which establishes the given initial velocity  $\dot{x}_1$ . In an electric case, it would correspond to oscillations started in a simple  $\mathcal{E}RS$  circuit with a current of known strength flowing steadily through the inductor  $\mathcal{L}$ , from a local voltaic battery. At  $t = 0$ , the battery is suddenly disconnected, leaving the reactor to discharge into the empty condenser. For these cases we consider the  $\omega, y, \dot{x}_1, P_1, W_1$  series of Fig. 171.

\* Bibliography 34 and 71.

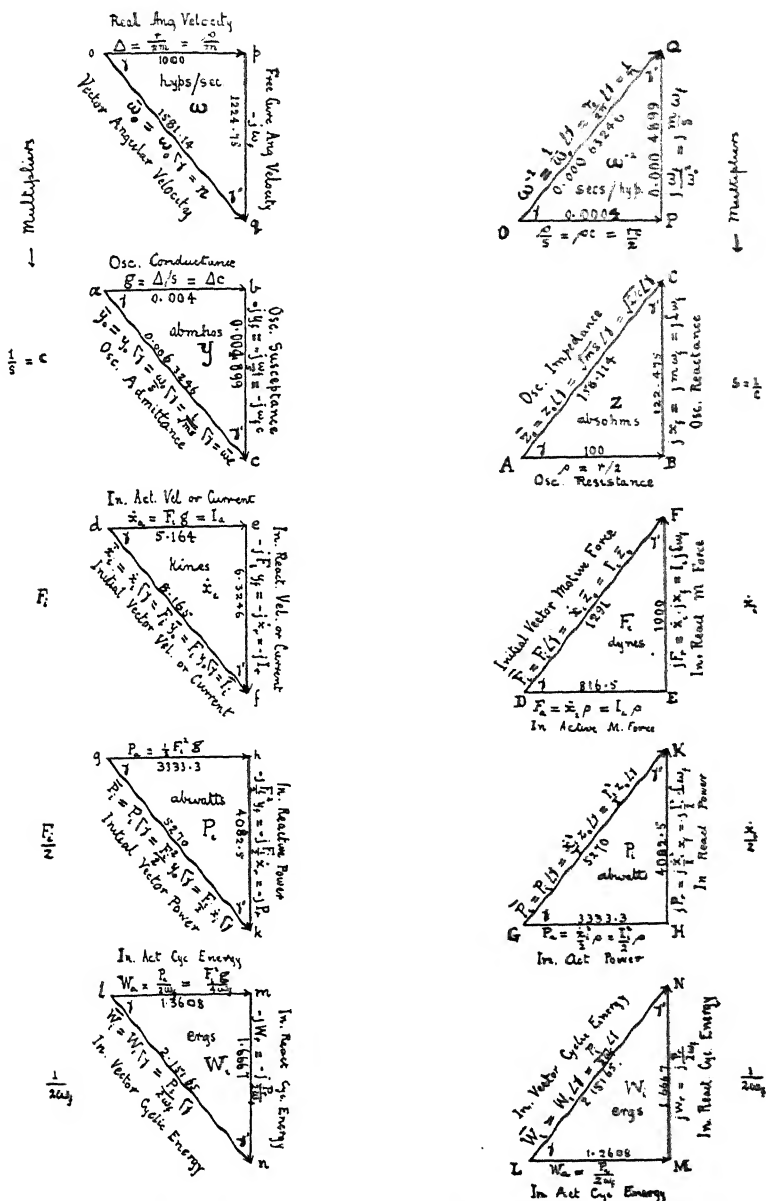


FIG. 171. Vector diagrams for damped periodic mechanical or electrical vibrations.  $B_0 = 0.632$ ,  $\gamma = -50^\circ 46' 6''$ ,  $\delta = 5.130$ .



**Vector  $\omega$  Diagram.** — Draw the right-angled triangle  $opq$ , with  $op$  horizontal, and to such a scale that its length is  $\Delta = r/2m$  (or  $r/2L$ ) hyp. per second. This represents the real or hyperbolic component of the decaying angular velocity  $\omega \propto \gamma$  of Fig. 167. Draw  $oq$ , of size  $\omega_0$ , and with the slope  $\gamma = \cos^{-1}(\Delta/\omega_0) = \cos^{-1}B_0$ . Then the third side  $pq$  is the imaginary component of the hyperbolic angular velocity; i.e., a real circular angular velocity  $-j\omega_f$ . Its size is  $\omega_f$ , the angular velocity of free vibration, in circular radians per second. With  $\Delta = 0$ ,  $pq = oq$ ,  $\omega_f = \omega_0$  and  $\gamma = 90^\circ$ .

In the case represented in Fig. 171, the system might have the constants last above specified; viz.,  $m = 0.1$  gm.,  $r = 200$  dynes per kine,  $s = 2.5 \times 10^6$  dynes per cm. Hence  $\omega_0 = \sqrt{2.5 \times 10^6} = 1581$  cir. rad. per sec., and  $\Delta = 1000$  hyp. rad. per sec. The corresponding electric case might be  $L = 0.1$  henry,  $r = 200$  ohms,  $s = 2.5 \times 10^6$  darafs, i.e., 4 microfarads. We then find  $pq$ , the angular velocity of free vibration, to be  $-j\omega_f = -j1224.75$  cir. rad. per sec. That is

$$(392) \quad \omega_f = \omega_0 \sin \gamma \quad \text{cir. radians per sec.,}$$

or

$$(393) \quad f_f = f_0 \sin \gamma \quad \text{cycles per sec.,}$$

and

$$(394) \quad u_f = \sin \gamma.$$

This would represent a highly damped system, because the oscillatory time constant would be  $\tau_0 = 1/\Delta = 0.001$  second; or the oscillations would fall to 1 eth in a millisecond, during which time only about 1/5th of an oscillatory cycle could be executed. Moreover  $\gamma = 50^\circ.46'.6''$  and  $B_0 = 0.632$ . Such a case, however, aptly illustrates the behavior of an oscillographic vibrator of low resonant frequency, operating in oil.

**Oscillatory Admittance or  $y$  Diagram.** — If we multiply the  $\omega$  diagram by  $c = 1/s$ , we obtain the corresponding  $y$  diagram, of oscillatory admittance,  $abc$ . This means that we may repeat the  $\omega$  triangle  $opq$ , but alter its scale of linear dimensions. The vector oscillatory admittance will now be  $ac$ , in this case 0.0063246 mechanical abmhos, or kines per dyne. The real component  $ab = \Delta/s$  may be called  $g$ , the oscillatory conductance, and the imaginary component  $-jy_f$ , the oscillatory susceptance. This is the susceptance which the spring offers to the impressed initial velocity  $\dot{x}_i$  at the actual free oscillation angular velocity  $\omega_f$ .

**Oscillatory Velocity  $\dot{x}_i$ ,  $\theta_i$  or Current Diagram  $I_i$ .** — If the damped system is set into oscillation with the actual initial velocity  $\dot{x}_r$ , or actual initial current  $I_r$ , then the side  $ef$  of the velocity triangle  $def$ , Fig. 171, must be given this value to scale, and the other two sides  $de$ , and  $df$  given proportional values, so as to keep the triangle  $def$  similar to  $opq$ , or  $abc$ . In other words, the scale of triangle  $opq$  must be altered in the ratio which will make  $ef$  have the correct initial velocity or current. In Fig. 171, this

initial value has been made 6.3246 kines; because it happens to be consistent with another case to be considered later. The velocity  $df$  is a fictitious vector velocity, useful for obtaining, by projection on the axis of  $ef$ , the instantaneous actual velocity, when rotated about center  $d$  with angular velocity  $\omega_f$ . Whereas the  $\omega$  diagram  $opq$ , and the  $y$  diagram  $abc$  are essentially stationary, the  $x$  or velocity diagram  $def$  may be regarded either as stationary or rotary.

The rotary application of the  $def$  triangle is illustrated in Fig. 172, where at the instant of release, or  $t = 0$ , the triangle starts from the position shown, and then rotates about center  $d$ , with uniform angular velocity  $\omega_f$ , in the direction of the arrow. The projection of  $df$  on the  $dX$  axis is then the actual initial velocity, assumed in this case as 6.3246 kines or  $do$ .

If there were no damping, i.e., if  $\Delta$  were zero, the path of the vector end  $f$ , rotating with angular velocity  $\omega_f$ , would be the circle  $fIJ$ , Fig. 172; but in the presence of damping, the path is the contracting equiangular spiral  $fmn$ . The positions of the rotating vector  $ef$  are indicated at successive sixteenths of a cycle. Instead of reaching the negative velocity  $d - X$ , the actual value is then  $db$ ; although the maximum negative value of velocity  $d4$  was reached at an earlier instant, when the rotating vector reached  $dn$ .

The velocity vector diagram  $def$ , Fig. 171, may thus be regarded either as a stationary diagram, to indicate the relative components, or as a rotary diagram, operated with angular velocity  $\omega_f$ , to indicate instantaneous values.

**Diagram of Damping Coefficients.** — It is not actually necessary, in Fig. 172, to draw in the equiangular spiral of velocity  $fmn$ . It is sufficient to draw the circle  $fIJ$  of undamped oscillation, and then apply to its instantaneous projections on  $OX$ , the proper corresponding values of the damping coefficient  $e^{-\Delta t}$ . These values may be obtained (1) by projection from a diagram of hyperbolic angular velocity as in Fig. 163, or (2) by the use of a table of logarithms, exponentials or

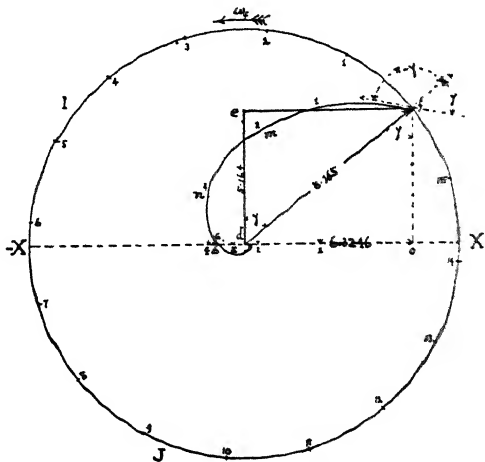


FIG. 172. Rotary-vector diagram of damped velocity or current.

other suitable functions, or (3) by the use of a damping-coefficient diagram, such as appears in Fig. 173. This is drawn on semi-logarithmic paper. The time abscissas are ruled at regular intervals, in the ordinary way. The damping-coefficient ordinates are ruled to logarithmic intervals, and may be marked off from a slide rule. The graph of  $e^{-\Delta t}$ , on such paper, is then always a straight line. In the case under consideration, the damping factor or coefficient at any time  $t$ , or time-phase angle, is found on the straight line 1A. At  $t = 0.001$  second, the value of the coefficient is seen to be 0.3679 or  $e^{-1}$ , and this should be applied to the projection of the circularly rotating vector in Fig. 172, after 1 millisecond. The result will then be the same as that given by the projection from the spiral  $fmn$  at the same instant.

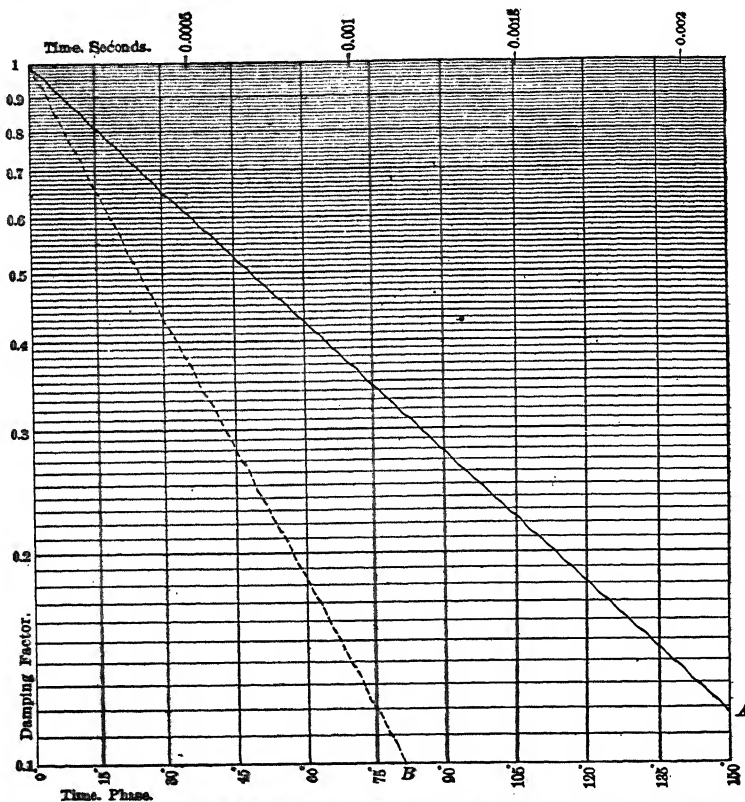


FIG. 173. Damping factors at different time-intervals after release.

**Logarithmic Decrement.** — The damping coefficient at time  $t$  being  $e^{-\Delta t}$ , the exponent is the logarithm of this coefficient to the Napierian

base  $e$ , and is commonly called the logarithm of the decrement or the *log decrement*,\* or "log dec." Denoting this by the symbol  $\delta$ , the log decrement at time  $t$  may be indicated as  $\delta_t$ , the damping factor or coefficient being  $e^{-\Delta t} = e^{-\delta_t}$ . The exponent is

$$(395) \quad \delta_t = \Delta t.$$

The simplest value of  $t$  to employ for the log decrement is perhaps the time  $t_1$ , during which the rotating radius vector passes over 1 radian.

It is

$$(396) \quad t_1 = \frac{1}{\omega_f} \quad \text{seconds.}$$

Denoting the corresponding log decrement for a radian by  $\delta_1$ ,

$$(397) \quad \delta_1 = \Delta t_1 = \frac{\Delta}{\omega_f} = \frac{B_0}{u_f}.$$

The most useful time interval is, however, that in which the rotating vector passes over 1 revolution or  $2\pi$  radians, i.e., the free periodic time  $T$ , or time of one cycle

$$(398) \quad T = \frac{2\pi}{\omega_f} = \frac{1}{f_f} \quad \text{seconds.}$$

Denoting the corresponding log decrement for a cycle by  $\delta_T$ ,

$$(399) \quad \delta_T = \Delta T = \frac{2\pi\Delta}{\omega_f} = \frac{\Delta}{f_f} = \frac{T}{\tau_0} = 2\pi \operatorname{ctn} \gamma = 2\pi \tan \gamma' = B_0 \cdot \frac{2\pi}{u_f}.$$

The term log decrement is ordinarily understood as meaning the log decrement for a cycle, when no other specification is given. With that understanding,  $\delta_T$  may be replaced by  $\delta$ , and when the damping is small,

$$(400) \quad \delta = 2\pi\gamma' = 2\pi B_0 = \frac{2\pi}{\Lambda_0} = \pi B_s = \frac{\pi}{\Lambda_s} = \frac{2\pi\rho}{z_0} = \frac{\pi r}{z_0}$$

where  $\gamma'$  is  $\pi/2 - \gamma$ , or the complement of the angle  $\gamma$ . In any system that oscillates freely, in the practical sense of having small damping, and executing many cycles before coming to rest,  $\gamma$  is necessarily nearly  $\pi/2$  radians, and  $\gamma'$  a relatively small angle, whose radian value is substantially the same as its sine or its tangent.

The angle  $\gamma'$  is thus a measure of the bluntness of resonance in an oscillating system, and indicates its degree of departure from a perfectly undamped or perpetual oscillator. It may be called the *phase defect* of the oscillation system. In an a.-c. circuit, i.e., a circuit of sustained oscillations, the phase defect of a condenser or other purely reactive device† is  $B_s$  and not  $B_0$ . It is sometimes called the *power-factor* of the circuit.

\* It might be better identified as a hyperbolic logarithm under the abbreviation "logh dec."

† Bibliography 78.

In any series of damped oscillations, like that presented by Fig. 140, the ratio of any two successive displacements in the same direction is  $\epsilon^{-\delta\tau} = \epsilon^{-\delta}$ ; so that if  $x_n$  and  $x_{n+1}$  are any two successive cyclic displacements in the same direction or of the same sign, we have  $\delta$  for the hyperbolic logarithm of their ratio, or

$$(402) \quad \log \frac{x_n}{x_{n+1}} = \delta,$$

and

$$(403) \quad \log \frac{x_n}{x_{n+1}} = 0.4343 \delta.$$

In any free vibrational system, the ratio  $x_n/x_{n+1}$ , and its logh decrement  $\delta$ , should be constant for all values of  $n$ , provided that the vibrations are of small amplitude. If  $\delta$  is observed to vary at different stages of amplitude decay, it is an evidence that the conditions in the system are not those assumed in our theory. Such mechanical cases present themselves when the resistance  $r$  is not simply proportional to the velocity, or when the elastance  $s$  is not simply proportional to the displacement. Electric cases also occasionally present themselves in which  $\delta$  is not constant during decay, when the resistance  $r$  varies, as when an arc is included in the path of discharge.

**Initial Vector Motive Force  $F_i$ .**—In the kinetically energized case, where the  $\omega$ ,  $y$ , and  $\dot{x}_i$  vector triangles have been drawn as above described, the ratio of the  $\dot{x}_i$  to the  $y$  triangle is  $F_i$ , the size of the initial vector displacement force. In the case considered, this ratio of corresponding sides in the  $\dot{x}_i$  and  $y$  triangles is 1291. This is the initial vector-displacement force in the mechanical case, or condenser emf. in the electric case. The vector relations of this force to the velocity or current are shown in Fig. 174. Here the  $\dot{x}_i$  triangle  $def$  occupies the same initial position as is indicated in Fig. 172, but the force  $\bar{F}_i$  assumes the vertical position  $O\bar{F}_i$ , coincident with the side  $de$ . The vector projection of this force on the reference axis  $OX$  is zero, at the moment  $t = 0$ . As time advances, and the vectors rotate in the direction of the arrow  $\omega_r$ , this projected value of  $\bar{F}_i$  becomes increasingly negative. In the mechanical case, the spring becomes bent and opposes resilient force. In the electric case, the condenser becomes negatively charged.

Associated with the force  $O\bar{F}_i$  of displacement in Fig. 174, is an equal vector force  $O\bar{E}_i$  of inertia, or of inductance. The angle  $\bar{F}_i O \bar{E}_i$  is  $2\gamma$ , or each of these two equal vector forces  $O\bar{F}_i$  and  $O\bar{E}_i$  makes the same angle  $\gamma$  with the vector velocity  $O\bar{I}_i$ . Its initial projection on the  $OX$  axis is 1264.9 volts, or dynes, in the positive direction. Immediately opposite to the velocity is a third vector force due to frictional resistance to velocity —  $\bar{I}_i$ , 1633 volts or dynes. The projection of this on the axis  $OX$  is — 1264.9 volts or dynes. These three vector forces  $O\bar{F}_i$ ,  $O\bar{E}_i$ , and  $O\bar{I}_i$









the set of diagrams in the right-hand column, Fig. 171, is to be preferred. This corresponds to the case where a simple emf. is suddenly discharged from or applied to a  $\mathcal{E}RS$  branch, initially without energy, or a simple vmf. is suddenly applied to a  $mrs$  vibrator initially at rest.

**Oscillatory Impedance Diagram.** — We first form the  $z_0$  triangle  $ABC$ , by taking the reciprocal of  $y$ ; or we first form the  $\omega^{-1}$  triangle  $OPQ$  by taking the reciprocal of  $\omega_0$ , and then multiply it by  $s$  to obtain the  $z_0$  triangle. The real component  $AB$  of the oscillatory impedance is  $\rho = r/2$ , the *oscillation resistance*. The hypotenuse  $AC$  is  $\sqrt{ms} = \sqrt{\mathcal{E}/c}$  abohms, corresponding to what is called the *surge impedance* of a circuit, but at the slope  $\gamma$ . The perpendicular  $BC$  is then the oscillatory reactance, or the reactance offered by the mass  $m$  at the free angular velocity  $\omega$ , actually developed. In the case considered, the oscillatory impedance is  $100 + j122.475 = 158.114 \angle 58^\circ 46' 6''$  ohms.

**Oscillatory VMF. or EMF. Vector Diagram.** — If the damped system is set into oscillation with the actual initial force  $F$ , volts or dynes, then the side  $EF$  of the force triangle  $DEF$ , Fig. 171, must be given this value to scale, and the other two sides  $DE$  and  $DF$  given proportional values, so as to keep the triangle  $DEF$  similar to  $ABC$ . Then  $DE$  will be the active component, or the initial emf. directed to overcoming  $Ir$  drop, or  $\dot{x}r$  resisting force.  $EF$  is the initial reactive emf. directed to overcoming the initial emf. of inertia, and also the actual initial impressed emf. in the condenser. The resultant  $DF$  is the total initial vector emf. The ratio of the actual initial force  $EF$  to the reactive impedance  $BC$  of the  $z$  triangle will then give the initial vector current  $I_i$  or velocity  $\dot{x}_i$  in the system. Thus, in the case considered, the initial impressed emf. being 1000 volts, the initial vector discharging current will be  $1000/122.475 = 8.165$  amperes, which is found at  $df$ , in the  $\dot{x}_i$  triangle. The reactive component of this, or  $ef = 6.3246$  amperes, was the actual initial discharging current in the corresponding kinetically energized case (Fig. 174).

The vmf. diagram may be considered not merely as stationary, for assigning initial vector relations, but also as rotatable, for assigning subsequent instantaneous relations. With the vertex  $F$  as center, rotate the triangle at the angular velocity  $\omega$ , and take projections on the  $FE$  axis. The example already considered may illustrate the application. A condenser of 4 microfarads is charged to an initial potential difference 1000 volts and then allowed to discharge at  $t = 0$ , through an inductance  $\mathcal{L}$  of 0.1 henry, and a total resistance  $r$  of 200 ohms. Find the conditions at any time  $t$ . In the mechanical case this is a spring of  $s = 250\,000$ , compressed by a force of 1000 dynes, and then suddenly released on a mass of 0.1 gm.

Here the numerical relations are represented in the  $\omega$  triangle  $opq$  of Fig. 171, and the impedance triangle  $ABC$  also applies. The emf. triangle  $DEF$  is then constructed, so that the initial reactive emf. is 1000 volts, this being the starting voltage at condenser terminals.



The vector  $O\bar{E}_i$ , Fig. 177, indicates the initial vector emf. of inertia, induced in the inductance  $\mathcal{L}$  or mass  $m$  by the discharge, in accordance with (408) or with Fig. 171. The projection  $OE$  on the  $X$  axis is the initial cemf. of inertia or self-induction. The vector  $O\bar{E}_i$  also rotates with angular velocity  $\omega_r$ . Its damped instantaneous projections on  $OX$ , after 1, 2, and 3 milliseconds, are indicated below the  $X$  axis at 1, 2, and 3 respectively.

Each of the rotating vectors  $O\bar{F}_i$  and  $O\bar{E}_i$  contributes an initial active component along  $O\bar{I}_i$  equal to  $DE$ , Fig. 171, or 816.5 volts. The sum of these two active components is initially 1633 volts along the direction  $O\bar{I}$ . The initial resistance vector cemf. or  $\bar{I}_i r$  drop is represented by the up-right line  $OR$ , of 1633 volts, with its associated equiangular spiral. The first three millisecond positions are shown on this spiral, and likewise these projections on the  $X$  axis. It will be seen that the  $Ir$  drop commences at zero, when  $t = 0$ , increases to a maximum near 640 volts in less than 2 milliseconds and then subsides rapidly.

The three emf. vectors  $O\bar{F}_i$ ,  $O\bar{E}_i$ , and  $OR$ , of displacement, inertia and resistance drop, rotate together in fixed circular phase relations. Considered as undamped, or rotating in circles, they maintain equilibrium at all times. Being damped by the application of one and the same damping coefficient  $e^{-\Delta t}$ , their damped vector values, in rotating, must also remain in equilibrium. That is, the vectors rotating in the three spirals shown, must equilibrate at all times. Finally, their vector instantaneous projections on the  $OX$  axis must also equilibrate at all times.

Taking the vector instantaneous current diagram  $def$ , from Fig. 171, and applying this current at the position  $\bar{I}_i$ , according to Fig. 177, we rotate this initial vector current of 8.165 amperes as shown in the triangle  $def$ , with the angular velocity  $\omega_r$ , or attach it to the rotating emf. system, midway between  $O\bar{F}_i$  and  $O\bar{E}_i$ . The vector  $O\bar{I}$  may be conceived of as rotating in a circle, undamped, but subject to a separately applied damping coefficient  $e^{-\Delta t}$ ; or, an equiangular spiral (not shown), of angle  $\gamma$  may be constructed upon it, and rotation effected in this spiral. Instantaneous projections, in either case, on the  $X$  axis, will determine the corresponding instantaneous currents. Or the instantaneous currents may be obtained, by taking the projections of the emf. vector  $OR$  on  $OX$ , reversing them in sign, and dividing by  $r$ .

It may be noted that whereas in the a.-c. circuit of sustained vibrations, the vector current is always in quadrature with the reactive emfs., and therefore takes no power from or into them, in the damped oscillatory circuit of free vibrations, these two vector reactive emfs.,  $O\bar{F}_i$  and  $O\bar{E}_i$ , Fig. 177, are each inclined at an angle  $\gamma$  with the current, and each of them delivers power to the current. That is, the stores of potential energy in the condenser and inductor are both drawn upon to supply the energy dissipated in resistance.

**Rotating Power Diagram.** — If we multiply the *DEF* diagram, Fig. 171, by  $\hat{x}_t/2$ , at zero slope, we obtain the initial vector-power diagram *GHK*. This is identical with the power diagram *ghk* previously obtained, except that the slope  $\gamma$  is reversed. This apparent discrepancy may be explained by remembering that the *GHK* power diagram is obtained with reference to velocity standard phase, or zero slope in  $\hat{x}$ , whereas the *ghk* power diagram is obtained with reference to vmf. standard phase or zero slope in  $F_t$ . The oscillatory power is actually developed at a phase intermediate between  $F_t$  and  $\hat{x}$ , so that, leading one, it must lag the other.

The initial vector active power is 3333 watts and reactive power 4802.5. We may rotate the triangle *GHK*, about the vertex *K*, at the angular velocity  $2\omega_j$ , as indicated in Fig. 175. The undamped or circularly revolving vectors *Ka*, *KH* and *KG*, will then project upon the *X* axis the instantaneous values of undamped active, reactive, and total power. Or, we may use and rotate the *ghk* triangle instead, starting from the position indicated in Fig. 175. The undamped power will oscillate between the projected limits  $O\bar{p}_t = +8603.3$ , and  $O\bar{p}_t = -1936.6$  watts, respectively the sum and difference of the base and hypotenuse in the power triangles *GHK* and *ghk*. The undamped reactive power will vary between the limits  $+4082.5$  and  $-4082.5$  watts. The undamped active or dissipative power will vary between the projected limits  $O\bar{p}_a = 6666.6$  watts. Since, however, the emf.  $O\bar{E}_t$ , Fig. 177, also develops active power on the current equally with  $O\bar{F}_t$ , the total undamped active power will range over twice this amount, or 13333 watts. Instantaneous projections of these undamped powers may be made on the *X* axis when the diagram rotates at angular velocity  $2\omega_j$ .

The damping coefficient of power to be applied to the projected powers in Fig. 176 is, as already stated in connection with Fig. 173,

$$(404) \quad e^{-2\Delta t} = e^{-\frac{r}{m}t} = e^{-\frac{2t}{\tau_0}} = e^{-\frac{t}{\tau_s}}.$$

Figure 178 shows the undamped sinusoidal values of the various quantities in the system, before applying the damping coefficients. The corresponding diagram of damped values appears in Fig. 179. It will be seen in the latter that the current rises to a maximum of 3.04 amperes in about 0.0006 second.

In Fig. 178, the sinusoid  $\bar{u}$  represents the projection value of the rotating vector emf.  $O\bar{F}_t$  at condenser terminals. This appears to reach 1291 volts, but the damping coefficient actually prevents it from rising above the initial value of 1000. Similarly the sinusoid  $\bar{e}$  represents the projection of the rotating vector  $O\bar{E}_t$  of reactance or self-induction. These sinusoids,  $\bar{u}$  and  $\bar{e}$  being out of phase with the current, are divided each into two components  $u_r$ ,  $u_i$  and  $e_r$ ,  $e_i$ , the former being in phase with the current, the latter in quadrature therewith. The maximum cyclic values

of  $u_r$  and  $e_r$  will be 816.5 volts each, as in Fig. 177, and the maximum cyclic values of  $\bar{u}_1$  and  $\bar{e}_1 = 1000$  volts each. The undamped power of

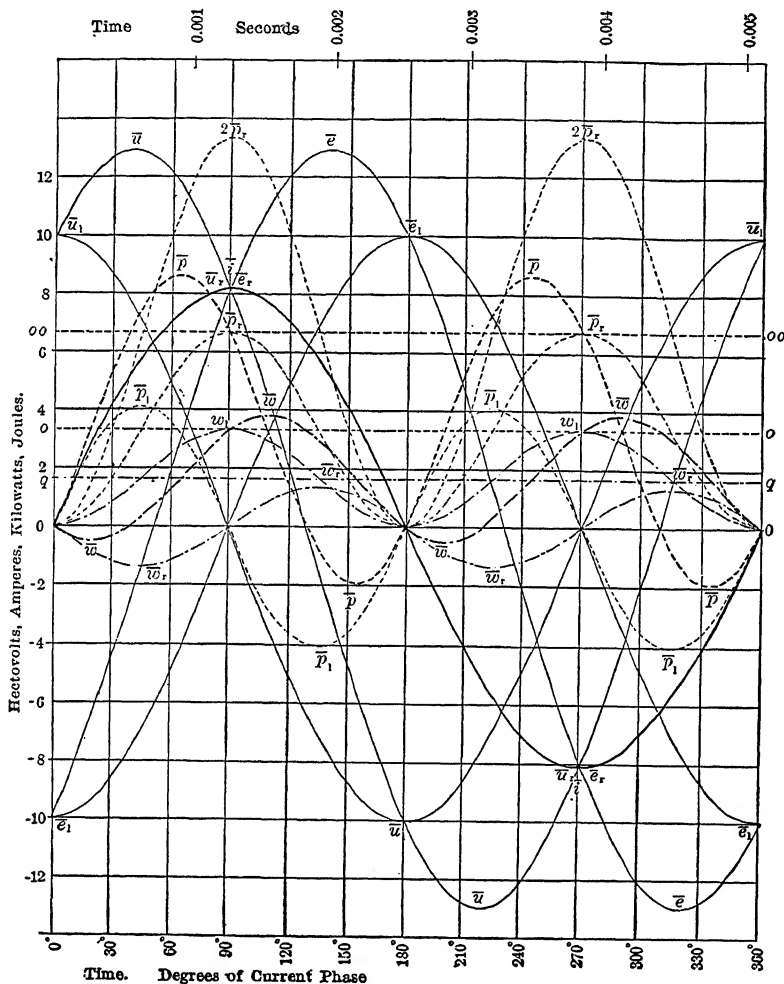


FIG. 178. Curves of potential difference, current, power, and energy in simple oscillating-current circuit containing resistance, leaving damping out of account.

the cophase components  $\bar{i}$  and  $\bar{u}_r$  is the double-frequency  $p_r$  of 3333.3 watts amplitude about the zero line  $oo$ , itself elevated 3333.3 watts. The power of  $\bar{i}$  and  $\bar{e}_r$  will be an identical sinusoid. The total power of cophase components is thus the sinusoid  $2\bar{p}_r$  of 6666.6 watts amplitude, about the

zero line  $oo$ ,  $oo$ , itself elevated 6666.6 watts. The reactive power expended by the quadrature voltage component of  $\bar{u}_1$  upon the current  $\bar{i}$ , is the double-frequency sinusoid  $\bar{p}_1$  of 4082.5 watts as at  $HK$ , Fig. 171. This power is in the magnetic field of the reactance. The total power exerted by  $\bar{u}$  upon  $\bar{i}$  is the heavy double-frequency sinusoid  $\bar{p}$ , of 5270 watts amplitude, about the zero line  $oo$  elevated 3333.3 watts.

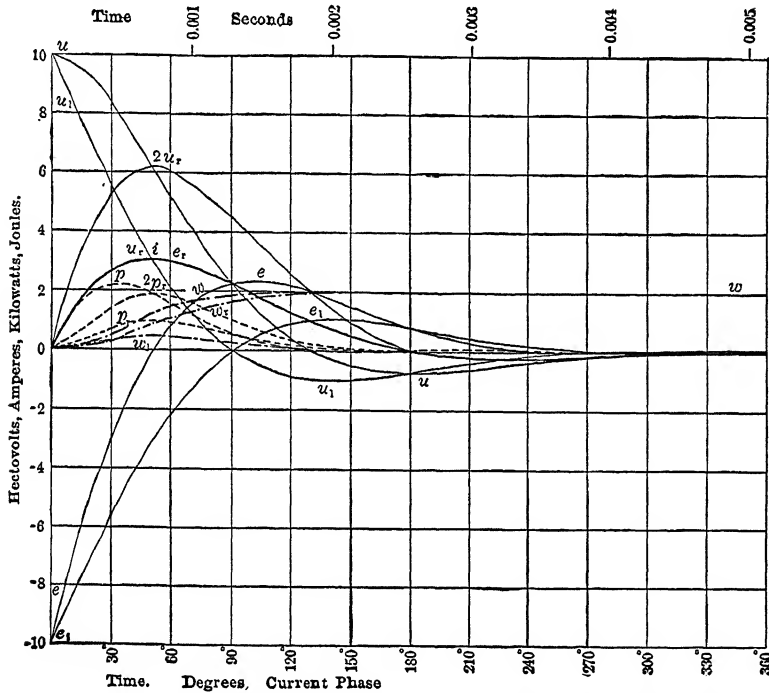


FIG. 179. Curves of potential difference, current, power, and energy in simple oscillating-current circuit containing resistance after applying damping-factors to the ordinates of Fig. 178.

The undamped energy of reactance magnetic flux is the double frequency sinusoid  $w_1$ , of 1.66 joules amplitude, about the zero line  $qq$ , itself elevated 1.66 joules. The undamped energy of dissipation in resistance due to  $\bar{u}_r$  and  $\bar{i}$  is the double-frequency sinusoid  $w_r$ , of 1.3608 joules, as in the  $W_4$  diagrams of Fig. 171. An identical sinusoid would represent the energy of dissipation due to  $\bar{e}_r$  and  $\bar{i}$ ; so that the total unattenuated energy of dissipation would be a double-frequency sinusoid of 2.7216 joules amplitude. The total undamped energy of  $\bar{u}$  acting on  $\bar{i}$  is the heavy double-frequency sinusoid  $\bar{w}$ , of 2.151 65 joules amplitude, about the zero line  $qq$ .

If we apply the attenuation-factors of Fig. 173 to the ordinates of Fig. 178, that is, multiplying the currents and voltages by  $\epsilon^{-\Delta t}$ , while multiplying the powers and energies by  $\epsilon^{-2\Delta t}$ , we obtain the curves of Fig. 179. This diagram represents the actual succession of events in the oscillating-current circuit. The potential difference at terminals falls along  $u$ . The emf. of self-induction pursues the opposite curve  $e$ . The current follows the heavy line  $i$ , reaching a maximum of 3.04 amperes near to  $45^\circ$  of its phase, or 0.00064 second after release. The components of voltage in phase with the current ( $u_r$  and  $e_r$ ) both coincide with its curve. The quadrature components of voltage are  $u_1$  and  $e_1$ . The total component of voltage in phase with the current follows the curve marked  $2u_r$ . The power curve  $p$  reaches a maximum of 2200 watts at about  $60^\circ$  of its phase. This power rapidly subsides, and only crosses the zero line in feeble measure. The total dissipative power is shown by the curve  $2p_r$ .

The energy in the inductance follows the curve  $w_1$ . This corresponds to  $w_1$  in Fig. 178, after applying the factor  $\epsilon^{-2\Delta t}$ . The total energy dissipated in the resistance, and the total energy expended by the condenser follow the curves  $w_r$  and  $w$ , respectively.

**Algebraic Scalar Relations.** — In dealing with damped oscillations, it is sometimes convenient to refer to algebraic rather than to geometric relations. Retaining the electric case, if we charge the condenser to  $F_r$  volts initial potential difference and discharge it at  $t = 0$ , the condenser potential difference at time  $t$  seconds is

$$(405) \quad \begin{aligned} f &= F_r \csc \gamma \epsilon^{-\Delta t} \cdot \sin (\omega_f t + \gamma) \\ &= F_t \epsilon^{-\Delta t} \cdot \sin (\omega_f t + \gamma) \end{aligned} \quad \text{dynes or volts,}$$

where  $F_t$  is the size of the vector motive force in the emf. diagram  $DEF$ , Fig. 171.

The instantaneous velocity or current is

$$(406) \quad \begin{aligned} \dot{x} \text{ or } i &= \frac{F_r}{s} \omega_0 \csc \gamma \cdot \epsilon^{-\Delta t} \cdot \sin \omega_f t = \frac{F_t}{z_0} \epsilon^{-\Delta t} \cdot \sin \omega_f t \\ &= I_t \epsilon^{-\Delta t} \cdot \sin \omega_f t \end{aligned} \quad \text{amp. or kines,}$$

where

$$(407) \quad I_t = \frac{F_r}{L\omega_f} = \frac{F_r}{m\omega_f} = \frac{F_t}{z_0} = \frac{F_t}{s} \omega_0 = F_t y_0 \quad \text{amp. or kines.}$$

Retaining, in what follows, only the electric unit of each dual case, the instantaneous emf. of inertia or self-induction in the system is

$$(408) \quad e = F_r \csc \gamma \epsilon^{-\Delta t} \cdot \sin (\omega_f t - \gamma) = F_t \epsilon^{-\Delta t} \cdot \sin (\omega_f t - \gamma) \quad \text{volts.}$$

The instantaneous power of the condenser or spring is

$$(409) \quad \begin{aligned} p_e = fi &= \frac{F_t I_t}{2} \epsilon^{-2\Delta t} \{ \cos \gamma - \cos (2\omega_f t + \gamma) \} \\ &= F_t I_t \epsilon^{-2\Delta t} \sin \omega_f t \cdot \sin (\omega_f t + \gamma) \end{aligned} \quad \text{watts.}$$

The instantaneous power of the inductor or mass is

$$(410) \quad p_i = ei = \frac{F_i I_i}{2} \epsilon^{-2\Delta t} \{\cos \gamma - \cos (2\omega_f t - \gamma)\} \\ = F_i I_i \epsilon^{-2\Delta t} \sin \omega_f t \cdot \sin (\omega_f t - \gamma) \quad \text{watts.}$$

The total instantaneous power of the system is

$$(411) \quad p = p_c + p_i = F_i^2 g \cdot \epsilon^{-2\Delta t} (1 - \cos 2\omega_f t) \\ = I_i^2 \rho \epsilon^{-2\Delta t} (1 - \cos 2\omega_f t) \quad \text{watts.}$$

The instantaneous elastic energy of the system, taking  $W_i = MN = mn$ , Fig. 171, is

$$(412) \quad w_c = \frac{F_i^2}{4s} \epsilon^{-2\Delta t} \{1 - \cos (2\omega_f t + 2\gamma)\} \\ = W_i \epsilon^{-2\Delta t} \{1 - \cos (2\omega_f t + 2\gamma)\} \quad \text{joules.}$$

The instantaneous inertia energy is

$$(413) \quad w_i = \frac{F_i^2}{4s} \epsilon^{-2\Delta t} (1 - \cos 2\omega_f t) = W_i \epsilon^{-2\Delta t} (1 - \cos 2\omega_f t) \quad \text{joules.}$$

The instantaneous total system energy is

$$(414) \quad w = w_c + w_i = 2 W_i \epsilon^{-2\Delta t} \{1 - \cos (2\omega_f t + \gamma) \cos \gamma\} \quad \text{joules.}$$

The initial energy in the system is

$$(415) \quad W_i = \frac{F_i^2}{2s} \sin^2 \gamma = 2 W_i \sin^2 \gamma = \frac{F_r^2}{2s} \quad \text{joules.}$$

The total instantaneous dissipated energy is

$$(416) \quad W_d = W_i - w = \frac{F_i^2}{2s} [\sin^2 \gamma - \{1 - \cos (2\omega_f t + \gamma) \cos \gamma\} \epsilon^{-2\Delta t}] \\ \text{joules.}$$

After  $m$  complete energy cycles,  $\cos (2\omega_f t + \gamma) = \cos \gamma$  and  $t = \frac{mT}{2}$ ; so that

$$(417) \quad W_d = \frac{F_i^2}{2s} \{\sin^2 \gamma (1 - \epsilon^{-\Delta m T})\} = W_i (1 - \epsilon^{-\Delta m T}) \quad \text{joules.}$$

The total energy dissipated in the first energy cycle when  $m = 1$  and  $t = T/2$  is

$$(418) \quad w_1 = W_i (1 - \epsilon^{-\Delta T}) = W_i (1 - \epsilon^{-\delta}) \quad \text{joules.}$$

The dissipation in the first, second, third, etc., energy cycles is

$$(419) \quad w_1, w_1 \epsilon^{-\delta}, w_1 \epsilon^{-2\delta}, \text{ etc.} \quad \text{joules.}$$

The total ultimate energy dissipated is thus

$$(420) \quad W_i = w_1 (1 + \epsilon^{-\delta} + \epsilon^{-2\delta} + \dots) = \frac{w_1}{1 - \epsilon^{-\delta}} \quad \text{joules.}$$

With the values in the case considered of  $F_i = 1291$ ,  $F_r = 1000$ ,  $c = 4 \times 10^{-6}$ ,  $\omega_f = 1224.75$ ,  $\gamma = 50^\circ 46'$ ,  $\Delta = 1000$ ,  $T = 0.00513$ ,  $W_i = 2$ , we have for the attenuation factor of one power period, or semi-period of potential difference,  $\epsilon^{-\delta} = 0.005917$ . The energy dissipated in resistance



during the first energy cycle is thus  $2 \times 0.994083 = 1.988166$  joules. The second cycle dissipates  $0.005917 \times 1.988166 = 0.0119$  joule. Each successive cycle dissipates 0.5917 per cent of the amount dissipated in the last preceding cycle. It is thus evident that in a heavily damped oscillatory motion, a relatively large fraction of the initial energy is rejected from the system in the first half-cycle of motive force or velocity, i.e., the first complete energy cycle.

**Comparative Relations between Potentially and Kinetically Energized Oscillations.** — If we compare the vector diagram of Fig. 174 of damped oscillations in a kinetically energized system ( $I^2\mathcal{E}/2$  or  $\dot{x}_t^2 m/2$ ) with that (Fig. 177) of the same system potentially energized ( $F_r^2/(2s)$  or  $F_r^2/(2s)$ ), with the same stock of energy, in this case 4 joules, we shall see that the two vector diagrams differ from each other only in phase. The vector system in the kinetically energized system of Fig. 174 is the same as that of the potentially energized system of Fig. 178, but leads the latter by  $(\pi - \gamma)$  in phase. Moreover, whether the initial stock of energy is communicated in a velocity, or in the elastic compression of a spring, it is evident that during the oscillatory discharge, the energy remaining in the system is rapidly changing between the kinetic and potential forms, so that the only difference in the initial rotating-vector system must relate to their phases with respect to the axis of reference. If the system is kinetically energized, the first phenomenon is velocity or current, and the elastic force of spring compression or condenser voltage develops in the next stage. If, however, the system is potentially energized, as by a compressed spring or charged condenser, the order of the phenomena at starting is reversed. The same set of vector diagrams can be used in either case. The algebraic relations of the kinetically energized system thus become (see Fig. 174)

$$(421) \quad f = -F_r \csc \gamma \cdot e^{-\Delta t} \cdot \sin \omega_f t = -F_t \cdot e^{-\Delta t} \cdot \sin \omega_f t \quad \text{volts or dynes,}$$

$$(422) \quad i = -I_t \cdot e^{-\Delta t} \cdot \sin (\omega_f t - \gamma) \quad \text{amp. or kines,}$$

$$(423) \quad e = -F_r \csc \gamma \cdot e^{-\Delta t} \cdot \sin (\omega_f t - 2\gamma) \\ = -F_t \cdot e^{-\Delta t} \cdot \sin (\omega_f t - 2\gamma) \quad \text{volts or dynes,}$$

where

$$F_r = I_t m \omega_f = I_r \csc \gamma \cdot m \omega_f \quad \text{volts or dynes.}$$

The three vectors  $f$ ,  $i$ , and  $e$ , forming at all times an equilibrating system, rotate rigidly together at angular velocity  $\omega_f$ , commencing at time  $t = 0$  from the positions shown in Fig. 174. After they have advanced through an angle  $\gamma$ , they will occupy the same positions as in Fig. 178, but inverted. After advancing through  $180^\circ + \gamma$ , their positions will be as in Fig. 178 directly. This inversion is due to the fact that when potentially energized,  $F_t$  is taken as positive, whereas, when kinetically energized,  $\dot{x}_t$  is taken as positive, and  $F_t$  as negative.

If a vibration system has its initial stock of energy partly in the potential, and partly in the kinetic form, the vector diagram of Fig. 178 can be prepared to scale for the potential stock, and that of Fig. 174 to the same scale for the kinetic stock. The two vector systems being superposed with the same line  $OX$  of reference, the vector sum will represent the vector state of the composite system for instantaneous projections.

**Oscillatory Displacement.** — Since the elastic force in the system is always  $-sx$ , the mechanical displacement  $x$ , or the electric charge in the condenser, is always in direct proportion to this force  $f$ . Hence, if the system considered were the vibrator of an oscillograph, the angular displacement of the vibrator, as indicated by the deflected beam of light at any instant, would be in direct proportion to the instantaneous projection of the rotating vector  $\bar{F}$ , Figs. 174 or 177. In the case considered, with a bluntness  $B_0 = 0.632$ , such as might readily be developed in an oil-damped oscillographic vibrator, the photographically recorded movement of the vibrator after being deflected by a steady current which was then suddenly interrupted, should correspond to the curve  $u$ , Fig. 179, which crosses the zero line near to  $t = 0.0018$  second, and after reaching  $-100$  volts, near  $t = 0.0026$  second, comes very nearly to rest at  $t = 0.004$  second. This shows that with such a vibrator, a transient wave of rectangular form would actually leave a record of the reversing wave form  $uu$ . A vibrator of greater bluntness  $B_0$  and damping constant  $\Delta$  would move from an initial deflection to rest more quickly and directly, but no mechanical vibrator could pass instantly from full initial deflection to complete rest. In other words, no simple *mrs* vibrator can ever be expected to execute a strictly rectangular wave form of displacement, even if it could be subjected to a strictly rectangular wave of impressed force. (See Fig. 105.)

**Reversal Time.** — By reference to Figs. 178 and 179, it may be observed that in the potentially energized case, the elastic force reverses in a time  $\tau_r = (\pi - \gamma)/\omega_f$  seconds from the start, and which may be called the *reversal time* of the force. Thereafter it will reverse every  $\pi/\omega_f$  or  $T/2$  seconds. The velocity or current will also reverse regularly every  $T/2$  seconds from the start. In the case considered,  $\tau_r = 0.00184$  second, and  $T/2 = 0.002565$  second.

In the kinetically energized case, the current or velocity reverses after  $\gamma/\omega_f$ , or  $0.00072$  second and thereafter every  $T/2$  seconds. The elastic force  $f$  also reverses regularly every  $T/2$  seconds from the start.

## FREE UNDAMPED VIBRATION. LIMITING CASE OF NEGLECTIBLE RESISTANCE

In practice, free vibrations are always damped in the absence of regenerative devices or amplifiers. Nevertheless, the damping in some vibration systems is relatively small. An example is furnished by an ordinary acoustic tuning fork freely vibrating in air. Tuning forks can be made which, with a frequency of 15~, fall in amplitude to  $1/e^{10}$  in about 7 seconds, or have a  $\Delta$  of  $1/7$ . The logarithmic decrement of the damping is thus  $1/(15 \times 7)$ , or 0.01, approximately; so that the amplitude falls off only about 1 per cent in each cycle. The vector diagrams for such vibrations approximate more closely to those of undamped vibrations than to those of the heavily damped vibrations discussed numerically in the last chapter. The undamped case, therefore, deserves separate consideration.

Phase Relations of  $\left\{ \begin{array}{l} \text{Displacement, Velocity, and Inertia Force} \\ \text{Quantity, Current, and Induced CEMF} \end{array} \right\}$ . —

In the damped vibrator, we have seen that  $\gamma$ , being the slope of the angular velocity or of the motion's equiangular spiral, the vector displacement (Figs. 169 and 170) lags the vector velocity by  $(\pi - \gamma)$ , while the vector acceleration leads the velocity by  $(\pi - \gamma)$ . In the undamped vibrator,  $\gamma = \pi/2$  radians or  $90^\circ$ , so that the phase relations are those of Fig. 156; namely, that the displacement is in lagging quadrature ( $\pi/2$  radians behind) the velocity, while the acceleration is in leading quadrature therewith ( $\pi/2$  radians ahead).

The angular velocity of the undamped free vibration  $\omega_f$  is identical with  $\omega_0 = \sqrt{s/m}$ , the resonant angular velocity. In the case of the above mentioned tuning fork, the difference between  $\omega_f$  and  $\omega_0$  would be less than 2 parts per million, and  $\gamma$  would be only  $6'$  short of  $90^\circ$  ( $\gamma = 89^\circ 54'$ ).

**Stationary Vector Diagrams.** — The ten stationary-vector diagrams of Fig. 171 reduce to the corresponding straight-line diagrams of Fig. 180, for the undamped case. These are easily understood by comparison with Fig. 171, in view of the discussion in the last chapter. The numerical values are for the same case as before, but with  $r = 0$ ; that is,  $m = 0.1$  gm.,  $s = 2.5 \times 10^5$  dynes/cm.,  $F_r = 1000$  dynes. Again,  $\mathcal{E} = 0.1$  henry,  $s = 2.5 \times 10^5$  darafs,  $F_r = 1000$  volts.

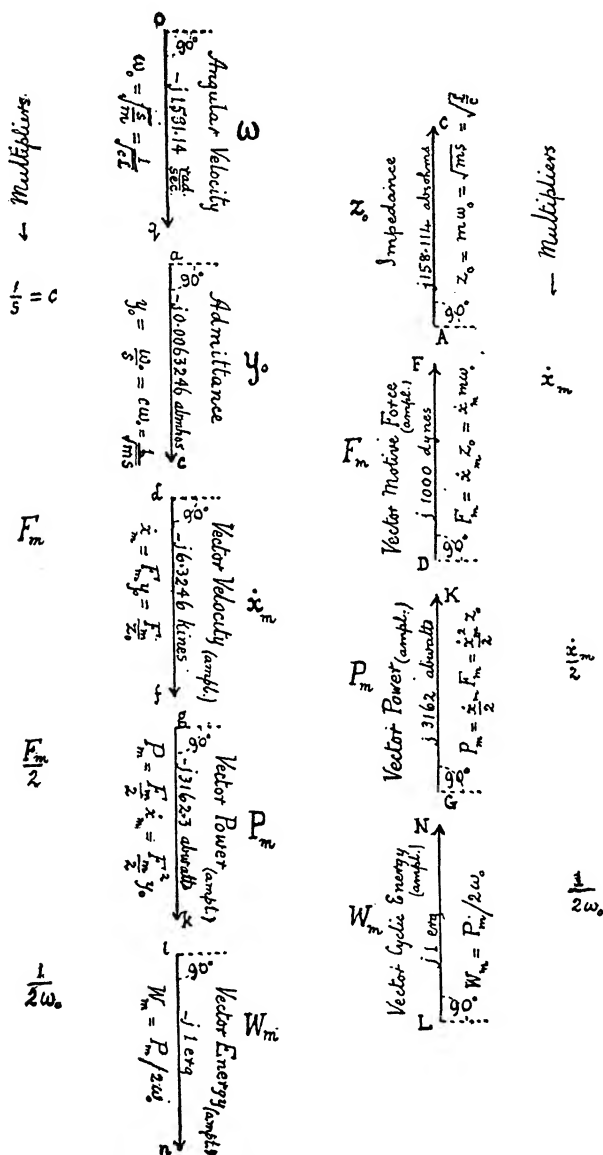


FIG. 180. Vector diagrams of undamped simple mechanical or electric oscillations.

**Rotative Force and Velocity Diagrams.** — In Fig. 180, the three diagrams  $\omega$ ,  $y_0$  and  $z_0$  are essentially stationary; but the remaining five diagrams may be regarded as either stationary or rotary, like the corresponding diagrams of Fig. 171.

Figure 181 is a rotary-vector diagram for the case considered, where  $\omega_r = \omega_0 = 1581.14$  radians per second  $= 251.646 \sim$ . Here,  $-XOX$

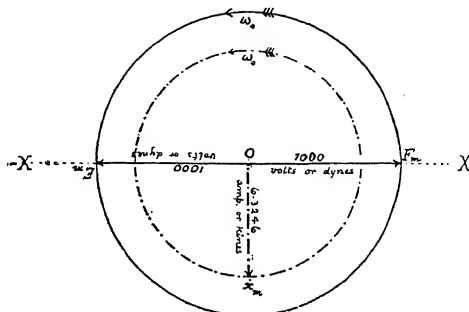


FIG. 181. Rotary-vector diagram of undamped vibration.

being the axis of reference through the center of rotation, the conditions are represented for a potentially energized case at time  $t = 0$ . The initial discharging force is  $OF_m = F_i = F_r = 1000$  volts or dynes. The initial inertia force or emf. of self-induction  $OE_m = E_i = E_r = 1000$  volts or dynes. The vector current  $I_m$  or  $\dot{x}_m$  is 6.3246 kins or

amperes. The initial value of this, as projected on  $-XOX$ , is zero. The two rotating vector forces  $OF_m$  and  $OE_m$  are the only forces in action, because there can be no resisting force or  $Ir$  drop. The angular velocity of all three vectors  $OE_m$ ,  $OI_m$  and  $OF_m$ , is  $\omega_0$ , as shown by the arrow.

If the system is kinetically and not potentially energized, so that it starts at  $t = 0$ , with an initial current  $I_m$  or velocity  $\dot{x}_m$ , and without initial force  $F_m$ , then the vector system of Fig. 181 should have its reference axis rotated clockwise through  $90^\circ$ , so that  $OX$  should coincide with  $O\dot{x}_m$ . The regular rotation of the vectors at angular velocity  $\omega_0$  will then project, on the new reference axis, the correct instantaneous values.

**Rotative Undamped Power Diagrams.** — If we rotate either of the two  $P$  diagrams  $GK$  or  $gk$ , Fig. 180, about the  $G$  or  $g$  point, at the angular velocity  $2\omega_0$ , and take instantaneous projections on the  $X$  axis, we can determine the instantaneous power of the system. It reaches the alternate maxima of  $+P_i$  and  $-P_i$  watts. The vector should occupy the position shown in Fig. 180 at time  $t = 0$ . Projections on the  $OX$  axis will then give instantaneous values of the condenser power. The inductor instantaneous power can be obtained by reversing the rotating  $P$  vector, or changing its phase by  $180^\circ$ .

**Rotative Undamped Energy Diagram.** — If we rotate either of the two  $W$  diagrams  $LN$  or  $ln$ , Fig. 180, about the  $L$  or  $l$  point, at the angular velocity  $2\omega_0$ , and take instantaneous projections on the  $Y$  axis, we can determine the instantaneous energy in the condenser and in the inductor. These projections are shown in Fig. 182. Here a circle  $LSC$ , of radius

$SC$ , equal to the initial stock of energy  $W_m$  ergs or joules, is rotated, with rolling, at angular velocity  $2\omega_0$  up the  $Y$  axis. The orthogonal projection of the center  $S$ , on the  $Y$  axis, will mark times or time phase angles. The orthogonal projection of the point  $C$  of the rotating circle, on the  $X$  axis, will mark the corresponding instantaneous elastic energy  $Oc = f^2/2s$ . Similarly, the projection on  $X$  of the point  $L$  will mark the corresponding instantaneous kinetic energy  $m\dot{x}^2/2$ , or  $\mathcal{L}i^2/2$ . Finally, the projection  $s$ , on  $OX$ , of the center  $S$  in the rotating and rolling circle, will mark the corresponding instantaneous half sum of potential and kinetic energies, or what may be described as the semi-system energy. In the undamped cases considered, this projected semi-system energy  $Os$  remains constant at either 1 erg, or 1 joule.

The path of the moving point  $C$  becomes the cycloid  $CC$ , and the path of the moving point  $L$  becomes the similar cycloid  $LLL$ . These cycloids differ by  $180^\circ$  in phase. The dotted arrows indicate the successive positions of the rotating vectors  $SC$  and  $SL$ , for successive intervals of  $30^\circ$  in time phase, or one-twelfth of an energy cycle. The first two positions, as well as their  $OX$  projections, are denoted by the corresponding small numerals. This diagram is the analogue in the undamped case of Fig. 176 in the case of damped oscillations, and also of a corresponding rotating and rolling vector-diagram in the sustained alternating or forced-oscillation case.\*

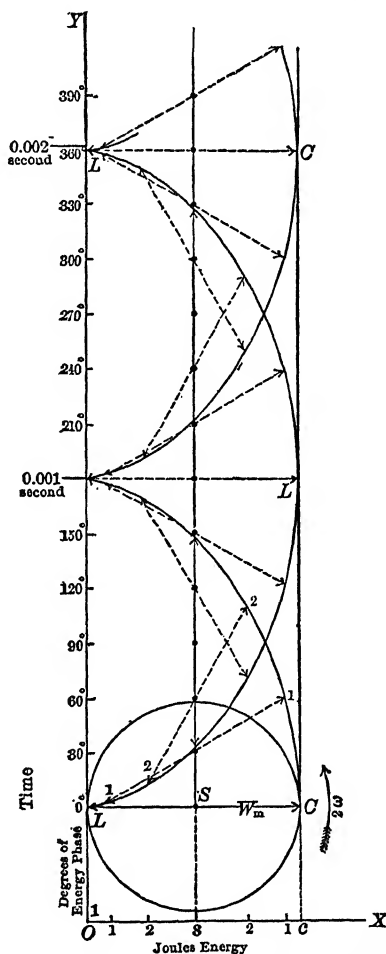


Fig. 182. Rotating and rolling vector-diagram of the condenser energy, the inductance energy, and the system energy in a resistanceless oscillating-current circuit.

\* Bibliography 71, page 135

Figure 183 represents the instantaneous values of emf., current, power, and energy for the potentially energized electric case considered, abscissas being measured both in time and in time phase, ordinates being in the appropriate electric units. It will be seen that the heavy sinusoid  $u$  of condenser emf. completes one cycle within the diagram, commencing at  $t = 0$ , with 1000 volts. The self-induced emf.  $e$  has equal amplitude

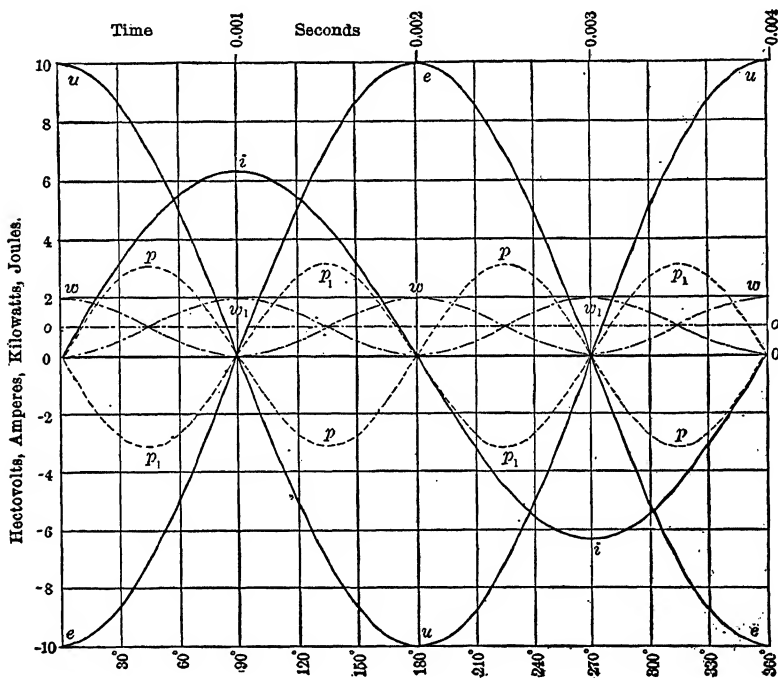


FIG. 183. Analysis of potential difference, current, power, and energy in a simple resistanceless discharging circuit.

and opposite phase. The sinusoidal current  $i$  reaches a maximum of 6.3246 amperes, in quadrature with the emfs. The condenser power  $p$  is a sinusoid of double frequency and 3162.3 watts amplitude. The inductively reactive power  $p_1$  is a similar sinusoid of the same amplitude and opposite phase. The condenser energy  $w$  is initially a maximum at 2 joules. It is a sinusoid of double frequency about the zero line  $oo$ , itself raised one joule. The kinetic energy, or magnetic energy, is the similar sinusoid  $w_1$  of opposite phase.

**Algebraic Scalar Relations of Undamped Oscillations.** — Taking the force as of standard phase (max. cyclic value at  $t = 0$ ), which would be appropriate to the potentially energized case, we have

$$(424) \quad i = F_m y_0 \sin \omega t, \quad \dot{x} = F_m y_0 \sin \omega t \quad \text{amp. or kines,}$$

$$(425) \quad p_c = \frac{F_m^2}{2} y_0 \sin 2\omega t, \quad p_c = \frac{F_m^2}{2} y_0 \sin 2\omega t \quad \text{watts or abwatts,}$$

$$(426) \quad w_c = \frac{F_m^2}{4\omega} y_0 \cos 2\omega t, \quad w_c = \frac{F_m^2}{4\omega} y_0 \cos 2\omega t \quad \text{joules or ergs,}$$

where  $p_c$  and  $w_c$  are the elastic power and energy, respectively. The values of  $p_i$  and  $w_i$ , the kinetic power and energy, are the negatives of  $p_c$  and  $w_c$ , respectively.

Taking the current or velocity as the standard of phase, which would be appropriate to the kinetically energized case, we have

$$(427) \quad e = I_m z_0 \sin \omega t, \quad \dot{f} = \dot{x}_m z_0 \sin \omega t \quad \text{volts or dynes,}$$

$$(428) \quad -p_c = \frac{I_m^2}{2} z_0 \sin 2\omega t, \quad -p_c = \frac{\dot{x}_m^2}{2} z_0 \sin 2\omega t \quad \text{watts or abwatts,}$$

$$(429) \quad -w_c = \frac{I_m^2}{4\omega} z_0 \cos 2\omega t, \quad -w_c = \frac{\dot{x}_m^2}{4\omega} z_0 \cos 2\omega t \quad \text{joules or ergs,}$$

$$(435) \quad p_i = \frac{I_m^2}{2} z_0 \sin 2\omega t, \quad p_i = \frac{\dot{x}_m^2}{2} z_0 \sin 2\omega t \quad \text{watts or abwatts,}$$

$$(431) \quad w_i = \frac{I_m^2}{4\omega} z_0 \cos 2\omega t, \quad w_i = \frac{\dot{x}_m^2}{4\omega} z_0 \cos 2\omega t \quad \text{joules or ergs.}$$

The preceding equations are often useful in dealing with damped oscillations as furnishing first approximations, especially when the damping is very small.

**Reinforced Oscillations.** — In dealing with a regenerative system, or a system of reinforced vibrations, we assume that when the mass  $m$  is given an initial displacement  $x$ , the simple harmonic vibration automatically introduces a simple harmonic reinforcement into the system, this reinforcement being capable of sustaining the vibration in spite of frictional resistance, by tapping a suitable connected source of energy. Let us assume that the cyclic magnitude of the reinforcement is some function  $\psi(x)$  of  $x$ , the maximum cyclic displacement of the mass. The connections of the system are such that the reinforcement has a definite phase with respect to the displacement. If this phase is favorable, the reinforcement will sustain the vibration indefinitely, at a maximum cyclic amplitude which will depend (1) upon the phase relation just mentioned, and (2) upon the reinforcement function  $\psi(x)$ .



Figure 184 is a vector diagram of the case drawn in accordance with Fig. 156, except that instead of taking the displacement  $x$  as standard of phase, we take the resilient force  $OC$ . This force being  $-sx$ , as already described, this is equivalent to a shift of  $180^\circ$  in the phase standard. The resilient force  $OC$  or  $sx$  is now taken as positive on the real axis, the inertia force  $OA$  is  $m\omega^2x$ ; and the resistance force  $OD$  becomes  $j\omega r x$ .  $OF$  is the reinforcement, of size  $\psi(x)$ , and lagging  $\beta^\circ$  in phase behind the resilient

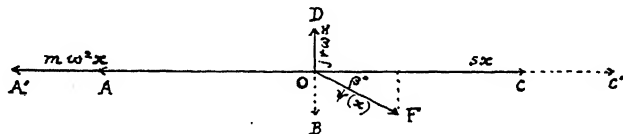


FIG. 184. Vector diagram of reinforced vibrations.

force  $OC$ . Then the real component  $\psi(x) \cos \beta$  acts in aid of the resilient force, or causes the resilience to be artificially increased, if  $\beta$  is less than  $90^\circ$ . In Fig. 184, the resilient force is virtually increased from  $OC$  to  $OC'$ . In order to maintain equilibrium between the resilient and inertia forces, the angular velocity  $\omega$  must increase until  $m\omega^2x$  reaches  $OA'$ . The imaginary component  $-j\psi(x) \sin \beta$  is the net reinforcement which equilibrates the frictional force  $OD = j\omega r x$ . Summing up forces along the real axis, we find

$$(432) \quad sx + \psi(x) \cos \beta = m\omega^2x \quad \text{volts or dynes,}$$

whence

$$(433) \quad \omega^2 = \frac{s}{m} + \frac{\psi(x)}{mx} \cos \beta \quad \left( \frac{\text{radians}}{\text{sec}} \right)^2,$$

or

$$(434) \quad \omega^2 = \omega_0^2 + \frac{\psi(x)}{mx} \cos \beta \quad \left( \frac{\text{radians}}{\text{sec.}} \right)^2,$$

This means that if  $\beta$  lies between  $0^\circ$  and  $90^\circ$ ,  $\omega$  is greater than the resonant frequency  $\omega_0$ . If  $\beta$  lies between  $90^\circ$  and  $180^\circ$ ,  $\omega$  is less than  $\omega_0$ . In the particular case where  $\beta = 90^\circ$ ,  $\omega = \omega_0$ .

Summing up forces along the imaginary axis, we have

$$(435) \quad r\omega x = \psi(x) \sin \beta \quad \text{volts or dynes.}$$

If we divide  $\cos \beta$  from (434) by  $\sin \beta$  from (435), we find

$$(436) \quad \cot \beta = \frac{\omega^2 - \omega_0^2}{2 \Delta \omega} = \frac{u^2 - 1}{2 B_0 u},$$

where  $\Delta$  is  $r/(2m)$ , and  $B_0 = \Delta/\omega_0$ , as in preceding Chapters. This equation is the same as (238). It means that the value of  $B_0$  involved by the phase lag  $\beta$  of the reinforcement happens to be identical with the value that is produced by an externally and independently impressed force acting at the same phase displacement. In other words, so long as the

phase of the impressed force is the same with respect to the resilient force, it is a matter of indifference to the angular velocity produced whether the force is independent, or is interlinked with the system.

Again, from (436), we obtain

$$(437) \quad \omega^2 - 2\Delta\omega \operatorname{ctn} \beta = \omega_0^2 \quad (\text{radians/sec.})^2,$$

whence

$$(438) \quad \omega = \sqrt{\omega_0^2 + \Delta^2 \operatorname{ctn}^2 \beta} + \Delta \operatorname{ctn} \beta \quad \text{radians/sec.},$$

or

$$(439) \quad u = \sqrt{1 + B_0^2 \operatorname{ctn}^2 \beta} + B_0 \operatorname{ctn} \beta,$$

which agrees with (233). This means that if the phase angle  $\beta$  of the reinforcement is fixed by the connections of the system, the frequency ratio  $u$  selected by the system is independent of the reinforcement function  $\psi(x)$ . If the reinforcement function is powerful, the vibrations will sustain themselves with relatively large maximum cyclic amplitude  $x$ , and relatively large maximum cyclic velocity  $\dot{x}$ . If the reinforcement function is weak, the vibrations will sustain themselves with relatively small  $x$  and  $\dot{x}$ ; but in any case, the frequency ratio  $u = \omega/\omega_0 = f/f_0$  will be the same, and will be equal to that produced in the system when it is actuated by an independent force maintaining the same phase  $\beta$ .

In the particular and most favorable case when  $\beta = 90^\circ$ , we have  $u = 1$ , and  $\omega = \omega_0 = \sqrt{s/m}$ ; i.e., the sustained frequency is identical with the resonant frequency. Moreover, the amplitude of the net reinforcement  $OB$ , Fig. 184, will then be a maximum.

Consequently, commencing with  $\beta = 0^\circ$ , the vibrations cannot be self-sustaining. With the lag angle  $\beta$  a little greater than  $0^\circ$ , feeble sustained oscillations are possible at a relatively high frequency and value of  $u$ . If the lag angle  $\beta$  increases,  $u$  diminishes, and  $x$  increases in accordance with the relation

$$(440) \quad x = \frac{\psi(x) \sin \beta}{r\omega} \quad \text{max. cy. cm. or coulombs.}$$

When  $\beta$  nearly reaches  $90^\circ$ ,  $x$  reaches its maximum. When  $\beta$  attains  $90^\circ$ ,  $u = 1$ . As  $\beta$  increases towards  $180^\circ$ ,  $u$  diminishes, and so also does  $x$ . When  $\beta$  reaches  $180^\circ$ ,  $u$  is a minimum and  $x$  vanishes, so that vibration cannot be self-sustained. Between  $\beta = 180^\circ$ , and  $\beta = 360^\circ$ , no vibrations can be self-sustained.

If we assume that  $\psi(x)$  is simply proportional to the  $n$ th root of  $x$ , that is, that

$$(441) \quad \psi(x) = ax^{\frac{1}{n}} \quad \text{dynes,}$$

where  $a$  is a specific force factor, and if  $\beta = 90^\circ$ , we have

$$(442) \quad x = \frac{ax^{\frac{1}{n}}}{r\omega} \quad \text{max. cy. cm.,}$$

or

$$(443) \quad x = \left( \frac{a}{r\omega} \right)^{\frac{n}{n-1}} \quad \text{max. cy. cm.}$$

In case  $\psi(x)$  is proportional to  $\sqrt{x}$ ,  $n = 2$ , and at  $\beta = 90^\circ$ ,

$$(444) \quad x = \left( \frac{a}{r\omega} \right)^2 \quad \text{max. cy. cm.}$$

All of the preceding results can be applied to the case of the humming telephone discussed in Chapter XXIII. The curves in Fig. 148 were computed for different assumed values of  $\Delta$ , with  $n = 2$ . The actual force factor of the humming-telephone system employed was not determined, but the observations are in fair agreement with the theory. The same theory applies to the somewhat more complicated system of a vacuum-tube oscillator.\*

\* Bibliography 82 and 84.

## APPENDIX VII

### FREE OVERDAMPED VIBRATION OF A SIMPLE SYSTEM. ULTRAPERIODIC VIBRATION

When we have seen in Appendix VI that a simple vibratory system, mechanical or electric, will oscillate, or will execute cyclically reversing displacements, if its damping factor  $\Delta$  is numerically less than its resonant angular velocity  $\omega_0$ , that is, if its oscillatory bluntness  $B_0$  is less than unity. The free angular velocity of the damped vibrations was shown to be

$$(445) \quad \omega_f = \sqrt{\omega_0^2 - \Delta^2} = \omega_0 \sqrt{1 - B_0^2} = \omega_0 \sin(\cos^{-1} B_0) = \omega_0 \sin \gamma \quad \frac{\text{cir. rad.}}{\text{sec.}}$$

If, however,  $\Delta$  exceeds  $\omega_0$ , or  $B_0$  exceeds unity, this becomes

$$(446) \quad \omega_f = j\sqrt{\Delta^2 - \omega_0^2} = j\omega_0\sqrt{B_0^2 - 1} \quad \frac{\text{cir. rad.}}{\text{sec.}},$$

or the circular angular velocity  $\omega_f$  becomes imaginary. An imaginary circular angular velocity may, however, be regarded as equivalent to a real hyperbolic angular velocity,\* which we may denote by  $\Omega$ ; so that

$$(447) \quad \Omega = \sqrt{\Delta^2 - \omega_0^2} = \omega_0 \sqrt{B_0^2 - 1} \quad \frac{\text{hyp. rad.}}{\text{sec.}}$$

The motion in the overdamped case may thus still be regarded as having an angular velocity in the generalized sense; but a simple vibrator, overdamped, no longer has a real period or a frequency. Its period and its frequency become imaginary. Figure 185 indicates vectorially the transition from a circular to a hyperbolic angular velocity, as the damping factor  $\Delta$  increases in a simple system of given resonant  $\omega_0$ . This figure may be looked upon as an extension of Fig. 167. Here the circular quadrant  $OUC$  is scaled to have a radius of  $\omega_0 = \sqrt{s/m}$  circular radians per second. We have already seen that if  $\Delta = 0$ , the undamped angular velocity will then be  $OU$ . If  $\Delta$  be made  $OA$  hyps. per second, a perpendicular to  $OX$  from  $A$  will intersect the quadrant at  $a$ . The vector  $\omega$  in Fig. 171 will now be  $Oa = \omega_0 \angle \gamma = \Delta - jOa'$ , or the circular angular velocity will fall from  $OU$  to  $Oa'$ , as already described in connection with Fig. 167.

\* The writer who first called attention to a hyperbolic angular velocity in the discharge of an overdamped  $\mathcal{E}RS$  system was A. Macfarlane, Bibliography 14.

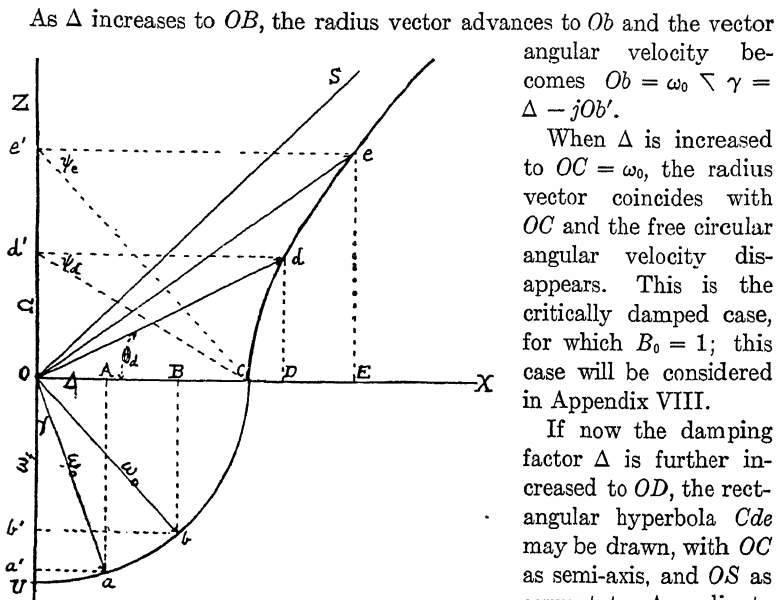


FIG. 185. Diagram of free angular velocities in periodic and ultraperiodic systems.

Then  $Dd = Od'$  is the hyperbolic angular velocity of the vibration, associated with the damping constant  $\Delta = OD$ . Thus we have

$$\Omega = \sqrt{\Delta^2 - \omega_0^2} = \omega_0 \sqrt{B_0^2 - 1},$$

$$(448) \quad = \omega_0 \sinh (\cosh^{-1} B_0) = \omega_0 \sinh \theta = \omega_0 \sinh (gd^{-1}\psi) \quad \frac{\text{hyp. rad.}}{\text{sec.}},$$

where  $\theta$  is the hyperbolic angle of the sector  $OCd$ , in hyp. radians. Similarly, if  $\Delta$  be increased to  $OE$ , the hyp. angular velocity is correspondingly increased to  $Oe'$ , associated with the damping constant  $OE$ .

In Fig. 185, if we draw a straight line from  $C$  to  $d'$ , the circular angle  $Cd'd$  may be denoted by  $\psi$ , for the hyp. sector  $Cod$ .\* This is called the *gudermannian angle*, or *gudermannian*, of the sector, and is usually written

$$(449) \quad \psi = gd \theta \quad \text{cir. radians.}$$

As is explained in textbooks on hyperbolic functions, the gudermannian of any hyperbolic angle  $\theta$  increases from 0 to  $\pi/2$  circular radians, or

\* This particular geometric method of finding the gudermannian of a hyp. sector is due to the late Dr. G. F. Becker.

from  $0^\circ$  to  $90^\circ$ , as  $\theta$  increases from zero to infinity. It is connected with  $\theta$  in very remarkable but well-known ways; namely,

$$(450) \quad \sin \psi = \tanh \theta$$

$$(451) \quad \cos \psi = \operatorname{sech} \theta$$

$$(452) \quad \sec \psi = \cosh \theta$$

$$(453) \quad \tan \psi = \sinh \theta.$$

Thus the sine, cosine, and tangent of a hyperbolic angle can be found from the ordinary trigonometric tables of circular angles, by first finding the gudermannian belonging to  $\theta$ . Conversely,  $\theta$  may be defined in terms of  $\psi$ , by (449), in the notation

$$(454) \quad \theta = gd^{-1} \psi \quad \text{hyps.}$$

It is often convenient to use this notation and mode of thought, because, if we can readily assign the value of the gudermannian  $\psi$  in Fig. 185, we do not need to construct the hyperbola  $Cde$ , in order to find the hyperbolic angle  $\theta$ .

We may readily find the gudermannian  $\psi$  in any ultraperiodic case, where  $\omega_0$  and  $\Delta$  are known. In Fig. 186, at diagram  $\Omega$ , draw  $op$  equal to  $\Delta$ , say along the  $OX$  axis, and in the  $XY$  plane. Construct upon  $op$  the semicircle  $oqp$ . Mark off with center  $o$ , a chord  $oq$  equal to  $\omega_0$ . Then  $qp$  will represent, to scale, the size of the hyperbolic angular velocity  $\Omega$ , for the vibration considered. We then have

$$(455) \quad \Omega = \sqrt{\Delta^2 - \omega_0^2} = \omega_0 \sinh \theta = \omega_0 \tan \psi = \omega_0 \operatorname{ctn} \psi' \quad \begin{array}{l} \text{hyps.} \\ \text{sec.} \end{array}$$

Moreover, in the right triangle  $oqp$ , the angle  $qop$  is  $\psi$ , the gudermannian of the corresponding hyperbolic angle in Fig. 185. The opposite angle  $qpo$  is  $\psi'$ , the gudermannian complement. As  $\Delta/\omega_0 = B_0$  increases from 1 to infinity, it is evident that from the construction that  $\psi$  increases from 0 to  $\pi/2$  radians, and  $\psi'$  diminishes correspondingly from  $\pi/2$  to 0.

It may be observed that a simple vibration system as previously defined, when overdamped, may be regarded conveniently as having a hyperbolic angular velocity  $\Omega$ , and this is not periodic. In more complicated dynamic systems, however, cases present themselves in which  $\Omega$  is a complex hyperbolic angular velocity, with periodic intervals of  $2\pi j$ . The general case of overdamped vibratory motion may thus include periods; although the simple vibratory system here considered, when overdamped, has no periods. It seems therefore more rational to describe underdamped motion as *periodic*, overdamped as *ultraperiodic*, and the intermediate limiting case of  $\Delta = \omega_0$  as *aperiodic*. We shall use these terms accordingly. Most writers, however, describe aperiodic motion as including all cases in which  $\Delta$  is greater than  $\omega_0$ ; or in which no circular angular velocity occurs.

Figure 186 gives a set of ultraperiodic stationary-vector diagrams corresponding to Figs. 158a, 171, and 180 for the periodic case. The  $\Omega$  triangle has been worked out for the particular case:

$$\begin{aligned} m &= 0.1 \text{ gm}, & s &= 0.25 \times 10^6 \text{ dynes/cm.}, & r &= 500 \text{ dynes/kine}, \\ & & \rho &= 250 \text{ dynes/kine}, \\ \text{or } \mathcal{L} &= 0.1 \text{ henry}, & s &= 0.25 \text{ megadaraf}, & r &= 500 \text{ ohms}, \\ & & \rho &= r/2 = 250 \text{ ohms}. \end{aligned}$$

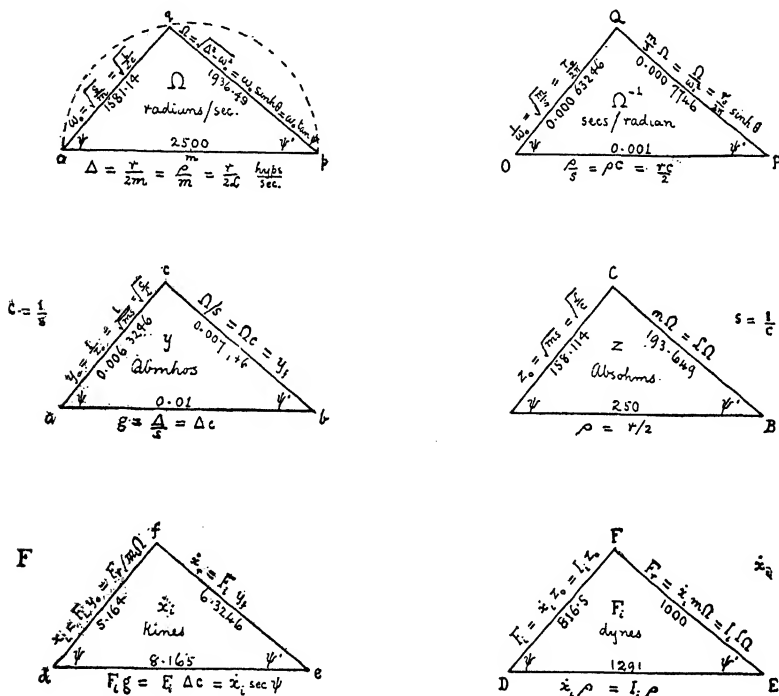


FIG. 186. Ultraperiodic motion diagrams.

Here  $\omega_0 = 1581.14$  cir. radians per second,  $\Delta = 2500$  hyp. radians per second. As explained in connection with Fig. 185, we draw  $op$  to scale to represent  $\Delta = 2500$ , and in a semicircle on  $op$  as diameter, draw the chord  $oq$  to represent  $\omega_0$ . The chord  $pq$  then represents the hyperbolic angular velocity of the motion, or 1936.49 hyps. per second. The angle  $\psi$  is  $50^\circ 46' 6''$ , and happens to be the same as the angle  $\gamma$  in the triangles of Fig. 171. It is the gudermannian of the hyperbolic angle  $\theta$ , in the construction of Figs. 185 and 186. Whereas the triangles of Fig. 171 are plane-vector triangles and subject to the arithmetic relations of complex quantities, the triangles of Fig. 185 are of scalar significance only. There are many analogies, however, between the two series.

**Ultraperiodic Admittance.** — If we multiply the  $\Omega$  triangle of Fig. 186 by  $c = 1/s$ , we obtain the similar triangle  $abc$  of admittance. The side  $ac$  measures, to a suitable scale, the surge admittance  $y_0$  of the periodic state; in this case 6.3246 millimhos. The side  $ab$  scales the conductance  $g = \Delta c$ . The side  $bc$  scales the susceptance  $y_f = \Omega c = 7.746$  millimhos.

**Initial Current or Velocity.** — Multiplying the  $y$  triangle by  $F_i$ , the initial motive force, we obtain the triangle  $def$ . The side  $df$  scales the initial radius vector current  $\dot{x}_i$  or  $\bar{I}_i$ . The side  $de$  scales the component  $F_{ig} = 8.165$  amperes. The side  $ef$  scales the reactive component  $I_r = 6.3246$  amperes.

**Ultraperiodic Impedance.** — Multiplying the  $\Omega^{-1}$  triangle by  $s$ , we obtain the impedance triangle  $z$ . The base  $AB$  is  $\rho$ , half the total resistance in the system. The side  $AC$  scales the surge impedance  $z_0 = \sqrt{ms}$ . The side  $BC$  then scales the quantity  $m\Omega$  which may, by analogy, be called the *ultraperiodic reactance*.

**Initial Motive Force.** — The  $DEF$  triangle is obtained from the  $z$  triangle by multiplying with  $I_i$  or  $\dot{x}_i$ , the initial radius-vector current or velocity. The side  $DF$  then scales the initial radius-vector motive force, the side  $DE$  the initial voltage expended on  $\rho$ , the semi-resistance, the side  $EF$  the initial voltage expended on the reactance  $\Omega$ .

**Ultraperiodic Vector Diagram for Potential Energy Case.** — Figure 187 indicates the vector diagram for an ultraperiodic case of a mechanical or electric system energized potentially, or by displacement, and released at the instant represented ( $t = 0$ ). The lower rectangular hyperbola  $c'B'Afc$  has the semi-axis  $OA$ , and asymptotes  $Os'$ ,  $Os'$ . The upper curve  $c'b'abc$  is the other half of the complete hyperbola. The upper curve  $E'DE$  is also a rectangular hyperbola drawn to the same asymptotes  $Os$ ,  $Os$ ; but with semi-axis  $OD$ .

At the moment  $t = 0$ , or initial instant of a system potentially energized, as by spring compression, and suddenly released, there are three vector forces to consider; namely  $OF_i$ , the initial vector motive force that starts the motion or discharges,  $OG$ , the vector inertia force, and  $OD$ , the vector force of frictional resistance  $-x_i r$ .

The vector initial force  $F_i$  makes a hyperbolic angle  $\theta$  as obtained in Fig. 185, with the axis  $OA$ . The angle  $AF'F_i$  is the gudermannian  $\psi$ , corresponding thereto. The vector  $OG$  is the initial counterforce of inertia. The two initial vectors  $OF_i$  and  $OG$  are equally inclined to the axis  $OA$ , which is the direction of the initial vector velocity  $\dot{x}_i$ . Opposite to  $OA$  is the initial vector retarding force  $OD$  or  $-r\dot{x}_i$ .

The three vector forces  $OF_i$ ,  $OG$  and  $OD$ , lying in the plane  $XOY$ , are in equilibrium. All three rotate about the center  $O$  with the uniform hyperbolic angular velocity  $\Omega$  hyps. per second, in the directions of the arrows. The extremities of the vectors  $OG$  and  $OF_i$  lie on the hyperbola  $c'A_c$ , while the extremity of  $OD$  lies on the hyperbola  $E'DE$ . Each vector





The rotary-vector diagram, Fig. 187, for hyperbolic damped angular velocity  $\Omega$ , corresponds to rotary-vector diagram, Fig. 177, for circular velocity  $\omega$ . In each case, the damping coefficient  $\epsilon^{-\Delta t}$  has to be applied at the instantaneous value of  $t$ . The projections  $OF'$ ,  $Of'$ , etc., go on increasing indefinitely with time, as the vector  $OF$  advances over the hyperbola  $Afc$ ; but the effect of the factor  $\epsilon^{-\Delta t}$  on these projections is always to bring them steadily back towards  $O$ .

Not only therefore are the three hyperbolically rotating vectors  $OG$ ,  $OF$ , and  $OD$  in continuous equilibrium, but the sum of their projections at any instant, such as  $Og'$ ,  $Of'$ ,  $Od'$  retains equilibrium. The same is true after the damping coefficient  $\epsilon^{-\Delta t}$  has been applied to all three of them. The damped-vector system rapidly shrinks to the center  $O$ .

An examination of Fig. 187 will show that the velocity  $\dot{x}$ , or current  $I$ , never changes sign, since the vector  $OD$  always moves in the same direction over its hyperbola. Its projected size, however, after applying the damping coefficient  $\epsilon^{-\Delta t}$ , rises to a maximum, and then dwindles to zero, — after an indefinitely long period. The elastic motive force of the spring acting on the system — or its electric prototype, the emf. of the condenser — likewise keeps the same direction throughout the discharge. The inertia force, however, or cemf. of self-induction, does change sign. It reverses at the instant when the vector  $OG$  crosses the axis  $OA$ .

It may be observed that in forced oscillations, or in the alternating-current circuit, the vector force of inertia, or emf. of self-induction, is always in quadrature with the vector of velocity or current, and therefore there is no continuous work done by one upon the other. In free vibration, however, whether periodic or ultraperiodic, it is evident from Figs. 177 and 187, that the vector inertia force is inclined to the vector current at an acute angle, so that the former continues to work on the latter during the discharge.

The hyperbolic vector diagram is presented in Fig. 188 for the particular electric or mechanical case already specified, retaining the electric analogue. Here, the  $4 \mu f$  condenser is charged to a potential difference  $\bar{U}_t = F_r = 1000$  volts, and discharged through  $r = 500$  ohms, and  $\mathcal{L} = 0.1$  henry, at  $t = 0$ . It will be observed that the triangle  $\bar{I}_t \bar{U}_t O$ , is the same as the  $DEF$  triangle of Fig. 186. The angle  $\psi$  of  $50^\circ 46' 06''$  is the gudermannian of the angle  $\theta = 1.03172$  hyps., or  $\theta = gd^{-1}(50^\circ 46' 06'')$ . From Tables of real hyperbolic functions, this value of  $\theta$  can be found without depending upon the graphic accuracy of Fig. 188, where  $\cosh \theta = 1291/816.5 = 1.5811$ , and  $\sinh \theta = 1000/816.5 = 1.2247$ , whence, by Tables,  $\theta = 1.03172$ . It is easy to see that at time  $t = 0$ , the projected or undamped value of the condenser potential difference is  $OU_t = 816.5 \sinh \theta = 816.5 \times 1.2247 = 1000$  volts, which is the initial condenser potential difference  $F_r$ , Fig. 186. At any subsequent time  $t$  seconds, the undamped projected value is  $816.5 \sinh (\Omega t + \theta)$ , where  $\Omega t$  is the hyperbolic



The initial vector  $O\bar{E}_i$  is drawn in Fig. 188 to match  $O\bar{U}_i$ . It advances, as time goes on, along the hyperbola towards  $\bar{I}_i$ , by the arrowhead steps 1, 2, 3, etc. After 5 such ten-thousandth second steps, the vector crosses the semidiameter  $O\bar{I}_i$ , and its projection on the  $X$  axis will change sign. The damped curve  $1' 2' 3'$  is also indicated. The emf. of self-induction, which at first opposes the current in the system, will thus reverse and subsequently help to propel the current, although in a stage where its size has become much reduced.

The initial frictional-force vector  $-I_i r$  is shown reversed, or below the  $X$  axis in Fig. 188, in order to save space. It is made to move clockwise to simulate the effect of reversal in direction. Its instantaneous positions in the damped curve and these projections on the  $X$  axis are indicated.

If we fit the  $def$  triangle of Fig. 186 into the space  $\bar{I}_i U_i O$ , Fig. 188, we find that the initial vector value of the discharging current  $O\bar{I}_i$  is 5.164 amperes, and its initial projection on  $X$  is zero. This current vector also moves along the hyperbola in the direction  $H'$ , with angular velocity  $\Omega$ . Its damped projection along  $OX$  undergoes no change in sign. Its size may be inferred from the projection of  $-\bar{I}_i r$ .

**Algebraic Scalar Relations of Ultraperiodic Motion.** — The algebraic values of  $u$ ,  $e$ , and  $i$  may be written down from an examination of Fig. 188. They correspond to formulas (405) to (408) of the periodic case.

The instantaneous actual condenser potential difference is

$$(456) \quad f = F_r \operatorname{ctn} \psi \cdot \epsilon^{-\Delta t} \cdot \sinh(\Omega t + \theta) = F_i \epsilon^{-\Delta t} \cdot \sinh(\Omega t + \theta) \\ = F_i \epsilon^{-\Delta t} \cdot \sinh(\Omega t + g d^{-1} \psi) \quad \text{volts,}$$

where  $F_r$  is  $FE$ , the initial actual potential difference, and  $F_i$  the size of  $DF$  the semi-axis vector potential difference of Fig. 186, or 816.5 volts.

$$(457) \quad i = I_i \cdot \epsilon^{-\Delta t} \cdot \sinh \Omega t \quad \text{amperes,}$$

where

$$(458) \quad I_i \text{ or } \dot{x}_i = \frac{F_r}{m\Omega} = \frac{U_r}{E\Omega} = \frac{F_i}{z_0} = \frac{U_i}{z_0} \quad \text{amperes.}$$

$I_i$  scales  $df$  or 5.164 amperes, Fig. 186.

The instantaneous actual emf. of self-induction is

$$(459) \quad e = F_r \operatorname{ctn} \psi \cdot \epsilon^{-\Delta t} \cdot \sinh(\Omega t - \theta) = F_i \cdot \epsilon^{-\Delta t} \cdot \sinh(\Omega t - \theta) \quad \text{volts.}$$

The instantaneous power of the condenser in the system is

$$(460) \quad p = fi = F_i I_i \cdot \epsilon^{-2\Delta t} \cdot \sinh \Omega t \cdot \sinh(\Omega t + \theta) \quad \text{watts.}$$

It may be noted that the cemf.  $e$  changes sign, or reverses, when

$$(461) \quad \Omega t = \theta \quad \text{hypers.}$$

so that the time required to reverse the cemf. is

$$(462) \quad \tau_r = \frac{\theta}{\Omega} \quad \text{seconds.}$$

This reversal time is an important property of the ultraperiodic system. In the case considered it is

$$\frac{1.03172}{1936.49} = 0.0005328 \text{ second.}$$

No second reversal occurs. The reversal in  $e$  occurs simultaneously with the recession, or passage of  $i$  through a maximum. It corresponds to the reversal of current in the kinetically energized ultraperiodic case.

The apparent resistance of the circuit to the discharging potential difference is, from (456) and (457)

$$(463) \quad z = \frac{f}{i} = \rho + \mathcal{E}\Omega \operatorname{ctnh} \Omega t \quad \text{ohms.}$$

This impedance is always real. It commences at an infinite value, and tends rapidly to the value  $(\rho + \mathcal{E}\Omega)$  ohms.

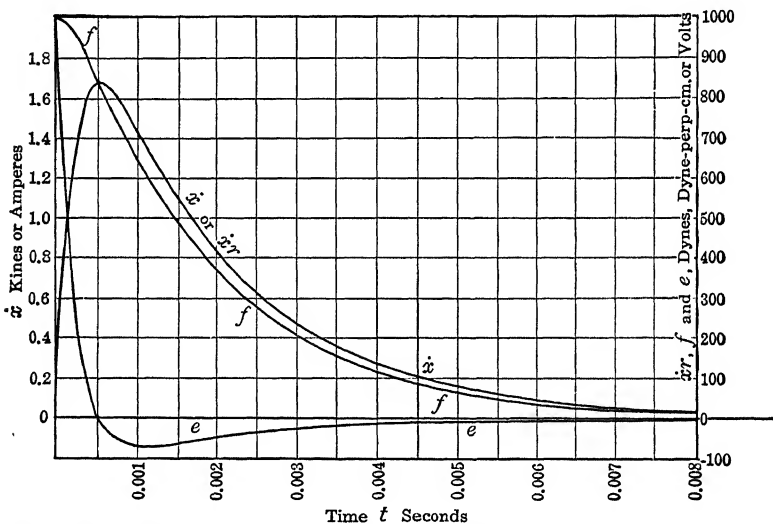


FIG. 189. Ultraperiodic motion for potentially energized system having constants  $s = 250,000$ ,  $m = 0.1$ ,  $r = 500$ ,  $\omega_0 = 1581$ ,  $\theta = 1.0317$ ,  $\Delta = 2500$ ,  $\Omega = 1936$ ,  $\psi = 50^\circ 46'$ ,  $B_0 = 1.581$ ,  $F_r = 1000$ ,  $\tau_r = 0.00053$ .

**Algebraic Scalar Relations obtained from Exponentials.** — We have derived the values of the ultraperiodic forces current and power from the hyperbolic analogue (Fig. 187) to the circular vector diagram (Fig. 177). They are usually derived, however, from the fundamental equation

$$(464) \quad q \text{ or } x = A\epsilon^{-t(\Delta-\Omega)} + B\epsilon^{-t(\Delta+\Omega)} \quad \text{coulombs or cm.}$$

which is also a solution of the fundamental differential equation. For the case of initial potential energy,

$$q = Q = F_r c = F_r / s,$$

and  $i = \dot{q} = 0$ , at  $t = 0$ . Consequently

$$(465) \quad f = \frac{F_r}{2\Omega} (\Delta + \Omega) \epsilon^{-t(\Delta - \Omega)} - \frac{F_r}{2\Omega} (\Delta - \Omega) \epsilon^{-t(\Delta + \Omega)} \quad \text{volts,}$$

$$(466) \quad i = \frac{Q}{2\Omega} \omega_0^2 \cdot \epsilon^{-t(\Delta - \Omega)} - \frac{Q}{2\Omega} \omega_0^2 \cdot \epsilon^{-t(\Delta + \Omega)} \quad \text{amperes,}$$

$$(467) \quad e = \frac{F_r}{2\Omega} (\Delta - \Omega) \epsilon^{-t(\Delta - \Omega)} - \frac{F_r}{2\Omega} (\Delta + \Omega) \epsilon^{-t(\Delta + \Omega)} \quad \text{volts ;}$$

or, in the case considered,

$$(468) \quad f = 1145.5 \epsilon^{-t(\Delta - \Omega)} - 145.5 \epsilon^{-t(\Delta + \Omega)} \quad \text{volts,}$$

$$(469) \quad i = 2.582 \epsilon^{-t(\Delta - \Omega)} - 2.582 \epsilon^{-t(\Delta + \Omega)} \quad \text{amperes,}$$

$$(470) \quad e = 145.5 \epsilon^{-t(\Delta - \Omega)} - 1145.5 \epsilon^{-t(\Delta + \Omega)} \quad \text{volts.}$$

The hyperbolic formulas (456) to (459) are probably easier to use in computations, except for large hyperbolic angles and values of  $t$ .

Figure 189 gives the values of  $f$ ,  $e$ ,  $i$ , and  $\dot{v}$  for the case considered, taking either set of formulas. It will be seen that the condenser potential difference  $f$  falls at first slowly for the first few ten-thousandths second, then rapidly, and finally very slowly towards zero.

The curve of  $i$  or of  $\dot{v}$  is the differential curve of  $f$ . It reaches a maximum value at 0.00053 second, the *reversal time* for the system. The curve of  $e$  commences at the initial value of  $f$ , but falls more rapidly, changes sign at 0.00053 second, and then slowly ascends to zero. The  $e$  curve is a first derived curve of the  $\dot{v}$  curve, or a second derived curve of the  $f$  curve.

**Kinetically Energized Ultraperiodic System.** — Just as in the periodic case, the initial vector diagram Figure 174, for the kinetically energized system differs only in phase from that (Fig. 177) for the potentially energized system, so in the ultraperiodic case, the two hyperbolic vector diagrams differ only in phase, if the initial stock of energy is the same.

A set of connections for the electric case are shown in Fig. 191. A low-resistance reactor is energized by the battery  $E$  through the ammeter  $A$ . At time  $t = 0$ , the switch  $S$  is suddenly and sparklessly opened.

The case of the same ultraperiodic circuit or mechanical system that has already been considered is presented by initial vector diagram in Fig. 190. It corresponds to Fig. 174 for the periodic case. The vector current  $OB$  makes a hyperbolic angle  $\theta$  hyps. with  $OA$ , the semi-axis of the hyperbola  $HAH'$ . The vector emf. of inertia  $OG$  makes a hyperbolic angle of  $2\theta$  hyps. with  $OA$ . The vector  $OD$  of  $Ir$  is in opposite phase to  $OB$ . The initial vector of condenser potential difference starts on the semi-axis

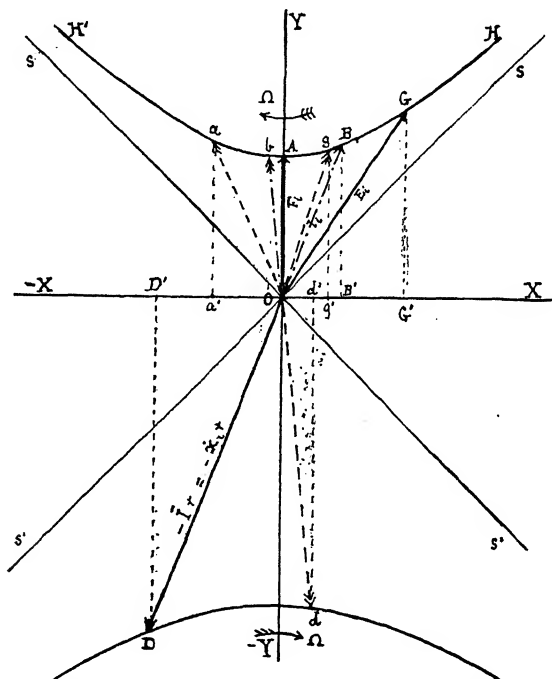


FIG. 190. Rotary-vector diagram of ultraperiodic vibration kinetically energized.

O.A. As time goes on, both  $I_r$  and  $E_i$  will cross the semi-axis  $OA$ , and their damped projections on the  $OX$  axis will reverse in sign. The projection of  $F_i$  will not reverse in sign.

After a lapse of time  $t$  equal to the reversal time  $\tau_r = \theta/\Omega$ , the vectors of the system will all coincide with the reverse of Fig. 187, or the inverse of Fig. 190 will coincide with Fig. 187, showing that the essential difference between the two diagrams is a matter of phase only, after taking into account the fact that  $f$  should be reckoned as negative in the case of Fig. 190, since it opposes a + current discharge, while in the case of Fig. 187,  $f$  is positive, since it propels the + current discharge.

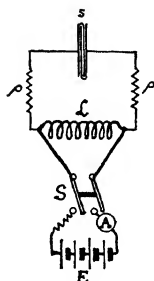


FIG. 191. Diagram of connections for kinetically energizing a simple ERS circuit with an initial current by ammeter  $A$ , before suddenly opening at switch  $S$ .

Algebraic Scalar Relations of Kinetically Energized Ultraperiodic System. — Referring to Fig. 190 for the damped projections of the hyperbolically rotating vectors, we have,

$$(471) \quad f = -I_r z_o \operatorname{ctn} \psi \cdot e^{-\Delta t} \cdot \sinh \Omega t = -F_t \cdot e^{-\Delta t} \cdot \sinh \Omega t \quad \text{volts,}$$

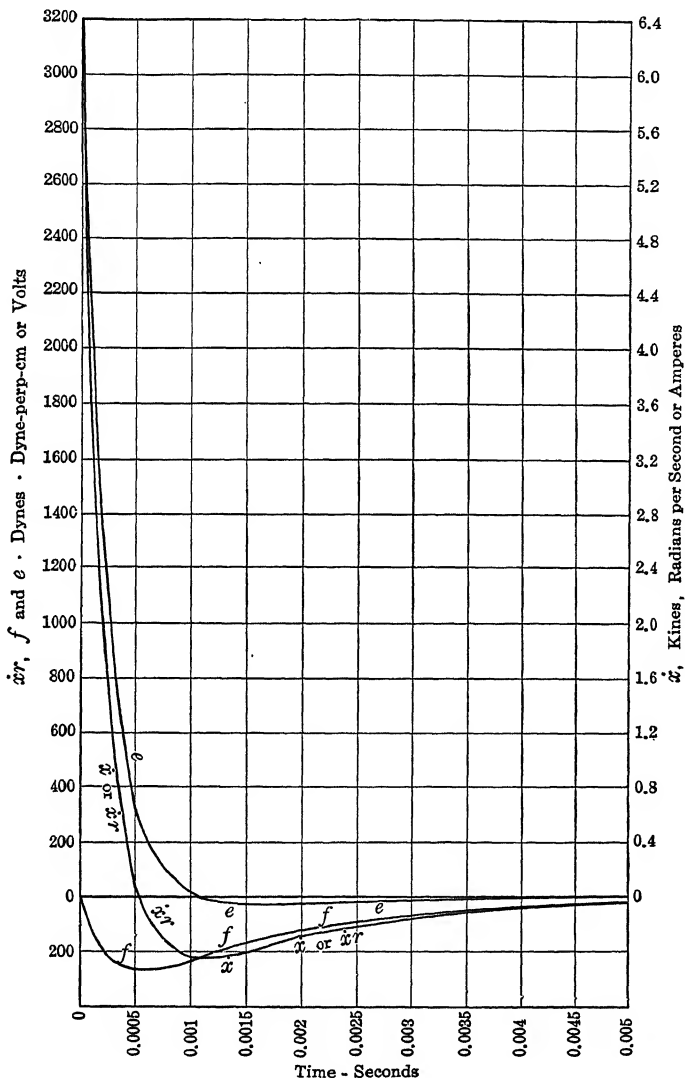


Fig. 192. Ultraperiodic motion for kinetically energized system having the same constants as in Fig. 189.  $I_r$  or  $\dot{x}_r = 6.3246$ .



$$(472) \quad i \text{ or } \dot{x} = -I_t \cdot \epsilon^{-\Delta t} \cdot \sinh(\Omega t - \theta) = -I_r \operatorname{ctn} \psi \epsilon^{-\Delta t} \cdot \sinh(\Omega t - \theta) \quad \text{amperes,}$$

where

$$(473) \quad I_t = \frac{U_r}{\mathcal{E}\Omega} = \frac{F_r}{m\Omega} = \frac{U_t}{z_0} = \frac{F_t}{z_0} = I_r \operatorname{ctn} \psi \quad \text{amperes}$$

$$(474) \quad e = -I_r z_0 \operatorname{ctn} \psi \cdot \epsilon^{-\Delta t} \cdot \sinh(\Omega t - 2\theta) = -F_t \cdot \epsilon^{-\Delta t} \cdot \sinh(\Omega t - 2\theta) \quad \text{volts,}$$

$I_r$  being the initial actual current of discharge. See (456)-(459).

The equivalent exponential expressions are found from (464), by taking  $q = 0$  when  $t = 0$ , and  $\dot{q} = i = -I_r$  when  $t = 0$ . These give

$$(475) \quad f = -\frac{I_t g}{2\Omega} \{ \epsilon^{-t(\Delta - \Omega)} - \epsilon^{-t(\Delta + \Omega)} \} \quad \text{volts,}$$

$$(476) \quad i = I_r \left\{ \left( \frac{\Delta - \Omega}{2\Omega} \right) \epsilon^{-t(\Delta - \Omega)} - \left( \frac{\Delta + \Omega}{2\Omega} \right) \epsilon^{-t(\Delta + \Omega)} \right\} \quad \text{amperes,}$$

$$(477) \quad e = -\frac{\mathcal{E}I_t}{2\Omega} \{ (\Delta - \Omega)^2 \epsilon^{-t(\Delta - \Omega)} - (\Delta + \Omega)^2 \epsilon^{-t(\Delta + \Omega)} \} \quad \text{volts.}$$

If we plot  $f$ ,  $e$ ,  $i$ , and  $\dot{x}$  as ordinates against time as abscissas, we obtain the graphs of Fig. 192. Here  $e$  and  $\dot{x}$  both commence at the value 3162 volts. The current  $i$  commences at 6.3246 amperes, which conveys the same initial stock of energy (2 joules) as in the preceding case of 1000 volts potential difference.

At the reversal time 0.00053 second, the current  $i$ , and the potential difference reverse. The inertia force  $e$  does not reverse until twice the reversal time has elapsed.

In this case, the system dissipates energy more rapidly from the kinetic start than from the potential start; the residual current, after say 0.002 second, being decidedly less than at that elapsed time in Fig. 189.

It is evident from a consideration of Figs. 190 and 192 that it is inaccurate to assert that the current cannot reverse in an overdamped discharge. The current and cemf. both reverse in the case of Figs. 190, 191, and 192. The cemf. reverses in the case of Figs. 188 and 189. The elastic force  $f$  alone retains the same direction throughout.

Any ultraperiodic case of mixed potential and kinetic energization can be dealt with quantitatively by showing each part separately, and then adding the component results.

## APPENDIX VIII

### FREE CRITICALLY DAMPED VIBRATION. APERIODIC VIBRATION

When  $\rho$ , the semiresistance of the system, is just equal to the surge resistance  $z_0 = \sqrt{L/c} = \sqrt{ms}$ , the oscillatory bluntness  $B_0 = 1$ , and the system is aperiodic, or intermediate between the periodic and ultraperiodic states. There is then neither a circular angular velocity  $\omega_f$ , nor a hyperbolic angular velocity  $\Omega$ .

Since a plane intersecting a right cone, in passing from the position where the curve of intersection is a circle to that where the curve of intersection is a hyperbola, must pass through a position where it is a parabola, it might be surmised that since a circular angular velocity applies to the periodic case, and a hyperbolic angular velocity to the ultraperiodic case, a parabolic angular velocity may apply to the intermediate aperiodic case, with a corresponding parabolic vector diagram. Such a diagram has indeed been proposed.\* It will suffice for our purposes, however, if we treat the aperiodic state as the limiting case either of the periodic state on the one hand, or of the ultraperiodic state on the other. In following each of these limiting cases we may derive the same results.

**Aperiodic System Potentially Energized, as Limiting Case of Periodic System.** — When in the  $\omega$  diagram of Fig. 171, we make the limiting value of  $\omega_0$  approach  $\Delta$ , the diagram nearly degrades into a single straight line. In Fig. 193, this diagram is presented in a preliminary stage, with  $\omega_f$  small but still easily recognizable. In the limiting case the value of  $\Delta = \omega_0$  may be indicated as  $\Delta_0$ . The angle  $\gamma$  shrinks to zero. If we consider a simple  $mrs$  or  $\mathcal{E}RS$  system, potentially energized by bending and releasing the spring in the one case, or charging the condenser and closing its circuit in the other, we may, following (405), write the instantaneous elastic force in the form

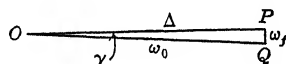


FIG. 193. Aperiodic case as limiting condition of o. c. circuit, when  $\Delta = \omega_0$ . Stationary vector-diagram of  $\omega_0$ .

$$(478) \quad f = F_r \cdot \csc \gamma \cdot e^{-\Delta t} \cdot \sin(\omega_f t + \gamma) \quad \text{dynes or volts,}$$

where  $F_r$  was the actual initial force at  $t = 0$ . Here we may substitute (see Fig. 193)  $1/\gamma$  for  $\csc \gamma$ , and  $\Delta_0 \gamma$  for  $\omega_f$ . Moreover, since  $(\omega_f t + \gamma)$  is a small angle, we may substitute  $(\omega_f t + \gamma)$  for  $\sin(\omega_f t + \gamma)$ . Consequently (478) becomes

$$(479) \quad \begin{aligned} f &= \frac{F_r}{\gamma} \cdot e^{-\Delta_0 t} (\Delta_0 \gamma t + \gamma) \\ &= F_r \cdot e^{-\Delta_0 t} (\Delta_0 t + 1) = F_r \cdot e^{-\Delta_0 t} (\omega_0 t + 1) \quad \text{volts or dynes.} \end{aligned}$$

\* Macfarlane, Bibliography 14, p. 179.

Similarly, we obtain from (406) and the formulas which immediately follow it, the displacement

$$(480) \quad x = -\frac{F_r}{s} \cdot \epsilon^{-\Delta_0 t} (\Delta_0 t + 1) \quad \text{cm. or coulombs.}$$

The velocity is

$$(481) \quad \dot{x} = \frac{F_r}{s} \Delta_0^2 t \cdot \epsilon^{-\Delta_0 t} = \frac{F_r}{m} t \cdot \epsilon^{-\Delta_0 t} \quad \text{kines or amp.}$$

The resistance counter force is

$$(482) \quad -\dot{x}r = -2F_r \cdot \Delta_0 t \cdot \epsilon^{-\Delta_0 t} \quad \text{dynes or volts.}$$

The inertia counter force is

$$(483) \quad e = -\ddot{x}m = F_r \cdot \epsilon^{-\Delta_0 t} (\Delta_0 t - 1) \quad \text{dynes or volts.}$$

It may be noted that in these expressions for  $f$ ,  $\dot{x}$ ,  $\dot{x}r$  and  $e$ , undamped, or before applying the damping coefficient  $\epsilon^{-\Delta_0 t}$ , all add equal increments in equal times.

The instantaneous power developed by the spring or condenser is

$$(484) \quad p_c = f\dot{x} = \frac{F_r^2}{m} \cdot \epsilon^{-2\Delta_0 t} \cdot t(\Delta_0 t + 1) \quad \text{abwatts or watts.}$$

The instantaneous power of the reactive inertia force is

$$(485) \quad p_m = -e\dot{x} = \ddot{x}m\dot{x} = \frac{F_r^2}{m} \cdot \epsilon^{-2\Delta_0 t} \cdot t(\Delta_0 t - 1) \quad \text{abwatts or watts.}$$

The dissipatory power of resistance is

$$(485a) \quad \dot{x}^2 r = p_c + p_m = \frac{2F_r^2}{m} \Delta_0 t^2 \cdot \epsilon^{-2\Delta_0 t} \quad \text{abwatts or watts.}$$

The velocity  $\dot{x}$  or current  $i$  reaches a maximum, according to (481), when  $t = 1/\Delta_0 = 1/\omega_0 = \tau_0$  secs, when  $\Delta_0 t = 1$ , and

$$(486) \quad \dot{x} = \frac{F_r}{m} \cdot \tau_0 \cdot \epsilon^{-1} = \frac{F_r}{s} \Delta_0 \epsilon^{-1} \quad \text{kines or amp.,}$$

where  $\tau_0$  is the oscillatory time constant  $m/\rho$  or  $\mathcal{E}/\rho$  seconds. The elastic force  $f$  diminishes towards zero without change of sign. The inertia force  $e$  reverses direction, however, at  $t = \tau_0$ , and thereafter propels instead of opposing the current. Hence in an aperiodic system, the reversal time  $\tau_r$  is equal to  $\tau_0$ . In the case considered,  $\tau_r = \tau_0 = 0.000632$  second.

**Aperiodic System Potentially Energized as Limiting Case of an Ultraperiodic System.** — Considering the tri-

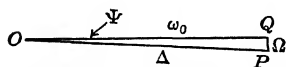


FIG. 194. Aperiodic case as limiting condition of ultraperiodic circuit, when  $\omega_0 = \Delta$ . Stationary vector-diagram of  $\Omega$ .

angle of Fig. 186, when  $\Delta$  approaches  $\omega_0$ , the triangle approaches collapse into a straight line with  $\Omega = 0$ . In Fig. 194, a preliminary stage is indicated with  $\Omega$  small. Then, repeating (456), the expression for the instantaneous elastic

force during discharge at time  $t$  from the initial application, is

$$(487) \quad f = \frac{F_r}{\sinh \theta} \cdot \epsilon^{-\Delta_0 t} \cdot \sinh(\Omega t + \theta) = F_r \cdot \text{ctn } \psi \cdot \epsilon^{-\Delta_0 t} \cdot \sinh(\Omega t + \theta)$$

dynes or volts.

Here  $\text{ctn } \psi$  becomes  $1/\psi$ , and  $\sinh(\Omega t + \theta) = \Omega t + \theta$ , also  $(\Omega t + \theta) = \Delta_0 \psi t + \psi$ , so that at the limit,

$$(488) \quad f = F_r \cdot \epsilon^{-\Delta_0 t} (\Delta_0 t + 1) \quad \text{dynes or volts,}$$

which agrees with (479). Equations (480) to (485) follow at once.

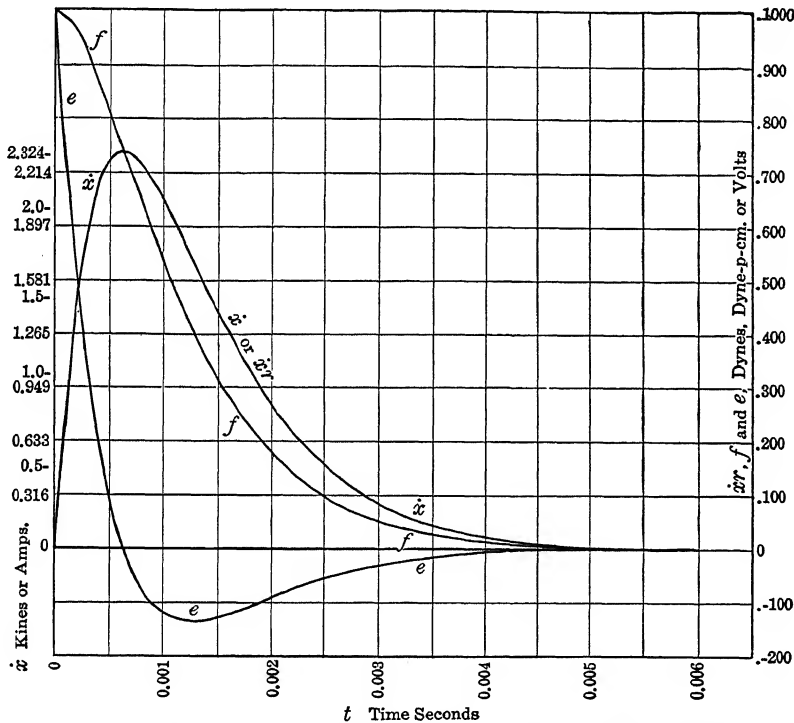


FIG. 195. Aperiodic motion for potentially energized system having the constants:  $s = 250,000$ ,  $m = 0.1$ ,  $r = 316.228$ ,  $\omega_0 = 1581.14 = \Delta_0$ ,  $B_0 = 1.0$ ,  $F_r = 1000$ ,  $\tau_r = \tau_0 = 0.000632$  sec.

In the case considered,  $F_r = 1000$ , and  $\Delta_0 = 1581.15$ ,  $r = 316.228$ ,  $\rho = 158.114$ . Figure 195 gives the graphs of  $f$ ,  $\dot{x}$ ,  $\ddot{x}$ , and  $e$  for this case. It will be observed that  $\ddot{x}$  reaches a maximum of 735 dynes or volts, at  $t = 0.000632$  second. The corresponding velocity or current is 2.3243 kynes or amperes.

If the system is energized kinetically with an initial velocity  $\dot{x}_i$  or  $I_i$  at  $t = 0$ , we obtain from (471)-(474)

$$(489) \quad i \text{ or } \dot{x} = -I_r \cdot e^{-\Delta_0 t} (\Delta_0 t - 1) \quad \text{amp. or kines,}$$

$$(490) \quad -\dot{x}r = 2I_r z_0 \cdot e^{-\Delta_0 t} (\Delta_0 t - 1) \quad \text{volts or dynes,}$$

$$(491) \quad f = -I_r \cdot z_0 \cdot e^{-\Delta_0 t} \cdot \Delta_0 t \quad \text{volts or dynes,}$$

$$(492) \quad e = -I_r \cdot z_0 \cdot e^{-\Delta_0 t} (\Delta_0 t - 2) \quad \text{volts or dynes.}$$

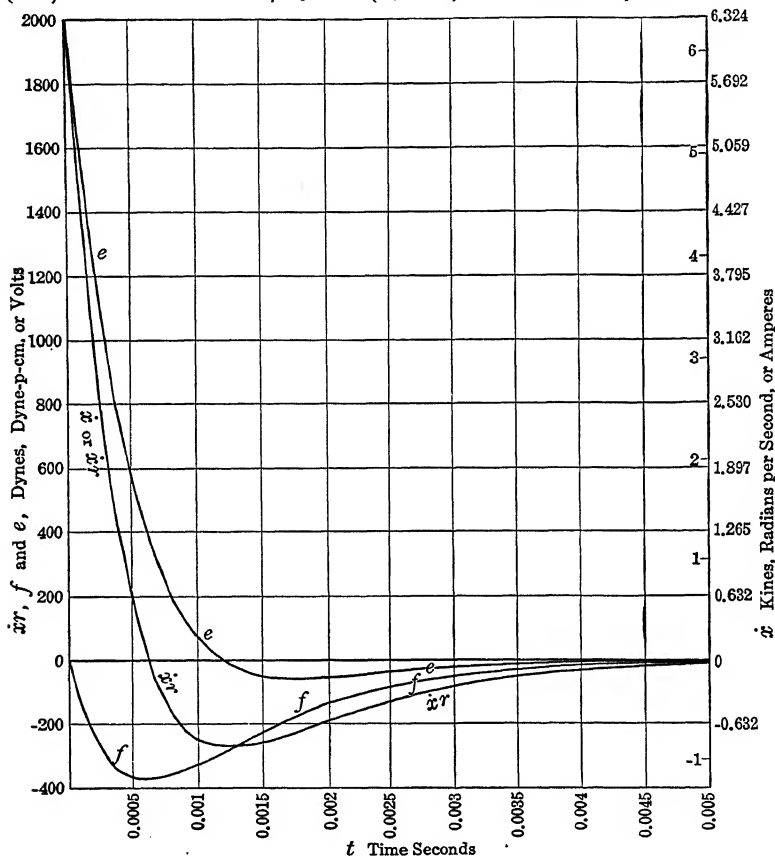


FIG. 196. Aperiodic motion for kinetically energized system having the same constants as in Fig. 195.  $I_i$  or  $\dot{x}_i = 6.3246$ .

The initial current  $I_r$  for the aperiodic system above considered, if energized kinetically to the same amount (2 joules), as in the potentially energized case, is 6.3246 amperes. Figure 196 shows the values of  $f$ ,  $e$ ,  $\dot{x}$ , and  $\dot{x}r$  for this case. It will be seen that the current reverses direction when  $t = \tau_0 = 0.000632$  second, and the inertia force changes sign when  $t = 2\tau_0$ ; but  $f$  does not change sign.

Figure 196a is an oscillogram of the discharge of an inductance through a condenser and a nearly aperiodic quantity of total resistance. The inductance was initially energized by sending a current of 0.078 amperes through it. The circuit elements are approximately the same as those dealt with in Fig. 196, but the exciting current and the energy are much smaller. In the first 0.01 second, the inductance is energized by closing it upon a pair of 115-volt mains through a resistance of 1475 ohms total resistance, the connections being substantially as shown in Fig. 191. Shortly before the end of this 0.01 sec. interval, the charging switch is opened, allowing the inductance to discharge through the condenser and resistance. The current following the curve *aa*, falls rapidly and reverses after 0.001 second to  $-0.006$  amperes. The shape of this curve agrees

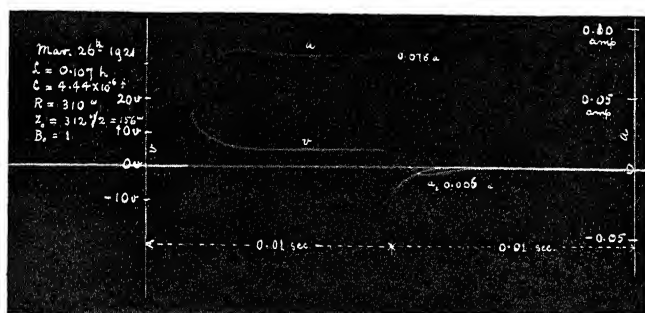


FIG. 196a. Oscillogram of current and voltage at terminals of an inductance of 0.107 henry and 53 ohms, connected substantially as in Fig. 191, and discharging, after 0.01 second, through a condenser of 4.44 microfarads, and a total resistance of 310 ohms. Circuit approximately aperiodic.  $\tau_0 = 0.0007$  second.  $B_0 = 1$ .

fairly well with the  $\dot{x}$  curve in Fig. 196. According to the theory of Fig. 196, however, the current should reverse to a negative maximum of about 0.01 ampere. The oscillatory time constant of the circuit in Fig. 196a being 0.0007 second, the current should pass through zero at that time after rupture. In the oscillogram, it passes through zero about 0.0010 second after rupture. These discrepancies may be accounted for by the fact that the arc at the circuit-opening switch probably did not completely extinguish until about 0.0004 second after switch contact rupture, as is shown by the sudden change in the shape of the voltage curve *v* at that time. This voltage *v* was measured across the terminals of the inductance and not across the terminals of the condenser, which accounts for the difference between its curve and that of curve *f*, Fig. 196. That is, the voltage *v* includes most of the  $IR$  drop as well as the potential difference across the condenser.

**Reversal Times in Vibrators of the same  $m$  and  $s$  but with Different Bluntness  $B_0$ .** — From what has been shown in this and preceding Chapters, it will be evident that the reversal time  $\tau_r$  of current  $i$  for a given  $mrs$  kinetically energized vibrator, or of cemf.  $e$  in a potentially energized vibrator, in which  $r$  is varied, is  $\gamma/\omega_r$  in the periodic case,  $t_0$  in the aperiodic case and  $\theta/\Omega$  in the ultraperiodic case. In the case considered, the periodic reversal time was 0.00072 sec., the aperiodic reversal time 0.00063 second, and the ultraperiodic reversal time 0.00053. As the resistance  $r$  is increased the reversal time diminishes, but not in a simple ratio.

**Comparison between Periodic and non-Periodic Damped Vibrations.** — Periodic vibrations are characterised by successive reversals of the forces and velocity, although, when there is heavy damping, the amplitude of these reversals may be so small as to escape detection. Non-periodic vibrations may be either aperiodic ( $B_0 = 1$ ) or ultraperiodic ( $B_0 > 1$ ). As is suggested by an examination of the cases presented in Figs. 191–192 and 195–196, there may be but little difference between the curves of  $f$ ,  $e$ , and  $\dot{x}$  in these two cases. An essential difference is, however, found in the reversal time  $\tau_r$ , which is just  $\tau_0$  in the aperiodic case, and less than  $\tau_0$  in ultraperiodic cases.

A closer approximation may, however, be secured to a rectangular type of wave (see Fig. 105) in the action of damped periodic vibrator ( $B_0 < 1$ ) than in that of the same vibrator non-periodic ( $B_0 \leq 1$ ).

Table XXII collects and presents, in a convenient form, the formulas which have been obtained for expressing the principal instantaneous quantities during discharge. The numbers attached to these various formulas in the text are included in the table. Each of the eight sets of formulas conform to the fundamental equation:—

$$(493) \quad \left. \begin{aligned} xs + \dot{x}r + \ddot{x}m &= 0 \\ qs + \dot{q}r + \ddot{q}L &= 0 \end{aligned} \right\} \quad \text{inst. volts or dynes } \angle.$$

**Free Vibrations in Charging or Energizing a System.** — We have hitherto discussed the vibrations that may occur in a  $mrs$  system in any periodic or non-periodic state, during discharge or release of its energy. Certain rotary-vector diagrams have been arrived at as representative in each. It may be noted that the same vector diagrams are applicable also to the transient phenomena that occur when a  $mrs$  system is charged or energized, either potentially, as by bending the driving spring, or kinetically, as by delivering a velocity by impulse.

If in the simple  $\mathcal{E}RS$  branch circuit of Fig. 27, assumed to be initially energyless, we suddenly impress a steady continuous emf.  $F$ , volts on the mains  $mm'$ ,  $m$  being positive to  $m'$ , then, if the condenser in its subsequent discharge will deliver a current from  $s$  to  $r$ , or upwards, as a conventionally + current, the initial charging current from  $m$  to  $m'$  will be a – current.

The charge of electricity or electric displacement will be  $-$ , in order that  $\dot{q}$  may be initially minus, commencing at zero and terminating at  $-F_r/s$  coulombs. The initial value of  $f$  must therefore be minus. If the resistance  $\rho$  is less than  $z_0$ , the charging vibration will be periodic, and the vector diagram of Fig. 177 may be used, if inverted, i.e., with the direction  $03$  as the positive direction of the  $X$  axis. Thus, if the constants of the circuit are the same as those for which Fig. 177 was prepared ( $\rho = 100$ ,  $\mathcal{L} = 0.1$ ,  $s = 250\,000$ ), the vector diagram of that figure is applicable with a change of  $180^\circ$  in reference phase, if the impressed voltage  $F_r$ , at  $t = 0$ , is 1000. In Fig. 179, the emf. must be read as commencing at zero and ending at 1000 volts. The current  $i$  must also be read with reversed sign. The other curves remain unaltered. Similar remarks apply to the aperiodic and ultraperiodic cases.

The charging vibrations of a simple electric or mechanical system differ only from its discharging vibrations, in regard to phase direction, the absolute numerical values of the elastic force  $f$ , of the displacement  $x$ , and of the elastic energy remaining the same.

The principal scalar algebraic formulas for computing the charging transients in a simple  $\mathcal{LRS}$  or  $mrs$  system are collected in Table XXII, for the undamped, damped periodic, aperiodic and ultraperiodic cases.

**Vibrations in a Single RMS System with Divided Elements.** — If we have a single circuit (Fig. 197) containing a plurality of condensers, of resistances or of reactances, and subject to either charging or discharging vibrations, we may refer the system to an equivalent single system, Fig. 198, having the same total elastance  $s = s_1 + s_2 + s_3 \dots$ , total resistance  $r = r_1 + r_2 + r_3 \dots$ , and total inductance  $\mathcal{L} = \mathcal{L}_1 + \mathcal{L}_2 + \mathcal{L}_3 \dots$ . Some resistance or resistances may be hertzian, or radiation resistances, while the others may be joulean resistances, which dissipate their energy in heat. The only important difference between the cases of Figs. 197 and 198 will lie in the effects of initial charges in a particular condenser or condensers.

Let one of the condensers, say  $s_1$ , Fig. 197, be initially charged with a quantity  $Q_1$  coulombs, and to an initial potential of  $Q_1 s_1$  volts, the rest of the system being without charge. Then, after release, the discharge of the condenser  $s_1$  will charge the other condensers oppositely, in such a manner as to check the oscillation. The oscillations will take place about a condition of voltage equilibrium, such that the emf. of the discharging condenser is equal and opposite to the sum of the emfs. in the other condensers. If the quantity necessary to flow through the circuit in order to attain the condition of emf. equilibrium is  $q_e$  coulombs, then

$$(494) \quad (Q_1 - q_e)s_1 = q_e(s_2 + s_3) \quad \text{volts,}$$

or

$$(495) \quad q_e = Q_1 \frac{s_1}{s_1 + s_2 + s_3} = Q_1 \frac{s_1}{s} \quad \text{coulombs.}$$



TABLE XXII

Formulas for instantaneous values of {condenser voltage} {current  $i$ } {emf. of self-induction} {elastic force  $f$ } {velocity  $\dot{x}$ } {inertia force  $e$ } of a discharging {LBS} system at time  $t$  secs. after release, and energized either potentially or kinetically.  $F_r$  = initial elastic force,  $I_r$  = initial current or velocity.  $z_0 = \sqrt{fs} = \sqrt{ms}$ ,  $\Delta = \frac{r}{2m} = \frac{\rho}{m}$ ,  $\omega_0 = \sqrt{s/m}$ ,  $B_0 = \Delta/\omega_0 = \rho/z_0$ ,  $\omega_f = \rho/z_0$ ,  $\omega_f = \omega_0\sqrt{1 - B_0^2} = \omega_0 \sin \gamma$ ,  $\Delta_0 = \omega_0$ ,  $\Omega = \omega_0 \sqrt{B_0^2 - 1} = \omega_0 \sinh \theta = \omega_0 \tan \psi$ .

UNDAMPED VIBRATIONS		DAMPED VIBRATIONS		
Periodic ( $B_0 = 0$ )	Periodic ( $B_0 < 1$ )	Aperiodic ( $B_0 = 1$ )	Ultraperiodic ( $B_0 > 1$ )	
$f = -I_r z_0 \sin \omega_0 t$ (427)	$f = -\frac{I_r}{\sin \gamma} z_0 \cdot e^{-\Delta t} \cdot \sin \omega_f t$ (421)	$f = -I_r z_0 \cdot e^{-\Delta_0 t} \cdot \Delta_0 t$ (491)	$f = -\frac{I_r}{\sinh \theta} z_0 \cdot e^{-\Delta t} \cdot \sinh \Omega t$ (471)	Kinetically Energized by $I_r$ or $\dot{x}_r$
$e = -I_r z_0 \sin \left( \omega_0 t - 2 \frac{\pi}{2} \right)$ (427)	$e = -\frac{I_r}{\sin \gamma} z_0 \cdot e^{-\Delta t} \cdot \sin (\omega_f t - 2 \gamma)$ (423)	$e = -I_r z_0 \cdot e^{-\Delta_0 t} \cdot (\Delta_0 t - 2)$ (492)	$e = -\frac{I_r}{\sinh \theta} z_0 \cdot e^{-\Delta t} \cdot \sinh (\Omega t - 2 \theta)$ (474)	
$\dot{x} = -I_r \cdot \sin \left( \omega_0 t - \frac{\pi}{2} \right)$ (427)	$\dot{x} = -\frac{I_r}{\sin \gamma} \cdot e^{-\Delta t} \cdot \sin (\omega_f t - \gamma)$ (422)	$\dot{x} = -I_r \cdot e^{-\Delta_0 t} \cdot (\Delta_0 t - 1)$ (493)	$\dot{x} = -\frac{I_r}{\sinh \theta} \cdot e^{-\Delta t} \cdot \sinh (\Omega t - \theta)$ (472)	Potentially Energized by $F_r$
$f = F_r \sin \left( \omega_0 t + \frac{\pi}{2} \right)$ (427)	$f = \frac{F_r}{\sin \gamma} \cdot e^{-\Delta t} \cdot \sin (\omega_f t + \gamma)$ (405)	$f = F_r \cdot e^{-\Delta_0 t} \cdot (\Delta_0 t + 1)$ (479)	$f = \frac{F_r}{\sinh \theta} \cdot e^{-\Delta t} \cdot \sinh (\Omega t + \theta)$ (456)	
$e = F_r \sin \left( \omega_0 t - \frac{\pi}{2} \right)$ (427)	$e = \frac{F_r}{\sin \gamma} \cdot e^{-\Delta t} \cdot \sin (\omega_f t - \gamma)$ (408)	$e = F_r \cdot e^{-\Delta_0 t} \cdot (\Delta_0 t - 1)$ (483)	$e = \frac{F_r}{\sinh \theta} \cdot e^{-\Delta t} \cdot \sinh (\Omega t - \theta)$ (450)	
$\dot{x} = \frac{F_r}{z_0} \cdot \sin \omega_0 t$ (424)	$\dot{x} = \frac{F_r}{m \omega_f} \cdot e^{-\Delta t} \cdot \sin \omega_f t$ (406)	$\dot{x} = \frac{F_r}{m \Delta_0} \cdot e^{-\Delta_0 t} \cdot \Delta_0 t$ (481)	$\dot{x} = \frac{F_r}{m \Omega} \cdot e^{-\Delta t} \cdot \sinh \Omega t$ (457)	
$I_r = \frac{F_r}{z_0} = m \omega_0$	$I_r = \frac{F_r}{m \omega_f}$	$I_r = \frac{F_r}{m \omega_0} \cdot \Delta_0$	$I_r = \frac{F_r}{m \Omega}$	

This is the oscillatory part of the charge in  $s_1$ . The remainder would reside permanently in the condensers, if there were no dielectric leakage. Since the passage of  $q_e$  coulombs attains the point of equilibrium about which oscillation takes place, the first swing, neglecting damping, carries  $2q_e$  coulombs through the circuit.

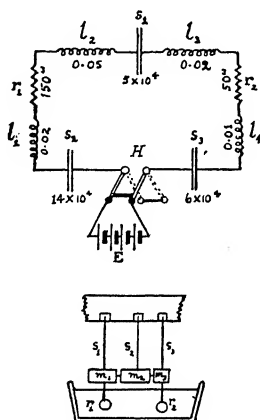


FIG. 197. Single electric and mechanical  $\mathcal{ERS}$  systems, with divided elements.

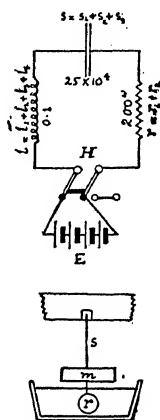


FIG. 198. Single electric and mechanical  $\mathcal{ERS}$  systems with equivalent single elements.

Of the initial stock of energy  $W = Q_1^2 s_1 / 2$  joules, the portion subject to oscillation, neglecting damping, is

$$(496) \quad W \frac{s_1}{s_1 + s_2 + s_3} = W \frac{s_1}{s} \quad \text{joules.}$$

This portion is alternately electric and magnetic energy. The remainder persists in the electric form, disregarding leakage.

If the impressed voltage  $E$ , instead of being applied initially to the component condenser  $s_1$ , were applied initially to the equivalent resultant condenser  $s$  of Fig. 198, whose elastance is the sum of the component elastances, the charge taken by  $s$  would be

$$(497) \quad q_e = Q_1 \frac{s_1}{s} \quad \text{coulombs,}$$

and the energy of the charge would be

$$(498) \quad W_e = W \frac{s_1}{s} \quad \text{joules.}$$

But we have seen that these are precisely the amounts of oscillation-charge and oscillation-energy available in the case of the charged component condenser. Hence we obtain the following rule for the treatment

of composite simple series circuits, with component condenser discharges: Form the equivalent single-element series circuit (Fig. 198). Impress the same initial emf. on the single condenser  $s$ , as would be impressed on the component condenser. The discharging oscillations of the single-element will then be identical with those that would occur in the composite system. After the oscillations have subsided, there will be, however, in the composite system, a residual electric energy to take into account, which does not appear in the equivalent single-element system.

Thus in the case of Fig. 16, let  $s_1 = 5 \times 10^4$ ,  $s_2 = 14 \times 10^4$ ,  $s_3 = 6 \times 10^4$  darafs,  $l_1 = 0.02$ ,  $l_2 = 0.05$ ,  $l_3 = 0.02$ ,  $l_4 = 0.01$  henry,  $r_1 = 150$  ohms,  $r_2 = 50$  ohms, and let an initial charge of 0.02 coulomb be given to  $s_1$  by an impressed emf. of 1000 volts, the other elements being without charge. The initial electric energy of the system  $W = 10$  joules. To find the oscillation of the system, we form the equivalent single-element system (Fig. 198) with  $s = 25 \times 10^4$  darafs,  $l = 0.1$  henry,  $r = 200$  ohms, and impress 1000 volts initially on the condenser  $s$ . This will take a charge of 0.004 coulomb, and an electric energy of 2 joules. These are the oscillation-charge and oscillation-energy of the composite system considered. The oscillations of the system are the same as those indicated in Figs. 175 to 179. After the oscillations have subsided, there will be a residual energy of 8 joules in the system, neglecting dielectric leakage, 0.016 coulomb at 800 volts in  $s_1$ ,  $-0.004$  coulomb at  $-560$  volts in  $s_2$ , and  $-0.004$  coulomb at  $-240$  volts in  $s_3$ .

Figures 197 and 198 indicate at their lower parts corresponding mechanical systems, in which elastic springs  $s$ , when deformed, set up the impressed elastic forces, the masses  $m$  correspond to the inductances, and the vanes  $r$ , immersed in a suitable liquid, mainly provide the frictional resistance. If one only of the three springs in Fig. 197 is deformed, say  $s_2$ , the system, after performing damped vibrations, will come to rest with deformation in all three at an equilibrium position.

## APPENDIX IX

### ON THE ANALOGIES BETWEEN SOUND-WAVE TRANSMISSION ALONG A UNIFORM ACOUSTIC TUBE CONDUCTOR AND ELECTROMAGNETIC-WAVE TRANSMISSION ALONG A UNI- FORM ELECTRIC LINE CONDUCTOR

We may assume that when a telephone receiver, actuated as an acoustic generator, sings a pure tone steadily into a long smooth straight tube of  $S$  sq. cm. internal cross-section, arranged as in Fig. 90, the sound waves traveling along the tube are plane waves, and that the effects on them of friction at the walls of the tube may be neglected. Even if the actual conditions do not conform closely with these postulates, the results thus arrived at may safely be regarded as first approximations.

The distance of any cross-section of the tube from the generator diaphragm, measured along the axis, may be expressed as  $l$  cm. The clamping-circle diameter of the receiver diaphragm may first be supposed to be equal to the internal diameter of the tube. The very small vibratory displacement of the air, in a sound wave, from its normal quiescent position, measured parallel to the axis, in the direction of increasing  $l$ , may be denoted by  $x$  cm. Since  $x$ , in the assumed case of a pure tone and simple harmonic vibration, may be taken as the projection, at time  $t$  seconds, on the tube axis, of the rotating plane vector

$$(499) \quad x = x_m \epsilon^{j\omega t} \quad \text{instantaneous cm. } \angle,$$

where  $\omega$  is the impressed angular velocity of rotation, and  $x_m$  is the maximum cyclic vibratory displacement, the vibratory velocity of a transverse layer of air in the tube, also measured along the axis, and in the direction of increasing  $l$ , is

$$(500) \quad \frac{\partial x}{\partial t} = \dot{x} = j\omega x_m \epsilon^{j\omega t} = j\omega x = \dot{x}_m \epsilon^{j\omega t} \quad \text{inst. kins or cm./sec. } \angle.$$

The velocity  $\dot{x}$  is also a plane-vector quantity, capable of being dealt with by the rules of complex arithmetic. Likewise, the vibratory acceleration will be

$$(501) \quad \frac{\partial^2 x}{\partial t^2} = \ddot{x} = j\omega x_m \epsilon^{j\omega t} = j\omega \dot{x} = -\omega^2 x_m \epsilon^{j\omega t} = -\omega^2 x$$

inst. kins/sec. or cm./sec.<sup>2</sup>  $\angle$ .

These equations indicate that in the steady state the acceleration is in leading quadrature to the velocity, which, in turn, is in leading quadrature to the displacement.

The *linear mass*, or mass of air normally occupying 1 cm. length of tube, will be

$$(502) \quad m = S\rho \frac{\text{gm.}}{\text{linear cm.}},$$

where  $\rho$  is the density (gm./c.c.) of the quiescent air in the tube at its actual temperature and its normal pressure intensity  $p_0$  dynes per sq. cm.

The fundamental dynamic equation expressing the instantaneous acceleration of a thin layer of air  $\partial l$  cm. long, having a mass  $m\partial l$  grams, is

$$(503) \quad m\ddot{x} \partial l = -\partial F \quad \text{dynes } \angle,$$

where  $+\partial F$  is the excess of total pressure on the far side of the layer above that on the near side; or

$$(504) \quad m\ddot{x} = S\rho\ddot{x} = -\frac{\partial F}{\partial l} \quad \frac{\text{dynes}}{\text{linear cm.}} \angle,$$

and \*

$$(505) \quad \rho\ddot{x} = -\frac{\partial p}{\partial l} \quad \frac{\text{dynes/sq. cm.}}{\text{linear cm.}} \angle,$$

where  $p$  is the excess of the pressure intensity  $p_0$  dynes per sq. cm. on the far side of the layer above that on the near side.

It is also a well known acoustic condition† that

$$(506) \quad \ddot{x} = v^2 \frac{\partial^2 x}{\partial l^2} \quad \frac{\text{kines } \angle}{\text{sec.}},$$

where  $v$  is the velocity of transmission of sound in the tube, along its axis, in kines.

From (501) and (503)

$$(507) \quad \partial F = -\dot{x} (j m \omega) \partial l \quad \text{rms. dynes } \angle.$$

This expresses the relation between a small difference of alternating pressure  $\partial F$  across an elementary length  $\partial l$  of the tube conductor, and the simultaneous vibratory velocity  $\dot{x}$  of the element. It corresponds to the well known relation between the difference of alternating electric pressure of emf.  $\partial E$ , across an elementary length  $\partial l$  of a line conductor, and the simultaneous alternating current  $I$  in the element

$$(508) \quad \partial E = -I (j \mathcal{L} \omega) \partial l \quad \text{rms. volts } \angle,$$

where  $\mathcal{L}$  is the linear inductance of the conductor in henries per km., and the linear resistance  $r$  of the conductor is ignored. Here  $\omega$  is the angular velocity of the impressed electric pressure, and  $l$  is the length of line in km., measured outwards from the generating end.

Again, from (504) and (506), we have

$$(509) \quad -\frac{\partial F}{\partial l} = m v^2 \frac{\partial^2 x}{\partial l^2} \quad \frac{\text{dynes}}{\text{linear cm.}} \angle.$$

\* Lamb's Hydrodynamics, p. 458, Eq. (3).

† *Ibid.*, Eq. (6).

Integrating, we find

$$(510) \quad F = -mv^2 \frac{\partial x}{\partial l} + \text{constant} \quad \text{dynes } \angle.$$

The constant of integration vanishes, and may be dropped, because  $F$ , the pressure deviation from the normal pressure  $F_0$  over a cross-section of the tube vanishes when  $\partial x / \partial l = 0$ . Hence,

$$(511) \quad F \partial l = -mv^2 \partial x \quad \text{cm.-dynes } \angle.$$

Differentiating with respect to time, we find

$$(512) \quad \frac{\partial F}{\partial t} \partial l = \dot{F} \partial l = -mv^2 \partial \dot{x} \quad \frac{\text{cm.-dynes}}{\text{sec.}} \angle,$$

or

$$(513) \quad j\omega F \partial l = -mv^2 \partial \dot{x} \quad \frac{\text{cm.-dynes}}{\text{sec.}} \angle,$$

and

$$(514) \quad \partial \dot{x} = -\frac{j\omega}{mv^2} F \partial l \quad \text{rms. kines } \angle.$$

The quantity  $mv^2$  may be replaced by  $s$ , the total elastic force resisting compression, expressed in ergs per cm. of displacement over the section, so that the instantaneous differential increase in vibrational velocity over an element of length  $\partial l$  is

$$(515) \quad \partial \dot{x} = -F \left( j \frac{\omega}{s} \right) \partial l \quad \text{rms. kines } \angle.$$

The quantity  $s$  is the *normal adiabatic elastic force*  $Sp'_0 = S\gamma p_0$ , of the medium over the section,  $\gamma$  being the ratio of specific heats, and  $p_0$  the quiescent pressure intensity in the medium. The last equation corresponds to the well known equation of differential increase in alternating current  $\partial I$ , over an element of conductor length  $\partial l$ ; namely

$$(516) \quad \partial I = -E(j\omega c) \partial l = -E \left( j \frac{\omega}{s} \right) \partial l \quad \text{rms. amperes } \angle,$$

where  $c$  is the linear capacitance of the conductor in farads per km., and  $s$  is its reciprocal. In this case, the linear leakance  $g$  of the conductor is ignored.

Since the complete electric-conductor equations for (508) and (516), including  $r$  and  $g$ , are

$$(517) \quad \partial E = -I(r + jL\omega) \partial l = -Iz \partial l \quad \text{rms. volts } \angle,$$

and

$$(518) \quad \partial I = -E \left( g + j \frac{\omega}{s} \right) \partial l = -Ey \partial l \quad \text{rms. amperes } \angle,$$

we may reasonably assume that the corresponding equations for the acoustic conductor, including frictional resistance along the tube and losses due to imperfect elasticity, are, from (507) and (515),

$$(519) \quad \partial F = -\dot{x}(r + j\omega m) \partial l = -\dot{x}z \partial l \quad \text{rms. dynes } \angle,$$

and

$$(520) \quad \partial \dot{x} = -F \left( g + j \frac{\omega}{s} \right) \partial l = -F y \partial l \quad \text{rms. kines } \angle.$$

In electric conductors, the linear dissipation constants  $r$  and  $g$  are accepted as constant at any single impressed frequency, whatever values may pertain to  $E$  and  $I$ ; but they are known to change when the impressed frequency is varied over a wide range. Similarly, in acoustic tubes, the linear dissipation constants  $r$  and  $g$  are perhaps constant at any single frequency, although they may vary when the frequency is varied. Numerous measurements will have to be collected before the acoustic dissipation constants of a tube can be determined with precision.

The known equations of electric propagation along uniform lines are applicable, following the above theory, to acoustic propagation along uniform tubes, when hydrostatic difference of pressure  $F$  is substituted for electric difference of pressure  $E$ , vibratory displacement  $x$  for alternating quantity  $q$ , vibratory velocity  $\dot{x}$  for alternating current  $I$ , linear mass  $m$  for linear inductance  $\mathcal{L}$ , linear frictional resistance  $r$  for linear electric resistance  $r$ , linear acoustic elasticity loss  $g$  for linear electric leakance  $g$ , and elastic force  $s$  for  $s$ , the reciprocal of the linear capacitance.

Table XXIII gives a comparison between electric and acoustic quantities for the case of negligible losses in transmission.

Table XXIV gives some comparative data for electric and acoustic conductors, still assumed as having no losses, but freed at the distant end.

Table XXV gives similar comparative data for the general case of conductors having linear losses of known values.

**Surge-impedance Density.** — In regard to Table XXIII, it may be noted that the acoustic surge impedance density has no counterpart in the ordinary theory of electric lines.

The value of the surge-impedance density, by (529), is  $\sqrt{\rho p'}$ , where  $\rho$  is the density of quiescent air at  $0^\circ\text{C}$ ., and the standard pressure of  $10^6$  bars or dynes per sq. cm. The value of  $p'_0 = \gamma p_0$  may be taken as  $1.41 \times 10^6$  bars, and  $\rho = 1.276 \times 10^{-3}$ . Consequently  $\mathfrak{z} = \sqrt{17.99 \times 10^2} = 42.4$  mechanical abohms per sq. cm. of tube cross-section, under the standard condition of 1 megabar pressure ( $10^6$  dynes per sq. cm.) and  $0^\circ\text{C}$ . If the actual pressure of the quiescent air in the tube is  $p_0$  bars, and the actual temperature is  $t^\circ\text{C}$ ., the surge-impedance density becomes

$$(521) \quad \mathfrak{z} = \frac{42.4 \sqrt{p_0 \times 10^{-6}}}{\sqrt{1 + 0.00366 t}} \quad \frac{\text{mechanical abohms}}{\text{sq. cm.}} \angle,$$

or for values not exceeding  $25^\circ\text{C}$ .,

$$(522) \quad \mathfrak{z} = \frac{42.4 \times \sqrt{p_0 \times 10^{-6}}}{1 + 0.00183 t} \quad \frac{\text{mechanical abohms}}{\text{sq. cm.}} \angle.$$

TABLE XXIII  
PROPERTIES OF ELECTRIC AND ACOUSTIC LINES WITH NEGLIGIBLE LOSSES  $r=g=0$   
 $r=g=0$

QUANTITY	ELECTRIC	ACOUSTIC
Linear hyperbolic angle	$\alpha = j\omega \sqrt{\mathcal{L}c} = j\omega \sqrt{\frac{\mathcal{L}}{s}} = j\frac{\omega}{v}$ $= j\frac{2\pi}{\lambda} = j\alpha_2$ hyps. $\angle$ km.	$\alpha = j\omega \sqrt{\frac{m}{s}} = j\frac{\omega}{v} = j\omega \sqrt{\frac{\rho}{p_0}}$ $= j\frac{2\pi}{\lambda} = j\alpha_2$ hyps. $\angle$ cm.
Hyperbolic angle of conductor	$\theta = L\alpha = j2\pi \frac{L}{\lambda}$ hyps. $\angle$	$\theta = L\alpha = j2\pi \frac{L}{\lambda}$ hyps. $\angle$
Wave length	$\lambda = \frac{2\pi}{\alpha_2} = j\frac{2\pi}{\alpha}$ km.	$\lambda = \frac{2\pi}{\alpha_2} = j\frac{2\pi}{\alpha}$ cm.
Velocity of propagation	$v = \frac{\omega}{\alpha_2} = j\frac{\omega}{\alpha} = f\lambda$ km. sec.	$v = \frac{\omega}{\alpha_2} = j\frac{\omega}{\alpha} = \sqrt{\frac{p_0'}{\rho}} = \sqrt{\frac{s}{m}} = f\lambda$ kines
Surge impedance	$z_0 = \sqrt{\frac{\mathcal{L}}{c}} = \sqrt{\mathcal{L}s} = \frac{s}{v}$ ohms	$z_0 = \sqrt{ms} = \frac{s}{v} = S_3 = S\sqrt{p_0'\rho}$ mechanical abohms
Surge-impedance density	$\frac{Z_P}{Z_A} = \frac{\tanh \delta_P}{\tanh \delta_A}$ numeric $\angle$	$\mathfrak{z} = \frac{z_0}{S} = \frac{\sqrt{ms}}{S} = \sqrt{\frac{\rho s}{S}} = \sqrt{p_0'\rho}$ dynes kine cm. <sup>2</sup>
Impedance ratio for P and A	$\frac{Z_P}{Z_A} = E_A I_A$ watts $\angle$	$\frac{Z_P}{Z_A} = \frac{\tanh \delta_P}{\tanh \delta_A}$ numeric $\angle$
Power at A	$P_A = E_A I_A = \frac{E_A^2}{z_0}$ watts	$P_A = F_A x_A$ abwatts $\angle^*$
Power at A, when $L = \infty$	$P_A = E_A I_A = \frac{E_A^2}{z_0}$ watts $\angle$	$P_A = F_A x_A = \frac{F_A^2 v}{s} = x_A^2 m v = S p k v = S e^2 p v$ abwatts $\angle^*$

\* In (531) and (532), either  $E_A$  and  $P_A$  or  $I_A$  and  $x_A$  must be taken without slope.



TABLE XXIV

NEGLECTIBLE LOSSES AND DISTANCE END FREE.

$$r = g = 0. \quad \delta_B = j \frac{\pi}{2} = j \underline{1}$$

$$r = g = 0$$

QUANTITY	ELECTRIC	ACOUSTIC	
Impedance at point $P$	$Z_P = \sqrt{\mathcal{L}} \tanh j (L_2 \alpha_2 + \underline{1})$ ohms $\angle$ $= -j \sqrt{\mathcal{L}} \text{cs ctn} \left( 2 \pi \frac{L_2}{\lambda} \right)$ ohms $\angle$ $= -j \sqrt{\mathcal{L}} \text{cs ctn} (L_2 \alpha_2)$ ohms $\angle$	$Z_P = \sqrt{ms} \tanh (j L_2 \alpha_2 + j \underline{1})$ mech. abohms $\angle$ $= -j \sqrt{ms} \text{ctn} \left( 2 \pi \frac{L_2}{\lambda} \right)$ $= -j \sqrt{ms} \text{ctn} (L_2 \alpha_2)$	(533) (534) (535)
Impedance ratio for $P$ and $A$	$Z_P = \frac{\text{ctn} (L_2 \alpha_2)}{\text{ctn} (L \alpha_2)}$ numeric $Z_A = \frac{\text{ctn} (L \alpha_2)}{\text{sin} (L_2 \alpha_2)}$ numeric	numeric	(536)
Current Velocity	$I_P = \frac{\text{sin} (L \alpha_2)}{\text{sin} (L_2 \alpha_2)}$ numeric $I_A = \frac{\text{cos} (L_2 \alpha_2)}{\text{cos} (L \alpha_2)}$ numeric	numeric	(537)
Voltage Pressure	$E_P = \frac{\text{cos} (L \alpha_2)}{\text{cos} (L_2 \alpha_2)}$ numeric $E_A = \frac{j E_A}{\sqrt{\mathcal{L}} \text{cs ctn} (L \alpha_2)}$ amperes $\angle$	numeric	(538)
Current Velocity	$I_A = \frac{j E_A}{\sqrt{\mathcal{L}} \text{cs ctn} (L \alpha_2)}$ amperes $\angle$ $E_B = \frac{E_A}{\text{cos} (L \alpha_2)}$ volts	$\dot{x}_A = \frac{j F_A}{\sqrt{ms} \text{ctn} (L \alpha_2)}$ kines $\angle$ $F_B = \frac{F_A}{\text{cos} (L \alpha_2)}$ dynes	(539) (540)

TABLE XXV  
PROPERTIES OF ELECTRIC AND ACOUSTIC LINES WHEN LOSSES ARE NOT NEGLIGIBLE

QUANTITY	ELECTRIC	ACOUSTIC	
Linear hyperbolic angle	$\alpha = \sqrt{yz} = \sqrt{(r+j\mathcal{L}\omega)} \left( g + j\frac{\omega}{s} \right)$ $\frac{\text{hyp.}}{\text{km.}}$ $= \alpha_1 + j\alpha_2$	$\alpha = \sqrt{yz} = \sqrt{(r+jm\omega)} \left( g + j\frac{\omega}{s} \right)$ $\frac{\text{hyp.}}{\text{cm.}}$ $= \alpha_1 + j\alpha_2$	(541)
Hyp. angle of conduct or Wave length	$\theta = L\alpha = L(\alpha_1 + j\alpha_2) = \theta_1 + j\theta_2$ $\frac{\text{hyp.}}{\text{km.}}$ $\lambda = \frac{2\pi}{\alpha_2}$ km.	$\theta = L\alpha = L(\alpha_1 + j\alpha_2) = \theta_1 + j\theta_2$ $\frac{\text{hyp.}}{\text{cm.}}$ $\lambda = \frac{2\pi}{\alpha_2}$ cm.	(542) (543)
Velocity of propagation	$v = \frac{\omega}{\alpha_2}$ km. $\frac{\text{km.}}{\text{sec.}}$	$v = \frac{\omega}{\alpha_2}$ cm. $\frac{\text{cm.}}{\text{sec.}}$	(544)
Surge impedance	$z_0 = \sqrt{\frac{z}{y}} = \sqrt{\frac{r+j\mathcal{L}\omega}{g+j\omega/s}}$ ohms $\angle$	$z_0 = \sqrt{\frac{z}{y}} = \sqrt{\frac{r+jm\omega}{g+j\omega/s}}$ dynes $\angle$ $\frac{\text{dyne}}{\text{cm.}}$	(545)
Impedance at point P	$Z_P = z_0 \tanh \delta_P$ ohms $\angle$	$Z_P = z_0 \tanh \delta_P$ dynes $\angle$ $\frac{\text{dyne}}{\text{cm.}}$	(546)
Impedance ratio for P and A	$\frac{Z_P}{Z_A} = \frac{\tanh \delta_P}{\tanh \delta_A}$ numeric $\angle$	$\frac{Z_P}{Z_A} = \frac{\tanh \delta_P}{\tanh \delta_A}$ numeric $\angle$	(547)
Current } ratio for P and A	$\frac{I_P}{I_A} = \frac{\cosh \delta_P}{\cosh \delta_A}$ numeric $\angle$	$\frac{I_P}{I_A} = \frac{\cosh \delta_P}{\cosh \delta_A}$ numeric $\angle$	(548)
Voltage } ratio for P and A	$\frac{E_P}{E_A} = \frac{\sinh \delta_P}{\sinh \delta_A}$ numeric $\angle$	$\frac{E_P}{E_A} = \frac{\sinh \delta_P}{\sinh \delta_A}$ numeric $\angle$	(549)
Pressure }			(550)

A rigid disk diaphragm of  $S$  sq. cm. on each face, vibrating with uniform amplitude over its surface, so as to generate plane waves in the tube indefinitely long, would develop on each face a surge resistance of

$$(550a) \quad z_0 = \frac{42.4 S \sqrt{p_0} \times 10^{-3}}{1 + 0.00183 t} \quad \text{mechanical abohms } \angle .$$

## APPENDIX X

### RELATIONS BETWEEN TWO PLANE VECTORS WITH DISPLACED REFERENCE AXES

**Proposition Concerning the Plane Vector**  $|\rho| \angle \alpha^\circ$ . The plane vector  $|\rho| \angle \alpha^\circ$  satisfies the equation

$$|\rho| \angle \alpha^\circ = |\rho| \angle (2\beta^\circ + \alpha^\circ) - 2 \sin \beta |\rho| \angle (90^\circ + \alpha^\circ + \beta^\circ).$$

In Fig. 199,  $OA$  is a plane vector, or geometric complex quantity of any convenient size  $\rho$ , taken at standard phase, or zero slope. It may be denoted by  $\rho_A$ .  $OB$  is a similar plane vector of the same size, distinguished by the symbol  $\rho_B$ . Its slope is  $-2\beta^\circ$ .  $OC$  is a vector denoted by  $\rho_c$ , of size  $\rho$ , and drawn perpendicular to  $Od$ , the bisector of the angle  $AOB$ .

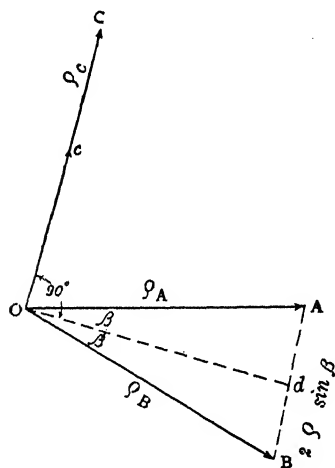


FIG. 199. System of three coordinated vectors  $\rho_A$ ,  $\rho_B$ , and  $\rho_c$ , all referred to  $OA$  as phase axis.

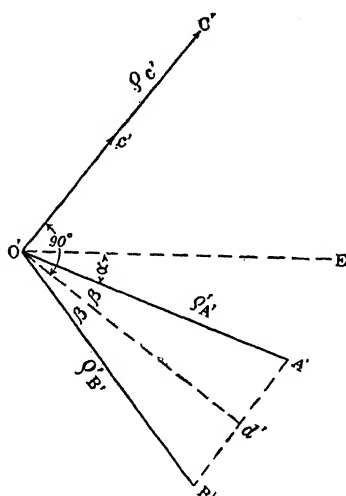


FIG. 200. Same system of three vectors rotated negatively through angle  $\alpha$ .

Then, because  $BA$  expressed vectorially is  $2|\rho| \sin \beta \angle (90^\circ - \beta^\circ)$ , and is equal to the vector  $OC$ , we have the vector relation

$$(551) \quad \rho_B = \rho_A - 2 \sin \beta \cdot \rho_c \quad \text{length units } \angle.$$

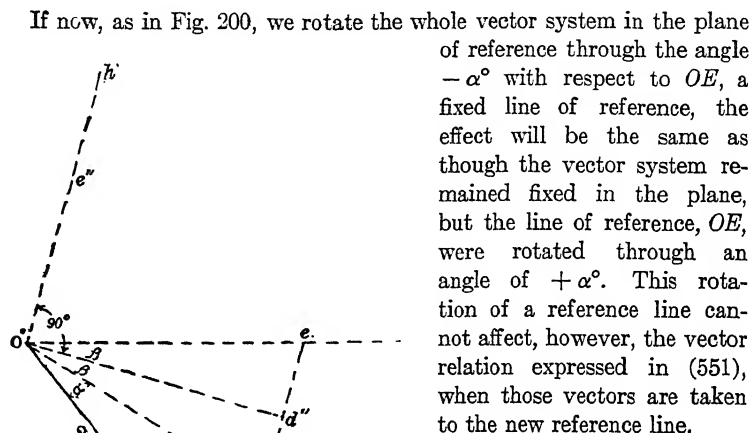


FIG. 201. Single vector  $\rho$ , specifiable in slope with respect to three coordinate reference axes  $Oe$ ,  $Om$ , and  $Oh$ .

respectively. Thus in Fig. 202,

$$(552) \quad |\rho_m| \angle \alpha^\circ = |\rho_e| \angle (2\beta^\circ + \alpha^\circ) - |\rho_h| 2 \sin \beta \angle (90^\circ + \alpha^\circ + \beta^\circ).$$

Since this relation holds for the vectors themselves, it must also hold for their real components, and for their imaginary components as well.

The power circle of Fig. 54 corresponds to Fig. 201, while the interpretations of 120 are referable to the construction of Fig. 202.

For a more detailed demonstration the reader may refer to the original paper.\*

If now, as in Fig. 200, we rotate the whole vector system in the plane of reference through the angle  $-\alpha^\circ$  with respect to  $OE$ , a fixed line of reference, the effect will be the same as though the vector system remained fixed in the plane, but the line of reference,  $OE$ , were rotated through an angle of  $+\alpha^\circ$ . This rotation of a reference line cannot affect, however, the vector relation expressed in (551), when those vectors are taken to the new reference line.

But the three vectors of (551) may be regarded as one and the same vector  $\rho$ , Fig. 201, expressed with respect to each of three initial lines  $O''m$ ,  $O''e$ , and  $O''h$ , and then denoted by  $\rho_m$ ,  $\rho_e$ , and  $\rho_h$ ,

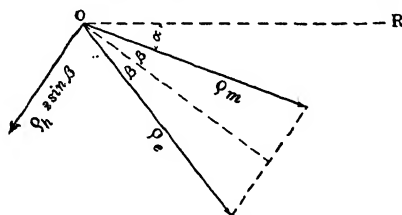


FIG. 202. System of three coordinated vectors,  $\rho_e$ ,  $\rho_m$ , and  $\rho_h \cdot 2 \sin \beta$ , similar to those of Fig. 200, referred to  $OR$  as phase axis.

\* Bibliography 79.

## APPENDIX XI

### GRAPHS OF SCALAR VELOCITIES AND DISPLACEMENTS

**Velocity-Resonance Curves of Simple MRS. Systems under Varied Impressed Frequency.** — Resonance curves play so prominent a part in the phenomena of forced vibrations, in either mechanical or electric systems, that they deserve special consideration.

Referring to (69), the vector rms. velocity  $\dot{x}$  established by a steady vmf. of rms. value  $F$ , taken as at standard phase, is

$$(553) \quad \dot{x} = \frac{F}{z} = \frac{F}{r + j(m\omega - s/\omega)} \quad \text{rms. kins } \angle.$$

When the impressed angular velocity takes the maximum value  $\dot{x}_0$ , we have

$$(554) \quad \dot{x}_0 = \frac{F}{r} \quad \text{rms. kins } \angle.$$

The ratio of the vector velocity at impressed  $\omega$ , to the maximum vector velocity at resonant  $\omega_0$ , may be called the *vector velocity ratio*, and is

$$(555) \quad \frac{\dot{x}}{\dot{x}_0} = \frac{1}{1 + j\left(\frac{m\omega - s/\omega}{r}\right)}.$$

Denoting the frequency ratio  $\omega/\omega_0$  by  $u$ , as in preceding chapters,

$$(556) \quad \frac{\dot{x}}{\dot{x}_0} = \frac{1}{1 + j\left\{\frac{mu\omega_0 - s/(u\omega_0)}{r}\right\}} = \frac{1}{1 + j\frac{\Lambda_0}{2}\left(u - \frac{1}{u}\right)} = \frac{1}{1 + j\Lambda_0 \sinh y},$$

where  $\Lambda_0$  is the sharpness of resonance  $\omega_0/\Delta$ , and  $y = \log h u$ . This expression becomes unity when  $u = 1$ , and falls to an indefinitely small value with either  $u = 0$ , or  $u = \infty$ . If we are interested only in the scalar value, or size, of this velocity ratio, we may denote it by  $\nu$ , and

$$(557) \quad \nu = \left| \frac{\dot{x}}{\dot{x}_0} \right| = \frac{1}{\sqrt{1 + \frac{\Lambda_0^2}{4}\left(u - \frac{1}{u}\right)^2}} = \frac{1}{\sqrt{1 + \Lambda_0^2 \sinh^2 y}}.$$

**Specific Velocity Resonance Curves.** — If we plot the *scalar velocity ratio*  $\nu$  as ordinates, for any simple *£RS* or *mrs* system, at varying values of  $u$  as abscissas, we obtain the ordinary well known *specific resonance curve*, with its maximum ordinate as 1, which is presented at  $u = 1$ .

Curve I, Fig. 203, is such a curve for the particular case of  $\Lambda_0 = 10$ , or  $B_0 = 0.1$ . It will be observed that the curve is necessarily asymmetric, about its maximum ordinate. It is always steeper on the low-frequency side ( $u < 1$ ). If, however, we plot values of  $\nu$  as ordinates against values of  $y$ , or  $\log u$ , as abscissas, it is evident from the form of (557) in respect to  $y$ , that the graph of  $\nu$  will be symmetric with respect to the maximum or unity ordinate. The same condition will apply, whether we use napierian or common logarithms of  $u$ , in marking off abscissas. In other words, if we plot the scalar velocity ratio, or current ratio,  $\nu$ , against the common logarithm of the frequency ratio ( $\log u$ ), the graph will be symmetric about the maximum ordinate. This is indicated in the broken curve II, Fig. 203, for the case of  $\Lambda_0 = 10$ , already considered. It is sometimes advantageous to plot an observed series of resonant values of velocity or current in this manner, so as to secure a graph that is theoretically symmetric about the middle ordinate. Errors in the observations are then likely to reveal themselves as departures from symmetry in the curve.

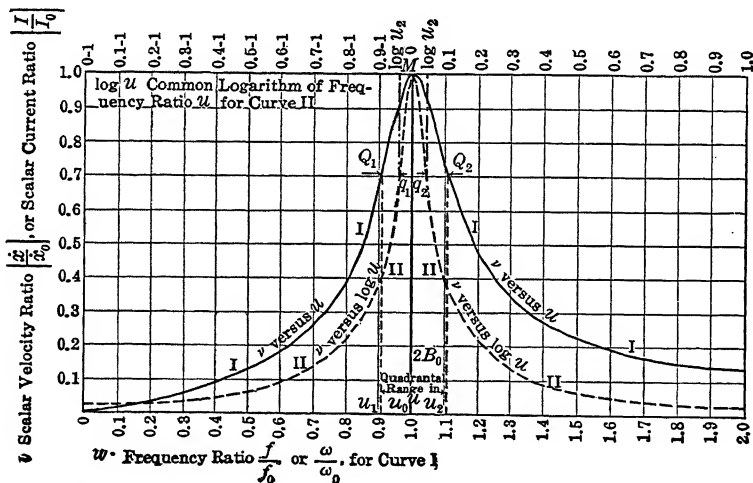


FIG. 203. Specific resonance curves under constant impressed vmf. and varied frequency.  $B_0 = 0.1$ ,  $\Lambda_0 = 10$ , showing symmetry and asymmetry with respect to the maximum resonant ordinate  $u_0 M$ . Ordinates scalar per unitage of  $\begin{cases} \text{velocity} \\ \text{current} \end{cases}$  at resonance. Abscissas frequency ratio  $f/f_0 = u$  for Curve I. Log frequency ratio or  $\log u$  for Curve II.

**Symmetrical Specific Current Resonance Curves of  $\nu$  versus  $u$  on Semi-logarithmic Paper.** — Instead of plotting  $\nu$  against  $\log u$ , or  $\log h u$ , we may plot  $\nu$  against  $u$  on semi-logarithmic paper, as is shown in Fig. 204 for the same case. This curve will be symmetric. It is advantageous for many purposes

to plot, in this manner, resonant velocity or resonant current curves under constant vmf. and varied frequency. The graphs so obtained are not only symmetric, but they are also readily comparable. It is not necessary, however, to use specific resonance curves of  $\nu$  and  $u$ . If we plot  $|\dot{x}|$  or  $I$ , as ordinates, against impressed frequency  $f$  as abscissas, the curve of simple resonance on semi-logarithmic paper will be symmetric, and only altered in position and in scale with respect to the  $\nu$  versus  $u$  curve.

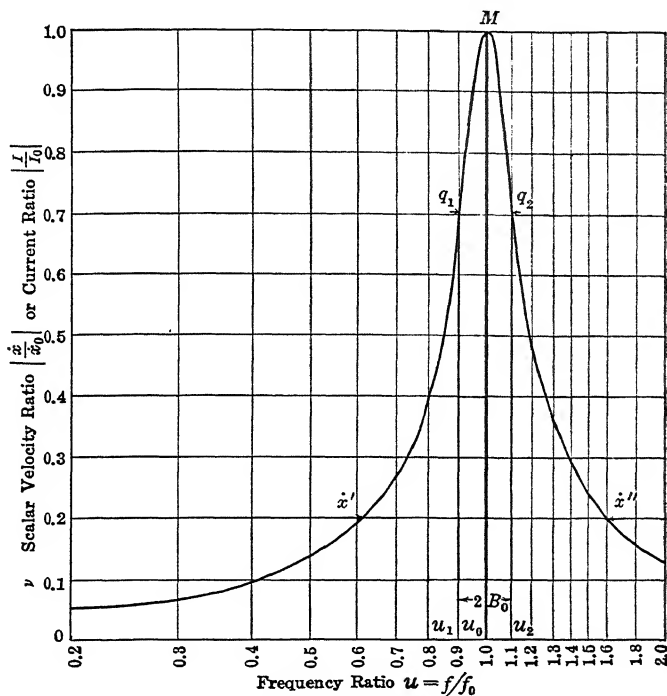


FIG. 204. Specific resonance curve for a case of  $B_0 = 0.1$  drawn on semi-logarithmic paper and symmetric with respect to the ordinate  $u_0 M$  of resonance. Ordinates  $\nu$ . Abscissas  $u$ .

**Quadrantal Range and Resonant Bluntness read from Specific Velocity or Current Resonance Curves.** — The quadrantal values of velocity or current,  $\dot{x}_1$ ,  $\dot{x}_2$ , or  $I_1$ ,  $I_2$ , always lie on the graphs of Figs. 203 or 204, at the points whose ordinates are 0.707 or  $2^{-1/2}$ . The abscissas of these points mark off either  $u_1$  and  $u_2$ , or  $\log u_1$  and  $\log u_2$ , as the case may be. Thus, for the case considered,  $u_1 = 0.905$ , and  $u_2 = 1.105$ . We know from (208), that  $B_0 = (u_2 - u_1)/2$ . In this case  $B_0 = (1.105 - 0.905)/2 = 0.1$ .

All simple resonances obeying (553), when plotted as in Fig. 204, differ only in respect to their  $\Lambda_0$ , as is manifest from an inspection of (557).



Any two such systems having the same resonant sharpness, will possess the same  $\nu$  versus  $u$  curve of specific resonance. Conversely, from an inspection of any such curve,  $\Lambda_0$  and  $B_0$  can be determined, because the quadrantal velocity ratios  $u_1$  and  $u_2$  may be ascertained directly and the range of  $u$  comprised between them will always be  $2B_0 = B_g$ .

When the system has very sharp resonance, as in the ordinary case of a vibration galvanometer, the two quadrantal frequency ratios  $u_1$  and  $u_2$  approach each other closely, as we have seen in connection with Fig. 139, and  $u_2 = 1 + B_0$ .

**Specific Current-Squared Resonance Curves of  $\nu^2$  versus  $\log u$ , or  $\nu^2$  versus  $\log u$ , in Radio Engineering.** — In radio engineering, the resonance curves are commonly read on instruments having scales graduated not to  $I$  the current, but to  $I^2$ , the square of the current, in the circuit under test. In such cases the scalar current square at resonance in a simple  $\mathcal{LRS}$  loosely coupled secondary circuit is

$$(558) \quad I_0^2 = \left(\frac{F}{r}\right)^2 \quad (\text{amperes})^2$$

and the scalar current squared at any other impressed frequency is

$$(559) \quad |I^2| = \left|\frac{F}{z}\right|^2 \quad (\text{amperes})^2,$$

The scalar current ratio is then, by (556)-(557),

$$(560) \quad \left|\frac{I}{I_0}\right|^2 = \nu^2 = \frac{1}{I + \frac{\Lambda_0^2}{4} \left(u - \frac{1}{u}\right)^2} = \frac{1}{1 + \Lambda_0^2 \sinh^2 y}.$$

Here again the graph of  $\nu^2$  versus  $u$  is asymmetric with respect to the maximum ordinate, but the graph  $\nu^2$  versus  $\log u$  is symmetric thereto.

Figure 205 presents the specific resonance graph of  $\nu^2$  versus  $u$ , drawn on semi-logarithmic paper, to produce the same effect as the graph of  $\nu^2$  versus  $\log u$ . The curve is drawn for the same sharpness of resonance as Fig. 204, i.e.,  $\Lambda_0 = 10$ . It is a symmetric curve, steeper than that of Fig. 204. The quadrantal frequency ratios  $u_1$  and  $u_2$  are now found at the points  $q_1$  and  $q_2$  on the curve, where the scalar  $\nu^2$  is 0.5, or has half the height of the maximum ordinate of resonance  $u_0 M$ . This property of the  $\nu^2$  versus  $u$  or  $\nu^2$  versus  $\log u$  curve is very easy to remember.

Radio resonance curves are commonly drawn with abscissas in wave lengths  $\lambda$ . If we denote the resonant wave length by  $\lambda_0$ ; then  $\lambda/\lambda_0 = 1/u$ . Consequently a curve of  $\nu^2$  versus  $\log (\lambda/\lambda_0)$  will be symmetric and will be a reversed curve of  $\nu^2$  versus  $\log u$ , thus permitting  $B_0$  to be read from it in the manner indicated by Fig. 205.

**Fundamental Geometry of Current Resonance Curves.** — Referring to formula (557), it will be seen that in the particular case of  $\Lambda_0 = 1$ , or the aperiodic case, we obtain

$$(561) \quad \nu = \frac{1}{\cosh y} = \frac{1}{\cosh (\log h u)} = \operatorname{sech} y = \operatorname{sech} (\log h u).$$

This means that in the aperiodic case, the specific resonance graph, drawn either to  $\log u$  abscissas on plain rectangular paper, or to  $u$  abscissas

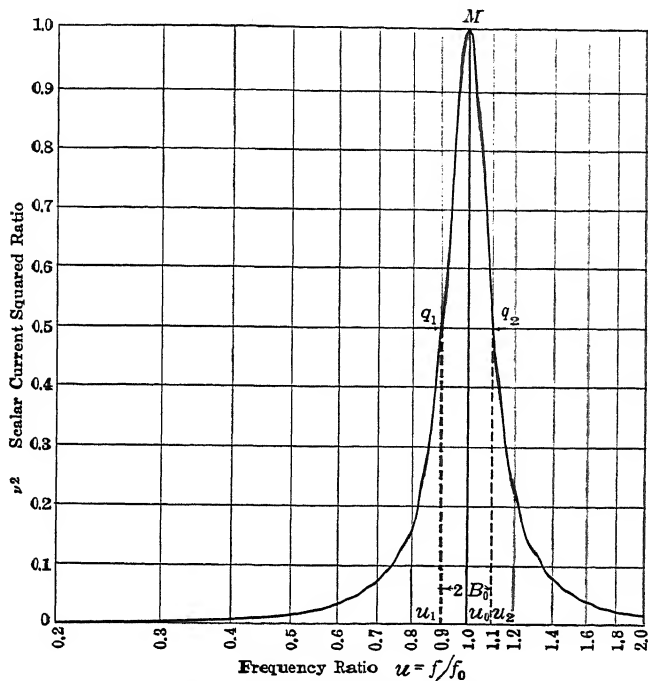


FIG. 205. Graph of scalar current-square ratio versus  $u$ , on semi-logarithmic paper, for  $B_0 = 0.1$ .

on semilogarithmic paper, is a simple curve of hyp. secants. This is shown in Fig. 206, which presents the specific resonance curve  $\nu$  versus  $\log u$ , for any aperiodic *ERS*, or *mrs* system ( $B_0 = 1$ ). The curve is drawn on semilogarithmic paper, and the abscissas are values of  $u$  on the logarithm scale. The corresponding values of  $\log h u$  are marked off on the top scale of abscissas. The graph is a curve of hyp. secants of these upper-scale abscissas.

If in (557) or (560), we make

$$(562) \quad \Lambda_0 \sinh (\log h u) = \Lambda_0 \sinh y = \sinh y',$$

then  $\nu$  in those formulas becomes

$$(563) \quad \nu = \frac{1}{\sqrt{1 + \sinh^2 y'}} = \frac{1}{\cosh y'} = \operatorname{sech} y'.$$

In the general case, therefore,  $\nu$  is still indirectly related to the curve of secants of Fig. 206, and might thus be constructed from a knowledge of  $\Lambda_0$ .

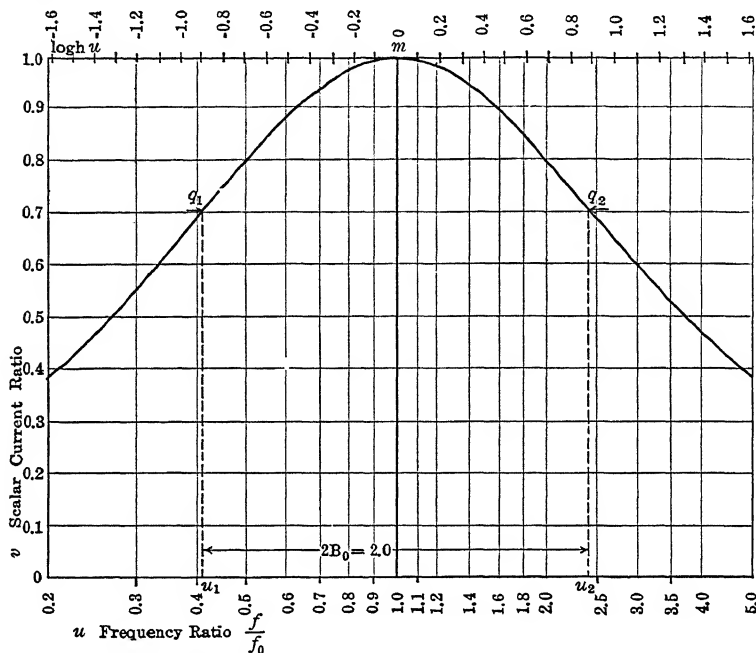


FIG. 206. Graph of  $\nu$  for the case  $B_0 = 1$ , also graph of  $\operatorname{sech} (\log h u)$ .

**Quadrantal Values of  $u$  in Velocity or Current Resonance Curves. —**

Since  $\nu = 1/\sqrt{2}$ , at either of the two quadrantal values  $u_1$  or  $u_2$ , of the frequency ratio, we obtain from (557)

$$(564) \quad \Lambda_0 \sinh y = 1,$$

at either quadrantal value, and also

$$(565) \quad \sinh (\log h u) = \sinh y = B_0.$$

Thus, in Fig. 206, the upper quadrantal value  $u_2$  occurs at  $\log h u = 0.8814$ , the hyp. sine of which is unity. Moreover, from (565), for any value of  $B_0$ ,

$$(566) \quad u_1 = \sqrt{1 + B_0^2} - B_0,$$

$$(567) \quad u_2 = \sqrt{1 + B_0^2} + B_0$$

which agree with (233), (242) and (247). These formulas enable us to predetermine directly the quadrantal points on a resonance curve for variable  $u$  when the resonant sharpness or bluntness are forthcoming.

When  $B_0 < 0.01$ , these formulas become

$$(567a) \quad u_1 = 1 - B_0,$$

$$(567b) \quad u_2 = 1 + B_0,$$

to a precision higher than 1 in 20,000. When  $B_0 < 0.025$ , we may still use the approximations

$$(567c) \quad u_1 = 1 - B_0 + B_0^2/2,$$

$$(567d) \quad u_2 = 1 + B_0 + B_0^2/2,$$

ordinarily to a precision higher than 1 in 1000.

**Summary of Deductions concerning Specific Velocity or Current Resonance Curves under Varied Impressed Frequency.** — Summing up the deductions reached in this Appendix, as well as in preceding Chapters,

concerning specific resonance curves  $\frac{\dot{x}}{\dot{x}_0}, \frac{\dot{x}_m}{\dot{x}_{m0}}, \frac{I}{I_0}, \frac{I_m}{I_{m0}}$ , in a simple  $\mathcal{E}RS$  or  $mrs$

system, under varied impressed frequencies steadily maintained, we have found that the plane-vector locus of such a curve is a circle, as in Fig. 29. The scalar locus of  $v$  versus  $u$  is a symmetric curve on semi-logarithmic paper, like that of  $v$  versus  $\log u$  on plain paper, and is a hyp. secant curve, either directly as in (561) or indirectly, as in (563). The resonant bluntness of the system can be ascertained from the curves.

**Graph of Scalar Displacements.** — In determining the motional impedance of a telephone receiver, or vibration galvanometer, we measure specific velocity ratios. Similarly, in determining the admittance of a simple  $\mathcal{E}RS$  system, under constant impressed voltage but varied frequency, we measure its specific current ratio. When, however, we measure the amplitude of vibration, as on a telephone diaphragm with an amplitude measurer (Fig. 62), or on a vibration galvanometer (Fig. 139), or again on an oscillograph galvanometer (Figs. 124–127), we deal with mechanical displacements  $x$  or  $\theta$ . In electric cases, we deal with electric displacements or electric quantities  $q$ . Figures 115–117 are vector specific-displacement diagrams, in that they enable the vector displacement at frequency ratio  $u$  to be determined with respect to the maximum vector displacement, for any given value of resonant bluntness  $B_0$ . We propose to give further consideration here to scalar graphs of displacement, or of specific displacement, such as Figs. 81 and 124.

The displacement  $x$  from (221) and (224) is

$$(568) \quad x = \frac{F}{(s - m\omega^2) + j r \omega} = \frac{F}{m\{\omega_0^2 - \omega^2 + j 2 \Delta \omega\}} \quad \text{cm } \angle.$$

The size or scalar value of this is

$$(569) \quad |x| = \frac{F}{m \sqrt{(\omega_0^2 - \omega^2)^2 + (2 \Delta \omega)^2}} = \frac{F}{m \omega_0^2 \sqrt{(1 - u^2)^2 + (2 B_0 u)^2}} \\ = \frac{F}{s \sqrt{(1 - u^2)^2 + (2 B_0 u)^2}} \quad \text{cm.}$$

Here  $|x|$  is readily shown to reach a maximum when  $u = \sqrt{1 - 2B_0^2} = u_d$ . Denoting this maximum value of displacement at  $u_d$  by  $|x_d|$ , we have

$$(570) \quad |x_d| = \frac{F}{s \sqrt{1 - u_d^2}} = \frac{F}{2 B_0 s u_d} \quad \text{cm.}$$

The ratio of any displacement  $|x|$  at impressed angular velocity  $\omega$ , to the maximum value  $|x_d|$  at the maximum displacement value  $u_d$ , is

$$(571) \quad \nu' = \frac{|x|}{|x_d|} = \sqrt{\frac{1 - u_d^4}{(1 - u^2)^2 + (2 B_0 u)^2}} = 2 B_0 \sqrt{\frac{1 - B_0^2}{(1 - u^2)^2 + (2 B_0 u)^2}} \\ = \frac{2 B_0 u_d}{\sqrt{(1 - u^2)^2 + (2 B_0 u)^2}}.$$

If we plot values of  $\nu'$  as ordinates against values of  $u$  as abscissas, we obtain a specific resonant displacement curve, such as that in Fig. 207, which is drawn for the case  $B_0 = 0.1$ . It is a resonance curve, in the sense that it rises to a sharp maximum near  $u_0 = 1$ , when  $B_0$  is small. It is also a specific-displacement curve, because it is drawn to a maximum ordinate of 1.0, when  $u = u_d$ .

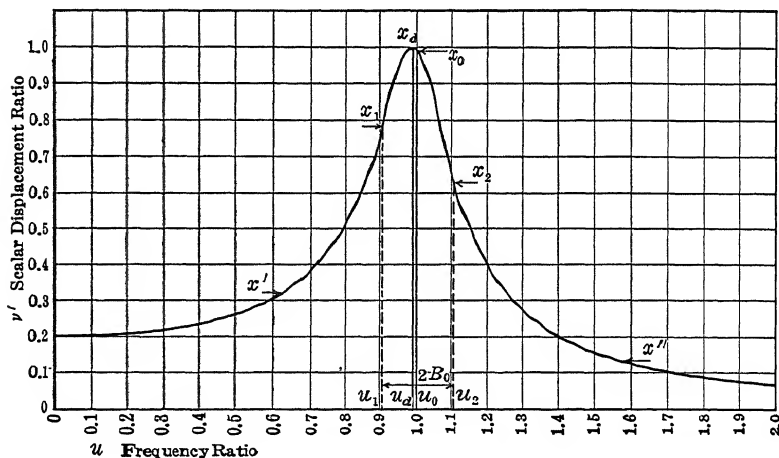


Fig. 207. Specific resonant displacement curve  $\left| \frac{x}{x_d} \right|$  or  $\left| \frac{q}{q_d} \right|$  or  $\left| \frac{\theta}{\theta_d} \right|$  with varied frequency and constant impressed vmf. for the case of  $B_0 = 0.1$  or  $\Delta_0 = 10$ .

The curve is asymmetric about its maximum ordinate, and droops towards the high-frequency side. In the case presented in Fig. 207, the maximum displacement being 1.0 at  $u = u_d = 0.995$ , that at resonance, or  $u_0$ , is 0.995. At the lower quadrantal frequency ratio  $u_1$ , the ratio  $\nu_1$  is 0.777, and at the upper quadrantal frequency ratio  $u_2$ ,  $\nu_2 = 0.6375$ .

The same type of specific resonant displacement curve applies to (1) the mechanical maximum cyclic rectilinear displacement in a simple *mrs* rectilinear system, such as a vibrating telephone diaphragm. Here  $\nu' = x/x_d$ .

(2) The mechanical maximum cyclic angular displacement in a rotary vibration system, such as that of an oscillograph or vibration galvanometer. In this case  $\nu' = \theta/\theta_d$ .

(3) The electric maximum cyclic quantity displacement in a simple *ERS* system of bluntness  $B_0$ . Here  $\nu' = q/q_d$ .

#### Relations between Velocity and Displacement Resonance Curves. —

If we operate on the curve of Fig. 207, by multiplying each ordinate by its abscissa  $u$ , we repeat the resonant velocity curve  $I$  of Fig. 203, except that the maximum ordinate will not be 1.0, but 0.995, the value of the ordinate  $u_0$  in 207. If we then reduce all the ordinates in Curve  $I$ , Fig. 203, by 0.995, the two will completely coincide. Thus, at  $u = 0.5$ , in Fig. 207, we have  $\nu'_{0.5} = 0.2630$ . Consequently  $\nu_{0.5} = 0.2630 \times 0.5 = 0.1315$ , on the basis of  $\nu_0 = 1.0$ ; but  $\nu'_0 = 0.995$  at  $u_0 = 1.0$  in Fig. 207, so that on this basis  $\nu_{0.5} = 0.1315/0.995 = 0.1322$ . This is the value of  $\nu$  designated in Fig. 203 on curve  $I$  at  $u = 0.5$ .

In any simple displacement resonance curve,  $x$  versus  $\omega$ , or  $x$  versus  $f$ , such as  $ABCD$ , Fig. 81, we obtain the corresponding velocity resonance curve of the system, by multiplying each ordinate by the angular velocity  $\omega$  pertaining to it. This follows from the last two expressions in (224).

**Maxima of Displacement Resonance Curves.** — We have already seen that current or velocity resonance curves,  $I$  versus  $u$ , have their maximum at resonance ( $\omega = \omega_0$ , or  $u = u_0 = 1$ ). Displacement resonance curves, however, have their maxima at a lower frequency  $\omega_d = \omega_0 \sqrt{1 - 2B_0^2}$ ; or  $u_d = \sqrt{1 - 2B_0^2}$ . When  $B_0$  exceeds 0.2, the difference becomes very noticeable (see Fig. 125). When, on the other hand,  $B_0$  is less than 0.05, as in vibration galvanometers, the difference between  $u_d$  and  $u_0$  becomes trivial, and the maximum deflection occurs virtually at resonance, or  $\omega_0$ . In Fig. 207, with  $B_0 = 0.1$ , the difference is still readily perceptible, since  $u_d = 0.99$ . The frequency of maximum displacement is approximately 1 per cent less than the frequency of resonance. The maximum specific cyclic displacement at resonance  $x_0$  is 0.995, or five per mil less than the maximum.

**Displacements corresponding to Equal Velocities on Each Side of Resonance.** — If we take any pair of equal scalar maximum cyclic velocities,  $|\dot{x}'|$  and  $|\dot{x}''|$ , from opposite sides of the resonant maximum, such as those shown in Fig. 204, at frequency ratios  $u' = 0.62$ , and  $u'' = 1.61$ , respectively, then, from (224)

$$(572) \quad \omega' |x'| = \omega'' |x''| \quad \text{Kines,}$$

where  $(x')$  and  $(x'')$  are the corresponding maximum cyclic displacements. Dividing both sides by  $\omega$ , we obtain

$$(573) \quad u' |x'| = u'' |x''| \quad \text{cm.,}$$

or

$$(574) \quad \left| \frac{x''}{x'} \right| = \frac{u'}{u''} = \frac{\omega'}{\omega''} = \frac{f'}{f''};$$

i.e., the ratio of the two displacements will be the reciprocal of the ratio of the frequencies at which the equal velocities occur. In the case considered, see Fig. 207,

$$\left| \frac{x'}{x''} \right| = \frac{0.325}{0.125} = 2.60 = \frac{1.61}{0.62} = \frac{u''}{u'}.$$

**Quadrantal Displacements.** — It is sometimes useful to deduce the quadrantal frequency ratios, and hence the resonant bluntness  $B_0$  of the system, from a curve of specific-displacement resonance, such as Fig. 207. In that case, we may utilize the relations obtained in the last paragraph. We have seen that the velocity or current conditions require that

$$(575) \quad v_1 = \left| \frac{\dot{x}_1}{\dot{x}_0} \right| = \frac{1}{\sqrt{2}} = v_2 = \left| \frac{\dot{x}_2}{\dot{x}_0} \right|,$$

and by (224)

$$(576) \quad \frac{\omega_1}{\omega_0} \left| \frac{x_1}{x_0} \right| = u_1 \left| \frac{x_1}{x_0} \right| = \frac{1}{\sqrt{2}} = \frac{\omega_2}{\omega_0} \left| \frac{x_2}{x_0} \right| = u_2 \left| \frac{x_2}{x_0} \right|.$$

Consequently

$$(577) \quad u_1 |x_1| = \frac{|x_0|}{\sqrt{2}} \quad \text{cm.,}$$

and

$$(578) \quad u_2 |x_2| = \frac{|x_0|}{\sqrt{2}} \quad \text{cm.}$$

Here  $|x_0|$  is the displacement at resonance, or  $u_0$ , as obtained from the displacement curve. Having ascertained the value of  $|x_0|/\sqrt{2}$ , we find by successive trials, a value of  $u_1$ , such that when multiplied by its ordinate, the product is  $|x_0|/\sqrt{2}$ . The same process is applied to find  $u_2$  and  $|x_2|$ . These are the two quadrantal values, and the distance between them is the quadrantal range. Thus, in Fig. 207,  $|x_0| = 0.995$ , so that  $|x_0|/\sqrt{2} = 0.704$ . We find that at  $u_1 = 0.905$ , where  $|x_1|$  is 0.777, their product is 0.704, so that these are respectively the lower quadrantal frequency ratio and the displacement. Similarly, at  $u_2 = 1.105$ , and  $|x_2| = 0.637$ ,  $u_2 |x_2| = 0.704$ , so that these are the upper quadrantal frequency ratio, and displacement ratio, respectively. These agree with Fig. 204, and  $2B_0 = 1.105 - 0.905 = 0.2$ .

**Symmetric Displacement Resonance Curves.** — The curve of specific displacement, as indicated in the case of Fig. 207, is asymmetric. An examination of formula (571) reveals, however, a symmetry in the relation of  $\nu'$  on each side of the maximum, if the abscissas are taken to  $u^2$ , or to the squares of the frequency ratios. Recasting Fig. 207 on this basis, we obtain the symmetric curve of Fig. 208. It is sometimes useful to plot displacement curves in this way, from laboratory observations, because any accidental errors in the series are likely to reveal themselves by their departure from symmetry in the resulting curve.

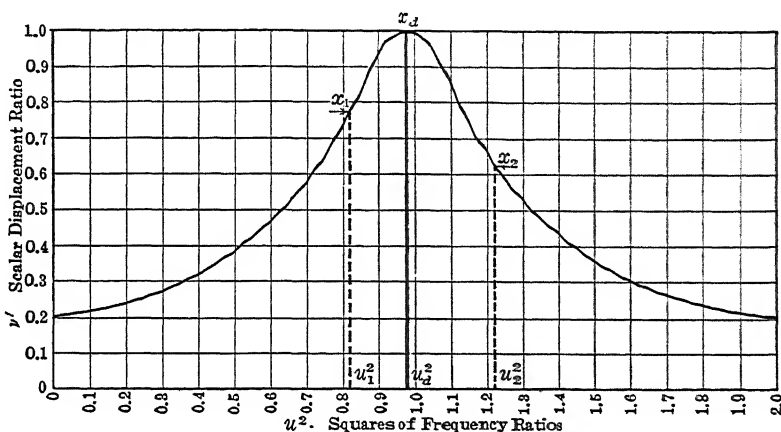


FIG. 208. Symmetric curve of specific resonant displacement drawn to squares of frequency ratios as abscissas. The curve is symmetric about the maximum ordinate  $\left| \frac{x_d}{x_d} \right| = 1.0$ , at  $u^2_d = 0.98$ .  $B_0 = 0.1$ .

It is hardly necessary to point out that since the displacement curve does not commence at zero, when the impressed frequency is very low, and, on the other hand, approaches zero at a very great impressed frequency, the symmetry of the curve can only extend as far as the duplicate initial ordinate.

In a similar way, if scalar displacements  $|x|$  are plotted against the squares of the frequencies which produce them, the resulting curve should be symmetric.

The quadrantal frequencies or frequency ratios may be ascertained from the curve by a procedure analogous to that described in connection with Fig. 207. That is, we may use (577) and (578), if we take the square roots of the abscissas for  $u_1$  and  $u_2$ , instead of the abscissas themselves. Thus in Fig. 208,  $\sqrt{0.819} \times 0.777 = 0.995/1.414 = 0.704$ , establishing  $u_1^2$  and  $|x_1|$ , and  $\sqrt{1.221} \times 0.637 = 0.995/1.414 = 0.704$ , establishing  $u_2^2$  and  $|x_2|$ .



**Equality of Displacements.**—It follows from a consideration of Fig. 208, that if two different impressed frequencies  $f'$ ,  $f''$ , or angular velocities  $\omega'$ ,  $\omega''$ , produce equal maximum cyclic displacements in a simple *mrs* system,

$$(579) \quad \frac{(\omega')^2 + (\omega'')^2}{2} = \omega_d^2 \quad \left( \frac{\text{rad.}}{\text{sec.}} \right)^2,$$

or

$$(580) \quad \frac{(f')^2 + (f'')^2}{2} = f_d^2 \quad \left( \frac{\text{cycles}}{\text{sec.}} \right)^2.$$

## APPENDIX XII

### DATA ON PROPORTIONALITY BETWEEN FRICTIONAL TORQUE AND ANGULAR VELOCITY IN VIBRATION INSTRUMENTS

As has been pointed out in preceding Chapters, one of the principal postulates in the theory of forced vibrations is the constancy of the mechanical resistance  $r$  to the motion of the vibrator, throughout the range of velocity employed. If  $r$  is constant, the retarding force or torque, as the case may require, will be  $\dot{x}r$ , or  $\dot{\theta}r$ , and will be in direct proportion to the linear velocity  $\dot{x}$ , or the angular velocity  $\dot{\theta}$ . If, on the contrary, the mechanical resistance  $r$  is not constant, within the required limits of accuracy and range of development, the retarding force of torque will involve higher powers of the velocity than the simple first power. This postulate is as fundamental to the mechanical system, as is the constancy of resistance in a metallic conductor (at constant temperature), to the application of Ohm's law. As there seems to be very little literature upon the constancy of  $r$ , some measurements were made on an oscillographic vibrator.

Formula (227) shows that if an oscillograph vibrator is operated steadily at its resonant frequency  $f_0$ , the displacement impedance has the size  $r\omega_0$ . Consequently, if  $r$  is constant, this impedance will be constant, and independent of the amount of displacement produced. If therefore the impressed vmt., at resonant frequency, is varied over a wide range, the maximum cyclic displacement produced should be directly proportional to this vmt. In other words, if the specific deflection, or radians deflection per ampere, of an oscillograph remains constant, at resonant frequency, over a considerable range in the actuating current  $I$ , it shows that  $r$  remains constant over that range.

Figure 209 indicates graphically the specific deflection obtained with an air-damped vibrator having the following dimensions. Strip length 23 mm., width 0.25 mm., thickness 0.018 mm. Size of mirror fastened at the midlength of the strips, approximately 1 mm. square.

The frequency of resonance of this vibrator was found to be 4130 ~, by the Lissajous-figure method described in Chapter XIX. Measured alternating currents, between 18 and 62 milliamperes in rms. strength, were passed through the instrument at this resonant frequency, and the maximum deflections produced by the reflected optical beam from the mirror were successively measured. The ratio of deflection to rms.

current, or specific deflection, over this range, is seen to produce a horizontal straight line in the diagram, within the limits of observational error. It therefore

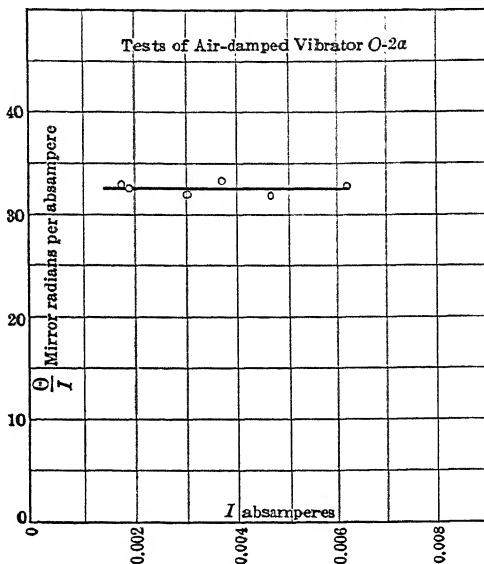


FIG. 209. Tests to detect variations in resistance torque to the motion of an oscillographic vibrator over a considerable range of displacement. (Prior.)

limits within which  $r$  can be taken as constant for engineering purposes. Judging from measurements of frictional resistance at higher velocities, it would appear that above some definite limit, the resistance  $r$  begins to depart sensibly from a constant value.

appears that the value of  $r$  was constant for the instrument, within that degree of precision. The current could not be conveniently reduced below 18 milliamperes, without loss of precision in measurement, nor could it be increased beyond 62 milliamperes (0.0062 abampere), without danger of stretching the strips by the heat produced.

More extensive and more precise measurements, conducted in this manner, on oscillograph vibrators immersed in different damping fluids, might indicate the complete

## APPENDIX XIII

### HARMONIC ANALYSIS SCHEDULES

We have already considered, in Chapter XXI, the corrections which are applicable to the various harmonic components of a complex wave, owing to the inertia of the oscillographic vibrator which recorded it. We may here consider briefly a suitable process for analyzing such a wave into its components.

The subject of harmonic analysis into Fourier components is very large, and its literature is extensive.\* We may confine ourselves here only to a consideration of a single well known method — the schedule method — and a particular schedule for evaluating odd harmonics up to the 17th, inclusive. It will be understood that when numerous oscillograms have to be analyzed, as a matter of daily routine, it becomes desirable to use some mechanical device for effecting the analyses automatically, whereas, when only an occasional oscillogram has to be dealt with, it is often inconvenient to install and maintain such mechanism. The schedule method is then convenient to follow.

**Odd Harmonics and Even Harmonics.** — Electric waves supplied by alternators are usually symmetric with respect to the zero line. That is, the negative half-waves are the images, as in a mirror, of the positive half-waves. This means, according to a well known theorem, that such waves contain only odd harmonic frequencies (1st, 3d, 5th, etc.), or at least that the even harmonic frequencies, or harmonics, are ordinarily negligibly small. Schedules for the harmonic analysis of waves from alternators deal, therefore, only with odd harmonics. On the other hand, electric waves supplied by oscillators, and also the records of acoustic waves, contain both even and odd harmonics, so that we may consider one 17-harmonic schedule for odd-component alternator waves, and one 11-harmonic schedule for even and odd components of a general wave. We may describe the fundamental frequency, in every case, as the first harmonic frequency or *first harmonic*.

**Schedule for Odd Terms only up to and including the Seventeenth Harmonic.** — Table XXVI gives the 17-harmonic schedule for odd terms. This schedule was originally drawn up at the City and Guilds of London Technical College. The schedule carries its own directions, but by way

\* See Dellenbaugh, Bibliography 88, in a paper that contains a good bibliographic index of Harmonic Analysis up to 1920.

TABLE XXVI

*Schedule for Harmonic Analysis:* Odd terms only; 18 ordinates to be taken from curve every ten degrees from  $0^\circ$  to  $180^\circ$  [N.B. As half periods are similar, the zero-line will be drawn midway between highest and lowest points.]

- (1) Divide the half-periods into 18 equal parts, and measure the 17 ordinates  $y_1 y_2 y_3 \dots y_{17}$ ;  $y_0$  and  $y_{18}$  being each zero.
- (2) Arrange these 17 ordinates in two rows, the first from right to left, the second from left to right, as under, and then take sums and differences.

First Row	$y_1$	$y_2$	$y_3$	$y_4$	$y_5$	$y_6$	$y_7$	$y_8$	$y_9$
Second Row	$y_{17}$	$y_{16}$	$y_{15}$	$y_{14}$	$y_{13}$	$y_{12}$	$y_{11}$	$y_{10}$	
Sums	$s_1$	$s_2$	$s_3$	$s_4$	$s_5$	$s_6$	$s_7$	$s_8$	
Differences	$d_1$	$d_2$	$d_3$	$d_4$	$d_5$	$d_6$	$d_7$	$d_8$	

Used for sine terms  
Used for cosine terms

- (3) Group numbers, as under, for use in obtaining 3d, 15th and 9th harmonics.

For SINE-TERMS Third and Fifteenth		For COSINE-TERMS Third and Fifteenth	
Sums	$s_1$ $s_6$ $-s_7$	$s_2$ $s_4$ $-s_8$	$s_3$ $-s_9$
	$a_1$	$a_2$	$a_3$
Ninth		Ninth	
Sum		Sum	
		$a_1$ $-a_8$	$a_4$
		Sums	
		$-d_8$ $-d_4$ $d_2$	$-d_7$ $-d_5$ $-$
		$b_1$	$b_2$
		Sum	
		$b_3$ $-b_1$	$b_4$

- (4) Enter the above numbers in their places, as in the table below, and on entering multiply each by the sine of the angle set down in the left-hand column. Find totals of first and second columns, and then take the sums and differences. Divide through by 9.

ANGLE	SINE	1st and 17th	3d and 15th	5th and 13th	7th and 11th	9th	1st and 17th	3d and 15th	5th and 13th	7th and 11th	9th
10°	0.1737	$s_1$		$-s_7$	$-s_6$		$d_8$		$-d_2$	$d_4$	
20°	0.3420	$s_2$		$s_8$	$-s_3$		$d_6$	$b_1$	$d_6$	$d_1$	
30°	0.5000		$a_1$								
40°	0.6428	$s_4$		$s_8$	$s_7$	$s_2$	$d_5$		$d_1$	$-d_7$	
50°	0.7660	$s_5$	$a_2$	$-s_6$	$s_6$		$d_3$	$b_2$	$-d_3$	$-d_3$	
60°	0.8660			$s_9$	$-s_4$	$s_1$	$d_1$		$-d_4$	$d_7$	$b_4$
70°	0.9397	$s_7$	$a_3$		$-s_3$	$-s_2$		$b_3$			
80°	0.9848	$s_9$									
90°	1.0000										
Total 1st Column											
Total 2d Column											
Sums		$\frac{9}{9} A_1$	$\frac{9}{9} A_3$	$\frac{9}{9} A_5$	$\frac{9}{9} A_7$	$\frac{9}{9} A_9$	$\frac{9}{9} B_1$	$\frac{9}{9} B_3$	$\frac{9}{9} B_5$	$\frac{9}{9} B_7$	$\frac{9}{9} B_9$
Differences		$\frac{9}{9} A_{17}$	$\frac{9}{9} A_{15}$	$\frac{9}{9} A_{13}$	$\frac{9}{9} A_{11}$	$\frac{9}{9} A_9$	$\frac{9}{9} B_{17}$	$\frac{9}{9} B_{15}$	$\frac{9}{9} B_{13}$	$\frac{9}{9} B_{11}$	$\frac{9}{9} B_9$

(5) Result  $y = A_1 \sin \theta + A_3 \sin 3\theta + A_5 \sin 5\theta + A_7 \sin 7\theta + A_9 \sin 9\theta + A_{11} \sin 11\theta + A_{13} \sin 13\theta + A_{15} \sin 15\theta + A_{17} \sin 17\theta + B_1 \cos \theta + B_3 \cos 3\theta + B_5 \cos 5\theta + B_7 \cos 7\theta + B_9 \cos 9\theta + B_{11} \cos 11\theta + B_{13} \cos 13\theta + B_{15} \cos 15\theta + B_{17} \cos 17\theta$ .

(6) Check result by following rules  $B_1 - A_3 + A_5 - A_7 + A_9 - A_{11} + A_{13} - A_{15} + A_{17} = 0$   
 $A_1 - A_3 + A_5 - A_7 + A_9 - A_{11} + A_{13} - A_{15} + A_{17} = y_0$ .

Great care must be taken throughout as to + and - signs. To reduce chances of error, space should be left in the blank schedules for first entering the values in their proper places, and with their proper signs; and secondly, for entering them again after multiplying each by the corresponding sine in the left-hand column.

(7) Compound A and B components of the several harmonics, and find their respective lags by the rules  $A'_1 = \sqrt{A_1^2 + B_1^2}$ ;  
 $\tan \alpha_1 = \frac{B_1}{A_1}$ , etc., for insertion in the equation  $\psi = A'_1 \sin (\theta + \alpha_1) + A'_3 \sin (3\theta + \alpha_3) + \dots$

	1st	3d	5th	7th	9th	11th	13th	15th	17th
$A'$	0.5666	0.0932	0.0411	0.0235	0.0149	0.0097	0.0062	0.0035	0.0011
$\alpha$	0°	0°	0°	0°	0°	0°	0°	0°	0°

The numerical values here given for  $A'$  pertain to the case of Figs. 210-211 and Table XXVII.

TABLE XXVII  
Example of the Application of the Schedules in Table XXVI for the Semicircular wave case of Fig. 210

Arranging Ordinates:									
First Row									
Second Row									
0.2291	0.2291	0.3143	0.3727	0.4157	0.4479	0.4714	0.4875	0.4969	0.5000
0.2291	0.2291	0.3143	0.3727	0.4157	0.4479	0.4714	0.4875	0.4969	0.5000
Sums		0.6286		0.8314		0.9428		0.9938	
Differences		0.6286		0.8314		0.9428		0.9938	
Grouping									
0.4582		0.6286		0.7454		0.8314		0.9428	
0.8058		0.8314		0.5000		0.5000		0.5000	
1.3540		1.4600		— 0.5000		— 0.5000		— 0.5000	
— 0.9750		— 0.9938		— 0.5000		— 0.5000		— 0.5000	
0.3790		0.4662		0.2454		0.1336		0.0858	
Sums		0.4662		0.2454		0.1336		0.0858	

*Remarks.* It is often advantageous to prepare, in advance, the blank schedules of Table XXVI. They may conveniently be prepared by making blueprints from a tracing. The half-wave to be analyzed is then laid out as in Fig. 210, and the seventeen equidistant ordinates, measured off on it, are inscribed in the blueprint schedule, together with their sums  $s$  and differences  $d$ , as they are shown in Table XXVII above. Denoting these respective sums and differences by the symbols  $s_1, s_2, \dots, s_{17}$  and  $d_1, d_2, \dots, d_{17}$  indicated on page 414, they are entered in the schedule, as at the upper part of page 417, and are then multiplied each by the sine coefficient of its horizontal row. They then appear as in the lower part of that page. The additions and subtractions being made by columns, as directed on page 415, the  $A$  and  $B$  coefficients are derived as shown at the bottom of page 417.

Since the semicircular wave of Fig. 210 presents no cosine terms, being symmetric with respect to its central ordinate  $v$ , no differences  $d$  appear in the schedule. That part of the computation which deals with cosine terms does not therefore need to be shown on page 417.

Entering:	1st and 17th	3rd and 15th	5th and 13th	7th and 11th	9th
0.1737	0.4582		- 0.9750	- 0.8058	
0.3420	0.7454	0.3790	0.7454	- 0.7454	
0.5000					
0.0428	0.8314		0.9938	0.6286	
0.7660	0.8958	0.4062	0.4582	0.9750	
0.8000	0.9428		- 0.9428	0.9428	
0.0397	0.0750		- 0.8958	0.4582	
0.0848	0.5000	0.2454	0.5000	- 0.5000	
1.0000	0.9938		0.6286	- 0.8314	0.1336
Multiplying by sines					
	0.0796	0.2150	- 0.1694	- 0.1556	
	0.3727	0.1895	0.3727	- 0.3727	
	0.8862		0.3510	0.7469	
	0.0163	0.4038	- 0.8418	0.4306	
	0.5000	0.2454	0.5000	- 0.5000	0.1336
				- 0.8188	
Total 1st Column	2.5548	0.4340	0.2126	0.1492	
Total 2d Column	2.5449	0.4038	0.1571	0.0620	
Sums	5.9997	0.8387	0.3697	0.2112	
Differences	0.0099	0.0311	0.0555	0.0672	
Divide by 9 . . .	$A_1 = 0.5806$ $A_{17} = 0.0011$	$A_3 = 0.0932$ $A_{15} = 0.0335$	$A_5 = 0.0411$ $A_{13} = 0.0062$	$A_7 = 0.0235$ $A_{11} = 0.0097$	$A_9 = 0.0136$ $A_{19} = 0.0136$

FOR SINE-TERMS



of illustration, we may apply it to the evaluation of the harmonics in a simple semicircular wave form, as shown in Fig. 210. The 17 ordinates have here been computed to four digits.

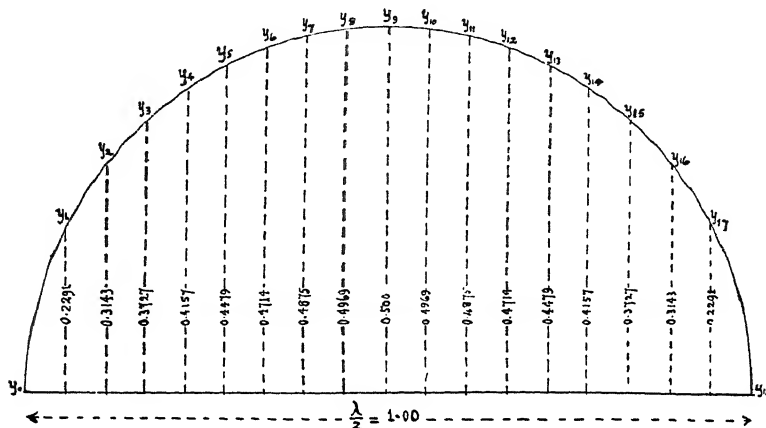


FIG. 210. Semicircular half-wave prepared for 17-term schedule analysis by ordinates measured at 18 ten-degree points, along base taken as of unit length.

The steps in the computation of this case are indicated in Table XXVII. It will be observed that because the initial and final ordinates,  $y_0$  and  $y_{18}$ , are taken as zero at the points where the wave cuts the zero line, and also because the half-wave is symmetric about the central ordinate  $y_9$ , there are no cosine terms. The analysis is as follows:

$$(581) \quad 0.5666 \sin \theta + 0.0932 \sin 3\theta + 0.0411 \sin 5\theta + 0.0235 \sin 7\theta \\ + 0.0149 \sin 9\theta + 0.0097 \sin 11\theta + 0.0062 \sin 13\theta \\ + 0.0035 \sin 15\theta + 0.0011 \sin 17\theta.$$

The theoretical analysis is \*

$$(582) \quad J_1\left(\frac{\pi}{2}\right) \cdot \sin \theta - \frac{1}{3} J_1\left(\frac{3\pi}{2}\right) \cdot \sin 3\theta \\ + \frac{1}{5} J_1\left(\frac{5\pi}{2}\right) \cdot \sin 5\theta - \frac{1}{7} J_1\left(\frac{7\pi}{2}\right) \sin 7\theta + \dots$$

where  $J_1(x)$  means the first order Bessel function of  $x$ , or

$$(583) \quad J_1(x) = \frac{x}{2} \left\{ 1 - \frac{1}{1!2!} \left(\frac{x}{2}\right)^2 + \frac{1}{2!3!} \left(\frac{x}{2}\right)^4 - \frac{1}{3!4!} \left(\frac{x}{2}\right)^6 + \dots \right\}$$

The expression (582), when 1.570795 replaces  $\pi/2$ , takes the form

$$(584) \quad 0.56682 \sin \theta + 0.0939 \sin 3\theta + 0.0423 \sin 5\theta + 0.0252 \sin 7\theta \\ + 0.0171 \sin 9\theta + 0.0123 \sin 11\theta \dots$$

\* Bibliography 22.

as far as the 11th harmonic term, inclusive. This means that the amplitude of the  $n$ th harmonic of a semicircle is the  $n$ th part of the first-order Bessel function of  $n$  quadrants expressed in radian measure. This Bessel function harmonic analysis applies not only to the semicircle, but also to any semiellipse which can be derived from a semicircle by simple projection. If the projection ratio is say  $b$ , then each harmonic of the semiellipse has  $b$  times the amplitude of the corresponding semicircular harmonic.

Figure 211 shows the semicircular half wave as a heavy curve and the successive harmonics, up to the 7th, inclusive, both separately and in superposition.

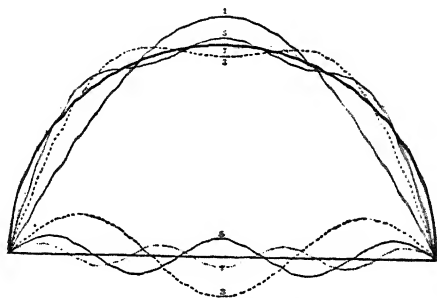


FIG. 211. Harmonic analysis and synthesis of a semicircular half wave, up to the seventh harmonic inclusive.

If we take the calculated value of 0.56682 the fundamental frequency as unity, the two series, as far as the 11th harmonic, compare as follows:

HARMONIC	1st	3rd	5th	7th	9th	11th
By Theory . . . . .	1.0	0.1656	0.0745	0.0444	0.0302	0.022
By Schedule . . . . .	0.9994	0.1644	0.0725	0.0415	0.0263	0.017
Difference . . . . .	0.0006	0.0012	0.0020	0.0029	0.0039	0.005

It will be seen that none of these differences exceed 5 per mil of the fundamental. The reason for their existence is that the harmonic schedule is based on the assumption that there are no harmonics above the seventeenth. The presence of the actual higher harmonics vitiates the computation.

In practice, the technique of oscillography rarely permits of a measurement of the measured ordinates to three significant digits without considerable uncertainty in the last figure. The curve is not defined with sufficient sharpness, as a rule, to enable very accurate measurements of ordinates to be made, so that the precision indicated in the above example is seldom attained in the laboratory.

For many purposes, shorter schedules covering a smaller number of harmonic terms may suffice. Roughly speaking, the time required to

work out a schedule increases as the square of the number of terms which it includes.

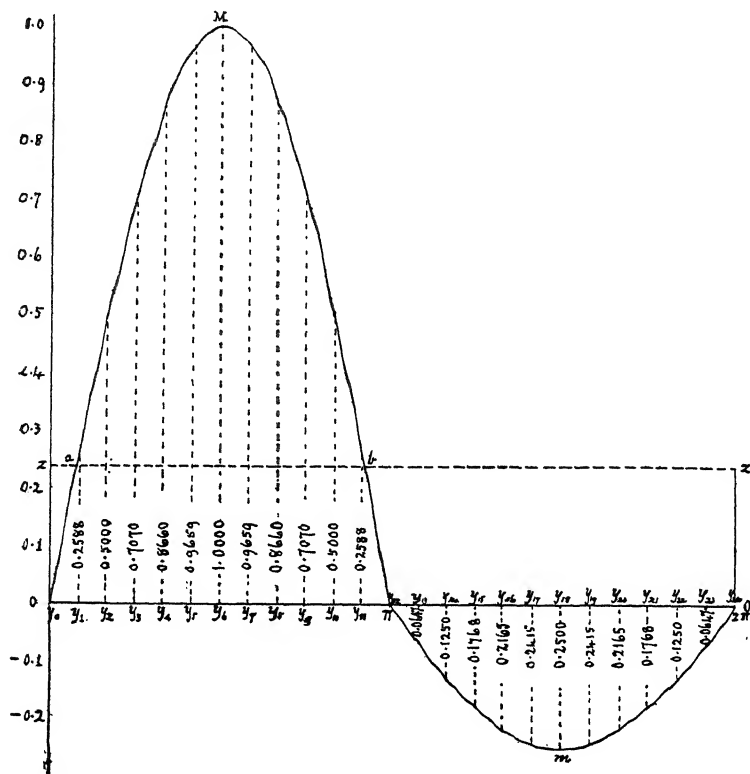


FIG. 212. Curve of  $1 \sin \theta_0 \pi + 0.25 \sin \theta_x^2 \pi$ , arranged for schedule analysis.

**Schedule for Both Even and Odd Terms, up to and including the Eleventh Harmonic.**—Table XXVIII gives a schedule, worked out by Dr. H. O. Taylor,\* for dealing with both odd and even harmonics up to and including the eleventh. A particular wave is presented in Fig. 212 for analysis by way of example. It consists of two sinusoidal half-waves in succession, with amplitudes of 1.0 and 0.25 respectively. The theoretical analysis of this asymmetric wave is

$$(585) \quad y = \frac{3}{2\pi} \left\{ \frac{1}{2} + \frac{5\pi}{12} \sin \theta - \frac{1}{1.3} \cos 2\theta - \frac{1}{3.5} \cos 4\theta - \frac{1}{5.7} \cos 6\theta \right. \\ \left. - \frac{1}{7.9} \cos 8\theta - \frac{1}{9.11} \cos 10\theta - \dots \right\}$$

\* Bibliography 57a.

or

$$(586) \quad y = 0.23873 + 0.625 \sin \theta - 0.15915 \cos 2\theta - 0.03183 \cos 4\theta \\ - 0.01363 \cos 6\theta - 0.00985 \cos 8\theta - 0.00482 \cos 10\theta \dots$$

The results of the schedule analysis as shown in Tables XXVIII and XXIX are

$$(587) \quad y = 0.23735 + 0.625 \sin \theta - 0.1619 \cos 2\theta - 0.0347 \cos 4\theta \\ - 0.0168 \cos 6\theta - 0.0110 \cos 8\theta - 0.0088 \cos 10\theta - \dots \text{numeric.}$$

In Fig. 212, the dotted line  $zabz'$ , parallel to the base, marks the ordinate 0.23873, and also divides the curve into two equal areas.

The numerical checks supplied at the end of the schedule are necessarily only approximate. They are rigidly correct only in cases where there are no harmonics higher than the tenth.

*Schedule for Harmonic Analysis:* Odd and even terms, according to the Fourier Series:

$$y = B_0 + A_1 \sin \omega t + A_2 \sin 2\omega t + A_3 \sin 3\omega t + \dots + A_{11} \sin 11\omega t \\ + B_1 \cos \omega t + B_2 \cos 2\omega t + B_3 \cos 3\omega t + \dots + B_{11} \cos 11\omega t.$$

- (1) Divide a full period into twenty-four equal parts of  $15^\circ$  each, and measure the twenty-four successive ordinates  $y_1, y_2, y_3, \dots, y_{24}$ .  $y_{24}$  should correspond to  $y_0$ , the initial ordinate, which is not scheduled.
- (2) Arrange these twenty-four ordinates in two rows, as below. Write down their sums and differences.

	$y_1$	$y_2$	$y_3$	$y_4$	$y_5$	$y_6$	$y_7$	$y_8$	$y_9$	$y_{10}$	$y_{11}$	$y_{12}$		
	$y_{24}$	$y_{23}$	$y_{22}$	$y_{21}$	$y_{20}$	$y_{19}$	$y_{18}$	$y_{17}$	$y_{16}$	$y_{15}$	$y_{14}$	$y_{13}$		
Sums	$S_0$	$S_1$	$S_2$	$S_3$	$S_4$	$S_5$	$S_6$	$S_7$	$S_8$	$S_9$	$S_{10}$	$S_{11}$	$S_{12}$	for cosine terms (B)
Differences		$d_1$	$d_2$	$d_3$	$d_4$	$d_5$	$d_6$	$d_7$	$d_8$	$d_9$	$d_{10}$	$d_{11}$		for sine terms (A)

- (3) Enter the above sums and differences, with their proper signs, in the following schedules, multiplying each by the sine of the angle set down in the left hand of each row. Find the totals of the first and second columns and take their sums and differences, preserving the signs of the latter. Divide throughout by 12.

Determine the coefficients  $A_i$  from schedule (A) by the relations  $A_i = D_i/12$ , where  $D_i = \Delta_i - \Delta'_i$  in schedule (A).

Determine  $B_0$  from  $B_0 = \Sigma S/24$ , i.e., the sum of the 13 values  $S_0, \dots, S_{12}$ , divided by 24.

Determine the remaining coefficients  $B_i$  from the relations  $B_i = D_i/12$ , where  $D_i = \Delta_i - \Delta'_i$  in schedule (B).

Checks:

$y_{24} = S_0 = \Sigma B$  or the sum of all the  $B$  coefficients from  $B_0$  to  $B_{11}$  inclusive.  
 $y_{12} = S_{12} = \Sigma B'' - \Sigma B'$  where  $\Sigma B''$  represents the sum of the even coefficients from  $B_0 \dots$  to  $B_{10}$  inclusive, and  $\Sigma B'$  represents the sum of the odd coefficients from  $B_1 \dots$  to  $B_{11}$  inclusive.

$$y_6 = A_1 - A_3 + A_5 - A_7 + A_9 - A_{11} + B_0 - B_2 + B_4 - B_6 + B_8 - B_{10}.$$

$$y_{18} = -A_1 + A_3 - A_5 + A_7 - A_9 + A_{11} + B_0 - B_2 + B_4 - B_6 + B_8 - B_{10}.$$

The assumption involved in these computations is that there are no harmonics higher than the eleventh.

TABLE XXVIII  
*Sine Terms (A)*

ANGLE	SINE	1ST OR FUNDAMENTAL	2D HARMONIC	3D HARMONIC	4TH HARMONIC	5TH HARMONIC	6TH HARMONIC
15°	0.2588	$d_1 + d_{11}$	$d_1 + d_6$	$d_1 + d_3$		$d_6 + d_7$	
30°	0.5000	$d_2 + d_{10}$		$d_2 + d_3 + d_{11}$		$d_2 + d_{10}$	
45°	0.7070	$d_3 + d_9$		$d_3 + d_6 + d_7$		$d_3 + d_9$	
60°	0.8660	$d_4 + d_8$	$d_2 + d_4$	$d_2 + d_3 + d_{10}$	$d_1 + d_2 + d_3 + d_6 + d_{10} + d_{11}$	$d_4 + d_8$	
75°	0.9659	$d_5 + d_7$		$d_5 + d_{10}$		$d_5 + d_{11}$	
90°	1.0000	$d_6$	$d_3$	$d_3 + d_6$		$d_6$	$d_3 + d_6 + d_{11}$
		$\Delta_1$	$\Delta_3$	$\Delta_5$	$\Delta_4$	$\Delta_5$	$\Delta_6$
		$\Delta'_1$	$\Delta'_2$	$\Delta'_3$	$\Delta'_4$	$\Delta'_5$	$\Delta'_6$

ANGLE	SINE	7TH HARMONIC	8TH HARMONIC	9TH HARMONIC	10TH HARMONIC	11TH HARMONIC
15°	0.2588	$d_6 + d_7$			$d_1 + d_5$	$d_1 + d_{11}$
30°	0.5000		$d_2 + d_{10}$		$d_7 + d_{11}$	$d_2 + d_{10}$
45°	0.7070		$d_3 + d_9$	$d_1 + d_3 + d_5 + d_{11}$		$d_3 + d_9$
60°	0.8660	$d_4 + d_8$	$d_1 + d_4 + d_7 + d_{10}$	$d_2 + d_3 + d_6 + d_7$	$d_8 + d_{10}$	$d_4 + d_8$
75°	0.9659	$d_5 + d_{11}$				
90°	1.0000	$d_6$		$d_6$	$d_3$	$d_6 + d_7$
		$\Delta_7$	$\Delta_8$	$\Delta_9$	$\Delta_{10}$	$\Delta_{11}$
		$\Delta'_7$	$\Delta'_8$	$\Delta'_9$	$\Delta'_{10}$	$\Delta'_{11}$

## Cosine Terms (B)

ANGLE	SINE	1ST OR FUNDAMENTAL	2D HARMONIC	3D HARMONIC	4TH HARMONIC	5TH HARMONIC	6TH HARMONIC
15°	0.2588	$S_6$ $S_4$	$S_2 + S_{10}$ $S_4 + S_8$		$S_1 + S_6$ $+ S_7 + S_{11}$	$S_1$ $S_4$	
30°	0.5000	$S_7$ $S_3$			$S_2 + S_4$ $+ S_6 + S_{10}$	$S_{11}$ $S_6$	
45°	0.7070	$S_8$ $S_2$		$S_1 + S_7$ $+ S_9$		$S_9$ $S_{10}$	
60°	0.8660	$S_{10}$ $S_6$	$S_1 + S_{11}$ $S_5 + S_7$			$S_3$ $S_2$	
75°	0.9659	$S_{11}$ $S_7$	$S_0 + S_{12}$ $S_6$	$S_0 + S_8$ $S_4 + S_{12}$	$S_0 + S_6$ $+ S_{12}$	$S_5$ $S_0$	$S_7$ $S_{12}$
90°	1.0000	$S_{12}$ $S_8$			$S_8 + S_9$	$S_0 + S_4$ $+ S_8 + S_{12}$	$S_2 + S_6$ $+ S_{10}$
		$\Delta_1$ $\Delta'_1$	$\Delta_2$ $\Delta'_2$	$\Delta_3$ $\Delta'_3$	$\Delta_4$ $\Delta'_4$	$\Delta_5$ $\Delta'_5$	$\Delta_6$ $\Delta'_6$

ANGLE	SINE	7TH HARMONIC	8TH HARMONIC	9TH HARMONIC	10TH HARMONIC	11TH HARMONIC
15°	0.2588	$S_{11}$ $S_4$			$S_2 + S_{10}$ $S_4 + S_8$	$S_6$ $S_3$
30°	0.5000	$S_8$ $S_2$	$S_1 + S_2 + S_4 + S_6$ $+ S_7 + S_8 + S_{10} + S_{11}$			$S_7$ $S_4$
45°	0.7070	$S_8$ $S_{10}$		$S_3 + S_6$ $+ S_{11}$	$S_6 + S_7$ $S_8 + S_{11}$	$S_9$ $S_3$
60°	0.8660	$S_{10}$ $S_6$				$S_2$ $S_{10}$
75°	0.9659	$S_7$ $S_0$	$S_0 + S_3 + S_6 + S_9 + S_{12}$ $\Delta_8$	$S_0 + S_8$ $S_4 + S_{12}$	$S_0 + S_{12}$ $S_6$	$S_{11}$ $S_0$
90°	1.0000	$\Delta_7$ $\Delta'_7$	$\Delta'_8$	$\Delta_9$ $\Delta'_9$	$\Delta_{10}$ $\Delta'_{10}$	$\Delta_{11}$ $\Delta'_{11}$

TABLE XXIX.—HARMONIC ANALYSIS OF THE WAVE REPRESENTED IN FIG. 212 FOR BOTH ODD AND EVEN TERMS

	0	1	2	3	4	5	6	7	8	9	10	11	12
	0	0.2588	0.5000	0.7071	0.8060	0.9659	1.0000	0.9659	0.8060	0.7071	0.5000	0.2588	0
	0	-0.0047	-0.1250	-0.1708	-0.2165	-0.2415	-0.2500	-0.2415	-0.2165	-0.1708	-0.1250	-0.0047	
<i>S</i>	0	0.1941	0.3750	0.5303	0.6495	0.7244	0.7500	0.7244	0.6495	0.5303	0.3750	0.1941	0
<i>d</i>	0	0.3235	0.6250	0.8839	1.0825	1.2074	1.2500	1.2074	1.0825	0.8839	0.6250	0.3235	0

	Sine	$A_1$	$A_3$	$A_5$	$A_7$	$A_9$	$A_{11}$	$A_{13}$
15°	0.2588	0.1075						
30°	0.5000	0.6250	0.7064					
45°	0.7071	1.2500	1.7076	1.7076				
60°	0.8660	1.8750	1.4790	1.4790	2.8040			
75°	0.9659	2.3235	0.8839	0.8839	2.8040	2.8040		
90°	1.0000	2.5000	3.1283	3.1283	2.8040	2.8040	2.8040	
		7.5000	3.1283	2.9576	2.8040	2.8040	2.8040	15°
		0	0 = $D_1$	0 = $D_3$	0 = $D_5$	0 = $D_7$	0 = $D_9$	30°
		7.5000 = $D_1$	0 = $A_1$	0 = $A_3$	0 = $A_5$	0 = $A_7$	0 = $A_9$	45°
		0.6250 = $A_1$						60°

	Sine	$A_7$	$A_9$	$A_{11}$	$A_{13}$	$A_{15}$	$A_{17}$	$A_{19}$
15°	0.2588	0.6250						
30°	0.5000	1.2500	1.7076	1.7076	0.7654			
45°	0.7071				0.7654	0.7654		
60°	0.8660	1.8750	2.8040	2.8040	1.4790	1.4790	1.8750	
75°	0.9659	2.3235	2.8040	2.8040	0.8839	0.8839	2.3235	60°
90°	1.0000	2.5000	3.1283	3.1283	2.8040	2.8040	3.1283	75°
		3.1250	2.9576	2.9576	3.1283	3.1283	2.9576	90°
		3.1250	0 = $D_7$	0 = $D_9$	0 = $D_{11}$	0 = $D_{13}$	0 = $D_{15}$	
		0 = $A_7$	0 = $A_9$	0 = $A_{11}$	0 = $A_{13}$	0 = $A_{15}$	0 = $A_{17}$	

$$\Sigma S = 5.6966; B_0 = \Sigma S/24 = 0.23735$$

Sine	$B_1$	$B_2$	$B_3$	$B_4$	$B_5$	$B_6$
15°	0.1875	0.1875				15°
30°	0.2588	0.3750	1.0247	0.9185	0.0502	
45°	0.5000	0.3248		1.0245	0.3248	
	0.7071	0.3750			0.3750	45°
60°	0.8660	0.3248			0.3248	
75°	0.9659	0.1875	0.6495		0.6997	60°
90°	1.0000	0	1.0247		0	75°
	1.0000	1.3006	1.6742	0.7500	1.7745	1.2900
	1.3006	2.6543	1.6742	1.6385	1.7745	1.5000
	0 = $D_1$	0 = $D_2$	0 = $D_3$	2.0851	0 = $D_5$	-0.2010 = $D_6$
	0 = $B_1$	-1.9431 = $D_8$	0 = $B_3$	-0.4166 = $D_4$	0 = $B_5$	-0.0168 = $B_6$
		-0.1619 = $B_7$		-0.0347 = $B_1$		

Sine	$B_7$	$B_8$	$B_9$	$B_{10}$	$B_{11}$
15°	0.0502				0.1875
30°	0.3248	1.9430	1.0247	0.3750	0.3248
45°	0.5000			0.6495	0.3750
	0.7071				0.3750
60°	0.8660	1.8106	0.6495	1.2548	0.3248
75°	0.9659	1.9430	1.0247	0.3750	0.1875
90°	1.0000	1.8106	1.0247	0.6495	0.1875
	1.0000	1.7745	1.6742	1.7357	1.3996
	1.7745	1.6742	1.6742	1.6298	1.3996
	0 = $D_7$	0 = $D_8$	0 = $D_9$	0 = $D_{10}$	0 = $D_{11}$
	0 = $B_7$	-0.1324 = $D_8$	0 = $B_9$	-0.0088 = $D_{10}$	0 = $B_{11}$
		-0.0110 = $B_8$			



## FURTHER EXPERIMENTAL TESTS OF MODES OF DIAPHRAGM VIBRATION

The following data concerning the observed modes and frequencies of vibration of Klaxon-horn diaphragms have been kindly contributed by Prof. V. Karapetoff from tests made at Cornell University. The tests were made on diaphragms for "industrial horns," which are similar to "automobile horns," but larger.

A Klaxon horn, as commonly employed on automobiles, has a standard form of circular diaphragm of japanned sheet steel, champed around its edge by a pair of flat steel clamping rings. The rings are compressed by six equidistant screws, which pass through corresponding holes in the edge of the diaphragm. At its center is riveted a steel boss for ratchet agitation. The dimensions of a sample industrial-horn diaphragm were:

Diameter of diaphragm . . . . .	13.8 cm.
Diameter of clamping circle . . . . .	11.4 cm.
Thickness of diaphragm (over japan) . . . . .	0.59 mm.
Approximate mass of central boss load . . . . .	7.5 gm.

Figure 213 shows such a diaphragm, clamped in a horizontal frame over

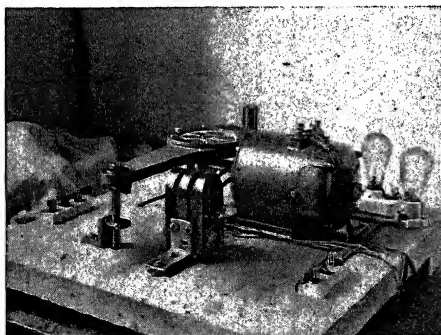


FIG. 213. Vibration tests of Klaxon horn diaphragm.

a motor-driven ratchet wheel. The speed of the motor, and thus the frequency of the impressed vmf., was measured by means of the associated magneto generator.

The motor was driven electrically at adjustable speeds. The diaphragm was thus maintained in corresponding forced vibration. At certain particular speeds, the plate responded definitely. These definite responses were recognized, partly by the emitted acoustic tone, and partly by the pattern formed by grains of sand strewn on the diaphragm surface.

A number of diaphragms were tested in the manner. A set of results obtained with one diaphragm selected at random, are given in Fig. 214.

Abscissas indicate impressed vmf. frequency, and ordinates the estimated intensity of response. The circle, at the top of each ordinate, shows the mode of vibration, as read from the same pattern. In this instance, the diaphragm gave a maximum response, on its first mode, at 390 ~, with a very loud tone. It also gave feeble response, in its first mode, at 130, 195, and 1110 ~. At 420 ~ it responded loudly in its

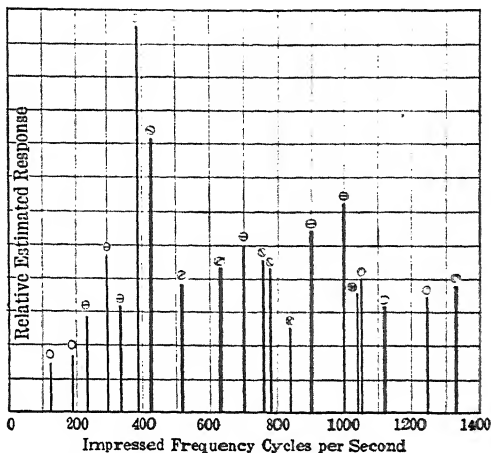


FIG. 214. Modes of vibration of diaphragm of Klaxon horn at different impressed frequencies. (Karapetoff.)

second mode with one nodal diameter. Other and feeble responses, in this mode, were obtained at 230, 300, 330, 520, 700, 753, 790, and 900 ~. In some of these cases, the nodal diameter assumed one direction, and in others another. Occasionally, a nodal diameter would be seen to swing periodically. The second mode, with two nodal diameters, was noticed at 830 ~, and with three diameters at 1040 ~. The third mode, with a single nodal circle, was observed at 1240 ~ and 1330 ~. A combination of 2d and 3d modes is shown at 1040 ~. One or two other mixed forms of vibration were also found.

Similar tests, with other diaphragms, gave results of the same type, but the frequencies of response were by no means identical. They often differed very considerably. It is clear that no great reliance in quantitative detail can be placed upon the frequencies or frequency ratios of these different modes, probably because of asymmetries in loading, thickness, quality, and clamping of the diaphragms. The results clearly indicate, however, that with relatively powerful vmfs. impressed upon a circularly clamped diaphragm, various modes of vibration may be set up at sharply selective frequencies, and that such a diaphragm is very sensitive to small departures from geometric and dynamic symmetry.

## LIST OF SYMBOLS EMPLOYED

$A$	force factor of a telephone receiver (dynes/rms. abampere $\angle$ ); also force factor of an oscillograph or vibration galvanometer $\frac{\text{dynes-p.-cm.}}{\text{rms. abampere}} \angle$
$A_1, A_2, A_3, A'_1, A'_2, A'_3$	Fourier harmonic amplitudes (amperes or volts).
$a$	clamping radius of a diaphragm (cm.); also radius of a disk (cm.); also a force factor in reinforced vibrations.
$a, b, c$	empirical constants in expression for damped resistance of a receiver (ohms).
$\alpha$	an angle or slope (radians or degrees).
$\alpha_1, \alpha_2, \alpha_3$	slopes of oscillograph correction factors (degrees).
$\alpha_1, \alpha_2$	quadrantal values of slope (radians).
$\alpha = (\alpha_1 + j\alpha_2)$	in acoustic impedance of an air tube, the linear hyperbolic angle of the tube (hyps. per cm. $\angle$ ).
$\alpha_1, \alpha_2$	real and imaginary components of linear hyp angle (hyp. and cir. radians).
$\alpha_n$	phase angle of vibration around a plate diaphragm (radians).
$B_1, B_2, B_3$	Fourier harmonic amplitudes (amperes or volts).
$B_s = 1/\Delta_s = 2B_0$	sustained resonant bluntness of a system based on $\tau_s$ (numeric).
$B_0 = 1/\Delta_0$	oscillatory resonant bluntness of a system based on $\tau_0$ (numeric).
$\mathcal{B}$	flux density in a magnetic circuit (gausses).
$\mathcal{B}_0$	permanent magnetic flux density in mag. cct. (gausses).
$\mathcal{B}_{im}$	maximum cyclic flux density in mag. cct. due to an alt. current (max. cyc. gaussess).
$\mathcal{B}_i$	effective flux density in a mag. cct. due to an alt. current (rms. gaussess).
$b$	thickness of a plate diaphragm (cm.).
$b, b$	mechanical susceptance (mechanical abmhos) or susceptance to torque.
$\beta^\circ$	slope of a complex quantity (degrees); in particular, slope of flux lag in receiver magnetic cct. (degrees); also a time-phase lag angle (radians or degrees).
$C = 1/D$	correction factor of an oscillographic vibrator (numeric $\angle$ ).
$C_1, C_2, C_3$	sizes of correction factors for oscillographic harmonic terms (numeric).
$c$	capacitance of a condenser (farads or abfarads); also linear capacitance of a line conductor (farads/km.); also a constant of diaphragm material (cm./ $\sqrt{\text{sec.}}$ ).

$c = 1/s$	inelastance of a mechanical vib. system (cm., dyne) or radian dyne-p.-cm.).
$\gamma$	a circular angle (radians or degrees); also in acoustic-conductor theory, the ratio 1.41 of specific heats in air, constant pressure to constant volume (numeric).
$D = 1/C$	deviation factor of an oscillograph (numeric $\angle$ ).
$d$	a differential; also in amplitude exploration, the length of the luminous reflected band (cm.).
$\Delta = r/2 m$	damping factor of a vib. system (hyp./sec.).
$\Delta_0$	aperiodic value of $\Delta$ when numerically equal to $\omega_0$ (hyps./sec.).
$\delta, \delta_T$	logh decrement of a damped vibration (numeric); also the deviation ( $u - 1$ ) for a sharp vibrator (numeric).
$\delta_t, \delta_i$	logh decrement of a damped vibration at time $t$ , and after one radian revolution (numerics).
$\delta_{2\pi}$	logh decrement of a damped vibration in one cycle or after $2\pi$ radians (numeric).
$\delta_A, \delta_P$	position angles of the sending end, and of a point $P$ on an acoustic or electric conductor (hyps. $\angle$ ).
$E$	electromotive force in a system (rms. volts or abvolts).
$E_a$	absorption emf. in pr. cct., due to action of sec. cct. (rms. volts $\angle$ ).
$E_A, E_P, E_B$	emf. at sending end, at an intermediate point, and at the receiving end, of line conductor (volts $\angle$ ).
$e$	emf. (abvolts); also instantaneous motive inertia force in a damped system (dynes or volts); also a time-phase in plate-diaphragm vibration (secs.).
$e_r$	emf. produced by resistance (rms. volts $\angle$ ).
$\epsilon = 2.718 \dots$	Napierian base (numeric).
$\eta' = r/r'$	mech. efficiency of diaphragm (numeric).
$\eta'' = R'/R''$	gross efficiency of receiver (numeric).
$\eta = \eta'\eta''$	net efficiency of receiver (numeric).
$\eta'_0, \eta''_0, \eta_0$	values of $\eta'$ , $\eta''$ , and $\eta$ at apparent resonance (numeric).
$F$	total magnetic tractive force on a diaphragm (dynes).
$F_0$	permanent magnetic tractive force on diaphragm (dynes).
$F_{im}$	maximum cyclic magnetic tractive force, or vmf., on diaphragm due to current (max. cyc. dynes).
$F_i$	effective tractive force or vmf. on diaphragm, due to current (rms. dynes).
$F_r$	vibromotive force or torque impressed on a system (rms. dynes $\angle$ or rms. dyne-p.-cm. $\angle$ ).
$F_m$	maximum cyclic value of $F_r$ (dynes $\angle$ , or dyne-p.-cm. $\angle$ ).
$F_a$	absorption vmf. due to action of secondary system (rms. dynes $\angle$ ).
$F_A, F_P, F_B$	vibromotive force over section of acoustic conductor, at sending end, at intermediate point $P$ , and at receiving end (rms. dynes $\angle$ ).
$F_2$	vmf. in secondary system (rms. dynes $\angle$ ).

$F_i$	size of initial vector force in a damped system (dynes or volts).
$F_r$	size of initial actual force in a damped system (dynes or volts).
$\mathcal{F}_0$	permanent mmf. in mag. ckt. (gilberts).
$\mathcal{F}_{im}$	mmf. in mag. ckt. due to alt. current (max. cyc. gilberts).
$\mathcal{F}_c$	mmf. of demagnetization (gilberts).
$\mathcal{F}_x$	eff. mmf. of displacement (rms. gilberts $\angle$ ).
$\mathcal{F}$	eff. resultant mmf. in mag. ckt. (rms. gilberts $\angle$ ).
$f$	specific mag. tractive force on diaphragm (dynes/cm. <sup>2</sup> ).
$f, \mathbf{f}$	instantaneous vmf. or vmt. on a system (dynes, or dyne-p.-cm.).
$f$	frequency (cycles/sec.).
$f_0, f_1, f_2$	frequency of resonance, lower and upper quadrantal values (cy. per sec.).
$f'_0, f''_0$	resonant frequency of a diaphragm after being loaded (cycles/sec.).
$f_s, f_d, f_f, f_{12}$	initial, maximum admittant, free and midquadrantal impressed frequency (cycles/sec.).
$f_{rm}$	mech. force due to resistance (max. cyc. dynes $\angle$ ).
$f_r$	mech. force due to resistance (rms. dynes $\angle$ ).
$g$	linear conductance of an electric conductor (mhos/km.).
$g \mathbf{g}$	mech. conductance, or conductance torque; also linear acoustic conductance (mech. abmho/cm.) conductance (mech. abmhos.).
$\gamma = 1.41$	ratio of specific heats in air (numeric); also an angle in a vector triangle (radians).
$\gamma' = \frac{\pi}{2} - \gamma$	the complement of the angle $\gamma$ (cir. radians).
$\mathcal{H}_c$	demagnetizing force (gilberts/cm.).
$\mathcal{H}'_c$	total demagnetizing force (gilberts/cm.).
$\theta$	displacement of a rot. vib. system (rms. radians $\angle$ ).
$\theta_m$	displacement of a rot. vib. system (max. cyc. radians $\angle$ ).
$\theta_i$	initial displacement of rot. vib. system (radians)
$\theta_t$	displacement at time $t$ (radians).
$\dot{\theta}$	angular velocity of rot. vib. system (rms. radians/sec.).
$\dot{\theta}_m$	angular vel. of rot. vib. system (max. cyc. radians/sec.).
$\theta = \theta_1 + j\theta_2$	line angle of a conductor el. or acous. (hyp. $\angle$ ).
$\theta$	in theory of angular velocity, $\cosh^{-1} B_0$ (hyp.).
$\theta'$	in oscillography, specific deflection of mirror (max. cyc. radians/rms. abampere).
$\theta'_m$	in oscillography, specific deflection of mirror (max. cyc. radians/max. cyc. abampere).
$\mathcal{J} = \phi$	current in magnetic circuit (maxwells per sec. $\angle$ ).
$I$	alt. current (rms. amp. or abamperes $\angle$ ).
$I_m$	alt. current (max. cyc. abamperes $\angle$ ).
$i$	instantaneous alt. current (abamperes); also $\sqrt{-1}$ in plate vibration theory.

$I_1, I_2$	pr. and sec. currents (rms. amp. or abamperes $\angle$ ).
$I_a$	virtual current of absorption in pr. ect. due to action of sec. ect. (rms. amp. or abamperes $\angle$ ).
$I_{1a}$	current in pr. ect. as effected by action of sec. ect. (rms. amp. or abamp. $\angle$ ).
$I_A$	current at sending end of conducting a.-c. line (amperes $\angle$ ).
$I_m$	current in receiver winding (max. cyc. abamperes).
$I$	eff. alt. current strength in receiver (rms. abamperes).
$J_n$	Bessel's function of the $n$ th order (numeric).
$j = \sqrt{-1}$	
$k = \sqrt{\omega/c}$	a constant of diaphragm material ( $\text{cm.}^{-1}$ ).
$k_s$	elasticity constant of diaphragm material (dynes/ $\text{cm.}^2$ ).
$k_m$	density constant of diaphragm material ( $\text{gm./c.c.}$ ).
$k_{sm}$	a constant of diaphragm material (ergs/ $\text{gm.}$ ) $^{\frac{1}{2}}$ .
$k = p/p'$	acoustic compression, or ratio of rms. diminution in volume to quiescent volume (numeric).
$L$	length of mean flux path in mag. ect. ( $\text{cm.}$ ); also length of an electric conductor ( $\text{km.}$ ) or acoustic conductor ( $\text{cm.}$ ); also distance between mirror and screen of oscillograph ( $\text{cm.}$ ).
$L_2$	distance from point $P$ to far end of el. or acoustic conductor ( $\text{km.}$ or $\text{cm.}$ ).
$\mathcal{L}$	inductance of receiver coil (henries or abhenries).
$\mathcal{L}_0$	vector inductance of receiver coil at apparent resonance (henries or abhenries $\angle$ ).
$\mathcal{L}''$	apparent inductance of a receiver free (henries or abhenries).
$l$	inductance of a branch circuit (henries or abhenries); also length of mirror radius arm ( $\text{cm.}$ ).
$\lambda$	wave length in el. or acous. conductor ( $\text{km.}$ or $\text{cm.}$ ); also a boundary-condition constant for plate diaphragms (numeric).
$M$	total mass of diaphragm within clamping circle ( $\text{gm.}$ ); also magnification factor of optical explorer (numeric).
$m$	equivalent mass of simple linear vibrator ( $\text{gm.}$ ); also number of complete energy cycles of a damped vibrator (numeric).
$m$	linear mass of air in an acoustic tube conductor ( $\text{gm. per linear cm.}$ ).
$m$	moment of inertia of simple rotational vibrator ( $\text{gm.-cm.}^2$ ).
$m'$	central load attached to a diaphragm ( $\text{gm.}$ ).
$m_1$	equivalent polar mass of a diaphragm ( $\text{gm.}$ ).
$m_0$	equivalent central mass of a diaphragm ( $\text{gm.}$ ); also mass of a rotational vibrator ( $\text{gm.}$ ).
$\mu$	magnetic permeability (gausses/gilberts per $\text{cm.}$ ); also mutual inductance or mutual mass between a pair of primary and secondary systems (henries, abhenries or grams); also symbol for a micron or $10^{-6}$ meter.

$N$	total number of turns in a receiver winding (numeric).
$N'$	fictitious number of displacement turns (abamp./cm. or gilberts/cm.).
$n$	number of nodal diameters in a vibrating plate diaphragm (numeric); also number of rings into which a vibrating plate may by assumption be divided, in order to find the central equivalent mass (numeric); also a complex angular velocity (hyp. per. sec. $\angle$ ); also the root index of a force factor in sustained vibration (numeric).
$\nu$	scalar ratio of current or velocity at any impressed frequency, to the maximum or resonant value (numeric).
$\nu'$	scalar ratio of quantity or displacement at any impressed frequency, to the maximum value at $f_a$ (numeric).
$P = EI$	vector power in simple a.-c. circuit (abwatts $\angle$ ); also a constant of amplitude-magnitude for a plate diaphragm (cm.).
$P_e = P_{ea} + jP_{er}$	electric power of motional-power circle (abwatts $\angle$ ).
$P_h = P_{ha} + jP_{hr}$	hysteretic power of motional-impedance circle (abwatts/2 sin $\beta$ $\angle$ ).
$P_i = P_a - jP_r$	initial vector power of a damped vib. system (abwatts $\angle$ ).
$P''_m = P''_{ma} + jP''_{mr}$	gross motional power of motional-power circle (abwatts $\angle$ ).
$P''_{mo}$	gross motional power at apparent resonance (abwatts $\angle$ ).
$P'_{ma} = \dot{x}^2 r'$	motional active power expended in displacement (abwatts).
$P_{ma} = \dot{x}^2 r$	net active power output (abwatts).
$P'' = P''_a + jP''_r = \mathcal{F}\dot{\phi}/4\pi$	vector power expended in mag. cct., diaphragm free (abwatts $\angle$ ).
$P_i = \mathcal{F}\dot{\phi}/4\pi$	vector power expended in electromagnetic cct. (abwatts $\angle$ ).
$P_i'' = \mathcal{F}_i\dot{\phi}/4\pi$	vector power in same cct., diaphragm free (abwatts $\angle$ ).
$p = N'/N$	turns ratio of a receiver (abamp./cm.); also ratio $r_2/r_1$ of resistance in coupled systems (numeric); also $Y^2/X$ the parameter of a parabola.
$p = F/S$	pressure intensity deviation from normal on surface of a diaphragm (dynes/sq. cm.).
$p_c$	power in a spring or condenser of a damped system (abwatts or watts).
$p$	power in a mass or inductance of a damped system (abwatts or watts).
$p_0$	hydrostatic pressure in quiescent air of acoustic conductor (dynes/sq. cm.).
$p'_0 = \gamma p_0$	adiabatic hydrostatic pressure in quiescent air of tube (dynes/sq. cm.).
$\pi = 3.1415 \dots$	(numeric).
$\phi$	angle between mirror and diaphragm (degrees); also flux in magnetic circuit (maxwells).

$\phi_0$	permanent mag. flux in receiver mag. cct. (maxwells).
$\phi_{im}$	mag. flux in mag. cct. due to alt. current (max. cyc. maxwells).
$\phi_e$	effective mag. flux in mag. cct. due to alt. current (rms. maxwells).
$\phi_z$	effective mag. flux in mag. cct. due to displacement (rms. maxwells).
$Q$	initial electric charge of a condenser (coulombs).
$q$	electric quantity or displacement (coulombs or ab-coulombs); also Young's modulus for plate diaphragm material (dyne/cm. <sup>2</sup> ).
$\dot{q} = i$	current in el. cct. (amp. or abamp.).
$q_e$	equilibrium charge in a series of condensers (coulombs).
$R_1$	resistance of a receiver winding or of a vibration galvanometer, to direct current (ohms).
$R$	resistance of a receiver winding, diaphragm damped (ohms or abohms).
$R''$	resistance of a receiver winding, diaphragm free (ohms or abohms).
$R' = R'' - R$	motional resistance of a receiver winding (ohms or abohms).
$R'_0 =  Z'_0 $	size of a diametral motional impedance at app. resonance (abohms).
$r$	electric resistance of branch a.-c. cct. (abohms); also radius of a point on a diaphragm from its center (cm.).
$r, r$	mech. resistance of a simple linear or rot. vibrator (mech. abohms).
$r'$	virtual mech. res. of displacement (mech. abohms or dynes/kine).
$r'' = r + r'$	gross mech. res. of a receiver diaphragm (mech. abohms).
$r_a = (\mu\omega)^2/r_2$	virtual res. of sec. system as apparent in pr. system at sec. resonance (el. or mech. abohms).
$\mathcal{R}_0$	reluctance of air-gaps to permanent mag. flux (oersteds).
$\rho$	size of a polar complex number (numeric) and radius vector length in polar coordinates (cm.); also density of quiescent air or other gas in an acoustic conductor (gm./c.c.); also density of plate diaphragm material (gm./cm. <sup>3</sup> ); also in oscillation theory, half the resistance $r$ of a system (ohms or abohms).
$S$	active surface of either pole of receiver magnet (sq. cm.); also cross-sectional area of a tube (sq. cm.).
$s = 1/c$	electric elastance of a condenser (abdarafs).
$s s$	mechanical elastance of a simple linear or rot. vibrator (dynes/cm. or dyne-p.-cm./radian).
$s'$	virtual mech. elastance of diaphragm displacement (dynes/cm.).
$s'' = s - s'$	gross mech. elastance of a diaphragm (dynes/cm.).
$\sigma$	elect. impedance of a terminal load (abohms $\angle$ ); also

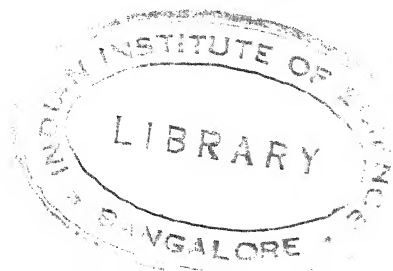


	acoustic impedance of an open tube end (mech. abohms $\angle$ ); also Poisson's ratio for plate diaphragm material (numeric).
$T$	periodic time of a complete free vibration (seconds).
$t$	time elapsed (seconds).
$t_e$	time to fall to $1/e$ th (seconds).
$t^{\circ}$	temperature of gas in acoustic conductor (deg. C.).
$\tau'$	torque (dyne-p.-cm.).
$\tau_0 = 2 \mathcal{E}/r = 2 m/r = 1/\Delta$	oscillatory time constant of system (secs.).
$\tau_s = \mathcal{E}/r = m/r = 1/2 \Delta$	non-oscillatory or sustained time constant (seconds).
$\tau_r$	time required for non-periodic reversal in free vibration (seconds).
$u = f/f_0$	ratio of impressed to resonant frequency (numeric).
$u_d, u_1, u_2, u_0, u_f$	values of $u$ at max. displacement, quadrants, resonance and free vibration (numeric).
$u', u''$	two frequency ratios producing equal velocities (numeric).
$v = \omega/\alpha_1$	group velocity of transmitting waves in el. or acoustic conductor (km./sec. or cm./sec.).
$\Lambda_0 = 1/B_0 = \omega_0/\Delta$	oscillatory sharpness of resonance (numeric).
$\Lambda_s = 1/B_s = \Lambda_0/2 \left\{ \begin{array}{l} \\ = \omega_0/2 \Delta \end{array} \right\}$	sustained sharpness of resonance (numeric).
$W$	kinetic energy of a vib. system (max. cyc. ergs).
$W_e$	elastic potential energy of a vib. system (max. cyc. ergs).
$W_d$	initial energy in a damped system (ergs or joules).
$W_k$	kinetic energy of a vib. diaphragm (max. cyc. ergs).
$w$	work done by a torque (ergs).
$w_1$	displacement of diaphragm over pole (max. cyc. cm.); also energy left in a damped system after one cycle (ergs or joules).
$w_r$	instantaneous local displacement of diaphragm (cm.); also max. cyclic local displacement (cm.).
$w_{rm}$	local displacement of diaphragm (max. cyc. cm.).
$w_d$	rms. displacement of diaphragm (rms. cm.).
$w_0$	displacement of diaphragm over center (max. cyc. cm.).
$w_{nr}$	instantaneous displacement at point on a plate diaphragm (cm.).
$\dot{w}$	local vib. velocity of diaphragm (max. cyc. kines).
$w_0$	central vib. velocity of diaphragm (max. cyc. kines).
$w_1$	polar vib. velocity of diaphragm (max. cyc. kines).
$\ddot{w}_0$	central acceleration of diaphragm (max. cyc. kines/sec.).
$w_e, w_i, w_d$	energy in elastic member, inertia member, and dissipation of a damped system (ergs or joules).
$X$	length of polar air gap entrefer (cm.); also coordinate of a curve.
$X$	damped reactance of a winding (ohms or abohms $\angle$ ).
$X''$	free reactance of a receiver winding (ohms or abohms $\angle$ ).
$X' = X'' - X$	motional reactance of a receiver (ohms or abohms).

$\mathcal{X}$	vector reactance of a receiver winding (ohms or abohms $\angle$ ).
$x$	displacement of a simple linear vibrator (rms. cm. $\angle$ ).
$x_c$	displacement of the center of an exploring mirror (cm.).
$x_m$	displacement of the center of an exploring mirror (max. cyc. cm.).
$x_t$	displacement of the center of an exploring mirror after lapse of $t$ secs. (cm.).
$x_{mo}, \dot{x}_{mo}$	displ. and velocity at the center of an exploring mirror, at resonance (max. cyc. cm.) (max. cyc. kines).
$x_0, \dot{x}_0$	displacement and velocity at center of diaphragm (cm. $\angle$ , kines $\angle$ ).
$\bar{x}, \dot{\bar{x}}$	rms. displacement and velocity over entire surface of diaphragm (cm. $\angle$ , kines $\angle$ ).
$\dot{x}, \ddot{x}$	velocity and acceleration of diaphragm or thin layer of air (rms. kines $\angle$ , rms kines/sec. $\angle$ ).
$\dot{x}_m, \ddot{x}_m$	sizes of velocity and acc. of diaphragm or air layer (max. cyc. kines $\angle$ ) (max. cyc. kines/sec. $\angle$ ).
$\dot{x}_r$	velocity of simple vibrator (rms. kines).
$\dot{x}_d$	an initial velocity of a disturbed vibratory system (kines).
$\dot{x}_1, \dot{x}_2$	velocities of pr. and sec. vibrators in coupling (rms. kines $\angle$ ).
$\dot{x}_{1a}$	velocity of pr. vibrator in presence of secondary action (rms. kines $\angle$ ).
$\dot{x}_a = \dot{x}_1 - \dot{x}_{1a}$	virtual absorption vel. of pr. vibrator due to sec. action (rms. kines $\angle$ ).
$\dot{x}_a$	active component of initial velocity (kines).
$\dot{x}_r$	reactive component of initial velocity (kines).
$x$	net mech. reactance of diaphragm (mech. abohms $\angle$ ).
$x'$	virtual mech. reactance of displacement (mech. abohms $\angle$ ).
$x_1, x_2$	acoustic reactance on sides of diaphragm (mech. abohms $\angle$ ).
$Y$	ordinate of a curve.
$Y' = 1/Z'$	motional admittance of a receiver (mhos $\angle$ or abmhos $\angle$ ).
$y = 1/z$	admittance to velocity of a system (mech. abmhos $\angle$ or kines per dyne $\angle$ ).
$y' = 1/z'$	displacement admittance of a vibrator (rms. mech. abmhos $\angle$ or radians/dyne-p.-cm. $\angle$ ).
$y'_s, y'_1, y'_0, y'_2$	initial, lower-quadrantal, resonant, and upper-quadrantal disp. admittance (rms. radians/dyne-p.-cm. $\angle$ ).
$y'_a, y'_f, y'_{12}$	maximum admittant, free and mid-quadrantal disp. adm. (rms. radians/dyne-p.-cm. $\angle$ ).
$y$	linear admittance of electric conductor (ohms/w. km.); also logh $u$ in the theory of resonance (numeric).
$y$	linear admittance in the theory of acoustic conductors (mech. abmhos/cm. $\angle$ ).
$y' = \Lambda_0 \logh u$	in the theory of resonance (numeric).

$y'' = 1/z''$	gross mech. admittance to velocity, of diaphragm (mech. abohms $\angle$ ).
$\psi = x^\circ$	a force function of the displacement amplitude $x$ .
$\psi = g i \theta$	germanmian of a hyperbolic angle $\theta$ (cir. radians or degrees).
$\psi' = \pi/2 - \psi$	germanmian complement of a hyp. angle (cir. radians or degrees).
$Z$	a-c. damped impedance of receiver winding (ohms or abohms $\angle$ ).
$Z''$	a-c. free impedance of same winding (ohms or abohms $\angle$ ).
$Z' = Z'' - Z$	notional impedance (ohms or abohms $\angle$ ).
$Z_0$	diametral or resonant impedance (ohms or abohms $\angle$ ).
$z$	mech. impedance to velocity (dynes kine $\angle$ ); also net mech. imp. of diaphragm (dynes kine $\angle$ ); also linear mech. impedance of acoustic conductor (abohms/cm. $\angle$ ).
$z$	linear impedance of electric conductor (ohms/w.km. $\angle$ ).
$z_v$	virtual mech. impedance of diaphragm due to its vibration in mag. field (mech. abohms $\angle$ ).
$z_1, z_2$	primary and secondary coupled cct. impedance (ohms or abohms $\angle$ ).
$z_1, z_2$	primary and secondary coupled cct. impedance (mech. abohms $\angle$ ).
$z_1, z_2, z$	acoustic impedance on sides 1 and 2 of diaphragm and their vector sum (mech. abohms $\angle$ ).
$z_a, z_a$	apparent elec. and mechanic imp. in pr. system due to effect of secondary system (el. or mech. abohms $\angle$ ).
$z_{1a} = z_1 + z_a$	primary cct. impedance including sec. reaction (abohms $\angle$ ).
$z_{1a} = z_1 + z_a$	primary system impedance including sec. reaction (mech. abohms $\angle$ ).
$z'$	total mech. impedance on a diaphragm (mech. abohms).
$z_0$ or $z_0$	surge impedance of el. or acoustic conductor (ohms $\angle$ or abohms $\angle$ ).
$z'' = r'' + jx''$	total or gross mech. impedance of a diaphragm (mech. abohms $\angle$ ).
$z_1, z_2, z$	acoustic impedance densities on side 1 and 2 of a diaphragm, and their vector sum (acoustic abohms/sq. cm. $\angle$ ).
$\omega = 2\pi f$	impressed angular velocity on system (cir. rad./sec.).
$\omega_0, \omega_1, \omega_0, \omega_2$	initial, lower-quadrantal, resonant, and upper-quadrantal impressed angular velocities (rad./sec.).
$\omega_0, \omega_f, \omega_{12}$	max. admittant, free and mid-quadrantal ang. vel. (rad./sec.).
$\omega_0''$	gross resonant angular velocity, taken as equivalent to $\omega_0$ (rad./sec.).
$\omega_1, \omega_{12}$	ang. velocities oppositely situated in mot. imp. circle (rad./sec.).

$\omega_0$	ang. vel. of resonance with loaded diaphragm (rad. sec.).
$\omega' = \omega_f$	ang. vel. of free vibration (rad. sec.).
$ Q $	size or length of a plane vector quantity $Q$ .
$\infty$	infinity.
$\approx$	approximately equals.
$\log x$	common logarithm of $x$ , to base 10.
$\log_h x$	hyperbolic logarithm of $x$ , to napierian base $e$ .
$\sim$	sign for cycles per second.
$\angle$	sign denoting a plane vector or complex quantity.
a.-c., d.-c.	abbreviations for "alternating-current" and "direct-current."
ab	prefix signifying a C. G. S. magnetic unit.
cmf.	counter-magnetomotive force.
emf.	electromotive force.
hyp.	contracted form of "hyperbolic radian."
rms.	root of mean square.
vmf.	vibromotive force.
vmt.	vibromotive torque.
w. km.	wire km.



# BIBLIOGRAPHY

1. MÖBIUS, *Ges. Werke*, II, p. 245, 1855.
2. M. J. LISSAJOUS, "Mémoire sur l'Etude Optique des Mouvements Vibratoires," *Ann. de Chemie et de Physique* (3) 51, p. 147, 1857.
3. D. E. HUGHES, "On the Physical Action of the Microphone," *Journ. Soc. Telegraph Engineers and Electricians*, London, Vol. XII, 1883, pp. 245-250.
4. J. CLERK MAXWELL, *Electricity and Magnetism*, 1888.
5. A. S. HIBBARD, *The Electrical World*, N.Y., Sept. 19, 1890.
6. J. A. EWING, *Magnetic Induction in Iron and other Metals*, London, 1892.
7. O. HEAVISIDE, *Electromagnetic Theory*, Vol. I, London, 1893. *Electrical Papers*, Vols. I and II, London, 1892.
8. BEDELL AND CREHORE, *Alternating Currents*, New York, 1893.
9. A. E. KENNELLY, "Impedance," *Trans. Am. Inst. Elect. Engrs.* Vol. X, pp. 175-232, April 18, 1893.
- 9a. C. STEINMETZ, "Complex Quantities and their use in Electrical Engineering," *Proc. Int. El. Congress of Chicago*, Aug. 1893, pp. 33-76.
10. A. BLONDEL, *Comptes Rendus*, 1893, Vol. CXVI, pp. 502 and 748.
11. A. E. KENNELLY, "Impedances of Mutually Inductive Circuits," *The Electrician*, London, 31, Oct. 27, 1893, pp. 699-700.
12. LORD RAYLEIGH, *Theory of Sound*, Vol. I, 1894, pp. 147, 352, 366, 473.
13. GEO. F. FITZGERALD, "On the Effect of Leakage on Wave Propagation in Telegraph Wires, or Mr. Oliver Heaviside's Theory Explained by Analogy," *The Electrician*, May 25, 1894, pp. 106-108.
14. A. MACFARLANE, "Application of Hyperbolic Analysis to the Discharge of a Condenser," *Trans. A. I. E. E.*, 1897, Vol. 14, p. 163.
15. W. DUDELL, "Oscillographs," *British Assoc. Adv. Sc.*, Toronto, 1897, also *The Electrician*, Vol. XXXIV, p. 636.
16. E. J. HOUSTON AND A. E. KENNELLY, "A Contribution to the Theory of Demagnetisation," *Elcc. World*, Vol. 25, p. 582.
17. F. GILL, "Note on a Humming Telephone," *Journ. of the Institution of Electrical Engineers*, London, 1901-02, Vol. XXXI, No. 153, pp. 388-399.
18. W. WIEN, *Ann. d. Physik*, 4, 1901, p. 450.
19. R. KEMPF-HARTMANN, *Ann. d. Physik*, 8, pp. 481-538, June 1902.
20. A. BLONDEL, "Théorie des Oscillographes," *L'Eclair. El.*, Oct. 25, 1902, pp. 115-125.
21. W. WIEN, *Ann. d. Physik*, 18, pp. 1049-1053, Dec. 1905.
22. A. E. KENNELLY, "The Harmonic Analysis of the Semicircle and of the Ellipse," *Annals of Mathematics*, 2 Ser., Vol. 7, No. 2, Jan. 1906.
23. A. E. H. LOVE, *The Mathematical Theory of Elasticity*, 2 Ed., p. 305, 1906.
24. H. ABRAHAM, "Rendement Acoustique du Téléphone," *Comptes Rendus*, 144, April 29, 1907, pp. 906-908.

25. H. POINCARÉ, "Etude du Récepteur Téléphonique," *L'Eclairage Elec.*, 50, Feb. 16, Feb. 23, Mar. 9, Mar. 16, 1907, pp. 221-372.
26. A. CAMPBELL, "On the Measurement of Mutual Inductances by the Aid of a Vibration Galvanometer," *Phil. Mag.*, p. 404, May 14, 1907.
27. F. K. VREELAND, *Phys. Rev.*, 27, p. 286, 1908.
28. E. H. BARTON, *Text Book of Sound*, pp. 146, 211, Sec. 146, Macmillan Co., 1908.
29. W. L. UPSON, "Investigation of the Phenomena of 'The Humming Telephone'." A thesis towards the degree of Master of Science in Elect. Engineering, Harvard University, 1908.
30. A. E. KENNELLY AND W. L. UPSON, "The Humming Telephone," *Proc. Am. Phil. Soc.*, 47, pp. 329-365, July 1908.
31. W. DUDDELL, "Bifilar Vibration Galvanometer," *Phil. Mag.*, pp. 168-179, July 1909 and *The Electrician*, 63, pp. 620-622, July 30, 1909.
32. A. WINKELMANN, *Handbuch der Physik*, Vol. 2, Leipzig, 1909.
33. F. WENNER, "A Theoretical and Experimental Study of the Vibration Galvanometer," *Bull. Bur. of Stand.*, 6, No. 3, p. 347, Feb. 1910.
- 33a. F. R. WATSON, "An Apparatus for Measuring Sound," *Phys. Rev.*, 30, Apr. 1910, pp. 471-473.
34. A. E. KENNELLY, "Vector Power in Alternating-Current Circuits," *Trans. A. I. E. E.*, 29, pp. 1233-1267, June 1910.
35. H. LAMB, *The Dynamical Theory of Sound*, London, 1910.
36. A. E. KENNELLY, "Vector Diagrams of Oscillating-Current Circuits," *Proc. Am. Ac. Arts and Sc.*, 46, Jan. 1911.
- 36a. J. A. FLEMING, "Some Oscillograms of Condenser Discharges and a Simple Theory of Coupled Oscillatory Circuits," *Proc. Phys. Soc. London*, Apr. 1913, p. 217.
37. G. W. PICKARD, "Telephone Receiver Efficiency," *Western Electrician*, May 6, 1911, 56, p. 899.
- 37a. G. A. CAMPBELL, "Cisoidal Oscillations," *Trans. A. I. E. E.*, Apr. 1911, Vol. XXX, Part II, pp. 873-909.
- 37b. P. THOMAS, "Method of Improving the Sensitiveness of the Telephone Detector in A. C. Null Measurements," *Journ. Frank. Inst.*, 174, Dec. 1912, pp. 679-682.
38. A. E. KENNELLY, *The Application of Hyperbolic Functions to Electrical-Engineering Problems*. University of London Press, 1911. McGraw-Hill Book Co., N.Y., 1916.
39. CH. F. MEYER AND J. B. WHITEHEAD, "The Vibrations of Telephone Diaphragms," *Trans. A. I. E. E.*, 31, II, pp. 1397-1418, 1912.
40. A. E. KENNELLY AND G. W. PIERCE, "The Impedance of Telephone Receivers as affected by the Motion of Their Diaphragms," *Proc. Am. Ac. Arts and Sc.*, 48, No. 6, 1912, pp. 111-151. Also *El. World*, N.Y., Sept. 14, 1912; also *B. A. Adv. Sc. Report*, Dundee, 1912.
41. S. BUTTERWORTH, "On the Vibration Galvanometer and its Application to Induction Bridges," *Proc. Phys. Soc. London*, 24, pp. 75-94, Jan. 1912.
42. G. D. SHEPARDSON, "Equivalent Frequency of Telephone Currents," Thesis in Library of Harvard University, Cambridge, 1912.
43. J. R. A. W. SALAMONS, on "Some Points in the Use and the Theory of the Oscillograph," *The Electrician*, 69, June 1912, pp. 357-360.
44. F. WENNER, "Characteristics and Applications of Vibration Galvanometers," *Trans. A. I. E. E.*, 31, Part I, June 25, 1912, pp. 1243-1254.

- 44a. A. GUYAU, "An Interference Oscillograph," *Comptes Rendus*, 156, Mar. 10, 1913, pp. 777-779, also *Journ. de Phys.*, 4, Mar. 1914.
45. H. F. HAWORTH, "Vibration-Galvanometer Design," *Proc. Phys. Soc., London*, 25, pp. 261-272, May 1913.
46. A. CAMPBELL, "On Vibration Galvanometers of Low Effective Resistance," *Proc. Phys. Soc., London*, 26, Dec. 1913, pp. 120-126.
- 46a. H. ABRAHAM, "Probable Advances in the Reception of Weak Signals in Long Distance Radio Telegraphy," *Bull. Soc. Int. El.*, 4 Mar. 1914, pp. 295-305.
47. S. BUTTERWORTH, "On a Null Method of Testing Vibration Galvanometers," *Proc. Phys. Soc., London*, 26, April 1914, pp. 264-273.
- 47a. H. ABRAHAM, A. DUFOUR AND G. FERRIE, "Sur une Methode de Mesure Directe de la Durée de Propagation des Ondes de T. S. F. à la Surface du Globe," *Comptes Rendus*, 159, July 6, 1914, pp. 38-40.
48. H. A. AFFEL AND O. C. HALL, "Telephone-Receiver Characteristics," Thesis El. Eng. Dept., Mass. Inst. Technology, 1914.
49. J. A. FLEMING, "The Predetermination of the Current and Voltage at the Receiving End of a Telephone or Other Alternating-current Line," *Jour. Inst. Elec. Engrs.*, Vol. 52, No. 236, pp. 717-723, May 1914.
50. R. L. JONES, "Simple Vibratory Systems and Their Impedance Analysis," Unpublished Memorandum, Eng. Dept. Western El. Co., New York, Sept. 1914.
51. A. GUYAU, "The Telephone Receiver," *Jour. de Phys.*, 4, June 1914, pp. 480-492.
52. AUG. GUYAU, *Le Téléphone Instrument de Mesure*, Paris, Gau. Vill., 1914.
53. L. W. CHUBB, "The Analysis of Periodic Waves," *The Electric Journal*, Feb. 1914, pp. 91-96.
54. L. W. CHUBB, "Polar and Circular Oscillograms and their Practical Application," *The Electric Journal*, 1914, pp. 262-267.
55. L. BOUTHILLON AND L. DROUET, "Etude Expérimentale du Récepteur Téléphonique," *Comptes Rendus*, 158, p. 1568, June 2, 1914 and *La Revue Electrique*, Oct. 16, pp. 294-295, 1914, also *Lum. Elec.* 26, July 14, 1914, p. 26.
56. A. E. KENNELLY AND H. O. TAYLOR, "Explorations over Vibrating Surfaces of Telephonic Diaphragms under Simple Impressed Tones," *Proc. Am. Phil. Soc.*, Vol. 44, May 1915, pp. 96-136.
- 56a. E. W. MARCHANT, "Methods of Measuring the Strength of Wireless Signals," *Electrician*, 75, May 28, 1915, pp. 267-270, June 4, 1915, pp. 309-311.
57. A. E. KENNELLY, F. D. EVERETT, AND A. A. PRIOR, "Thermal Insulation Tests of Electric Ovens," *El. World*, N.Y., March 27, 1915.
- 57a. H. O. TAYLOR, "A Mechanical Process for Constructing Harmonic Analysis Schedules for Waves having Even and Odd Harmonics," *The Physical Review*, 6, No. 4, Oct. 1915, pp. 303-311.
58. A. E. KENNELLY AND H. A. AFFEL, "The Mechanics of Telephone-Receiver Diaphragms, as Derived from their Motional-Impedance Circles," *Proc. Am. Ac. Arts and Sc.*, 51, No. 8, Nov. 1915.
59. A. E. KENNELLY, "The Impedances, Angular Velocities, and Frequencies of Oscillating-Current Circuits," *Proc. I. R. E.*, Nov. 1915, pp. 1-32.
60. A. E. KENNELLY AND H. O. TAYLOR, "Some Properties of Vibrating Telephone Diaphragms," *Proc. Am. Phil. Soc.*, Vol. 55, 1916, pp. 415-460.

61. J. A. FLEMING, "The Principles of Electric Wave Telegraphy and Telephony," 3rd Ed., 1916, p. 347.
62. H. G. CRANE AND C. L. DAWES, "Construction of a Lecture-Room Oscillograph," *El. World*, N.Y., 67, p. 424, Feb. 19, 1916.
63. B. S. COHEN AND J. G. HILL, "Long-Distance and Cable Telephony," *Inst. P. O. Elec. Engrs.*, 1916.
64. B. S. COHEN, "Telephonometry," *The Electrician*, 77, May 26, and June 2, 1916, pp. 244-245, 277-279.
65. G. W. O. HOWE, "The Amplitude and Phase of the Higher Harmonics in Oscillographs," *Proc. I. E. E.*, 54, 1916, pp. 19-28.
66. M. LATOUR, "Theory of Telephone Receiver," *La Lum. Elec.*, 33, June 17 and July 22, 1916.
67. G. D. SHEPARDSON, "Telephone Apparatus," Appleton & Co., 1917.
68. A. BLONDEL ET F. CARBONAY, "Analyse Harmonique des Differences de Potentiel Alternatives par la Resonance Mechanique d'un Barreau de Fer Aimanté," *Ann. de Phys.*, Sept. 1917, pp. 97-158.
69. H. O. TAYLOR, "Motional-Impedance Circle of the Telephone Receiver," *Proc. Radio Club of America*, June 1917.
70. H. TOURNAYRE, "Théorie du Téléphone," *L'Industrie Electrique*, July 25, Aug. 10, 1917.
71. A. E. KENNELLY, "Artificial Electric Lines, their Theory, Mode of Construction and Uses," McGraw-Hill Book Co., New York, 1917.
72. A. E. KENNELLY, "Some Experiments on the Effects of Changes in Diaphragm Thickness on the Characteristics of a Telephone Receiver," *Journ. Franklin Inst.*, Nov. 1917, 184, pp. 723-726.
73. J. MILLS, "Radio Communication," McGraw-Hill Book Co., 1917, pp. 26-35.
74. W. H. ECCLES, "Wireless Telegraphy and Telephony," D. Van Nostrand Co., 1918, pp. 347-350.
- 74a. H. O. TAYLOR, "Telephone Receivers and Radio Telegraphy," *Proc. Inst. Rad. Eng.*, 6, 1918, p. 37.
75. M. LATOUR, "Note sur les Pertes dans les Tôles de Fer aux Frequences Elevées," *Révue Gen. de l'EL.*, 3, April 13, 1918, pp. 539-543.
- 75a. H. NUKIYAMA, "The Energetics of Telephone Receivers," *M. I. T. Report*, May 1918.
76. A. BLONDEL, "Sur l'Analyse harmonique directe de l'onde des courants alternatifs par Resonance Mécanique ou Electrique," *Ann. de Phys.*, 10, 1918, pp. 195-354.
77. I. B. CRANDALL, "The Air-damped Vibrating System: Theoretical Calibration of the Condenser Transmitter," *Phys. Rev.*, 1918, p. 449.
- 77a. J. ZENNECK, "Ueber Telephonische Messungen an einem drahtlosen Empfänger," *Jahrb. d. D. Tel.* 12, 1918, pp. 443-450.
78. J. H. DELLINGER, "The Measurement of Radio Frequency Resistance, Phase Difference, and Decrement," *Proc. I. R. E.*, Feb. 1919, pp. 27-59.
79. A. E. KENNELLY AND H. NUKIYAMA, "Electromagnetic Theory of the Telephone Receiver," *Proc. A. I. E. E.*, Mar. 14, 1919, pp. 491-539.
80. L. V. KING, "On the Determination of the Electrical and Acoustic Characteristics of Telephone Receivers," *Journ. Franklin Inst.*, May 1919, pp. 613-625, also *Yearbook of Wireless Telegraphy*, 1919, p. 926.
81. W. HAHNEMANN AND H. HECHT, "Der Mechanisch-Akustische Aufbau eines Telephons," *Ann. d. Phys.*, 1919, No. 21, pp. 454-480.



82. W. H. ECCLES, "Vector Diagrams of Some Oscillatory Circuits used with Thermionic Tubes," *Proc. Physical Soc. London*, Vol. XXXI, Part III, Apr. 15th, 1919, pp. 137-149.

82a. A. G. WEBSTER, "Acoustical Impedance and the Theory of Horns and of the Phonograph," *Proc. Nat. Ac. of Sci.*, May 8, 1919, pp. 275-282.

82b. BUREAU OF STANDARDS, "Telephone Receivers for Wireless Telegraphy and Telephony," Research. *El. Rev.* (Chicago) 75, Nov. 22, 1919, p. 800. Also "Wireless Telephone Receivers," *El. Rev. London*, 86, Jan. 2, 1920, p. 19.

83. A. E. KENNELLY, R. N. HUNTER, AND A. A. PRIOR, "Oscillographs and their Tests," *Proc. A. I. E. E.*, Feb. 20, 1920, pp. 1-45.

83a. V. KARAPETOFF, "Diaphragms and Sound Measurement — the Phonodeik," *Tel. Engineer*, 23, Feb. 1920, pp. 15-16.

84. R. A. HEISING, "The Audion Oscillator," *Journal A. I. E. E.*, May 1920.

84a. A. E. KENNELLY AND E. VELANDER, "Potentiometer Measurements at Telephone Frequencies," *Proc. Am. Phil. Soc.*, 58, Apr. 1919, pp. 97-132.

84b. M. PIRANI AND P. PASCHEN, "Measurement of Sensitiveness Efficiency of Telephone Receivers," *El. World*, 75, Mar. 27, 1920, p. 744.

85. P. G. AGNEW, "A New Form of Vibration Galvanometer," *Scientific Papers of the Bureau of Standards*, No. 370, March 12th, 1920.

85a. C. V. DRYSDALE, "The Eleventh Kelvin Lecture," *Journ. Inst. Elec. Engrs. London*, July 1920, 58, p. 591.

86. H. MORI, "Study of Motional Impedance in Receivers," *Denki Hyoron*, 8, 1920, Nos. 1, 2 and 3.

87. A. E. KENNELLY AND K. KUROKAWA, "Acoustic Impedance," *Proc. Am. Ac. Arts & Sc.*, Vol. 56, Feb. 1921, pp. 1-42.

88. F. S. DELLENBAUGH, "An Electromechanical Device for Rapid Schedule Harmonic Analysis of Complex Harmonic Waves," *Proc. Am. Inst. El. Engrs.*, February 1921, 40, No. 2, pp. 135-143.

89. R. L. WEGEL, "Theory of Magneto-Mechanical Systems as applied to Telephone Receivers and Similar Structures" *Journ. A. I. E. E.*, 40, Oct. 1921, No. 10, pp. 791-802.

90. H. FLETCHER AND R. L. WEGEL, "The Frequency Sensitivity of Normal Ears," *Proc. Nat. Ac. Sc.*, 8, No. 1, Jan. 1922, pp. 5-6, also *Phys. Rev.*, June 1922.

91. H. FLETCHER, "The Nature of Speech and its Interpretation," *Jour. Frank. Inst.*, 193, June 1922, No. 6, pp. 729-747.

92. I. B. CRANDALL AND D. MACKENZIE, "Analysis of the Energy Distribution in Speech," *Phys. Rev.*, 19, No. 3, Mar. 1922.

93. R. L. WEGEL, "The Physical Characteristics of Audition and Dynamical Analysis of the External Ear," *Bell System Technical Journal*, Vol. 1, No. 2, Nov. 1922, pp. 56-68.

94. V. O. KNUDSEN, "Sensibility of the Ear to Small Differences of Intensity and Frequency," *Phys. Rev.* 21, 2nd Ser., Jan. 1923, pp. 84-102.

95. K. KUROKAWA, "Measurement of Acoustic Constants of Cloth," *Journal of the Institute of Electrical Engineers of Japan*, Feb. 1923, pp. 1-27.

# INDEX OF SUBJECTS

Ab; prefix to a "practical" unit, 49  
 Abohm, mechanical or electrical, 49  
 Absorption emf. in primary circuit, 161  
 Absorption graphs of primary velocity, 166  
 Absorption loop in motional-impedance circle, 159  
 Absorption vmf. in primary due to secondary systems, 161  
 Acoustic damping device for telephone receivers, 65  
 Acoustic impedance, 167  
   method of evaluating, 171  
   over a flexible diaphragm, 169  
   of an air column in tube, 172  
 Acoustic-impedance density, 168  
 Acoustic impedance and motional impedance, 170  
 Acoustic resistance, 168  
 Acoustic surge impedance, 178  
 Acoustic vmfs. on diaphragm, 22  
 Active mechanical output of diaphragm, 104  
 Active and reactive electric power, 103  
 Adiabatic elastic force, 391  
 Admittance to displacement, 221, 226  
 Admittance to velocity or to current, 58  
 Air-damped vibrators, 251  
 Amplitude explorer, magnification factor of, 21  
 Amplitude measurer, 118  
 Amplitude measurer for increased precision, 130  
 Analogies between acoustic tube and electric line transmission, 389  
 Analysis and correction of oscillograms, 262  
 Analysis of the motional-impedance circle, 99  
 Angle of reactance deviation in a telephone receiver, 69  
 Angle of vector reactance, 102  
 Angular velocities, real or hyperbolic, 327  
   complex, 328  
   generalized complex, 334  
   of a simple mechanical or electric system, 325  
   quadrantal, 99

Angular velocity  
   circular locus of, 214  
   impedance to, 212  
   of a rotational vibrating system, 206  
   of vibration or of alternation, 43  
   sub-resonant, 315  
   super-resonant, 317  
 Aperiodic system, 219  
 Aperiodic vibration, 379  
 Application to architectural acoustics, 189  
 Architectural acoustics, application of motional impedance to, 189  
 Asymmetry of specific deflection-frequency curves, 253  
 Baldwin telephone receivers, 2, 4  
 Bell bipolar receivers, 2  
 Bell head receivers or watch-case receivers, 2  
 Bell monopolar receivers, 2  
 Bell telephone receivers, 2  
 Bessel-function harmonic analysis of semicircle, 418  
 Best values of bluntness for an oscillograph, 255  
 Bibliography, 438  
 Bifilar oscillographs, 196  
 Bifilar vibration galvanometers, 266  
 Bluntness of resonance, 217  
 Central equivalent mass of diaphragm, 32, 34, 308  
 Circular locus of angular velocity, 214  
 Circular orbit, simple velocity in, 325  
 Classification of diaphragms — membranes and plates, 12  
 Collected numerical data on analyzed receiver, 126  
 Complex angular velocities, 328  
   applied to transient vibrations, 331  
   complex pairs of, 330  
 Complex numbers  
   in electrical engineering literature, 55  
   sizes and slopes of, 56  
 Constants of an oscillograph vibrator, 236  
 Contour lines of equal vibration amplitude, 22

- Correction and analysis of oscillograms, 262
- Correction data for marking upon oscillograms, 265
- Correction factor of oscillogram, 263
- Counter mmf. in permanent magnetic circuit, 7
- Coupled-system primary-velocity graphs, 166
- Critically damped free vibration, 379
- Current sensitivity of vibration galvanometer, 268
- Currents or velocities, quadrantal, 404
- Curve of motional admittance, 176
- Damped periodic vibration, 336
- Damping-coefficient diagram, 339
- Damping constant, 331
  - of a diaphragm, 101
- Damping device for use with telephone receivers, 63
- Damping factor, 340
- Damped impedance
  - locus of, 67
  - of telephone receiver, 61
  - vector diagram of, 69
- Damped vibration, vector diagram of, 332
- Data determinable from the motional-impedance circle, 112
- Data secured on particular receivers, 124
- Decrement, logarithmic, 340
- Demagnetizing force, 7
- Density of acoustic impedance, 168
- Deviation factor of oscillograph, 230
- Diagram of damping coefficients or damping factors, 339
- Diaphragm elasticity measurement, static apparatus for, 38
- Diaphragm, epsilonic time interval of, 102
- Diaphragm vibration
  - amplitude distribution, 15
  - experimental tests of, 426
- Displacement admittance, 221, 226
- Displacement-admittance curve, 96
- Displacement-admittance graph, 227
- Displacement-admittance locus, 84, 98
- Displacement contours over diaphragms, 22
- Displacement
  - elastic coefficient of receiver diaphragm, 93
  - flux locus, 82
  - impedance, 221
  - mechanical resistance of receiver diaphragm, 93
  - of diaphragm, vector locus of, 97
  - quadrantal, 407
  - resonance curves, symmetrical, 409
  - tractive force on receiver diaphragm, 91
- Displacement-impedance parabolas, 222
- Displacement magnetic flux in telephone receiver, 82
- Disturbing influences tending to distort motional-impedance circle, 94
- Dot differential, with respect to time, 45
- Dynamical model for illustrating motional velocity, 157
- Dyne-perpendicular-cm., 207
- Ear acoustic load, 184
- Effects of changes in thickness of diaphragm on its characteristics, 193
- Effect of loading a diaphragm with a central mass, 34
- Effect of size of wire on receiver constants, 128
- Efficiency
  - gross, of receiver at resonance, 106
  - net, of receiver at resonance, 106
- Elastance of a receiver diaphragm, gross, displacement, and net, 93
- Elastance coefficient, mechanical, 50
- Elastance, electric, 44
- Elastic constants of diaphragms from static deflections, 40
- Elastic potential energy of simple vibration, 47
- Elastic reactance, mechanical, 50
- Elastic restoring force of simple vibration, 46
- Elastic restoring torque, 210
- Electric power in receiver, vector diagram of, 86
- Electrical theory of coupled circuits, 160
- Electromagnetic vmfs. on diaphragm, 22
- Electromotive force generated in a vibration galvanometer, 278
- Energy and power, vibratory, 317
- Epsilonic time interval of a diaphragm, 102
- Equivalent mass of diaphragm, 32, 33, 34
- Equivalent mass of diaphragm, central and polar, 307, 308
- Equivalent single central elastic force of a diaphragm, 37
- Exploration of vibration amplitude over diaphragms, 22
- Exploration of vibration over thin glass diaphragms, 29

- Explorer optical system, 20
- Explorer supports, 18
- Extinguishing resistance of humming-telephone circuits, 294
- Figures, Lissajous, 238
- Force diagrams vector, for a receiver, 89
- Force factor, vector, in a receiver, 88
- Force of mechanical resistance, 48
- Forced vibration, steady-state vector diagrams of, 319
- Forced vibrations of a diaphragm under simple impressed emf., 42
- Formulas for free vibration in tabular form, 386
- Formulas for oscillographic displacement admittance, 229
- Free damped vibrations, 336
- Free impedance of telephone receiver, 61
- Free impedance series, 71
- Free impedance vector diagram, 80
- Free overdamped or ultraperiodic oscillations, 365
- Free undamped oscillations, 356
- Free vibrations in charging a system, 384
- Frequency of apparent resonance of a receiver diaphragm, 77
- Frequency, quadrantal range of, 56
- Frequencies, quadrantal, 99
- Frequency ratio, 213
- Fundamental constants in receiver, methods for determining, 115
- Fundamental geometry of current resonance curves, 403
- Generalized complex angular velocities, 334
- Graphs of scalar velocity and displacement, 399
- Gravest mode of circular plate vibration, 13
- Gross efficiency of receiver at resonance, 106
- Gross elastic coefficient of receiver diaphragm, 93
- Gross mechanical admittance, 96
- Gross mechanical displacement of diaphragm, 97
- Gross mechanical resistance of receiver diaphragm, 93
- Gudermannian angle, 366, 367
- Gudermannian complement, 367
- Harmonic analysis schedules, 413
- Humming cycle, 293
- Humming telephone, 287
  - action, outline theory of, 296
  - circuit, extinguishing resistance in, 294
  - effects of shortening air-tube, 288
- Hyperbolic or real angular velocities, 327
- Hysteretic power axes, 105
- Imaginary axis or axis of imaginaries, 51
- Impedance, acoustic, 167
  - motional, 74
- Impedance diagrams, mechanical, 182
- Impedance ratio and efficiency of receivers, 129
- Impedance to angular velocity, 212
- Impedance to displacement, 221
  - parabolic, 222
- Inertia damping device for telephone receivers, 64
- Inertia reactance torque, 212
- Influence of diaphragm dimensions on its constants, 191
- Influences that affect the constants of a receiver, 134
- Inverse parabola of displacement admittance, 228
- Kine or centimeter per second, 45
- Kinetic energy of simple vibration, 46
- Lily-pad graphs of distorted primary velocity or current, 164
- Linear mass, 390
- Lissajous figures, 238
- Loading the diaphragm of a receiver, 115
- Logarithmic decrement, 340
- Magnetic amplifying power of receiver permanent magnet, 10, 11
- Magnetic circuit power, 108
- Magnetic currents and fluxes in magnetic circuit, 110
- Magnetomotive force diagram in receiver, 82
- Magnetomotive force, structural, of permanent magnet, 7
- Magnification factor of amplitude explorer, 21
- Mass reactance, mechanical, 49
- Maximum admittant frequency of a vibrator, 232
- Maximum of displacements resonance curve, 407
- Measurement of electric impedance of receivers, 61
- Measurement of mechanical resistance in fluids, 188
- Measurement of vibration amplitude at resonance, 116
- Mechanical abohm defined, 49

- Mechanical abmho, 58
- Mechanical conductance, 214
- Mechanical displacement, 96
- Mechanical efficiency of receiver at resonance, 106
- Mechanical elastic reactance, 50
- Mechanical impedance of diaphragm at variable frequency, 53
  - diagrams, 182
  - graph for a motional-impedance, 185
  - in polar and rectangular coördinates, 54
  - to velocity, 51
- Mechanical mass reactance, 49
- Mechanical resistance, 48
  - coefficient, dimensions of, 49
  - force, 48
- Mechanical resonance, 47
- Mechanical susceptance, 214
- Method for evaluating acoustic impedance, 171
- Methods for determining fundamental constants, in receiver, 115
- Mica-diaphragm receiver, 4
- Mode of vibration of a telephone diaphragm, 12, 13
- Moment of inertia, 209
- Motional-admittance curve, 176
- Motional impedance, 74
  - and acoustic impedance, 170
  - circle, 76
  - circle, analysis of, 99
  - circle, data determinable from, 112
  - circle, quadrantal points of, 99
  - circle, influences tending to distort, 94
  - circle of reference, 185
  - data, without the measurement of damped impedances, 79
  - of receiver pressed against ear, 184
  - vectors, 73
- Motional power diagram of receiver, 102
- Mutual mass of coupled mechanical systems, 161
- Natural frequency of diaphragm as affected by thickness, 193
- Net efficiency of receiver at resonance, 106
- Net elastic coefficient of receiver diaphragm, 93
- Net mechanical resistance of receiver diaphragm, 93
- Odd and even harmonics, 413
- Ohm's law extended to vibrations and to alternating currents, 56
- Optical system used with explorer, 19
- Organ pipe as source of vml., 23
  - standards, application of theory to, 31
- Oscillations reinforced, 297
- Oscillograms, 199
  - analysis and correction of, 262
  - correction data for marking upon, 205
  - correction factor of, 263
  - polar, 202
  - rectangular, 202
  - steady, 199
  - transient, 199
- Oscillograph
  - best bluntness for, 255
  - correction factor of, 230
  - damped, free and motional impedance of, 256
  - deviation factor of, 230
  - motional power in, 257
  - specific deflection of, 245, 246
  - tests, 243
  - vibrator, 198
- Oscillographs, bifilar, 196
  - unifilar, 196
- Oscillographmeter, 237
- Oscillatory displacement of a damped oscillator freely vibrating, 355
- Oscillatory energy diagram, 344
- Oscillatory impedance diagram, 346
- Oscillatory time constant, 218
- Overtones, Bessel, 13
- Parabolas of displacement impedance, 222
- Partial modes of plate vibration, 14
- Periodic vibration of a damped system, 336
- Permanent magnet of receiver, functions of, 6
- Plane vectors with displaced reference axes, 397
- Polar equivalent mass of diaphragm, 33, 308
- Polar equivalent mass coefficient of diaphragm, 34
- Polar oscillograms, 202
- Potentially and kinetically energized oscillations, 354
- Power diagram, motional, of receiver, 102
- Power and energy, vibratory, 317
- Power in a magnetic circuit, 108
- Principal impressed angular velocities of vibratory system, 231
- Properties of damped impedance locus, 67
- Proportionality between frictional torque and angular velocity, 411

Quadrantal angular velocities, 99  
 Quadrantal currents or velocities, 404  
 Quadrantal displacements, 407  
 Quadrantal frequency ratios, 214  
 Quadrantal frequencies, 99  
 Quadrantal frequencies, upper and lower, 56  
 Quadrantal points of motional-impedance circle, 99  
 Quadrantal range of frequency, 56  
  
 Radius of gyration, 209  
 Ratio, frequency, 213  
 Rayleigh Bessel-curve of vibration amplitude, 27  
 Rayleigh Bessel-function theory of plate free vibration, 303  
 Rayleigh-bridge connections for telephone receiver tests, 62  
 Reactance, acoustic, 168  
     mechanical, of elastance, 50  
     mechanical, of mass, 49  
 Reactance deviation angle of telephone receiver, 69  
 Real or hyperbolic angular velocities, 327  
 Reciprocating-engine vibrations and resonant effects, 60  
 Rectangular oscillograms, 202  
 Reed vibration galvanometers, 266  
 Reinforce, 297  
 Reinforced oscillations, 297, 361  
 Resistance  
     acoustic, 168  
     mechanical, 48  
     of a receiver diaphragm, gross, displacement and net, 93  
     torque, 211  
     bluntness of, 217  
     mechanical, 47  
     sharpness of, 217  
 Resonance curve  
     of diaphragm, 25  
     geometry of, 403  
     specific, 399  
 Resonant angular velocity, 313  
 Resonant range of diaphragm, as affected by thickness, 193  
 Reversal time of a damped oscillator freely vibrating, 355  
 Reversal times in vibrators with different bluntness, 384  
 Root-mean-square and maximum-cyclic vibration velocities, 45  
 Rotational velocity, 207  
 Rotational vibration system, angular velocity of, 206  
 Rotative damped vector power diagram, 343

Scalar displacement and velocity graphs, 399  
 Scalar displacement graphs, 405  
 Scalar velocity and displacement graphs, 399  
 Schedules of harmonic analysis, 413  
 Secondary distortions of motional-impedance circles, 142  
 Semicircle harmonic analysis, 418  
 Semilogarithmic paper resonance curves, 400  
 Semiquadrature, 216  
 Shaft out-of-balance vibrations, 60  
 Shaft, unbalanced rotating, vibration of, 321  
 Sharpness of resonance, 217  
 Simple harmonic motion and associated uniform circular motion, 43  
 Simple velocity of a particle in a circular orbit, 325  
 Simple vibration, elastic restoring force of, 46  
 Simple vibration, Kinetic energy of, 46  
 Simple vibrator theory, 311  
 Size and slope of complex numbers, 56  
 Sources of diaphragm vmf., 22  
 Specific deflection of oscillograph, 245, 246  
 Specific resonance curves, 399  
 Spiral vector diagram of expanding or contracting vibrations, 329  
 Steady oscillograms, 199  
 Steady-state vector diagrams of forced vibration, 319  
 Stiffness, 44  
 Stiffness coefficient of a diaphragm, 37  
 Structural mmf. of permanent magnet, 7  
 Sub-resonant angular velocity, 315  
 Super-resonant angular velocity, 317  
 Surge impedance, acoustic, 178  
 Surge impedance density, acoustic, 392  
 Symbols, list of, 428  
 Symmetrical displacement resonance curves, 409  
 System, aperiodic, 219  
  
 Table of comparative electrical and mechanical units, 208  
 Technique for measuring vibration amplitude at resonance, 120  
 Telephone receiver, damping devices for use with, 63  
     free and damped impedance of, 61  
     vector emf. diagram, 81  
     reactance deviation angle of, 69  
     vector force, diagrams of, 80  
 Temperature effects on diaphragm vibration amplitudes, 29

- Terminal acoustic impedance, 181
- Tests of oscillograph, 243
- Theory of equivalent mass of a diaphragm, 307
- Time constant, oscillatory, 218
- Time interval, epsilonic, of a diaphragm, 102
- Torque, elastic restoring, 210
  - of inertia reactance, 212
  - resistance, 211
  - vibromotive, 206
- Torsional-pendulum model for illustrating motional velocity, 156
- Tractive force of displacement on receiver diaphragm, 91
- Transient initial velocity, 319
- Transient oscillograms, 199
- Transient vibrations, application of complex angular velocities to, 331
- Transient with given initial velocity or current, 336
- Tuning a receiver by varying acoustic air column, 187
- Ultrapariodic admittance, 369
- Ultrapariodic angular velocity, 368
- Ultrapariodic impedance, 369
- Ultrapariodic or overdamped oscillations, 365
- Ultrapariodic reactance, 369
- Ultrapariodic vector diagrams, 368
- Ultrapariodic vibration, 200
- Unbalanced rotating shaft, vibration of, 321
- Undamped vibration, 332
- Unifilar oscillographs, 196
- Unifilar vibration galvanometers, 266
- Uniform circular motion and associated simple harmonic motion, 43
- Units, table of comparative, 208
- Variations in air-chamber of receiver, effect on motional-impedance circle, 139
- Variations in air pressure, effect on receiver motional-impedance circle, 140
- Variations in clamping the cap, effect on receiver motional-impedance circle, 134
- Variations in temperature, effect on receiver motional-impedance circle, 138
- Vector angular-velocity circular locus, 214
- Vector damped emf. diagram, 70
- Vector diagram of damped impedance, 69
  - of damped vibration, 332
  - of electric power in receiver, 86
  - of free impedance, 80
  - of magnetic flux in receiver, 85
  - of mmf. in receiver, 82
- Vector emf. diagram of receiver, 81
- Vector force diagrams of the telephone receiver, 80, 89
  - diagram with two vmfs., 90
  - factor in a receiver, 88
- Vector motional emf., 98
- Vector motional impedance, 73
- Vector power diagram of receiver, 102
- Vector reactance of a receiver, 69
- Vector reactance angle, 102
- Velocities or currents, quadrantal, 404
- Velocity of vibration, initial transient, 319
- Velocity, rotational, 207
- Vibrating system, rotational, angular velocity of, 206
- Vibration-amplitude curves along a diaphragm radius, 28
- Vibration explorer, 16
- Vibration galvanometers, 265
  - deflection graph of, 275
  - emf. generated in, 278
  - fundamental constants of, 268
  - measurement of damping constant, 280
  - measurement of motional impedance, 279
  - methods of tuning, 269
  - motional-impedance and velocity circles of, 274
  - power absorbed in, 278
  - use of instrument transformer with, 285
  - working constants of, 267
- Vibration, ultrapariodic, 200
- Vibration, undamped, 332
- Vibrations in a system having divided elements, 385
- Vibratory displacement, 45
- Vibratory power and energy, 317
- Vibratory velocity, 45
- Vibromotive force (vmf.), 6, 10
- Vibromotive torque, 206
- Virtual absorption impedance of secondary in primary, 160
- Virtual vibratory velocity of absorption, 162
- Vmf., sources of for actuating diaphragm, 22
- Wreeland oscillator connections for telephone receiver tests, 62
- Wax bridge damping device for telephone receivers, 65

## INDEX OF NAMES

(The bold-face figures indicate Bibliography references.)

- |   |   |
|---|---|
| <p>Abraham, H., <b>24</b>, <b>46a</b>, <b>47a</b>, 38<br/>           Affel, H. A., <b>48</b>, <b>58</b>, 40, 115, 116<br/>           Agnew, P. G., <b>85</b>, 266, 271</p> <p>Barton, E. H., <b>28</b>, 13, 31<br/>           Becker, G. F., 366<br/>           Bedell, F., <b>8</b>, 49<br/>           Bell, G., 1, 2, 6<br/>           Bessel, F. W., 13, 27, 30, 303<br/>           Blondel, A., <b>10</b>, <b>20</b>, <b>68</b>, <b>76</b>, 196, 266<br/>           Bouthillon, L., <b>55</b>, 440<br/>           Bush, V., <b>66a</b>, 335<br/>           Butterworth, S., <b>47</b>, 440</p> <p>Calder, C. H., 192<br/>           Campbell, A., <b>46</b>, 440<br/>           Campbell, G. A., <b>37a</b>, 310, 335<br/>           Carbonay, F., <b>68</b>, 441<br/>           Chubb, L. W., <b>53</b>, <b>54</b>, 202<br/>           Clerk-Maxwell, J., <b>4</b>, 439<br/>           Cohen, B. S., <b>63</b>, <b>64</b>, 441<br/>           Crandall, I. B., <b>77</b>, <b>92</b>, 441<br/>           Crane, H. G., <b>62</b>, 239<br/>           Crehore, A. C., <b>8</b>, 49</p> <p>Dawes, C. L., <b>62</b>, 239<br/>           Dellenbaugh, F. S., <b>79</b>, <b>88</b>, 225<br/>           Dellinger, J. H., <b>78</b>, 341<br/>           Drouet, L., <b>55</b>, 440<br/>           Drysdale, C. V., <b>85a</b>, 266, 270<br/>           Duddell, W., <b>15</b>, 197, 266, 270, 274<br/>           Dufour, A., <b>47a</b>, 440</p> <p>Eccles, W. H., <b>42a</b>, <b>74</b>, <b>82</b>, 335<br/>           Everett, F. D., <b>57</b>, 440<br/>           Ewing, J. A., <b>6</b>, 8</p> <p>Ferrié, G., <b>47a</b>, 440<br/>           Fitzgerald, G. F., <b>13</b>, 439<br/>           Fleming, J. A., <b>36a</b>, <b>49</b>, <b>61</b>, <b>55</b>, <b>56</b>, 335<br/>           Fletcher, H., <b>90</b>, <b>91</b>, 442<br/>           Fourier, J. B. J., 413</p> <p>Gill, F., <b>17</b>, 287</p> | <p>Grinstead, 55<br/>           Gudermann, C., 366<br/>           Guyau, A., <b>44a</b>, <b>51</b>, <b>52</b>, 440</p> <p>Hahnemann, W., <b>81</b>, 441<br/>           Hall, O. C., <b>48</b>, 440<br/>           Haworth, H. F., <b>45</b>, 440<br/>           Heaviside, O., <b>7</b>, <b>6</b>, <b>56</b>, <b>58</b>, 335<br/>           Hecht, H., <b>81</b>, 441<br/>           Heising, R. A., <b>84</b>, 442<br/>           Hibbard, A. S., <b>5</b>, 287<br/>           Hill, J. G., <b>63</b>, 441<br/>           Howe, G. W. O., <b>65</b>, 441<br/>           Hughes, D. E., <b>3</b>, 287<br/>           Hunter, R. N., <b>83</b>, 442</p> <p>Jackson, D. C., 205<br/>           Jones, R. L., <b>50</b>, 217</p> <p>Karapetoff, V., <b>83a</b>, 426<br/>           Kempf-Hartmann, R., <b>19</b>, 439<br/>           King, L. V., <b>80</b>, 441<br/>           Knudson, V. O., <b>94</b>, 442<br/>           Kurokawa, K., <b>87</b>, 175</p> <p>Lamb, H., <b>35</b>, 13, 14, 187, 390<br/>           Latour, M., <b>66</b>, <b>75</b>, 441<br/>           Lissajous, J., <b>2</b>, 238<br/>           Love, A. E. H., <b>23</b>, 439</p> <p>Macfarlane, A., <b>14</b>, 365, 379<br/>           MacKenzie, D., <b>92</b>, 442<br/>           Marchant, O. W., <b>56a</b>, 440<br/>           Meyer, C. F., <b>39</b>, <b>6</b>, 11<br/>           Mills, J., <b>73</b>, 441<br/>           Möbius, A. F., <b>1</b>, 59<br/>           Mori, H., <b>86</b>, 159, 300, 302</p> <p>Northrup, E. F., 265, 269<br/>           Nukiyama, H., <b>75a</b>, <b>79</b>, 91</p> <p>Ohm, G. S., <b>56</b></p> <p>Paschen, P., <b>84b</b>, 442</p> |
|---|---|



Pickard, G. W., 37, 439  
Pierce, G. W., 40, 63, 78  
Pirani, M., 84b, 442  
Poincaré, H., 25, 89, 80  
Prior, A. A., 57, 83, 412

Rayleigh, Lord, 12, 12, 13, 27, 29, 62,  
66, 173, 191, 280, 303

Salamons, J. R. A. W., 43, 439  
Shepardson, G. D., 67, 441  
Silsbee, F. B., 272  
Steinmetz, C., 9a, 55

Taylor, H. O., 56, 57a, 60, 69, 16, 23, 24,  
31, 143, 157, 160, 194, 274, 310

Tournayre, H., 70, 441

Upton, W. L., 29, 30, 287, 301

Velander, E., 84a, 442

Vreeland, F. K., 27, 22, 62, 243,

Webster, A. G., 82a, 167

Wegel, R. L., 89, 90, 93, 442

Wenner, F., 33, 279, 285, 286

Wheatstone, C., 62

Whitehead, J. B., 39, 6

Wien, W., 18, 21, 439

Winkelmann, A., 32, 440

Zenneck, J., 77a, 441